Distribution Agreement

In presenting this thesis or dissertation as a partial fulfillment of the requirements for an advanced degree from Emory University, I hereby grant Emory University and its agents the non-exclusive license to archive, make accessible, and display my thesis or dissertation in whole or in part in all forms of media, now or hereafter known, including display on the world wide web. I understand that I may select some access restrictions as part of the online submission of this thesis or dissertation. I retain all ownership rights to the copyright of the thesis or dissertation. I also retain the right to use in future works (such as articles or books) all or part of this thesis or dissertation.

Signature:

Aaron T. Bosse Date

C-H Functionalization Inspired Total Synthesis and New Donor/Acceptor Carbenes for Asymmetric C-H Functionalization

By

Aaron T. Bosse

Doctor of Philosophy

Chemistry

Huw M. L. Davies, Ph.D.

Advisor

Simon B. Blakey, Ph.D.

committee member

William M. Wuest, Ph.D.

committee member

Accepted:

Kimberly Jacob Arriola, Ph.D.

Dean of the James T. Laney School of Graduate Studies

Date

C-H Functionalization Inspired Total Synthesis and New Donor/Acceptor Carbenes for Asymmetric C-H Functionalization

By

Aaron T. Bosse
B.A., College of the Holy Cross, 2017

Advisor: Huw M. L. Davies, Ph.D.

An abstract of
A dissertation submitted to the Faculty of the
James T. Laney School of Graduate Studies of Emory University
in partial fulfillment of the requirements for the degree of
Doctor of Philosophy
in Chemistry
2022

Abstract

C-H Functionalization Inspired Total Synthesis and New Donor/Acceptor Carbenes for Asymmetric C-H Functionalization

By Aaron T. Bosse

Dirhodium(II)-catalyzed C-H insertion by donor/acceptor carbenes has become a powerful tool for catalyze controlled C-H functionalization. The Davies lab has spent decades developing various ligands to alter the steric and electronic profile of dirhodium tetracarboxylate catalyst, resulting in a "toolbox" of catalysts for a wide array of selective C-H functionalization reactions. The first chapter gives an overview of rhodium carbene chemistry, along with their applications in natural product synthesis.

The second chapter discusses the application of the newest generation of dirhodium tetracarboxylate catalysts applied to the total synthesis of (-)-cylindrocyclophane A. These C_2-symmetric natural products have a fascinating molecular architecture featuring a [7.7]paracyclophane ring. I developed and accomplished a route encompassing 6 C-H functionalization steps and primarily constructing the carbon skeleton through these steps. Four enantioselective carbene-induced C-H functionalizations to generate the six stereogenic centers, two palladium-catalyzed C-H functionalizations of diazocarbonyl compounds, and four directed C-H acetoxylations. Currently I am on the final step in the synthesis where completion of this work will represent a pinnacle for what C-H functionalization can achieve in total synthesis.

The third chapter describes the successful completion of an enantioselective formal synthesis of (-)-aflatoxin B_2. The route developed here highlights two impressive C-H functionalization methodologies enabling a completely novel strategy to this family of natural products. Chiral dirhodium-mediated C-H insertion not only establishes a key benzylic stereocenter with high enantioselectivity but also installs the appropriate functionality for the annulation of the C-ring. Following the carbene insertion, carbonyl-directed bis C-H acetoxylation site-selectively introduces the appropriate oxidation functionality needed. Together, these crucial transformations provide direct access to the tricyclic core of (-)-aflatoxin B_2 and highlight the considerable potential of site-selective C−H functionalizations in natural product synthesis.

The fourth and final chapter details the development of α-aryl-α-diazoketones for highly selective intermolecular C-H functionalization. The inspiration for this work stems from the desire to expand the chemical space one can access with our rhodium carbene technology. We hypothesized the ketone functionality could function as a surrogate for chiral alcohols and amines, greatly expanding on the established work with aryl diazoacetates. Optimization of the ketone/catalyst pairing lead us to a highly selective system using an aryl ketone and Rh_2(*S*-TPPTTL)$_4$. Following functionalization, we demonstrated this new ketone handle can be used to synthesize chiral benzylamides, allowing access to new chemical space unseen by the previous diazoesters.

C-H Functionalization Inspired Total Synthesis and New Donor/Acceptor Carbenes for Asymmetric C-H Functionalization

By

Aaron T. Bosse

B.A., College of the Holy Cross, 2017

Advisor: Huw M. L. Davies, Ph.D.

A dissertation submitted to the Faculty of the
James T. Laney School of Graduate Studies of Emory University
in partial fulfillment of the requirements for the degree of
Doctor of Philosophy
in Chemistry
2022

Acknowledgements

We've all had an amazing mentor that has touched our lives and changed them forever. For me, I've been luckily to experience guidance from two amazing individuals. The first is Prof. Andre Isaacs, who without him I would not be writing this dissertation. I first met Andre in my undergraduate years where I was incredibly lucky to join his lab, without having him previously as a lecture professor. In my two years of research with him, not only did he open my eyes to the wonders of organic synthesis but instilled in me a confidence that I could become an organic chemist. Without Andre's continuous support to this day, I would not have believed in my-self and that I could go to graduate school and get a Doctorate in organic chemistry. Andre taught me to persevere through challenges and critically think about how to solve problems. He gave me all the skills I would need to succeed in graduate school, not only conceptual topics but how to conduct research in an efficient and meticulous manner. Most importantly, he believed in me.

From this life changing experience, I decided to enter graduate school at Emory University where I would meet my second life changing mentor, Prof. Huw Davies. As a graduate research advisor, he continued the mentorship started by Andre and helped me succeed my goal of becoming an organic chemist. Huw is not only a caring professor that genuinely wants his students to succeed, but also a master at his ability to shape and navigate projects. However, the most impressive skill that I was able to witness and learn from Huw is his ability to lead and inspire people through the Center for Selective C-H Functionalization (CCHF). The feedback and instructions I received from Huw have been indispensable for my personal and professional growth as a chemist. In all my conversations with Huw about navigating my projects, I always left the meeting learning better ways to analyze data and execute the best possible plan. Additionally, not only did Huw mentor me in science and leadership he also assisting me in building a network of

scientists that will and has impacted my career forever. Huw positioned me in a role as a leader in the CCHF, enabling me to connect with many scientists across the country. This not only built my network but helped me understand chemistry from a larger perspective. I am beyond thank full for all that he has done for me and will be forever grateful for everything that he has done for me.

As the first connection Huw enable for me, Prof. Brian Stoltz has not only been my main collaborator through my Ph.D. but also a secondary mentor. Brian has always been there to support our project and help me think about how to break and build molecules. Even though I am not a part of his group, I am incredibly thankful to receive mentorship and guidance from one of the best synthetic chemists in the world. I also want to thank his kindness in opening his lab to me for a month and letting me immerse myself in his group. I would also like to thank Professor Erik Sorensen for being a wonderful collaborator and continuously challenging the way I think about synthetic strategies. Beyond my two collaborators I would also like to thank my committee members Professor Bill Wuest, Professor Simon Blakey and Professor Nate Jui. All of them have been incredibly helpful at my time at Emory, assisting me in developing the skills I need to succeed after Emory.

During my time at Emory not only have I interacted with amazing professors but have been helped by several other people. I first would like to thank Dan Morton, Rio Febrian and Rachael Hall. All these people are part of the management team for the CCHF and have become instrumental roles in my personal growth. Whenever I needed guidance all of them went above and beyond to help me in whatever I need. After I took the role of Student Leadership Counsel Chair for the CCHF, Rio and Rachael were both there to help me succeed in this new role and I would not have been successful without them.

Of course, working in the Davies lab would not have been such an amazing experience without all the group members I had the chance to interact with over the years. Not only were they my co-workers, but several have now become close friends in my life. Most importantly I would like to thank my mentor Dr. Wenbin Liu. When I first joined the lab Wenbin was always there for me to help me get adjusted and learn everything I needed to succeed. Even after she graduated, she still always gave me guidance when I ask for it. She probably doesn't know it but without her tutelage my lab hands would not be as good as they have become. I would also like to thank Maizie Lee for being an incredible lab mate, bay mate, and friend. Bo Wei and Yannick Boni both joined the lab together when I did, and they have been an incredible cohort to work with. I feel so fortunate to have had the privilege to experience grad school together with them and will always treasure their friendship. Lastly, Terrence Nguyen has been an amazing collaborator and mentee, who has challenged by viewpoint on how to conduct and think about research. Thank you Terrence for helping me bring our project to completion and being a wonderful mentee. All my success in the Davies lab would not be possible without the past and present group members and I am so fortunate to have had lab's input and feedback these past five years.

Throughout my time at Emory, I not only was able to make many friends, but I also was able to find my best friend. Ingrid Wilt is without a doubt the biggest supporter and best partner I could ask for. I am sure I would not have made it through grad school without her help and continuous support. Ingrid has shown me what it means to be a kind caring person through her actions and words. No one has ever pushed and challenged me like Ingrid. She has helped me become the person I am today, and I am so grateful that she has become a part of my life. Not only do I have her but our two amazing animals, Buddy and Loaf, who have become the support system I need after a tough day in lab.

Lastly, I would like to thank all my friends and family. My Ph.D. journey would not be possible without the support I receive from my parents. Since I was a child, they always supported what I wanted to do and for that I will always grateful. Not only did they support my ambitions but that gave me the tools I need to succeed by teaching me so many life skills. They also sacrificed more than I could know so that I could pursue my dreams. Mom and Dad, I love you so much and I can never thank you enough for all that you've done. Beyond my parents my brother and grandparents have also been incredibly helpful and supportive in my journey. I feel so fortunate to be blessed by an amazing brother that has and will always have my back. And my wonderful grandparents that have loved and supported me through my journey. Finally, I would like to thank my first chemistry teacher ever, Mrs. Trotochaud. Her AP Chemistry class in high school was my first experience of chemistry and it was her teaching that made me excited about the topic. It was her that put me on the path of science and got me interested and wanting to study chemistry in college. Without such a positive experience in high school I don't think I would be in the position I am in today.

For Andre and my parents

Table of Contents

List of Figures

List of Schemes

List of tables

List of Abbreviations

A	acceptor
ACN	acetonitrile
Ac	acetyl
AcOH	acetic acid
APCI	atmospheric pressure chemical ionization
Ar	aryl
Bn	benzyl
Boc	*tert*-butyloxycarbonyl
Bu	butyl
CBS	Corey–Bakshi–Shibata catalyst
CCHF	NSF Center for Selective C-H Functionalization
CMD	concerted metal-deprotonation
D	donor
DBU	1,8-diazabicycloundec-7-ene
DCC	*N*,*N*′-dicyclohexylcarbodiimide
1,2-DCE	1,2-dichloroethane
DCM	dichloromethane
DG	directing group
DIBAL-H	diisobutylaluminium hydride
DMAP	N,N-4-(dimethylamino)pyridine
DMF	dimethylformamide
DMSO	dimethyl sulfoxide

DYKAT	dynamic kinetic asymmetric transformation
dr	diastereomeric ratio
ee	enantiomeric excess
EDCI	1-Ethyl-3-(3-dimethylaminopropyl)carbodiimide
EDG	electron-donating group
Et	ethyl
EtOAc	ethyl acetate
Et_3N	triethylamine
equiv	equivalents
ESI	electrospray ionization
EWG	electron-withdrawing group
g	gram
h	hour
HATU	hexafluorophosphate azabenzotriazole tetramethyl uranium
Het	heteroaromatic
hexene	*trans*-2-hexene
HFIP	1,1,1,3,3,3-hexafluoroisopropanol
HFL	Hofmann-Löffler-Freytag
HPLC	high performance liquid chromatography
HRMS	high-resolution mass spectrometry
HWE	Horner-Wadsworth-Emmons
hv	light
IR	infrared spectroscopy
KOH	potassium hydroxide

L_n	ligand
LiOH	lithium hydroxide
LCMS	liquid chromatography–mass spectrometry
m	*meta*
M	metal
Me	methyl
min	minute
MOA	mechanism of action
mol	mole
mmol	millimoles
mg	milligram
m.p.	melting point
Ms	Mesyl
M.S.	molecular sieves
NMR	nuclear magnetic resonance
N.D.	not detected
N.R.	no reaction
NSI	nanospray ionization
***o*-NBSA**	*ortho*-nitrobenzenesulfonyl azide
OMe	methoxy
o	*ortho*
p	*para*
***p*-ABSA**	*para*-acetamidobenzenesulfonyl azide

P	protecting group
Ph	phenyl
Phth	phhalimide
PIDA	(Diacetoxyiodo)benzene
PKS	polyketide synthase
Rh_2[*R*-3,5-di(*p*-^{t}BuPh)TPCP]$_4$	Rh_2(*R*-DiBic)$_4$
Rh_2[*R*-3,5-tris(*p*-^{t}BuPh)TPCP]$_4$	Rh_2(*R*-TriBic)$_4$
RCM	ring-closing olefin metathesis
rr	regioisomericf ratio
r.t.	room temperature
SAR	structure activity relationship
SI	supplemental information
TES	triethylsilane
TBDPS	*tert*-butyl diphenyl silane
TBS	*tert*-butyldimethylsilyl
TCE	2,2,2-trichloroethoxycarbonyl
temp	temperature
TMDS	tetramethyldisiloxane
TMTOH	Me_3SnOH
TPCP	triarylcyclopropanecarboxylate
TFA	trifluoroacetic acid
TFE	2,2,2-trifluoroethoxycarbonyl
TFT	trifluorotoluene

TFAA	trifluoroacetic anhydride
THF	tetrahydrofuran
TIPS	triisopropylsilyl
TLC	thin layer chromatography
TMS	trimethylsilyl
Troc	2,2,2-trichloroethoxycarbonyl
Ts	tosyl
Zn	zinc

Chapter 1

Introduction to Selective C-H Functionalization via Dirhodium Carbenes and Applications in Total Synthesis

---

1.1. Site-selective C-H Functionalization

After decades of experimentation and failure, C-H Functionalization has emerged as a practical technology for the streamlined synthesis of complex molecules.[1-7] Traditionally organic chemistry has been limited to transformations through functional group manipulation. Energetic and electronic differences between functional groups and C-H bonds are needed for a selective reaction to take place. Utilizing functional groups limits the chemical space one can access, as well as increases the step count and cost to a valuable molecule.[8] Alternatively, C-H functionalization proceeds through direct reaction of a C-H bond, removing the need for an additional functional group handle. Yet the ubiquity of the C-H bond in organic molecules reveals the defining challenge for the field, namely site-selectivity.[1, 3, 4, 6, 9-18] Out of this problem of functionalizing a single C-H bond, two solutions have been developed.

One of the first solutions developed is to control the reaction selectivity through the substrate itself. Radical reactions have achieved site-selectivity through intramolecular hydrogen transfer via the Hofmann-Löffler-Freytag (HLF) reaction.[19-24] While an effective strategy, the HFL reaction is limited to the inherent bias of the substrate and thus a specific C-H bond 5 atoms away. Moving to transitional metal catalysts, extensive work has been done on exploring and developing directing groups to control the metal's insertion into a specific C-H bond by chelation of the directing group with the metal.[9, 25-29] Initial development of directing groups utilized strong directing groups that tightly bind to the metal.[30, 31] While these gave great selectivity, they only

worked with specific directing groups and installing/removal of them added unnecessary steps in a synthesis.[32] Recently, Jin-Quan Yu has pioneered a new idea of weakly coordinating directing groups.[9, 33] These functional groups, such as simple carbonyls, now reversibly bind the metal enabling a wide array of directing groups, that theoretically could be any functional group.[34]

The second solution to site-selectivity in C-H Functionalization is catalyst control.[35-39] Enzymes, which in biological systems are known to be exquisitely selective for a specific substrate and reaction, have now been engineered to work in a flask.[40-42] Directed evolution, pioneered by Francis Arnold, is where an enzyme is fed a certain non-natural substrate, then evolved over several iterations to be highly selective for the desired transformation.[42] Beyond enzymes, privileged transitions metals combined with special ligands, have become another effective platform for catalyst-controlled C-H functionalization.[10] Excitingly, this system has the potential to be general for catalyst-controlled selective C-H functionalization by the development of ligands for various C-H bonds. The ultimate outcome of this strategy would be the creation of a "toolbox" with an array of catalysts with different ligands, each with a defined steric and electronic profile to tune the selectivity.

To date, one of the most powerful transformations of this type is the catalyst-controlled C-H functionalization and C-C bond formation using metal carbenes.[6, 10, 15] The traditional way a carbene is formed is through the decomposition of a diazo compound by various metals, typically copper or rhodium.[43] The metal carbene is generated *in situ* when the diazo compound approaches the electrophilic catalyst, extruding nitrogen to form the transient carbene.[15] The metal carbene then inserts itself into a C-H bond through a concerted hydride abstraction event (Scheme 1.1).[15] Due to the partial positive charge build-up in the transition state for the C-H insertion, the site on the substrate that best stabilizes the intermediate will preferably be functionalized. However,

depending on the steric environment around the catalyst, ligands can force the carbene under catalyst control, reacting with sites not typically preferred by the substrate.[10]

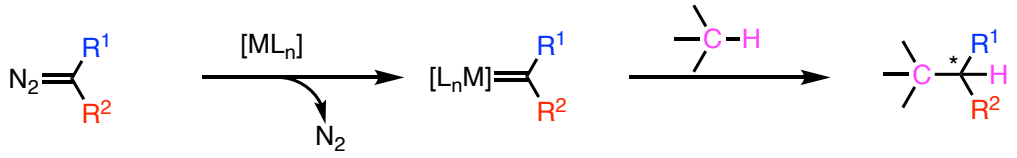

Scheme 1.1 General mechanism for metal carbene formation and C-H functionalization

1.2. Dirhodium Carbene Chemistry and Catalyst Toolbox

There are a variety of metals that decompose diazo compounds, however dirhodium (II) complexes are the most efficient for metal carbene transformation.[44, 45] These dirhodium carbenes have been spectroscopically shown to be similar to group VI Fischer carbenes, and computational data indicates the rhodium carbene is extremely electrophilic, allowing C-H bonds to act as nucleophiles.[46-48] This links the stability and selectivity of rhodium carbenes to the electronic properties on the diazo substrate, allowing one to tune the reactivity based on the substituents (Figure 1.1). These diazo compounds, carbene precursors, have been classified into five groups.[43] Acceptor carbenes with one or two electron-withdrawing groups attached demonstrate limited selectivity for intermolecular C-H functionalization due to the high reactivity of the unstable metal carbene.[13] In contrast, donor carbenes with one or two electron-donating groups attached, stabilizes the carbene which lowers reactivity but increases selectivity.[43] Therefore, to find the goldilocks zone of reactivity, the Davies group developed donor/acceptor carbenes.[49, 50] The acceptor group keeps the reactivity while the donor group attenuates the carbene's electrophilicity by donating electron density into the empty *p*-orbital of the carbene carbon.[45, 51]

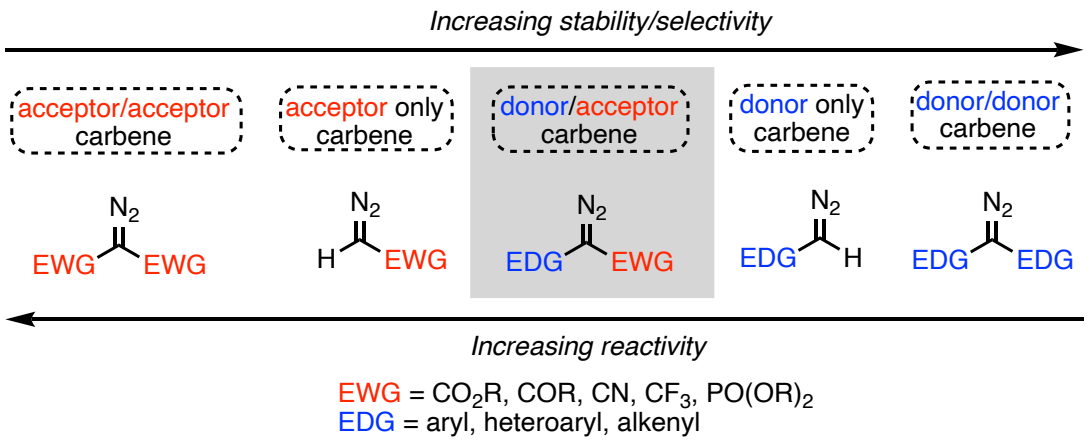

Figure 1.1 Dirhodium carbene classes

Once the donor/acceptor diazos were found to be the superior carbene source, several dirhodium catalyst have been developed for site- and stereoselective C-H functionalization. While the electronics on the diazo is critical for selective reactivity, equally as important is the ligand scaffold around the metal. In the Davies group, we have developed three generations of dirhodium tetracarboxylate catalysts, each with their own selectivity profile (Figure 1.2). The first-generation catalysts have chiral sulfonyl proline ligands.[52-54] The most broadly used, $Rh_2(DOSP)_4$, includes a dodecyl sulfonyl proline ligand, allowing solubility in non-polar solvents increasing its performance.[52] Notably, $Rh_2(DOSP)_4$, functions well across a wide range of C-H bonds, preferring activated bonds either benzylic, allylic, or adjacent to oxygen or nitrogen.[44] Other proline-based catalysts, like $Rh_2(biDOSP)_4$, include a linker between the proline rings rigidifying the catalyst, in hopes to improve the reaction profile. However, $Rh_2(biDOSP)_4$ was never fully explored due to the difficulty of the synthesis and the use of *tert*-butyllithium.[55] The second class of catalysts is phthalimido-based and originally developed by Hashimoto, the most significant being $Rh_2(PTTL)_4$ and $Rh_2(TCPTTL)_4$, used for enantioselective amidation.[56-59] Impressed by the results with these catalysts the Davies lab developed $Rh_2(PTAD)_4$ and $Rh_2(TCPTAD)_4$ to use with our

donor/acceptor carbenes. The synthesis of these two catalysts leverages the selectivity of Rh_2(DOSP) to functionalize the adamantane scaffold, providing a new catalyst with increased site-selectivity and reactivity.[60, 61] The adamantyl group is bulkier than the *tert*-butyl group, blocking the bottom face of the catalyst, increasing asymmetric induction in the C-H insertion step. These second-generation catalysts were designed to be readily diversified through a variety of chiral amino acids for the ligand synthesis. Most recently, Rh_2(TPPTTL)$_4$, was developed as the newest member in this generation for the desymmetrization of cyclohexane derivatives.[62] The third generation of catalysts feature chiral triarylcyclopropane ligands.[63, 64] Just as Rh_2(PTAD)$_4$ was inspired by C-H functionalization of adamantane using Rh_2(DOSP)$_4$, the third generation is prepared through asymmetric cyclopropanation of 1,1-diphenylethylene using the first- or second-generation catalysts (JT-28).[65-68] These ligands are called **T**ri**P**henyl**C**yclo**P**ropanecarboxylates (TPCP), many of which are sterically congested allowing for unseen selectivity from the previous generations. Crucially, these catalysts have a highly modular route and can display a wide range of conformations, resulting in novel selectivity.

1st Generation: Chiral prolinate ligands

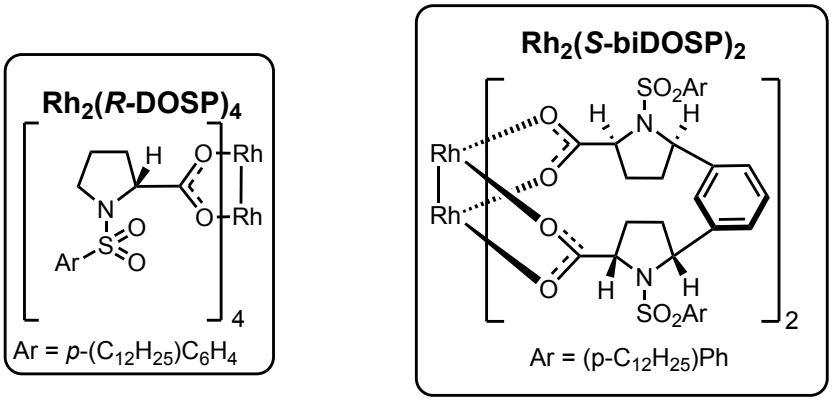

2nd Generation: Phthalimide-protected chiral amino acid ligands

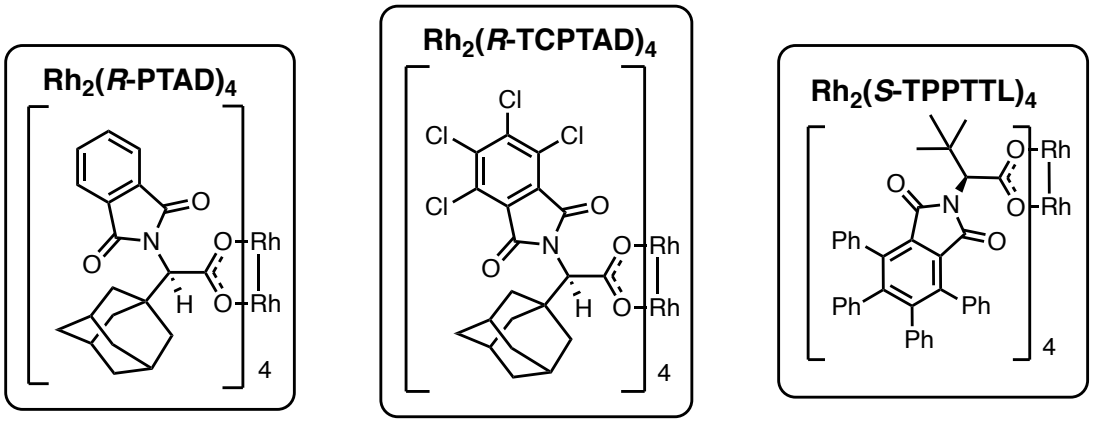

3rd Generation: Chiral triarylcyclopropane ligands

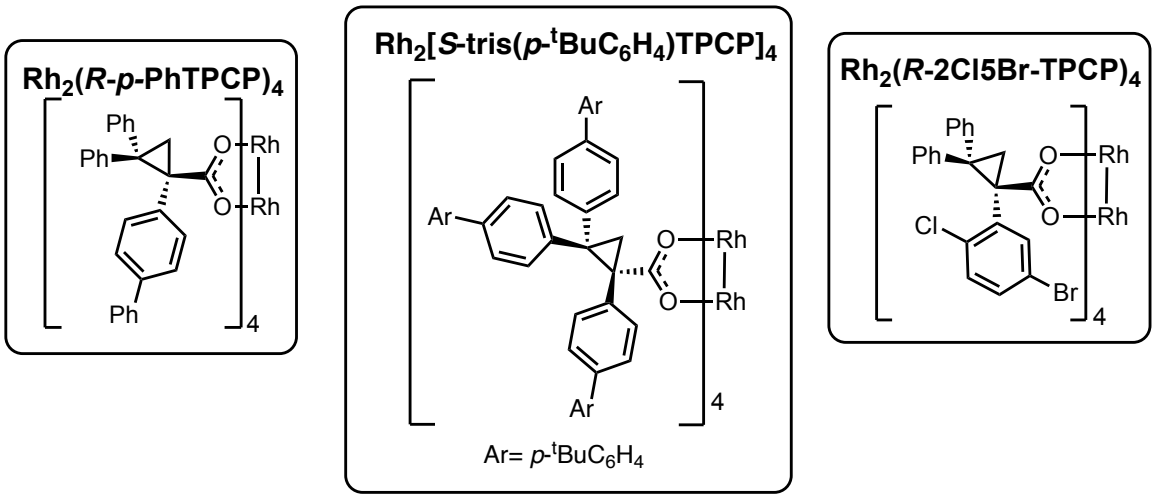

Figure 1.2 Representative dirhodium catalysts used in the Davies group

With the catalyst toolbox expanding we now have catalysts capable of functionalizing C-H bonds that are difficult or previously impossible to react with. Each dirhodium catalyst was developed to distinguish between C-H bonds with no electronic bias and only slight steric differences, shown eloquently in the branched hydrocarbon model in Figure 1.3. This selectivity paradigm is illuminated in the reactions of 2-methylpentane with donor/acceptor diazoacetates and our newest catalysts. Using Rh_2[*R*-3,5-di(*p*-^{t}BuPh)TPCP]$_4$ (or Rh_2(*R*-DiBic)$_4$) this bulky catalyst is capable of inserting the carbene into the most accessible methylene C-H bond of the substrate.[68] Since the catalyst itself contains an elaborate triphenylcyclopropane (TPCP) ligand, high diastereo- and enantioselectivity can be achieved without substantial steric difference around the C-H bond in the substrate. After the creation of this catalyst, further efforts in the lab have allowed successful site-selective C-H functionalization at the most accessible tertiary C-H bond by Rh_2(*R*-TCPTAD)$_4$, and primary C-H bond by Rh_2[*R*-3,5-tris(*p*-^{t}BuPh)TPCP]$_4$ (or Rh_2(*R*-TriBic)$_4$).[65, 66] These results demonstrate the power of dirhodium (II) tetracarboxylate catalysts in their ability to override substrate control in favor of catalyst preference. Beyond hydrocarbons the scope of these catalysts has been demonstrated on more complex targets, such as steroid derivatives.

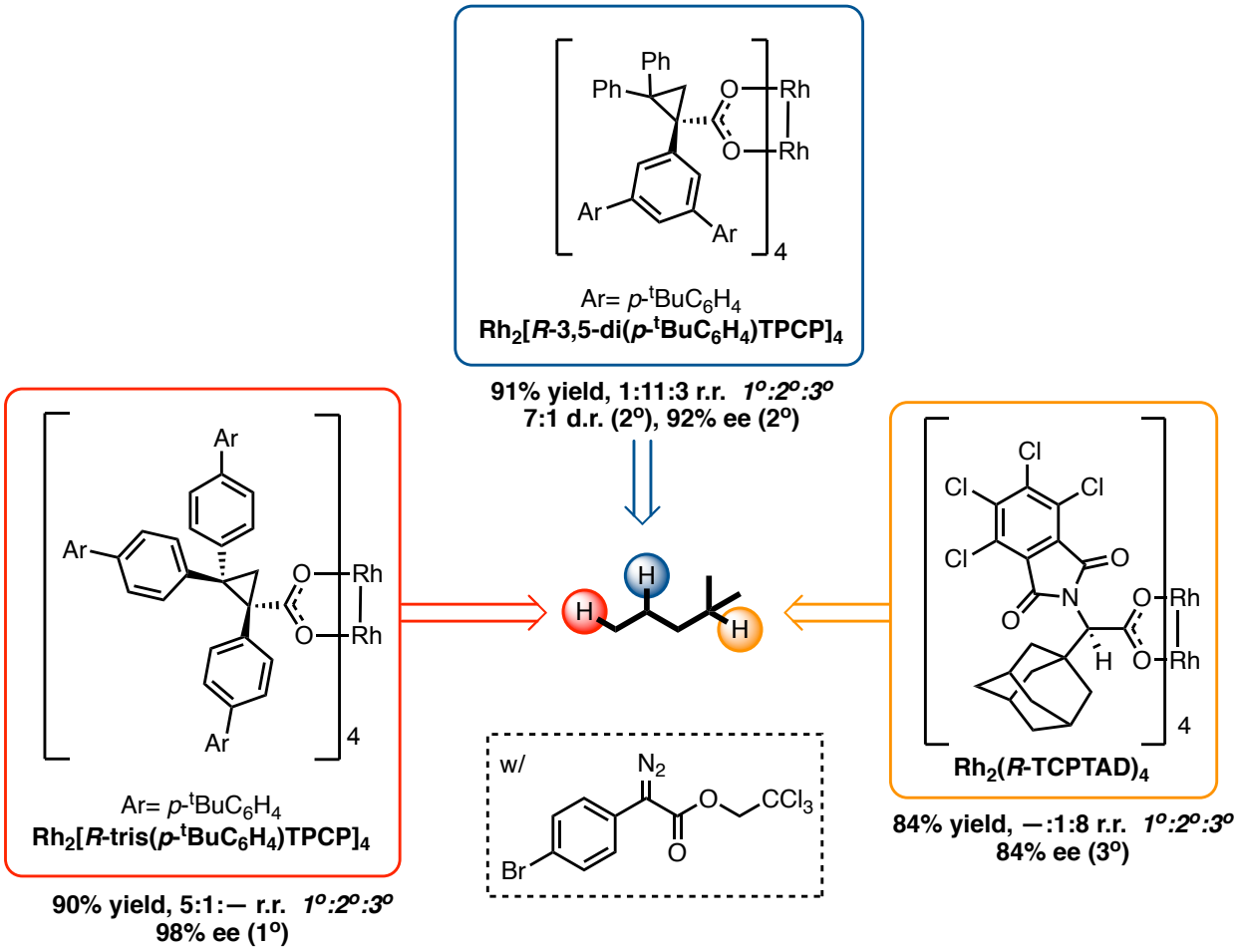

Figure 1.3 General site selectivity of Davies catalyst toolbox

Recently, the Davies group has been able to push the site-selectivity even further with the disclosure of a new TPCP catalyst. This novel catalyst has an *ortho*-Cl substituent on one of the phenyl rings that not only changes the overall geometry but has a unique site-selectivity.[67] The catalyst, Rh_2(*R*-2-Cl-5-BrTPCP)$_4$, is capable of completely overcoming the electronic bias in a substrate and will functionalize the most accessible C2 methylene C-H bond, even in the presence of electronically activated methylene C-H bonds (Scheme 1.2). Not only is the reaction highly regioselective but also enantio- and diastereoselective. Additionally, the complementary site-selectivity at the benzylic position can be achieved with Rh_2(*R*-TCPTAD)$_4$. It is hypothesized that

the *ortho*-Cl based catalyst is sterically more encumbered and therefore prefers the most sterically accessible methylene proton. Furthermore, the *ortho*-Cl substituent is essential in changing the symmetry of the complex to C_4, while other TPCP catalysts tend to adopt D_2 or C_2 symmetry.[10] Moving beyond simple hydrocarbons, the rhodium carbene chemistry has been applied in the synthesis of bioactive pharmaceuticals, such as Ritalin and Effexor.[13, 69, 70] Even more impressive, this technology has been used in the synthesis of natural products.

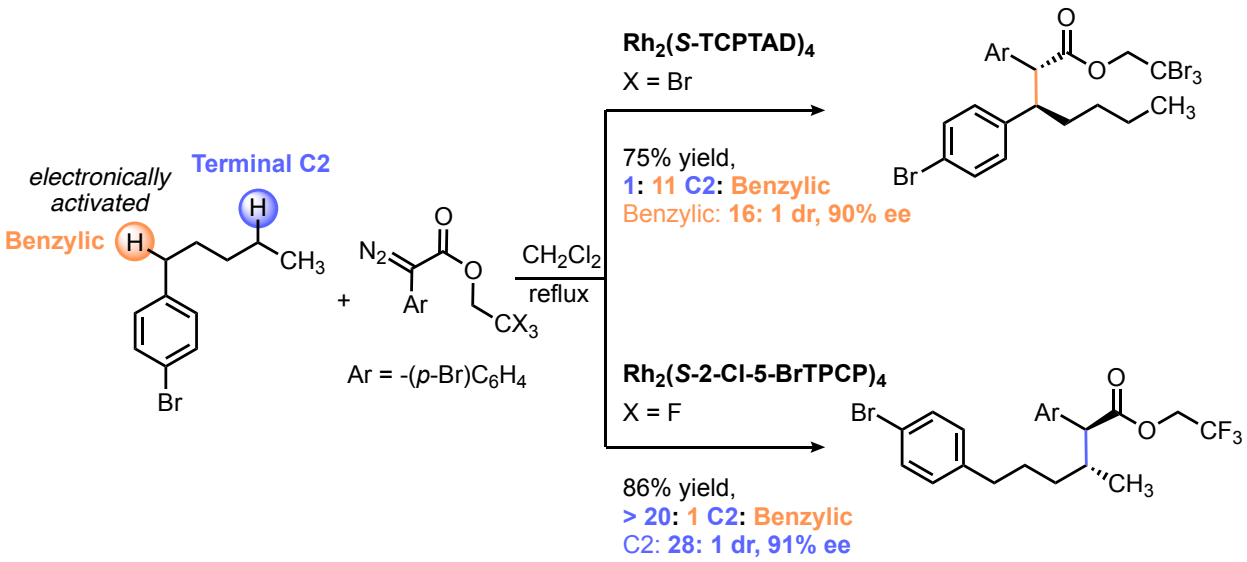

Scheme 1.2 Complementary site-selectivity of Rh_2(*R*-2-Cl-5-BrTPCP)$_4$ and Rh_2(*R*-TCPTAD)$_4$

1.3. Applications of Dirhodium Carbene Chemistry in Total Synthesis

The ability to develop a novel methodology and then apply the technology to natural product synthesis will always be the penultimate demonstrate of its utility. Over the decades of developing new dirhodium catalysts, the Davies lab has been highly successful in applying these catalysts to total synthesis endeavors. This thesis will discuss the five most recent syntheses tackled by the Davies lab leveraging C-H functionalization strategies made possible by dirhodium (II) tetracarboxylate catalysts.

In 2006, the first-generation catalyst, Rh_2(*R*-DOSP)$_4$, was successfully used in the synthesis of (-)-colombiasin A (Scheme 1.3).[71] Using a vinyldiazoacetate, the key step in the synthesis is a C-H activation/Cope rearrangement that kinetically resolves a stereocenter as well as forms two new ones. Incredibly this step also goes with remarkably high diastereoselectivity and high enantioselectivity (>20:1 dr, >95% ee). The result of this impressive transformation is a 14-step synthesis where the key carbene step sets three stereogenic centers in a single reaction.

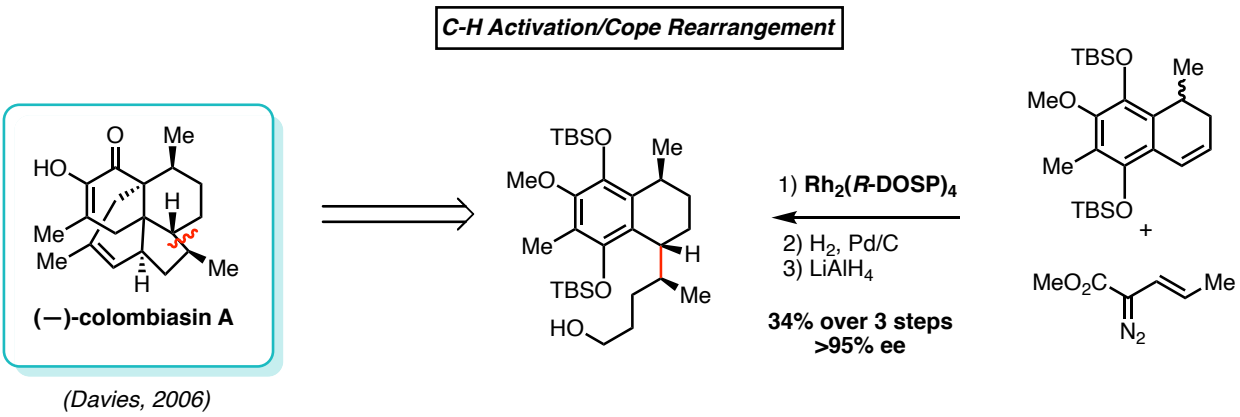

Scheme 1.3 Key step in the total synthesis of (-)-colombiasin A

The second-generation of catalysts, Rh_2(*R*-PTAD)$_4$ was successfully used in the synthesis of (-)-5-epi-vibsanin E (Scheme 1.4).[72] Rh_2(*R*-PTAD)$_4$ enables highly efficient [4+3] cycloaddition with dienes, which was leveraged to form a cycloheptane in the key step. Formally a [4+3] cycloaddition proceeds through first cyclopropanation of the diene by a vinyldiazoacetate, followed by a Cope rearrangement to form the enantioenriched cycloheptane. This step not only forms a difficult medium size ring, but also a quaternary stereocenter with high enantioselectivity (90% ee). The result of this transformation is an 18-step route where the key rhodium catalyzed step allows rapid assembly of the tricyclic core.

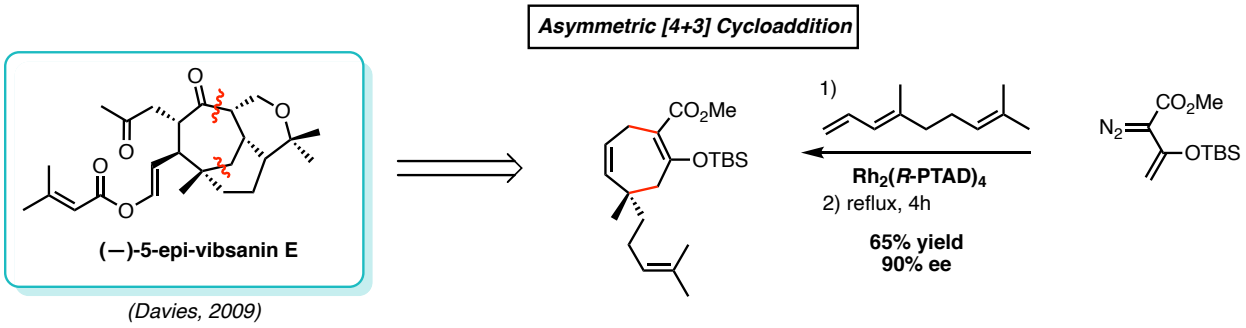

(Davies, 2009)

Scheme 1.4 Key step in the total synthesis of (-)-5-epi-vibsanin E

Continuing with the success of the second-generation catalysts, the next synthesis utilizes Rh_2(*R*-PTTL)$_4$ in a C-H functionalization of an activated C(sp^3)-H bond. In a collaboration with the Yu group, we sought to apply multiple C-H activation steps in a row to access the core scaffold in the natural product lithospermic acid.[73] In a short C-H activation/C-O cyclization sequence, the core dihydrobenzofuran architecture can be assembled (Scheme 1.5). The C-H functionalization proceeds through the insertion of a benzylic methylene adjacent to a silyl protected alcohol. This doubled activated proton allows for efficient hydride abstraction, combined with the ligand scaffold to yield a highly selective step (>97:3 dr, 95% ee). While the authors did not make the actual natural product, the strategy demonstrated allows for rapid formation of the core scaffold.

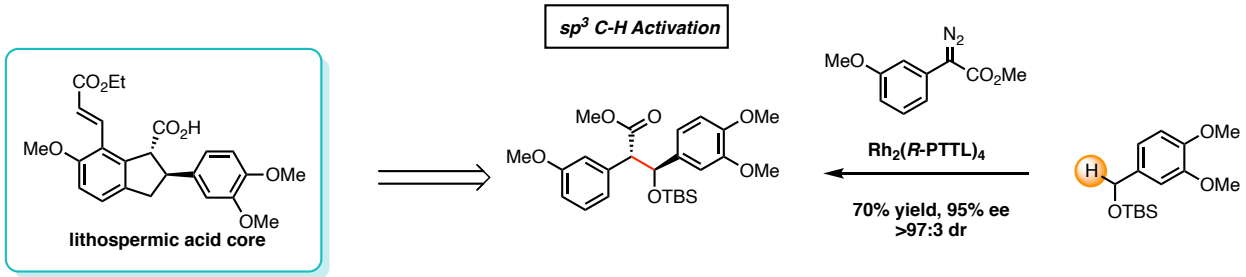

(Davies/Yu, 2013)

Scheme 1.5 Key step in the synthesis of lithospermic acid core

The next synthesis moves from the traditional focus of the Davies lab on C(sp^3)-H functionalization to C(sp^2)-H functionalization. In 2015, the Davies lab partnered with the Itami group to tackle the synthesis of dictyodendrin A.[74] Using Rh_2(*S*-TCPTAD)$_4$ the team was able to do a double C(sp^2)-H activation of the protons on the pyrrole core (Scheme 1.6). An initial C-H cross coupling followed by the double carbene C-H insertion, enabled a rapid construction of the core architecture, demonstrating how C-H functionalization logic can streamline synthesis. The result is a formal synthesis that is 12-steps in the longest linear sequence.

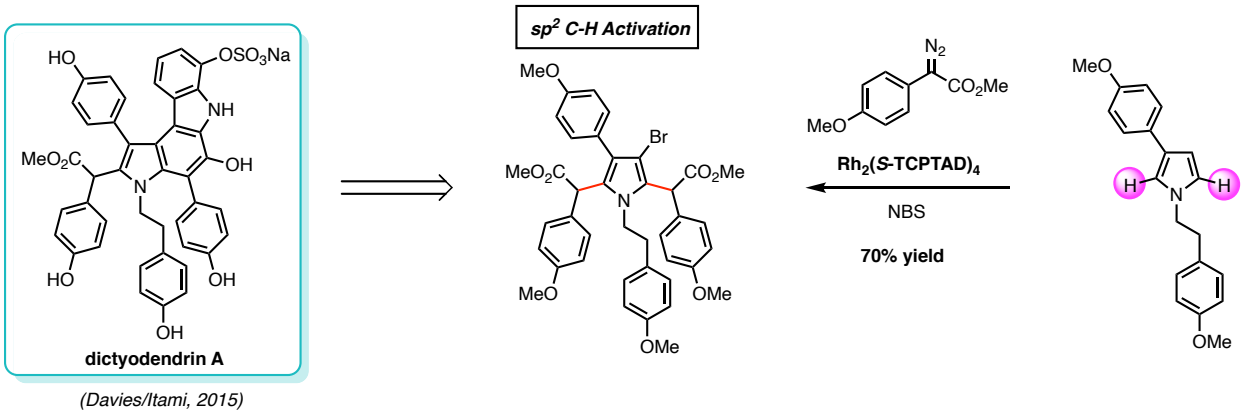

Scheme 1.6 Key step in the Total Synthesis of dictyodendrin A

The final total synthesis, and most recent attempt by the Davies lab, is the construction of the indoxamycin core.[75] In this strategy, the most ambitious C-H functionalization is attempted with bicyclo[3.3.0]octane used as the coupling partner. Previously discussed routes either undergo a formal sigmatropic rearrangement (Scheme 1.3/1.4) or functionalize an incredibly activated C-H bond (Scheme 1.5) where it is the only one that can react. In this system with bicyclo[3.3.0]octane the substrate now has multiple sites of C-H bonds that could be activated. Thus, catalyst control using a dirhodium catalyst from our toolbox would be critical for success. Using Rh_2(*S*-PTAD)$_4$ the researchers were able to develop not only a reaction that was incredibly

regioselective but also highly diastereoselective (Scheme 1.7, >20:1 rr, >20:1 dr). Following a directed C-H activation Heck coupling, in two steps the densely functionalized architecture found in the indoxamycin natural products was formed.

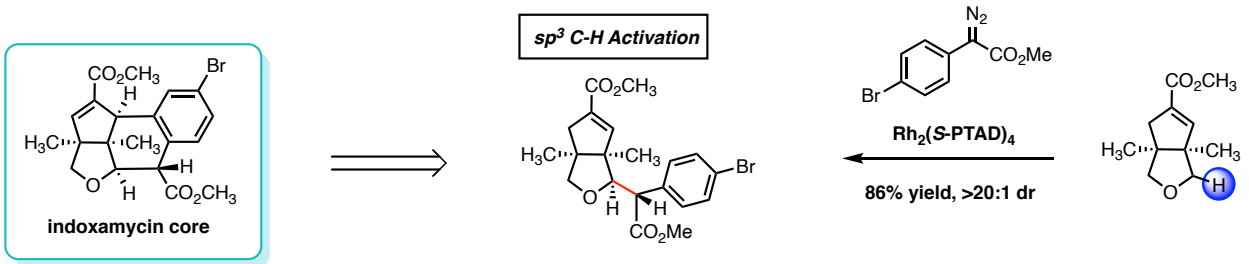

(Davies/Yu/Sorensen, 2016)

Scheme 1.7 Key step in the synthesis of indoxamycin core

1.4. Conclusion

The development of dirhodium (II) carbene chemistry has exploded over the past decade. It has moved from an organometallic novelty to a serious and powerful strategy for the synthesis of small molecules or complex targets. The ability to access new chemical space instantly and with high regio-, enantio- and diastereocontrol is unmatched by most methods. This ability is demonstrated the best in the many examples of natural product synthesis using donor/acceptor diazoacetates. In these selected examples, the C-H functionalization serves as a linchpin step that not only streamlines the routes but creates dense stereochemically rich functionality in a single step. However, all the previous strategies shown previous only us the first and second generations of catalysts and are limited to activated C-H bonds. There has yet to be an endeavor using the newest third generation of catalysts and attempting unactivated C-H functionalization in a total synthesis project.

The focus of this dissertation will describe the utilization of the newest dirhodium (II) tetracarboxylate catalysts in the synthesis of two natural products. Chapter 2 will detail the most

ambitious application of the dirhodium technology, namely the streamlined synthesis of (-)-cylindrocyclophane A using C-H functionalization logic. Chapter 3 will elaborate on how the strategy to (-)-cylindrocyclophane A was able to be adapted to a formal enantioselective synthesis of (-)-aflatoxin B_2. Lastly, chapter 4 will go over the development of new donor/acceptor carbene precursors, name α-aryl-α-diazoketones.

1.5. References

1. Gutekunst, W. R.; Baran, P. S., C–H functionalization logic in total synthesis. *Chem. Soc. Rev.* **2011,** *40* (4), 1976-1991.
2. McMurray, L.; O'Hara, F.; Gaunt, M. J., Recent developments in natural product synthesis using metal-catalysed C–H bond functionalisation. *Chem. Soc. Rev.* **2011,** *40* (4), 1885-1898.
3. Yamaguchi, J.; Yamaguchi, A. D.; Itami, K., C-H Bond Functionalization: Emerging Synthetic Tools for Natural Products and Pharmaceuticals. *Angew. Chem. Int. Ed.* **2012,** *51* (36), 8960-9009.
4. Wencel-Delord, J.; Glorius, F., C–H bond activation enables the rapid construction and late-stage diversification of functional molecules. *Nat. Chem.* **2013,** *5* (5), 369-375.
5. Hartwig, J. F., Evolution of C–H Bond Functionalization from Methane to Methodology. *J. Am. Chem. Soc.* **2016,** *138* (1), 2-24.
6. Davies, H. M. L.; Morton, D., Recent Advances in C–H Functionalization. *J. Org. Chem.* **2016,** *81* (2), 343-350.
7. Abrams, D. J.; Provencher, P. A.; Sorensen, E. J., Recent applications of C–H functionalization in complex natural product synthesis. *Chem. Soc. Rev.* **2018,** *47* (23), 8925-8967.
8. Bream, R. N.; Clark, H.; Edney, D.; Harsanyi, A.; Hayler, J.; Ironmonger, A.; Mc Cleary, N.; Phillips, N.; Priestley, C.; Roberts, A.; Rushworth, P.; Szeto, P.; Webb, M. R.; Wheelhouse, K., Application of C–H Functionalization in the Development of a Concise and Convergent Route to the Phosphatidylinositol-3-kinase Delta Inhibitor Nemiralisib. *Org. Process Res. Dev.* **2021,** *25* (3), 529-540.
9. Meng, G.; Lam, N. Y. S.; Lucas, E. L.; Saint-Denis, T. G.; Verma, P.; Chekshin, N.; Yu, J.-Q., Achieving Site-Selectivity for C–H Activation Processes Based on Distance and Geometry: A Carpenter's Approach. *J. Am. Chem. Soc.* **2020,** *142* (24), 10571-10591.
10. Davies, H. M. L.; Liao, K., Dirhodium tetracarboxylates as catalysts for selective intermolecular C–H functionalization. *Nat. Rev. Chem.* **2019,** *3* (6), 347-360.
11. Godula, K.; Sames, D., C-H Bond Functionalization in Complex Organic Synthesis. *Science* **2006,** *312* (5770), 67-72.
12. Noisier, A. F. M.; Brimble, M. A., C–H Functionalization in the Synthesis of Amino Acids and Peptides. *Chem. Rev.* **2014,** *114* (18), 8775-8806.

13. Davies, H. M. L.; Du Bois, J.; Yu, J.-Q., C–H Functionalization in organic synthesis. *Chem. Soc. Rev.* **2011,** *40* (4), 1855-1856.
14. Ye, J.; Lautens, M., Palladium-catalysed norbornene-mediated C–H functionalization of arenes. *Nat. Chem.* **2015,** *7* (11), 863-870.
15. Davies, H. M. L.; Manning, J. R., Catalytic C–H functionalization by metal carbenoid and nitrenoid insertion. *Nature* **2008,** *451* (7177), 417-424.
16. Kärkäs, M. D., Electrochemical strategies for C–H functionalization and C–N bond formation. *Chem. Soc. Rev.* **2018,** *47* (15), 5786-5865.
17. Revathi, L.; Ravindar, L.; Fang, W.-Y.; Rakesh, K. P.; Qin, H.-L., Visible Light-Induced C−H Bond Functionalization: A Critical Review. *Adv. Synth. Catal.* **2018,** *360* (24), 4652-4698.
18. Wei, Y.; Hu, P.; Zhang, M.; Su, W., Metal-Catalyzed Decarboxylative C–H Functionalization. *Chem. Rev.* **2017,** *117* (13), 8864-8907.
19. Yang, M.; Su, B.; Wang, Y.; Chen, K.; Jiang, X.; Zhang, Y.-F.; Zhang, X.-S.; Chen, G.; Cheng, Y.; Cao, Z.; Guo, Q.-Y.; Wang, L.; Shi, Z.-J., Silver-catalysed direct amination of unactivated C–H bonds of functionalized molecules. *Nat. Commun.* **2014,** *5* (1), 4707.
20. O'Broin, C. Q.; Fernández, P.; Martínez, C.; Muñiz, K., N-Iodosuccinimide-Promoted Hofmann–Löffler Reactions of Sulfonimides under Visible Light. *Org. Lett.* **2016,** *18* (3), 436-439.
21. Wappes, E. A.; Fosu, S. C.; Chopko, T. C.; Nagib, D. A., Triiodide-Mediated δ-Amination of Secondary C−H Bonds. *Angew. Chem. Int. Ed.* **2016,** *55* (34), 9974-9978.
22. Choi, G. J.; Zhu, Q.; Miller, D. C.; Gu, C. J.; Knowles, R. R., Catalytic alkylation of remote C–H bonds enabled by proton-coupled electron transfer. *Nature* **2016,** *539* (7628), 268-271.
23. Becker, P.; Duhamel, T.; Martínez, C.; Muñiz, K., Designing Homogeneous Bromine Redox Catalysis for Selective Aliphatic C−H Bond Functionalization. *Angew. Chem. Int. Ed.* **2018,** *57* (18), 5166-5170.
24. Bao, X.; Wang, Q.; Zhu, J., Copper-catalyzed remote C(sp3)–H azidation and oxidative trifluoromethylation of benzohydrazides. *Nat. Commun.* **2019,** *10* (1), 769.
25. Lyons, T. W.; Sanford, M. S., Palladium-Catalyzed Ligand-Directed C−H Functionalization Reactions. *Chem. Rev.* **2010,** *110* (2), 1147-1169.
26. Zhang, F.; Spring, D. R., Arene C–H functionalisation using a removable/modifiable or a traceless directing group strategy. *Chem. Soc. Rev.* **2014,** *43* (20), 6906-6919.
27. He, J.; Wasa, M.; Chan, K. S. L.; Shao, Q.; Yu, J.-Q., Palladium-Catalyzed Transformations of Alkyl C–H Bonds. *Chem. Rev.* **2017,** *117* (13), 8754-8786.
28. Saint-Denis Tyler, G.; Zhu, R.-Y.; Chen, G.; Wu, Q.-F.; Yu, J.-Q., Enantioselective C(sp3)–H bond activation by chiral transition metal catalysts. *Science* **2018,** *359* (6377), eaao4798.
29. Shang, M.; Feu Karla, S.; Vantourout Julien, C.; Barton Lisa, M.; Osswald Heather, L.; Kato, N.; Gagaring, K.; McNamara Case, W.; Chen, G.; Hu, L.; Ni, S.; Fernández-Canelas, P.; Chen, M.; Merchant Rohan, R.; Qin, T.; Schreiber Stuart, L.; Melillo, B.; Yu, J.-Q.; Baran Phil, S., Modular, stereocontrolled Cβ–H/Cα–C activation of alkyl carboxylic acids. *PNAS* **2019,** *116* (18), 8721-8727.
30. Tomberg, A.; Muratore, M. É.; Johansson, M. J.; Terstiege, I.; Sköld, C.; Norrby, P.-O., Relative Strength of Common Directing Groups in Palladium-Catalyzed Aromatic C−H Activation. *iScience* **2019,** *20*, 373-391.

31. Dutta, U.; Maiti, D., Emergence of Pyrimidine-Based meta-Directing Group: Journey from Weak to Strong Coordination in Diversifying meta-C–H Functionalization. *Acc. Chem. Res.* **2022,** *55* (3), 354-372.
32. Mahamudul Hassan, M. M.; Mondal, B.; Singh, S.; Haldar, C.; Chaturvedi, J.; Bisht, R.; Sunoj, R. B.; Chattopadhyay, B., Ir-Catalyzed Ligand-Free Directed C–H Borylation of Arenes and Pharmaceuticals: Detailed Mechanistic Understanding. *J. Org. Chem.* **2022**.
33. Engle, K. M.; Mei, T.-S.; Wasa, M.; Yu, J.-Q., Weak Coordination as a Powerful Means for Developing Broadly Useful C–H Functionalization Reactions. *Acc. Chem. Res.* **2012,** *45* (6), 788-802.
34. Li, G.; Wan, L.; Zhang, G.; Leow, D.; Spangler, J.; Yu, J.-Q., Pd(II)-Catalyzed C–H Functionalizations Directed by Distal Weakly Coordinating Functional Groups. *J. Am. Chem. Soc.* **2015,** *137* (13), 4391-4397.
35. Thu, H.-Y.; Tong, G. S.-M.; Huang, J.-S.; Chan, S. L.-F.; Deng, Q.-H.; Che, C.-M., Highly Selective Metal Catalysts for Intermolecular Carbenoid Insertion into Primary C□H Bonds and Enantioselective C□C Bond Formation. *Angew. Chem. Int. Ed.* **2008,** *47* (50), 9747-9751.
36. Díaz-Requejo, M. M.; Pérez, P. J., Coinage Metal Catalyzed C−H Bond Functionalization of Hydrocarbons. *Chem. Rev.* **2008,** *108* (8), 3379-3394.
37. Roizen, J. L.; Zalatan, D. N.; Du Bois, J., Selective Intermolecular Amination of C-H Bonds at Tertiary Carbon Centers. *Angew. Chem. Int. Ed.* **2013,** *52* (43), 11343-11346.
38. Gormisky, P. E.; White, M. C., Catalyst-Controlled Aliphatic C–H Oxidations with a Predictive Model for Site-Selectivity. *J. Am. Chem. Soc.* **2013,** *135* (38), 14052-14055.
39. Clark, J. R.; Feng, K.; Sookezian, A.; White, M. C., Manganese-catalysed benzylic C(sp3)–H amination for late-stage functionalization. *Nat. Chem.* **2018,** *10* (6), 583-591.
40. Dydio, P.; Key, H. M.; Hayashi, H.; Clark, D. S.; Hartwig, J. F., Chemoselective, Enzymatic C–H Bond Amination Catalyzed by a Cytochrome P450 Containing an Ir(Me)-PIX Cofactor. *J. Am. Chem. Soc.* **2017,** *139* (5), 1750-1753.
41. Zwick, C. R.; Renata, H., Remote C–H Hydroxylation by an α-Ketoglutarate-Dependent Dioxygenase Enables Efficient Chemoenzymatic Synthesis of Manzacidin C and Proline Analogs. *J. Am. Chem. Soc.* **2018,** *140* (3), 1165-1169.
42. Zhang, R. K.; Chen, K.; Huang, X.; Wohlschlager, L.; Renata, H.; Arnold, F. H., Enzymatic assembly of carbon–carbon bonds via iron-catalysed sp3 C–H functionalization. *Nature* **2019,** *565* (7737), 67-72.
43. Doyle, M. P.; McKervey, M. A.; Ye, T., Modern catalytic methods for organic synthesis with diazo compounds: From cyclopropanes to ylides. *Wiley, New York* **1998**.
44. Davies, H. M. L.; Beckwith, R. E. J., Catalytic Enantioselective C−H Activation by Means of Metal−Carbenoid-Induced C−H Insertion. *Chem. Rev.* **2003,** *103* (8), 2861-2904.
45. Davies, H. M. L.; Panaro, S. A., Effect of Rhodium Carbenoid Structure on Cyclopropanation Chemoselectivity. *Tetrahedron* **2000,** *56* (28), 4871-4880.
46. Berry, J. F., The role of three-center/four-electron bonds in superelectrophilic dirhodium carbene and nitrene catalytic intermediates. *Dalton Trans.* **2012,** *41* (3), 700-713.
47. Nakamura, E.; Yoshikai, N.; Yamanaka, M., Mechanism of C−H Bond Activation/C−C Bond Formation Reaction between Diazo Compound and Alkane Catalyzed by Dirhodium Tetracarboxylate. *J. Am. Chem. Soc.* **2002,** *124* (24), 7181-7192.
48. Kornecki Katherine, P.; Briones John, F.; Boyarskikh, V.; Fullilove, F.; Autschbach, J.; Schrote Kaitlin, E.; Lancaster Kyle, M.; Davies Huw, M. L.; Berry John, F., Direct

Spectroscopic Characterization of a Transitory Dirhodium Donor-Acceptor Carbene Complex. *Science* **2013,** *342* (6156), 351-354.
49. Davies, H. M. L.; Smith, H. D.; Korkor, O., Tandem cyclopropanation/Cope rearrangement sequence. Stereospecific [3 + 4] cycloaddition reaction of vinylcarbenoids with cyclopentadiene. *Tetrahedron Lett.* **1987,** *28* (17), 1853-1856.
50. Davies, H. M. L.; Hansen, T., Asymmetric Intermolecular Carbenoid C−H Insertions Catalyzed by Rhodium(II) (S)-N-(p-Dodecylphenyl)sulfonylprolinate. *J. Am. Chem. Soc.* **1997,** *119* (38), 9075-9076.
51. Hansen, J.; Autschbach, J.; Davies, H. M. L., Computational Study on the Selectivity of Donor/Acceptor-Substituted Rhodium Carbenoids. *J. Org. Chem.* **2009,** *74* (17), 6555-6563.
52. Davies, H. M. L.; Bruzinski, P. R.; Lake, D. H.; Kong, N.; Fall, M. J., Asymmetric Cyclopropanations by Rhodium(II) N-(Arylsulfonyl)prolinate Catalyzed Decomposition of Vinyldiazomethanes in the Presence of Alkenes. Practical Enantioselective Synthesis of the Four Stereoisomers of 2-Phenylcyclopropan-1-amino Acid. *J. Am. Chem. Soc.* **1996,** *118* (29), 6897-6907.
53. Davies, H. M. L.; Bruzinski, P. R.; Fall, M. J., Effect of diazoalkane structure on the stereoselectivity of rhodium(II) (S)-N-(arylsulfonyl)prolinate catalyzed cyclopropanations. *Tetrahedron Lett.* **1996,** *37* (24), 4133-4136.
54. L. Davies, H. M., Dirhodium Tetra(N-arylsulfonylprolinates) as Chiral Catalysts For Asymmetric Transformations of Vinyl- and Aryldiazoacetates. *Eur. J. Org. Chem.* **1999,** *1999* (10), 2459-2469.
55. Davies, H. M. L.; Kong, N., Synthesis and evaluation of a novel dirhodium tetraprolinate catalyst containing bridging prolinate ligands. *Tetrahedron Lett.* **1997,** *38* (24), 4203-4206.
56. Hashimoto, S.-i.; Watanabe, N.; Sato, T.; Shiro, M.; Ikegami, S., Enhancement of enantioselectivity in intramolecular C-H insertion reactions of α-diazo β-keto esters catalyzed by chiral dirhodium(II) carboxylates. *Tetrahedron Lett.* **1993,** *34* (32), 5109-5112.
57. Yamawaki, M.; Tsutsui, H.; Kitagaki, S.; Anada, M.; Hashimoto, S., Dirhodium(II) tetrakis[N-tetrachlorophthaloyl-(S)-tert-leucinate]: a new chiral Rh(II) catalyst for enantioselective amidation of C□H bonds. *Tetrahedron Lett.* **2002,** *43* (52), 9561-9564.
58. Saito, H.; Oishi, H.; Kitagaki, S.; Nakamura, S.; Anada, M.; Hashimoto, S., Enantio- and Diastereoselective Synthesis of cis-2-Aryl-3-methoxycarbonyl-2,3-dihydrobenzofurans via the Rh(II)-Catalyzed C−H Insertion Process. *Org. Lett.* **2002,** *4* (22), 3887-3890.
59. Tsutsui, H.; Abe, T.; Nakamura, S.; Anada, M.; Hashimoto, S., Practical Synthesis of Dirhodium(II) Tetrakis[N-phthaloyl-(S)-tert-leucinate]. *Chem. Pharm. Bull.* **2005,** *53* (10), 1366-1368.
60. Reddy, R. P.; Davies, H. M. L., Dirhodium Tetracarboxylates Derived from Adamantylglycine as Chiral Catalysts for Enantioselective C−H Aminations. *Org. Lett.* **2006,** *8* (22), 5013-5016.
61. Reddy, R. P.; Lee, G. H.; Davies, H. M. L., Dirhodium Tetracarboxylate Derived from Adamantylglycine as a Chiral Catalyst for Carbenoid Reactions. *Org. Lett.* **2006,** *8* (16), 3437-3440.
62. Fu, J.; Ren, Z.; Bacsa, J.; Musaev, D. G.; Davies, H. M. L., Desymmetrization of cyclohexanes by site- and stereoselective C–H functionalization. *Nature* **2018,** *564* (7736), 395-399.

63. Qin, C.; Boyarskikh, V.; Hansen, J. H.; Hardcastle, K. I.; Musaev, D. G.; Davies, H. M. L., D2-Symmetric Dirhodium Catalyst Derived from a 1,2,2-Triarylcyclopropanecarboxylate Ligand: Design, Synthesis and Application. *J. Am. Chem. Soc.* **2011,** *133* (47), 19198-19204.
64. Qin, C.; Davies, H. M. L., Role of Sterically Demanding Chiral Dirhodium Catalysts in Site-Selective C–H Functionalization of Activated Primary C–H Bonds. *J. Am. Chem. Soc.* **2014,** *136* (27), 9792-9796.
65. Liao, K.; Pickel, T. C.; Boyarskikh, V.; Bacsa, J.; Musaev, D. G.; Davies, H. M. L., Site-selective and stereoselective functionalization of non-activated tertiary C–H bonds. *Nature* **2017,** *551* (7682), 609-613.
66. Liao, K.; Yang, Y.-F.; Li, Y.; Sanders, J. N.; Houk, K. N.; Musaev, D. G.; Davies, H. M. L., Design of catalysts for site-selective and enantioselective functionalization of non-activated primary C–H bonds. *Nat. Chem.* **2018,** *10* (10), 1048-1055.
67. Liu, W.; Ren, Z.; Bosse, A. T.; Liao, K.; Goldstein, E. L.; Bacsa, J.; Musaev, D. G.; Stoltz, B. M.; Davies, H. M. L., Catalyst-Controlled Selective Functionalization of Unactivated C–H Bonds in the Presence of Electronically Activated C–H Bonds. *J. Am. Chem. Soc.* **2018,** *140* (38), 12247-12255.
68. Liao, K.; Negretti, S.; Musaev, D. G.; Bacsa, J.; Davies, H. M. L., Site-selective and stereoselective functionalization of unactivated C–H bonds. *Nature* **2016,** *533* (7602), 230-234.
69. Davies, H. M. L.; Hopper, D. W.; Hansen, T.; Liu, Q.; Childers, S. R., Synthesis of methylphenidate analogues and their binding affinities at dopamine and serotonin transport sites. *Bioorg. Med. Chem. Letters* **2004,** *14* (7), 1799-1802.
70. Davies, H. M. L.; Ni, A., Enantioselective synthesis of β-amino esters and its application to the synthesis of the enantiomers of the antidepressant Venlafaxine. *Chem. Comm.* **2006,** (29), 3110-3112.
71. Davies, H. M. L.; Dai, X.; Long, M. S., Combined C−H Activation/Cope Rearrangement as a Strategic Reaction in Organic Synthesis: Total Synthesis of (−)-Colombiasin A and (−)-Elisapterosin B. *J. Am. Chem. Soc.* **2006,** *128* (7), 2485-2490.
72. Schwartz, B. D.; Denton, J. R.; Lian, Y.; Davies, H. M. L.; Williams, C. M., Asymmetric [4 + 3] Cycloadditions between Vinylcarbenoids and Dienes: Application to the Total Synthesis of the Natural Product (−)-5-epi-Vibsanin E. *J. Am. Chem. Soc.* **2009,** *131* (23), 8329-8332.
73. Wang, H.; Li, G.; Engle, K. M.; Yu, J.-Q.; Davies, H. M. L., Sequential C–H Functionalization Reactions for the Enantioselective Synthesis of Highly Functionalized 2,3-Dihydrobenzofurans. *J. Am. Chem. Soc.* **2013,** *135* (18), 6774-6777.
74. Yamaguchi, A. D.; Chepiga, K. M.; Yamaguchi, J.; Itami, K.; Davies, H. M. L., Concise Syntheses of Dictyodendrins A and F by a Sequential C–H Functionalization Strategy. *J. Am. Chem. Soc.* **2015,** *137* (2), 644-647.
75. Bedell, T. A.; Hone, G. A. B.; Valette, D.; Yu, J.-Q.; Davies, H. M. L.; Sorensen, E. J., Rapid Construction of a Benzo-Fused Indoxamycin Core Enabled by Site-Selective C−H Functionalizations. *Angew. Chem. Int. Ed.* **2016,** *55* (29), 8270-8274.

Chapter 2

Streamlined Approach to (−)-Cylindrocyclophane A through C-H Functionalization Logic

---

2.1. Introduction to Cylindrocyclophanes

2.1.1. Isolation and Structure determination

Since their first introduction by Cram and Steinberg in 1951, [m.n]paracyclophanes have inspired chemists with their fascinatingly unique bridge aromatic architectural complexity.[1] It wasn't until 1990 that the first [7.7]paracyclophanes were isolated by Moore and co-workers from two species of terrestrial blue-green algae, *Cylindrospermum licheniforme* Kutzing and *Nostoclickia* (Roth) Bornet.[2] In this isolation report both cylindrocyclophane A and nostocyclophane D were reported as the first [7.7]paracyclophane natural products.[2] Since this initial report, teams lead by Jimmy Orjala and Sabine Mundt, have isolated dozens of other [7.7]paracyclophane natural product. These new natural products are the ribocyclophanes,[3] carbamidocyclophanes,[4, 5] and merocyclophanes,[6, 7] which join the cyclindrocyclophanes[8] and nostocyclophanes[9] as the five subclasses of [m.n]paracyclophane natural products (Figure 2.1). However, since this work focuses on the synthesis of (-)-cylindrocyclophane A, only discussion of the cylindrocyclophane subclass will be detailed. The absolute configuration of (-)-cylindrocyclophane A was determined by NMR spectral analysis.[8] The ^{13}C spectrum only included 18 carbons, while the HRMS assigned a molecular formula of $C_{36}H_{56}O_6$, therefore alluding to a molecule with a two-fold axis of symmetry. To assign the absolute configuration ^{1}H NMR and DEPT experiments were performed on the (*R*)- and (*S*)-Mosher esters of the benzylic alcohols with the four phenolic groups methylated, resulting in the elucidation of (-)-cylindrocyclophane A.[8]

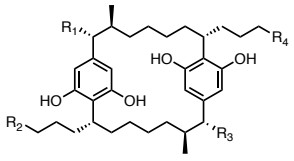

Cylindrocyclophane Core

	R_1	R_2	R_3	R_4
A	OH	CH_3	OH	CH_3
B	OH	CH_3	OAc	CH_3
C	OH	CH_3	H	CH_3
D	OAc	CH_3	OAc	CH_3
E	OAc	CH_3	H	CH_3
F	H	CH_3	H	CH_3
A_1	OH	CH_3	OH	CH_2Cl
A_2	OH	CH_3	OH	$CHCl_2$
A_3	OH	CH_2Cl	OH	$CHCl_2$
A_4	OH	$CHCl_2$	OH	$CHCl_2$
C_1	OH	CH_3	H	CH_2Cl
C_2	OH	CH_3	H	$CHCl_2$
C_3	OH	CH_2Cl	H	$CHCl_2$
C_4	OH	$CHCl_2$	H	$CHCl_2$
F_4	H	$CHCl_2$	H	$CHCl_2$
A_{B4}	OH	$CHBr_2$	OH	$CHBr_2$

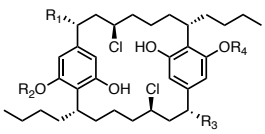

Nostocyclophane Core

	R_1	R_2	R_3	R_4
A	OCH_3	gylcoside	OCH_3	glycoside
B	OCH_3	H	OCH_3	glycoside
C	OH	H	OCH_3	H
D	OCH_3	H	OCH_3	H

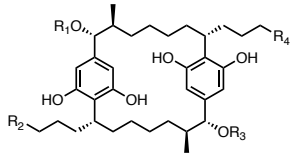

Carbamidocyclophane Core

	R_1	R_2	R_3	R_4
A	$CONH_2$	$CHCl_2$	$CONH_2$	$CHCl_2$
B	$CONH_2$	CH_2Cl	$CONH_2$	$CHCl_2$
C	$CONH_2$	CH_3	$CONH_2$	$CHCl_2$
D	$CONH_2$	CH_3	$CONH_2$	CH_2Cl
E	$CONH_2$	CH_3	$CONH_2$	CH_3
F	H	$CHCl_2$	$CONH_2$	$CHCl_2$
G	Ac	$CHCl_2$	$CONH_2$	$CHCl_2$
H	$CONH_2$	CH_3	H	CH_3
I	$CONH_2$	CH_3	H	CH_2Cl
J	$CONH_2$	CH_2Cl	$CONH_2$	CH_2Cl
K	$CONH_2$	CH_3	H	$CHCl_2$
L	$CONH_2$	CH_2Cl	H	$CHCl_2$

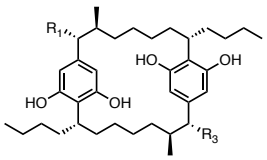

Ribocyclophane Core

	R_1	R_2
A	ribose	ribose
B	ribose	OH
C	ribose	H
D	ribose	OAc

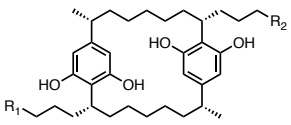

Merocyclophane Core

	R_1	R_2
A	CH_3	CH_3
C	CH_3	OH
D	OH	OH

Figure 2.1 Molecular architecture of the [7.7]paracyclophane natural products

During their initial isolation, the cylindrocyclophanes were evaluated for biological activity and were found to exhibit promising cytotoxicity against KB and LoVo tumor cell lines at <20 μg/ml.[2] Years later, after the isolation of additional subclasses of [7.7]paracyclophanes, many were shown to have cytotoxic activity towards various cancer cell lines: HT-29 (colon cancer cells), FI (human amniotic epithelial cells), MCF7 (breast adenocarcinoma cells), OVCAR3 (ovarian epithelial cancer), MDA-MB-231 (human breast cancer cells), and MDA-MB-435 (human melanoma cells), with IC_{50}'s in the range of 0.1-5 μM.[10-12] Additionally, they displayed antimicrobial activity against Gram-positive pathogens with minimum inhibitory concentrations (MIC's) in the range of 0.1-2 μM toward resistant Gram-positive bacteria, methicillin-resistant

staphylococcus *aureus* (MRSA), along with activity against S. *pneumoniae* with MIC's between 0.2-3 μM (Table 2.1).[10-12] The most promising of the natural products reveal antimicrobial activity with MIC's at around 50-fold lower than their corresponding IC_{50} value against non-tumorigenic cell line HaCaT. Demonstrating the possibility for selective antimicrobial activity over general cytotoxicity.

Compound		Antimicrobial testing *Gram-positive*		Cytotoxic testing
		MRSA MIC (μM)	S. *pneumoniae* MIC (μM)	HaCaT IC_{50} (μM)
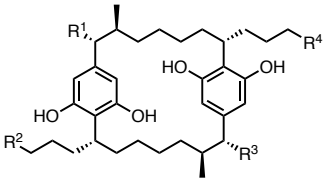 Cylindrocyclophane Core	**A**: R^1= R^3= OH, R^2= R^4= CH_3 **D**: R^1= R^3= OAc, R^2= R^4= CH_3 **A_1**: R^1= R^3= OH, R^2= CH_3, R^4= CH_2Cl **A_2**: R^1= R^3= OH, R^2= CH_3, R^4= $CHCl_2$ **A_3**: R^1= R^3= OH, R^2= CH_2Cl, R^4= $CHCl_2$ **A_4**: R^1= R^3= OH, R^2= R^4= $CHCl_2$	**A**: MIC 0.1-1.1 μM **D**: MIC 0.9 μM **A_1**: MIC 1.02 μM **A_2**: MIC 0.96 μM **A_3**: MIC 0.45 μM **A_4**: MIC 0.43 μM	**A**: MIC 0.3-2.2 μM **D**: MIC 2.4 μM **A_1**: MIC 2.1 μM **A_2**: MIC 1.99 μM **A_3**: MIC 0.92 μM **A_4**: MIC 0.87 μM	**A**: IC_{50} 5.0 ± 1.9 μM **D**: IC_{50} 11 ± 1 μM **A_1**: IC_{50} 11.3 μM **A_2**: IC_{50} 11.5 μM **A_3**: IC_{50} 8.6 μM **A_4**: IC_{50} 9.3 μM

Table 2.1 Biological activity of select cylindrocyclophanes

2.1.2. Biosynthesis of Cylindrocyclophane

Lead by the team that first isolated (-)-cylindrocyclophane A, Moore and co-workers tried to elucidate the biosynthetic pathway by feeding ^{2}H, ^{13}C, and ^{18}O-labeled sodium acetates to *C. lichenforme* cultures.[13] While NMR analysis of isolated metabolites resulted in a proposed pathway, the team was unable to unravel the key dimerization event to form the macrocyclic structure. It would not be until 2012 when Balskus and co-workers identified the cylindrocyclophane (*cyl*) biosynthetic gene cluster in *C. licheniforme*.[14] Furthermore, they were able to characterize several components of the polyketide synthase (PKS) machinery, and in 2017 complete the biosynthetic pathway to (-)-cylindrocyclophane F.[15-18] While this work focuses on (-)-cylindrocyclophane A, the biosynthetic pathway to F is the same approach to A and therefore relevant to the discussion here.

The biosynthesis starts with decanoic acid **2.1** converting to the decanoyl-acyl carrier protein (ACP) thioester **2.2** (Scheme 2.1).[17] From there, the next transformation is the key step uncovered by the Balskus lab. Decanoyl-CylB thioester **2.2** is regioselectivity and enantioselectively chlorinated by halogenase CylC to give chlorodecanoyl thioester **2.3**. With the chlorinated substrate in hand, CylD-CylH catalyzes enzymatic reactions through a type I PKS assembly in the presence of malonyl-CoA to convert **2.3** into intermediate **2.4**. This intermediate then undergoes resorcinol formation yielding **2.5** by malonyl-CoA under type III PKS CylI enzymatic catalysis. Lastly, CylK functions as an alkylating enzyme promoting the double S_n2 dimerization forming (-)-cylindrocyclophane F.

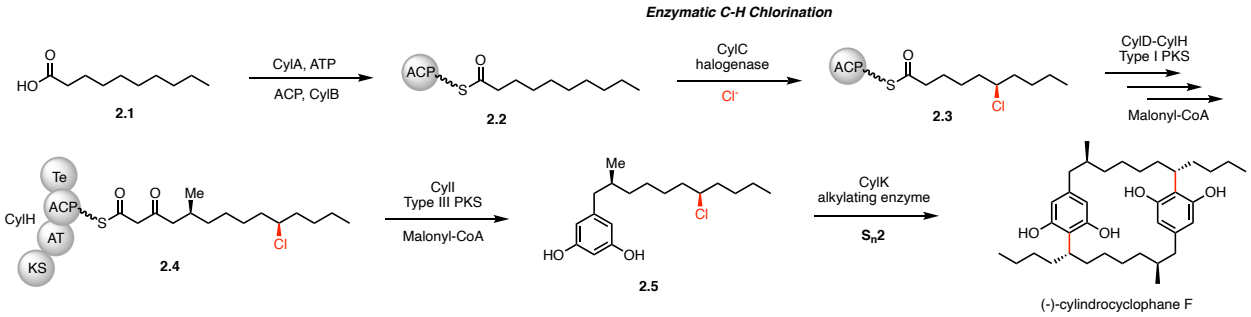

Scheme 2.1 Biosynthesis of (-)-cylindrocyclophane F

2.1.3. Previous Total Syntheses of (-)-Cylindrocyclophane A

The unique molecule architecture combined with promising biological activity has generated considerable synthetic interest of these compounds. To date, three major syntheses have been developed to (-)-cylindrocycophane A.[19-22] Historically, the approach has been the same, using the inherent C_2-symmetry in the natural product as a functional handle for a convergent strategy bringing two identical components together. The three approaches that will be outlined here all use different dimerization techniques, as well as unique strategies to build their monomers. While all the routes display considerable chemical innovation, they all have several limitations.

First, all of them rely on building an advanced fragment and then dimerization of the two identical fragments. Thus, limiting only the synthesis of symmetrical paracyclophanes. Furthermore, none of the strategies are ideally suited for the synthesis of analogs because the diversification would have to occur early in the synthesis. Lastly, the routes all require lengthy step count between 16 to 24 linear steps, or 21 total steps in the shortest route. Thus, a streamlined and modular route would not only allow for a shorter synthesis but flexibility to create analogs to study the SAR and MOA, both of which have been limited by the synthesis. For all three routes, the focus will be on the general strategy and endgame as those components relate the most to the approach that will be outlined in the results and discussion section.

The first total synthesis of (-)-cylindrocylophane A was accomplished in 2000 by Hoye and co-workers.[21] Exploiting the C_2-symmetry of the macrocycle, the team's strategy hinges on a late-stage Horner-Wadsworth-Emmons (HWE) coupling to provide the cyclic dimer (Scheme 2.2). The synthesis of the monomer utilizes a commercially available lipase enzyme (Amano P-30) to kinetically resolve an alcohol. From there they perform an Ireland-Claisen rearrangement to set the first benzylic stereocenter. After several functional group manipulation, the HWE reaction provided the macrocycle in 55% yield. The final stereocenter is set after the macrocyclization by an asymmetric hydroboration using a hindered monoisopinocampheyl borane derived from (+)-alpha-pinene. With the final stereocenter set, the endgame for Hoye includes a simple demethylation of the methoxy groups on the resorcinol subunit. This demethylation of the resorcinol framework is a key late-stage reaction that will be seen in the other strategies and will be relevant to the endgame discussed in the results and discussion section. Through this strategy Hoye and co-workers synthesized the natural product in 24 linear steps, making it the longest route to date.

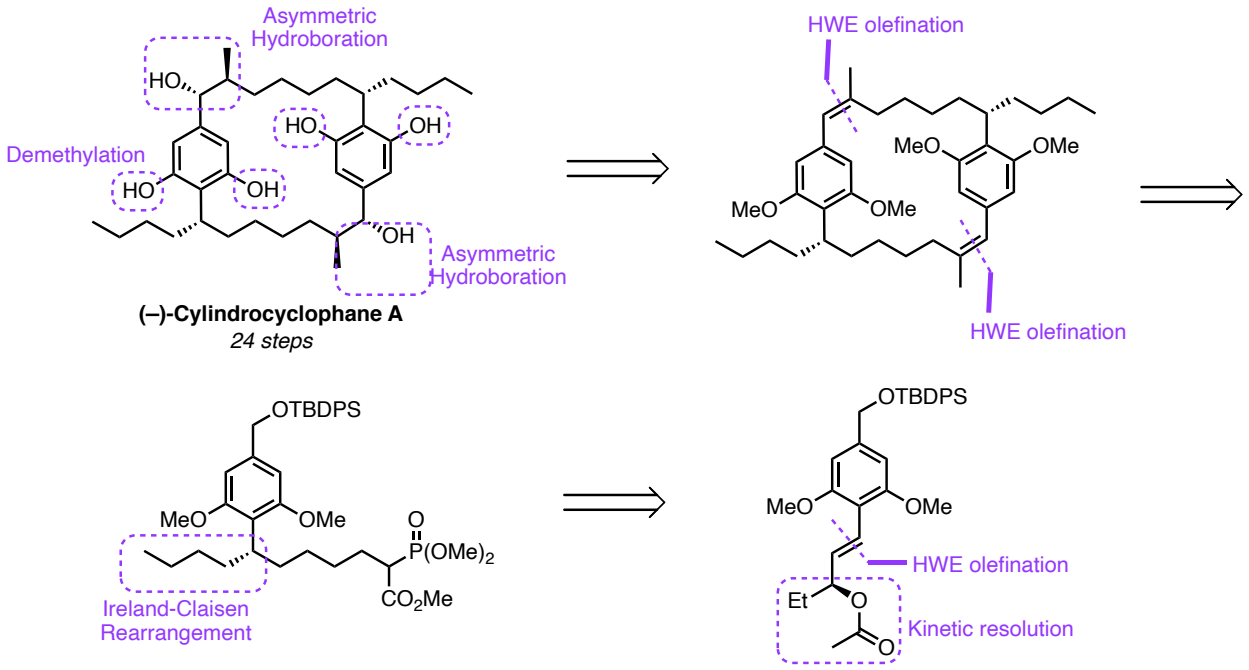

Scheme 2.2 Hoye's synthesis of (-)-cylindrocyclophane A

In back-to-back publications, the next synthesis of (-)-cylindrocyclophane A came out right when the Hoye route was published, from the team of Smith and co-workers.[19, 20] The synthesis hinges on a key ring-closing olefin metathesis (RCM) to form the 22-membered macrocycle (Scheme 2.3). Building the monomer subunit needed for the RCM reaction, the team forms the resorcinol ring through a Danheiser benzannulation. To create the stereocenters, both Evans and Myers auxiliaries are used to set all the stereocenters in the natural product. When faced with the crux macrocyclization, Smith optimized the Schrock molybdenum-based catalyst to form the macrocycle in 77% yield. With the ring formed, Smith's endgame focuses on removal of the TES protecting group, hydrogenation of the alkenes from the RCM and final demethylation of the resorcinol framework. Key to this endgame is keeping the phenols masked as methoxy group until the final step as the free resorcinol compound can easily be oxidized to the quinone. Through this

strategy Smith and co-workers were able to form the natural product in 16 linear steps with an 8.1% overall yield, resulting in the shortest synthesis to date.

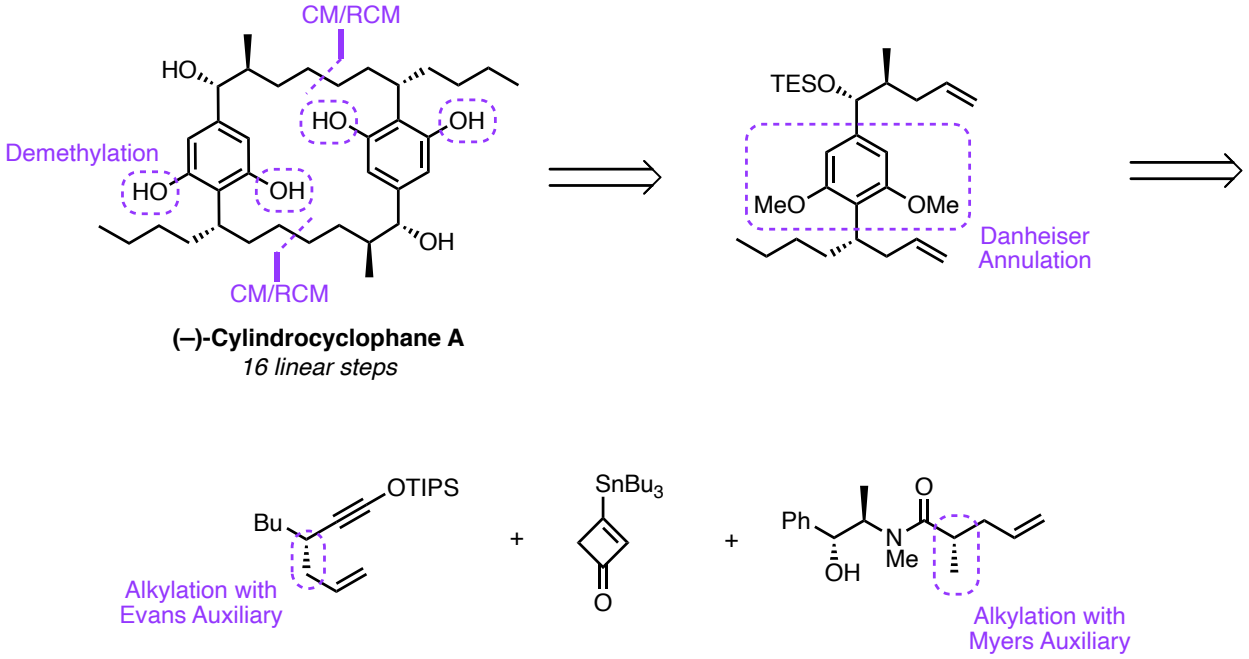

Scheme 2.3 Smith's synthesis of (-)-cylindrocyclophane A

The final and most recent total synthesis of (-)-cylindrocyclophane A comes ten years after the first two from Nicolaou and co-workers.[22] Unique to this approach is a convergent route to both (-)-cylindrocyclophane A and F from one late stage building block. The key dimerization used by Nicolaou is a Ramber-Bäcklund olefination that forms the macrocycle in a 51% yield over two steps (Scheme 2.4). To synthesize the monomer for the dimerization, the key step uses a CBS reduction that then directs a diastereoselective hydrogenation. Post-macrocycle formation, the final two stereocenters are set with the same approach employed by Hoye via asymmetric hydroboration. Since the endgame used by Nicolaou is the same approach employed by Hoye and Smith, namely demethylation of the resorcinol, this highlights the difficulty of handling the free phenols.[21, 22] Like both previous routes, demethylation of the methoxy groups on the resorcinol is

the final step in the synthesis, clearly highlighting the need to mask the phenols until the end. Through this strategy Nicolaou and co-workers synthesize (-)-cylindrocyclophane A in 22 linear steps.

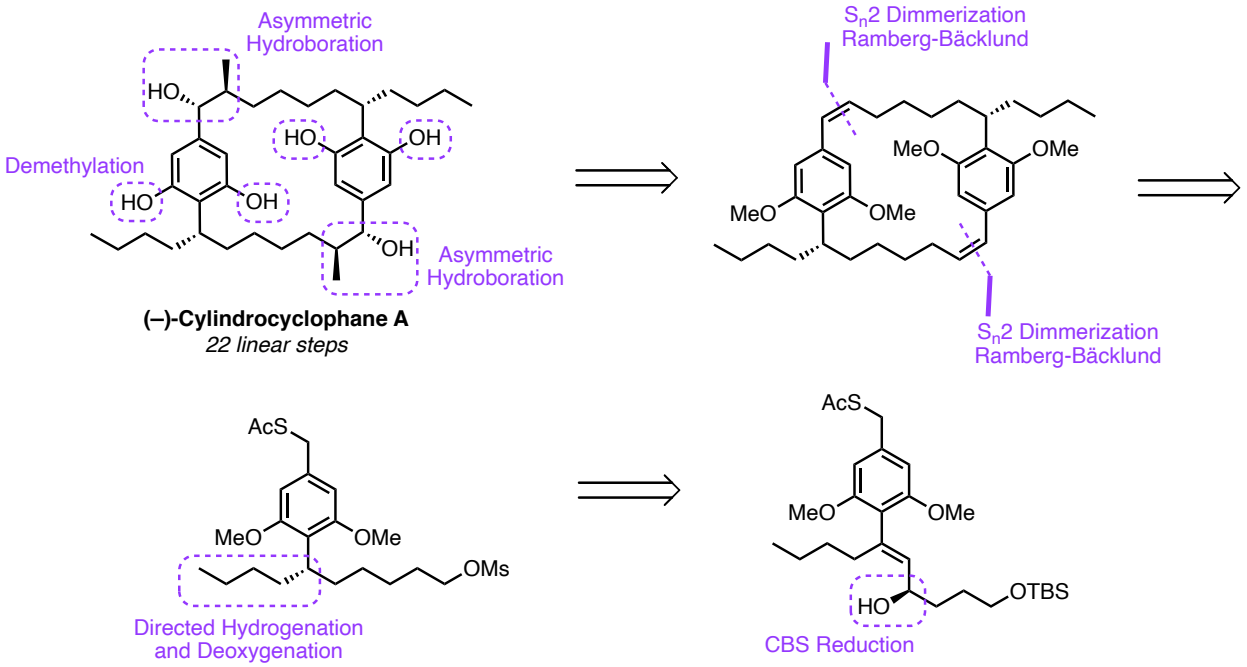

Scheme 2.4 Nicolaou's synthesis of (-)-cylindrocyclophane A

2.1.4. A C-H Functionalization Strategy to (-)-Cylindrocyclophane A

The importance of the inherent symmetry in cylindrocyclophane can be seen since all the past total syntheses use it as a synthetic handle. Therefore, the approach outlined here leverages the C_2-symmetry as a functional handle in my synthetic design of the natural product. However, what makes my approach unique, compared to the others, is the C-H functionalization strategy used to create the core structure, which allows for rapid building of complexity. Furthermore, while all previous routes focus on one natural product, a C-H functionalization approach would in theory be flexible and modular, allowing access to the other sub-classes of [m.n]paracyclophanes and analogs for studying SAR and MOA.

In 2016, Kuangbiao Liao and co-workers from the Davies lab developed a new chiral dirhodium catalyst, Rh_2(3,5-di(p-tBuC_6H_4)TPCP)$_4$ (or Rh_2(*R*-DiBic)$_4$), that is selective for the most accessible methylene C(sp^3)-H bond in a molecule (Scheme 2.5a).[23] During the presentation on this new methodology at a NSF CCHF meeting, Dr. Brian Stoltz suggested a novel retrosynthetic disconnection of the cylindrocyclophane core that would highlight both the power of C-H functionalization as an enabling technology and would allow for a new efficient synthesis of (-)-cylindrocyclophane A (Scheme 2.5b). Thus, a collaboration was initiated between the Davies and Stoltz group to take on this ambitious plan. To accomplish this transformation, insertion into a terminal methylene C(sp^3)-H bond would need to be preferred over the benzylic activated methylene C(sp^3)-H. Further catalyst development studies by Wenbin Liu in the Davies group identified *ortho*-chlorotriarylcyclopropanecarboxylate (TPCP) ligands, which generated a superior catalyst to accomplish this feat.[24] A representative example of a reaction with this catalyst can be found in Chapter 1 Scheme 1.2.

a. Breakthrough methodology

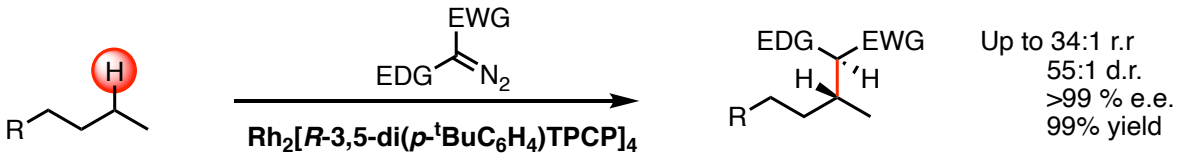

b. Key disconnection

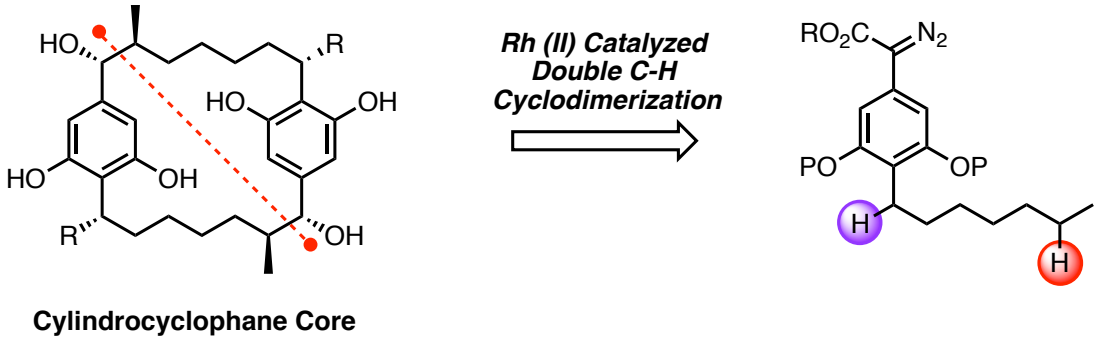

Cylindrocyclophane Core

Scheme 2.5 Enabling methodology and key disconnection on cylindrocyclophane

With multiple catalyst at our disposal, the Davies laboratory has established a strong precedent for the ability to construct the core of (-)-cylindrocyclophane A via C-H activation. Additionally, the literature is sparse in using C-H activation in creating macrocyclic rings, with one example coming from the White group where an allylic C-H bond is oxidatively activated to form a macrocycle.[25, 26] Another recent example comes from the Baran group where two aromatic C-H bonds are coupled together through a copper mediated oxidative process.[27] Thus, not only would this strategy to (-)-cylindrocyclophane A be a more efficient and modular synthesis than any other route previously developed, but it would also advance C-H insertion technology for preparing medium and macrocyclic rings in an unprecedented cyclization event.

Encouraged by the promising new catalyst, Rh_2(*R*-2-Cl-5-BrTPCP)$_4$, an ambitious disconnection of (-)-cylindrocyclophane A was developed that relies on utilizing 12 C-H functionalization reactions (Figure 2.2). Four enantioselective carbene-induced C-H functionalizations to generate the six stereogenic centers,[24, 28] four palladium-catalyzed C-H functionalizations of diazocarbonyl compounds,[29] and four directed C-H acetoxylations.[30, 31] Not only would this synthesis represent a massive jump in streamlining the synthesis to all [7.7]paracyclophane natural products, but additionally the modularity of the route imparted by the C-H functionalization logic now allows for future studies to probe the SAR and MOA to systematically study the pharmacological profile.

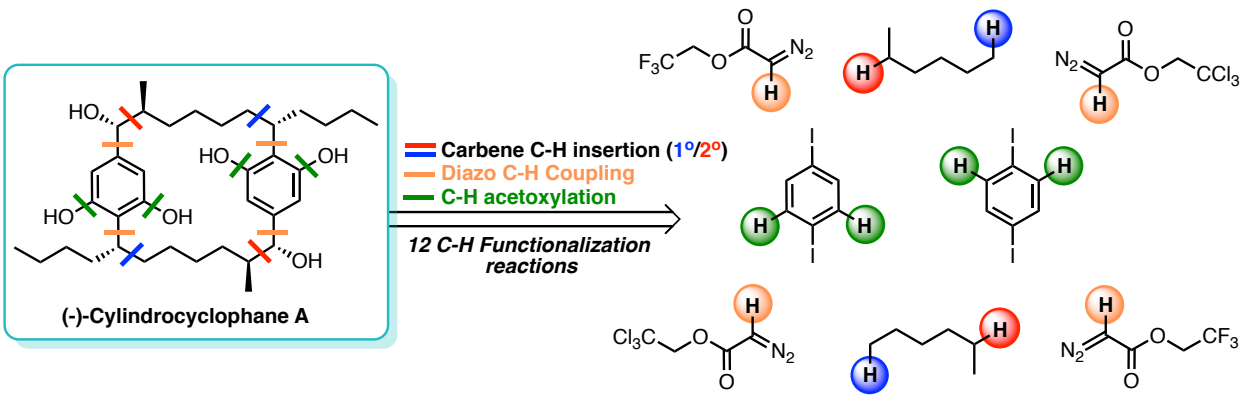

Figure 2.2 A C-H functionalization approach to (-)-cylindrocyclophane A

This chapter will cover the progress to the synthesis of (-)-cylindrocyclophane A using C-H functionalization logic. A discussion on the various strategies and current endgame will be presented.

2.2. Results and Discussion

2.2.1. Model Synthesis of the [7.7]Paracyclophane core

Embarking on this ambitious endeavor, the first question that needed to be addressed was whether the macrocyclic framework could be synthesized by carbene insertion using our dirhodium technology. To validate the hypothesis, a model study was conducted where all the functionality in the natural product is stripped away (Scheme 2.6). The purpose of this study was to focus in on if using our carbene methodology can build the [7.7]paracyclophane core via C-H functionalization without interference from other functional groups.

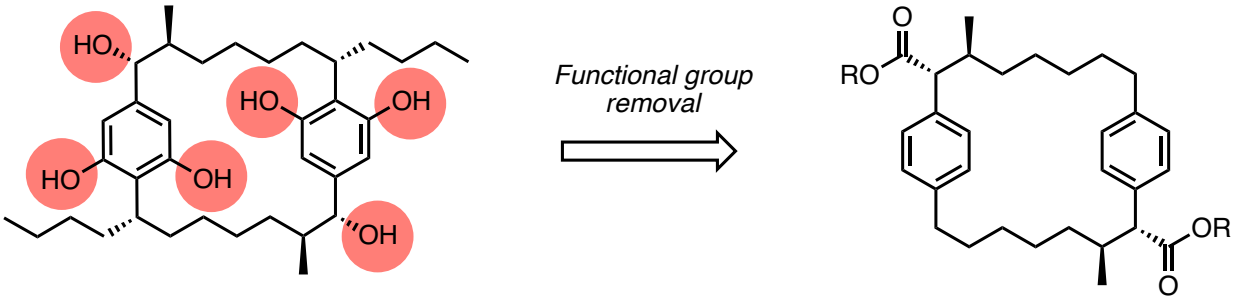

(–)-Cylindrocyclophane A **Model Paracyclophane Target**

Scheme 2.6 Model study target compound and strategy

The model study starts with commercially available aryl iodide **2.6**. Then the first step is a palladium-catalyzed cross coupling of the aryl iodide **2.6** with the diazoacetate $\mathbf{2.7_X}$ to form the aryldiazoacetate $\mathbf{2.8_X}$ in 87% yield for both TCE and TFE diazoacetates.[29] Next, the first key carbene-induced C-H functionalization between $\mathbf{2.8_{Cl}}$ and **2.6** was screened under a variety of conditions (Table 2.2). Using previously established standard conditions, the first variable screened was the catalyst.[23] Looking at the available catalysts in the Davies toolbox, only two catalysts can selectively functionalize unactivated methylene C-H bonds. Analyzing the reaction with Rh_2(*R*-DiBic)$_4$ resulted in an unselective reaction where the regioselectivity for the C2 methylene C-H bond versus the benzylic C-H bond was only 1:1.[11] When the reaction was conducted with Rh_2(*R*-2-Cl-5-BrTPCP)$_4$ the regioselectivity excitingly increased to 11:1

(C2:benzylic). Additionally, the product **2.9$_{Cl}$** was generated in 47% yield with 75% ee and >20:1 dr.[24] Unfortunately, unwanted formation of a byproduct was lowering the yield and overall efficiency. Analyzing the byproducts showed me the major byproduct was insertion into water, along with dimerization of the donor/acceptor diazo. To minimize dimerization the reaction was conducted at room temperature, however this just shut down any reactivity (Table 2.2, entry 3). Next, concentration was looked at, which lowering or increasing it also did not improve the yield (Table 2.2, entry 4+5). Then the solvent was optimized by distillation and adding 4Å molecular sieves (4Å MS) to the reaction. Excitingly this greatly minimized byproduct formation from water engaging the carbene and increased the yield to 66% (Table 2.2, entry 6). The final variable that was optimized was the diazo itself, where switching from the TCE (**2.8$_{Cl}$)** to TFE (**2.8$_{F}$)** group led to not only a jump in yield but drastic increase in selectivity to >30:1 rr, >20:1 dr and 91% ee for **2.9$_{F}$** (Table 2.2, entry 7).[24] With this step fully optimized it was now time to move to the key macrocyclization.

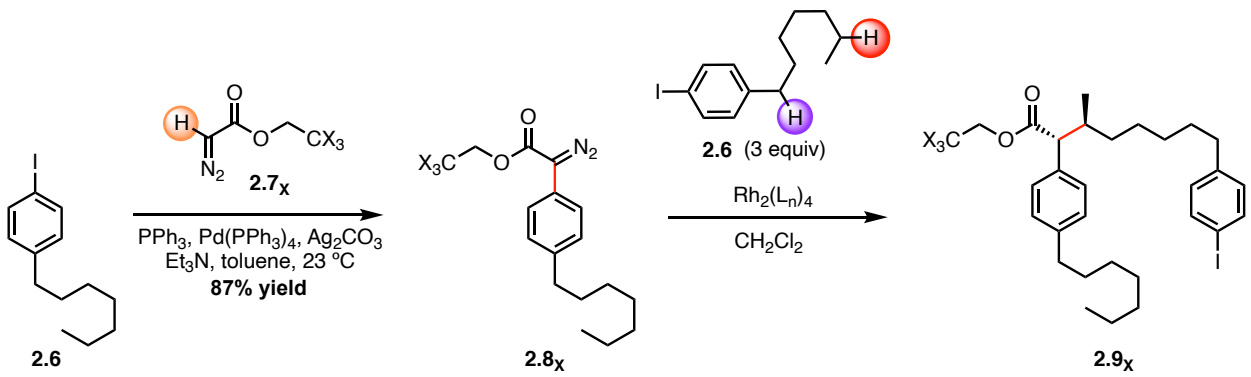

Entry	Catalyst	Conc. (M)	X	Additive	Temp	Yield	Prod: Byproduct[a]	rr (2°:benzylic)	dr/ee
1	Rh_2(*R*-DiBic)$_4$	0.13	Cl	-	40°C	-	-	1:1	-
2	Rh_2(*R*-2Cl5Br-TPCP)$_4$	0.13	Cl	-	40°C	47%	2:1	11:1	>20:1 /75%
3	Rh_2(*R*-2Cl5Br-TPCP)$_4$	0.13	Cl	-	rt	-	-	-	-
4	Rh_2(*R*-2Cl5Br-TPCP)$_4$	0.05	Cl	-	40°C	15%	1:2.5	11:1	>20:1 /75%
5	Rh_2(*R*-2Cl5Br-TPCP)$_4$	0.2	Cl	-	40°C	25%	1:1	11:1	>20:1 /75%
6[b]	Rh_2(*R*-2Cl5Br-TPCP)$_4$	0.13	Cl	4Å MS	40°C	66%	10:1	11:1	>20:1 /75%
7[b]	Rh_2(*R*-2Cl5Br-TPCP)$_4$	0.13	F	4Å MS	40°C	83%	>20:1	>30:1	>20:1 /91%

[a]Byproducts observed are dimerization and O-H insertion. [b]DCM was distilled over CaH_2, under argon, over molecular sieves.

Table 2.2 Optimization of the model study intermolecular C-H insertion

After optimizing the first half of the model system, the next step was to take product **2.9$_F$** further to screen macrocyclization conditions. A second palladium-catalyzed reaction[29] with **2.9$_F$** and **2.7$_X$** gave the next carbene precursor **2.10$_X$** in 81% yield for both TCE and TFE diazoacetates, which subsequently underwent screening via dirhodium catalyzed conditions (Table 2.3). Based on previous results, Rh_2(*R*-2-Cl-5-BrTPCP)$_4$ was chosen as the only catalyst compatible with the system, and that the reaction would require refluxing conditions and rigorously dry of the solvent.[24] When the optimization was initiated, inspiration from known macrocyclizations that perform

under high dilution conditions, such as RCM reactions, were used as a precedent.[32] Varying catalyst loading from 1 to 5 mol % unfortunately lead to no product formation (Table 2.3, entry 1+2). Undeterred by the result it was hypothesized if more concentrated conditions would work, therefore increasing the concentration excitingly formed some of the desired product **2.11$_{Cl}$** (Table 2.3, entry 3)! Notably, White and co-workers experienced the same effect with their palladium-catalyzed macrolactonization, where White hypothesized high dilutions are unnecessary because the catalyst dictates the maximum concentration.[26] However, at this stage the reaction was irreproducible, and the major byproducts generated were insertion of the donor/acceptor diazo into water along with polymerization of the diazo. Switching from the **2.10$_{Cl}$** to **2.10$_{F}$** diazoacetate and distilling the solvent instead of degassing it improved the dr from 3:1 to 5.6:1 for product **2.11$_{F}$** and minimized the byproduct formation slightly. Yet the reaction was still not reproducible, and the yield poor (Table 2.3, entry 4). Adding HFIP to the reaction, which historically has been used to improve the selectivity of dirhodium carbene transformation,[33] unfortunately did not improve the reaction either and it seemed as if there were no more variables to change (Table 2.3, entry 5). It was hypothesized that insertion into water was outcompeting the C-H functionalization in the small scale which the screen was conducted. Therefore, we postulated that increasing the scale of the reaction would minimize the background reaction and thus increase the yield. Conducting the reaction on 1.0 mmol scale incredibly doubled the yield to 68%, as well as drastically suppressed byproduct formation (Table 2.3, entry 6). Furthermore, increasing the scale of the reaction also lead to a reproducible result. Excitingly, due to the symmetrical structure of the product, the asymmetric induction is amplified in the second C-H functionalization through the Horeau principle, and **2.11$_{F}$** is produced in >99% ee with good yield, although this comes at the expense of a lower level of overall diastereoselectivity.[34] Notably, this macrocyclization is the first example

of an enantioselective macrocyclization by means of functionalization of an unactivated C(sp^3)-H bond.[24]

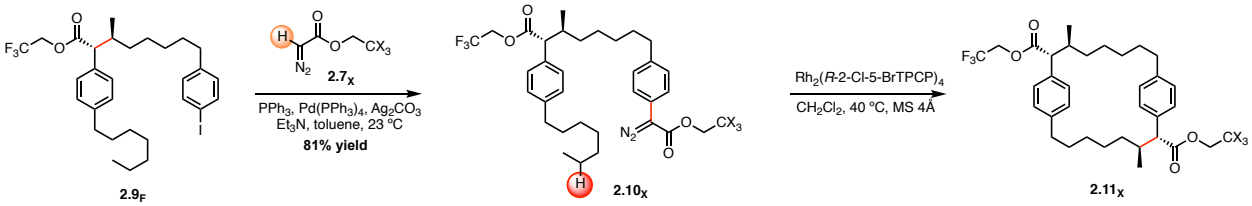

Entry	Catalyst Loading	Conc. (M)	X	Additive	Solvent purification	Yield	Prod: Byproduct[a]	dr/ee
1	1 mol %	0.004	Cl	4Å MS	Degassed	0%	-	-
2	5 mol %	0.004	Cl	4Å MS	Degassed	0%	-	-
3	1 mol %	0.02	Cl	4Å MS	Degassed	0-23%	2:1	3:1/-
4	1 mol %	0.02	F	4Å MS	Distilled Fresh	0-24%	4:1 - 8:1[b]	5.6:1/ -
5	1 mol %	0.02	F	4Å MS /HFIP	Distilled Fresh	0-29%	6:1-12:1[b]	5.6:1/ -
6[c]	1 mol %	0.02	F	4Å MS	Distilled Fresh	68%	>20:1	5.6:1/ >99%

[a]Major byproduct observed is O-H insertion with some polymerization. [b]Inconsistent ratio, not reproducible. [c]Reaction done on 1mmol scale.

Table 2.3 Optimization of the model study C-H macrocyclization

With the proof-of-principle validated, we now knew that our carbene methodology could form the [7.7]paracyclophane framework in good yields with incredibly high regio-, diastero- and enantioselectivity. Even more encouraging was that a stepwise route was developed to build the macrocycle, allowing diversity on the scaffold that the previous routes could not access. However, there was still interest in a direct dimerization approach of aryl diazoacetate **2.8F** to the model paracyclophane **2.11F** (Scheme 2.7). While this approach would not allow for the synthesis of unsymmetrical cyclophanes, this strategy would be a landmark result for our methodology as in a

single step two C-C bonds and four stereocenters would be formed. Unfortunately, after exhaustive screening of conditions, only dimerization and polymerization of the donor/acceptor diazo **2.8$_F$** was observed. Only in one case did the reaction create any product, interestingly it was a reverse set up where the catalyst was added directly to the refluxing diazo. Yet this resulted in a low yield of 16% with impurities remaining after purification. Moving forward it was decided that the stepwise approach would be the most reliable and reproducible for the synthesis.

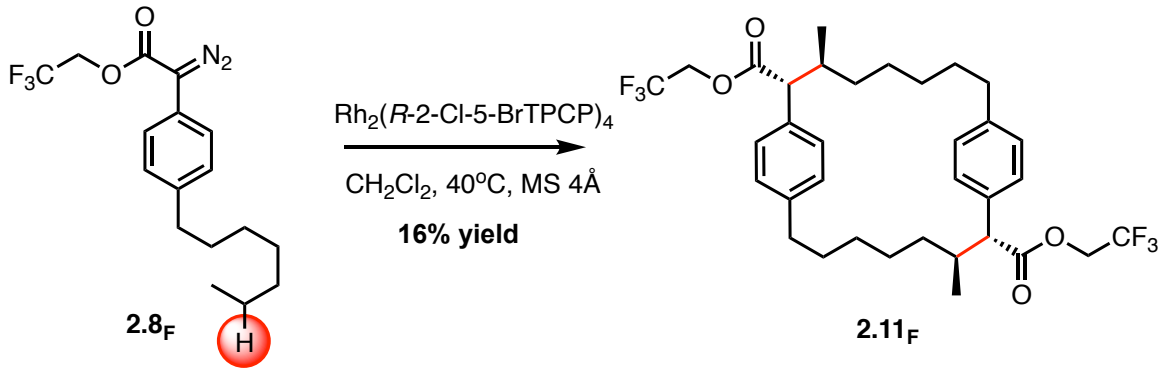

Scheme 2.7 Dimerization strategy to [7.7]paracyclophane core

Once the initial hypothesis was validated the next step was to probe the compatibility of the carbene chemistry with a more functionalized substrate. This new model system consisted of a protected resorcinol compound **2.12** in the form of acetoxy groups. This substrate **2.12** would allow analysis of functional group compatibility with our carbene technology, specifically the resorcinol protected acetoxy functionality. Due to the difficulty of synthesizing the aryl iodide starting material **2.12**, which was made by my collaborator Elizabeth Goldstein, only one initial pass has been attempted on this more functionalized model system (Scheme 2.8). Palladium-catalyzed reaction[29] on **2.12** with **2.7$_F$** gave the carbene precursor **2.13**, which was ready to be subjected under the previously optimized conditions from Table 2.2. Upon conducting the reaction, it was found to be able to do the intermolecular C-H insertion yielding **2.14**, however the

diastereoselectivity drastically suffers, switching from >20:1 to 1:1.5. Even more critically, the dr switches and favors the minor diastereomer that does not match the natural product (see chapter 2 SI). We hypothesized that incorporating the 2,6-acetoxy functionality sterically crowds the carbene pocket, resulting in the dr switching. Thus, this distinctly told me that the acetoxy functional groups could not be pre-installed before formation of the macrocycle, and this result will be key to designing the synthetic strategy.

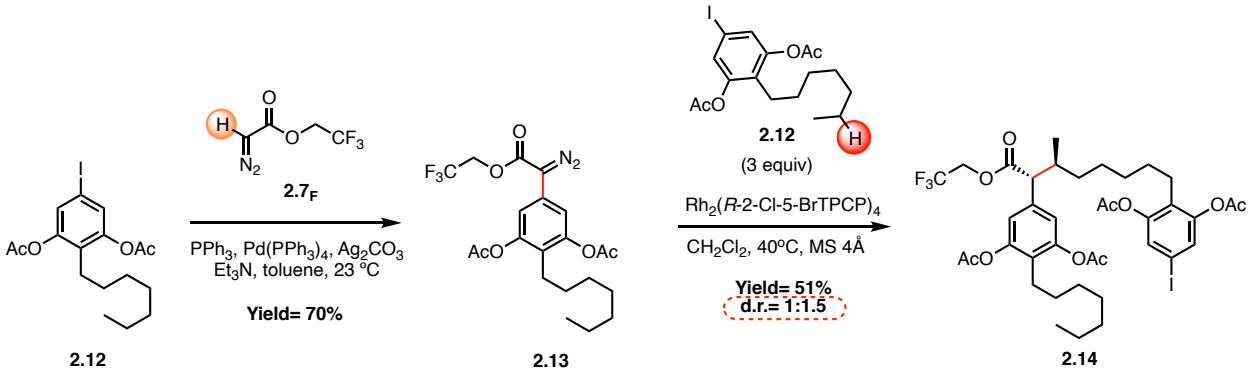

Scheme 2.8 Model study on resorcinol protected substrate

In summary, we were able to demonstrate the newly developed Rh_2(*R*-2-Cl-5-BrTPCP)$_4$ catalyst can assemble the [7.7]paracyclophane framework in good yield with excellent selectivity (Scheme 2.9).[24] Notably, the yield for the macrocyclization was able to be increased after repeating and scaling the reaction even more from 68% to 73% yield. Moving forward, application of the model studies were used to develop a retrosynthesis to (-)-cylindrocyclophane A based on the results.

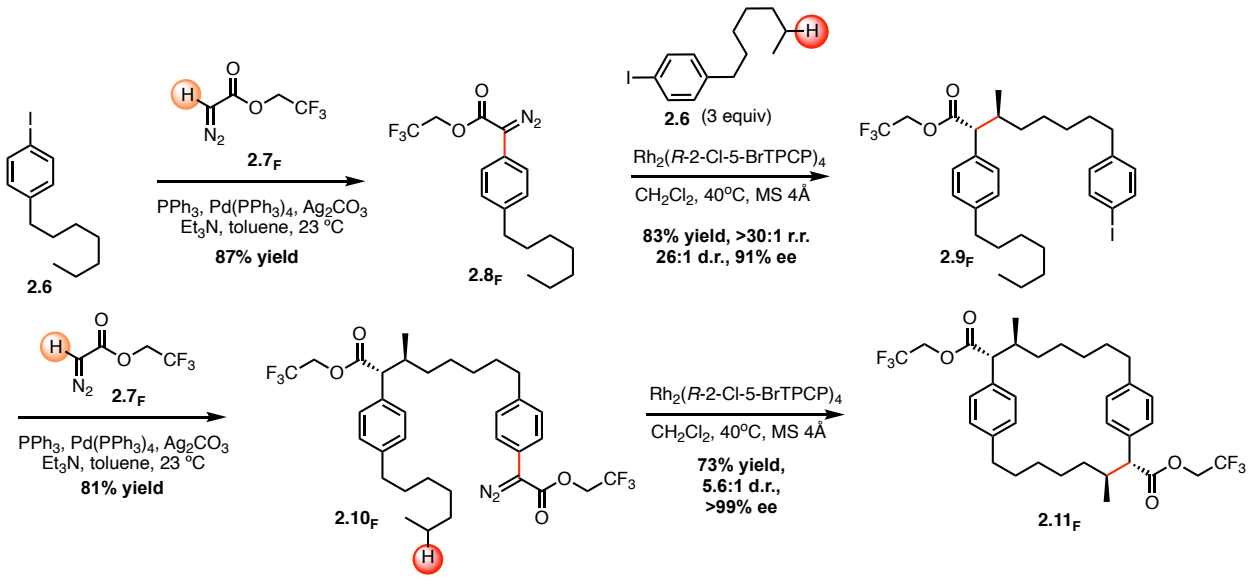

Scheme 2.9 Summary of the model study to the [7.7]paracyclophane architecture

2.2.2. Retrosynthetic Analysis

The first-generation approach that was developed is by far the most ambitious and shortest route proposed to the natural product (Scheme 2.10). The proposed route starts with known aryl diazoacetate **2.15** and an ambitious primary insertion with the methyl C(sp^3)-H bond in *n*-hexane to set the first stereocenter.[35] Following the insertion, the ester is then converted to the Weinreb amide **2.16**, which is posed to direct a double C-H acetoxylation[30, 31] forming **2.17**. Reduction of the amide **2.17** to the ketone and palladium catalyzed C-H functionalization[29] would afford the diazo compound **2.18**. This diazo compound **2.18** is now posed to do a double C-H cyclodimerization to form the macrocyclic compound **2.19**. The final steps would involve a chemoselective reduction of the ketone, then hydrolysis of the TFE ester before oxidative decarboxylation to yield structure **2.20**. The last step would be global hydrolysis of the six acetoxy groups yielding (-)-cylindrocyclophane A in 9 steps from the starting aryl diazoacetate **2.15**.

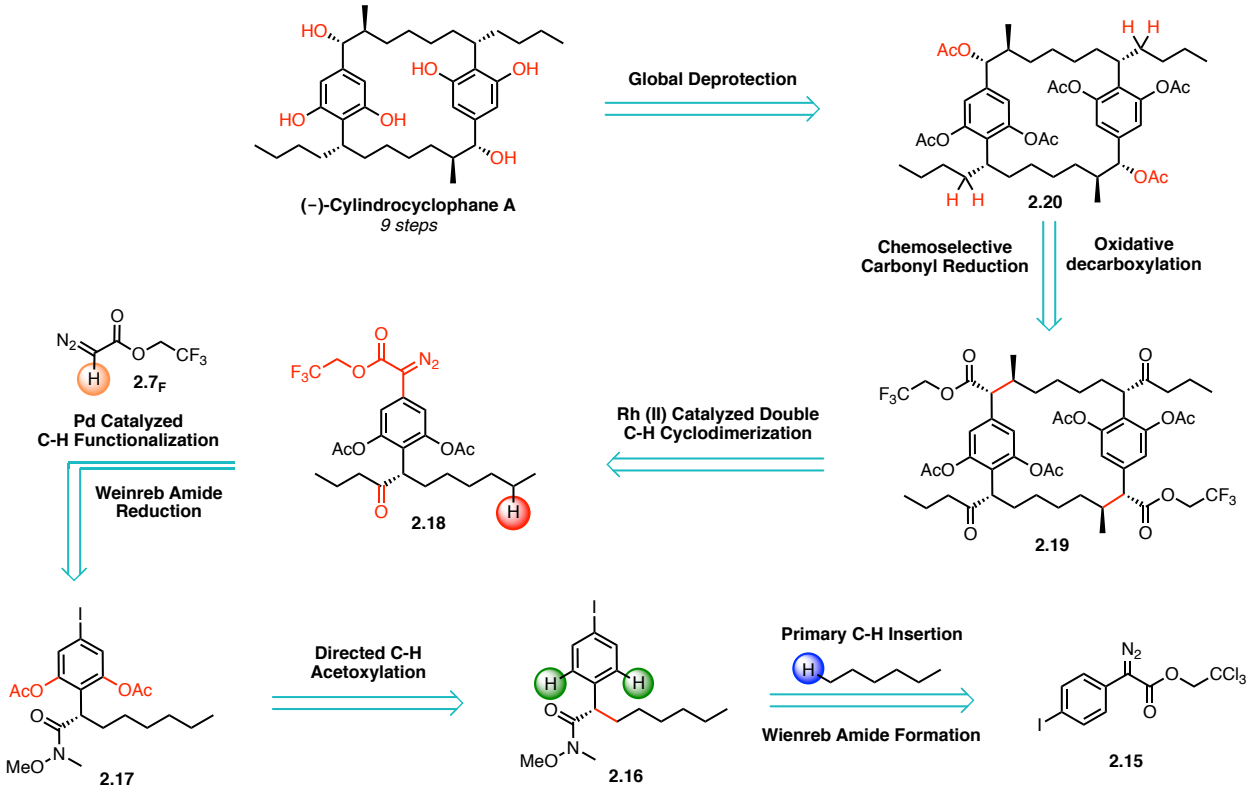

Scheme 2.10 First-generation retrosynthetic analysis of (-)-cylindrocyclophane A

While this retrosynthesis was the original strategy for the natural product, completion of the model studies gave key insight that allowed for revision of the strategy. First, C-H acetoxylation before the macrocycle is formed will not be viable due to the regioselectivity issue uncovered in the model system in Scheme 2.8. Thus, directed C-H acetoxylation would have to happen post-macrocycle formation. Next, since the Weinreb amide will be utilized to conduction the acetoxylation, it needs to be formed and reduced after the macrocycle is formed. Alternatively, one can envision using our TCE or TFE functionality to direct the C-H acetoxylation, over the Weinreb amide as the directing group. However, when these functionalities were screened in a model system to see if they could competently perform the reaction, all of them failed to produce any product (Scheme 2.11). Therefore, the Weinreb amide is the only functional group reported to

perform the desired C-H acetoxylation.[30] Additionally, incorporation of the Weinreb amide on the starting diazo or before the macrocycle is formed is also not viable, as the Weinreb amide functional group incorporates extra activated protons that interfere with rhodium carbene reactions, even with Rh_2(*R*-2-Cl-5-BrTPCP)$_4$. Finally, direct dimerization of a donor/acceptor diazo compound directly to the macrocycle gave minimal desired product in the simple model **2.11$_F$**, and therefore would not work in the complicated diazo proposed in Scheme 2.10.

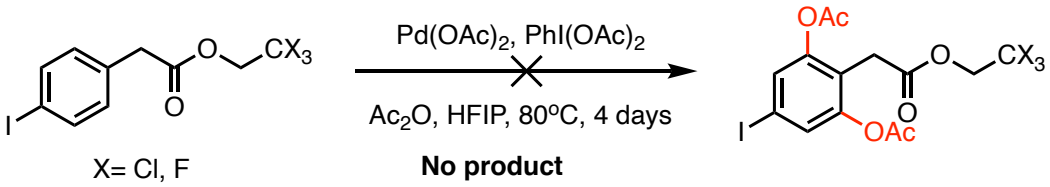

Scheme 2.11 Failed alternative directing groups for C-H acetoxylation

With this information in hand, the strategy to (-)-cylindrocyclophane A was revised. Considering all that was discussed above, a less ambitious and more reasonable second-generation approach to (-)-cylindrocyclophane A is proposed (Scheme 2.12). The modified route starts with the same aryl diazoacetate **2.15**, which can be synthesized from the corresponding phenylacetic acid derivative (see chapter 2 SI), followed by primary insertion on *n*-hexane.[35] After the initial carbene insertion, the same C-H functionalization sequence used in the model will be performed to build up the macrocycle **2.23** quickly. Once the macrocycle **2.23** is formed, selective hydrolysis of the Troc group can be performed followed by amide coupling to yield the Weinreb amide **2.24**. The amide **2.24** then can undergo the directed four-fold C(sp^2)-H acetoxylation[30] forming the late-stage macrocycle **2.25**. At this stage several endgames could be envisioned, namely hydrolysis/oxidative decarboxylation of the TFE group, Grignard reduction of the amide to the ketone, and finally reduction of the ketone to the alkane forming (-)-cylindrocyclophane A.

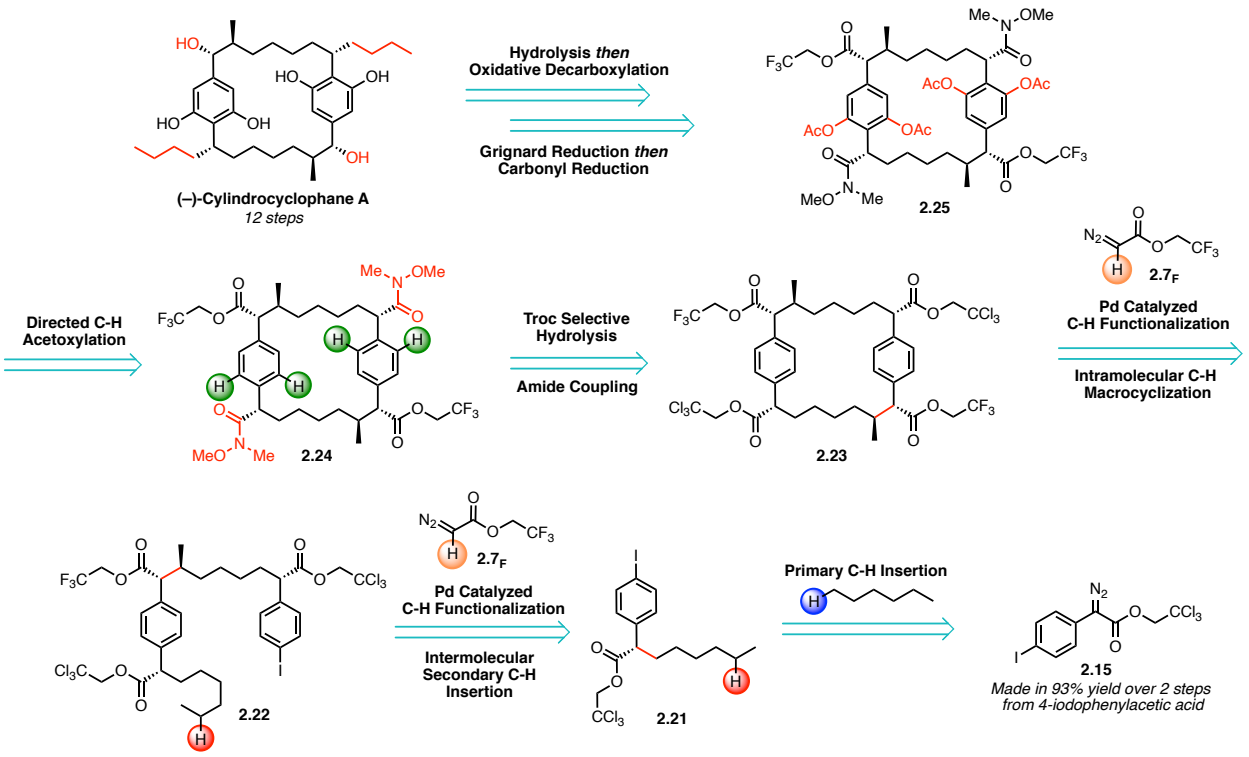

Scheme 2.12 Second-generation retrosynthetic analysis of (-)-cylindrocyclophane A

2.2.3. Studies Toward the Synthesis of (-)-Cylindrocyclophane A

At this stage with successful synthesis of the model paracyclophane **2.11$_F$**, and a retrosynthesis to the natural product, it was time to move forward with the route proposed in Scheme 2.12. The synthesis of aryl diazoacetate **2.15** starts from the commercially available 4-iodophenylacetic acid, DCC coupling and Regitz diazo transfer with *o*-NBSA results in the diazo **2.15** in 93% yield over 2 steps (see chapter 2 SI).[36] With the starting diazo **2.15** in hand, we moved forward with optimizing the primary methyl C-H insertion on *n*-hexane. Analyzing our catalyst toolbox, only one catalyst at the time could functionalize unactivated methyl C(sp^3)-H bonds, Rh_2[*R*-3,5-tris(*p*-^{t}BuPh)TPCP]$_4$ (or Rh_2(*R*-TriBic)$_4$).[35] Conducting the reaction under the published conditions resulted in a poorly regioselective reaction (Scheme 2.13). The reaction gave a 52% yield and a mixture of regioisomers in a 1:1.4 ratio (**2.21 : 2.26)** favoring the methylene

insertion over the methyl. Furthermore, this mixture was completely inseparable via flash chromatography. Therefore, the ambitious primary insertion on *n*-hexane was not going to be a viable path to set the first stereocenter.

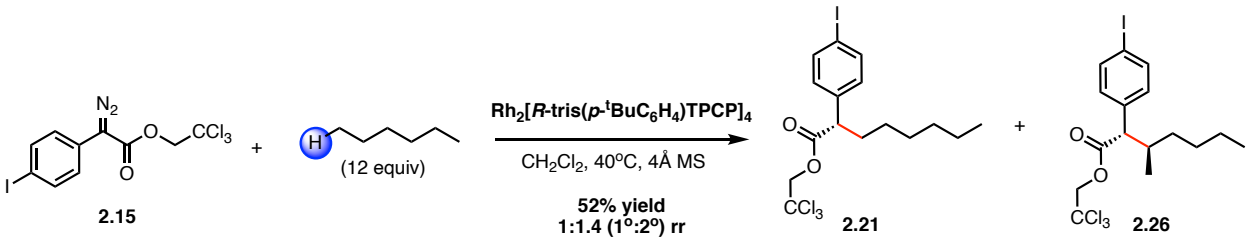

Scheme 2.13 Primary C-H insertion on *n*-hexane

Undeterred by the unselective C-H functionalization with *n*-hexane, a new strategy that would overcome this limitation was developed. The solution we arrived at is conducting the reaction on *trans*-2-hexene (hexene) instead of *n*-hexane. Switching to hexene now converts that terminal methyl proton to an activated C(sp^3)-H bond through allylic stabilization during the C-H abstraction transition state. Since the desired C-H bond is now activated, not only does this increase the chance for a selective reaction, but it also allows other catalyst in the Davies toolbox to be screened. With several primary selective catalysts available, notably all are in the third generation TPCP class of catalyst, the two best catalysts were tested, again Rh_2(*R*-TriBic)$_4$ and now Rh_2(*R*-*p*-PhTPCP)$_4$ (or Rh_2(*R*-BPCP)$_4$).[28, 35] Screening both catalysts under the previously reported conditions resulted in an impressive result from both catalyst (Scheme 2.14). Surprisingly, both catalysts gave identical results. Nearly quantitative yield of 96% yield and almost perfect selectivity of >20:1 rr and 97% ee for **2.27**. Rh_2(*R*-BPCP)$_4$ was chosen as that optimum catalyst, due to ease of its ligand synthesis over Rh_2(*R*-TriBic)$_4$.[35] Notably, this reaction was capable of being scaled up to 25g scale where the catalyst loadings can be dropped to 0.25 mol %.

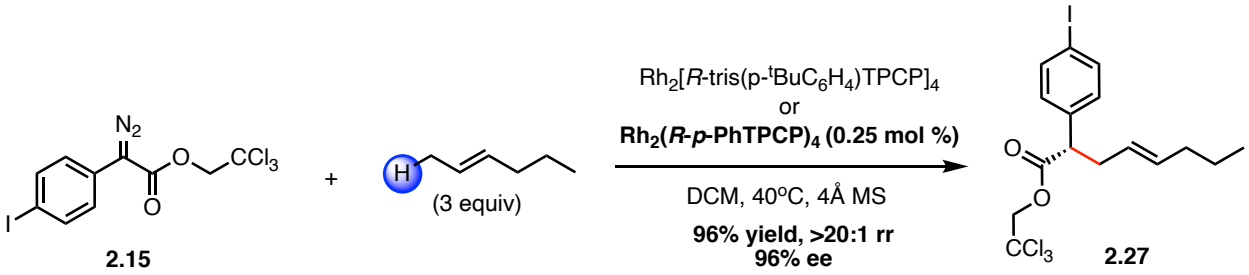

Scheme 2.14 Primary C-H insertion on *trans*-2-hexene

With the primary insertion of hexene optimized, enabling an excellent way to make an almost enantiopure starting material setting the crucial first stereocenter in the synthesis, the next problem was hydrogenation of the resultant alkene **2.27**. Normally hydrogenating a disubstituted alkene is quite facile, however the aryl iodide in my system presented another challenge. Since most transition metals used in hydrogenation reactions are also metals that can oxidatively add into aryl iodide moieties, there was a need to find orthogonal conditions to hydrogenate the alkene. Looking to the literature three catalysts were chosen that seemed like they could perform the desired reaction (Table 2.4). Screening the three catalysts, the first one evaluated was Adam's catalyst (Table 2.4, entry 1).[37] Under these conditions the alkene was successfully hydrogenated to **2.21**, however cleavage of the aryl iodide was also detected. Additionally, the hydrogenated product with and without the iodide is inseparable via column chromatography. Using Wilkinsin's catalyst led to no reactivity at all (Table 2.4, entry 2).[38] However, the last catalyst tried was Crabtree's catalyst, yielding quantitative hydrogenation yielding **2.21** with no detected iodide cleavage (Table 2.4, entry 3).[39, 40]

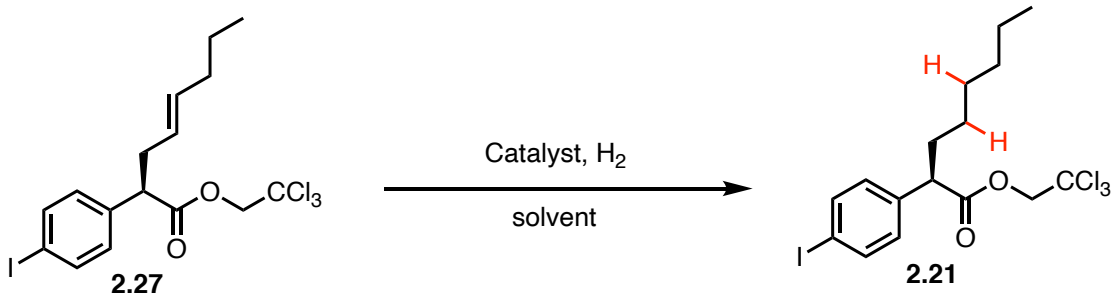

Entry	Catalyst	solvent	yield (%)
1	PtO_2	EtOH	84[a]
2	$[RhCl(PPh_3)_3]$	benzene	0
3	**$[Ir(cod)(PCy_3)(py)]PF_6$**	**CH_2Cl_2**	**>99**

[a]Isolated with small quantities of the dehalogenated product

Table 2.4 Hydrogenation catalyst screen

After successful hydrogenation, the next stage was to carry the pseudo-hexane functionalized product **2.21** forward through the macrocycle formation sequence outlined in the model study. Taking aryl iodide **2.21** under the standard palladium-catalyzed C-H cross coupling conditions[29] with $\mathbf{2.7_F}$ resulted in the diazoacetate compound **2.28** that is now posed for the next key carbene C-H functionalization (Scheme 2.15). Taking diazo **2.28** and reacting it with the previous aryl iodide **2.21**, under the optimized conditions from Table 2.2, resulted in the intermolecular C-H insertion product **2.22**.[24] Notably, to obtain good reactivity the aryl iodide **2.21** must be used in excess as a C-H trap in the reaction. However, we found that the unreacted material from purification could be recycled and resubjected to the reaction with no loss to selectivity. This was a valuable discovery as this is important material with a stereocenter already set. The optimized conditions from the model studied resulted in an excellent reaction that performs in

good yield up to 68%, with excellent selectivity of >20:1 rr and 95:5:< 5:< 5 dr for **2.22**. Regio- and relative diastereoselectivity can be determined from the crude ^{1}H NMR of the reaction, while the diastereoselectivity ratio caused by the catalyzed was determined by chiral HPLC (see chapter 2 SI).

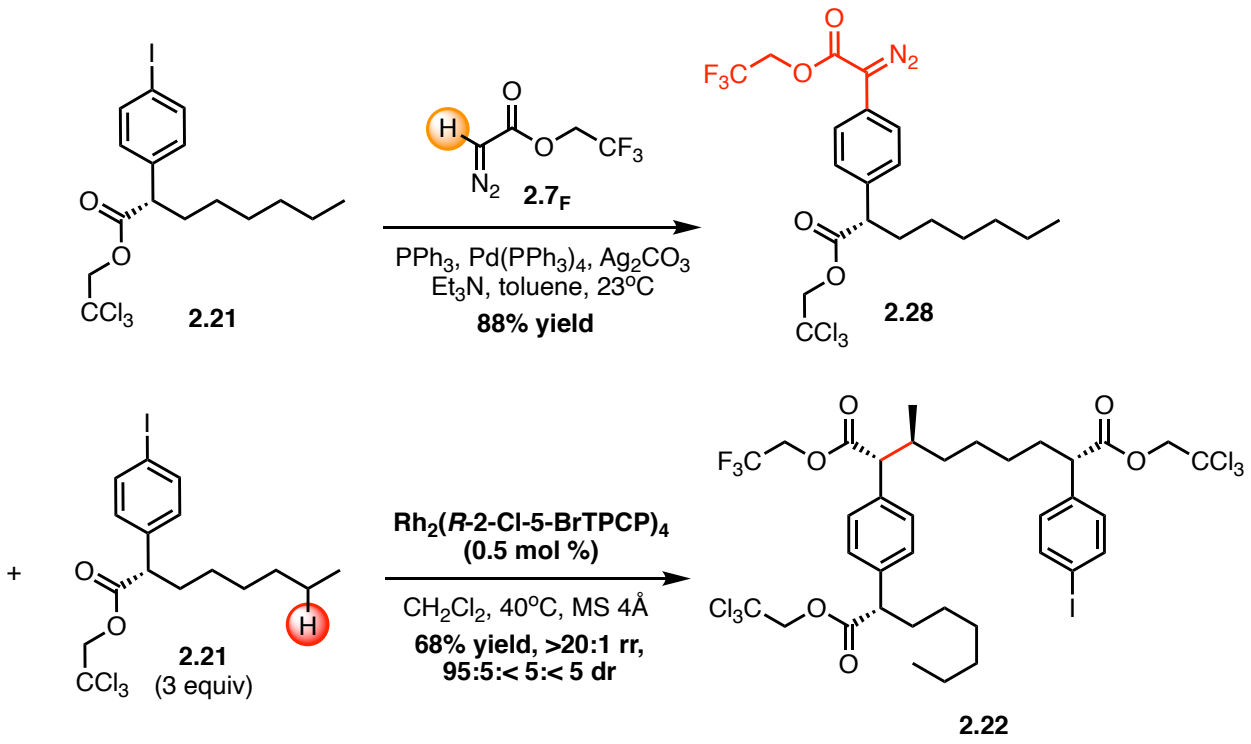

Scheme 2.15 Diazo cross coupling and intermolecular C-H insertion

Moving intermolecular C-H insertion product **2.22** forward, surprisingly the final sequence of the macrocyclization turned out to be very difficult to reproduce and optimize. Aryl iodide **2.22** was subjected under the standard palladium-catalyzed C-H cross coupling conditions[29] with **2.7F**, which surprisingly yielded an irreproducible result (Scheme 2.16). Under these conditions yields were generated up to 77% for diazoacetate **2.29**, however other times it would result in no product at all. After analyzing the reaction and the reagents used, we noticed that when the reaction did not work there would be no silver mirror in the round bottom flask that was seen when the reaction

worked. Since at this point, a fresh bottle of palladium tetrakis was being used, along with dry solvents and freshly prepared substrates, it was hypothesized that the silver carbonate purity and source would be key to a reproducible reaction. After screen various silver carbonate sources, we found that only silver carbonate purchased from Strem would enable a reproducible reaction up to 77% yield for **2.29**.

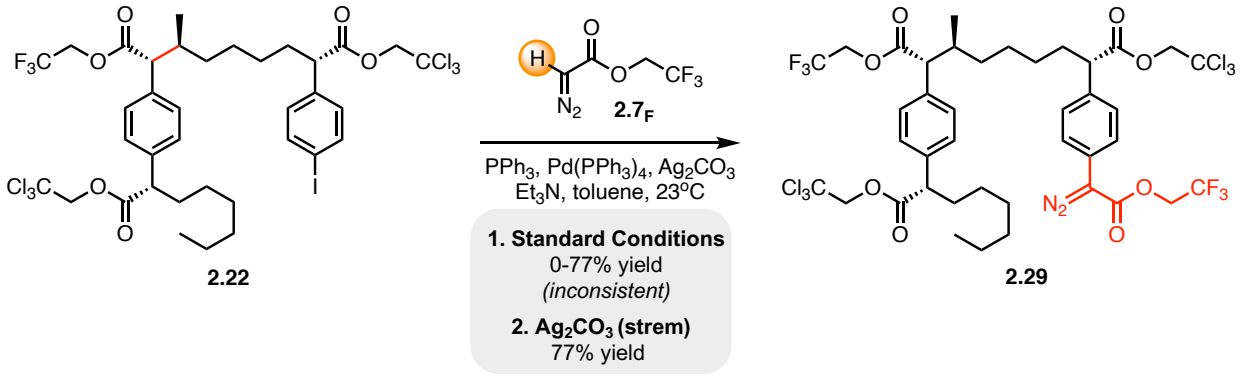

Scheme 2.16 Late-stage palladium-catalyzed C-H cross coupling

Finally, with diazoacetate **2.29** in hand the stage was set for the key macrocyclization. Subjecting diazo **2.29** under the optimized macrocyclization conditions from Table 2.3, again led to a surprising result. Under these conditions the reaction was irreproducible with inconsistent yields between 0-20% in 8:1 dr for **2.23** (Scheme 2.17).[24] This inconsistent result even persisted with my rigorously dry conditions and scale up technique that was developed from the model study (Table 2.3). The problem was solved by making physical observations in lab. After carefully synthesizing and purifying diazo **2.29**, the compound was stored in a -20 ºC freezer overnight to be used in the C-H macrocyclization reaction the next day. After storage overnight in the freezer we noticed the compound had significant bubbles from diazo decomposition. Realizing that to synthesize this diazo **2.29** the previous two steps used transition metals, namely rhodium and palladium, where trace metals could be lingering around after purification destroying the diazo

2.29. Therefore, to address this hypothesis diazo **2.29** was freshly prepared and immediately subjected to the dirhodium catalyzed macrocyclization. Excitingly in this first attempt the yield jumped to 70% for **2.23**! Furthermore, using freshly prepared diazo **2.29** allowed for the reaction to be reproducible. Even though the reaction only performs in 8:1 dr this compound is easily recrystallized to a single diastereomer. Lastly, the macrocyclization for **2.23** is under the Horeau principle[34] and performs with >99% ee, which is confirmed through X-ray crystallography that demonstrates all six stereocenters are set and they all match the stereochemistry in (-)-cylindrocyclphane A (see chapter 2 appendix SI).[2]

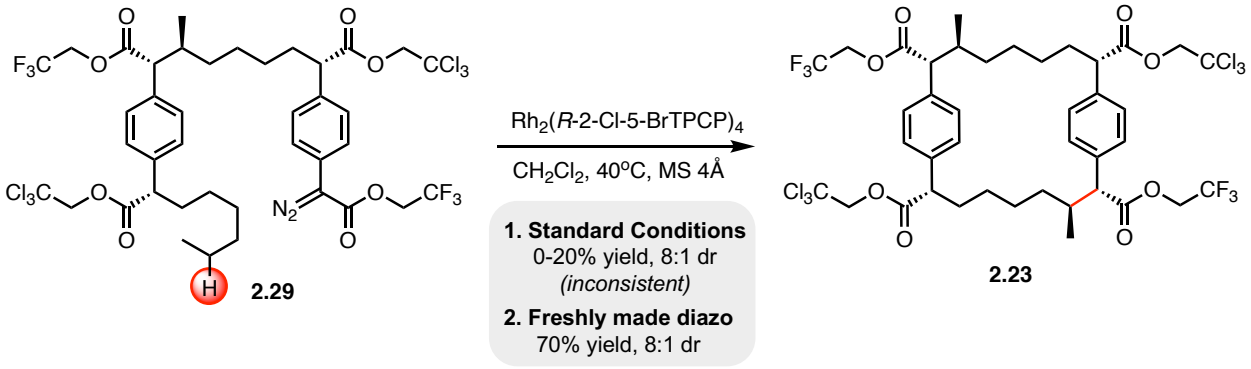

Scheme 2.17 Key macrocyclization using Rh_2(*R*-2-Cl-5-BrTPCP)$_4$

After successful macrocycle formation and optimization of the key step, the next stage was investigating functional group manipulations around the macrocycle. Taking macrocycle **2.23** and subjecting it under zinc/acetic acid conditions allows for chemoselective hydrolysis of the Troc group over the TFE ester yielding **2.30** (Scheme 2.18).[41] The key to the exquisite chemoselectivity is the mechanism for hydrolysis, which zinc facilitates homolysis of the weaker carbon-chlorine bond over the carbon-fluorine bond. While the reaction takes four days to go to completion it performs in quantitative yield and needs no purification before the next step.

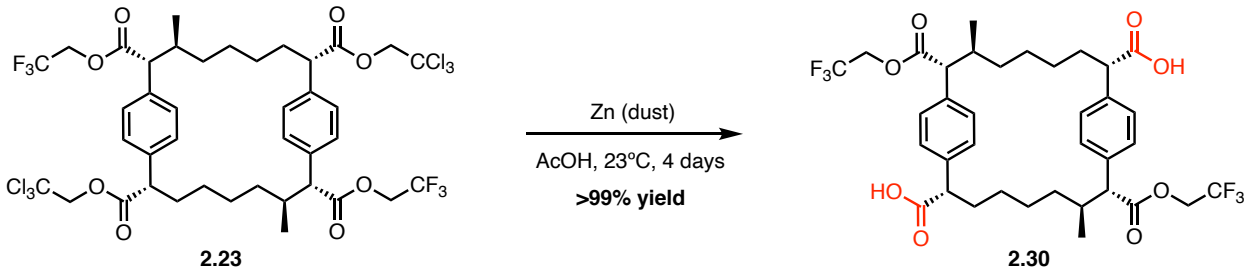

2.23 **2.30**

Scheme 2.18 Chemoselective Troc hydrolysis

With carboxylic acid **2.30** in hand, the compound was subjected to amide coupling conditions. Since there are an abundant amount of amide coupling conditions in the literature, the most robust procedures were screened to see which one would perform the best (Table 2.5). Starting with the Appel-type conditions,[42, 43] this gave a promising yield of 71% for **2.24** (Table 2.5, entry 1). However, a small impurity always remained after column chromatography, therefore, we moved on to other coupling conditions. EDCI coupling conditions[44] led to poor yield of 35%, while excitingly HATU catalyzed conditions[45] formed the Weinreb amide **2.24** in excellent yield of 83% (Table 2.5, entry 2+3).

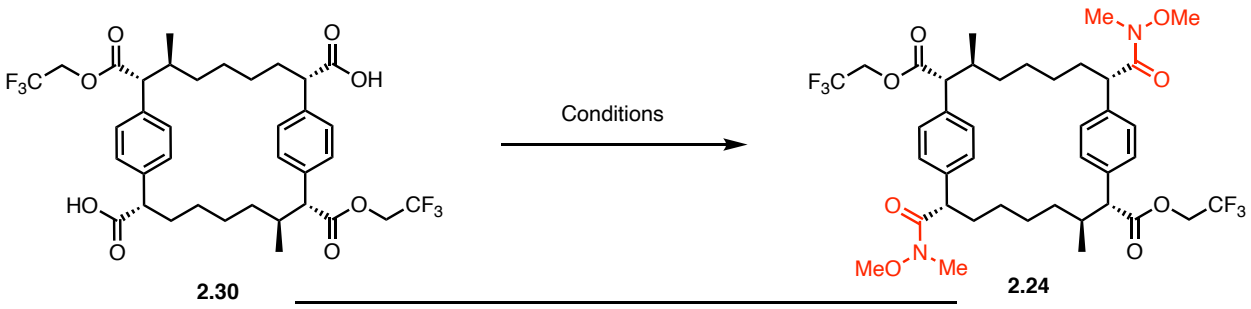

2.30 **2.24**

Entry	Conditions	yield (%)
1	HNMeOMe•HCl, PPh_3 CBr_4, pyridine, CH_2Cl_2	71[a]
2	HNMeOMe•HCl, EDC DMAP, Et_3N, DMF	35
3	**HNMeOMe•HCl, HATU DIPEA, DMF**	**85**

[a]Trace unknown impurity detected in ^1H NMR after purification

Table 2.5 Weinreb amide coupling screen

Now that optimized conditions were found for the formation of Weinreb amide **2.24** the final key C-H functionalization step could be attempted. While bis-acetoxylation is known on simple substrates,[30] this ambitious four-fold C-H acetoxylation has never been attempted and would push the directed C-H functionalization to its limit. Subjecting amide **2.24** under the literature conditions for C-H acetoxylation excitingly formed the desired product **2.25** after 3 days (Scheme 2.19). Unsurprisingly the reaction also creates all the acetoxylated isomers on the way to the tetra-functionalized product, resulting in an incredibly difficult purification. However, some of the desired product **2.25** can be purified out and the resulting mixture of isomers can be re-subjected to the reaction conditions and purified out again. After 2 cycles of the reaction, both 3-day long, the desired product **2.25** can be isolated in up to 61% yield.

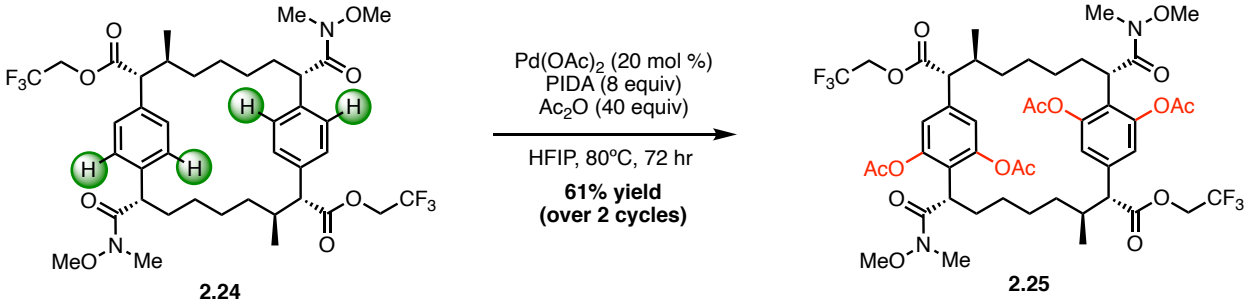

Scheme 2.19 Directed C-H acetoxylation on the macrocycle

While this is a working route and enables formation of the product **2.25** that can be carried forward, a more efficient procedure would be desired. Thus, collaboration with the Yu group here was essential as they were able to suggest and send me a critical pyridine sulfonic acid ligand **2.31** that they suggested would greatly accelerate the rate-determining step of the reaction.[31] The pyridine sulfonic acid ligand **2.31** coordinates to the palladium atom, forcing an acetate ligand off,

making the palladium complex cationic speeding up the concerted metal-deprotonation (CMD) C-H functionalization step. Using ligand **2.31** greatly increased the efficiency of the rection the first time it was utilized. With the ligand the reaction goes to completion in 24 hours and in that single pass generates a 77% yield for **2.25** (Scheme 2.20). Not only does the ligand **2.31** decrease the time of the reaction for six days to one day, but it also greatly improves the purification of the macrocycle **2.25** as only the tetra and tri acetoxylated isomers are formed.

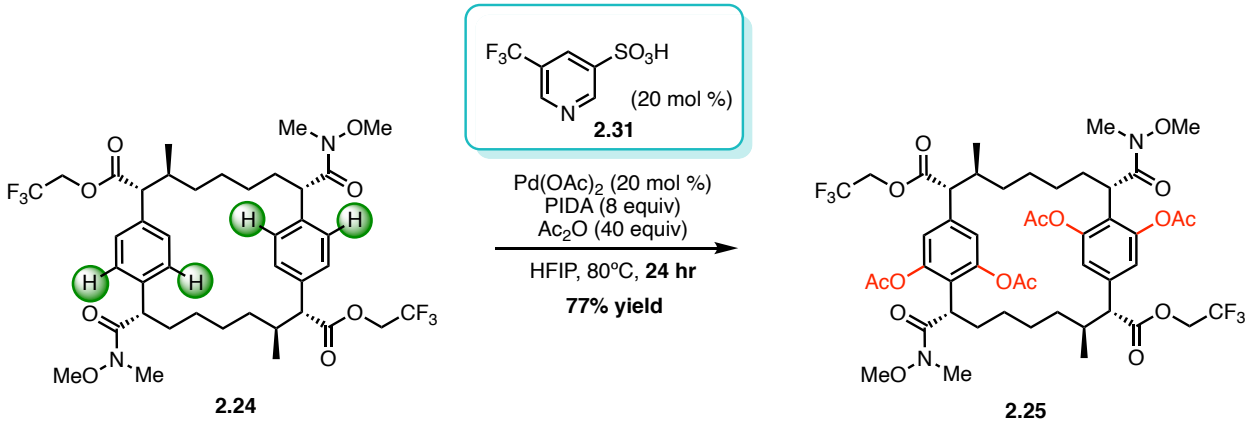

Scheme 2.20 Directed C-H acetoxylation with pyridine sulfonic acid ligand

With the final proposed C-H functionalization step completed in the synthesis, all that remains are functional group manipulations around the macrocycle. It was envisioned at this stage a chemoselective hydrolysis of the all the esters over the Weinreb amide would be possible. While the ester should be more electrophilic than the amide, a model study was conducted to make sure the hydrolysis would be selective for the esters and not epimerize the stereocenters. In this vein, Me_3SnOH (TMTOH) hydrolysis conditions were chosen, which was developed by Nicolaou to hydrolyze esters with highly epimerizable stereocenters.[46] Attempting the reaction on the two models led to selective hydrolysis on macrocycle **2.32** and TFE ester **2.34** (Scheme 2.21). Hydrolysis of macrocycle **2.32** to resorcinol **2.33** elucidated the chemoselectivity of the acetoxy

groups over the Weinreb amide on the macrocycle. While hydrolysis of TFE ester **2.34** to carboxylic acid **2.35** shows the TFE ester is also compatible under these hydrolysis conditions.

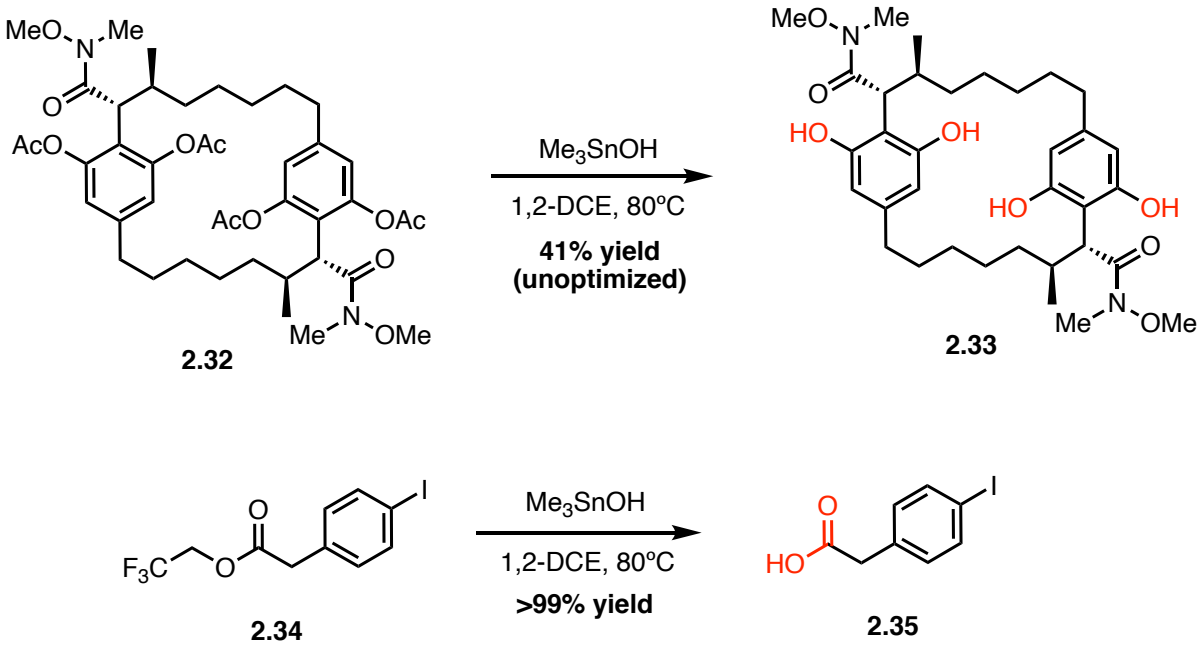

Scheme 2.21 Model hydrolysis reactions

After successful demonstration of the hydrolysis in the two models, we confidently moved to testing the reaction with material at the front end of the synthesis. Taking macrocycle **2.25** and subjecting it to the TMTOH hydrolysis conditions surprisingly led to an unselective reaction (Scheme 2.22). Varying the equivalents, temperature, time, concentration and work up all lead to either degradation or over hydrolysis with loss of the Weinreb amide peaks in the ^{1}H NMR. Moving to other base or acid catalyzed conditions (Scheme 2.22) led to the same result.[47-52] Again, under any of the new conditions, varying the equivalents, temperature, time, concentration and work up all lead to either no reaction, degradation or over hydrolysis. Clearly a selective reaction on the esters of substrate **2.25** to **2.36** was not going to work, and it was time to think of an alternative strategy.

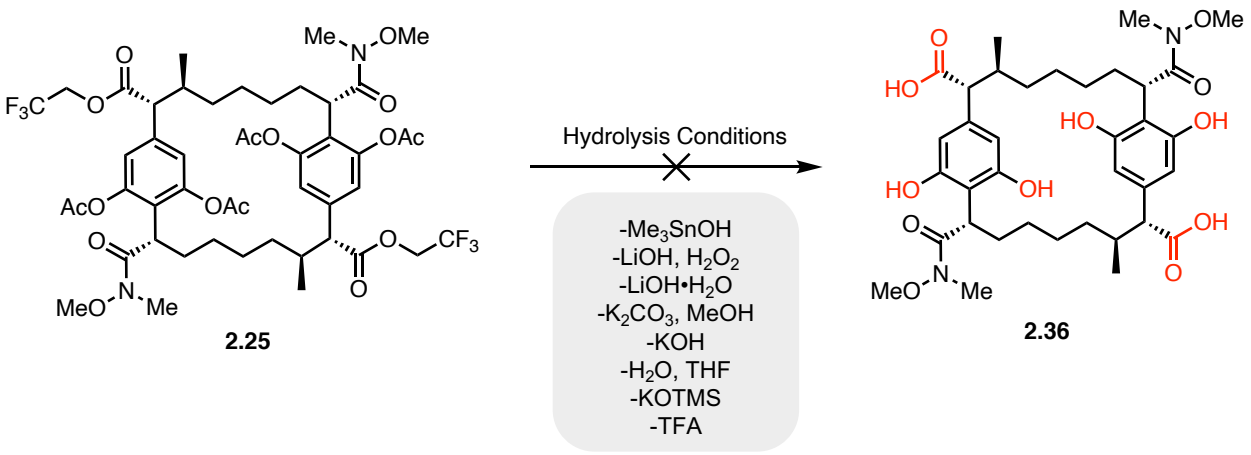

Scheme 2.22 Failed late-stage hydrolysis on the macrocycle

My previous hypothesis was that the esters in macrocycle **2.25** should be more electrophilic and react first, but clearly that was not the experimental result. Since all the attempts failed to selectively hydrolyze the esters, it was hypothesized if it would be possible to chemoselectively reduce the Weinreb amide over the esters to form aldehyde **2.37**. While the amide should be a less reactive functional group to nucleophilic attack, on the flip side it should be more nucleophilic than the esters due to the imidate resonance structure. Therefore, harnessing the nucleophilicity of the amide could potentially lead to preferential reduction yielding **2.37**. After searching the literature for precedented conditions, the Schwartz reagent was chosen as one of the most robust amide reduction reactions.[53] Unfortunately, using the Schwartz reagent led to no reduction of the amide **2.25** (Table 2.6). Either purchasing the Schwartz reagent (Table 2.6, entry 1), making it fresh[54] (Table 2.6, entry 2), or generating it *in situ*[55] (Table 2.6, entry 3) all led to no reaction on the amide and loss of the acetoxy functionality seen in the crude ^{1}H NMR. Lastly, trying $Mo(CO)_6$ catalyzed hydrosilylation led to only recovery of the starting material **2.25**.[56] With only failed results from the ester hydrolysis or amide reduction attempts the endgame strategy was re-evaluate.

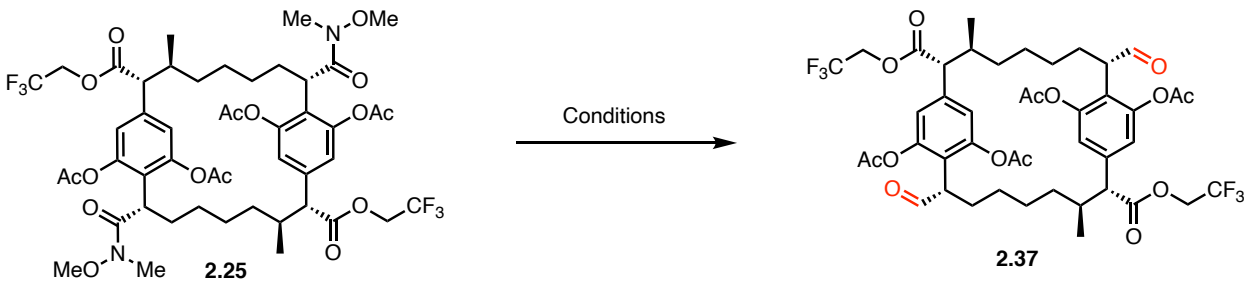

Entry	Conditions	yield (%)
1	$Cp_2Zr(H)Cl_2$ *(purchased)*	Over reduction
2	$Cp_2Zr(H)Cl_2$ *(made fresh)*	Over reduction
3	$Cp_2Zr(H)Cl_2$ (generated *in situ)*	Over reduction
4	$Mo(CO)_6$, TMDS	No reaction

Table 2.6 Amide reduction screen

2.2.4. Third-Generation Retrosynthetic Analysis

With a slew of bad results, it was at this point that we decided to re-analyze the endgame strategy. It was hypothesized that attempting the hydrolysis on the polyfunctionalized product **2.25** potentially has too many functional groups for a selective reaction. Therefore, to overcome the unselective reaction, we decided to try the hydrolysis before conducting the C-H acetoxylation on the molecule to reduce the number of functional groups (Scheme 2.23). For simplicity in the retrosynthesis shown here (Scheme 2.23) the previous steps that are already established were omitted. The new strategy laid out here starts with TFE hydrolysis on macrocycle **2.24**, affording the carboxylic acid **2.38** that is primed for oxidative decarboxylation. After inversion of the carboxylic acid group the directed four-fold C-H acetoxylation will be performed to give macrocycle **2.39**. At this stage all that is left is Grignard reduction to add the final carbons in (-)-cylindrocyclophane A, followed by reduction of the ketone to the alkane. The approached outlined

here would end up being 13 steps from the known aryldiazoacetate and 15 linear steps in the longest sequence from commercially available material.

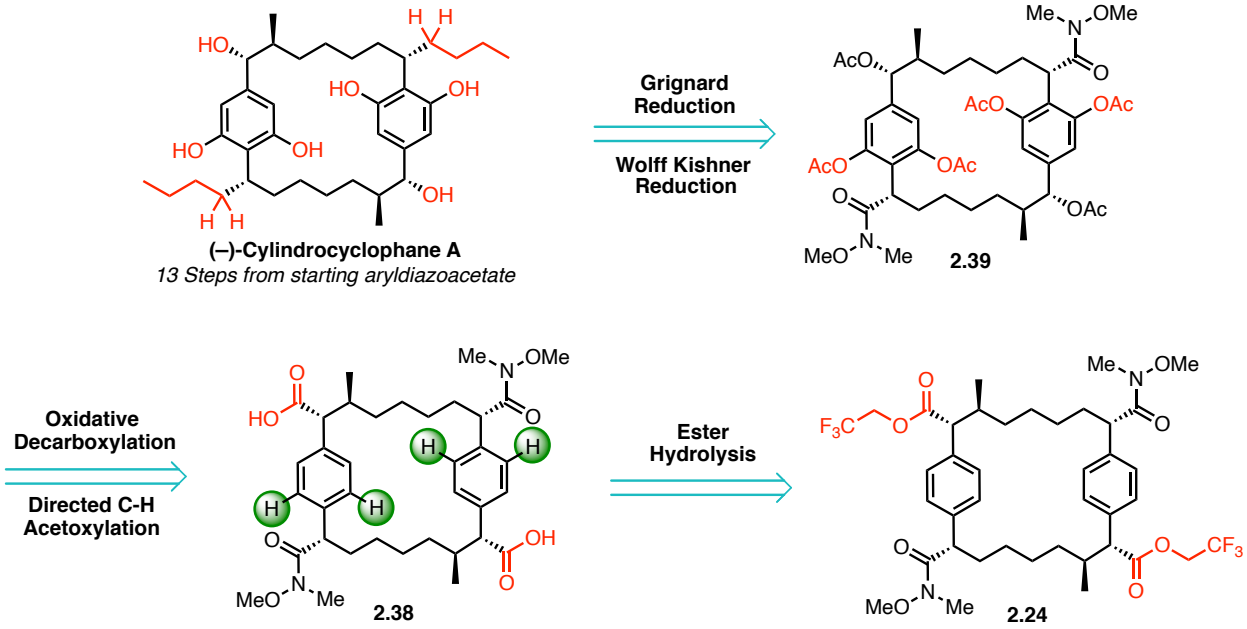

Scheme 2.23 Third-generation endgame retrosynthetic analysis

2.2.5. Final Approach to (-)-Cylindrocyclophane A

Excited by the new endgame strategy, we embarked on trying the newly proposed hydrolysis on the simpler macrocycle **2.24**. Subjecting macrocycle **2.24** to lithium hydroxide (LiOH) hydrolysis conditions incredibly gave 97% yield for **2.38** (Scheme 2.24)! Simply stirring the macrocycle **2.24** open to air overnight yielded a chemoselective reaction that requires no purification afterwards. The one downside to this approach was that the LiOH does slightly epimerize the stereocenter adjacent to the newly formed acid **2.38**. However, this turns out to be not important as the following reaction is the photoredox decarboxylation that destroys and reforms the stereocenter.

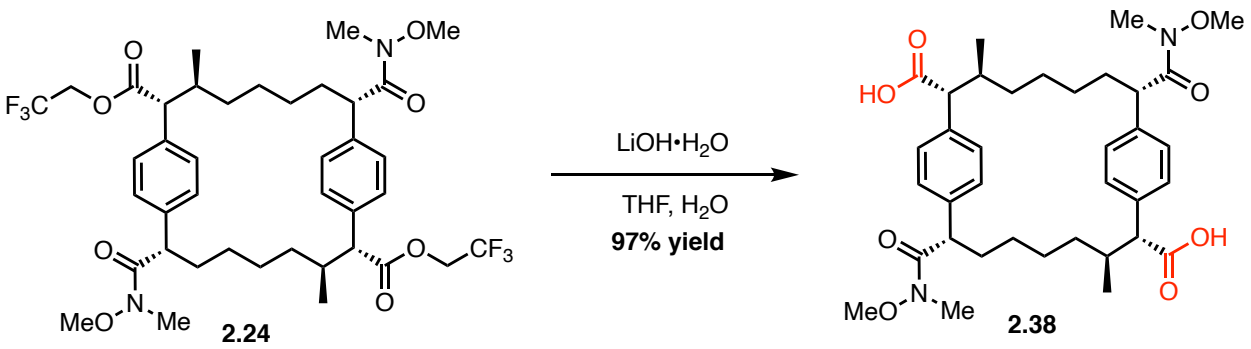

Scheme 2.24 Hydrolysis of the TFE esters

After successful hydrolysis the carboxylic acid **2.38** was now in hand to attempt the oxidative decarboxylation. Originally the idea was developed from classic conditions that utilize lead tetraacetate.[57-60] However, while the synthesis was being worked on over the years a recent photoredox catalyzed reaction came out that replaces the classic conditions with a modern variant.[61] Instead of lead tetraacetate, these new conditions utilize an acridinium based photocatalyst and copper (II) acetate. The proposed mechanism starts with blue light excitation of the photocatalyst, which then can facilitate radical decarboxylation. That resultant radical can then recombine with copper then reductively eliminate the product. A key aspect for why this specific oxidative decarboxylation method was chosen is that the authors proposed radical recombination with copper. Since the mechanism for this transformation goes through a radical, destroying the stereocenter already set, we hypothesized that the radical recombining with a large atom, such as copper, versus oxygen in another report,[62, 63] would allow for facial selectivity from the adjacent stereocenter.

Subjecting the macrocyclic carboxylic acid **2.38** to a small-scale test reaction with the organophotoredox conditions excitingly generated the product **2.40** in around 20% unoptimized yield. However, after this initial result, attempts to repeat the reaction were unsuccessful.

Undeterred by the irreproducible reaction the photoredox literature was studied to learn more about reactions of this type to optimize the transformation.[64] The first variable that found to be important was light penetration. Since these reactions were run on small scale (5-10mg), the reaction needed to be diluted significantly, as well as use minimal 4Å MS to minimize blue light scattering. The next variable that was unraveled was the amount of photocatalyst that needs to be added. Again, due to the small scale of the reaction, too much of the acridinium organophotocatalyst was being added, which can result in self quenching. Lastly, rigorously sparging the reaction to remove all the oxygen was critical as well for an effective reaction.[65] Testing the reaction again now that all these variables have been analyzed, we were pleasantly surprised to not only have the reaction reproducible but achieve an 52% yield for **2.40** (Scheme 2.25). Even more excitingly the reaction performs in 9:1 dr favoring the major diastereomer I need to make (-)-cylindrocyclophane A (see chapter 2 SI). The one limitation from this reaction is that it does not scale up at all and the largest scale achieved was up to 70 mg.

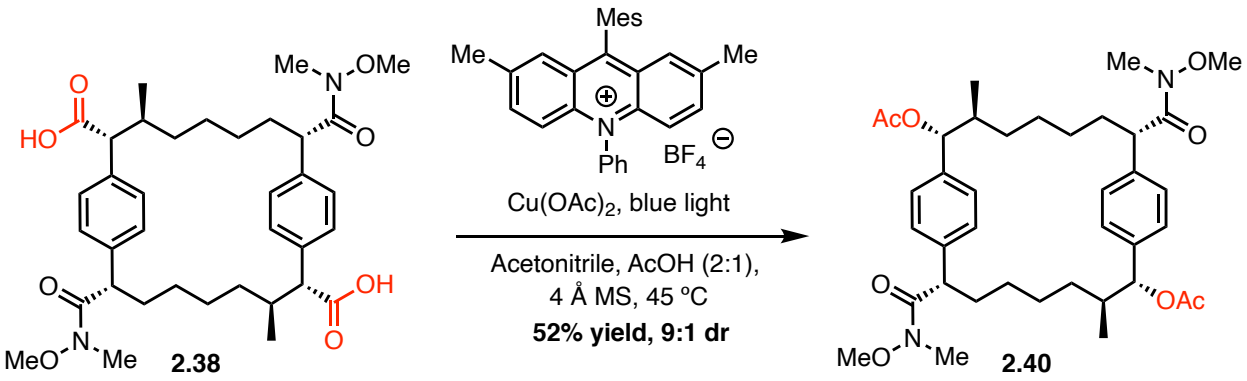

Scheme 2.25 Photoredox catalyzed decarboxylation acetoxylation

With carboxy inversion compound **2.40** in hand, the material was carried forward to the final C-H functionalization reaction. While the four-fold directed C-H acetoxylation worked on macrocycle **2.24**, we were unsure how effective the reaction would be on this modified substrate

2.40. Taking the optimized ligand **2.31** catalyzed conditions[31] from the second-generation route (Scheme 2.20), macrocycle **2.40** was subjected to the reaction conditions. Luckily, no further optimization was needed as the previously optimized conditions worked beautifully here (Scheme 2.26). While this substrate takes two days instead of one to go to completion, no re-subjection of the isomer mixture is needed as a 60% yield for **2.39** is generated in the first cycle.

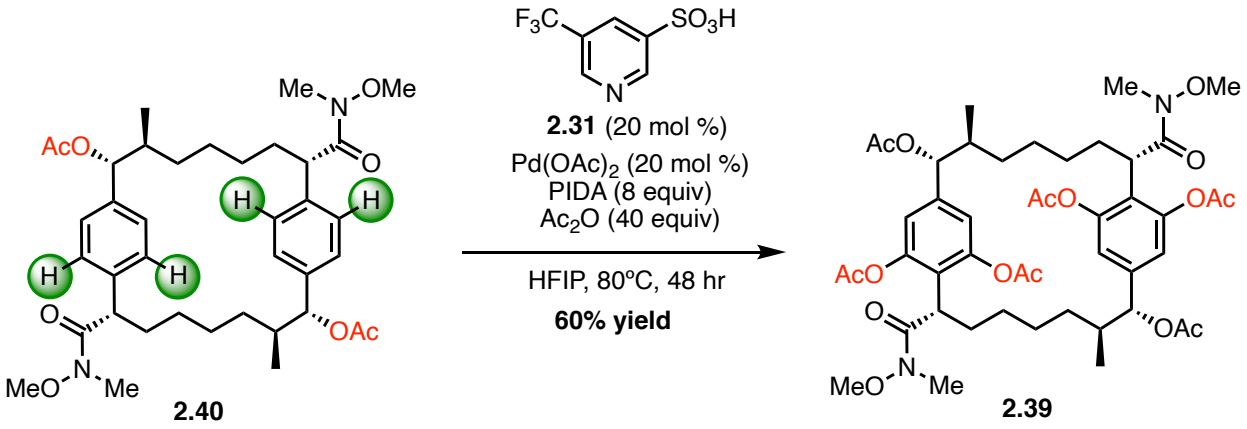

Scheme 2.26 Directed four-fold C-H acetoxylation third-generation route

Only two steps away from the (-)-cylindrocyclophane A, we moved to the final reductions in the synthesis. After C-H acetoxylation to form macrocycle **2.39**, the next step proposed is global reduction via Grignard addition. The hypothesis is that by running the Grignard reduction with a vast excess of Grignard, the Grignard would be able to deprotect all the acetoxy functional groups and reduce the Weinreb amide to the ketone. However, since all the previous syntheses of cylindrocyclophane had phenol deprotection as the final step, we were unsure if the phenols would be stable enough for purification. Upon subjecting the macrocycle **2.39** to the Grignard conditions on small-scale (1mg), the desired product **2.41** was exciting found via mass hit by HRMS (Scheme 2.27). Yet, due to the miniature scale of the reaction the product **2.41** could never be seen in the ^{1}H NMR or isolate it via prepLC. Even with the promising mass hit result we were hesitant to scale

the reaction up to increase the chances of isolation. Therefore, macrocycle **2.39** was tested against a few other reactions before moving to a model.

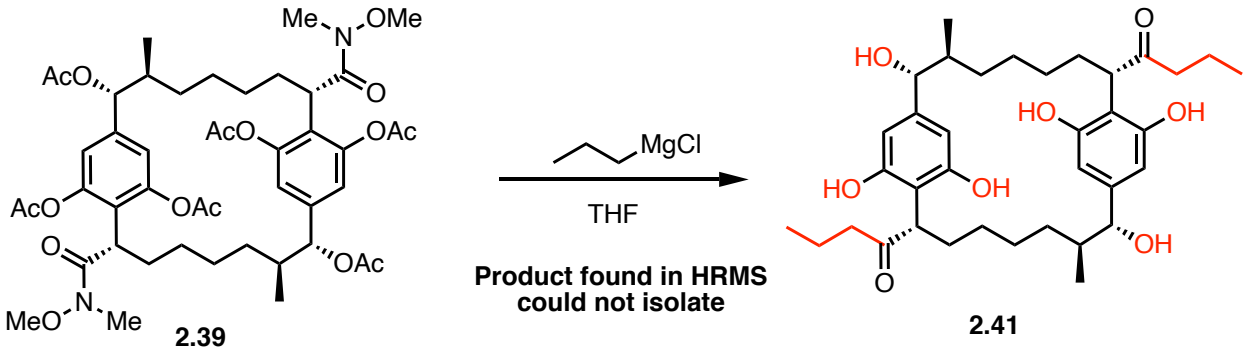

Scheme 2.27 Global Grignard reduction attempt

Since we didn't know if the Grignard wasn't working due to stability or purification of the free phenols, additional chemoselective reactions were found that would selectively reduce the Weinreb amide **2.39**, leaving the acetoxys intact. Since the Schwartz reduction failed in the similar system before (Table 2.6), we searched for other chemoselective reactions. The first reaction attempted was reduction via MgAB reagent (Scheme 2.28).[66] The MgAB reagent is a modified borohydride reagent that was disclosed in a publication to selectively reduced amides in the presence of esters. However, after synthesizing the MgAB reagent and subjecting the conditions to my macrocycle **2.39**, complete destruction of the starting material was found, with no signs of my macrocycle seen in the ^{1}H NMR. The next reaction attempted was activation of the amide via ethyl triflate, followed by reduction of the imidate via LiAlH(O*t*-Bu)$_3$ (Scheme 2.28).[67] Unfortunately, in every attempt the Weinreb amide was still present in the crude ^{1}H NMR, with unselective reactions happening on the acetoxy functional groups. The final conditions tried was reduction with DIBAL-H, with the hope of reducing the Weinreb amide to the aldehyde and

deprotection of the acetate groups to the alcohol (Scheme 2.28). However, this reaction led to a product that was insoluble in all NMR solvents and no mass hit in the HRMS.

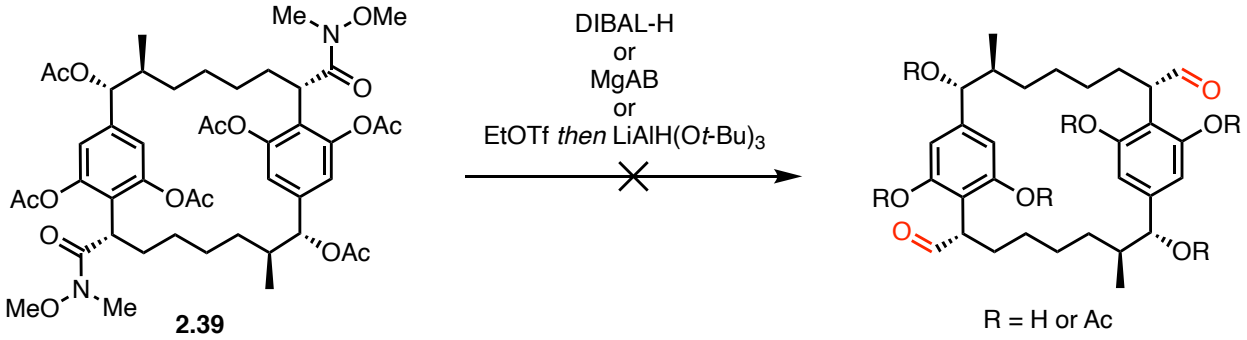

Scheme 2.28 Failed late-stage Weinreb amide reductions on the macrocycle

After several failed attempts to reduce macrocycle **2.39** it was clear a new strategy was needed. Therefore, to validate the best endgame to (-)-cylindrocyclophane A we decided to screen reactions on a model system to pinpoint the reactivity desired without the complication of the macrocycle.

2.2.6. Endgame Strategies and Model Studies for Late-Stage Transformations

At this stage we couldn't tell if the reactions just weren't compatible with the 2,6-acetoxy functionality in the system, or if the issue is with the macrocycle's steric hindrance or solubility. To test the endgame strategies, a model system was synthesized using material early in the synthetic route (Scheme 2.29). This model would allow testing if selective reduction on the notoriously difficult 2,6-disubstituted aromatic system would be possible. Taking the pseudo-hexane functionalized product **2.21** under zinc/acetic acid hydrolysis conditions[41] quantitatively hydrolyzed the Troc group to the carboxylic acid **2.42**. The resultant carboxylic acid **2.42** can be coupled with HATU to generate Weinreb amide **2.43** in 78% yield,[45] which is subsequently subject

to the directed double C-H acetoxylation.[30] Since the model is a simpler substrate than the macrocycle, the pyridine sulfonic acid ligand **2.31** is not needed here, forming the bisacetoxylated product **2.44** in 58% yield.

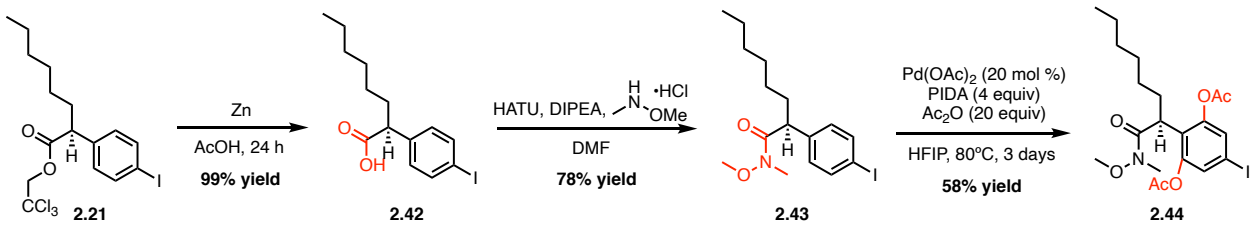

Scheme 2.29 Synthesis of the model compound to probe endgame strategies

With the model substrate in hand, the reactions we chose to explore were amide activation then imidation/reduction[67] and Petasis ofefination/alkylation.[68-70] While these strategies were explored Tyler Casselman tested iridium catalyzed hydrosilylation conditions.[71] Unfortunately, all attempts by Tyler Casselman failed to generate the desired aldehyde, resulting in over reduction to the amine. Since these results were conducted by Tyler Casselman and are not relevant to the current endgame they will not be shown here. The first reaction explored was the amide activation/reduction sequence with **2.44** (Scheme 2.30).[67] This reaction is a recent JOC publication where the authors report a selective reduction of 2,6-disubstituted benzamides in the presence of other electrophilic functional groups, including esters. With a promising precedent the reaction was explored with several different activating reagents used in the paper (Scheme 2.30). However, in all cases, regardless of the activating agent, preferential reduction of the acetoxy group occurred. This either generated the free phenol **2.45**, or the phenol would cyclize on the amide forming lactone **2.46**. Since this reaction was monitored by LCMS and analyzed by crude ^{1}H NMR, no isolated yields were obtained.

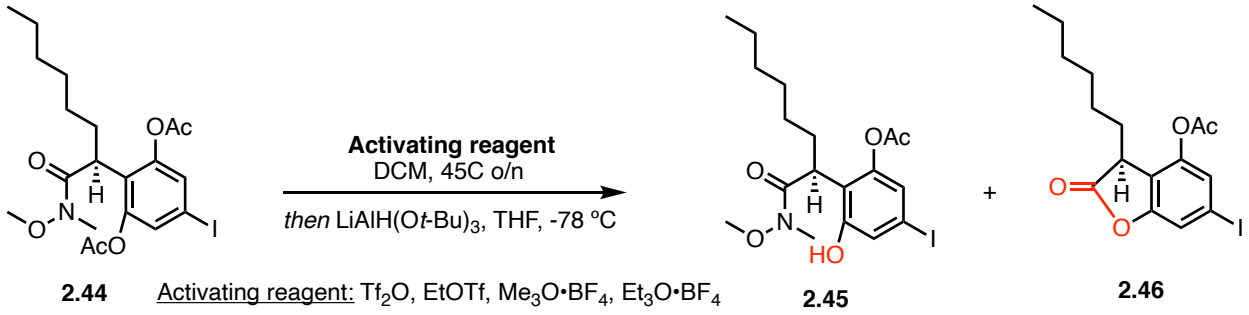

2.44 Activating reagent: Tf_2O, EtOTf, $Me_3O{\cdot}BF_4$, $Et_3O{\cdot}BF_4$ **2.45** **2.46**

Scheme 2.30 Model study on amide activation/imidate reduction

After failure to preferentially activate the Weinreb amide over the acetoxys, we turned to Petasis olefination/alkylation.[68-70] The hypothesis here is the amide should preferentially react with the titanium complex forming the enamine, which can then be subjected to alkylation to form the desired ketone product. Subjecting the model **2.44** to the Petasis reagent excitingly generated a mass hit by LCMS for the enamine **2.48**, however following alkylation and acid work up yielded no product detection via LCMS for the desired ketone (Scheme 2.31). It turns out that the mass for the enolization of the acetoxy (**2.47**) is the same mass for enamine formation (**2.48**). After acidic work up the enol is hydrolyzed to the phenol, which cyclizes on the amide forming the lactone **2.46** seen in the previous strategy. This was validated through LCMS and ^{1}H NMR analysis of the crude reaction. While not the desired reactivity, both strategies in Schemes 2.30 and 2.31 allow illumination of the hypothesis. Namely, the acetoxy groups will always preferentially react in this system over the Weinreb amide.

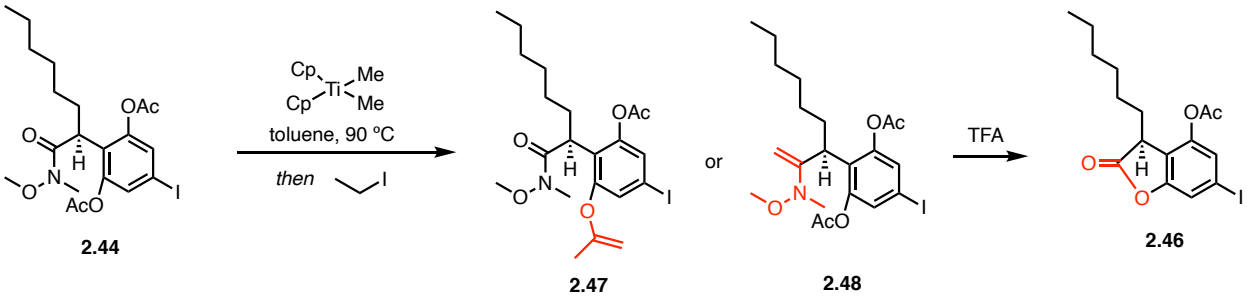

2.44 **2.47** **2.48** **2.46**

Scheme 2.31 Model study on Petasis olefination/alkylation

While the hypothesis was disproven with the model system, these studies gave key insight into the endgame strategy. We discovered that no matter what conditions we tried to reduce the Weinreb amide, the acetoxy group will always react first. Thus, chemoselective reduction of the Weinreb amide is unattainable in this system. With this knowledge in hand, we decided to turn our efforts back to the Grignard reduction on the macrocycle. Since purification and isolation of the Grignard product **2.41** was previously impossible, collaboration with the Stoltz lab was instrumental to utilize their analytical expertise to see if we could solve the purification issue. At Caltech not only was the LCMS mass hit from the Grignard reduction reproduced, but we were also even able to isolate the product **2.41** via prepLC (Scheme 2.32)! Currently Tyler Casselman is working on optimizing the Grignard reduction and the subsequent ketone reduction to synthesize (-)-cylindrocyclophane A.

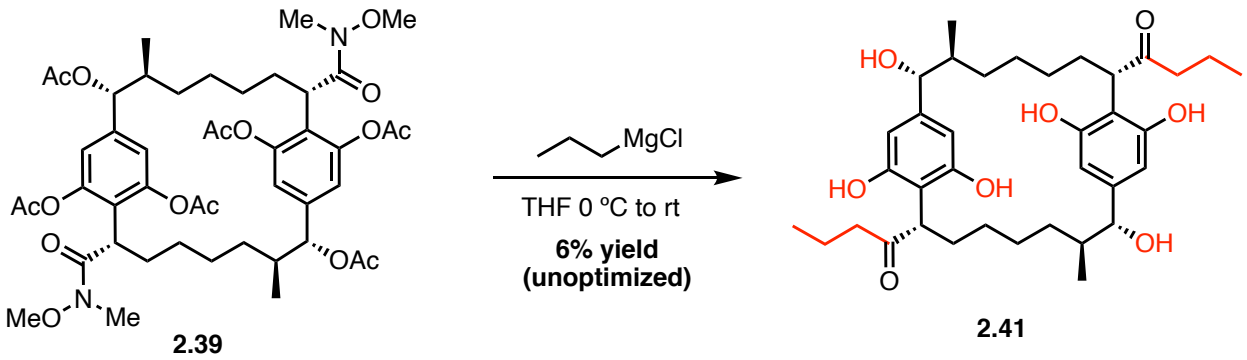

Scheme 2.32 Successful late-stage Grignard reduction on the macrocycle

At last, with one step to go, we currently are focused on the final reduction needed to synthesize (-)-cylindrocyclophane A. For the final step we proposed condensation of the ketone **2.**41 with *p*-toluenesulfonyl hydrazide to form the hydrazone, which can be subsequently reduce

to the alkane via hydride reduction with sodium cyanoborohyride (Scheme 2.33).[72-75] Currently Tyler Casselman is working on studying and optimizing the final reduction against model compound **2.44**. Once successful conditions are found Tyler Cassleman will then move to conducting the reaction on the macrocycle **2.41**. Ultimately, we hope that by the time this dissertation is submitted the proposed total synthesis of (-)-cylindrocyclophane A outlined here will close to completion.

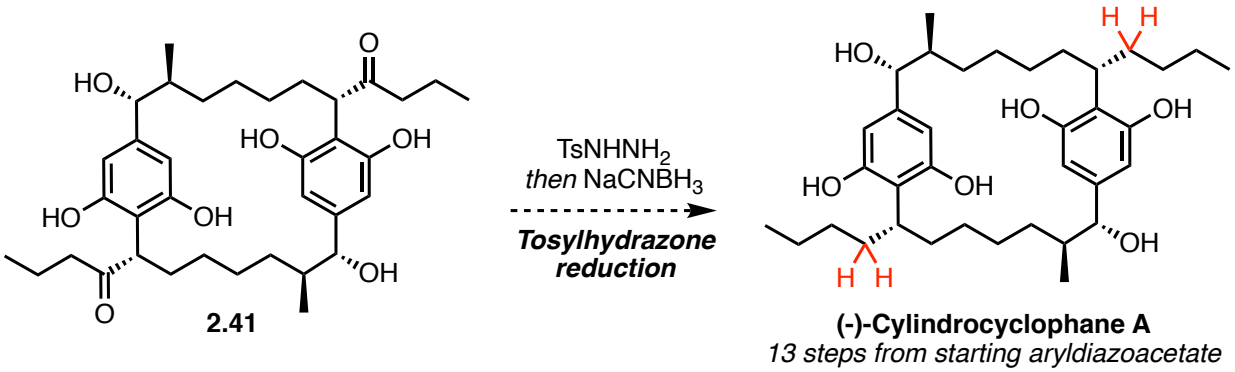

Scheme 2.33 Proposed final step to synthesize (-)-cylindrocyclophane A

2.3. Conclusion

In conclusion a novel synthesis to (-)-cylindrocyclophane A was developed using C-H functionalization logic. Completion of this work would represent a major milestone in total synthesis, encompassing 6 C-H functionalization steps and primarily constructing the carbon skeleton through these steps. The proposed synthetic approach described herein is versatile and can access a wide variety of [7.7]paracyclophane derivatives and their analogs, previously inaccessible with traditional synthetic methods. In the future, the modular route disclosed here will allow for SAR and MOA analysis to probe the promising biological activity and determine if this class of compounds warrants further development as potential drug candidates. At the beginning of the project, a model study of the [7.7]paracyclophane core was completed where the model

[7.7]paracyclophane was formed in >99% enantiopurity with an overall yield of 46% from the starting aryldiazoacetate. Notably, this macrocyclization is the first example of an enantioselective macrocyclization by means of functionalization of an unactivated C(sp^3)-H bond, pushing the boundaries of not only the C-H functionalization field, but representing a novel entry to macrocyclic rings. With the proof of principle validated we conducted several additional model studies to determine the best route to the natural product, resulting in the work discussed here. With the optimal route unraveled, 14 out of the 15 total steps have been achieved, including the four-fold acetoxylation, indicating successful use of all the desired C-H functionalization steps. We anticipate that this project will serve as a pinnacle for what C-H functionalization can achieve in total synthesis, acting as a model for future total syntheses utilizing C-H functionalization logic.

2.4. Distribution of Credit

My role in this project was the lead researcher to explore the synthesis of (-)-cylindrocyclophane A using C-H functionalization logic. The initial model study and synthesis of **2.11$_F$** was disclosed in a JACS publication in 2018.[24] I mentored an undergraduate Camila Suarez during part of the studies, and she contributed to some of the steps under my direction. Specifically, Camila was key in synthesizing the starting aryl diazoacete **2.15** and acceptor only diazoacetate **2.7$_F$**. Additionally, she conduction the primary C-H insertion with hexene (**2.27**) and the following hydrogenation (**2.21**). Elizabeth Goldstein and Tyler Casselman from the Stoltz group also contributed to some components of the project and their contributions will be acknowledged when discussed. The last results in section **2.2.6.** were conducted by myself as a visiting scholar at Caltech in Dr. Brian Stoltz's lab. Finally, Hoojon Park from the Yu lab contributed to this project

by synthesizing and sending me the pyridine sulfonic acid ligand **2.31**. A manuscript of the current work in this chapter is currently being written by myself.

2.5. References

1. Cram, D. J.; Steinberg, H., Macro Rings. I. Preparation and Spectra of the Paracyclophanes. *J. Am. Chem. Soc.* **1951,** *73* (12), 5691-5704.
2. Moore, B. S.; Chen, J. L.; Patterson, G. M. L.; Moore, R. E.; Brinen, L. S.; Kato, Y.; Clardy, J., [7.7]Paracyclophanes from blue-green algae. *J. Am. Chem. Soc.* **1990,** *112* (10), 4061-4063.
3. May, D. S.; Kang, H.-S.; Santarsiero, B. D.; Krunic, A.; Shen, Q.; Burdette, J. E.; Swanson, S. M.; Orjala, J., Ribocyclophanes A–E, Glycosylated Cyclophanes with Antiproliferative Activity from Two Cultured Terrestrial Cyanobacteria. *J. Nat. Prod.* **2018,** *81* (3), 572-578.
4. Bui, H. T.; Jansen, R.; Pham, H. T.; Mundt, S., Carbamidocyclophanes A-E, chlorinated paracyclophanes with cytotoxic and antibiotic activity from the Vietnamese cyanobacterium Nostoc sp. *J. Nat. Prod.* **2007,** *70* (4), 499-503.
5. Luo, S.; Kang, H. S.; Krunic, A.; Chlipala, G. E.; Cai, G.; Chen, W. L.; Franzblau, S. G.; Swanson, S. M.; Orjala, J., Carbamidocyclophanes F and G with Anti-Mycobacterium tuberculosis Activity from the Cultured Freshwater Cyanobacterium Nostoc sp. *Tetrahedron letters* **2014,** *55* (3), 686-689.
6. Kang, H. S.; Santarsiero, B. D.; Kim, H.; Krunic, A.; Shen, Q.; Swanson, S. M.; Chai, H.; Kinghorn, A. D.; Orjala, J., Merocyclophanes A and B, antiproliferative cyclophanes from the cultured terrestrial Cyanobacterium Nostoc sp. *Phytochemistry* **2012,** *79*, 109-15.
7. May, D. S.; Chen, W. L.; Lantvit, D. D.; Zhang, X.; Krunic, A.; Burdette, J. E.; Eustaquio, A.; Orjala, J., Merocyclophanes C and D from the Cultured Freshwater Cyanobacterium Nostoc sp. (UIC 10110). *J. Nat. Prod.* **2017,** *80* (4), 1073-1080.
8. Moore, B. S.; Chen, J.-L.; Patterson, G. M. L.; Moore, R. E., Structures of cylindrocyphanes a-f. *Tetrahedron* **1992,** *48* (15), 3001-3006.
9. Chen, J. L.; Moore, R. E.; Patterson, G. M. L., Structures of nostocyclophanes A-D. *J. Org. Chem.* **1991,** *56* (14), 4360-4364.
10. Chlipala, G. E.; Sturdy, M.; Krunic, A.; Lantvit, D. D.; Shen, Q.; Porter, K.; Swanson, S. M.; Orjala, J., Cylindrocyclophanes with proteasome inhibitory activity from the Cyanobacterium Nostoc sp. *J. Nat. Prod.* **2010,** *73* (9), 1529-1537.
11. Preisitsch, M.; Harmrolfs, K.; Pham, H. T.; Heiden, S. E.; Fussel, A.; Wiesner, C.; Pretsch, A.; Swiatecka-Hagenbruch, M.; Niedermeyer, T. H.; Muller, R.; Mundt, S., Anti-MRSA-acting carbamidocyclophanes H-L from the Vietnamese cyanobacterium Nostoc sp. CAVN2. *J Antibiot* **2015,** *68* (3), 165-77.
12. Preisitsch, M.; Heiden, S. E.; Beerbaum, M.; Niedermeyer, T. H. J.; Schneefeld, M.; Herrmann, J.; Kumpfmüller, J.; Thürmer, A.; Neidhardt, I.; Wiesner, C.; Daniel, R.; Müller, R.; Bange, F.-C.; Schmieder, P.; Schweder, T.; Mundt, S., Effects of Halide Ions on the Carbamidocyclophane Biosynthesis in Nostoc sp. CAVN2. *Mar. Drugs* **2016,** *14* (1), 21.

13. Bobzin, S. C.; Moore, R. E., Biosynthetic origin of [7.7]paracyclophanes from cyanobacteria. *Tetrahedron* **1993,** *49* (35), 7615-7626.
14. Nakamura, H.; Hamer, H. A.; Sirasani, G.; Balskus, E. P., Cylindrocyclophane Biosynthesis Involves Functionalization of an Unactivated Carbon Center. *J. Am. Chem. Soc.* **2012,** *134* (45), 18518-18521.
15. Nakamura, H.; Balskus, E. P., Using Chemical Knowledge to Uncover New Biological Function: Discovery of the Cylindrocyclophane Biosynthetic Pathway. *Synlett* **2013,** *24* (12), 1464-1470.
16. Nakamura, H.; Wang, J. X.; Balskus, E. P., Assembly line termination in cylindrocyclophane biosynthesis: discovery of an editing type II thioesterase domain in a type I polyketide synthase. *Chem. Sci.* **2015,** *6* (7), 3816-3822.
17. Nakamura, H.; Schultz, E. E.; Balskus, E. P., A new strategy for aromatic ring alkylation in cylindrocyclophane biosynthesis. *Nat. Chem. Biol.* **2017,** *13* (8), 916-921.
18. Martins, T. P.; Rouger, C.; Glasser, N. R.; Freitas, S.; de Fraissinette, N. B.; Balskus, E. P.; Tasdemir, D.; Leão, P. N., Chemistry, bioactivity and biosynthesis of cyanobacterial alkylresorcinols. *Nat. Prod. Rep.* **2019,** *36* (10), 1437-1461.
19. Smith, A. B.; Kozmin, S. A.; Adams, C. M.; Paone, D. V., Assembly of (−)-Cylindrocyclophanes A and F via Remarkable Olefin Metathesis Dimerizations. *J. Am. Chem. Soc.* **2000,** *122* (20), 4984-4985.
20. Smith, A. B., 3rd; Adams, C. M.; Kozmin, S. A.; Paone, D. V., Total synthesis of (-)-cylindrocyclophanes A and F exploiting the reversible nature of the olefin cross metathesis reaction. *J. Am. Chem. Soc.* **2001,** *123* (25), 5925-37.
21. Hoye, T. R.; Humpal, P. E.; Moon, B., Total Synthesis of (−)-Cylindrocyclophane A via a Double Horner-Emmons Macrocyclic Dimerization Event. *J. Am. Chem. Soc.* **2000,** *122* (20), 4982-4983.
22. Nicolaou, K. C.; Sun, Y.-P.; Korman, H.; Sarlah, D., Asymmetric Total Synthesis of Cylindrocyclophanes A and F through Cyclodimerization and a Ramberg–Bäcklund Reaction. *Angew. Chem. Int. Ed.* **2010,** *49* (34), 5875-5878.
23. Liao, K.; Negretti, S.; Musaev, D. G.; Bacsa, J.; Davies, H. M. L., Site-selective and stereoselective functionalization of unactivated C–H bonds. *Nature* **2016,** *533* (7602), 230-234.
24. Liu, W.; Ren, Z.; Bosse, A. T.; Liao, K.; Goldstein, E. L.; Bacsa, J.; Musaev, D. G.; Stoltz, B. M.; Davies, H. M. L., Catalyst-Controlled Selective Functionalization of Unactivated C–H Bonds in the Presence of Electronically Activated C–H Bonds. *J. Am. Chem. Soc.* **2018,** *140* (38), 12247-12255.
25. Stang, E. M.; Christina White, M., Total synthesis and study of 6-deoxyerythronolide B by late-stage C–H oxidation. *Nat. Chem.* **2009,** *1*, 547.
26. Fraunhoffer, K. J.; Prabagaran, N.; Sirois, L. E.; White, M. C., Macrolactonization via Hydrocarbon Oxidation. *J. Am. Chem. Soc.* **2006,** *128* (28), 9032-9033.
27. Peters, D. S.; Romesberg, F. E.; Baran, P. S., Scalable Access to Arylomycins via C–H Functionalization Logic. *J. Am. Chem. Soc.* **2018,** *140* (6), 2072-2075.
28. Qin, C.; Davies, H. M. L., Role of Sterically Demanding Chiral Dirhodium Catalysts in Site-Selective C–H Functionalization of Activated Primary C–H Bonds. *J. Am. Chem. Soc.* **2014,** *136* (27), 9792-9796.
29. Fu, L.; Mighion, J. D.; Voight, E. A.; Davies, H. M. L., Synthesis of 2,2,2,-Trichloroethyl Aryl- and Vinyldiazoacetates by Palladium-Catalyzed Cross-Coupling. *Chem. Eur. J.* **2017,** *23* (14), 3272-3275.

30. Li, G.; Wan, L.; Zhang, G.; Leow, D.; Spangler, J.; Yu, J.-Q., Pd(II)-Catalyzed C–H Functionalizations Directed by Distal Weakly Coordinating Functional Groups. *J. Am. Chem. Soc.* **2015,** *137* (13), 4391-4397.
31. Park, H.; Li, Y.; Yu, J.-Q., Utilizing Carbonyl Coordination of Native Amides for Palladium-Catalyzed C(sp3)−H Olefination. *Angew. Chem. Int. Ed.* **2019,** *58* (33), 11424-11428.
32. Lecourt, C.; Dhambri, S.; Allievi, L.; Sanogo, Y.; Zeghbib, N.; Ben Othman, R.; Lannou, M. I.; Sorin, G.; Ardisson, J., Natural products and ring-closing metathesis: synthesis of sterically congested olefins. *Nat. Prod. Rep.* **2018,** *35* (1), 105-124.
33. Sharland, J. C.; Wei, B.; Hardee, D. J.; Hodges, T. R.; Gong, W.; Voight, E. A.; Davies, H. M. L., Asymmetric synthesis of pharmaceutically relevant 1-aryl-2-heteroaryl- and 1,2-diheteroarylcyclopropane-1-carboxylates. *Chem. Sci.* **2021,** *12* (33), 11181-11190.
34. Harned, A. M., From determination of enantiopurity to the construction of complex molecules: The Horeau principle and its application in synthesis. *Tetrahedron* **2018,** *74* (28), 3797-3841.
35. Liao, K.; Yang, Y.-F.; Li, Y.; Sanders, J. N.; Houk, K. N.; Musaev, D. G.; Davies, H. M. L., Design of catalysts for site-selective and enantioselective functionalization of non-activated primary C–H bonds. *Nat. Chem.* **2018,** *10* (10), 1048-1055.
36. Garlets, Z. J.; Sanders, J. N.; Malik, H.; Gampe, C.; Houk, K. N.; Davies, H. M. L., Enantioselective C–H functionalization of bicyclo[1.1.1]pentanes. *Nat. Catal.* **2020,** *3* (4), 351-357.
37. Jiang, Y.; Thomson, R. J.; Schaus, S. E., Asymmetric Traceless Petasis Borono-Mannich Reactions of Enals: Reductive Transposition of Allylic Diazenes. *Angew. Chem. Int. Ed.* **2017,** *56* (52), 16631-16635.
38. Jourdant, A.; González-Zamora, E.; Zhu, J., Wilkinson's Catalyst Catalyzed Selective Hydrogenation of Olefin in the Presence of an Aromatic Nitro Function: A Remarkable Solvent Effect. *J. Org. Chem.* **2002,** *67* (9), 3163-3164.
39. Xu, Y.; Mingos, D. M. P.; Brown, J. M., Crabtree's catalyst revisited; Ligand effects on stability and durability. *Chem. Comm.* **2008,** (2), 199-201.
40. Crabtree, R. H., Deactivation in Homogeneous Transition Metal Catalysis: Causes, Avoidance, and Cure. *Chem. Rev.* **2015,** *115* (1), 127-150.
41. Windholz, T. B.; Johnston, D. B. R., Trichloroethoxycarbonyl: a generally applicable protecting group. *Tetrahedron Lett.* **1967,** *8* (27), 2555-2557.
42. Vorbrüggen, H.; Krolikiewicz, K., A simple synthesis of Δ2-oxazines, Δ2-oxazines, Δ2-thiazolines and 2-substituted benzoxazoles. *Tetrahedron* **1993,** *49* (41), 9353-9372.
43. Al-Azani, M.; al-Sulaibi, M.; al Soom, N.; Al Jasem, Y.; Bugenhagen, B.; Al Hindawi, B.; Thiemann, T., The use of BrCCl3-PPh3 in Appel type transformations to esters, O-acyloximes, amides, and acid anhydrides. *C. R. Chim.* **2016,** *19* (8), 921-932.
44. Ghosh, A. K.; Shahabi, D., Synthesis of amide derivatives for electron deficient amines and functionalized carboxylic acids using EDC and DMAP and a catalytic amount of HOBt as the coupling reagents. *Tetrahedron Lett.* **2021,** *63*, 152719.
45. Carpino, L. A., 1-Hydroxy-7-azabenzotriazole. An efficient peptide coupling additive. *J. Am. Chem. Soc.* **1993,** *115* (10), 4397-4398.
46. Nicolaou, K. C.; Estrada, A. A.; Zak, M.; Lee, S. H.; Safina, B. S., A Mild and Selective Method for the Hydrolysis of Esters with Trimethyltin Hydroxide. *Angew. Chem. Int. Ed.* **2005,** *44* (9), 1378-1382.

47. Jin, M.; Adak, L.; Nakamura, M., Iron-Catalyzed Enantioselective Cross-Coupling Reactions of α-Chloroesters with Aryl Grignard Reagents. *J. Am. Chem. Soc.* **2015,** *137* (22), 7128-7134.
48. Lovri , M.; Cepanec, I.; Litvi , M.; Bartolin j , A.; Vinkovj , V., Scope and Limitations of Sodium and Potassium Trimethylsilanolate as Reagents for Conversion of Esters to Carboxylic Acids. *Croat. Chem. Acta* **2007,** *80*, 109-115.
49. Greszler, S. N.; Shelat, B.; Voight, E. A., Enabling Synthesis of ABBV-2222, A CFTR Corrector for the Treatment of Cystic Fibrosis. *Org. Lett.* **2019,** *21* (14), 5725-5727.
50. Beutner, G. L.; Cohen, B. M.; DelMonte, A. J.; Dixon, D. D.; Fraunhoffer, K. J.; Glace, A. W.; Lo, E.; Stevens, J. M.; Vanyo, D.; Wilbert, C., Revisiting the Cleavage of Evans Oxazolidinones with LiOH/H2O2. *Org. Process Res. Dev.* **2019,** *23* (7), 1378-1385.
51. Chakraborti, A. K.; Sharma, L.; Sharma, U., A mild and chemoselective method for deprotection of aryl acetates and benzoates under non-hydrolytic condition. *Tetrahedron* **2001,** *57* (45), 9343-9346.
52. Evans, D. A.; Britton, T. C.; Ellman, J. A., Contrasteric carboximide hydrolysis with lithium hydroperoxide. *Tetrahedron Lett.* **1987,** *28* (49), 6141-6144.
53. Spletstoser, J. T.; White, J. M.; Tunoori, A. R.; Georg, G. I., Mild and Selective Hydrozirconation of Amides to Aldehydes Using Cp2Zr(H)Cl: Scope and Mechanistic Insight. *J. Am. Chem. Soc.* **2007,** *129* (11), 3408-3419.
54. Buchwald, S. L.; LaMaire, S. J.; Nielsen, R. B.; Watson, B. T.; King, S. M., A Modified Procedure for the Preparation of Cp2Zr(H)Cl (Schwartz's Reagent). *Tetrahedron Lett.* **1987,** *28* (34), 3895-3898.
55. Zhao, Y.; Snieckus, V., A Practical in situ Generation of the Schwartz Reagent. Reduction of Tertiary Amides to Aldehydes and Hydrozirconation. *Org. Lett.* **2014,** *16* (2), 390-393.
56. Tinnis, F.; Volkov, A.; Slagbrand, T.; Adolfsson, H., Chemoselective Reduction of Tertiary Amides under Thermal Control: Formation of either Aldehydes or Amines. *Angew. Chem. Int. Ed.* **2016,** *55* (14), 4562-4566.
57. Hart, D. J.; Lee, C. S.; Pirkle, W. H.; Hyon, M. H.; Tsipouras, A., Asymmetric synthesis of .beta.-lactams and the carbapenem antibiotic (+)-PS-5. *J. Am. Chem. Soc.* **1986,** *108* (19), 6054-6056.
58. Aoyama, Y.; Uenaka, M.; Kii, M.; Tanaka, M.; Konoike, T.; Hayasaki-Kajiwara, Y.; Naya, N.; Nakajima, M., Design, synthesis and pharmacological evaluation of 3-benzylazetidine-2-one-based human chymase inhibitors. *Bioorg. Med. Chem.* **2001,** *9* (11), 3065-3075.
59. Reider, P. J.; Grabowski, E. J. J., Total synthesis of thienamycin: a new approach from aspartic acid. *Tetrahedron Lett.* **1982,** *23* (22), 2293-2296.
60. Macdonald, D. I.; Durst, T., A synthesis of trans-2-arylbenzocyclobuten-1-ols. *Tetrahedron Lett.* **1986,** *27* (20), 2235-2238.
61. Senaweera, S.; Cartwright, K. C.; Tunge, J. A., Decarboxylative Acetoxylation of Aliphatic Carboxylic Acids. *J. Org. Chem.* **2019,** *84* (19), 12553-12561.
62. Khan, S. N.; Zaman, M. K.; Li, R.; Sun, Z., A General Method for Photocatalytic Decarboxylative Hydroxylation of Carboxylic Acids. *J. Org. Chem.* **2020,** *85* (7), 5019-5026.
63. Song, H.-T.; Ding, W.; Zhou, Q.-Q.; Liu, J.; Lu, L.-Q.; Xiao, W.-J., Photocatalytic Decarboxylative Hydroxylation of Carboxylic Acids Driven by Visible Light and Using Molecular Oxygen. *J. Org. Chem.* **2016,** *81* (16), 7250-7255.

64. Griffin, J. D.; Zeller, M. A.; Nicewicz, D. A., Hydrodecarboxylation of Carboxylic and Malonic Acid Derivatives via Organic Photoredox Catalysis: Substrate Scope and Mechanistic Insight. *J. Am. Chem. Soc.* **2015,** *137* (35), 11340-11348.
65. Cartwright, K. C.; Lang, S. B.; Tunge, J. A., Photoinduced Kochi Decarboxylative Elimination for the Synthesis of Enamides and Enecarbamates from N-Acyl Amino Acids. *J. Org. Chem.* **2019,** *84* (5), 2933-2940.
66. Bailey, C. L.; Clary, J. W.; Tansakul, C.; Klabunde, L.; Anderson, C. L.; Joh, A. Y.; Lill, A. T.; Peer, N.; Braslau, R.; Singaram, B., Reduction of Weinreb amides to aldehydes under ambient conditions with magnesium borohydride reagents. *Tetrahedron Lett.* **2015,** *56* (5), 706-709.
67. Xiao, P.; Tang, Z.; Wang, K.; Chen, H.; Guo, Q.; Chu, Y.; Gao, L.; Song, Z., Chemoselective Reduction of Sterically Demanding N,N-Diisopropylamides to Aldehydes. *J. Org. Chem.* **2018,** *83* (4), 1687-1700.
68. Petasis, N. A.; Lu, S.-P., Methylenations of heteroatom-substituted carbonyls with dimethyl titanocene. *Tetrahedron Lett.* **1995,** *36* (14), 2393-2396.
69. Stork, G.; Brizzolara, A.; Landesman, H.; Szmuszkovicz, J.; Terrell, R., The Enamine Alkylation and Acylation of Carbonyl Compounds. *J. Am. Chem. Soc.* **1963,** *85* (2), 207-222.
70. Hanzawa, Y.; Kowase, N.; Momose, S.-i.; Taguchi, T., A Cp2TiCl2-Me3Al (1 : 4) reagent system: An efficient reagent for generation of allylic titanocene derivatives from vinyl halides, vinyl ethers and carboxylic esters. *Tetrahedron* **1998,** *54* (38), 11387-11398.
71. Nakajima, M.; Sato, T.; Chida, N., Iridium-Catalyzed Chemoselective Reductive Nucleophilic Addition to N-Methoxyamides. *Org. Lett.* **2015,** *17* (7), 1696-1699.
72. Xie, Z.; Song, Y.; Xu, L.; Guo, Y.; Zhang, M.; Li, L.; Chen, K.; Liu, X., Rapid Synthesis of N-Tosylhydrazones under Solvent-Free Conditions and Their Potential Application Against Human Triple-Negative Breast Cancer. *ChemistryOpen* **2018,** *7* (12), 977-983.
73. Kabalka, G. W.; Yang, D. T. C.; Baker, J. D., Deoxygenation of .alpha.,.beta.-unsaturated aldehydes and ketones via the catecholborane reduction of the corresponding tosylhydrazones. *J. Org. Chem.* **1976,** *41* (3), 574-575.
74. Kabalka, G. W.; Baker, J. D., New mild conversion of ketones to the corresponding methylene derivatives. *J. Org. Chem.* **1975,** *40* (12), 1834-1835.
75. Hu, Y.-J.; Gu, C.-C.; Wang, X.-F.; Min, L.; Li, C.-C., Asymmetric Total Synthesis of Taxol. *J. Am. Chem. Soc.* **2021,** *143* (42), 17862-17870.

Chapter 3

A C-H Functionalization Strategy Enables an Enantioselective Formal Synthesis of (-)-Aflatoxin B_2

3.1. Introduction

3.1.1. Isolation, Structure Determination and Biosynthesis

The aflatoxins (**3.1**-**3.4**) are mycotoxins and potent heptocarcinogenic polyketide natural products produced by the pathogenic fungi *Aspergillus flavus*, *Aspergillus versicolor*, and *Aspergillus parasiticus*.[1, 2] Biologically they are dangerous liver carcinogens, afflicting humans and animals that ingest contaminated grain flour, nuts, and corn. They gained notoriety in the 1960s by causing the mas turkey death in Great Britain.[2-4] However, their effects on tissues other than the liver is largely unknown as is the underlying mechanism for their biological activity. In their pure states, aflatoxins B and G fluoresce blue and green, respectively,[5] and their molecular structures were elucidated by the analytical studies of Büchi and co-workers[1, 6, 7] and confirmed by X-ray crystallographic analyses.[8] The aflatoxins contain a substituted coumarin framework fused to two dihydrofuran rings and either a cyclopentanone ring [e.g., aflatoxins B_1 (**3.1**) and B_2 (**3.2**)] or a δ-lactone ring [e.g., aflatoxins G_1 (**3.3**) and G_1 (3.4)] (Figure 3.1). The C-ring alkene of aflatoxins B_1 (**3.1**) and G_1 (**3.3**) heightens the mutagenicity of these compounds in relation to that of the dihydro counterparts.[9]

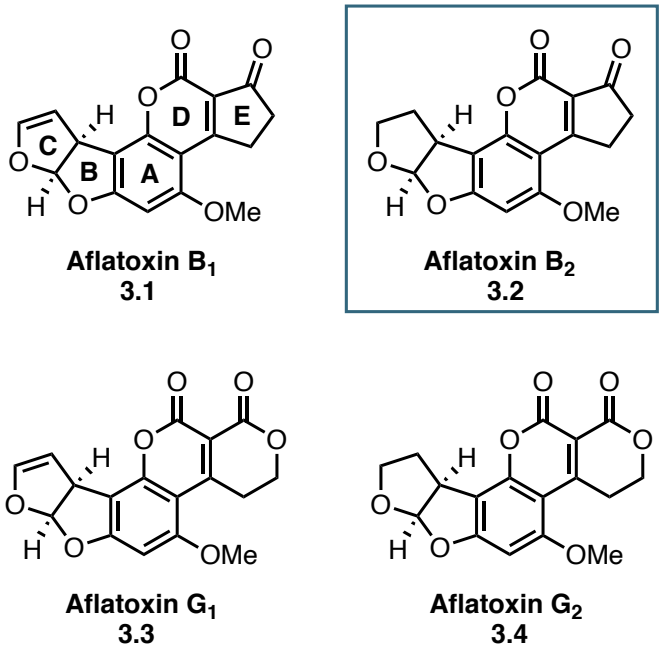

Figure 3.1 Aflatoxins B_1, B_2, G_1 and G_2

Aflatoxins are produced by a polyketide pathway that was first proposed by Birch in 1967 and at least 27 enzymatic reactions have been shown to be involved in this process.[10] Among natural products, it has long been considered that the biosynthesis of aflatoxin is one of the longest and most complex due to the high number of oxidative rearrangements it entails.[11] Therefore, the complete biosynthetic pathway is unknown at this time and only critical steps have been elucidated. In 1985 Dutton[12] characterized three critical oxidation steps/oxidative enzymes incorporated in the biosynthesis, including monooxygenases responsible for incorporating oxygen atoms and dioxygenases involved in ring-cleavage reaction. Finally, a Baeyer-Villiger type reaction is catalyzed by cytochrome P-450 enzymes responsible for inserting oxygen atoms between carbons.

3.1.2. Previous Enantioselective Syntheses of (-)-Aflatoxin B_2

The biological activity of these metabolites, along with their densely oxidized core, has inspired several total syntheses of the various aflatoxins. The landmark racemic syntheses were disclosed by Büchi[13, 14] and Roberts[15] in 1966 and 1968 respectively. Since these initial reports, the aflatoxins have served as a testing ground for novel synthetic strategies and methodologies over the past several decades. These efforts have culminated in several enantioselective syntheses,[16-23] many of which rely on constructing the ABC tricyclic core, followed by assembly of the D- and E-rings. With this in mind, this thesis will focus on the two major asymmetric syntheses relevant to the work disclosed here.

In 2003, Trost and co-workers[17] achieved the first asymmetric synthesis of aflatoxin B_1 and B_{2A}. The synthesis hinges on a key palladium-catalyzed dynamic kinetic asymmetric transformation (DYKAT) of a γ-acyloxybutenolide to establish the stereochemistry at the ring-junction acetal (Scheme 3.1). To synthesize their key coupling partners, the coumarin precursor was constructed via Pechmann reaction. Next, Trost uses their previously reported DYKAT methodology to set the chiral center of the B-ring with excellent enantioselectivity (>95% ee). Finally, the BC-ring is formed through an intramolecular Heck reaction. After several functional group manipulations, the synthesis of aflatoxin B_{2A} is complete, and after elimination of the hemiacetal, aflatoxin B_1 is formed in nine total steps.

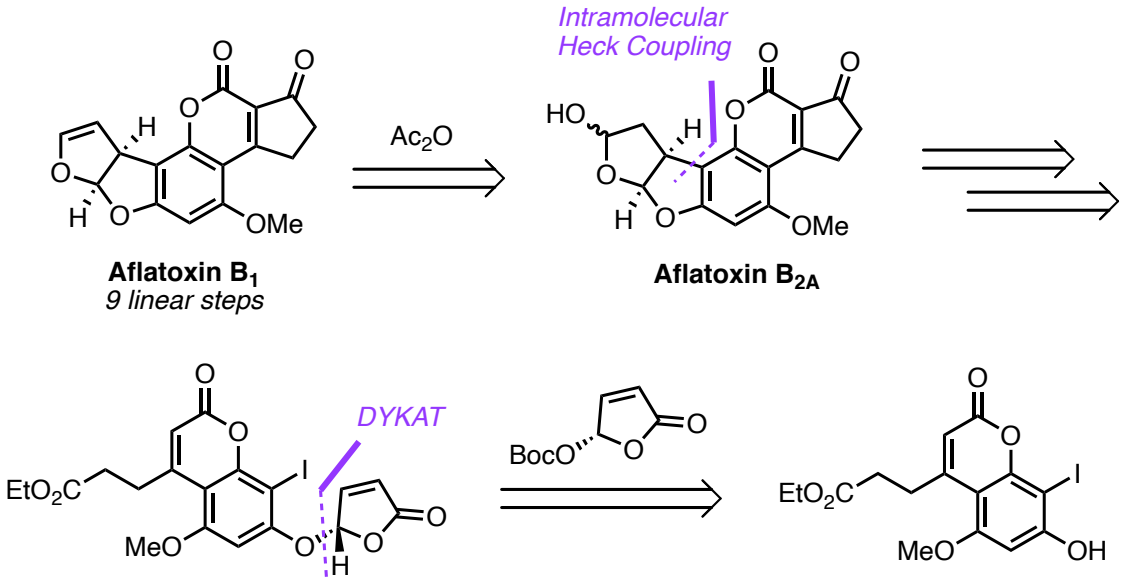

Scheme 3.1 Trost's asymmetric total synthesis of (-)-aflatoxin B_1 and B_{2A}

In 2005, Corey and co-workers[20] reported the first asymmetric synthesis of (-)-aflatoxin B_2. The key step in the route features a remarkable oxazaborolidinium-catalyzed [3+2] cycloaddition forming the ABC-ring system in a single step with excellent enantioselectivity (92% ee), which could be recrystallized up to enantiopurity (Scheme 3.2). The precursors for the cycloaddition are commercially available demonstrating a concise entry to the stereochemical rich core. Notably, the cycloaddition product obtained does not match the A-ring of Aflatoxin B_2, thus six functional group manipulations were needed to transpose the hydroxyl group over. However, this strategy was reported by Noland and follows Friedel–Crafts acylation, hydroxyl protection, 1,2-addition, DMP oxidation, oxygen insertion, saponification, and reduction. Finally, the DE-ring can be synthesized employing the conditions reported by Büchi,[24] enabling an eight-step linear synthesis of (-)-aflatoxin B_2.

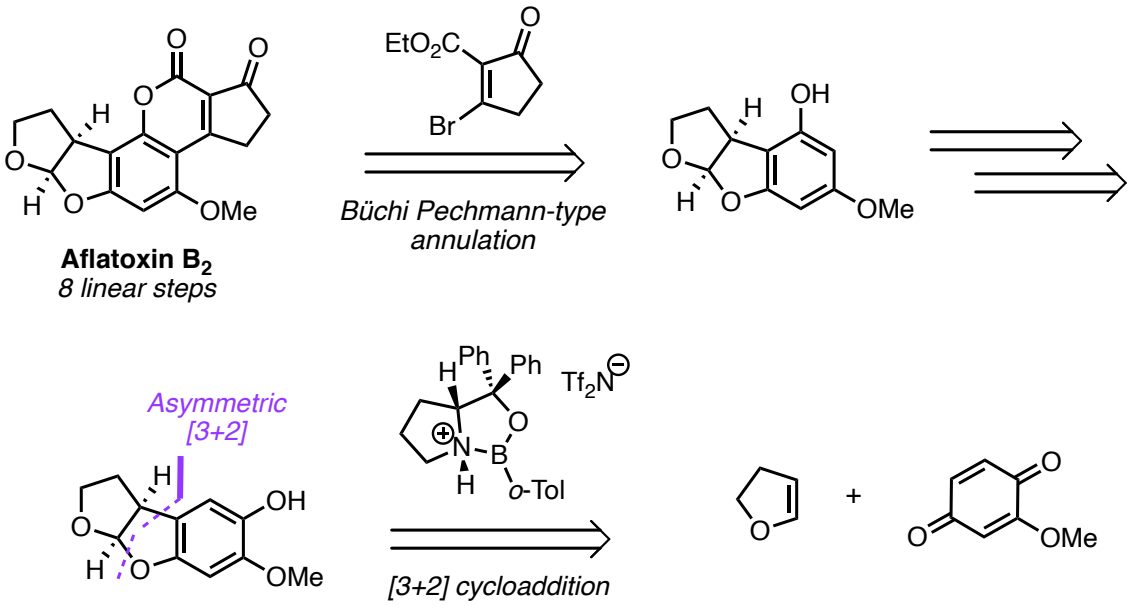

Scheme 3.2 Corey's asymmetric total synthesis of (-)-aflatoxin B_2

As a consequence of its highly oxidized nature and sensitive stereogenic centers, the furo[2,3-*b*]benzofuran core (**3.14)** has proven to be challenging to construct and continues to inspire innovative concepts for synthesis. Therefore, the approached outlined in this chapter will detailed a C-H functionalization strategy to the ABC-ring of (-)-aflatoxin B_2.

3.1.3. A C-H Functionalization Strategy to (-)-Aflatoxin B_2

Inspired by the successful four-fold acetoxylation in my cylindrocyclophane synthesis (see chapter 2), this formal synthesis came out of conversation between the Sorensen and Davies groups. However, before the collaboration started, the Sorensen lab had attempted a similar strategy to (-)-aflatoxin B_2 several years prior and failed. The original synthesis relied on a key C-H functionalization of 1,3-dioxolane **3.6** using a donor/acceptor diazoacetate **3.5**, and after a functional group manipulation to afford **3.8**, a directed C-H acetoxylation would be performed (Scheme 3.3). Unfortunately, this strategy failed in both key transformations. First, the insertion

of **3.5** into dioxolane **3.6** performs in low yield with decent enantioselectivity for the product **3.7**. The yield suffers because cyclic ethers tend to engage the rhodium carbenes in ylide chemistry, undergoing ring-expansion instead of C-H functionalization.[25] Second, the directed C-H bisacetoxylation failed to generate product **3.9** in all attempts. With failure of both key steps, this project was set aside until the technology needed to complete the synthesis was developed.

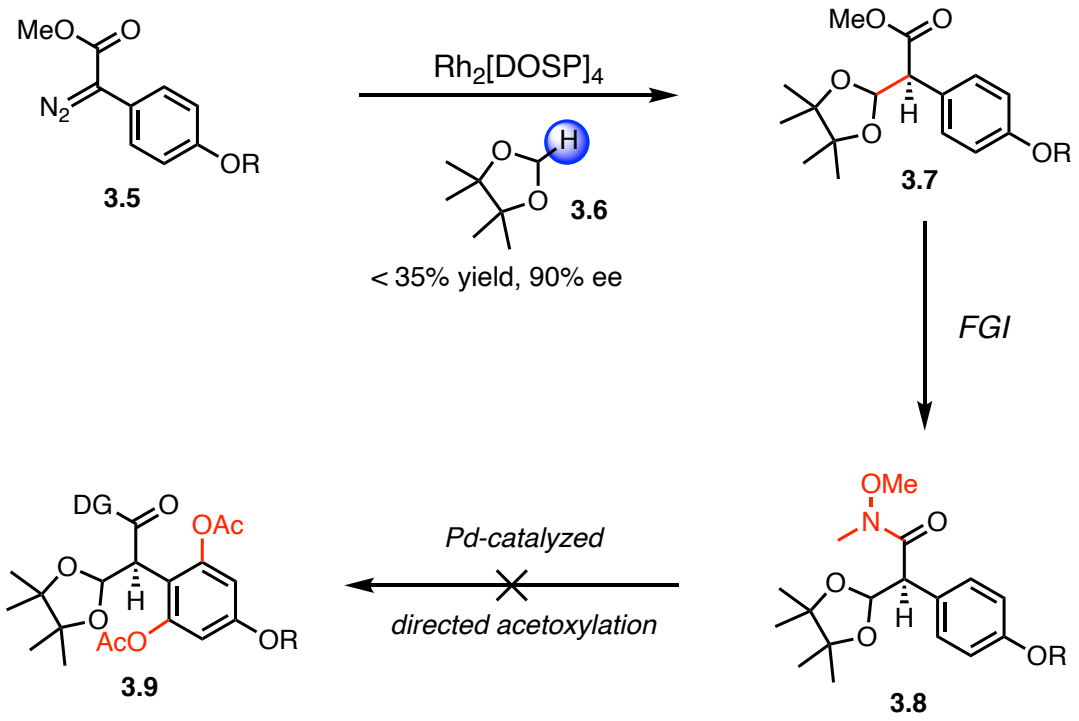

Scheme 3.3 Key C-H functionalization steps in the original strategy to (-)-aflatoxin B_2

Several years later, the Davies lab has now expanded their catalyst toolbox substantially,[26] as well as the Yu lab's directing group technology.[27-33] With the success of my multifold acetoxylation to (-)-cylindrocyclophane A (see chapter 2), using the newly developed pyridine sulfonic acid ligand,[28, 34, 35] the Sorensen lab realized this approach could be applied to their failed aflatoxin synthesis. Therefore, they reached out to initiate a collaboration to tackle this synthesis. However, one problem remained, the initial carbene C-H functionalization to set the first

stereocenter. In thinking about how to overcome this challenge, we realized that the efficient and selective primary C-H functionalization of *trans*-2-hexene, followed by oxidative cleavage of the alkene, could access the desired chemical space (Scheme 3.4).[36] Thus, not only was the multifold acetoxylation developed in Ch.2 instrumental in creating a successful route, but also the initial insertion into *trans*-2-hexene was also necessary to set the first stereocenter.

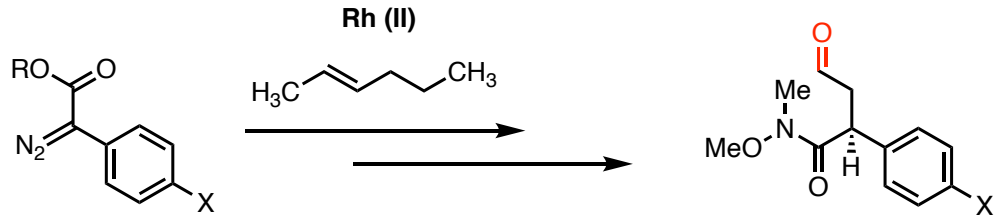

Scheme 3.4 Circumventing the dioxolane insertion

Going through the retrosynthetic analysis we envisioned a formal synthesis to the ABC-ring core that would be a single established step away from (-)-aflatoxin B_2. The route starts from a donor/acceptor diazoester **3.10** undergoing a dirhodium catalyzed C-H insertion of *trans*-2-hexene at the primary methyl C(sp^3)-H bond, establishing a key C-C bond and the benzylic stereocenter (Scheme 3.5).[37] Concomitantly, this would also install functionality to enable the eventual annulation of rings B and C. Enantioenriched **3.11** could thus be elaborated to key intermediate **3.12** through traditional functional group manipulations. To complete the oxidation pattern on the aromatic ring, we envisioned a carbonyl-directed bis-C−H palladation/oxidation to form **3.13**.[27, 28, 34, 35] In the wake of these transformations, we imagined that global protecting group cleavages and a partial reduction of the Weinreb amide moiety in **3.13** would generate a fleeting aldehyde (not shown) that will spontaneously cyclize to afford compound **3.14**, the penultimate intermediate towards (-)-aflatoxin B_2. Notably, the initial stereocenter set from the carbene insertion would control the stereochemistry of the cyclization. Thus, high control of the first

stereocenter will be crucial for high diastereoselectivity later in the route. With promising results from the (-)-cylindrocyclophane A synthesis we embarked on modifying them to synthesize (-)-aflatoxin B_2.

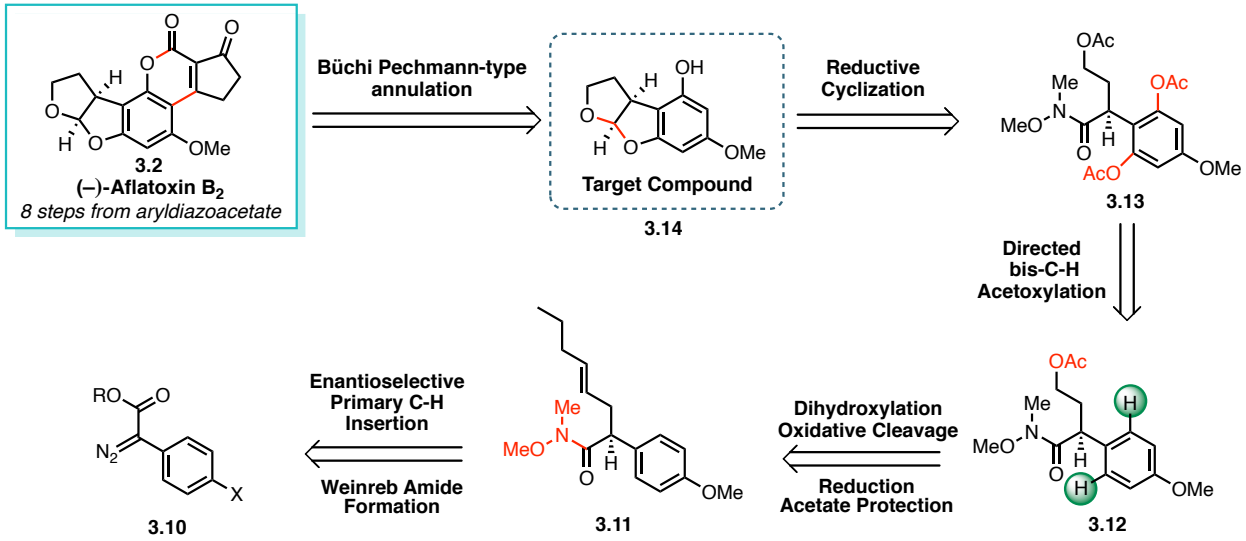

Scheme 3.5 Revised C-H functionalization strategy to (-)-aflatoxin B_2

3.2. Results and Discussion

3.2.1. Enantioselective Primary C-H Insertion

The execution of the synthesis commenced with the optimization of the enantioselective C-H insertion using dirhodium carbenes derived from aryl diazoacetates.[36, 37] With the impressive success of the nearly perfect reaction on *trans*-2-hexene in the cylindrocyclophane project (96% yield, 96% ee, >20:1 rr, see chapter 2), studies were conducted to apply this protocol to the aflatoxin synthesis. However, while the cylindrocyclophane synthesis utilized a *para*-iodo group on the donor side of the aryl diazoacetate, the route employed here would need a *para*-OMe found in aflatoxin. Based on the earlier optimizations of the *trans*-2-hexene insertion reaction, various donor/acceptors diazo compounds were evaluated with Rh_2(*R*-*p*-PhTPCP)$_4$ (Table 3.1). At the outset, we were concerned that the electron-rich nature of the *para*-OMe derivative might cause

deleterious dimerization of the rhodium carbene during attempts to perform the C−H insertion and set the benzylic stereocenter. We anticipated that *para*-halo-substituted carbenes **3.10a** - **3.10c** would react more efficiently, while also providing a functional handle for the introduction of the methoxy group at a later stage.[38] This maneuver, albeit less expeditious, would provide additional flexibility if the bis-C(sp^2)-H oxidation proved to be challenging on an electron-rich *para*-methoxyphenyl intermediate.

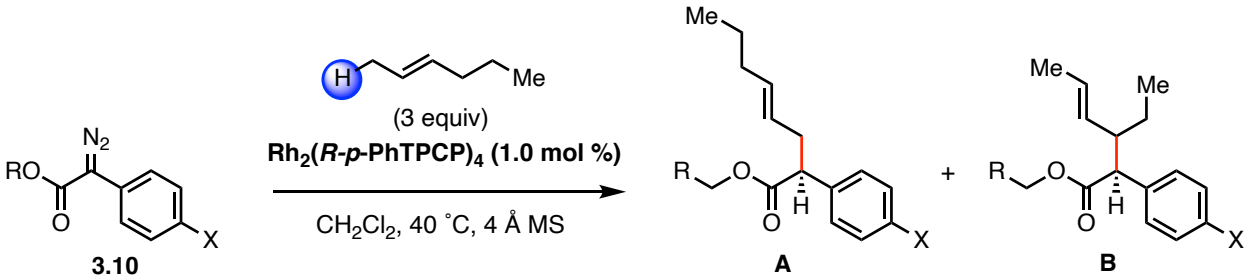

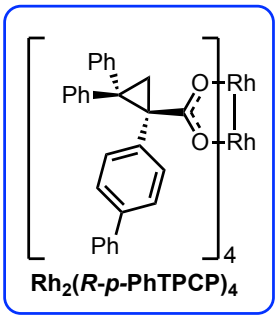

Entry	R	X	Yield	ee	rr (A:B)
1	CH_2CF_3	Cl (**3.10a**)	69	92	11:1
2	CH_2CCl_3	Cl (**3.10b**)	51	96	13:1
3	CH_2CCl_3	I (**3.10c**)	96	96	> 20:1
4	CH_2CF_3	OMe (**3.10d**)	59	96	11:1
5	CH_2CCl_3	OMe (**3.10e**)	47	96	10:1

Table 3.1 Enantioselective C-H insertion results with *trans*-2-hexene

Reactions with *para*-Cl diazoesters **3.10a** and **3.10b** furnished the desired insertion products in moderate to good yields and excellent enantio- and regioselectivity (Table 3.1, entries 1 and 2, respectively). Iodo-substituted derivative **3.10c** performed exceptionally well under the reaction conditions, providing the product in 96% yield and excellent enantioselectivity as a single detectable regioisomer (Table 3.1, entry 3). Gratifyingly, reactions with *para*-OMe diazoesters also delivered the desired insertion products, albeit with slightly diminished yields but excellent

enantioselectivity and good regioselectivity (Table 3.1, entries 4 and 5). The lower yields and selectivity obtained with diazoesters **3.10d** and **3.10e** demonstrate the sensitivity of this transformation to the electronics of donor/acceptor rhodium carbenes.

This brings up a key problem with *trans*-2-hexene, namely the allylic position creates a site-selectivity challenge between the primary and secondary C-H bonds. Critically, the desired aryldiazoacetates **3.10d** and **3.10e** both yield small amounts of the undesired regioisomer from the methylene insertion, that can't be purified out until later transformations. While this still allows for material to be moved forward, ideally, we would like to avoid the unwanted regioisomer. Early efforts to circumvent issues of regioselectivity using diazoacetate **3.10d** anethole furnished the insertion product **3.15** in moderate yields with high enantioselectivity (Scheme 3.6). However, this reaction produced more impurities than the reaction with *trans*-2-hexene, some of which could not be removed. Combined with the lower overall enantioselectivity compared to the *trans*-2-hexene insertion, this route was not explored further.

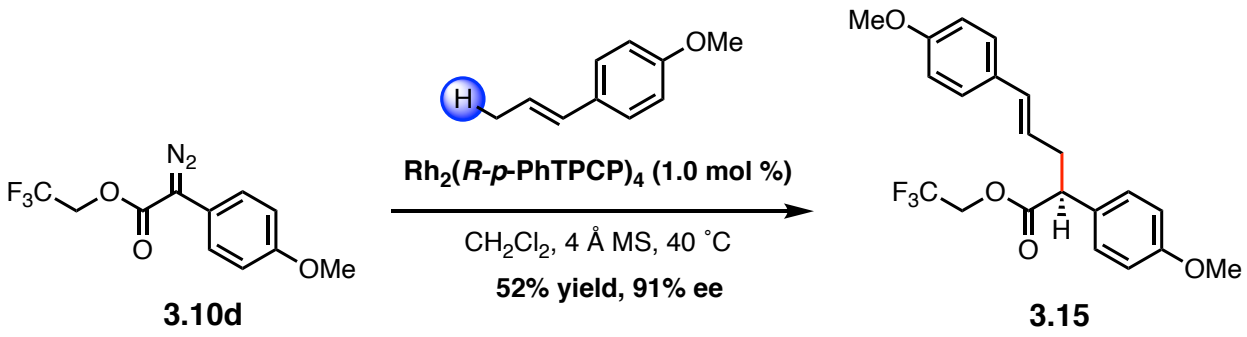

Scheme 3.6 C-H insertion with anethole

While the anethole reaction did not solve the regioselectivity issue we had another strategy that could solve this problem. The highly efficient and selective C−H insertion with diazo **3.10c** prompted efforts to install the methoxy group present in the natural product through C-O

coupling[38] and advance to the bis-C–H oxidation step. Even though this would add another step to the synthesis, the exquisitely selective reaction with diazo **3.10c** and *trans*-2-hexene would be the ideal entry to this strategy, thus encouraging our efforts to probe this strategy.

3.2.2. Investigating a C-O Coupling Strategy

Due to the superior results of *para*-iodo diazo **3.10c** over *para*-Cl diazos **3.10a** and **3.10b**, the functionalized *para*-iodo product **3.16** was decided to be carried forward to test the C-O coupling strategy. Using standard conditions, the Troc moiety was converted to the Weinreb amide (Scheme 3.7) through zinc/acetic acid hydrolysis[39] (96% yield) followed by HATU coupling[40] in 74% yield, albeit with slight erosion of ee due to the basic nature of the reaction (see chapter 3 SI). This material was then sent to Nick Falcone, who subjected the Weinreb amide to Buchwald's C-O coupling conditions[38] afforded the desired *para*-OMe derivative **3.11**. At this stage, Nick Falcone sent the Buchwald coupled product **3.11** back to the Davies lab for HPLC analysis. However, even though the desired product could be formed, the sensitive benzylic stereocenter racemized even further under the harsh basic and heating conditions required for the conversion to **3.11** (see chapter 3 SI). The erosion of enantiopurity while advancing **3.16** compelled us to revisit the insertion with *para*-OMe diazoester **3.10d**.

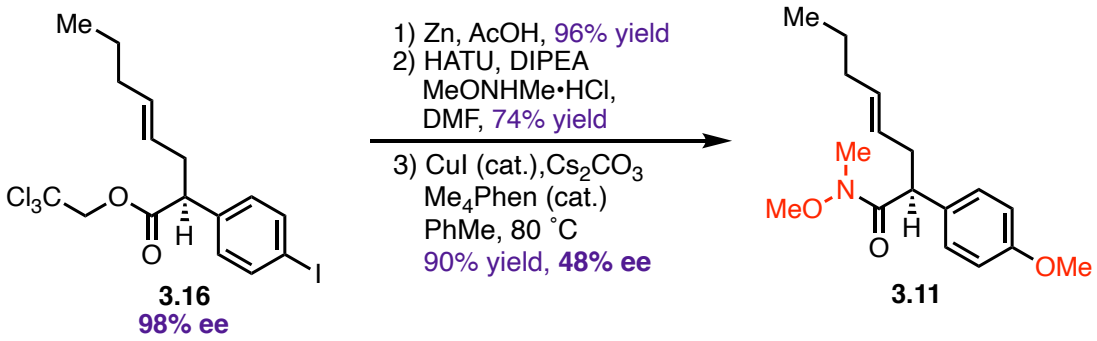

Scheme 3.7 Investigating a C-O coupling strategy

3.2.3. Completing the Enantioselective Formal Synthesis

Moving forward with our optimal diazoester **3.10d**, the donor/acceptor diazoacetate could be synthesized in two steps from the commercially available 4-methoxyphenylacetic acid in 76% yield over two steps (see chapter 3 SI). Subjecting diazoester **3.10d** to the C–H insertion, we found that the yield of this transformation could be improved to 71% on a multigram scale with 0.5 mol % catalyst loading (Scheme 3.8). Due to the TFE group being more labile than the Troc group, compound **3.18** can be directly converted to the Weinreb amide **3.11** in 70% yield with retention of stereochemistry, thereby setting the stage for the palladium-catalyzed bis-C(sp^2)-H acetoxylation. At this stage the amide **3.11** was shipped off to Nick Falcone in the Sorensen laboratory. Thus, the rest of the work outlined in this chapter is all work conducted by Nick Falcone alone.

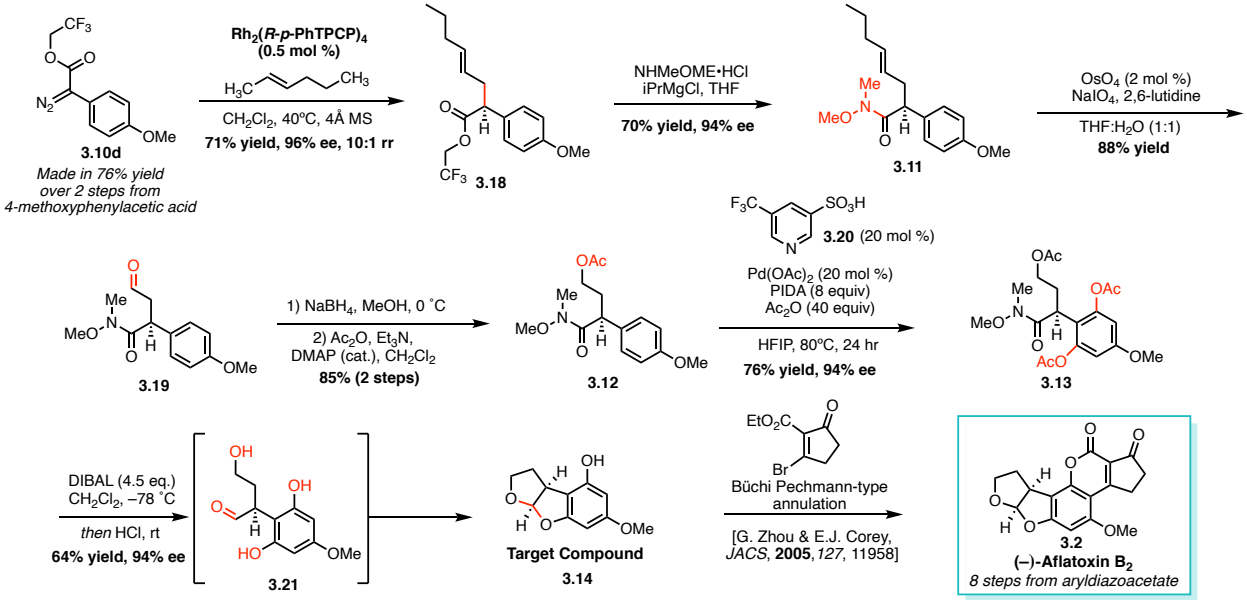

Scheme 3.8 Completing the enantioselective formal synthesis of (-)-aflatoxin B_2

Anticipating that the olefin in **3.11** would interfere with the C-H acetoxylation, we elected to elaborate the 2-hexenyl fragment to a suitable precursor for the C-ring in the natural product. Subjecting the alkene **3.11** under dihydroxylation conditions, followed by oxidative cleavage afforded us the aldehyde **3.19** in 88% yield.[41] Attempts to conduct the acetoxylation with aldehyde **3.19** unfortunately led to a complex mixture containing no detectable product. To overcome this, the aldehyde was converted to acetate ester **3.12** in 85% yield over two steps by reduction with sodium borohydride and acetate formation with acetic anhydride. At last, the stage was set for the pivotal bis-C(sp^2)-H oxidation. Upon exposure to Yu's palladium-catalyzed acetoxylation conditions,[27] using the pyridine sulfonic acid ligand **3.20**,[28, 34, 35] the desired product **3.13** was generated in 76% yield, with no erosion of enantioselectivity. Notably, Nick Falcone was able to use the exact conditions optimized for the cylindrocyclophane route (see chapter 2) with the substrate **3.12** to affect the desired transformation. Finally, treatment of **3.13** with excess diisobutylaluminum hydride (DIBAL-H) at a low temperature accomplished a selective monoreduction of the Weinreb amide and reductive cleavage of all three acetates. The Weinreb amide reduction liberated a putative aldehyde intermediate **3.21**, which spontaneously cyclized forming rings B and C in 64% yield, thus completing our formal synthesis of the penultimate precursor **3.14** to (-)-aflatoxin B_2.

3.3. Conclusion

In summary, a concise formal synthesis of (-)-aflatoxin B_2 has been achieved by a strategy that is reliant on three site-selective C-H functionalizations. The route developed here highlights two impressive C-H functionalization methodologies enabling a completely novel strategy to this family of natural products. Chiral dirhodium-mediated C-H insertion not only establishes a key

benzylic stereocenter with high enantioselectivity but also installs the appropriate functionality for the annulation of the C-ring. This reaction demonstrates the power of donor/acceptor carbenes to enable efficient access to complex chiral building blocks. Following the carbene insertion, carbonyl-directed bis-acetoxylation site-selectively introduces the appropriate oxidation functionality needed in the natural product. This eliminated the need for lengthy and troublesome late-stage manipulations on the central aromatic ring. Notably, the bis-acetoxylation was achieved under mild conditions, preserving the delicate benzylic stereogenic center. We anticipate that this mode of reactivity will find applications in the synthesis of other highly oxygenated complex molecules. Together, these crucial transformations provide direct access to the tricyclic core of (-)-aflatoxin B_2 and highlight the considerable potential of site-selective C−H functionalization in natural product synthesis.

3.4. Distribution of Credit

This project stems from cross talk between the Davies lab and Sorensen lab and was recently disclosed in an *Org. Lett.* publication.[42] The Sorensen lab initiated this collaboration after seeing results from my cylindrocyclophane work (see Ch.2) during one of our weekly meetings for the NSF CCHF. All the carbene reactions and optimizations were conducted by me as well as conversion of ester **3.18** to amide **3.11**. I then sent amide **3.11** to my collaborator Nick Falcone in the Sorensen lab, who conducted all the subsequent steps to our target compound **3.14**. Additionally, for the Buchwald C-O coupling study, I took ester **3.16** through the Zinc hydrolysis and HATU amide coupling, then sent that material to Nick Falcone who conducted the C-O coupling. To be consistent with our HPLC data, Nick Falcone then sent the Buchwald coupling product back to me for HPLC analysis. Finally, Hojoon Park from the Yu lab, synthesized the

pyridine sulfonic acid ligand **3.20**, which was sent to Nick Falcone who used it to conduct the acetoxylation using the conditions reported by me in the cylindrocyclophane study.

3.5. References

1. Asao, T.; Buchi, G.; Abdel-Kader, M. M.; Chang, S. B.; Wick, E. L.; Wogan, G. N., Aflatoxins B and G. *J. Am. Chem. Soc.* **1963,** *85* (11), 1706-1707.
2. Van Der Zijden, A. S. M.; Koelensmid, W. A. A. B.; Boldingh, J.; Barrett, C. B.; Ord, W. O.; Philp, J., Aspergillus Flavus and Turkey X Disease: Isolation in Crystalline Form of a Toxin responsible for Turkey X Disease. *Nature* **1962,** *195* (4846), 1060-1062.
3. Sargeant, K.; Sheridan, A. N. N.; O'Kelly, J.; Carnaghan, R. B. A., Toxicity associated with Certain Samples of Groundnuts. *Nature* **1961,** *192* (4807), 1096-1097.
4. Bianchini, A.; Bullerman, L. B., Mycotoxins I Classifiocation. *Encyclopedia of Food Microbiology (Second Edition)* **2014**, 854-861.
5. Hartley, R. D.; Nesbitt, B. F.; O'Kelly, J., Toxic Metabolites of Aspergillus Flavus. *Nature* **1963,** *198* (4885), 1056-1058.
6. Asao, T.; Büchi, G.; Abdel-Kader, M. M.; Chang, S. B.; Wick, E. L.; Wogan, G. N., The Structures of Aflatoxins B and G1. *J. Am. Chem. Soc.* **1965,** *87* (4), 882-886.
7. Brechbuehler-Bader, S.; Buechi, G.; Milne, G., The absolute configuration of the aflatoxins. *J. Org. Chem.* **1967,** *32* (8), 2641-2642.
8. Cheung, K. K.; Sim, G. A., Aflatoxin G1: Direct Determination of the Structure by the Method of Isomorphous Replacement. *Nature* **1964,** *201* (4925), 1185-1188.
9. Martin, C. N.; Garner, R. C., Aflatoxin B-oxide generated by chemical or enzymic oxidation of aflatoxin B1 causes guanine substitution in nucleic acids. *Nature* **1977,** *267* (5614), 863-865.
10. Birch, A. J., Biosynthesis of Polyketides and Related Compounds. *Science* **1967,** *156* (3772), 202-206.
11. Caceres, I.; Al Khoury, A.; El Khoury, R.; Lorber, S.; P. Oswald, I.; El Khoury, A.; Atoui, A.; Puel, O.; Bailly, J.-D., Aflatoxin Biosynthesis and Genetic Regulation: A Review. *Toxins* **2020,** *12* (3).
12. Dutton, M. F.; Ehrlich, K.; Bennett, J. W., Biosynthetic relationship among aflatoxins B1, B2, M1, and M2. *Appl. Environ. Microbiol.* **1985,** *49* (6), 1392-1395.
13. Büchi, G.; Foulkes, D. M.; Kurono, M.; Mitchell, G. F., The Total Synthesis o Racemic Aflatoxin B1. *J. Am. Chem. Soc.* **1966,** *88* (19), 4534-4536.
14. Buechi, G.; Foulkes, D. M.; Kurono, M.; Mitchell, G. F.; Schneider, R. S., Total synthesis of racemic aflatoxin B1. *J. Am. Chem. Soc.* **1967,** *89* (25), 6745-6753.
15. Roberts, J. C.; Sheppard, A. H.; Knight, J. A.; Roffey, P., Studies in mycological chemistry. Part XXII. Total synthesis of (±)-aflatoxin-B2. *J. Chem. Soc. C.* **1968,** (0), 22-24.
16. Civitello, E. R.; Rapoport, H., Synthesis of the Enantiomeric Furobenzofurans, Late Precursors for the Synthesis of (+)- and (-)-Aflatoxins B1, B2, G1, and G2. *J. Org. Chem.* **1994,** *59* (14), 3775-3782.

17. Trost, B. M.; Toste, F. D., Palladium Catalyzed Kinetic and Dynamic Kinetic Asymmetric Transformations of γ-Acyloxybutenolides. Enantioselective Total Synthesis of (+)-Aflatoxin B1 and B2a. *J. Am. Chem. Soc.* **2003,** *125* (10), 3090-3100.
18. Bando, T.; Shishido, K., Enantioselective Access to the Mycotoxin, Aflatoxin B2. *Synlett* **1997,** *1997* (06), 665-666.
19. Noland, W. E.; Kedrowski, B. L., Quinone Approaches toward the Synthesis of Aflatoxin B2. *Org. Lett.* **2000,** *2* (14), 2109-2111.
20. Zhou, G.; Corey, E. J., Short, Enantioselective Total Synthesis of Aflatoxin B2 Using an Asymmetric [3+2]-Cycloaddition Step. *J. Am. Chem. Soc.* **2005,** *127* (34), 11958-11959.
21. Huang, W.-L.; Raja, A.; Hong, B.-C.; Lee, G.-H., Organocatalytic Enantioselective Michael–Acetalization–Reduction–Nef Reaction for a One-Pot Entry to the Functionalized Aflatoxin System. Total Synthesis of (−)- Dihydroaflatoxin D2 and (−)- and (+)-Microminutinin. *Org. Lett.* **2017,** *19* (13), 3494-3497.
22. Wang, Z.; Zu, L., Organocatalytic enantioselective direct alkylation of phloroglucinol derivatives: asymmetric total synthesis of (+)-aflatoxin B2. *Chem. Comm.* **2019,** *55* (35), 5171-5174.
23. Marino, J. P.; Kieler, K. A.; Kim, M.-W., An enantioselective synthesis of (−)-4-hydroxy-6-methoxy-3a,8a-dihydrofuro[2,3-b]benzofuran: an advanced intermediate in the synthesis of (−)-aflatoxin B1 and G1. *Tetrahedron* **2011,** *67* (5), 837-841.
24. Buechi, G.; Weinreb, S. M., Total syntheses of aflatoxins M1 and G1 and an improved synthesis of aflatoxin B1. *J. Am. Chem. Soc.* **1971,** *93* (3), 746-752.
25. Jana, S.; Guo, Y.; Koenigs, R. M., Recent Perspectives on Rearrangement Reactions of Ylides via Carbene Transfer Reactions. *Chem. Eur. J.* **2021,** *27* (4), 1270-1281.
26. Davies, H. M. L.; Liao, K., Dirhodium tetracarboxylates as catalysts for selective intermolecular C–H functionalization. *Nat. Rev. Chem.* **2019,** *3* (6), 347-360.
27. Li, G.; Wan, L.; Zhang, G.; Leow, D.; Spangler, J.; Yu, J.-Q., Pd(II)-Catalyzed C–H Functionalizations Directed by Distal Weakly Coordinating Functional Groups. *J. Am. Chem. Soc.* **2015,** *137* (13), 4391-4397.
28. Park, H.; Li, Y.; Yu, J.-Q., Utilizing Carbonyl Coordination of Native Amides for Palladium-Catalyzed C(sp3)−H Olefination. *Angew. Chem. Int. Ed.* **2019,** *58* (33), 11424-11428.
29. Desai, L. V.; Stowers, K. J.; Sanford, M. S., Insights into Directing Group Ability in Palladium-Catalyzed C−H Bond Functionalization. *J. Am. Chem. Soc.* **2008,** *130* (40), 13285-13293.
30. Rit, R. K.; Yadav, M. R.; Sahoo, A. K., Pd(II)-Catalyzed ortho-C–H Oxidation of Arylacetic Acid Derivatives: Synthesis of Benzofuranones. *Org. Lett.* **2014,** *16* (3), 968-971.
31. Barysevich, M. V.; Laktsevich-Iskryk, M. V.; Krech, A. V.; Zhabinskii, V. N.; Khripach, V. A.; Hurski, A. L., Palladium-Catalyzed 2-(Neopentylsulfinyl)aniline Directed C–H Acetoxylation and Alkenylation of Arylacetamides. *Eur. J. Org. Chem.* **2020,** *2020* (8), 937-943.
32. Vijaykumar, M.; Punji, B., Pd(II)-Catalyzed Chemoselective Acetoxylation of C(sp2)–H and C(sp3)–H Bonds in Tertiary Amides. *J. Org. Chem.* **2021,** *86* (12), 8172-8181.
33. Kalepu, J.; Pilarski, L. T., Weinreb Amides as Directing Groups for Transition Metal-Catalyzed C-H Functionalizations. *Molecules* **2019,** *24* (5).
34. Park, H.; Yu, J.-Q., Palladium-Catalyzed [3 + 2] Cycloaddition via Twofold 1,3-C(sp3)–H Activation. *J. Am. Chem. Soc.* **2020,** *142* (39), 16552-16556.
35. Park, H.; Chekshin, N.; Shen, P.-X.; Yu, J.-Q., Ligand-Enabled, Palladium-Catalyzed β-C(sp3)–H Arylation of Weinreb Amides. *ACS Catal.* **2018,** *8* (10), 9292-9297.

36. Davies, H. M. L.; Du Bois, J.; Yu, J.-Q., C–H Functionalization in organic synthesis. *Chem. Soc. Rev.* **2011,** *40* (4), 1855-1856.
37. Qin, C.; Davies, H. M. L., Role of Sterically Demanding Chiral Dirhodium Catalysts in Site-Selective C–H Functionalization of Activated Primary C–H Bonds. *J. Am. Chem. Soc.* **2014,** *136* (27), 9792-9796.
38. Altman, R. A.; Shafir, A.; Choi, A.; Lichtor, P. A.; Buchwald, S. L., An Improved Cu-Based Catalyst System for the Reactions of Alcohols with Aryl Halides. *J. Org. Chem.* **2008,** *73* (1), 284-286.
39. Windholz, T. B.; Johnston, D. B. R., Trichloroethoxycarbonyl: a generally applicable protecting group. *Tetrahedron Lett.* **1967,** *8* (27), 2555-2557.
40. Carpino, L. A., 1-Hydroxy-7-azabenzotriazole. An efficient peptide coupling additive. *J. Am. Chem. Soc.* **1993,** *115* (10), 4397-4398.
41. Yu, W.; Mei, Y.; Kang, Y.; Hua, Z.; Jin, Z., Improved Procedure for the Oxidative Cleavage of Olefins by OsO4−NaIO4. *Org. Lett.* **2004,** *6* (19), 3217-3219.
42. Falcone, N. A.; Bosse, A. T.; Park, H.; Yu, J.-Q.; Davies, H. M. L.; Sorensen, E. J., A C–H Functionalization Strategy Enables an Enantioselective Formal Synthesis of (−)-Aflatoxin B2. *Org. Lett.* **2021,** *23* (24), 9393-9397.

Chapter 4

Aryl Diazoketones as New Donor/Acceptor Carbene Precursors for Highly Selective Intermolecular C-H Functionalization Reactions

---

4.1. Introduction

Donor/acceptor diazo compounds have been widely used for dirhodium(II)-catalyzed C-H functionalization reactions.[1-4] Out of all the different donor/acceptor diazo compound out there, aryl diazoacetates have emerged as a privileged scaffold for intermolecular C-H functionalization (Figure 4.1).[3] The exquisite selectivity comes from the subtle attenuation of the carbene by the aryl "donor group" and ester "acceptor group" and changing either one of these results in a fast drop in overall site- and stereoselectivity.[5, 6] Notably, incorporation of nitrogen or oxygen functionality as donor groups has been inaccessible due to the unstable nature of the diazo compounds themselves. To circumvent this problem, several landmark studies using 1,2,3-triazoles as carbene precursors has enable the incorporation of alpha-amino functionality in place of the ester acceptor group.[7-11] Furthermore, efforts to change the acceptor unit of the diazo leads to poor reactivity for intermolecular C-H insertion with not current examples in the literature. Thus, currently the state-of-the-art technology of intermolecular C-H insertion with diazo compounds is narrowly limited to aryldiazoacetates. However, their incomparable ability to access valuable and difficult to synthesis chiral building blocks warrants studies to expand the current diazo scope.[12-18] One of the key goals in this field is incorporation of valuable heteroatoms into the diazo scaffold. While this is not possible from the donor side, having a surrogate for the desired heteroatom on the acceptor side would be a notable advancement from the current technology. One such functional group that could be consider is a ketone over the tradition ester. While seemingly similar to the ester, the

lower oxidation state of the ketone allows for the potential of stereoretentive Baeyer-Villiger reactions[19] or Beckmann-rearrangements[20] to yield chiral oxygen or amino functionality.

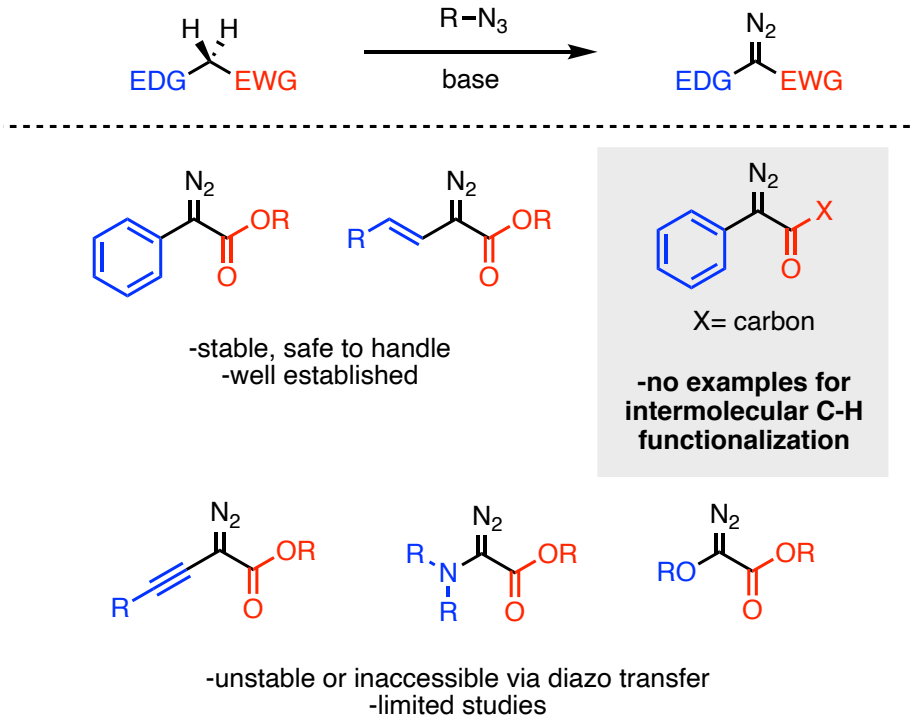

Figure 4.1 General synthesis and different forms of donor/acceptor diazo compounds

In searching the literature for reactions with diazoketones, the majority have been constrained to cyclopropanation reactions or ylide chemistry, with C–H insertion examples limited to highly activated and biased systems or intramolecular reactions.[21] In 2007, Tain and co-workers[22] reported an intramolecular C-H insertion to synthesize α-aryl cyclopentanones (Scheme 4.1). The scope of the reaction was very limited with only minor modifications on the aromatic substituent. Furthermore, yields for these reactions were only modest to good, and even though they were using a chiral catalyst (Rh_2(*S*-PTTL)$_4$) the enantioselectivity furnished poor ee's ranging from 44% to 49% ee.

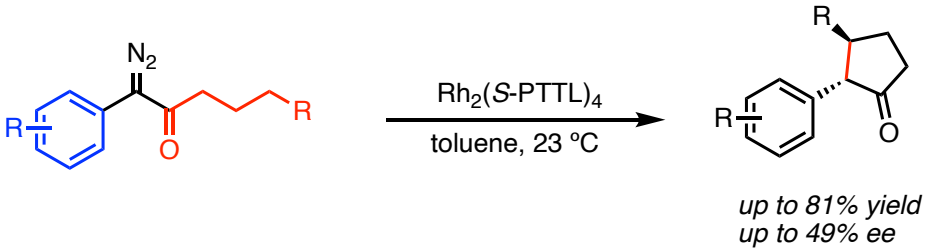

Scheme 4.1 Intramolecular C-H functionalization with α-aryl-α-diazoketone

Moving to ylide chemistry, a recent report in 2014 by Zhou and co-workers[23] disclosed an enantioselective N-H insertion (Scheme 4.2). Since reactions undergoing ylide chemistry generate an enol, chiral rhodium catalysts give no enantioselectivity and thus chiral phosphoric acids were used to achieve chiral induction in the proton-transfer step. Additionally, the researchers were able to demonstrate the utility of their reaction to generate unnatural chiral amino acids. The scope outlined by Zhou demonstrates decent breath of scope with excellent yields and high enantioselectivity up to 98% ee.

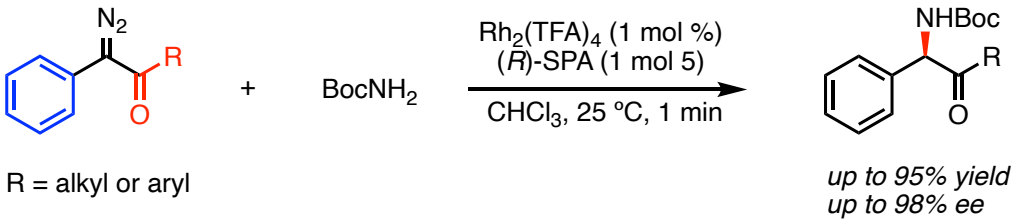

Scheme 4.2 Enantioselective ylide reaction with α-aryl-α-diazoketone

Lastly, the Charette group has done extensive work with cyclopropanation of various diazo compounds. In 2010 and 2011 they reported two separate reports on asymmetric intermolecular cyclopropanation with diazoketones (Scheme 4.3). The 2010 publications studied the use of additives with various diazoketones, looking at only acceptor/acceptor, either α-nitro-α-diazoketones or α-cyano-α-diazoketones (Scheme 4.3a).[24] They found additives were able to

increase the diastereoselectivity with the α-nitro diazo compound, but not with the α-cyano. However, chiral catalyst Rh_2(*S*-TCPTTL)$_4$ was used in the α-nitro case and achiral Rh_2(oct)$_4$ with the α-cyano, hinting the additives only display effects with chiral catalysts. Moving to the 2011 study, the team again focused on acceptor/acceptor diazoketones for highly diastereo- and enantioselective cyclopropanations with Rh_2(*S*-TCPTTL)$_4$.[25] However, they did screen one α-aryl-α-diazoketones, while having impressive diastereo- and enatioselectivity, the yield was poor in only 9% yield (Scheme 4.3b). The resulting products from their impressive scope furnished a variety of cyclopropane α- and β-amino acid derivatives. Thus, with few and far between examples of reactions with α-aryl-α-diazoketones, we are interested in applying our expanded catalyst toolbox in the hopes finding new carbene precursors for intermolecular C-H insertion.

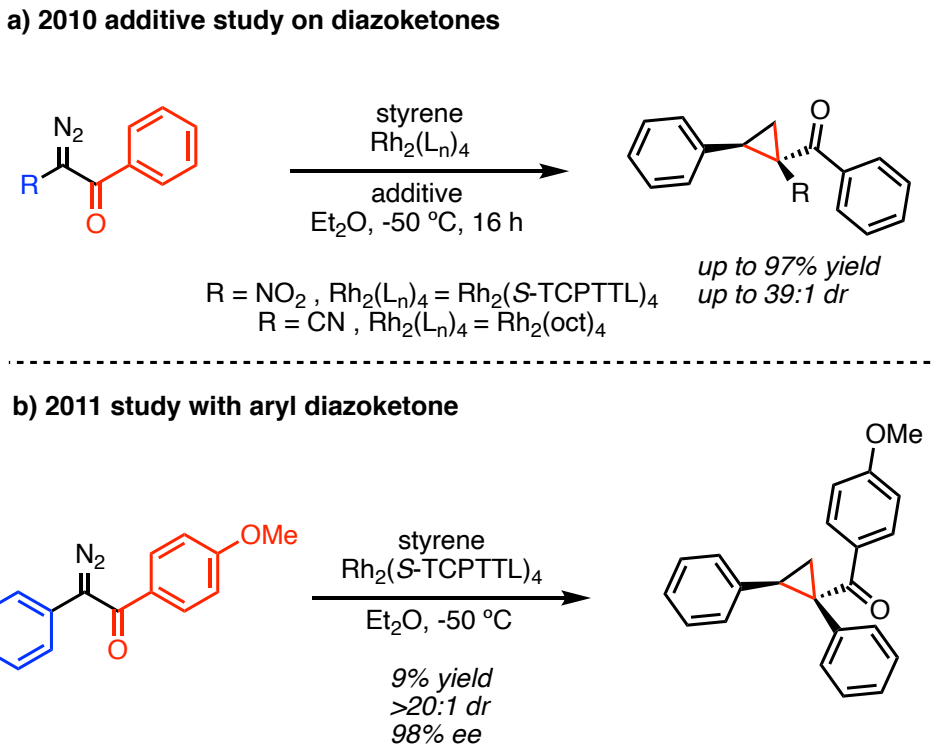

Scheme 4.3 Asymmetric intermolecular cyclopropantion with acceptor/acceptor diazoketones and α-aryl-α-diazoketone

While we have previously reported that aryl diazoketones are also competent donor/acceptor carbene precursors, the application was limited to cyclopropanation and the scope of alkene substrates was relatively narrow (Scheme 4.4).[26] While the scope was limited to only a handful of styrenal derivatives, the yields and diastero- and enantioselectivies were excellent for all the diazoketones when using Rh_2(*S*-PTAD)$_4$ as a catalyst – apart from phenyl substituted ketones. Notably, to achieve high asymmetric induction, the researchers utilized quite unusual alkynyl groups in the R^1 position. Furthermore, when this reaction was disclosed, it was the first reported example of intermolecular reactions with α-aryl-α-diazoketone. However, the only example of C-H functionalization using aryl diazoketones in the paper used cyclohexadiene as the substrate, which is one of the easiest substrates due to double electronic activation from the diene functionality. Therefore, one of the primary goals for this project was to expand our donor/acceptor carbene reactions toolbox and demonstrate the synthetic utility of the newly incorporated ketone functionality as opposed to an ester group.

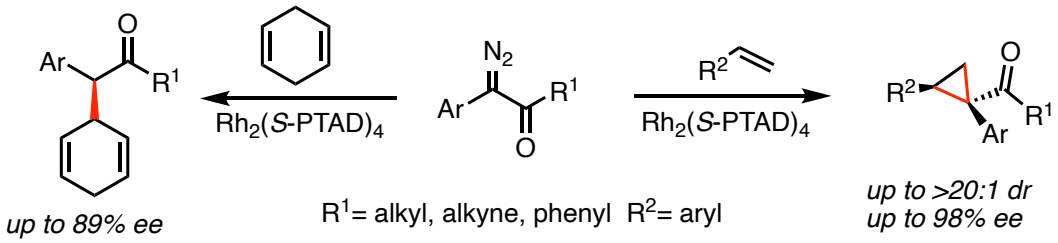

Scheme 4.4 Previously reported chemistry on aryl diazoketones as donor/acceptor carbene precursors

The motivation for this work comes from the ability of the ketone functionality to open new chemical space the ester acceptor group could not. On the outset of the project, we envisioned the ketone functional group could undergo a stereoretentive Baeyer-Villiger oxidation then

hydrolysis to form chiral alcohols. The other transformation we were interested in exploring was ketoxime formation followed by Beckmann-rearrangement to form chiral benzylamides (Scheme 4.5). The synthesis of chiral alcohols has been widely studied with a plethora of reactions available, one common example is the asymmetric reduction of a ketone.[27-33] The preparation of enantiopure benzylamides has also been heavily pursued in the chemical community due to their presence in a variety of biologically relevant compounds and synthetic versatility as building blocks.[34-37] The acylation of chiral amines is one of the principal methods for their preparation, and the most common reaction performed in the pharmaceutical industry.[34, 35, 38] New methods for their synthesis are constantly being developed, one such example is C-H insertion through nitrenes, via metal[1, 39-42] or enzymatic catalysis.[43-46] However, these approaches can be limited, either through the preparation of a chiral amine for acylation or limited functional group tolerance with nitrenes. In this chapter, a new way of synthesizing chiral benzylamides is reported that was enabled by a key C-H functionalization step using the recently discovered dirhodium catalyst, Rh_2(*S*-TPPTTL)$_4$, in conjunction with the use of donor/acceptor diazoketone compounds.

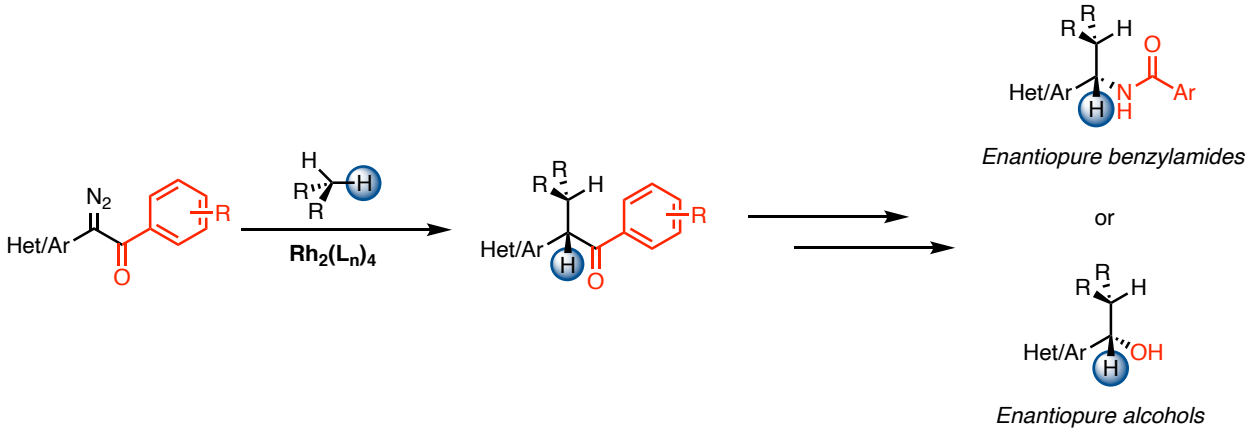

Scheme 4.5 Proposed modifications of C-H insertion products from reactions with α-aryl-α-diazoketones

4.2. Results and Discussion

4.2.1. Catalyst Screen and Reaction Optimization

Initial reaction optimization focused on the identification of an aryl diazoketone as an effective carbene precursor. Based off of previous work in our lab, *para*-bromophenyl methylketone **4.1** was chosen as a suitable diazo to screen against our catalyst library.[26] The diazo **4.1** was synthesized through Regtiz diazo transfer with *p*-ABSA in 82% yield. As a model substrate 4-ethyltoluene was chosen as an ideal substrate, which would allow evaluation of the site-selectivity for methyl vs. methylene C(sp^3)-H bonds. Upon extensive catalyst screening, temperature, solvent, and concentration optimization, the only catalyst that gave any of the desired product was Rh_2(*S*-TPPTTL)$_4$ (Table 4.1, entry 1). The product was formed only in trace yield (<5%), but excitingly in only one regio- and diastereomer for methylene C-H insertion. Modifying the electronics on the donor side of the diazo to the *p*-nitro compound **4.2** (found in our diazo library) led to no increase in the yield (Table 4.1, entry 12). Additionally, screening alkynyl diazos **4.3** and **4.4** found in our diazo library led to no product generation either (Table 4.1, entry 13+14). It was hypothesized that the diazoketones screened here might be too sterically small versus that standard ester, leading to unproductive pathways. To test this theory, tertbutyl diazoketone **4.5** was synthesized and screened with the optimum catalyst, but found it ineffective as well (Table 4.1, entry 15).

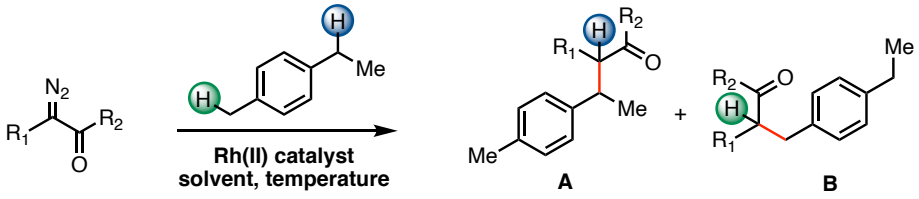

Entry	Compd.	R_1	R_2	Conc. (M)	Temp (°C)	Solvent	Catalyst	yield(%)
1	**4.1**	**(*p*-Br)Ph**	**Me**	**0.125**	**25**	**CH_2Cl_2**	**Rh_2(*S*-TPPTTL)$_4$**	**trace[a]**
2	4.1	(*p*-Br)Ph	Me	0.25	25	CH_2Cl_2	Rh_2(*S*-TPPTTL)$_4$	0
3	4.1	(*p*-Br)Ph	Me	0.125	40	CH_2Cl_2	Rh_2(*S*-TPPTTL)$_4$	0
4	4.1	(*p*-Br)Ph	Me	0.125	0	CH_2Cl_2	Rh_2(*S*-TPPTTL)$_4$	0
5	4.1	(*p*-Br)Ph	Me	0.125	25	TFT	Rh_2(*S*-TPPTTL)$_4$	0
6	4.1	(*p*-Br)Ph	Me	0.125	25	CH_2Cl_2	Rh_2(*S*-DOSP)$_4$	0
7	4.1	(*p*-Br)Ph	Me	0.125	25	CH_2Cl_2	Rh_2(*S*-PTTL)$_4$	0
8	4.1	(*p*-Br)Ph	Me	0.125	25	CH_2Cl_2	Rh_2(*R*-2-Cl 5-BrTPCP)$_4$	0
9	4.1	(*p*-Br)Ph	Me	0.125	25	CH_2Cl_2	Rh_2(*R*-DiBic)$_4$	0
10	4.1	(*p*-Br)Ph	Me	0.125	25	CH_2Cl_2	Rh_2(*R*-TriBic)$_4$	0
11	4.1	(*p*-Br)Ph	Me	0.125	25	CH_2Cl_2	Rh_2(*S*-TCPTTL)$_4$	0
12	4.2	(*p*-NO_2)Ph	Me	0.125	25	CH_2Cl_2	Rh_2(*S*-TPPTTL)$_4$	trace[a]
13	4.3	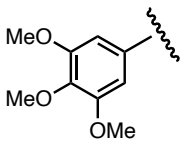	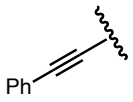	0.125	25	CH_2Cl_2	Rh_2(*S*-TPPTTL)$_4$	0
14	4.4	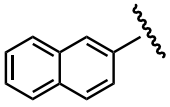	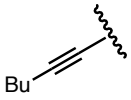	0.125	25	CH_2Cl_2	Rh_2(*S*-TPPTTL)$_4$	0
15	4.5	(*p*-Br)Ph	*t*Bu	0.125	25	CH_2Cl_2	Rh_2(*S*-TPPTTL)$_4$	0

[a]Products from the reactions with 4.1 and 4.2 were produced in >20:1 rr (A:B) and >20:1 dr

Table 4.1 Initial optimization of the C-H insertion with α-aryl-α-diazoketones

After extensive screening with poor results, clearly the model diazoketone had to be modified. While sterics weren't making a difference from the initial screen, electronic modifications were studied next. In thinking how the diazoketone could be modified to act similar to the diazoester, it was hypothesized in order to mimic an ester group increasing the electronic profile on the ketone would be beneficial. Thus, to achieve this the phenyl substituted ketone **4.6** was chosen. Under the previous conditions that generated trace product (Table 4.1, entry 1), the new diazo **4.6** was subjected to the rhodium catalyzed C-H insertion (Table 4.2). Excitingly, the yields not only jumped from <5% to 46%, but the reaction was exquisitely regio-, diastereo- and enantioselective for the methylene C-H bond (Table 4.2, entry 1). The exclusive methylene site selectivity could be attributed to the structural features of the catalyst that imparts a very defined way the rhodium-carbene interacts with the substrate. However, with the moderate yield we wanted to confirm that optimal catalyst was being used. Testing the related Rh_2(*S*-PTAD)$_4$ catalyst, previous used for aryl diazoketone cyclopropanation,[26] gave a low yield and only moderate selectivity (Table 4.2, entry 2). Furthermore, screening several other catalysts from the catalyst toolbox all led to worst enantioselectivity and poor ^{1}H NMR yields (Table 4.2, entries 3-7). Notably, at the same time catalysts were being screened, we also were studying various diazo compounds against the lead catalyst Rh_2(*S*-TPPTTL)$_4$. Since all the diazos routinely gave excellent regio-, diastereo- and enantioselective, the diazos available at the time were used for the catalyst screen. Hence, the switch to the *para*-Br **4.7** and *para*-CF_3 **4.8** diazos. Additionally, because these diazos give similar selectivity with only changes in yield (Table 4.3), we are confident with the results from the catalyst screen.

Validated that the optimum catalyst was in hand, we sought to change the solvent and concentration in hopes of increasing the yield. To avoid the potential for Wolff-rearrangement,

refluxing the reaction was avoided as heat is known accelerates the rearrangement.[47, 48] Running the reaction in TFT led to a drop in the yield (Table 4.2, entry 8). However, diluting the reaction increased the yield by about 10% (Table 4.2, entry 9). Finally, isolation of the major byproduct of the reaction allowed discovery that insertion of the carbene into oxygen, generating a diketone, was causing the modest yields.[49] Additionally, the diazoketone was found to be unstable in DCM, and after sitting in DCM overnight the diazo decomposes. Therefore, to circumvent this, the reaction and the diazoketone was degassed before adding the diazo to the mixture of catalyst and substrate. Furthermore, the diazo was added all at once instead of traditional slow addition to avoid decomposition in the DCM. With this procedure the optimization was completed achieving a 66% yield (Table 4.2, entry 10). Notably, using freeze-pump-thaw technique to set up the reaction led to the same result generated via sparging the reaction with Schlenk line technique. Therefore, we carried forward with sparging the reactions via Schlenk line technique as this is a simpler and faster protocol.

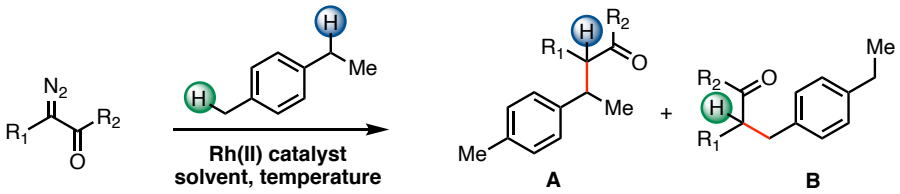

Entry	Compd.	R_1	R_2	Solvent	Conc. (M)	Catalyst	yield(%)	rr (A:B)	dr	ee(%)
1	4.6	Ph	Ph	CH_2Cl_2	0.125	Rh_2(*S*-TPPTTL)$_4$	46	>20:1	>20:1	99
2	4.7	Ph	(*p*-Br)Ph	CH_2Cl_2	0.125	Rh_2(*S*-PTAD)$_4$	15	2:1	>20:1	77
3	4.8	Ph	(*p*-CF_3)Ph	CH_2Cl_2	0.125	Rh_2(*S*-DOSP)$_4$	24[a]	>20:1	8:1	54
4	4.8	Ph	(*p*-CF_3)Ph	CH_2Cl_2	0.125	Rh_2(*S*-NTTL)$_4$	1[a]	>20:1	>20:1	32
5	4.8	Ph	(*p*-CF_3)Ph	CH_2Cl_2	0.125	Rh_2(*R*-TCPTAD)$_4$	13[a]	>20:1	>20:1	52
6	4.8	Ph	(*p*-CF_3)Ph	CH_2Cl_2	0.125	Rh_2(*R*-2-Cl 5-BrTPCP)$_4$	3[a]	5:1	>20:1	52
7	4.8	Ph	(*p*-CF_3)Ph	CH_2Cl_2	0.125	Rh_2(*S*-*p*BrTPCP)$_4$	4[a]	7:1	>20:1	86
8	4.8	Ph	(*p*-CF_3)Ph	TFT	0.125	Rh_2(*S*-TPPTTL)$_4$	30	>20:1	>20:1	-
9	4.8	Ph	(*p*-CF_3)Ph	CH_2Cl_2	0.0625	Rh_2(*S*-TPPTTL)$_4$	57	>20:1	>20:1	99
10[b]	**4.8**	**Ph**	**(*p*-CF_3)Ph**	**CH_2Cl_2**	**0.0625**	**Rh_2(*S*-TPPTTL)$_4$**	**66**	**>20:1**	**>20:1**	**99**

[a]Yields were determined by NMR with trichloroethylene as internal standard
[b]Reaction was degassed and the diazo added all at once

Table 4.2 Optimization of the C-H functionalization with the phenyl substituted diazoketones

4.2.2. Aryl Diazoketone Scope

Having identified that an aryl ketone is essential for a successful reaction, we moved to studying the diazo scope, modifying the functionality on both the donor and acceptor side. Notably, since the goal of the project is to convert the ketone to an alcohol or benzylamide, the focus was on modifying the donor side with minimal perturbations on the acceptor side. The synthesis of the diazoketones starts from the commercially available phenylacetic acid derivatives **4.9**, which under EDCI coupling conditions affords the Weinreb amide **4.10** (Scheme 4.6). Next, the amide is subjected to a Grignard addition, either using commercially available Grignards or Grignards

synthesized in the lab to yield ketone products **4.11**. Finally, the last step is the Regitz diazo transfer with *o*-NBSA to afford the aryl diazoketones **4.12**. Notably, this procedure had to be slightly modified from the established method. It was found that upon quenching the diazo transfer with saturated sodium ammonium chloride, the slightly acidic work-up would destroy the diazo. Thus, the work-up was removed from the procedure and by concentrating the crude down and purifying it instantly via basified flash chromatography, the diazoketone compounds could be cleanly and reproducibly isolated.

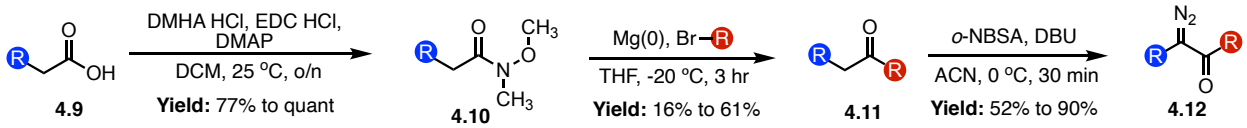

Scheme 4.6 General diazoketone synthesis prep

With the library of diazo compounds in hand, we moved to subjecting them to the optimized C-H insertion conditions against 4-ethyltoluene with Rh_2(*S*-TPPTTL)$_4$ (Table 4.3). Starting with exploring changes to the acceptor side, modification of the *para* position is well tolerated, displaying low yields with electron donating groups and good yields with electron withdrawing groups (Table 4.3, entries **4.13**, **4.14**, **4.15**, **4.17**, **4.18**). The improved result of the *para*-CF_3 diazo **4.8** can be rationalized by making the carbene slightly more electrophilic and reactive, finding the "sweet spot" of reactivity attributed to aryl diazoacetates. Bis-*para* substituted compound **4.19** also performed well, however a slight drop in enantioselectivity (90% ee) was seen as presumably the diazo could be interfering with the wall of the chiral catalyst. After the initial evaluation studies to generate the six products described above, the further optimization and evaluation of a range of aryl diazoketones was conducted by Terrence Nguyen and his complete results are summarized in Table 4.3. Terrence Nguyen started his study with *meta* substitution on

the acceptor side, which was tolerated in modest yields but excellent overall selectivity with *meta*-CF_3 product **4.20**. Unfortunately, substituting anything at the *ortho* position to the ketone shut down reactivity. Moving to the donor side, *para* substitution (Table 4.3, entries **4.21**, **4.22**, **4.23**, **4.24**) is tolerated well in low to modest yields. *Meta* substitution performs in low to modest yields as well (Table 4.3, entries **4.25**, **4.26**, **4.27**, **4.28**, **4.29**), notably the electron donating group performing better on the donor side over the acceptor side. Besides standard phenyl rings, naphthalene (Table 4.3, entry **4.30**) and excitingly 2-cloropyridine (Table 4.3, entry **4.31**) are both tolerated in fair to good yield, respectively. Unfortunately, *ortho* substituent on the donor ring is also not tolerated in the reaction, as well as *para*-Ph substitution on the donor ring, presumably due to a steric clash with the wall of the chiral catalyst. Notably, the regio- and diastereoselectivity is perfect across the board with all diazos in the scope performing in >20:1 rr and >20:1 dr. Additionally, the enantioselectivity is excellent as well ranging from 90% to >99% ee.

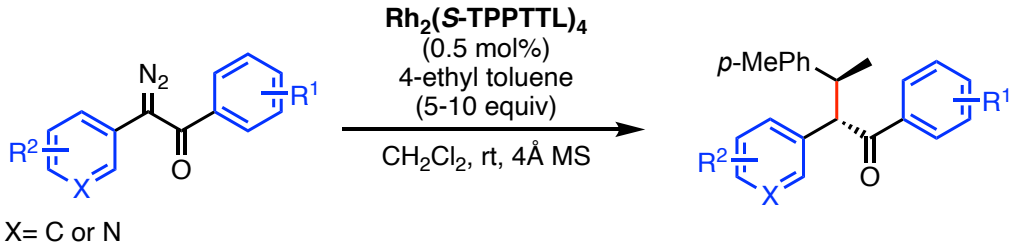

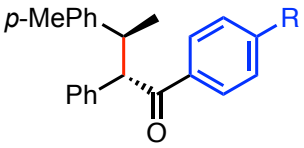

4.13. R = H, 64% yield, >20:1 r.r., >20:1 d.r., 99% e.e.
4.14. R = OMe, 30% yield, >20:1 r.r., >20:1 d.r., >99% e.e
4.15. R = CF_3, 66% yield, >20:1 r.r., >20:1 d.r., 99% e.e.
4.17. R = Br, 54% yield, >20:1 r.r., >20:1 d.r., >99% e.e.
4.18. R = F, 36% yield, >20:1 r.r., >20:1 d.r., >99% e.e.

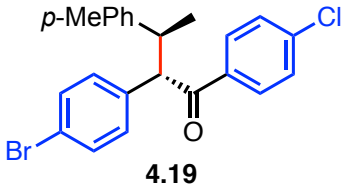

4.19
57% yield
>20:1 r.r.
>20:1 d.r.
90% e.e.

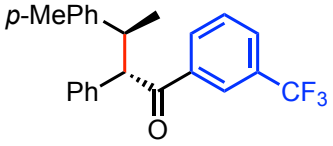

4.20
56% yield
>20:1 r.r.
>20:1 d.r.
>99% e.e.

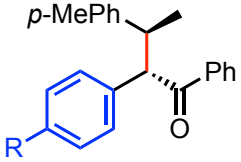

4.21. R = CF_3, 50% yield, >20:1 r.r., >20:1 d.r., 94% e.e.
4.22. R = F, 31% yield, >20:1 r.r., >20:1 d.r., 96%e.e.
4.23. R = Cl, 44% yield, >20:1 r.r., >20:1 d.r., 92% e.e.
4.24. R = Br, 39% yield, >20:1 r.r., >20:1 d.r., 94% e.e.

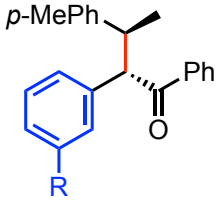

4.25. R = CH_3, 46% yield, >20:1 r.r., >20:1 d.r., 96% e.e.
4.26. R = F, 39% yield, >20:1 r.r., >20:1 d.r., 94%e.e.
4.27. R = Cl, 55% yield, >20:1 r.r., >20:1 d.r., 96% e.e.
4.28. R = Br, 40% yield, >20:1 r.r., >20:1 d.r., 92% e.e.
4.29. R = OMe, 52% yield, >20:1 r.r., >20:1 d.r., 99% e.e.

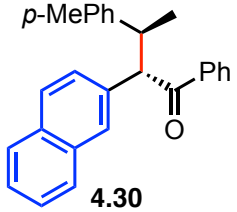

4.30
48% yield
>20:1 r.r.
>20:1 d.r.
98% e.e.

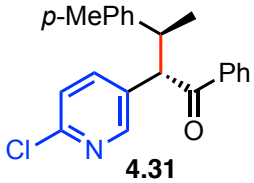

4.31
66% yield
>20:1 r.r.
>20:1 d.r.
>99% e.e.

Table 4.3 Scope of aryl diazoketone reactivity with 4-ethyltoluene

4.2.3. Substrate Scope

With the diazo scope now completed, we turned our attention to understanding the substrate scope. Analyzing the diazo scope, the *para*-CF_3 diazo **4.8** was chosen as the optimum diazo to move forward with for the substrate scope. It was reasoned that a *para*-CF_3 group would serve two purposes: 1) it attenuates an even more reactive carbene that could allow us to functionalize unactivated substrates, 2) critically it would facilitate regioselective Baeyer-Villiger oxidation or Beckmann-rearrangement in the next step by increasing the migratory aptitude of the secondary alkyl group in the ketone product. Thus, with the optimized catalyst, carbene precursor and reaction conditions in hand, we next sought to challenge the selectivity of the catalyst by exploring the scope of a variety of activated and unactivated substrates (Scheme 4.7). This study was conducted in collaboration with my undergraduate student mentee, Camilla Suarez.

Starting with the activated substrates, ethyl benzene derivates **4.15**, **4.32**, **4.33** all functioned well with good yield and excellent selectivity. The two allylic substrates **4.34** and **4.35** also were competent in the reaction resulting in good yields and excellent selectivity. Moving to the other benzylic substrates, indane **4.36** performed well, however, not only was the regioselectivity lower but this substrate had one of the lowest enantioselectivity in the scope with 81% ee. Both cyclobutane **4.37** and dihydrobenzofuran **4.38** are tolerated in fair to low yields respectively, with excellent regioselectivity but poor diastereoselectivity for the dihydrobenzofuran. Notably, cyclobutane **4.37** is related to a transient receptor potential vanilloid 3 antagonist developed by Abbvie.[50] Excitingly the highest yield obtained was with THF product **4.39** in 75% yield, however with modest diastereo- and enantioselectivity. Interestingly, changing from THF to tetrahydropyran yielded product **4.40** in low yields but excellent regio- and

enantioselectivity with modest diastereoselectivity. Moving to unactivated systems, cyclopentane **4.41** and cyclohexane **4.42** and **4.43** are all tolerated in fair to good yields respectively with perfect overall selectivity. Lastly, adamantane is tolerated in good yield with excellent selectivity for product **4.44**. Overall, our scope demonstrates a huge leap in reactivity with aryl diazoketones, unseen before in the literature.

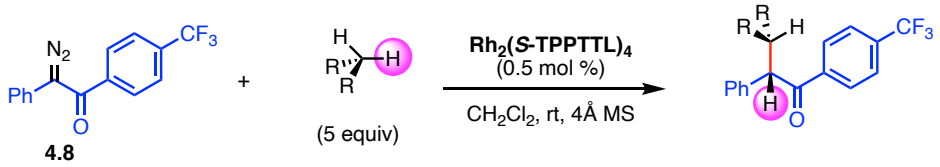

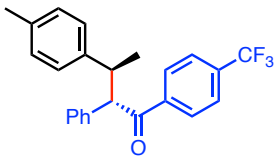

4.15
66% yield
>20:1 r.r.
>20:1 d.r.
99% e.e.

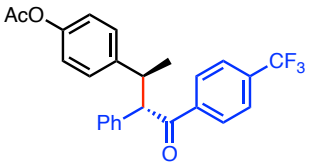

4.32
59% yield
>20:1 d.r.
99% e.e.

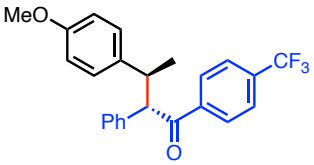

4.33
66% yield
>20:1 r.r.
>20:1 d.r.
91% e.e.

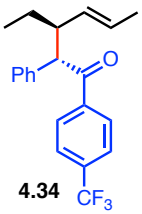

4.34
58% yield
>20:1 r.r.
>20:1 d.r.
>99% e.e.

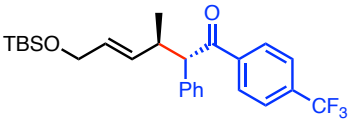

4.35
51% yield
7:1 r.r
>20:1 d.r.
95% e.e.

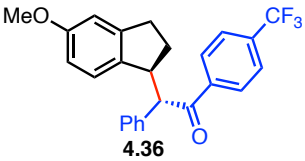

4.36
62% yield
13:1 r.r.
>20:1 d.r.
81% e.e.

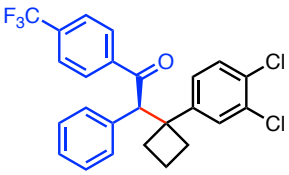

4.37
47%
>20:1 rr
>99% e.e.

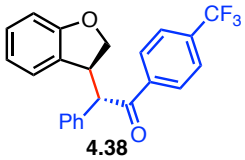

4.38
30% yield
>20:1 r.r.
3:1 d.r.
96% e.e.

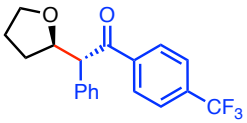

4.39
75% yield
>20:1 rr
7:1 d.r.
78% e.e.

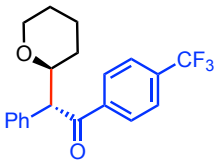

4.40
30% yield
>20:1 rr
10:1 dr
91% ee

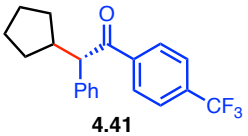

4.41
40% yield
99% e.e.

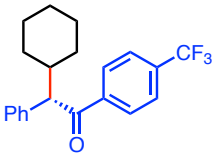

4.42
58% yield
99% e.e.

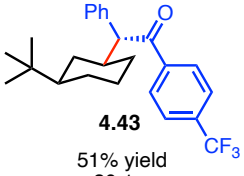

4.43
51% yield
>20:1 r.r.
>20:1 d.r.
>99% e.e.

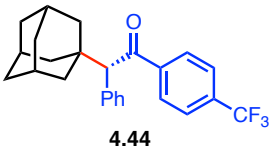

4.44
58% yield
>20:1 r.r
95% e.e.

Scheme 4.7 Substrate scope with *para*-CF_3 α-aryl-α-diazoketone

To demonstrate the impressive selectivity developed here with aryl diazoketones and Rh_2(*S*-TPPTTL)$_4$, we sought to compare the scope outlined here with known reactions with aryldiazoacetates (Scheme 4.8). Beginning with **4.15** and **4.45**, the yields and regioselectivity are identical, however the diastereo- and enantioselectivity selectivity found in **4.15** completely outclasses the reaction with Rh_2(*S*-DOSP)$_4$ and the corresponding aryldiazoaceate.[51] With acetate derivative **4.32** and **4.46**, yields are higher for the aryldiazoacetate, however overall selectivity is greatly improved using the diazoketone.[52] Comparing **4.33** and **4.47**, again yields are higher for the aryldiazoacetate, enantioselectivity is comparable, yet the dr is drastically increased (from 2:1 to >20:1) when using the diazoketone.[52] Moving to *trans*-2-hexene, **4.48** is formed in better yield than **4.34**, however **4.34** is notably exquisitely selective, whereas the aryldiazoacetate is formed in moderate yield and the authors note a poor mixture of diastereomers.[53] Allylic alcohol **4.49** is generated in better yield and enantioselectivity over **4.35**, while diastereoselectivity is greatly improved using the diazoketone.[11] Furthermore, both reactions (**4.49** and **4.35**) utilize Rh_2(*S*-TPPTTL)$_4$ indicating increase catalyst compatibility with diazoketones. Comparing cyclobutane **4.50** and **4.37** both using Rh_2(*S*-TPPTTL)$_4$, the aryldiazoacetate outperforms the diazoketone, with only moderately better enantioselectivity for **4.37**.[54] THF product **4.39** is generated in higher yield and diastereoselectivity compared to **4.51**.[55] However, interestingly this is one of the few cases where the diazoketone gives a higher yield but lower enantioselectivity compared to the aryldiazoacetate. Moving to the cyclic hydrocarbons, **4.41** is formed in higher enantioselectivity but lower yield compared to **4.52**.[56] Similarly, cyclohexane **4.42** and **4.53** are both generated in 99% ee, however higher yields are obtained with the aryldiazoacetate.[56] Diazoketone **4.8**

outperforms the classic reaction with the diazoester when *tert*-butyl cyclohexane (**4.43**) was used as the substrate.[56] Only one diastereomer (>20:1) was observed and formed in essentially complete enantioselectivity (>99% e.e.), while moderate diastereoselectivity (11:1) is reported with aryldiazoacetates (**4.54**) but higher yield. This result indicates that when an aryl diazoketone is used as the carbene source, the catalyst can achieve better kinetic resolution between the C-3 and C-5 C–H bonds and therefore give an improved desymmetrization reaction. The same trend follows the reaction with adamantane, product **4.44** gives better enantioselectivity but lower yield compared to **4.55**.[56] The indane (**4.36)**, dihydrobenzofuran (**4.38**) and tetrahydropyran (**4.40**) products have no known reactions in the literature with aryldiazoacetates and thus cannot be compared here. Currently these substrates are being screened against aryldiazoacetates and Rh_2(*S*-TPPTTL)$_4$ to compare the selectivity. Overall, the diazoketone substrate scope demonstrates that while yields are typically lower when using a diazoketone, the regio-, diastereo- and enantioselectivity is typically superior for most cases.

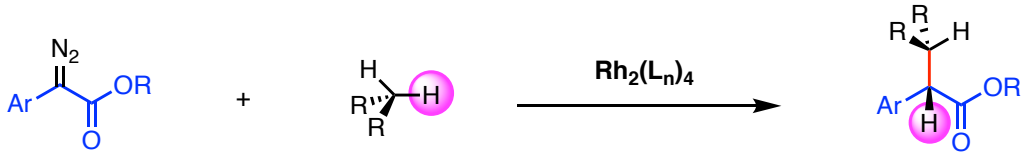

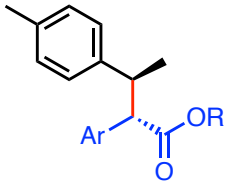

4.45

Rh_2(*S*-DOSP)$_4$
Ar = C_6H_4(*p*-Br)
R = $CH_2CH_2CCl_3$
66% yield, >20:1 rr,
3:1 dr, 81% ee

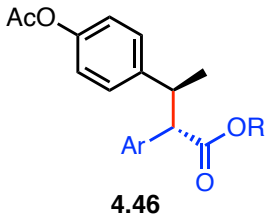

4.46

Rh_2(*S*-DOSP)$_4$
Ar = C_6H_4(*p*-Br)
R = CH_3
77% yield, 3.6:1 dr
86% ee

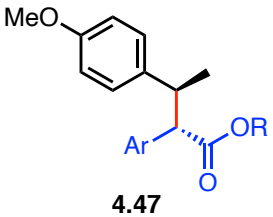

4.47

Rh_2(*S*-DOSP)$_4$
Ar = C_6H_4(*p*-Br)
R = CH_3
86% yield, 2.1:1 dr
89% ee

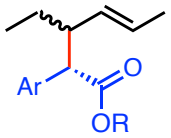

4.48

Rh_2(*S*-DOSP)$_4$
Ar = C_6H_4(*p*-Br)
R = CH_3
75% yield, 9:1 rr

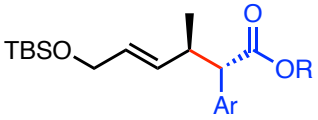

4.49

Rh_2(*S*-TPPTTL)$_4$
Ar = C_6H_4(*p*-Br)
R = $CH_2CH_2CF_3$
64% yield, >20:1 rr,
3.5:1 dr, 99% ee

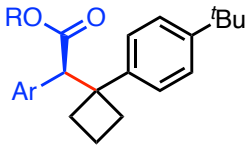

4.50

Rh_2(*S*-TPPTTL)$_4$
Ar = C_6H_4(*p*-Br)
R = $CH_2CH_2CCl_3$
71% yield, >20:1 rr
94% ee

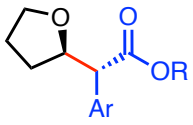

4.51

Rh_2(*S*-DOSP)$_4$
Ar = C_6H_5
R = CH_3
67% yield, 2.8:1 dr,
97% ee

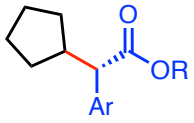

4.52

Rh_2(*S*-TPPTTL)$_4$
Ar = C_6H_4(*p*-Br)
R = $CH_2CH_2CCl_3$
73% yield, 97% ee

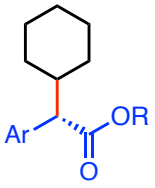

4.53

Rh_2(*S*-TPPTTL)$_4$
Ar = C_6H_4(*p*-Br)
R = $CH_2CH_2CCl_3$
79% yield, 99% ee

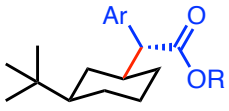

4.54

Rh_2(*S*-TPPTTL)$_4$
Ar = C_6H_4(*p*-Br)
R = $CH_2CH_2CCl_3$
80% yield, >20:1 rr,
11:1 dr, 95% ee

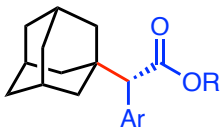

4.55

Rh_2(*S*-TPPTTL)$_4$
Ar = C_6H_4(*p*-Br)
R = $CH_2CH_2CCl_3$
72% yield, 90% ee

Scheme 4.8 Comparison of the substrate scope with aryldiazoacetates

While the scope outlined in Scheme 4.7 shows a wide variety of activated and unactivated substrates, several other compounds were not tolerated for C-H functionalization. Outlined below are a variety of substrates that were screened which were found to be unproductive for the reaction (Figure 4.2). Notably, a wide variety of nitrogen protected substrates (**4.56**, **4.57**, **4.58**, **4.59**, and **4.60**), either piperidine, pyrrole, indoline or exocyclic amines, were not tolerated at all in the reaction. Exploring different protecting groups (ex. Boc, Ts, Phth) gave no change in reactivity for any of the substrates. Attempting to diversify the cyclohexane results, adding a pendant TBS protected alcohol **4.61** resulted in loss of reactivity. Activated substrates *p*-cymene **4.62** and xylene **4.63** gave no product either, presumable to the catalyst preference for methylene C-H bonds, then methine over methyl.[56] Substrates with a balance of benzylic activation but deactivated with a ketone functionality, **4.64** and **4.65**, both gave no product, demonstrating the subtle effects electronics have on the system. Finally, linear alkane 2-methylpentane **4.66** gave no product at all and using hexane as a co-solvent only gave trace product. Overall, these failed substrates for C-H insertion elucidate the subtleties of the C-H functionalization reaction, showing a need for future catalyst development to expand the scope of reactivity for aryl diazoketones.

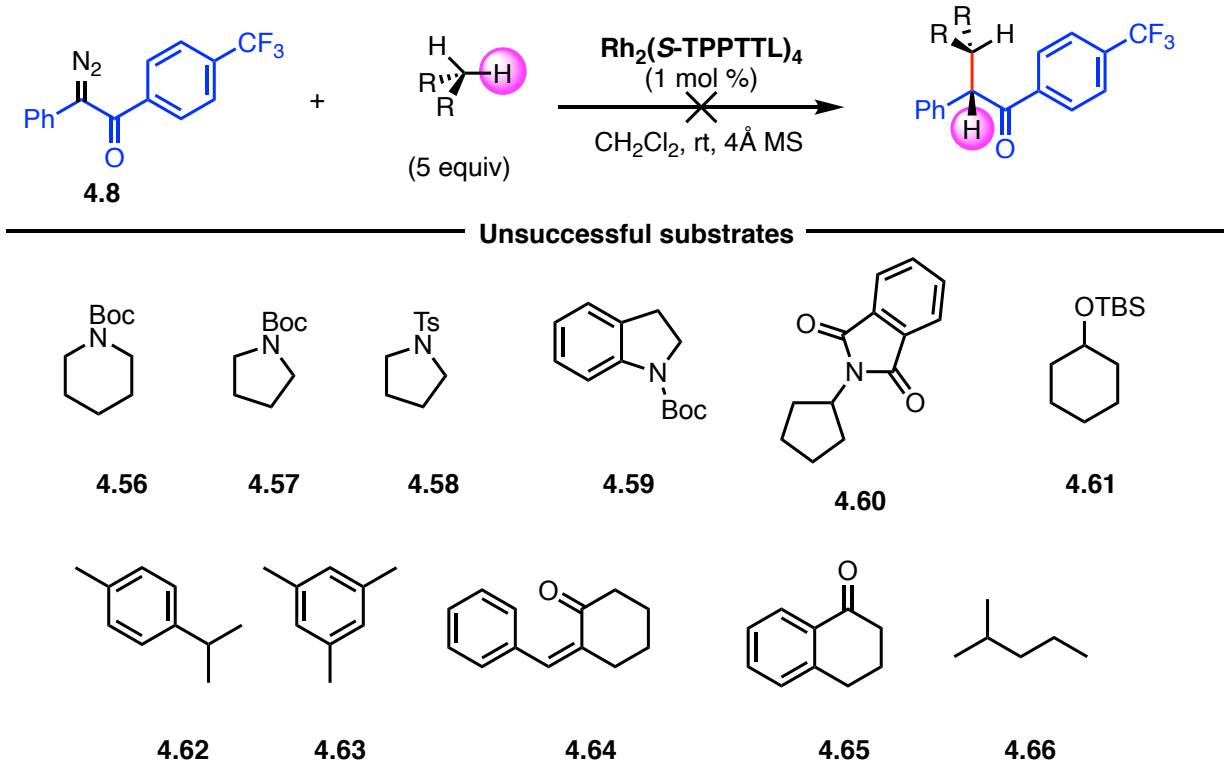

Figure 4.2 Failed substrates for C-H functionalization with aryl diazoketones

4.2.4. Derivatization of Aryl Diazoketone Products

Having established a robust profile of substrates competent under our new diazoketone carbene, we then sought to demonstrate its utility in post-functionalization transformations. Notably, the transformations outlined here are chemoselective for the ketone functional group and thus these compounds would not be accessible using our standard aryldiazoaceatate. Starting with a variety of our C-H insertion products we screened a plethora of Baeyer-Villiger oxidation conditions against these ketones. Since the majority of precedented Baeyer-Villiger oxidations utilized either cyclic ketones or sterically unhindered linear ones, we were unsure of how the steric profile on our C-H functionalization products would affect the reaction. Thus, we decided to screen the Baeyer-Villiger reaction against ketone **4.13** and **4.43**. Starting with the 4-ethyltoluene product

4.13, standard *m*CPBA conditions[57-59] or a variety of Lewis acid assisted H_2O_2 oxidations[60-62] gave no desired product **4.67** and complete recovery of starting material (Table 4.4).

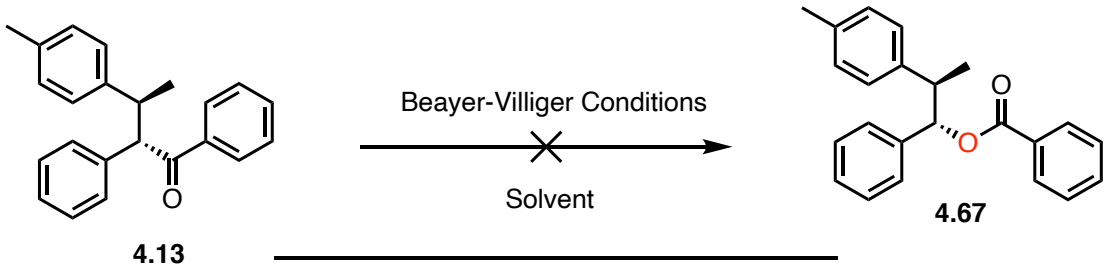

4.13 **4.67**

Entry	Conditions	yield (%)
1	*m*CPBA, CH_2Cl_2	0
2	$Bi(OTf)_3$, *m*CPBA, CH_2Cl_2	0
3	TFAA, H_2O_2	0
4	BCF, H_2O_2, DCE 50 °C	0
5	NaBARF, H_2O_2, DCE 50 °C	0
6	BF_3OEt_2, H_2O_2, DCE 50 °C	0

Table 4.4 Baeyer-Villiger oxidation screen against functionalized 4-ethyltoluene product

Moving to the *tert*-butyl cyclohexane product **4.43**, again a variety of *m*CPBA[57-59] or Lewis acid assisted H_2O_2 oxidations[60-63] gave no product **4.68** and complete recovery of starting material (Table 4.5). Even attempting the harshest known oxidation conditions, with either $AlCl_3$ (entry 8)[64] or TFAA (entry 9),[62] resulted only in recovery of starting material. Therefore, with no hint of product in any reaction, it was concluded that the C-H insertion products are too hindered for Baeyer-Villiger oxidation. This was further validated by Terrence Nguyen where he was able to conduct control experiments demonstrating the conditions we screened worked on the simple

substrates. Thus, validating the hypothesis that the products generated from the C-H functionalization reaction are too sterically hindered.

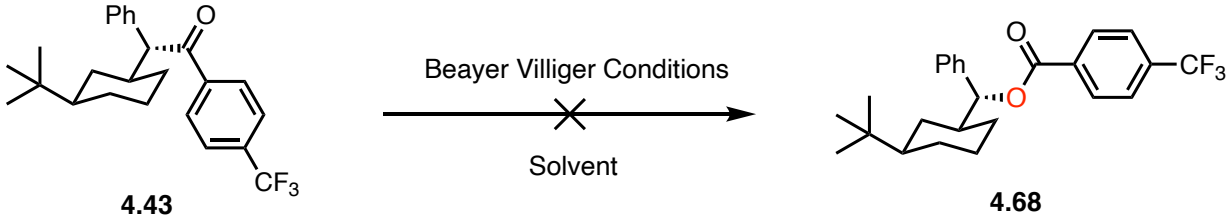

4.43 **4.68**

Entry	Conditions	yield (%)
1	*m*CPBA, $NaHCO_3$, CH_2Cl_2, 40 °C	0
2	*m*CPBA, $NaHCO_3$, DCE, 80 °C	0
3	*m*CPBA, HFIP CH_2Cl_2, phosphate buffer	0
4	NaBARF, H_2O_2, DCE, 50 °C	0
5	$LiB(C_6F_5)_4 \cdot 2.5Et_2O$, H_2O_2, DCE, 50 °C	0
6	2 $Na_2CO_3 \cdot 3\ H_2O_2$, TFA	0
7	$Bi(OTf)_3$, *m*CPBA, CH_2Cl_2	0
8	$AlCl_3$, H_2O_2, ethanol	0
9	TFAA, H_2O_2, Na_2HPO_4, CH_2Cl_2	0

Table 4.5 Baeyer-Villiger oxidation screen against functionalized *tert*-butylcyclohexane product

Undeterred by the failed Baeyer-Villiger oxidations, we turned our attention to the Beckmann-rearrangement. Due to the potential steric hindrance, that was seen in the Baeyer-Villiger oxidation attempts, we chose to carry forward the hexene functionalized product **4.34** through the Beckmann-rearrangement synthesis. Notably, Terrence Nguyen was the only one to

work on the Beckmann-rearrangement and therefore all the results that will be discussed were performed by him. The synthesis starts with the functionalized product **4.34** being subjected to ketoxime formation via condensation with hydroxylamine (Scheme 4.9). Formation of the ketoxime **4.69** performs in great yield (87%) and results in a mixture of *E/Z* isomers in a ratio of 3.8:1. Using the ^{1}H NMR we propose the minor isomer is the desired ketoxime that is desired to undergo Beckmann-rearrangment. Subjecting ketoxime **4.69** to Beckmann-rearrangement conditions[65] with tosyl chloride furnished a 20% yield for the desired benzylamide **4.70**. Since the desired ketoxime was approximately 20% of the E/Z mixture, it is hypothesized that the minor isomer quantitatively rearranges to the benzylamide, while the major ketoxime has an undesired reactivity. Currently we are trying to synthesize the desire ketoxime cleanly to test this hypothesis. Notably, the chiral benzylamide formed is generated in 96% ee with stereoretention. Excitingly Terrence Nguyen was able to confirm the absolute stereochemistry with an X-ray crystal structure.

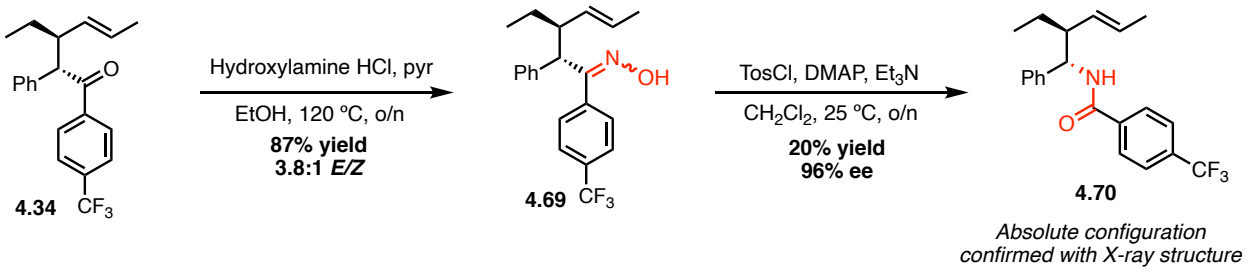

Scheme 4.9 Beckmann-rearrangement of C-H insertion product to access chiral benzylamides

4.3. Conclusion

In conclusion, we have developed a new donor/acceptor diazo compound competent in intermolecular C-H functionalization of a wide array of activated and unactivated C-H bonds. Optimization of the ketone/catalyst pairing led us to a highly selective system using an α-aryl-α-diazoketone and Rh_2(*S*-TPPTTL)$_4$, often outperforming what can be achieved with the established

aryldiazoacetate systems. Following functionalization, we demonstrated this new ketone handle can be used to synthesize chiral benzylamides, allowing access to new chemical space unseen by the previous diazoesters. However, this particular step needs further optimization for it to be broadly useful. This space includes a plethora of functionalized chiral building blocks with orthogonal handles, useful for medicinal chemistry libraries and total synthesis applications. Ultimately our aryl diazoketone expands our toolbox of carbenes compatible under dirhodium catalyzed C-H functionalization.

4.4. Distribution of Credit

The work reported in this chapter is in collaboration with several members from the Davies lab: Dr. Jiantao Fu, Camila Suarez and Terrence-Thang H. Nguyen. This project was initiated by myself in thinking about how I could utilize different donor/acceptor diazo compounds for the cylindrocyclophane synthesis. When optimizing the reaction, I achieved the breakthrough result with **4.6** discovering the necessity of an aryl ketone. I found the best catalyst was Rh_2(*S*-TPPTTL)$_4$, which was developed by Dr. Jiantao Fu, hence the two of us collaborated on this project as it stems from innovation from both of us. Dr. Jiantao Fu helped with the initial optimization and substrate scope, as well as some of the Baeyer-Villiger screening. Once he graduated, I mentored an undergraduate Camila Suarez during part of the studies, where she contributed to the rest of the substrate scope. Notably, all the reactions conducted by Dr. Jiantao Fu and Camila Suarez were all evaluated by me. Terrence Nguyen joined the project at the start of 2021 and was critical to finalizing the optimization and screening the diazoketone scope with 4-ethyltoluene. Terrence Nguyen synthesized the majority of the diazoketones, where together we looked at changes to the acceptor side, while only Terrence synthesized and evaluated modifications to the donor ring.

Additionally, Terrence Nguyen assisted in the Bayer-Villiger screening and was the sole person to evaluate the Beckmann-rearrangement. A manuscript is in preparation of the current findings in this chapter, and it has been co-written by me and Dr. Jiantao Fu.

4.5. References

1. Davies, H. M. L.; Manning, J. R., Catalytic C–H functionalization by metal carbenoid and nitrenoid insertion. *Nature* **2008,** *451* (7177), 417-424.
2. Davies, H. M. L., Finding Opportunities from Surprises and Failures. Development of Rhodium-Stabilized Donor/Acceptor Carbenes and Their Application to Catalyst-Controlled C–H Functionalization. *J. Org. Chem.* **2019,** *84* (20), 12722-12745.
3. Davies, H. M. L.; Liao, K., Dirhodium tetracarboxylates as catalysts for selective intermolecular C–H functionalization. *Nat. Rev. Chem.* **2019,** *3* (6), 347-360.
4. Davies, H. M. L.; Du Bois, J.; Yu, J.-Q., C–H Functionalization in organic synthesis. *Chem. Soc. Rev.* **2011,** *40* (4), 1855-1856.
5. Davies, H. M. L.; Panaro, S. A., Effect of Rhodium Carbenoid Structure on Cyclopropanation Chemoselectivity. *Tetrahedron* **2000,** *56* (28), 4871-4880.
6. Hansen, J.; Autschbach, J.; Davies, H. M. L., Computational Study on the Selectivity of Donor/Acceptor-Substituted Rhodium Carbenoids. *J. Org. Chem.* **2009,** *74* (17), 6555-6563.
7. Davies, H. M. L.; Alford, J. S., Reactions of metallocarbenes derived from N-sulfonyl-1,2,3-triazoles. *Chem. Soc. Rev.* **2014,** *43* (15), 5151-5162.
8. Kubiak, R. W.; Mighion, J. D.; Wilkerson-Hill, S. M.; Alford, J. S.; Yoshidomi, T.; Davies, H. M. L., Enantioselective Intermolecular C–H Functionalization of Allylic and Benzylic sp3 C–H Bonds Using N-Sulfonyl-1,2,3-triazoles. *Org. Lett.* **2016,** *18* (13), 3118-3121.
9. Garlets, Z. J.; Davies, H. M. L., Harnessing the β-Silicon Effect for Regioselective and Stereoselective Rhodium(II)-Catalyzed C–H Functionalization by Donor/Acceptor Carbenes Derived from 1-Sulfonyl-1,2,3-triazoles. *Org. Lett.* **2018,** *20* (8), 2168-2171.
10. Kubiak, R. W.; Davies, H. M. L., Rhodium-Catalyzed Intermolecular C–H Functionalization as a Key Step in the Synthesis of Complex Stereodefined β-Arylpyrrolidines. *Org. Lett.* **2018,** *20* (13), 3771-3775.
11. Vaitla, J.; Boni, Y. T.; Davies, H. M. L., Distal Allylic/Benzylic C−H Functionalization of Silyl Ethers Using Donor/Acceptor Rhodium(II) Carbenes. *Angew. Chem. Int. Ed.* **2020,** *59* (19), 7397-7402.
12. Davies, H. M. L.; Hopper, D. W.; Hansen, T.; Liu, Q.; Childers, S. R., Synthesis of methylphenidate analogues and their binding affinities at dopamine and serotonin transport sites. *Bioorg. Med. Chem. Letters* **2004,** *14* (7), 1799-1802.
13. Davies, H. M. L.; Ni, A., Enantioselective synthesis of β-amino esters and its application to the synthesis of the enantiomers of the antidepressant Venlafaxine. *Chem. Comm.* **2006,** (29), 3110-3112.
14. Davies, H. M. L.; Dai, X.; Long, M. S., Combined C−H Activation/Cope Rearrangement as a Strategic Reaction in Organic Synthesis: Total Synthesis of (−)-Colombiasin A and (−)-Elisapterosin B. *J. Am. Chem. Soc.* **2006,** *128* (7), 2485-2490.

15. Schwartz, B. D.; Denton, J. R.; Lian, Y.; Davies, H. M. L.; Williams, C. M., Asymmetric [4 + 3] Cycloadditions between Vinylcarbenoids and Dienes: Application to the Total Synthesis of the Natural Product (−)-5-epi-Vibsanin E. *J. Am. Chem. Soc.* **2009,** *131* (23), 8329-8332.
16. Wang, H.; Li, G.; Engle, K. M.; Yu, J.-Q.; Davies, H. M. L., Sequential C–H Functionalization Reactions for the Enantioselective Synthesis of Highly Functionalized 2,3-Dihydrobenzofurans. *J. Am. Chem. Soc.* **2013,** *135* (18), 6774-6777.
17. Bedell, T. A.; Hone, G. A. B.; Valette, D.; Yu, J.-Q.; Davies, H. M. L.; Sorensen, E. J., Rapid Construction of a Benzo-Fused Indoxamycin Core Enabled by Site-Selective C−H Functionalizations. *Angew. Chem. Int. Ed.* **2016,** *55* (29), 8270-8274.
18. Gutekunst, W. R.; Baran, P. S., C–H functionalization logic in total synthesis. *Chem. Soc. Rev.* **2011,** *40* (4), 1976-1991.
19. Renz, M.; Meunier, B., 100 Years of Baeyer–Villiger Oxidations. *Eur. J. Org. Chem.* **1999,** *1999* (4), 737-750.
20. Kaur, K.; Srivastava, S., Beckmann rearrangement catalysis: a review of recent advances. *New J. Chem.* **2020,** *44* (43), 18530-18572.
21. Arora, R.; Kashyap, K.; Mittal, A.; Kakkar, R., Synthesis and Reactions of Diazoketones. *Org. Prep. Proced. Int.* **2019,** *51* (2), 103-146.
22. Taber, D. F.; Tian, W., Rhodium-Catalyzed Intramolecular C−H Insertion of α-Aryl-α-diazo Ketones. *J. Org. Chem.* **2007,** *72* (9), 3207-3210.
23. Xu, B.; Zhu, S.-F.; Zuo, X.-D.; Zhang, Z.-C.; Zhou, Q.-L., Enantioselective N-H Insertion Reaction of α-Aryl α-Diazoketones: An Efficient Route to Chiral α-Aminoketones. *Angew. Chem. Int. Ed.* **2014,** *53* (15), 3913-3916.
24. Marcoux, D.; Lindsay, V. N. G.; Charette, A. B., Use of achiral additives to increase the stereoselectivity in Rh(ii)-catalyzed cyclopropanations. *Chem. Comm.* **2010,** *46* (6), 910-912.
25. Lindsay, V. N. G.; Nicolas, C.; Charette, A. B., Asymmetric Rh(II)-Catalyzed Cyclopropanation of Alkenes with Diacceptor Diazo Compounds: p-Methoxyphenyl Ketone as a General Stereoselectivity Controlling Group. *J. Am. Chem. Soc.* **2011,** *133* (23), 8972-8981.
26. Denton, J. R.; Davies, H. M. L., Enantioselective Reactions of Donor/Acceptor Carbenoids Derived from α-Aryl-α-Diazoketones. *Org. Lett.* **2009,** *11* (4), 787-790.
27. Lumbroso, A.; Cooke, M. L.; Breit, B., Catalytic Asymmetric Synthesis of Allylic Alcohols and Derivatives and their Applications in Organic Synthesis. *Angew. Chem. Int. Ed.* **2013,** *52* (7), 1890-1932.
28. Cho, B. T., Recent development and improvement for boron hydride-based catalytic asymmetric reduction of unsymmetrical ketones. *Chem. Soc. Rev.* **2009,** *38* (2), 443-452.
29. Liu, Y.-L.; Lin, X.-T., Recent Advances in Catalytic Asymmetric Synthesis of Tertiary Alcohols via Nucleophilic Addition to Ketones. *Adv. Synth. Catal.* **2019,** *361* (5), 876-918.
30. Moore, J. C.; Pollard, D. J.; Kosjek, B.; Devine, P. N., Advances in the Enzymatic Reduction of Ketones. *Acc. Chem. Res.* **2007,** *40* (12), 1412-1419.
31. Shende, V. S.; Singh, P.; Bhanage, B. M., Recent trends in organocatalyzed asymmetric reduction of prochiral ketones. *Catal. Sci. Technol.* **2018,** *8* (4), 955-969.
32. Chen, W.; Tan, C.-H.; Wang, H.; Ye, X., The Development of Organocatalytic Asymmetric Reduction of Carbonyls and Imines Using Silicon Hydrides. *Eur. J. Org. Chem.* **2021,** *2021* (21), 3091-3112.

33. Bøgevig, A.; Pastor, I. M.; Adolfsson, H., Highly Enantioselective Ruthenium-Catalyzed Reduction of Ketones Employing Readily Available Peptide Ligands. *Chem. Eur. J.* **2004,** *10* (1), 294-302.
34. Lundberg, H.; Tinnis, F.; Selander, N.; Adolfsson, H., Catalytic amide formation from non-activated carboxylic acids and amines. *Chem. Soc. Rev.* **2014,** *43* (8), 2714-2742.
35. Roughley, S. D.; Jordan, A. M., The Medicinal Chemist's Toolbox: An Analysis of Reactions Used in the Pursuit of Drug Candidates. *J. Med. Chem.* **2011,** *54* (10), 3451-3479.
36. DeCroos, P.; Han, Z. S.; Sidhu, K.; Lorenz, J.; Nummy, L.; Byrne, D.; Qu, B.; Xu, Y.; Wu, L.; Lee, H.; Roschangar, F.; Song, J. J.; Senanayake, C. H., Development of a Large-Scale Asymmetric Process for tert-Butanesulfinamide. *Org. Process Res. Dev.* **2019,** *23* (2), 263-268.
37. Rajput, P.; Sharma, A., Synthesis and biological importance of amide analogues. *J. Pharmacol Med. Chem.* **2018,** *2* (2), 22-31.
38. Piazzolla, F.; Temperini, A., Recent advances in chemoselective acylation of amines. *Tetrahedron Lett.* **2018,** *59* (27), 2615-2621.
39. Collet, F.; Dodd, R. H.; Dauban, P., Catalytic C–H amination: recent progress and future directions. *Chem. Comm.* **2009,** (34), 5061-5074.
40. Hayashi, H.; Uchida, T., Nitrene Transfer Reactions for Asymmetric C–H Amination: Recent Development. *Eur. J. Org. Chem.* **2020,** *2020* (8), 909-916.
41. Chiappini, N. D.; Mack, J. B. C.; Du Bois, J., Intermolecular C(sp3)−H Amination of Complex Molecules. *Angew. Chem. Int. Ed.* **2018,** *57* (18), 4956-4959.
42. Lebel, H.; Huard, K.; Lectard, S., N-Tosyloxycarbamates as a Source of Metal Nitrenes: Rhodium-Catalyzed C−H Insertion and Aziridination Reactions. *J. Am. Chem. Soc.* **2005,** *127* (41), 14198-14199.
43. Singh, R.; Kolev, J. N.; Sutera, P. A.; Fasan, R., Enzymatic C(sp3)-H Amination: P450-Catalyzed Conversion of Carbonazidates into Oxazolidinones. *ACS Catal.* **2015,** *5* (3), 1685-1691.
44. Athavale, S. V.; Gao, S.; Liu, Z.; Mallojjala, S. C.; Hirschi, J. S.; Arnold, F. H., Biocatalytic, Intermolecular C−H Bond Functionalization for the Synthesis of Enantioenriched Amides. *Angew. Chem. Int. Ed.* **2021,** *60* (47), 24864-24869.
45. Jia, Z.-J.; Gao, S.; Arnold, F. H., Enzymatic Primary Amination of Benzylic and Allylic C(sp3)–H Bonds. *J. Am. Chem. Soc.* **2020,** *142* (23), 10279-10283.
46. Liu, Z.; Arnold, F. H., New-to-nature chemistry from old protein machinery: carbene and nitrene transferases. *Curr. Opin. Biotechnol.* **2021,** *69*, 43-51.
47. Kirmse, W., 100 Years of the Wolff Rearrangement. *Eur. J. Org. Chem.* **2002,** *2002* (14), 2193-2256.
48. Phelps, R.; Orr-Ewing, A. J., Direct Observation of Ylide and Enol Intermediates Formed in Competition with Wolff Rearrangement of Photoexcited Ethyl Diazoacetoacetate. *J. Am. Chem. Soc.* **2020,** *142* (17), 7836-7844.
49. Zhang, C.; Wang, X.; Jiao, N., Copper-Catalyzed Aerobic Oxidative C—C Bond Cleavage of 1,3-Diaryl-diketones to Synthesize 1,2-Diketones. *ChemInform* **2014,** *45* (50).
50. Gomtsyan, A.; Schmidt, R. G.; Bayburt, E. K.; Gfesser, G. A.; Voight, E. A.; Daanen, J. F.; Schmidt, D. L.; Cowart, M. D.; Liu, H.; Altenbach, R. J.; Kort, M. E.; Clapham, B.; Cox, P. B.; Shrestha, A.; Henry, R.; Whittern, D. N.; Reilly, R. M.; Puttfarcken, P. S.; Brederson, J.-D.; Song, P.; Li, B.; Huang, S. M.; McDonald, H. A.; Neelands, T. R.; McGaraughty, S. P.; Gauvin, D. M.; Joshi, S. K.; Banfor, P. N.; Segreti, J. A.; Shebley, M.;

Faltynek, C. R.; Dart, M. J.; Kym, P. R., Synthesis and Pharmacology of (Pyridin-2-yl)methanol Derivatives as Novel and Selective Transient Receptor Potential Vanilloid 3 Antagonists. *J. Med. Chem.* **2016,** *59* (10), 4926-4947.
51. Wertz, B.; Ren, Z.; Bacsa, J.; Musaev, D. G.; Davies, H. M. L., Comparison of 1,2-Diarylcyclopropanecarboxylates with 1,2,2-Triarylcyclopropanecarboxylates as Chiral Ligands for Dirhodium-Catalyzed Cyclopropanation and C–H Functionalization. *J. Org. Chem.* **2020,** *85* (19), 12199-12211.
52. Davies, H. M. L.; Jin, Q.; Ren, P.; Kovalevsky, A. Y., Catalytic Asymmetric Benzylic C−H Activation by Means of Carbenoid-Induced C−H Insertions. *J. Org. Chem.* **2002,** *67* (12), 4165-4169.
53. Qin, C.; Davies, H. M. L., Role of Sterically Demanding Chiral Dirhodium Catalysts in Site-Selective C–H Functionalization of Activated Primary C–H Bonds. *J. Am. Chem. Soc.* **2014,** *136* (27), 9792-9796.
54. Garlets, Z. J.; Wertz, B. D.; Liu, W.; Voight, E. A.; Davies, H. M. L., Regio- and Stereoselective Rhodium(II)-Catalyzed C–H Functionalization of Cyclobutanes. *Chem* **2020,** *6* (1), 304-313.
55. Davies, H. M. L.; Hansen, T.; Churchill, M. R., Catalytic Asymmetric C−H Activation of Alkanes and Tetrahydrofuran. *J. Am. Chem. Soc.* **2000,** *122* (13), 3063-3070.
56. Fu, J.; Ren, Z.; Bacsa, J.; Musaev, D. G.; Davies, H. M. L., Desymmetrization of cyclohexanes by site- and stereoselective C–H functionalization. *Nature* **2018,** *564* (7736), 395-399.
57. ten Brink, G. J.; Arends, I. W. C. E.; Sheldon, R. A., The Baeyer−Villiger Reaction: New Developments toward Greener Procedures. *Chem. Rev.* **2004,** *104* (9), 4105-4124.
58. Alam, M. M.; Varala, R.; Adapa, S. R., Bi(OTf)3-Catalyzed Baeyer–Villiger Oxidation of Carbonyl Compounds with m -CPBA. *Synth. Commun.* **2003,** *33* (17), 3035-3040.
59. Wang, Y.; Wang, Q.; He, J.; Zhang, Y., Highly effective C–C bond cleavage of lignin model compounds. *Green Chem.* **2017,** *19* (13), 3135-3141.
60. Uyanik, M.; Ishihara, K., Baeyer–Villiger Oxidation Using Hydrogen Peroxide. *ACS Catal.* **2013,** *3* (4), 513-520.
61. Uyanik, M.; Nakashima, D.; Ishihara, K., Baeyer–Villiger Oxidation and Oxidative Cascade Reactions with Aqueous Hydrogen Peroxide Catalyzed by Lipophilic Li[B(C6F5)4] and Ca[B(C6F5)4]2. *Angew. Chem. Int. Ed.* **2012,** *51* (36), 9093-9096.
62. Burton, J. W.; Clark, J. S.; Derrer, S.; Stork, T. C.; Bendall, J. G.; Holmes, A. B., Synthesis of Medium Ring Ethers. 5. The Synthesis of (+)-Laurencin. *J. Am. Chem. Soc.* **1997,** *119* (32), 7483-7498.
63. Kjonaas, R. A.; Clemons, A. E., The Baeyer–Villiger Oxidation with Trifluoroacetic Acid and Household Sodium Percarbonate. *J. Chem. Educ.* **2008,** *85* (6), 827.
64. Lei, Z.; Ma, G.; Wei, L.; Yang, Q.; Su, B., Clean Baeyer–Villiger Oxidation Using Hydrogen Peroxide as Oxidant Catalyzed by Aluminium Trichloride in Ethanol. *Catal. Lett.* **2008,** *124* (3), 330-333.
65. White, J. D.; Choi, Y., Catalyzed Asymmetric Diels−Alder Reaction of Benzoquinone. Total Synthesis of (−)-Ibogamine. *Org. Lett.* **2000,** *2* (15), 2373-2376.

Experimental Section

5.1. General Considerations

Reactions were carried out under nitrogen in flame-dried unless otherwise specified. Dichloromethane, diethyl ether, tetrahydrofuran, and toluene were purified using a *Glass Contour Solvent System.* Dichloromethane used for C–H functionalization reactions was distilled under nitrogen from calcium hydride onto 4Å molecular sieves and stored under nitrogen for 24 h prior to use. Flash column chromatography was performed on Silicycle SiliaFlash P60 silica gel (60 Å pore size, 40–63 μm particle size, 230–400 mesh) and ACS reagent grade solvents. Reactions were monitored by thin layer chromatography (TLC) carried out on with aluminum-sheet or glass-backed silica gel plates, visualizing with UV light, and staining with aqueous KMnO4.

All ^{1}H NMR spectra were recorded at either 400 MHz, 500 MHz, or 600 MHz on Varian-400, Varian-500, or Bruker-600 spectrometers. ^{13}C NMR spectra were recorded at either 101 MHz, 126 MHz, or 151 MHz on Varian-400, Varian-500, or Bruker-600 spectrometers. ^{19}F NMR spectra were recorded at 282, 376 or 565 MHz on Varian-300, Varian-400 or Bruker-600 spectrometer. NMR spectra were obtained from solutions of $CDCl_3$ 0.03% TMS, C_6D_6, MeOD, and AcOD-d_4 with residual solvent serving as internal standard (7.26 ppm for ^{1}H or 0.00ppm and 77.16 ppm for ^{13}C in $CDCl_3$, 7.16 ppm for ^{1}H and 128.06 for ^{13}C in C_6D_6, 3.31 ppm for ^{1}H and 49.00 for ^{13}C in MeOD, and 2.04 ppm for ^{1}H and 20.0 for ^{13}C in AcOD-d_4). NMR shifts were reported in parts per million (d ppm). Abbreviations for signal multiplicity are as follow: s = singlet, d = doublet, t = triplet, q = quartet, m = multiplet, brs = broad singlet, dd = doublet of doublet, etc. Coupling constants (J values) were calculated directly from the spectra.

All reagents were purchased from commercial sources (Sigma Aldrich, Thermo Fisher, TCI Chemicals, AK Scientific, Oakwood Chemical, Acros Organics, Combi- Blocks, Strem, Enamine, and Santa Cruz Biotechnology) and used as received without purification. IR spectra were collected on a Nicolet iS10 FT-IR spectrometer (cm^{-1}). Optical rotations were measured on Jasco P-2000 polarimeters. Mass spectra were taken on a Thermo Finnigan LTQ-FTMS spectrometer with APCI, ESI or NSI by the Department of Chemistry at Emory University. Racemic standards were generated by performing reactions with the appropriate racemic dirhodium catalyst for the reaction by dissolving an equimolar mixture of the R and S catalyst in a minimal amount of dichloromethane and concentrating under vacuum. The enantiomeric excess (ee) was determined by High performance liquid chromatography analysis was performed on either Varian Prostar chiral HPL instrument, Agilent 1100 Technologies HPLC instruments, or Agilent Technologies 1290 Infinity UHPLC instrument, and the data outlined below varies in presentation based on the software used for each system. Chiral HPLC conditions were determined by obtaining separation of the racemic products generated using a mixture of the appropriate catalysts. The HPLC instruments used isopropanol/hexane gradient and commercial ChiralPak/ChiralCel columns from Daicel Chemical Industries, notably ChiralPak AD-H (5 μm particle size, 4.6 mm vs. 250 mm), ChiralCel OZ-H (5 μm particle size, 4.6 mm vs. 250 mm), and ChiralCel OD-H (5 μm particle size, 4.6 mm vs. 250 mm), ChiralCel AS-H (5 μm particle size, 4.6 mm vs. 250 mm), and ChiralCel OJ-H (5 μm particle size, 4.6 mm vs. 250 mm).

5.2. Experiment Section for Chapter 2

Substrates and reagents

The following compounds were prepared according to published procedures:

2,2,2-trifluoroethyl 2-diazoacetate[1]

Rh_2(*R*-2-Cl-5-BrTPCP)$_4$[2]

Rh_2[*R*-tris(*p*-^{t}BuC_6H_4)TPCP]$_4$[3]

Rh_2(*R*-p-ph-TPCP)$_4$[4]

5-(trifluoromethyl)-3-pyridinesulfonic acid[5] *(synthesized by Hojoon Park)*

2-heptyl-5-iodo-1,3-phenylene diacetate *(synthesized by Elizabeth Goldstein)*

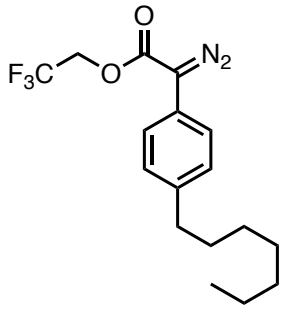

2,2,2-Trifluoroethyl 2-diazo-2-(4-heptylphenyl)acetate

A 250-ml round-bottom flask with stir bar was flame dried under vacuum. Once cool enough all solids were added first: PPh_3 (1.65 mmol, 0.1 equiv.), $Pd(PPh_3)_4$ (0.825 mmol, 0.05 equiv.) and Ag_2CO_3 (8.25 mmol, 0.5 equiv.). After solids added, the reaction vessel was purged with argon three times. Next the liquids were added: toluene (66 ml), Et_3N (21.5 mmol, 1.3 equiv.), 1-heptyl-4-iodobenzene (16.5 mmol, 1 equiv.), and finally the 2,2,2-trifluoroethyl 2-diazoacetate (21.5 mmol, 1.3 equiv.) was added last. The resulted mixture was stirred at room temperature (23 ^{o}C) for 5 h and then, filtered through a short silica plug (3.5 cm *diameter*, 5 cm *height*), eluting with ethyl acetate until elutes clear. The crude product was concentrated and purified by column chromatography (5% ether in pentane) to afford the product as a yellow oil (87% yield). This compound is disclosed in a publication.[2]

Rf = 0.71 (pentane/diethyl ether = 9/1);

^{1}H NMR (600 MHz, $CDCl_3$) δ 7.36 (d, *J* = 8.3 Hz, 2H), 7.22 (d, *J* = 8.2 Hz, 2H), 4.65 (q, *J* = 8.4 Hz, 2H), 2.60 (t, *J* = 7.6 Hz, 2H), 1.63 – 1.57 (m, 2H), 1.36 – 1.22 (m, 8H), 0.87 (t, *J* = 6.6 Hz 3H);

^{13}C NMR (125 MHz, $CDCl_3$) δ 163.4, 141.5, 129.1, 124.3, 122.9 (q, *J* = 277.6 Hz), 121.3, 60.3 (q, *J* = 36.9 Hz), 35.4, 31.7, 31.2, 29.1, 29.1, 22.6, 13.9 (The resonance resulting from the diazo carbon was not observed);

^{19}F NMR (282 MHz, $CDCl_3$) δ -73.9 (t, *J* = 8.4 Hz);

IR (neat) 2957, 2927, 2856, 2089, 1715, 1515, 1456, 1410, 1350, 1280, 1242, 1167, 1137, 1074, 1020, 974, 923, 839, 810, 733, 653 cm^{-1};

HRMS (+p NSI) calcd for $C_{17}H_{22}F_3N_2O_2$ $(M+H)^+$ 343.1628 found 343.08576.

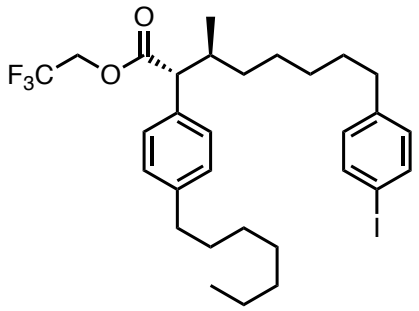

2,2,2-Trifluoroethyl (2*R*,3*S*)-2-(4-heptylphenyl)-8-(4-iodophenyl)-3-methyloctanoate

A 50-ml flame-dried round-bottom flask with condenser was charged with 4 Å MS and Rh_2(*R*-2-Cl-5-BrTPCP)$_4$ (0.02 mmol, 1.0 mol%) and then, purged three times with argon. 1-n-Heptyl-4-iodobenzene (6.29 mmol, 3.0 equiv.) and distilled CH_2Cl_2 (8 ml) were added next, then the mixture was heated to 40 ºC and refluxed for at least 15 min before addition of the diazo compounds. Next, 2,2,2-Trifluoroethyl 2-diazo-2-(4-heptylphenyl)acetate (2.09 mmol, 1.0 equiv.) was purged under argon in a 20-mL scintillation vial, then diluted with distilled CH_2Cl_2 (8 ml). Then, under reflux conditions and argon atmosphere, the diazo solution was added to the reaction vessel dropwise via syringe pump over 3 h. The reaction mixture was stirred at 40 ºC for another 30 min, and concentrated under vacuum for crude ^{1}H NMR. The crude product was purified by flash column chromatography (3% ether in pentane) to afford as an opaque oil (83% yield, >30:1 rr, 26: dr, 91% ee). This compound is disclosed in a publication.[2]

Note: Solvent must be carefully dried (distilled over CaH_2 and stored on activated 4 Å MS).

Rf = 0.71 (pentane/diethyl ether = 19/1);

$[\alpha]^{20}_D$: -18.6° (c = 1.00, $CHCl_3$, 91% ee);

^{1}H NMR (600 MHz, $CDCl_3$) δ 7.56 (d, *J* = 8.2 Hz, 2H), 7.20 (d, *J* = 8.0 Hz, 2H), 7.12 (d, *J*= 8.0 Hz 2H), 6.86 (d, *J*= 8.1 Hz, 2H), 4.55 (dq, *J* = 8.5, 4.1 Hz, 1H), 4.29 (dq, *J* = 8.5, 4.2 Hz, 1H), 3.32 (d, *J* = 10.9 Hz, 1H), 2.57 (t, *J*= 7.6 Hz, 2H), 2.45 (t, *J* = 7.7 Hz, 2H), 2.23 – 2.16 (m, 1H), 1.63 – 1.56 (m, 2H), 1.51 – 1.41 (m 2H), 1.34 – 1.23 (m, 10H), 1.22 – 1.09 (m, 4H), 1.00 (d, *J* = 6.7 Hz, 3H), 0.88 (t, *J* = 6.7 Hz, 3H);

^{13}C NMR (125 MHz, $CDCl_3$) δ 172.5, 142.3, 137.2, 134.1, 130.5, 128.6, 128.4, 123.0 (q, *J* = 277.2 Hz), 90.5, 60.2 (q, *J* = 36.5 Hz), 57.9, 36.2, 35.6, 35.3, 33.1, 31.8, 31.3, 31.0, 29.3, 29.2, 29.0, 26.0, 22.7, 17.7, 14.1;

^{19}F NMR (282 MHz, $CDCl_3$) δ -73.7 (t, *J* = 8.5 Hz);

IR (neat) 2927,2855,1753,1484,1464,1400,1278,1165,1128,1061,1006,979,824,793,737cm^{-1};

HRMS (+p NSI) calcd for $C_{30}H_{41}O_2IF_3$ $(M+H)^+$ 617.2098 found 617.20986;

HPLC (R,R-Whelk column, 0 % *i*-propanol in hexane, 1 mL min^{-1}, 1 mg mL^{-1}, 30 min, UV 210 nm) retention times of 14.9 min (major) and 17.6 min (minor) 91% ee with Rh_2(*R*-2-Cl-5-BrTPCP)$_4$.

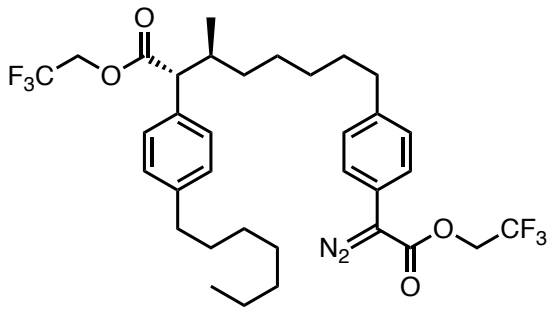

2,2,2-Trifluoroethyl (2*R*,3*S*)-8-(4-(1-diazo-2-oxo-2-(2,2,2-trifluoroethoxy)ethyl)phenyl)-2-(4-heptylphenyl)-3-methyloctanoate

A 50-ml round-bottom flask with stir bar was flame dried under vacuum. Once cool enough all solids were added first: PPh_3 (0.129 mmol, 0.1 equiv.), $Pd(PPh_3)_4$ (0.065 mmol, 0.05 equiv.) and Ag_2CO_3 (0.645 mmol, 0.5 equiv.). After solids added, the reaction vessel was purged with argon three times. Next the liquids were added: toluene (5.2 ml), Et_3N (1.67 mmol, 1.3 equiv.), 2,2,2-Trifluoroethyl (2*R*,3*S*)-2-(4-heptylphenyl)-8-(4-iodophenyl)-3-methyloctanoate (1.29 mmol, 1 equiv.), and finally the 2,2,2-trifluoroethyl 2-diazoacetate (1.67 mmol, 1.3 equiv.) was added last. The resulted mixture was stirred at room temperature (23 ^{o}C) for 5 h and then, filtered

through a short silica plug (3.5 cm *diameter*, 5 cm *height*), eluting with ethyl acetate until elutes clear. The crude product was concentrated and purified by column chromatography (2% ether in pentane) to afford product as a yellow oil (81% yield). This compound is disclosed in a publication.[2]

Rf = 0.45 (pentane/diethyl ether = 9/1);

^{1}H NMR (600 MHz, $CDCl_3$) δ 7.34 (d, *J* = 8.3 Hz, 2H), 7.21 (d, *J* = 8.1 Hz, 2H), 7.16 (d, *J* = 8.3 Hz, 2H), 7.12 (d, *J* = 8.1 Hz, 2H), 4.64 (q, *J* = 8.4 Hz, 2H), 4.55 (dq, *J* = 12.7, 8.5 Hz, 1H), 4.29 (dq, *J* = 12.7, 8.5 Hz, 1H), 3.32 (d, *J* = 10.5 Hz, 1H), 2.57 (t, *J*= 7.6 Hz, 2H), 2.51 (t, *J* = 7.7 Hz, 2H), 2.23 – 2.15 (m, 1H), 1.62 – 1.56 (m, 2H), 1.52 – 1.44 (m, 2H), 1.35 – 1.24 (m, 10H), 1.22 – 1.11 (m, 4H), 1.00 (d, *J* = 6.5 Hz, 3H), 0.87 (t, *J* = 7.0 Hz, 3H);

^{13}C NMR (125 MHz, $CDCl_3$) δ 172.5, 142.3, 141.3, 134.1, 129.2, 128.6, 128.4, 124.2, 123.0 (q, *J*= 277.7 Hz), 122.9 (q, *J*= 277.7 Hz), 121.3, 60.3 (q, *J*= 36.9 Hz), 60.2 (q, *J*= 36.6 Hz), 57.9, 36.2, 35.6, 35.3, 33.1, 31.8, 31.3, 31.1, 29.3, 29.2, 29.1, 26.0, 22.7, 17.7, 14.1;

^{19}F NMR (282 MHz, $CDCl_3$) δ -73.7 (t, *J* = 8.5 Hz), -73.9 (t, *J* = 8.3 Hz);

IR (neat) 2928, 2856, 2090, 1753, 1717, 1514, 1456, 1409, 1350, 1279, 1242, 1165, 1135, 1074, 976, 923, 839, 733 cm^{-1};

HRMS (+p NSI) calcd for $C_{34}H_{41}O_4N_2F_6$ $(M-H)^-$ 655.2976 found 655.29807;

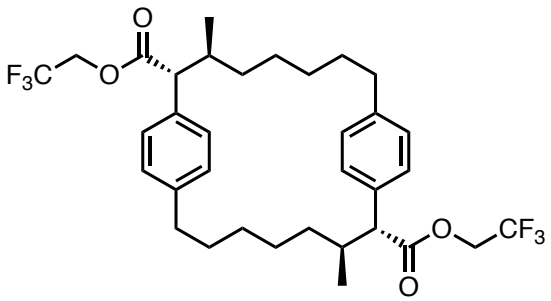

Bis(2,2,2-trifluoroethyl) (2*R*,3*S*,10*R*,11*S*)-3,11-dimethyl-1,9(1,4)-dibenzenacyclohexadecaphane-2,10-dicarboxylate

A 100-ml flame-dried round-bottom flask with condenser were charged with 4 Å MS and Rh_2(*R*-2-Cl-5-BrTPCP)$_4$ (0.01 mmol, 1.0 mol%), then purged three times under argon. Distilled CH_2Cl_2 (10.5 ml) was added using oven dried syringes, then the mixture was heated to 40 °C and

refluxed for at least 15 min before addition of the diazo compounds. Next, 2,2,2-Trifluoroethyl (2*R*,3*S*)-8-(4-(1-diazo-2-oxo-2-(2,2,2-trifluoroethoxy)ethyl)phenyl)-2-(4-heptylphenyl)-3-methyloctanoate (1.04 mmol, 1.0 equiv.) was purged under argon in a 20-mL scintillation vial, then diluted with distilled CH_2Cl_2 (10.5 ml). Then, under reflux conditions and argon atmosphere, the diazo solution was added to the reaction vessel dropwise via syringe pump over 3 h. The reaction mixture was stirred at 40 °C for another 30 min, and concentrated under vacuum for crude ^{1}H NMR. The crude product was purified by flash column chromatography (3% ether in pentane) to afford the product as a white solid (73% yield, 5.6:1 dr, >99% ee). This compound is disclosed in a publication.[2]

Note: Solvent must be carefully dried (distilled over CaH_2 and stored on activated 4 Å MS).

m.p. 141-143 °C

Rf = 0.45 (pentane/diethyl ether = 9/1);

$[\alpha]^{20}_D$: -11.0 ° (c = 1.00, $CHCl_3$, 5.6:1 d.r., >99% ee);

^{1}H NMR (600 MHz, $CDCl_3$) δ 7.16 (d, *J* = 8.0 Hz, 4H), 7.01 (d, *J* = 8.1 Hz, 4H), 4.55 (dq, *J* = 12.7, 8.5 Hz, 2H), 4.27 (dq, *J* = 12.7, 8.4 Hz, 2H), 3.21 (d, *J* = 11.4 Hz, 2H), 2.58 (dt, *J* = 13.1, 6.4 Hz, 2H), 2.42 (dt, *J* = 13.6, 7.6 Hz, 2H), 2.19 – 2.09 (m, 2H), 1.48 – 1.27 (m, 6H), 1.12 – 0.96 (m, 10H), 0.96 – 0.85 (m, 4H), 0.80 – 0.68 (m, 2H);

^{13}C NMR (151 MHz, $CDCl_3$) δ 172.7, 141.8, 134.4, 128.8, 128.2, 122.95 (q, *J* = 277.3 Hz), 60.21 (q, *J* = 36.5 Hz), 58.3, 36.4, 35.5, 32.7, 30.8, 28.3, 26.0, 17.7;

^{19}F NMR (282 MHz, $CDCl_3$) δ -73.7 (t, *J* = 8.5 Hz);

IR (neat) 2929, 2856, 1748, 1403, 1385, 1347, 1303, 1275, 1225, 1160, 1123, 1052, 981, 909, 838, 822, 740, 661 cm^{-1};

HRMS (+p NSI) calcd for $C_{30}H_{42}O_2IF_3$ $(M)^+$ 628.2987 found 628.29995;

HPLC [for better separation, the ester product was reduced to ((2*R*,3*S*,10*R*,11*S*)-3,11-dimethyl-1,9(1,4)-dibenzenacyclohexadecaphane-2,10-diyl)dimethanol, and the pure major diastereomer of the alcohol derivative was obtained via prep HPLC (Ascentis® C18 column, 80% acetonitrile in H_2O with 0.1% trifluoroacetic acid)]

(ADH column, 10 % *i*-propanol in hexane, 1.0 mL min^{-1}, 1 mg mL^{-1}, 80 min, UV 210 nm) retention times of 28.69 min (major) and 60.71 min (minor) >99% ee with Rh_2(*R*-2-Cl-5-BrTPCP)$_4$.

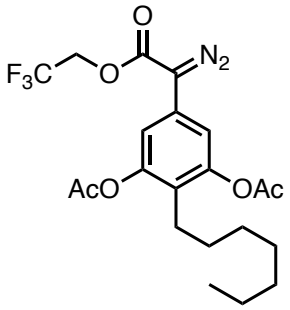

5-(1-diazo-2-oxo-2-(2,2,2-trifluoroethoxy)ethyl)-2-heptyl-1,3-phenylene diacetate

The procedure is adapted from the literature[1]: A 10-ml round-bottom flask with stir bar was flame dried under vacuum. Once cool enough all solids were added first: PPh_3 (6.3 mg, 23.9 μmol, 0.1 equiv.), $Pd(PPh_3)_4$ (13.8 mg, 12.0 μmol, 0.05 equiv.) and Ag_2CO_3 (33.0 mg, 0.12 mmol, 0.5 equiv.). After solids added, the reaction vessel was purged with argon three times. Next the liquids were added: toluene (1.0 ml), Et_3N (0.04 m, 0.311 mmol, 1.3 equiv.), 2-heptyl-5-iodo-1,3-phenylene diacetate (100 mg, 0.239 mmol, 1 equiv.), and finally the 2,2,2-trifluoroethyl 2-diazoacetate (52.2 mg, 0.311 mmol, 1.3 equiv.) was added last. The resulted mixture was stirred at room temperature (23 °C) for 5 h and then, filtered through a short silica plug (3.5 cm *diameter*, 5 cm *height*), eluting with ethyl acetate until elutes clear. The crude product was concentrated and purified by column chromatography (10% ether in pentane) to afford the product as a red oil (70% yield).

Rf = 0.63 (hexane/ether = 1:1)

^{1}H NMR (600 MHz, $CDCl_3$) δ 7.08 (s, 2H), 4.63 (q, *J* = 8.3 Hz, 2H), 2.40 (t, *J* = 7.78 Hz, 2H), 2.32 (s, 6H), 1.46 – 1.41 (m, 2H), 1.32 – 1.23 (m, 8H), 0.88 (t, *J* = 7.23 Hz, 3H).

^{13}C NMR (151 MHz, $CDCl_3$) δ 168.9, 162.6, 150.3, 125.8, 123.5, 122.7 (q, *J* = 277.5 Hz) 115.5, 60.3 (q, *J* = 37.0 Hz), 31.6, 29.5, 28.9, 28.9, 24.6, 22.6, 20.8, 14.1.

IR (neat) 2827, 2858, 2099, 1766, 1624, 1577, 1416, 1369, 1283, 1160, 1108, 1041, 1020, 975, 893, 840 cm^{-1}.

HRMS (+p ESI) calcd for $C_{21}H_{29}F_3N_3O_6$ $(M+NH4)^+$ 476.2003 found 476.2003

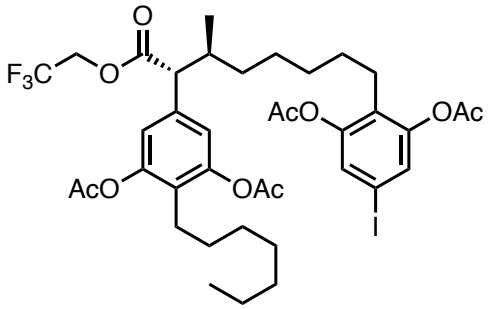

2-((6*S*,7*R*)-7-(3,5-diacetoxy-4-heptylphenyl)-6-methyl-8-oxo-8-(2,2,2-trifluoroethoxy)octyl)-5-iodo-1,3-phenylene diacetate

A 10-ml flame-dried round-bottom flask with condenser was charged with 4 Å MS and Rh_2(*R*-2-Cl-5-BrTPCP)$_4$ (3.92 mg, 2.05 μmol, 1.0 mol %) and then, purged three times with argon. 2-heptyl-5-iodo-1,3-phenylene diacetate (257 mg, 0.614 mmol, 3.0 equiv.) and distilled CH_2Cl_2 (0.8 ml) were added next, then the mixture was heated to 40 °C and refluxed for at least 10 min before addition of the diazo compounds. Next, 5-(1-diazo-2-oxo-2-(2,2,2-trifluoroethoxy)ethyl)-2-heptyl-1,3-phenylene diacetate (94 mg, 0.205 mmol, 1.0 equiv.) was purged under argon in a 20-mL scintillation vial, then diluted with distilled CH_2Cl_2 (0.8 ml). Then, under reflux conditions and argon atmosphere, the diazo solution was added to the reaction vessel dropwise via syringe pump over 3 h. The reaction mixture was stirred at 40 °C for another 30 min and concentrated under vacuum for crude ^{1}H NMR. The crude product was purified by flash column chromatography (5% ether in pentane) to afford the product as an opaque oil (51% yield, 1:1.5 dr).

Rf = 0.36 (hexanes/ether = 1:1)

$[\alpha]^{20}_D$: +1.9° (c = 0.8, $CHCl_3$)

^{1}H NMR (400 MHz, $CDCl_3$) δ 7.29 (s, 2H), 6.93 (s, 2H), 4.61 (dq, *J* = 12.7, 8.5 Hz, 1H), 4.28 (dq, *J* = 12.7, 8.4 Hz, 1H), 3.32 (d, *J* = 10.1 Hz, 1H), 2.38 (dd, *J* = 9.1, 6.7 Hz, 2H), 2.30 (s, 6H), 2.28 (s, 6H), 2.15 – 2.07 (m, 1H), 1.48 – 1.38 (m, 3H), 1.36 – 1.17 (m, 16H), 1.17 – 1.09 (m, 1H), 0.97 (d, *J* = 6.5 Hz, 3H), 0.88 (t, *J* = 7.0 Hz, 3H).

^{13}C NMR (151 MHz, $CDCl_3$) δ 171.6, 168.8, 168.7, 149.9, 149.6, 135.5, 129.2, 127.8, 127.0, 122.8 (q, *J* = 277.3 Hz), 120.3, 88.4, 60.3 (q, *J* = 36.6 Hz), 57.2, 36.7, 33.2, 31.6, 29.6, 29.5, 28.9, 28.8 (d, *J* = 2.2 Hz), 26.0, 24.7 (d, *J* = 7.1 Hz), 22.6, 20.8, 20.7, 17.3, 14.0.

^{19}F NMR (376 MHz, $CDCl_3$) δ -73.6 (dt, *J* = 12.9, 8.4 Hz).

IR (neat) 2928, 2858, 1768, 1595, 1572, 1464, 1431, 1402, 1369, 1278, 1190, 1131, 1109, 1041, 1021, 979, 909 cm^{-1}.

HRMS (+p ESI) calcd for $C_{38}H_{49}F_3IO_{10}$ $(M+H)^+$ 849.2324 found 849.2342

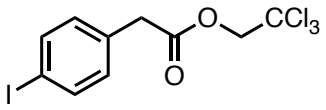

2,2,2-trichloroethyl 2-(4-iodophenyl)acetate

To a 250-ml round bottom flask purged with argon was added the 2,2,2-trichloroethyl 2-(4-iodophenyl)acetate (10.0 g, 38.2 mmol, 1 equiv), DMAP (467 mg, 3.8 mmol, 0.1 equiv), trichloroethanol (4.4 ml, 45.8 mmol, 1.2 equiv) and 84 ml of DCM. Then the reaction mixture was cooled to 0 ºC via ice bath. At 0 ºC, DCC (8.67 g, 42 mmol, 1.1 equiv) was dissolved in 42 ml of DCM and added slowly to the reaction over a few minutes. The reaction mixture was then stirred overnight. Then the reaction was filtered over celite, washing the solid with ether. The filtrate was concentrated and purified by flash column chromatography (hexane/ethyl acetate = 9/1) to provide a white solid (>99% yield). The physical and spectral data were identical to those previously reported for this compound.[6]

^{1}H NMR (400 MHz, $CDCl_3$) δ 7.69 – 7.65 (m, 2H), 7.10 – 7.05 (m, 2H), 4.75 (s, 2H), 3.71 (s, 2H).

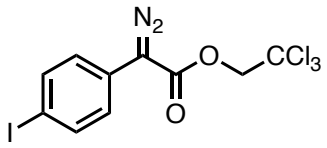

2,2,2-trichloroethyl 2-diazo-2-(4-iodophenyl)acetate

To a flame-dried 100-ml round-bottom flask purged under argon was added 2,2,2-trichloroethyl 2-(4-iodophenyl)acetate (5.0 g, 12.7 mmol, 1.0 equiv), 43 ml of acetonitrile and *o*-NBSA (4.35 g, 19.1 mmol, 1.5 equiv). Then the reaction was cooled to 0 ºC via ice bath and DBU (4.21 ml, 28 mmol, 2.2 equiv) was added dropwise at 0 ºC. The reaction was stirred for 1 hr at 0 ºC. Then the mixture was quenched with sat. NH_4Cl. The layers were separated and then extracted with ether (x3). The organic layer was washed with sat. brine, dried with $MgSO_4$ and concentrated under reduced pressure. The crude residue was purified by flash column chromatography (hexane/diethyl ether = 9/1) to provide an orange solid (93% yield). The physical and spectral data were identical to those previously reported for this compound.[6]

^{1}H NMR (600 MHz, $CDCl_3$) δ 7.73 – 7.70 (m, 2H), 7.28 – 7.23 (m, 2H), 4.91 (s, 2H).

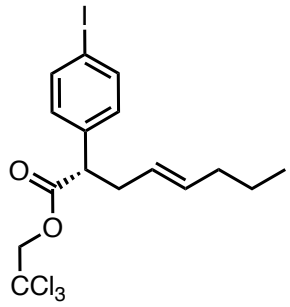

2,2,2-trichloroethyl (*S*,*E*)-2-(4-iodophenyl)oct-4-enoate

A 250-ml flame-dried round-bottom flask with condenser was charged with 4 Å MS and Rh_2(*R*-p-ph-TPCP)$_4$ (52 mg, 0.03 mmol, 0.25 mol%) and then, purged three times with nitrogen. *Trans*-2-hexene (4.5 ml, 35.8 mmol, 3.0 equiv.) and distilled CH_2Cl_2 (48 ml) were added next, then the

mixture was heated to 40 °C and refluxed for at least 10 min before addition of the diazo compounds. Next, 2,2,2-trichloroethyl 2-diazo-2-(4-iodophenyl)acetate (5.0 g, 11.9 mmol, 1.0 equiv.) was purged under nitrogen in a 100-mL round-bottom flask, then diluted with distilled CH_2Cl_2 (48 ml). Then, under reflux conditions and nitrogen atmosphere, the diazo solution was added to the reaction vessel dropwise via syringe pump, or addition funnel with larger scales, over 3 h. The reaction mixture was stirred at 40 °C for another 30 min and concentrated under vacuum for crude ^{1}H NMR. The crude product was purified by flash column chromatography (3% ether in petroleum ether) to afford the product as an opaque oil (96% yield, >20:1 rr, 96% ee). This compound is disclosed in a publication.[7]

Rf = 0.76 (hexane/diethyl ether = 9/1)

$[\alpha]^{20}_D$: +23.5° (c = 0.67, $CHCl_3$)

^{1}H NMR (600 MHz, $CDCl_3$) δ 7.65 (d, *J* = 8.3 Hz, 2H), 7.10 (d, *J* = 8.3 Hz, 2H), 5.50 (ddd, *J* = 15.1, 7.5, 6.0 Hz, 1H), 5.31 (ddd, *J* = 15.3, 7.7, 6.1 Hz, 1H), 4.73 (d, *J* = 12.0 Hz, 1H), 4.67 (d, *J* = 12 Hz, 1H), 3.69 (dd, *J* = 8.4, 7.0 Hz, 1H), 2.80 (dt, *J* = 15.0, 7.8 Hz, 1H), 2.50 (dt, *J* = 13.7, 7.0 Hz, 1H), 1.91 (q, *J* = 7.2 Hz, 2H), 1.31 (h, *J* = 7.3 Hz, 2H), 0.83 (t, *J* = 7.4 Hz, 3H).

^{13}C NMR (151 MHz, $CDCl_3$) δ 171.4, 137.7, 137.3, 134.0, 130.1, 125.6, 94.7, 93.1, 74.1, 51.5, 36.1, 34.5, 30.3, 29.6, 22.4, 13.5.

IR (neat) 2955, 2923, 2854, 2257, 1751, 1586, 1484, 1436, 1403, 1372, 1336, 1258, 1204, 1138, 1062, 1006, 968, 819, 801, 751, 718, 517, 498, 438 cm^{-1}.

HRMS (+p APCI) calcd for $C_{16}H_{19}Cl_3IO_2$ $(M+H)^+$ 474.9495 found 474.9489.

HPLC (ADH, 0.5 % *i*-propanol in hexane, 1 mL min^{-1}, 1 mg mL^{-1}, 30 min, UV 210 nm) retention times of 6.4 min (major) and 7.2 min (minor) 96% *e.e.* with Rh_2(*R*-p-PhTPCP)$_4$.

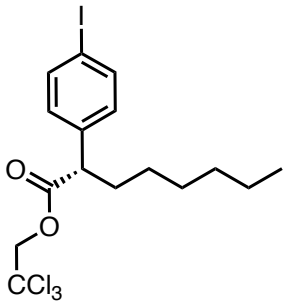

2,2,2-trichloroethyl (*S*)-2-(4-iodophenyl)octanoate

To a 500-ml round-bottom flask flame-dried and purged under nitrogen was added 2,2,2-trichloroethyl (*S*,*E*)-2-(4-iodophenyl)oct-4-enoate (5.37 g, 11.3 mmol, 1.0 equiv), crabtree's catalyst (90.9 mg, 113 μmol, 1.0 mol %) then DCM (113 mL). Then the atmosphere was exchanged with hydrogen and the reaction was run for 2 h. After 2 h crabtree's catalyst (90.9 mg, 113 μmol, 1.0 mol %) was added again and the atmosphere was exchanged with hydrogen then let stir overnight. The reaction mixture was then concentrated under vacuum and purified by flash column chromatography (10% ether in hexane) to afford the product as an opaque oil. (>99% yield).

Rf = 0.8 (hexane/diethyl ether = 9/1)

$[\alpha]^{20}_{D}$: +12.8° (c = 1.0, $CHCl_3$)

^{1}H NMR (600 MHz, $CDCl_3$) δ 7.65 (d, *J* = 8.2 Hz, 2H), 7.10 (d, *J* = 8.2 Hz, 2H), 4.74 (d, *J* = 12 Hz, 1H), 4.67 (d, *J* = 12.0 Hz, 1H), 3.62 (t, *J* = 7.7 Hz, 1H), 2.11 (dtt, *J* = 12.8, 8.3, 4.8 Hz, 1H), 1.81 (dtt, *J* = 12.8, 8.3, 4.8 Hz, 1H), 1.27 (dtt, *J* = 31.4, 14.0, 11.5, 5.0 Hz, 8H), 0.86 (t, *J* = 6.9 Hz, 3H).

^{13}C NMR (151 MHz, $CDCl_3$) δ 171.9, 137.8, 137.7, 130.1, 94.8, 93.0, 74.0, 51.1, 33.0, 31.5, 28.9, 27.3, 22.5, 14.0.

IR (neat) 2953, 2926, 2856, 1751, 1484, 1465, 1403, 1372, 1263, 1200, 1140, 1062, 1007, 821, 793, 758, 719, 572, 500 cm^{-1}.

HRMS (+p APCI) calcd for $C_{16}H_{21}Cl_3IO_2$ $(M+H)^+$ 476.9652 found 476.9646.

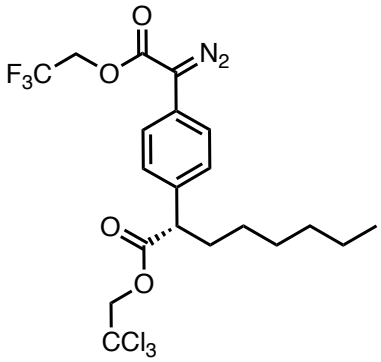

2,2,2-trichloroethyl (*S*)-2-(4-(1-diazo-2-oxo-2-(2,2,2-trifluoroethoxy)ethyl)phenyl)octanoate

The procedure is adapted from the literature[2]: A 250-ml round-bottom flask with stir bar was flame dried under vacuum. Once cool enough all solids were added first: PPh_3 (297 mg, 1.13 mmol, 0.1 equiv.), $Pd(PPh_3)_4$ (653 mg, 0.565 mmol, 0.05 equiv.) and Ag_2CO_3 (1.56 g, 5.65 mmol, 0.5 equiv.). After solids added, the reaction vessel was purged with nitrogen three times. Next the liquids were added: toluene (45 ml), Et_3N (2.05 ml, 14.7 mmol, 1.3 equiv.), 2,2,2-trichloroethyl (*S*)-2-(4-iodophenyl)octanoate (5.40 g, 11.3 mmol, 1.0 equiv.), and finally the 2,2,2-trifluoroethyl 2-diazoacetate (2.47 g, 14.7 mmol, 1.3 equiv.) was added last. The resulted mixture was stirred at room temperature (23 ^oC) for 5 h and then, filtered through a short silica plug (3.5 cm *diameter*, 5 cm *height*), eluting with ethyl acetate until elutes clear. The crude product was concentrated and purified by flash column chromatography (3% ether in hexane) to afford the product as a red oil (88% yield).

Rf = 0.47 (hexane/diethyl ether = 9/1)

$[\alpha]^{20}_D$: +6.4^o (c = 1.0, $CHCl_3$)

^{1}H NMR (600 MHz, $CDCl_3$) δ 7.45 – 7.37 (m, 4H), 4.75 – 4.67 (m, 2H), 4.65 (q, *J* = 8.3 Hz, 2H), 3.68 (t, *J* = 7.7 Hz, 1H), 2.14 (dt, *J* = 13.3, 8.5 Hz, 1H), 1.82 (dt, *J* = 13.3, 8.5 Hz, 1H), 1.35 – 1.19 (m, 8H), 0.86 (t, *J* = 6.9 Hz, 3H).

^{13}C NMR (151 MHz, $CDCl_3$) δ 172.1, 163.1, 136.4, 128.9, 124.2, 123.6, 122.0 (q, *J* = 277.2 Hz), 94.8, 74.0, 60.2 (q, *J* = 36.6 Hz), 51.0, 33.0, 31.5, 28.9, 27.3, 22.5, 14.0.

^{19}F NMR (565 MHz, $CDCl_3$) δ -73.9 (t, *J* = 8.3 Hz).

IR (neat) 2929, 2858, 2092, 1751, 1716, 1514, 1452, 1411, 1353, 1281, 1241, 1169, 1139, 1074, 974, 924, 838, 761, 720, 652, 572, 513, 427 cm^{-1}.

HRMS (+p ESI) calcd for $C_{20}H_{22}Cl_3F_3N_2O_4Na$ $(M+Na)^+$ 539.0495 found 539.0493.

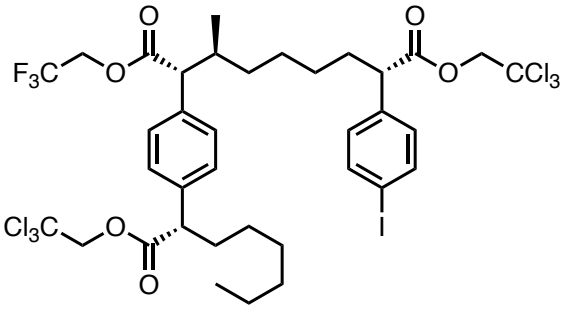

9-(2,2,2-trichloroethyl) 1-(2,2,2-trifluoroethyl) (2*R*,3*S*,8*S*)-8-(4-iodophenyl)-3-methyl-2-(4-((*S*)-1-oxo-1-(2,2,2-trichloroethoxy)octan-2-yl)phenyl)nonanedioate

A 100-ml flame-dried round-bottom flask with condenser was charged with 4 Å MS and Rh_2(*R*-2-Cl-5-BrTPCP)$_4$ (53.6 mg, 0.028 mmol, 1.0 mol %) and then, purged three times with nitrogen. 2,2,2-trichloroethyl (*S*)-2-(4-iodophenyl)octanoate (4.01 g, 8.40 mmol, 3.0 equiv.) and distilled CH_2Cl_2 (11 ml) were added next, then the mixture was heated to 40 °C and refluxed for at least 10 min before addition of the diazo compounds. Next, 2,2,2-trichloroethyl (*S*)-2-(4-(1-diazo-2-oxo-2-(2,2,2-trifluoroethoxy)ethyl)phenyl)octanoate (1.45 g, 2.80 mmol, 1.0 equiv.) was purged

under argon in a 20-mL scintillation vial, then diluted with distilled CH_2Cl_2 (11 ml). Then, under reflux conditions and nitrogen atmosphere, the diazo solution was added to the reaction vessel dropwise via syringe pump over 3 h. The reaction mixture was stirred at 40 ^oC for another 30 min and concentrated under vacuum for crude ^1H NMR. The crude product was purified by flash column chromatography (3% ether in hexane) to afford the product as an opaque oil. (68% yield, >20:1 rr, 95:5:< 5:< 5 dr).

Note 1: Solvent must be carefully dried (distilled over CaH_2 and stored on activated 4 Å MS).

Note 2: The drawn absolute and relative major stereochemistry is drawn based on analogy to the model system. Further confirmation of this assignment is achieved for x-ray structure of a later intermediate. Since chiral centers are already present in the substrates the asymmetric induction for the two new chiral centers formed by the catalyst is reported as diastereoselectivity. The diastereomeric ratio of the relative stereochemistry for the two new stereogenic centers was determined by the methyl shielding in the crude ^1H NMR. The diastereomeric ratio caused by the catalyst was determined by chiral HPLC. The product from the racemic catalyst was not cleanly sparable by HPLC, however both *S* and *R* catalyzed reactions were conducted to distinguish between the two peaks. The resolution was not great; thus, the racemic and *R*-chiral reactions were reduced by DIBAL-H to confirm the absolute diastereoselectivity. In the reduced HPLC the racemic catalyst has two peaks for the two major diastereomers but there are other contaminants in the HPLC, thus the assignment for the two major diastereomers (known for the anti) is assigned from the HPLC of the ester products with the *R* and *S* catalyst.

Rf = 0.21 (hexane/diethyl ether = 9/1)

$[\alpha]^{20}_D$: +3.8^o (c = 1.05, $CHCl_3$)

^{1}H NMR (600 MHz, $CDCl_3$) δ 7.64 (d, *J* = 8.1 Hz, 2H), 7.29 (d, *J* = 8.1 Hz, 2H), 7.24 (d, *J* = 8.1 Hz, 2H), 7.04 (d, *J* = 8.2 Hz, 2H), 4.77 – 4.62 (m, 4H), 4.53 (dq, *J* = 12.8, 8.4 Hz, 1H), 4.31 (dq, *J* = 12.8, 8.3 Hz, 1H), 3.66 (t, *J* = 7.7 Hz, 1H), 3.55 (t, *J* = 7.7 Hz, 1H), 3.33 (d, *J* = 10.5 Hz, 1H), 2.16 (dtq, *J* = 18.2, 8.9, 4.7, 3.9 Hz, 2H), 2.03 (dtd, *J* = 14.0, 8.9, 5.5 Hz, 1H), 1.86 – 1.77 (m, 1H), 1.69 (ddt, *J* = 19.3, 13.3, 6.1 Hz, 1H), 1.36 – 1.19 (m, 10H), 1.13 (dtt, *J* = 25.2, 15.4, 7.1 Hz, 4H), 0.98 (d, *J* = 6.6 Hz, 3H), 0.87 (h, *J* = 6.9 Hz, 3H).

^{13}C NMR (151 MHz, $CDCl_3$) δ 172.3, 172.1, 171.8, 137.7, 137.7, 137.6, 136.1, 130.0, 128.7, 128.4, 122.8 (q, *J* = 277.3 Hz), 94.9, 94.7, 93.0, 74.0, 73.9, 60.2 (q, *J* = 36.6 Hz), 57.7, 51.2, 50.9, 36.1, 33.0, 32.9, 32.9, 31.5, 28.9, 27.4, 27.3, 25.9, 22.5, 17.5, 14.1.

^{19}F NMR (376 MHz, $CDCl_3$) δ -73.7 (t, *J* = 8.3 Hz).

IR (neat) 2930, 2858, 2361, 1751, 1510, 1485, 1456, 1404, 1372, 1276, 1166, 1134, 1061, 1006, 979, 821, 753, 718, 572, 504, 493, 450, 430 cm^{-1}.

HRMS (+p ESI) calcd for $C_{36}H_{46}Cl_6F_3NIO_6$ $(M+NH4)^+$ 982.0453 found 982.0482.

HPLC [for better separation, the ester product was reduced with DIBAL-H to (2*R*,3*S*,8*S*)-2-(4-((*S*)-1-hydroxyoctan-2-yl)phenyl)-8-(4-iodophenyl)-3-methylnonane-1,9-diol] (ODH, 5.0 % *i*-propanol in hexane, 1.0 mL min^{-1}, 1.0 mg mL^{-1}, 90 min, UV 210 nm) retention times of 63.6 min (major) and 72.8 min (minor) 91% dr with Rh_2(*R*-2-Cl-5-BrTPCP)$_4$.

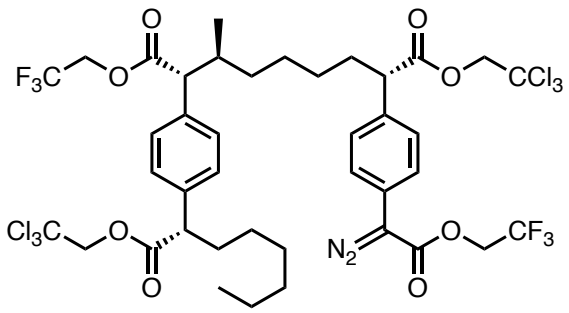

9-(2,2,2-trichloroethyl) 1-(2,2,2-trifluoroethyl) (2*R*,3*S*,8*S*)-8-(4-(1-diazo-2-oxo-2-(2,2,2-trifluoroethoxy)ethyl)phenyl)-3-methyl-2-(4-((*S*)-1-oxo-1-(2,2,2-trichloroethoxy)octan-2-yl)phenyl)nonanedioate

The procedure is adapted from the literature[2]: A 25-ml round-bottom flask with stir bar was flame dried under vacuum. Once cool enough all solids were added first: PPh_3 (34.8 mg, 0.133 mmol, 0.1 equiv.), $Pd(PPh_3)_4$ (76.6 mg, 0.066 mmol, 0.05 equiv.) and Ag_2CO_3 (183 mg, 0.663 mmol, 0.5 equiv.). After solids added, the reaction vessel was purged with nitrogen three times. Next the liquids were added: toluene (5.3 ml), Et_3N (0.240 ml, 1.72 mmol, 1.3 equiv.), 9-(2,2,2-trichloroethyl) 1-(2,2,2-trifluoroethyl) (2*R*,3*S*,8*S*)-8-(4-iodophenyl)-3-methyl-2-(4-((*S*)-1-oxo-1-(2,2,2-trichloroethoxy)octan-2-yl)phenyl)nonanedioate (1.283 g, 1.33 mmol, 1.0 equiv.), and finally the 2,2,2-trifluoroethyl 2-diazoacetate (289.8 mg, 1.72 mmol, 1.3 equiv.) was added last. The resulted mixture was stirred at room temperature (23 °C) for 5 h and then, filtered through a short silica plug (3.5 cm *diameter*, 5 cm *height*), eluting with ethyl acetate until elutes clear. The crude product was concentrated and purified by flash column chromatography (3% ether in hexane) to afford the product as a red oil (77% yield).

Rf = 0.79 (hexane/diethyl ether = 1/1)

$[\alpha]^{20}_D$: +4.3° (c = 0.8, $CHCl_3$)

^{1}H NMR (600 MHz, $CDCl_3$) δ 7.41 (d, *J* = 8.1 Hz, 2H), 7.34 (d, *J* = 8.2 Hz, 2H), 7.29 (d, *J* = 8.0 Hz, 2H), 7.25 (d, *J* = 8.0 Hz, 2H), 4.75 – 4.61 (m, 6H), 4.53 (dq, *J* = 12.7, 8.3 Hz, 1H), 4.31 (dq, *J* = 12.7, 8.3 Hz, 1H), 3.66 (t, *J* = 7.7 Hz, 1H), 3.61 (t, *J* = 7.7 Hz, 1H), 3.33 (d, *J* = 10.5 Hz, 1H), 2.15 (dddd, *J* = 22.7, 13.3, 9.9, 3.9 Hz, 2H), 2.09 – 2.01 (m, 1H), 1.86 – 1.77 (m, 1H), 1.77 – 1.66 (m, 1H), 1.36 – 1.20 (m, 10H), 1.19 – 1.07 (m, 4H), 0.98 (d, *J* = 6.5 Hz, 3H), 0.86 (t, *J* = 6.9 Hz, 3H).

^{13}C NMR (151 MHz, $CDCl_3$) δ 172.3, 172.1, 172.0, 163.1, 137.7, 136.2, 136.1, 128.8, 128.7, 128.4, 126.8, 122.9 (qd, *J* = 277.3, 3.9 Hz), 94.9, 94.8, 74.0, 73.9, 60.2 (qd, *J* = 36.7, 10.9 Hz), 57.7, 51.2, 50.9, 36.1, 33.0, 33.0, 32.9, 31.5, 28.9, 27.4, 27.4, 26.0, 22.5, 17.5, 14.0.

^{19}F NMR (376 MHz, $CDCl_3$) δ -73.7 (t, *J* = 8.4 Hz), -73.9 (t, *J* = 8.4 Hz).

IR (neat) 2930, 2858, 2361, 2093, 1750, 1718, 1514, 1410, 1353, 1280, 1242, 1166, 1137, 1074, 976, 838, 756, 719, 652, 571, 513, 484, 450, 435 cm^{-1}.

HRMS (+p ESI) calcd for $C_{40}H_{48}Cl_6F_6N_3O_8$ $(M+NH4)^+$ 1022.1477 found 1022.1523.

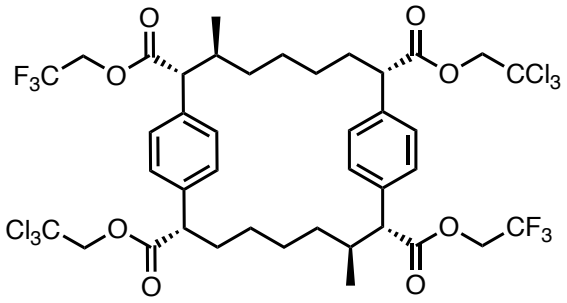

Macrocycle 2.23

A 100-ml flame-dried round-bottom flask with condenser were charged with 4 Å MS and Rh_2(*R*-2-Cl-5-BrTPCP)$_4$ (34.7 mg, 0.01 mmol, 1.0 mol%), then purged three times under nitrogen. Distilled CH_2Cl_2 (18 ml) was added using oven dried syringes, then the mixture was heated to 40 °C and refluxed for at least 10 min before addition of the diazo compounds. Next, 9-(2,2,2-trichloroethyl) 1-(2,2,2-trifluoroethyl) (2*R*,3*S*,8*S*)-8-(4-(1-diazo-2-oxo-2-(2,2,2-trifluoroethoxy)ethyl)phenyl)-3-methyl-2-(4-((*S*)-1-oxo-1-(2,2,2-trichloroethoxy)octan-2-yl)phenyl)nonanedioate (1.83 g, 1.82 mmol, 1.0 equiv.) was used immediately after its synthesis and purged under nitrogen in a 50-mL round-bottom flask, then diluted with distilled CH_2Cl_2 (18 ml). Then, under reflux conditions and nitrogen atmosphere, the diazo solution was added to the

reaction vessel dropwise via syringe pump over 3 h. The reaction mixture was stirred at 40 °C for another 30 min and concentrated under vacuum for crude ^{1}H NMR, showing the product was formed in 8:1 dr. The crude product was purified by flash column chromatography (10% ether in hexane) to afford the product as a white solid and single diastereomer (70% yield). Alternatively, the crude mixture can be recrystallized in 20% ether in hexane to yield the diastereopure product as a white solid (62% yield). The absolute configuration and relative configuration are determined by x-ray crystallography.

Note 1: Solvent must be carefully dried (distilled over CaH_2 and stored on activated 4 Å MS).

Note 2: The crude material obtained shows two diastereomeric signals in 8:1. The change in dr from the starting material is due to the Horeau principle. Recrystallization gave the desired diastereomer in 62% yield and the NMR appears as a signal diastereomer.

Rf = 0.46 (hexane/ethyl acetate = 4/1)

$[\alpha]^{20}_D$: -7.6° (c = 0.34, $CHCl_3$)

^{1}H NMR (600 MHz, $CDCl_3$) δ 7.21 (s, 8H), 4.73 (dd, *J* = 12.0, 1.0 Hz, 2H), 4.62 (dd, *J* = 12.0, 1.1 Hz, 2H), 4.53 (dq, *J* = 12.8, 8.4 Hz, 2H), 4.27 (dq, *J* = 12.7, 8.3 Hz, 2H), 3.52 (dd, *J* = 11.4, 4.4 Hz, 2H), 3.19 (d, *J* = 11.4 Hz, 2H), 2.14 – 2.07 (m, 2H), 1.97 – 1.82 (m, 4H), 1.49 – 1.39 (m, 2H), 1.00 (d, *J* = 6.4 Hz, 6H), 0.94 (qt, *J* = 12.5, 6.3 Hz, 4H), 0.76 (t, *J* = 12.8 Hz, 2H), 0.70 – 0.61 (m, 4H).

^{13}C NMR (151 MHz, $CDCl_3$) δ 172.1, 172.1, 136.8, 136.4, 128.6, 122.8 (q, *J* = 277.2 Hz), 94.8, 73.9, 60.2 (q, *J* = 36.7 Hz), 58.7, 51.4, 37.0, 33.8, 33.1, 27.9, 27.3, 17.8.

^{19}F NMR (376 MHz, $CDCl_3$) δ -73.7 (t, *J* = 8.5 Hz).

IR (neat) 2935, 2860, 1749, 1511, 1466, 1407, 1374, 1276, 1222, 1164, 1128, 1062, 979, 909, 835, 809, 762, 726, 645, 572, 539, 462, 450, 440, 431 cm^{-1}.

HRMS (+p ESI) calcd for $C_{40}H_{44}Cl_6F_6O_8$ $(M+H)^+$ 977.1150 found 977.1177.

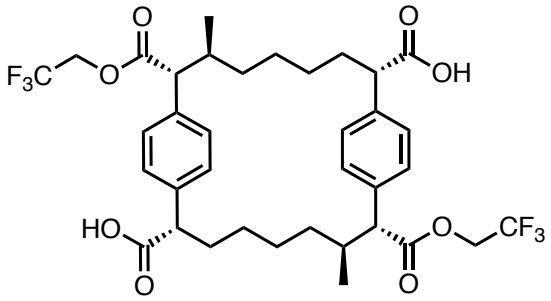

(2*S*,7*S*,8*R*,10*S*,15*S*,16*R*)-7,15-dimethyl-8,16-bis((2,2,2-trifluoroethoxy)carbonyl)-1,9(1,4)-dibenzenacyclohexadecaphane-2,10-dicarboxylic acid

To a 250-ml round-bottom flask was added macrocycle 2.23 (893 mg, 0.912 mmol, 1.0 equiv) then zinc (3.58 g, 54.7 mmol, 60 equiv) and acetic acid (46ml). Stir for 4 days at room temperature. The crude mixture was diluted with water then filtered washing with EtOAc. The eluent was then further diluted with EtOAc, then washed with water (x2), brine (x8), then dried with $MgSO_4$ and concentrated under reduced pressure. The crude product was clean by ^{1}H NMR and carried forward as a white solid (>99% yield).

Rf = 0.05 (hexane/ethyl acetate = 2/1)

$[\alpha]^{20}_D$: +13.9° (c = 0.8, EtOAc)

^{1}H NMR (600 MHz, $CDCl_3$) δ 7.20 (d, *J* = 7.5 Hz, 4H), 7.15 (d, *J* = 7.8 Hz, 4H), 4.55 (dq, *J* = 12.7, 8.4 Hz, 2H), 4.23 (dq, *J* = 12.8, 8.4 Hz, 2H), 3.39 (dd, *J* = 11.6, 4.2 Hz, 2H), 3.18 (d, *J* = 11.3 Hz, 2H), 2.11 – 2.03 (m, 2H), 1.87 (t, *J* = 13.0 Hz, 2H), 1.80 (dd, *J* = 12.3, 7.9 Hz, 2H), 1.46 – 1.37 (m, 2H), 0.99 (d, *J* = 6.3 Hz, 6H), 0.89 (q, *J* = 10.5, 9.7 Hz, 4H), 0.73 (t, *J* = 12.7 Hz, 2H), 0.68 – 0.52 (m, 4H).

^{13}C NMR (151 MHz, $CDCl_3$) δ 179.0, 176.5, 172.2, 171.2, 137.1, 136.3, 128.6, 122.9 (q, *J* = 277.2 Hz), 60.3 (q, *J* = 36.5 Hz), 58.7, 51.3, 37.2, 33.9, 33.0, 27.9, 27.3, 21.0, 20.6, 17.7, 14.2.

^{19}F NMR (376 MHz, $CDCl_3$) δ -73.7 (td, *J* = 8.5, 5.6 Hz).

IR (neat) 2933, 2858, 1749, 1705, 1511, 1468, 1407, 1385, 1275, 1225, 1167, 1128, 1058, 1021, 979, 910, 840, 731, 697, 660 cm^{-1}.

HRMS (-p ESI) calcd for $C_{36}H_{41}F_6O_8$ $(M-H)^-$ 715.2706 found 715.2703.

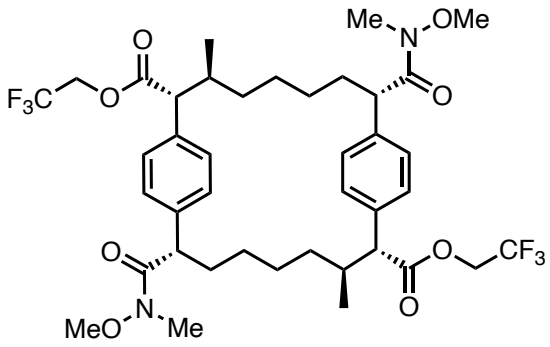

bis(2,2,2-trifluoroethyl) (2*R*,3*S*,8*S*,10*R*,11*S*,16*S*)-8,16-bis(methoxy(methyl)carbamoyl)-3,11-dimethyl-1,9(1,4)-dibenzenacyclohexadecaphane-2,10-dicarboxylate

To a 50-ml flame-dried round-bottom flask was added (2*S*,7*S*,8*R*,10*S*,15*S*,16*R*)-7,15-dimethyl-8,16-bis((2,2,2-trifluoroethoxy)carbonyl)-1,9(1,4)-dibenzenacyclohexadecaphane-2,10-dicarboxylic acid (988 mg, 1.38 mmol, 1.0 equiv) in N,N-dimethylformamide (7 ml). The mixture was then cooled to 0 ºC. HATU (1.57 g, 4.14 mmol, 3.0 equiv) and then N-ethyl-N-isopropylpropan-2-amine (1.92 mL, 11.0 mmol, 8.0 equiv) was added at 0 ºC. The reaction was then stirred for 20min at 0 ºC. Then N,O-dimethylhydroxylamine hydrochloride (403 mg, 4.14 mmol, 3.0 equiv) was added 0 ºC, then the reaction was stirred overnight and let warm to room temperature. The reaction was dilute with EtOAc and water, then separated and washed with brine (x8), dried with $MgSO_4$ and concentrated under reduced pressure. The crude product was

purified by flash column chromatography (25% EtOAc in hexane) to afford the product as a white solid (85% yield).

Rf = 0.53 (hexane/ethyl acetate = 1/1)

$[\alpha]^{20}_D$: -2° (c = 0.3, $CHCl_3$)

^{1}H NMR (600 MHz, $CDCl_3$) δ 7.17 (s, 8H), 4.46 (dq, *J* = 12.7, 8.5 Hz, 2H), 4.33 (dq, *J* = 12.7, 8.4 Hz, 2H), 3.79 (s, 2H), 3.36 (s, 6H), 3.16 (d, *J* = 11.4 Hz, 2H), 3.10 (s, 6H), 2.09 – 2.03 (m, 2H), 1.89 – 1.80 (m, 2H), 1.74 – 1.66 (m, 2H), 1.41 (t, *J* = 12.1 Hz, 2H), 0.99 (d, *J* = 6.4 Hz, 6H), 0.92 (qt, *J* = 11.5, 5.7 Hz, 4H), 0.80 (t, *J* = 12.9 Hz, 2H), 0.67 – 0.51 (m, 4H).

^{13}C NMR (151 MHz, $CDCl_3$) δ 172.2, 138.9, 135.7, 128.7, 128.5, 122.9 (q, *J* = 277.2 Hz), 61.1, 60.1 (q, *J* = 36.5 Hz), 58.8, 47.8, 37.1, 34.0, 33.6, 33.3, 32.2, 28.1, 27.5, 17.8.

^{19}F NMR (376 MHz, $CDCl_3$) δ -73.8 (t, *J* = 8.4 Hz).

IR (neat) 2934, 2857, 1751, 1656, 1510, 1409, 1382, 1274, 1164, 1126, 1056, 1022, 979, 909, 841, 803, 730, 646, 623, 566, 532, 452, 433, 424 cm^{-1}.

HRMS (+p ESI) calcd for $C_{40}H_{53}F_6N_2O_8$ $(M+H)^+$ 803.3706 found 803.3702.

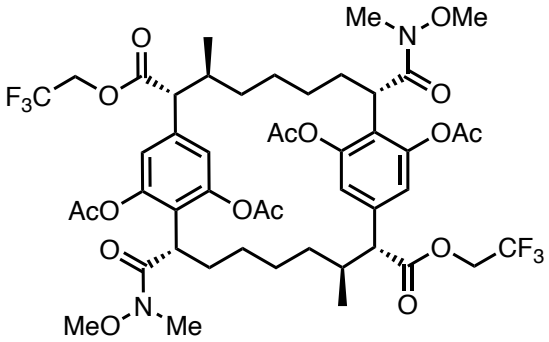

bis(2,2,2-trifluoroethyl) (2*R*,3*S*,8*S*,10*R*,11*S*,16*S*)-1^3,1^5,9^2,9^6-tetraacetoxy-8,16-bis(methoxy(methyl)carbamoyl)-3,11-dimethyl-1,9(1,4)-dibenzenacyclohexadecaphane-2,10-dicarboxylate

The procedure is adapted from the literature[7]: To a flame-dried 8-ml vial was added $Pd(OAc)_2$ (11.7 mg, 51.8 μmol, 20 mol %), $PhI(OAc)_2$ (669 mg, 2.07 mmol, 8.0 equiv), 5-(trifluoromethyl)-3-pyridinesulfonic acid X (11.7 mg, 51.8 μmol, 20 mol %), and bis(2,2,2-trifluoroethyl) (2*R*,3*S*,8*S*,10*R*,11*S*,16*S*)-8,16-bis(methoxy(methyl)carbamoyl)-3,11-dimethyl-1,9(1,4)-dibenzenacyclohexadecaphane-2,10-dicarboxylate (208.0 mg, 269.1 μmol, 1.0 equiv). Then HFIP (2.6 ml) and Ac_2O (0.98 ml, 10.4 mmol, 40 equiv) were added and the septum cap was exchanged with a Teflon septum-lined screw cap and heated to 80 °C for 24 h. The reaction was cooled to room temperature, diluted with EtOAc and filtered over celite. The eluent was concentrated under reduced pressured and purified by flash column chromatography (30% to 50% EtOAc in hexanes) to deliver the product as a tan solid (77% yield).

Rf = 0.34 (hexanes/EtOAc = 1:1)

$[\alpha]^{20}_D$: +38.5° (c = 0.85, $CHCl_3$)

^{1}H NMR (400 MHz, $CDCl_3$) δ 7.00 (d, *J* = 1.7 Hz, 2H), 6.89 (d, *J* = 1.7 Hz, 2H), 4.50 – 4.33 (m, 4H), 3.98 (dd, *J* = 12.0, 4.3 Hz, 2H), 3.16 (d, *J* = 11.4 Hz, 2H), 3.00 (s, 6H), 2.91 (s, 6H), 2.32 (s, 6H), 2.21 (s, 6H), 1.94 (qd, *J* = 12.8, 11.8, 3.6 Hz, 4H), 1.79 (ddd, *J* = 13.5, 9.5, 4.1 Hz,

2H), 1.51 – 1.37 (m, 3H),, 0.99 (d, *J* = 6.4 Hz, 6H), 0.95 – 0.78 (m, 5H), 0.73 – 0.61 (m, 2H), 0.52 (q, *J* = 12.3 Hz, 2H).

^{13}C NMR (101 MHz, $CDCl_3$) δ 172.9, 171.5, 168.7, 167.7, 149.3, 148.7, 136.3, 124.3, 122.7 (q, *J* = 277.5 Hz) 122.0, 119.1, 60.4, 60.0, 59.7, 58.3, 39.9, 37.7, 34.1, 31.9, 30.2, 28.0, 27.4, 21.2, 20.6, 17.8.

^{19}F NMR (376 MHz, $CDCl_3$) δ -73.8 (t, *J* = 8.4 Hz).

IR (neat) 2934, 2858, 1769, 1757, 1659, 1619, 1577, 1431, 1412, 1368, 1285, 1275, 1180, 1131, 1087, 1032, 979, 906, 842, 804, 730 cm^{-1}

HRMS (+p ESI) calcd for $C_{48}H_{58}F_6N_2O_{16}Na_2$ $[M+2Na-2H]^+$ 1078.3847 found 1078.5087

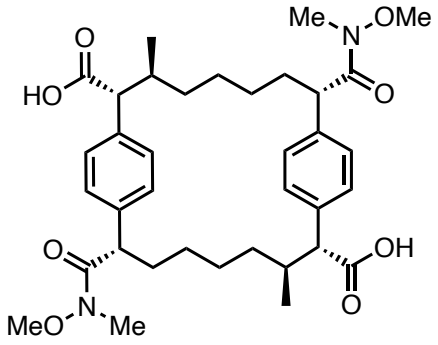

(2*R*,3*S*,8*S*,10*R*,11*S*,16*S*)-8,16-bis(methoxy(methyl)carbamoyl)-3,11-dimethyl-1,9(1,4)-dibenzenacyclohexadecaphane-2,10-dicarboxylic acid

To a 10-ml round-bottom was added bis(2,2,2-trifluoroethyl) (2*R*,3*S*,8*S*,10*R*,11*S*,16*S*)-8,16-bis(methoxy(methyl)carbamoyl)-3,11-dimethyl-1,9(1,4)-dibenzenacyclohexadecaphane-2,10-dicarboxylate (60.0 mg, 74.7 μmol, 1.0 equiv) then THF (1.5 ml) and water (1.5 ml) was added. Then lithium hydroxide hydrate (157 mg, 3.74 mmol, 50 equiv) was added to the reaction and then let stir at room temperature overnight. The reaction was diluted with water and acidify with

2M HCl. The product was extracted with EtOAc (x2), dried with $MgSO_4$ and concentrated under reduced pressure. The crude product was clean by ^1H NMR and carried forward as a white solid (97% yield).

Rf = 0.05 (dichloromethane/methanol = 9/1)

$[\alpha]^{20}_D$: +9.5° (c = 0.5, AcOH)

^1H NMR (600 MHz, MeOD) δ 7.25 (d, *J* = 7.7 Hz, 4H), 7.18 (d, *J* = 8.0 Hz, 4H), 3.90 (s, 2H), 3.50 (s, 6H), 3.11 (s, 6H), 3.04 (d, *J* = 11.3 Hz, 2H), 2.10 – 2.03 (m, 2H), 1.70 (ddt, *J* = 18.3, 13.2, 8.5 Hz, 4H), 1.50 – 1.41 (m, 2H), 1.03 (d, *J* = 6.3 Hz, 6H), 0.98 – 0.88 (m, 3H), 0.88 – 0.81 (m, 2H), 0.67 (dtd, *J* = 22.7, 11.9, 5.5 Hz, 4H).

^{13}C NMR (151 MHz, AcOD) δ 180.1, 176.1, 139.7, 138.8, 138.2, 137.9, 129.7, 61.8, 60.2, 52.3, 48.6, 37.4, 34.8, 34.1, 33.7, 32.7, 28.9, 28.0, 18.2, 14.3.

IR (neat) 2918, 2950, 2360, 2106, 1693, 1650, 1383, 1777, 989, 799, 668, 592 cm^{-1}.

HRMS (+p ESI) calcd for $C_{36}H_{50}N_2O_8Na$ $(M+Na)^+$ 661.3465 found 661.3452.

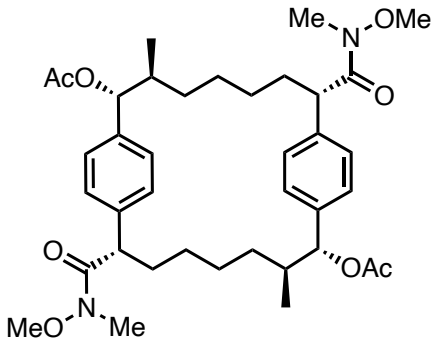

(2*R*,3*S*,8*S*,10*R*,11*S*,16*S*)-8,16-bis(methoxy(methyl)carbamoyl)-3,11-dimethyl-1,9(1,4)-dibenzenacyclohexadecaphane-2,10-diyl diacetate

The procedure is adapted from the literature[8]: To a flame-dried 8-ml vial purged under nitrogen (x3) was added 4 Å MS, $Cu(OAc)_2$ (42.6 mg, 235 μmol, 6.0 equiv), 9-mesityl-2,7-dimethyl-10-phenyl- acridinium tetrafluoroborate (0.5 mg, 1.0 μmol, 2.5 mol %), and (2*R*,3*S*,8*S*,10*R*,11*S*,16*S*)-8,16-bis(methoxy(methyl)carbamoyl)-3,11-dimethyl-1,9(1,4)-dibenzenacyclohexadecaphane-2,10-dicarboxylic acid (25.0 mg, 39.1 μmol, 1.0 equiv). Then acetonitrile (1.7 ml) and acetic acid (0.85 ml) was added to the reaction mixture. The reaction was then degassed via nitrogen bubbling for 10 min using an 18-gauge needle and another exit needle. The reaction was then sealed placed and two blue lights placed against the vial and wrapped in tin foil. The mixture was stirred under blue light for 48 h. The crude mixture was cooled to room temperature and filtered over celite eluting with EtOAc. The eluent was concentrated under vacuum, diluted with EtOAc and washed with water, then brine (x4), dried with $MgSO_4$ and concentrated under reduced pressure for crude ^{1}H NMR analysis, showing the product was formed in 9:1 dr. The crude product was purified by flash column chromatography (30% EtOAc in hexane) to afford the product as a white solid and single diastereomer by ^{1}H NMR (52% yield).

Rf = 0.33 (hexane/EtOAc = 1:1)

$[\alpha]^{20}_D$: +79.8° (c = 0.85, $CHCl_3$)

^{1}H NMR (600 MHz, $CDCl_3$) δ 7.22 – 7.14 (m, 8H), 5.17 (d, *J* = 10.5 Hz, 2H), 3.83 (s, 2H), 3.40 (s, 6H), 3.11 (s, 6H), 1.99 (s, 6H), 1.84 – 1.74 (m, 4H), 1.74 – 1.67 (m, 2H), 1.47 – 1.37 (m, 2H), 0.99 (d, *J* = 6.4 Hz, 6H), 0.95 – 0.85 (m, 4H), 0.65 (dddd, *J* = 49.4, 24.7, 12.2, 5.2 Hz, 6H).

^{13}C NMR (151 MHz, $CDCl_3$) δ 170.4, 138.6, 128.2, 127.6, 81.3, 61.2, 47.6, 38.9, 33.8, 32.7, 29.7, 28.0, 27.6, 21.2, 16.1.

IR (neat) 2934, 2857, 1736, 1660, 1510, 1465, 1373, 1240, 1019, 991, 970, 916, 801, 730, 600, 565 cm^{-1}.

HRMS (+p ESI) calcd for $C_{38}H_{55}N_2O_8$ $(M+H)^+$ 667.3958 found 667.3959.

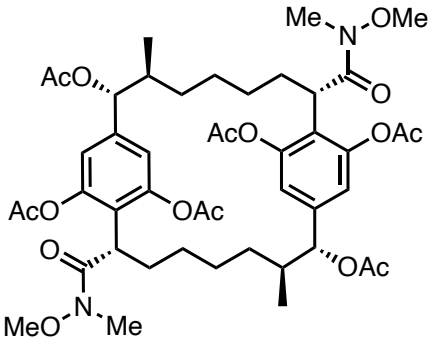

(2*S*,7*S*,8*R*,10*S*,15*S*,16*R*)-2,10-bis(methoxy(methyl)carbamoyl)-7,15-dimethyl-1,9(1,4)-dibenzenacyclohexadecaphane-1^2,1^6,9^3,9^5,8,16-hexayl hexaacetate

The procedure is adapted from the literature[7]: To a flame-dried 8-ml vial was added $Pd(OAc)_2$ (2.0mg, 9.0 µmol, 20 mol %), $PhI(OAc)_2$ (116 mg, 360 µmol, 8.0 equiv), 5-(trifluoromethyl)-3-pyridinesulfonic acid X (2.0mg, 9.0 µmol, 20 mol %), and (2*R*,3*S*,8*S*,10*R*,11*S*,16*S*)-8,16-bis(methoxy(methyl)carbamoyl)-3,11-dimethyl-1,9(1,4)-dibenzenacyclohexadecaphane-2,10-diyl diacetate (30.0 mg, 45.0 µmol, 1.0 equiv). Then HFIP (1.0ml) and Ac_2O (0.17 ml, 1.8 mmol, 40 equiv) were added and the septum cap was exchanged with a Teflon septum-lined screw cap and heated to 80 °C for 48 h. The reaction was cooled to room temperature, diluted with EtOAc and filtered over celite. The eluent was concentrated under reduced pressured and purified by flash column chromatography (50% EtOAc in hexanes) to deliver the product as a white solid (60% yield).

Rf = 0.47 (EtOAc/hexanes 3:1)

$[\alpha]^{20}_D$: +64° (c = 0.1, $CHCl_3$)

^{1}H NMR (600 MHz, $CDCl_3$) δ 6.97 (s, 2H), 6.86 (s, 2H), 5.20 (d, *J* = 10.0 Hz, 2H), 4.01 – 3.96 (m, 2H), 3.02 (s, 6H), 2.95 (s, 6H), 2.31 (s, 6H), 2.22 (s, 6H), 2.00 (s, 6H), 1.83 (p, *J* = 8.1 Hz, 5H), 1.73 – 1.65 (m, 3H), 1.45 (tt, *J* = 10.1, 5.7 Hz, 2H), 1.04 – 0.96 (m, 3H), 0.95 (d, *J* = 6.5 Hz, 6H), 0.82 – 0.77 (m, 3H), 0.66 – 0.57 (m, 2H).

^{13}C NMR (151 MHz, $CDCl_3$) δ 170.1, 169.0, 167.5, 149.1, 148.4, 139.4, 120.8, 117.8, 80.0, 59.9, 40.0, 39.2, 32.6, 30.3, 27.9, 27.3, 21.1, 21.1, 20.7, 15.7.

IR (neat) 2931, 2360, 1771, 1744, 1663, 1431, 1370, 1232, 1182, 1035, 900, 516 cm^{-1}.

HRMS (+p ESI) calcd for $C_{46}H_{63}N_2O_{16}$ $(M+H)^+$ 899.4178 found 899.4181.

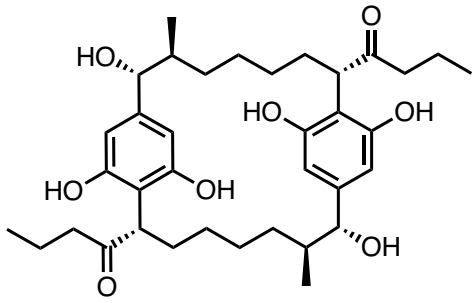

1,1'-((2*S*,7*S*,8*R*,10*S*,15*S*,16*R*)-1^{2},1^{6},9^{3},9^{5},8,16-hexahydroxy-7,15-dimethyl-1,9(1,4)-dibenzenacyclohexadecaphane-2,10-diyl)bis(butan-1-one)

To a flame-dried 4-ml vial purged under nitrogen (x3) was added (2*S*,7*S*,8*R*,10*S*,15*S*,16*R*)-2,10-bis(methoxy(methyl)carbamoyl)-7,15-dimethyl-1,9(1,4)-dibenzenacyclohexadecaphane-1^{2},1^{6},9^{3},9^{5},8,16-hexayl hexaacetate (5.0mg, 1 equiv, 5.6 μmol) then THF (0.11ml, 0.05 M). The mixture was then cooled to 0 °C in an ice bath for 10 min. At 0 °C propylmagnesium chloride (1.0 M in 2-Me-THF, 0.56ml, 100 equiv, 0.56 mmol) was added dropwise and the reaction was let warmed to room temperature overnight. The mixture was then cooled to 0 °C and quenched with water, acidified with sat. NH_4Cl, then extracted with EtOAc, washed with brine, dried with

$MgSO_4$ and concentrated under reduced pressure. The crude product was purified by prepLC (Agilent 1100 HPLC, 9.4x250 C8 column, 20% ACN/H_2O 0.5min at 2.5ml/min, 20-70% ACN for 6.5min at 5ml/min, 100% ACN for 1min) to deliver the product as a white solid (0.2 mg, 6% yield unoptimized).

Note: This compound is partially characterized as my collaborated Tyler Casselman is currently optimizing this step.

1H NMR (400 MHz, MeOD) δ 6.30 (s, 2H), 6.18 (s, 2H), 3.90 (dd, *J* = 10.4, 4.8 Hz, 2H), 3.79 (d, *J* = 9.7 Hz, 2H), 2.21 (td, *J* = 7.3, 1.9 Hz, 4H), 1.93 – 1.76 (m, 4H), 1.47 (h, *J* = 7.5, 5.2 Hz, 9H), 1.09 (d, *J* = 6.4 Hz, 6H), 1.04 – 0.96 (m, 2H), 0.77 (t, *J* = 7.4 Hz, 6H), 0.66 (dd, *J* = 11.7, 6.9 Hz, 2H).

HRMS (-p ESI) calcd for $C_{36}H_{52}O_8$ $(M-H)^-$ 611.3662 found 611.3604.

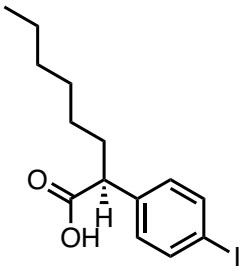

(*S*)-2-(4-iodophenyl)octanoic acid

To a 100-ml round-bottom flask was added 2,2,2-trichloroethyl (*S*)-2-(4-iodophenyl)octanoate (527 mg, 1.1 mmol, 1.0 equiv) then zinc (721 mg, 11.0 mmol, 10 equiv) and acetic acid (14ml). Stir for 24 h at room temperature. The crude mixture was diluted with water then filtered washing with EtOAc. The eluent was then further diluted with EtOAc, then washed with water

(x2), brine (x8), then dried with $MgSO_4$ and concentrated under reduced pressure. The crude product was clean by ^1H NMR and carried forward as a yellow oil (99% yield).

^1H NMR (600 MHz, $CDCl_3$) δ 7.65 (d, *J* = 8.1 Hz, 2H), 7.06 (d, *J* = 8.1 Hz, 2H), 3.48 (t, *J* = 7.7 Hz, 1H), 2.04 (tdd, *J* = 12.3, 8.4, 4.6 Hz, 1H), 1.74 (pd, *J* = 8.9, 8.3, 5.0 Hz, 1H), 1.34 – 1.16 (m, 8H), 0.86 (t, *J* = 7.0 Hz, 3H).

^{13}C NMR (151 MHz, $CDCl_3$) δ 178.9, 138.1, 137.7, 130.0, 92.9, 50.9, 32.9, 31.5, 28.9, 27.3, 22.5, 14.0.

IR (neat) 3023, 2953, 2924, 2855, 1710, 1586, 1484, 1416, 1401, 1378, 1275, 1227, 1204, 1182, 1122, 1063, 1006, 936, 815, 745, 724, 698 cm^{-1}.

HRMS (-p APCI) calcd for $C_{14}H_{18}IO_2$ $(M-H)^-$ 345.0351 found 345.0346.

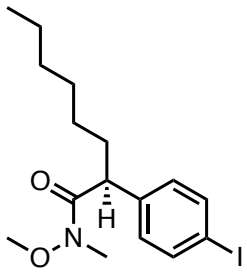

(*S*)-2-(4-iodophenyl)-*N*-methoxy-*N*-methyloctanamide

To a 50-ml flame-dried round-bottom flask was added (*S*)-2-(4-iodophenyl)octanoic acid (382 mg, 1.1 mmol, 1.0 equiv) in N,N-dimethylformamide (2.8 ml). The mixture was then cooled to 0 °C. HATU (503 mg, 1.32 mmol, 1.2 equiv) and then N-ethyl-N-isopropylpropan-2-amine (0.58 mL, 3.31 mmol, 3.0 equiv) was added at 0 °C. The reaction was then stirred for 20min at 0 °C. Then N,O-dimethylhydroxylamine hydrochloride (161 mg, 1.66 mmol, 1.5 equiv) was added 0 °C, then the reaction was stirred overnight and let warm to room temperature. The reaction was

dilute with EtOAc and water, then separated and washed with brine (x8), dried with $MgSO_4$ and concentrated under reduced pressure. The crude product was purified by flash column chromatography (20% ether in hexane) to afford the product as an opaque oil (78% yield).

Rf = 0.32 (hexanes/ether 2:1)

^{1}H NMR (600 MHz, $CDCl_3$) δ 7.62 (d, *J* = 8.3 Hz, 2H), 7.08 (d, *J* = 8.2 Hz, 2H), 3.92 (s, 1H), 3.51 (s, 3H), 3.15 (s, 3H), 2.07 – 1.97 (m, 1H), 1.72 – 1.63 (m, 1H), 1.31 – 1.19 (m, 8H), 0.85 (t, *J* = 6.8 Hz, 3H).

^{13}C NMR (151 MHz, $CDCl_3$) δ 174.2, 140.0, 137.5, 130.2, 92.1, 61.3, 47.0, 33.9, 32.2, 31.6, 29.1, 27.6, 22.5, 14.0.

IR (neat) 2930, 2853, 1742, 1659, 1483, 1459, 1380, 1177, 1115, 1060, 1006, 806, 627, 610 cm^{-1}.

HRMS (+p ESI) calcd for $C_{16}H_{25}INO_2$ $(M+H)^+$ 390.0852 found 390.0859.

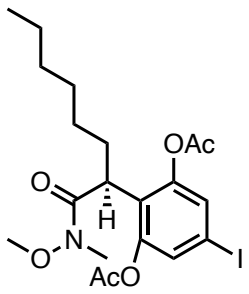

(*S*)-5-iodo-2-(1-(methoxy(methyl)amino)-1-oxooctan-2-yl)-1,3-phenylene diacetate

The procedure is adapted from the literature[9]: To a flame-dried 20-ml vial was added $Pd(OAc)_2$ (38.6 mg, 172 μmol, 20 mol %), $PhI(OAc)_2$ (1.11 g, 3.44 mmol, 4.0 equiv), and (*S*)-2-(4-iodophenyl)-*N*-methoxy-*N*-methyloctanamide (335 mg, 861 μmol, 1.0 equiv). Then HFIP (8.6 ml) and Ac_2O (1.63 ml, 117.2 mmol, 20 equiv) were added and the septum cap was exchanged

with a Teflon septum-lined screw cap and heated to 80 ºC for 72 h. The reaction was cooled to room temperature, diluted with EtOAc and filtered over celite. The eluent was concentrated under reduced pressured and purified by flash column chromatography (30% ether in hexanes) to deliver the product as a white solid (58% yield).

Rf = 0.33 (hexanes/ether 1:1)

^{1}H NMR (600 MHz, $CDCl_3$) δ 7.33 (s, 2H), 3.93 – 3.88 (m, 1H), 3.13 (s, 3H), 3.06 (s, 3H), 2.29 (s, 6H), 2.11 (dddd, *J* = 13.8, 10.5, 7.2, 4.6 Hz, 1H), 1.31 – 1.19 (m, 8H), 1.14 – 1.07 (m, 1H), 0.86 (t, *J* = 7.0 Hz, 3H).

^{13}C NMR (151 MHz, $CDCl_3$) δ 172.6, 168.5, 149.2, 129.8, 126.6, 89.1, 60.3, 39.9, 32.1, 31.7, 30.0, 29.2, 27.6, 22.6, 20.7, 14.1.

IR (neat) 2930, 1770, 1665, 1589, 1459, 1368, 1189, 1036, 907 cm^{-1}.

HRMS (+p ESI) calcd for $C_{20}H_{28}INO_6$ $(M+H)^+$ 506.1040 found 506.1031.

References

1. Fu, L.; Mighion, J. D.; Voight, E. A.; Davies, H. M. L., Synthesis of 2,2,2,-Trichloroethyl Aryl- and Vinyldiazoacetates by Palladium-Catalyzed Cross-Coupling. *Chem. Eur. J.* **2017,** *23* (14), 3272-3275.
2. Liu, W.; Ren, Z.; Bosse, A. T.; Liao, K.; Goldstein, E. L.; Bacsa, J.; Musaev, D. G.; Stoltz, B. M.; Davies, H. M. L., Catalyst-Controlled Selective Functionalization of Unactivated C–H Bonds in the Presence of Electronically Activated C–H Bonds. *J. Am. Chem. Soc.* **2018,** *140* (38), 12247-12255.
3. Liao, K.; Yang, Y.-F.; Li, Y.; Sanders, J. N.; Houk, K. N.; Musaev, D. G.; Davies, H. M. L., Design of catalysts for site-selective and enantioselective functionalization of non-activated primary C–H bonds. *Nat. Chem.* **2018,** *10* (10), 1048-1055.
4. Qin, C.; Davies, H. M. L., Role of Sterically Demanding Chiral Dirhodium Catalysts in Site-Selective C–H Functionalization of Activated Primary C–H Bonds. *J. Am. Chem. Soc.* **2014,** *136* (27), 9792-9796.
5. Park, H.; Chekshin, N.; Shen, P.-X.; Yu, J.-Q., Ligand-Enabled, Palladium-Catalyzed β-C(sp3)–H Arylation of Weinreb Amides. *ACS Catal.* **2018,** *8* (10), 9292-9297.

6. Garlets, Z. J.; Sanders, J. N.; Malik, H.; Gampe, C.; Houk, K. N.; Davies, H. M. L., Enantioselective C–H functionalization of bicyclo[1.1.1]pentanes. *Nat. Catal.* **2020,** *3* (4), 351-357.
7. Falcone, N. A.; Bosse, A. T.; Park, H.; Yu, J.-Q.; Davies, H. M. L.; Sorensen, E. J., A C–H Functionalization Strategy Enables an Enantioselective Formal Synthesis of (−)-Aflatoxin B2. *Org. Lett.* **2021,** *23* (24), 9393-9397.
8. Senaweera, S.; Cartwright, K. C.; Tunge, J. A., Decarboxylative Acetoxylation of Aliphatic Carboxylic Acids. *J. Org. Chem.* **2019,** *84* (19), 12553-12561.
9. Li, G.; Wan, L.; Zhang, G.; Leow, D.; Spangler, J.; Yu, J.-Q., Pd(II)-Catalyzed C–H Functionalizations Directed by Distal Weakly Coordinating Functional Groups. *J. Am. Chem. Soc.* **2015,** *137* (13), 4391-4397.

5.3. Experiment Section for Chapter 3

Substrates and reagents

The following compounds were prepared according to published procedures:

Rh_2(*R*-*p*-PhTPCP)$_4$[1]

General procedure for enantioselective C–H insertions with trans-2-hexene

A flame-dried flask with oven dried condenser was charged with 4 Å MS and Rh_2(*R*-*p*-PhTPCP)$_4$ (1.8 mg, 0.001 mmol, 1.0 mol %) and purged three times with nitrogen. (*E*)-hex-2-ene (110.2 µL, 0.90 mmol, 3.00 eq.) and distilled CH_2Cl_2 (1.15 mL) were added,[Note 1] and the mixture was heated to 40 ˚C and refluxed for 10 min before addition of the diazo compounds. In a separate flask the diazoester[Note 2] (0.30 mmol, 1.00 eq.) was dissolved in distilled CH_2Cl_2 (1.15 mL) under argon. Under refluxing conditions, the diazoester solution was added to the reaction vessel dropwise via syringe pump over 3 h. The reaction mixture was stirred at 40 ˚C for another 30 min and concentrated *in vacuo*. The crude product was purified by flash column chromatography (2% Et_2O/hexanes) to afford the corresponding insertion product as a clear oil.

Note 1: Solvent must be distilled over CaH_2 and stored over activated 4 Å MS.

Note 2: Diazoesters were prepared according to literature precedent.[2]

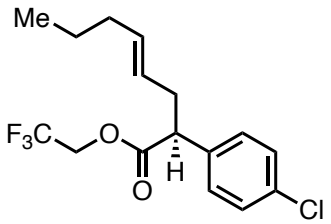

2,2,2-trifluoroethyl (*S*,*E*)-2-(4-chlorophenyl)oct-4-enoate

This compound was prepared according to the general procedure for C-H insertion with *trans*-2-hexene (69 mg, 69% yield, 92% ee, 11:1 rr).

R_f = 0.72 (10% Et_2O/hexanes)

[a]$^{20}_D$: +35.1° (c = 1.04, $CHCl_3$)

^{1}H NMR (600 MHz, $CDCl_3$): δ 7.30 (d, *J* = 8.5 Hz, 2H), 7.24 (d, *J* = 8.4 Hz, 2H), 5.48 (dtt, *J* = 15.0, 6.9, 1.3 Hz, 1H), 5.32 – 5.19 (m, 1H), 4.49 (dq, *J* = 12.7, 8.4 Hz, 1H), 4.38 (dq, *J* = 12.7, 8.4 Hz, 1H), 3.67 (dd, *J* = 8.6, 6.9 Hz, 1H), 2.79 – 2.70 (m, 1H), 2.46 (dtq, *J* = 13.5, 6.8, 1.2 Hz, 1H), 1.95 – 1.88 (m, 2H), 1.31 (h, *J* = 7.4 Hz, 2H), 0.83 (t, *J* = 7.4 Hz, 3H).

^{13}C NMR (151 MHz, $CDCl_3$): δ 171.6, 136.0, 134.1, 133.5, 129.3, 128.8, 125.4, 122.8 (q, *J* = 277.3 Hz), 60.4 (q, *J* = 36.6 Hz), 51.0, 36.4, 34.5, 22.3, 13.4.

^{19}F NMR (565 MHz, $CDCl_3$): δ -73.74 (t, *J* = 8.2 Hz).

HRMS (+p APCI) m/z: $[M + H]^+$ Calcd for $C_{16}H_{18}ClF_3O_2$ $[M+H]^+$ 335.1026; Found 335.1024

IR (neat): 2961, 2929, 2873, 1756, 1492 cm^{-1}

HPLC: The ester product was reduced to (*S*,*E*)-2-(4-chlorophenyl)oct-4-en-1-ol for better separation. (AD-H, *i*-PrOH/hexanes = 5/95, flow rate = 1.0 mL/min, l = 230 nm) t_r = 6.9 min (major), t_r = 9.3 min (minor).

Note: The corresponding ester was inseperable on chiral HPLC and there needed to be reduced to the corresponding primary alcohol to determine the ratio. Using $LiAlH_4$ the corresponding ester can be reduced to the alcohol without altering the enantiomeric ratio.

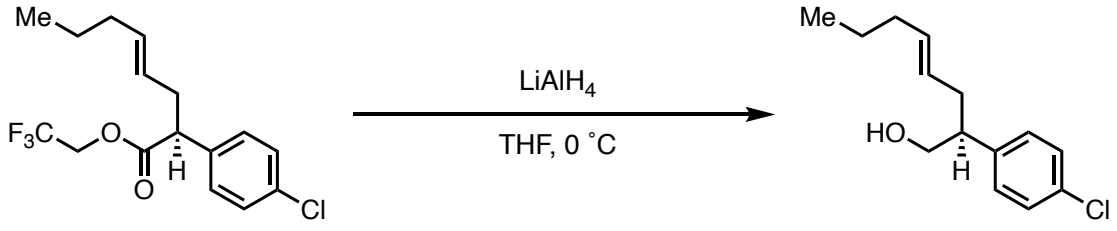

A flame dried flask purged under nitrogen was added the corresponding ester (0.2 mmol, 1.0 eq.) in THF (1 mL) and cooled to 0 ˚C via ice bath. Under nitrogen atmosphere, lithium aluminum hydride (1.0 M in THF, 1.0 mL, 1.0 mmol, 5.0 eq.) was added dropwise into the flask at 0 ˚C, and the mixture was allowed to warm to room temperature and stirred overnight. The reaction was quenched by adding 2.0 mL of 2.0 M aqueous HCl solution dropwise. The resulting solution was extracted by diethyl ether three times and dried over anhydrous sodium sulfate. The crude product was concentrated *in vacuo*, confirmed by ^{1}H NMR, and used for HPLC directly without purification.

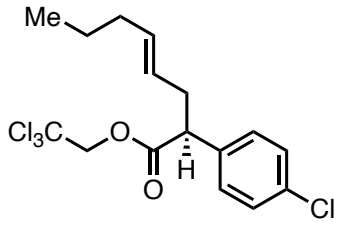

2,2,2-trichloroethyl (*S*,*E*)-2-(4-chlorophenyl)oct-4-enoate

This compound was prepared according to the general procedure for C-H insertion with *trans*-2-hexene (59 mg, 51% yield, 96% ee, 13:1 rr).

R_f = 0.75 (10% Et_2O/hexanes)

[a]$^{20}_D$: +26.6° (c = 1.0, $CHCl_3$)

^{1}H NMR (600 MHz, $CDCl_3$): **δ** 7.31 – 7.27 (m, 4H), 5.50 (dtt, *J* = 15.0, 6.8, 1.3 Hz, 1H), 5.31 (dtt, *J* = 15.3, 7.0, 1.4 Hz, 1H), 4.73 (d, *J* = 11.9 Hz, 1H), 4.68 (d, *J* = 12.0 Hz, 1H), 3.72 (dd, *J* = 8.4, 7.1 Hz, 1H), 2.81 (dddq, *J* = 15.1, 8.2, 7.1, 1.0 Hz, 1H), 2.55 – 2.46 (m, 1H), 1.91 (qt, *J* = 7.2, 1.0 Hz, 2H), 1.31 (h, *J* = 7.4 Hz, 2H), 0.83 (t, *J* = 7.4 Hz, 3H).

^{13}C NMR (151 MHz, $CDCl_3$): **δ** 171.5, 136.1, 134.0, 133.4, 129.5, 128.7, 125.6, 94.7, 74.1, 51.3, 36.1, 34.5, 22.7, 13.5.

HRMS (+p APCI) m/z: $[M + H]^+$ Calcd for $C_{16}H_{18}Cl_4O_2$ $[M+H]^+$ 383.0139; Found 383.0138.

IR (neat): 2957, 2928, 2872, 1750, 1491 cm^{-1}

HPLC: (OD-H, *i*-PrOH/hexanes = 1/99, flow rate = 0.1 mL/min, l = 210 nm) t_r = 49.6 min (major), t_r = 53.6 min (minor).

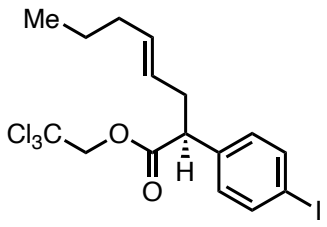

2,2,2-trichloroethyl (*S*,*E*)-2-(4-iodophenyl)oct-4-enoate

This compound was prepared according to the general procedure for C-H insertion with *trans*-2-hexene (137 mg, 96% yield, 96% ee, >20:1 rr).

R_f = 0.76 (10% Et_2O/hexanes)

$[a]^{20}_D$: +23.5° (c = 0.67, $CHCl_3$, 96% ee)

^{1}H NMR (600 MHz, $CDCl_3$): **δ** 7.65 (d, *J* = 8.3 Hz, 2H), 7.10 (d, *J* = 8.3 Hz, 2H), 5.50 (ddd, *J* = 15.1, 7.5, 6.0 Hz, 1H), 5.31 (ddd, *J* = 15.3, 7.7, 6.1 Hz, 1H), 4.73 (d, *J* = 12.0 Hz, 1H), 4.67 (d, *J* = 11.9 Hz, 1H), 3.69 (dd, *J* = 8.4, 7.0 Hz, 1H), 2.80 (dt, *J* = 15.0, 7.8 Hz, 1H), 2.50 (dt, *J* = 13.7, 7.0 Hz, 1H), 1.91 (q, *J* = 7.2 Hz, 2H), 1.31 (h, *J* = 7.3 Hz, 2H), 0.83 (t, *J* = 7.4 Hz, 3H).

^{13}C NMR (151 MHz, $CDCl_3$): **δ** 171.4, 137.7, 137.3, 134.0, 130.1, 125.6, 94.7, 93.1, 74.1, 51.5, 36.1, 34.5, 22.4, 13.5.

HRMS (+p APCI) m/z: $[M + H]^+$ Calcd for $C_{16}H_{19}Cl_3IO_2$ 474.9495; Found 474.9489.

IR (neat): 2955, 2923, 2854, 1751, 1138 cm^{-1}

HPLC: (AD-H, *i*-PrOH/hexanes = 0.5/99.5, flow rate = 1.0 mL/min, l = 210 nm) t_r = 6.4 min (major), t_r = 7.2 min (minor).

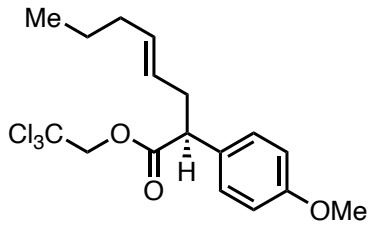

2,2,2-trichloroethyl (*S*,*E*)-2-(4-methoxyphenyl)oct-4-enoate

This compound was prepared according to the general procedure for C-H insertion with *trans*-2-hexene (36 mg, 47% yield, 96% ee, 10:1 rr).

R_f = 0.53 (10% Et_2O/hexanes)

[a]$^{20}_D$: +28.7° (c = 1.0, $CHCl_3$)

^{1}H NMR (600 MHz, $CDCl_3$): **δ** 7.27 (d, *J* = 8.7 Hz, 1H), 6.86 (d, *J* = 8.7 Hz, 1H), 5.51 (dtt, *J* = 15.0, 6.7, 1.3 Hz, 1H), 5.34 (dddt, *J* = 15.2, 7.8, 6.5, 1.4 Hz, 1H), 4.73 (d, *J* = 12.0 Hz, 1H), 4.66 (d, *J* = 12.0 Hz, 1H), 3.79 (s, 3H), 3.69 (dd, *J* = 8.8, 6.8 Hz, 1H), 2.85 – 2.76 (m, 1H), 2.49 (dtq, *J* = 14.2, 6.6, 1.2 Hz, 1H), 1.92 (qd, *J* = 6.9, 1.3 Hz, 2H),1.31 (h, *J* = 7.4 Hz, 2H), 0.83 (t, *J* = 7.4 Hz, 3H).

^{13}C NMR (151 MHz, $CDCl_3$): **δ** 172.1, 158.9, 133.5, 129.8, 129.1, 126.2, 113.9, 94.8, 74.0, 55.2, 51.1, 36.3, 34.5, 22.4, 13.5.

HRMS (+p APCI) m/z: $[M + H]^+$ Calcd for $C_{17}H_{21}Cl_3O_3$ $[M+H]^+$ 379.0635; found 379.0633.

IR (neat): 2956, 2929, 1749, 1610, 1510 cm^{-1}

HPLC: (OD-H, *i*-PrOH/hexanes = 1/99, flow rate = 0.5 mL/min, l = 210 nm) t_r = 10.3 min (major), t_r = 12.0 min (minor).

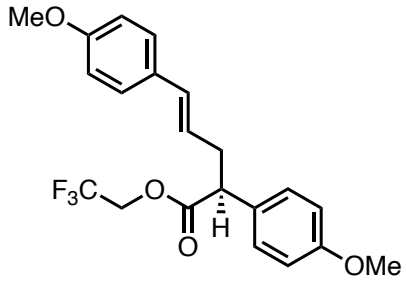

2,2,2-trifluoroethyl (*S*,*E*)-2,5-bis(4-methoxyphenyl)pent-4-enoate

A flame-dried flask with an oven-dried condenser was charged with 4 Å MS and Rh_2(*R*-*p*-PhTPCP)$_4$ (5.3 mg, 0.003 mmol, 1.0 mol %) and purged three times with nitrogen. Anethole (**S1**, 0.23 mL, 1.50 mmol, 5.0 eq.) and distilled CH_2Cl_2 (1.15 mL) were added,[Note 1] and the mixture was heated to 40 ˚C and refluxed for 10 min before addition of the diazoester. In a separate flask, diazoester **5a**[Note 2] (82.3 mg, 0.30 mmol, 1.0 eq.) was dissolved in distilled CH_2Cl_2 (1.15 mL) under argon. Under refluxing conditions, the diazoester solution was added to the reaction vessel dropwise via syringe pump over 3 h. The reaction mixture was stirred at 40 ˚C for another 30 min and concentrated *in vacuo*. The crude product was purified by flash column chromatography (10% Et_2O/hexanes) to afford the product as a clear oil (62.0 mg, 52% yield, 91% ee).

R_f = 0.71 (10% Et_2O/hexanes)

[a]$^{20}_D$: +53.2° (c = 0.67, $CHCl_3$, 96% ee)

^{1}H NMR (600 MHz, $CDCl_3$): **δ** 7.26 (d, *J* = 8.7 Hz, 2H), 7.22 (d, *J* = 8.7 Hz, 2H), 6.88 (d, *J* = 8.7 Hz, 2H), 6.82 (d, *J* = 8.7 Hz, 2H), 6.39 (d, *J* = 15.8 Hz, 1H), 5.95 (ddd, *J* = 15.7, 7.6, 6.6 Hz, 1H), 4.49 (dq, *J* = 12.7, 8.5 Hz, 1H), 4.39 (dq, *J* = 12.7, 8.4 Hz, 1H), 3.80 (s, 3H), 3.79 (s, 3H), 3.76 (dd, *J* = 8.7, 6.8 Hz, 1H), 2.94 (dddd, *J* = 14.3, 8.8, 7.6, 1.3 Hz, 1H), 2.66 (dtd, *J* = 14.4, 6.7, 1.5 Hz, 1H).

^{13}C NMR (151 MHz, $CDCl_3$): **δ** 172.1, 159.1, 159.0, 131.9, 129.9, 129.4, 128.9, 127.2, 123.9, 122.8 (d, *J* = 277.5 Hz), 114.1, 113.9, 60.4 (q, *J* = 36.6 Hz), 55.2, 55.2, 50.7, 36.8.

HRMS (-p APCI) m/z: [M - H]$^-$ Calcd for $C_{21}H_{21}F_3O_4$ [M-H]$^-$ 393.1392; found 391.1313

IR (neat): 2935, 2838, 1752, 1608, 1510 cm^{-1}

HPLC: (OD-H, *i*-PrOH/hexanes = 1/99, flow rate = 1.0 mL/min, l = 210 nm) t_r = 16.0 min (major), t_r = 22.9 min (minor).

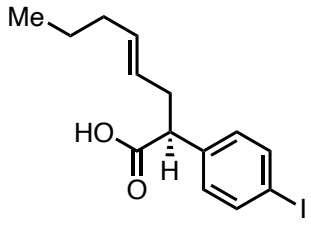

(*S*,*E*)-2-(4-iodophenyl)oct-4-enoic acid

To a round-bottom flask was added 2,2,2-trichloroethyl (*S*,*E*)-2-(4-iodophenyl)oct-4-enoate (2.940 g, 6.18 mmol, 1.00 eq.), zinc dust (4.041 g, 61.8 mmol, 10.0 eq.), and acetic acid (77.0 mL) then stirred for 18 h. The reaction mixture was diluted with water, then filtered through celite and eluted with EtOAc. The mixture was then diluted with EtOAc, washed with water two times, then brine eight times. The organic layers were dried over anhydrous sodium sulfate and concentrated *in vacuo*. The crude clear oil was taken forward directly without purification (2.04 g, 96% yield).

R_f = 0.52 (50% EtOAc/hexane)

[a]$^{20}_D$: +52.7° (c = 0.69, $CHCl_3$)

^{1}H NMR (600 MHz, $CDCl_3$): δ 7.62 (d, *J* = 8.2 Hz, 1H), 7.07 (d, *J* = 8.3 Hz, 1H), 5.46 – 5.38 (m, 1H), 5.33 – 5.25 (m, 1H), 3.97 (s, 1H), 3.50 (s, 2H), 3.14 (s, 2H), 2.72 (dt, *J* = 14.6, 7.6 Hz, 1H), 2.35 (dt, *J* = 14.0, 7.0 Hz, 1H), 1.90 (q, *J* = 7.1 Hz, 2H), 1.30 (h, *J* = 7.3 Hz, 2H), 0.82 (t, *J* = 7.4 Hz, 3H).

^{13}C NMR (151 MHz, $CDCl_3$): **δ** 178.3, 137.7, 133.9, 130.1, 125.7, 93.0, 51.4, 36.1, 34.5, 22.4, 13.5**.**

IR (neat): 3024, 2955, 2925, 2870, 1704 cm^{-1}

HRMS (+p APCI) m/z: $[M + H]^+$ Calcd for $C_{14}H_{17}O_2I$ 345.0351; Found 345.0348

HPLC: (AS-H, *i*-PrOH/hexanes = 5/95, flow rate = 1.0 mL/min, l = 210 nm) t_r = 6.4 min (minor), t_r = 7.7 min (major).

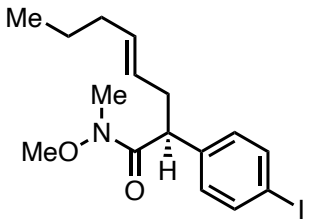

(*S*,*E*)-2-(4-iodophenyl)-*N*-methoxy-*N*-methyloct-4-enamide

To a flame-dried round-bottom flask was added (*S*,*E*)-2-(4-iodophenyl)oct-4-enoic acid (2.131 g, 6.19 mmol, 1.0 eq.) in *N*,*N*-dimethylformamide (15.5 mL). The reaction was cooled to 0 ˚C, and HATU (2.825 g, 7.43 mmol, 1.2 eq.) and *N*,*N*-diisopropylethylamine (3.23 mL, 2.66 mmol, 3.0 eq.) were added and the reaction was stirred for 20 min. *N*,*O*-dimethylhydroxylamine hydrochloride (0.905 g, 9.28 mmol, 1.5 eq.) was added and the reaction was warmed to room temperature slowly and stirred for 16 h. The mixture was diluted with EtOAc and water and the layers were separated. The organic phase was washed with brine eight times, dried over anhydrous sodium sulfate, and concentrated *in vacuo*. The crude residue was purified by flash column chromatography (20% Et_2O/hexanes) to afford the product as a clear oil (1.77 g, 74% yield).[Note 1]

Note 1: We found that the enantiopurity slightly eroded during the conversion of (*S*,*E*)-2-(4-iodophenyl)oct-4-enoic acid to (*S*,*E*)-2-(4-iodophenyl)-*N*-methoxy-*N*-methyloct-4-enamide

(80% ee) but elected to advance the material to investigate the viability of a C–O coupling strategy.

R_f = 0.37 (33% Et_2O/hexanes)

[a]$^{20}_D$: +41.6° (c = 0.50, $CHCl_3$)

^{1}H NMR (600 MHz, $CDCl_3$): **δ** 7.62 (d, *J* = 8.2 Hz, 1H), 7.07 (d, *J* = 8.3 Hz, 1H), 5.46 – 5.38 (m, 1H), 5.33 – 5.25 (m, 1H), 3.97 (br, 1H), 3.50 (s, 2H), 3.14 (s, 2H), 2.72 (dt, *J* = 14.6, 7.6 Hz, 1H), 2.35 (dt, *J* = 14.0, 7.0 Hz, 1H), 1.90 (q, *J* = 7.1 Hz, 2H), 1.30 (h, *J* = 7.3 Hz, 2H), 0.82 (t, *J* = 7.4 Hz, 3H).

^{13}C NMR (151 MHz, $CDCl_3$): **δ** 173.7, 139.5, 137.5, 133.1, 130.3, 126.9, 92.3, 61.4, 47.6, 37.0, 34.6, 32.2, 22.5, 13.5.

IR (neat): 2957, 2929, 2870, 1660, 1483 cm^{-1}

HRMS (+p APCI) m/z: $[M + H]^+$ Calcd for $C_{16}H_{22}O_2IN$ 388.0773; Found 388.0765.

HPLC: (AS-H, *i*-PrOH/hexanes = 1/99, flow rate = 1.0 mL/min, l = 230 nm) t_r = 6.3 min (minor), t_r = 7.9 min (major), 80% ee.

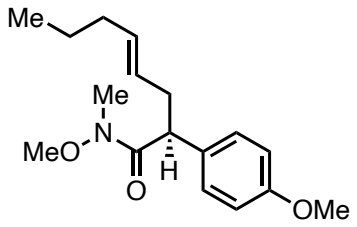

(*S*,*E*)-*N*-methoxy-2-(4-methoxyphenyl)-*N*-methyloct-4-enamide

The Buchwald C-O coupling[3] was conducted by Nick Falcone and HPLC data collected by Aaron Bosse.

Spectral data matched those obtained through direct C–H insertion/Weinreb amide formation.

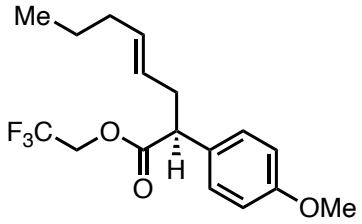

2,2,2-trifluoroethyl (*S*,*E*)-2-(4-methoxyphenyl)oct-4-enoate

A flame-dried round-bottom flask with oven dried condenser was charged with 4 Å MS and Rh_2(*R*-*p*-PhTPCP)$_4$ (0.05 mmol, 0.5 mol %) and then, purged three times with nitrogen. *Trans*-hex-2-ene (6.24 mL, 50.0 mmol, 5.0 eq.) and distilled CH_2Cl_2 (38.0 mL) were added,[Note 1] and the mixture was heated to 40 ˚C and refluxed for 10 min before addition of the diazo compounds. In a separate flask, the diazoester[Note 2] (2.742 g, 10.0 mmol, 1.0 eq.) was dissolved in distilled CH_2Cl_2 (38.0 mL) under argon. Under refluxing conditions, the diazoester solution was added to the reaction vessel dropwise via syringe pump over 3 h. The reaction mixture was stirred at 40 ˚C for another 30 min and concentrated *in vacuo*. The crude product was purified by flash column chromatography (2% Et_2O/hexanes) to afford the productas a clear oil (2.345 g, 71% yield, 96% ee, 11:1 rr).

Note 1: Solvent must be distilled over CaH_2 and stored over activated 4 Å MS.

Note 2: The diazoester was prepared according to literature precedent.[2]

R_f = 0.46 (10% Et_2O/hexanes)

[a]$^{20}_D$: +37.0˚ (c = 0.57, $CHCl_3$)

^{1}H NMR (600 MHz, $CDCl_3$): δ 7.22 (d, *J* = 8.7 Hz, 1H), 6.86 (d, *J* = 8.7 Hz, 1H), 5.49 (dtt, *J* = 15.0, 6.8, 1.3 Hz, 1H), 5.30 (dddt, *J* = 15.2, 7.7, 6.5, 1.4 Hz, 1H), 4.49 (dq, *J* = 12.7, 8.4 Hz, 1H), 4.35 (dq, *J* = 12.7, 8.4 Hz, 1H), 3.79 (s, 2H), 3.65 (dd, *J* = 8.9, 6.6 Hz, 1H), 2.79 – 2.70 (m, 1H), 2.49 – 2.41 (m, 1H), 1.96 – 1.87 (m, 1H), 1.32 (h, *J* = 7.4 Hz, 1H), 0.83 (t, *J* = 7.4 Hz, 2H).

^{13}C NMR (151 MHz, $CDCl_3$): **δ** 172.4, 159.2, 133.8, 129.9, 129.1, 126.1, 123.1 (q, *J* = 277.4 Hz), 114.2, 60.5 (q, *J* = 36.6 Hz), 55.4, 51.0, 36.7, 34.7, 22.5, 13.6.

^{19}F NMR (565 MHz, $CDCl_3$): **δ** -73.7 (t, *J* = 8.6 Hz).

IR (neat): 2959, 2931, 1754, 1611, 1165 cm^{-1}

HRMS (+p APCI) m/z: $[M + H]^+$ Calcd for $C_{17}H_{22}F_3O_3$ 331.1521; Found 331.1514.

HPLC: (OD-H, *i*-PrOH/hexanes = 1/99, flow rate = 0.5 mL/min, l = 210 nm) t_r = 11.0 min (minor), t_r = 13.4 min (major).

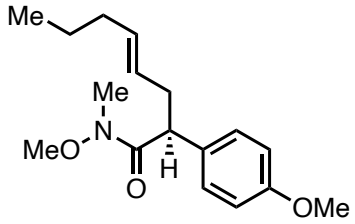

(*S*,*E*)-*N*-methoxy-2-(4-methoxyphenyl)-*N*-methyloct-4-enamide

To a flame-dried round-bottom flask under nitrogen was added 2,2,2-trifluoroethyl (*S*,*E*)-2-(4-methoxyphenyl)oct-4-enoate (2.330 g, 7.05 mmol, 1.0 eq.) and THF (141 mL). *N,O*-dimethylhydroxylamine hydrochloride (0.826 g, 8.46 mmol, 1.2 eq.) was added and the solution was cooled to 0 ˚C. Isopropylmagnesium chloride (2.0 M in THF, 10.6 mL, 21.2 mmol, 3.0 eq.) was added dropwise, and the reaction was warmed to room temperature and stirred for 13 h. This was quenched with saturated aqueous NH_4Cl, basified with 10% NaOH solution, and extracted with EtOAc three times. The combined organic layers were dried over anhydrous magnesium sulfate and concentrated *in vacuo*. The crude residue was purified by flash column chromatography (15% Et_2O/hexanes) to afford the product as a clear oil (1.438 g, 70% yield, 94% ee).

R_f = 0.31 (20% EtOAc/hexanes)

[a]$^{20}_{D}$: +72.1˚ (c = 0.62, $CHCl_3$)

^{1}H NMR (600 MHz, $CDCl_3$): **δ** 7.23 (d, *J* = 8.7 Hz, 2H), 6.83 (d, *J* = 8.7 Hz, 2H), 5.43 (dtt, *J* = 14.8, 6.7, 1.3 Hz, 1H), 5.32 (dtt, *J* = 15.3, 7.0, 1.4 Hz, 1H), 3.98 (s, 1H), 3.77 (s, 4H), 3.49 (s, 3H), 3.14 (s, 3H), 2.77 – 2.68 (m, 1H), 2.35 (dtd, *J* = 13.7, 6.9, 1.1 Hz, 1H), 1.91 (td, *J* = 7.0, 5.6 Hz, 2H), 1.31 (h, *J* = 7.3 Hz, 2H), 0.83 (t, *J* = 7.4 Hz, 3H).

^{13}C NMR (151 MHz, $CDCl_3$): **δ** 174.7, 158.6, 132.7, 132.1, 130.1, 129.3, 127.6, 114.0, 61.4, 55.3, 47.3, 37.4, 34.7, 32.3, 22.6, 13.7.

IR (neat): 2957, 2932, 1657, 1610, 1509, 1247 cm^{-1}

HRMS (+p APCI) m/z: $[M + H]^+$ Calcd for $C_{17}H_{26}O_3N$ 292.1913; Found 292.1908.

HPLC: (OD-H, *i*-PrOH/hexanes = 5/95, flow rate = 0.5 mL/min, l = 210 nm) t_r = 11.9 min (major), t_r = 13.6 min (minor).

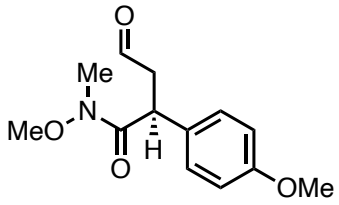

(*S*)-*N*-methoxy-2-(4-methoxyphenyl)-*N*-methyl-4-oxobutanamide

This reaction was conducted Nick Falcone and the reported data can be found in the corresponding publication.[4]

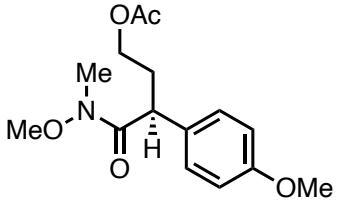

(*S*)-4-(methoxy(methyl)amino)-3-(4-methoxyphenyl)-4-oxobutyl acetate

This reaction was conducted Nick Falcone and the reported data can be found in the corresponding publication.[4]

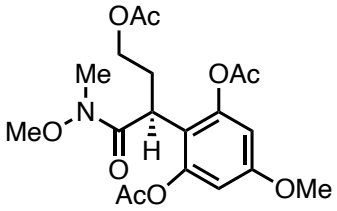

(*S*)-2-(4-acetoxy-1-(methoxy(methyl)amino)-1-oxobutan-2-yl)-5-methoxy-1,3-phenylene diacetate

This reaction was conducted Nick Falcone and the pyridine sulfonic acid synthesized by Hojoon park. The reported data can be found in the corresponding publication.[4]

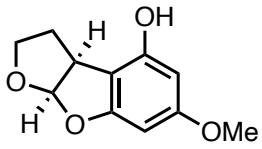

(3a*S*,8a*R*)-6-methoxy-2,3,3a,8a-tetrahydrofuro[2,3-*b*]benzofuran-4-ol

This reaction was conducted Nick Falcone and the reported data can be found in the corresponding publication.[4]

References

1. Qin, C.; Davies, H. M. L., Role of Sterically Demanding Chiral Dirhodium Catalysts in Site-Selective C–H Functionalization of Activated Primary C–H Bonds. *J. Am. Chem. Soc.* **2014,** *136* (27), 9792-9796.
2. Zhang, B.; Hollerbach, M. R.; Blakey, S. B.; Davies, H. M. L., C–H Functionalization Approach for the Synthesis of Chiral C2-Symmetric 1,5-Cyclooctadiene Ligands. *Org. Lett.* **2019,** *21* (24), 9864-9868.
3. Altman, R. A.; Shafir, A.; Choi, A.; Lichtor, P. A.; Buchwald, S. L., An Improved Cu-Based Catalyst System for the Reactions of Alcohols with Aryl Halides. *J. Org. Chem.* **2008,** *73* (1), 284-286.
4. Falcone, N. A.; Bosse, A. T.; Park, H.; Yu, J.-Q.; Davies, H. M. L.; Sorensen, E. J., A C–H Functionalization Strategy Enables an Enantioselective Formal Synthesis of (−)-Aflatoxin B2. *Org. Lett.* **2021,** *23* (24), 9393-9397.

5.4. Experiment Section for Chapter 4

Commercially available ketones

These ketones were purchased from commercial sources and used without purification:

1,2-diphenylethan-1-one

1-(4-bromophenyl)-2-phenylethan-1-one

1-(4-fluorophenyl)-2-phenylethan-1-one

Substrates and reagents

The following compounds were prepared according to published procedures:

Rh_2(*S*-TPPTTL)$_4$[1]

(*E*)-*tert*-butyldimethyl(pent-2-en-1-yloxy)silane[2]

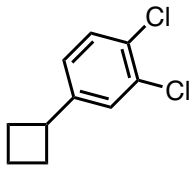

1,2-dichloro-4-cyclobutylbenzene

To a flame-dried round-bottom flask with findenser was charged with a stir-bar and oven- dried silver Mg turnings (646 mg, 1.5 equiv, 26.56 mmol). The RBF was sealed, flame-dried again, and backfilled with N_2 (x3). To the reaction vessel was added dry THF (1 molar) and was allowed to stir for over 30 minutes under N_2 line. Afterwards, 4-bromo-1,2-dichlorobenzene (4.0 g, 1 equiv, 17.71 mmol) was added drop-wise over 10 min (can be very exothermic after complete addition). The Grignard was stirred for 1 h then cooled to 0 ^oC via ice bath. Then cyclobutanone (800 mg, 1 equiv, 11.41 mmol) was added and the reaction was warmed to room temperature overnight. The crude mixture was quenched with saturated ammonium chloride,

extracted with ether (x2), then dried with $MgSO_4$, filtered, and concentrated in vacuo. The crude material was carried further without further purification.

^{1}H NMR (400 MHz, $CDCl_3$) δ 7.57 (d, *J* = 2.2 Hz, 1H), 7.42 (d, *J* = 8.3 Hz, 1H), 7.32 (dd, *J* = 8.3, 2.2 Hz, 1H), 2.52 – 2.45 (m, 2H), 2.39 – 2.29 (m, 2H), 2.09 – 1.98 (m, 1H), 1.71 (dtt, *J* = 11.5, 8.9, 7.5 Hz, 1H).

To a flame-dried 50 ml round-bottom purged under N_2 (x3) was added 1-(3,4-dichlorophenyl)cyclobutan-1-ol (1.0 g, 1 equiv, 4.6 mmol) and TFA (7.1 ml, 20 equiv, 92 mmol) then cooled to 0 ºC in an ice bath for 10 min. At 0 ºC triethylsilane (3.7 ml, 5 equiv, 23 mmol) was added dropwise then the mixture was warmed to room temperature and stirred overnight. The reaction was cooled to 0 ºC and quenched with saturated sodium bicarbonate, extracted with DCM, then dried with $MgSO_4$, filtered, and concentrated in vacuo. The crude material was purified by flash chromatography (hexanes) to yield a pink oil. The residue was then subjected to Kugelrohr distillation (0.5 mmHg, 100 ºC) for 20 min to remove excess silane resulting in the clean product as a clear oil (442 mg, 48% yield).

Rf = 0.76 (hexanes)

^{1}H NMR (600 MHz, $CDCl_3$) δ 7.34 (d, *J* = 8.2 Hz, 1H), 7.28 (d, *J* = 2.1 Hz, 1H), 7.03 (dd, *J* = 8.2, 2.1 Hz, 1H), 3.49 (p, *J* = 8.6 Hz, 1H), 2.34 (qt, *J* = 7.6, 2.2 Hz, 2H), 2.15 – 1.95 (m, 3H), 1.90 – 1.81 (m, 1H).

^{13}C NMR (151 MHz, $CDCl_3$) δ 146.5, 132.0, 130.0, 129.3, 128.3, 125.8, 39.3, 29.5, 18.1.

IR (neat) 2963, 2940, 2891, 2861, 1590, 1557, 1472, 1443, 1396, 1378, 1331, 1244, 1131, 1096, 1028, 920, 874, 816, 787, 709, 672, 590 cm^{-1}.

HRMS (+p APCI) cald for $C_{10}H_{10}Cl_2$ $[M+]^+$ 200.0160 found 200.0158.

General procedure A for the synthesis of Weinreb Amides

To a 55 mL test-tube with stir-bar was charged with the corresponding acetic acid (1 equiv.), N,O- dimethylhydroxylamine hydrochloride (1.5 equiv.), N-(3- Dimethylaminopropyl)-N′-ethylcarbodiimide hydrochloride (1.5 equiv.), and N,N-dimethylpyridin-4-amine (1.5 equiv.). To the solid mixture was added DCM (0.250 molar). The reaction mixture was allowed to stir overnight at room temperature. Afterwards, the organic layer was washed with 1M HCl and then the organic layer was dried with $MgSO_4$, filtered, and concentrated in vacuo to afford the corresponding Weinreb amide without further purification and clean by ^1H NMR. The materials were moved forwards to the next step without further characterization.

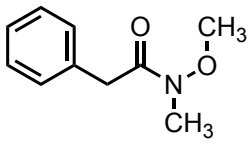

***N*-methoxy-*N*-methyl-2-phenylacetamide**

Prepared from general procedure A. To a 1L round-bottom flask with stir-bar was charged with the 2-phenylacetic acid (1 equiv., 734 mmol), N,O-dimethylhydroxylamine hydrochloride (1.5 equiv., 1.10 mol), N-(3-Dimethylaminopropyl)-N′-ethylcarbodiimide hydrochloride (1.5 equiv., 1.10 mol), and N,N-dimethylpyridin-4-amine (1.5 equiv., 1.10 mol). To the solid mixture was added DCM (0.250 molar). The corresponding compound is a transparent light-yellow oil (110 g, 614 mmol, 83% yield). The material was moved forwards to the next step without further characterization and physical and spectral data were identical to those previously reported for this compound.[3]

^1H NMR (400 MHz, $CDCl_3$) δ 7.34 – 7.27 (m, 4H), 7.27 – 7.20 (m, 1H), 3.77 (s, 2H), 3.59 (s, 3H), 3.18 (s, 3H).

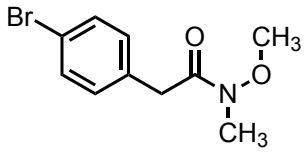

2-(4-bromophenyl)-*N*-methoxy-*N*-methylacetamide

Prepared from general procedure A. To a 55 mL test-tube with stir-bar was charged with 2-(4-bromophenyl)acetic acid (1 equiv., 5.00 mmol), N,O-dimethylhydroxylamine hydrochloride (1.5 equiv., 7.50 mmol), N-(3-Dimethylaminopropyl)-N′-ethylcarbodiimide hydrochloride (1.5 equiv., 7.50 mmol), and N,N-dimethylpyridin-4-amine (1.5 equiv., 7.50 mmol). To the solid mixture was added DCM (0.250 molar). The corresponding compound is a white solid (1.13 g, 4.38 mmol, 88% yield). The material was moved forwards to the next step without further characterization and physical and spectral data were identical to those previously reported for this compound.[3]

^{1}H NMR (400 MHz, $CDCl_3$) δ 7.44 (d, *J* = 8.4 Hz, 2H), 7.17 (d, *J* = 8.4 Hz, 2H), 3.72 (s, 2H), 3.63 (s, 3H), 3.19 (s, 3H).

Procedure to wash Magnesium Turnings:

1. 1) Add magnesium turnings to a large-fritted glass funnel.
2. 2) Pour 1-3M HCl onto magnesium turnings. This will effervesce the magnesium exposing a fresh Magnesium surface. **WARNING**: **this is an exothermic reaction**. Pour slowly and triturate the turnings so that the solution saturates the turnings. This step usually requires excess HCl solution until every single turning has a fresh silvery Mg surface.
3. 3) After you have washed the Mg, rinse the magnesium with excess ethanol to wash off any remaining aqueous solution while triturating.

4. 4) Dry your magnesium turnings by rinsing with excess diethyl ether while triturating.
5. 5) After you have dried your silver Mg turnings with the ether, you can store it in the oven at 130 ^{o}C.

Preparation of 1M Grignard Solutions:

To a flame-dried round-bottom flask with findenser was charged with a stir-bar and oven- dried silver Mg turnings (1.1 equiv.). The RBF was sealed and backfilled with N_2 (x3). To the reaction vessel was added dry THF (1 molar) and was allowed to stir for over 30 minutes under N_2 line. Afterwards, the desired halide (1 equiv.) was added drop-wise over 30 minutes [can be very exothermic after complete addition]. The solution was then placed in a sonicator and sonicated under N_2 balloon for over 3 hours. The desired 1M Grignard solution was then subjected to the Grignard addition.

General Procedure B for the synthesis of ketones

To a flame-dried round- bottom flask with stir-bar was added the corresponding Weinreb amide (1 equiv.), sealed and backfilled with N_2 (x3), and subsequently, dry THF (0.15 molar) was added to the sealed-vessel under N_2 balloon. The reaction mixture was cooled with 0 ^{o}C ice bath and allowed to stir for over 10 minutes. Subsequently to the cooled solution was added the corresponding 1M Grignard reagent (1.5 equiv.). The reaction mixture was allowed to stir overnight warming up to room temperature. To reaction mixture was quenched with excess saturated NH_4Cl solution, diluted with ethyl acetate, extracted with ethyl acetate (x3), the combined organic layers were dried with $MgSO_4$, filtered, and concentrated in vacuo. The crude material was subjected to flash chromatography hexanes/ethyl acetate. The collected fractions were concentrated in vacuo to afford the corresponding ketone.

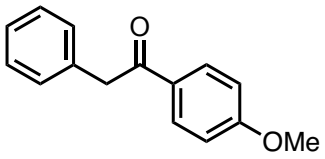

1-(4-methoxyphenyl)-2-phenylethan-1-one

1M Grignard solution prepared from Preparation of 1M Grignard Solutions. Magnesium (1.6 g, 2.5 equiv, 67 mmol) and 1-bromo-4-methoxybenzene (5.0 g, 3.3 mL, 1 equiv, 27 mmol) was used. The resultant Grignard solution is an opaque gray solution.

Ketone prepared from General Procedure B. N-methoxy-N-methyl-2-phenylacetamide (1.0 g, 1 Eq, 5.6 mmol) was used. The crude material was dry-loaded onto silica and subjected to flash chromatography hexanes/EtOAc (POI elutes at 20% EtOAc). The collected fractions were concentrated in vacuo to afford 1-(4-methoxyphenyl)-2- phenylethan-1-one (860 mg, 3.80 mmol, 68 %) tinged with yellow amorphous material and white crystals. The material was dissolved in minimal hexanes and allowed to recrystallize in -20 ^{o}C freezer in a sealed vial, filtered, and the solids collected and dried to afford 1-(4-methoxyphenyl)-2-phenylethan-1-one (860 mg, 3.80 mmol, 68 %) as white solids. The physical and spectral data were identical to those previously reported for this compound.[4]

^{1}H NMR (600 MHz, $CDCl_3$) δ 8.02 – 7.97 (m, 2H), 7.34 – 7.22 (m, 5H), 6.95 – 6.90 (m, 2H), 4.23 (s, 2H), 3.86 (s, 3H).

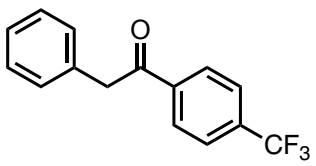

2-phenyl-1-(4-(trifluoromethyl)phenyl)ethan-1-one

1M Grignard solution prepared from Preparation of 1M Grignard Solutions. Magnesium (19.0 g, 1.1 equiv, 782 mmol) and 1-bromo-4-(trifluoromethyl)benzene (160 g, 98.6 mL, 1 equiv, 711 mmol) was used. The resultant Grignard solution is a dark brown solution.

Ketone prepared from General Procedure B. N-methoxy-N-methyl-2-phenylacetamide (10 g, 1 Eq, 44 mmol) was used. The crude material was dry-loaded onto silica and subjected to flash chromatography Hexanes:EtOAc (100 g column; 0% EtOAc 5 CV --> 0% - 100% 20 CV --> 100% 5CV; POI elutes at 70% EtOAc). The collected fractions were concentrated in vacuo. The amorphous orange material was resuspended in minimal amount of ethanol and filtered. The white solids were dried to afford 2-phenyl-1-(4- (trifluoromethyl)phenyl)ethan-1-one (20 g, 76 mmol, 85 %) as a white powder. The physical and spectral data were identical to those previously reported for this compound.[5]

^{1}H NMR (600 MHz, $CDCl_3$) δ 8.11 (ddt, J = 8.9, 1.9, 0.9 Hz, 2H), 7.72 (ddt, J = 8.4, 1.7, 0.8 Hz, 2H), 7.37 – 7.31 (m, 2H), 7.27 – 7.24 (m, 3H), 4.31 (s, 2H).

^{19}F NMR (376 MHz, $CDCl_3$) δ -63.2.

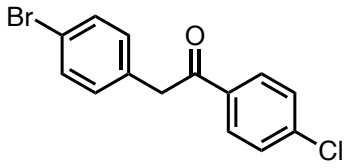

2-(4-bromophenyl)-1-(4-chlorophenyl)ethan-1-one

Ketone prepared from General Procedure B. (4-chlorophenyl) magnesium bromide (5.02 g, 23 mL, 1 molar, 1.5 equiv, 23.2 mmol) and 2-(4-bromophenyl)-N-methoxy-N- methylacetamide (4.0 g, 1 equiv, 15.5 mmol) was used. The crude material was dry-loaded onto silica and subjected to flash chromatography hexanes/EtOAc. The collected fractions were concentrated in vacuo to afford 2-(4-bromophenyl)-1-(4-chlorophenyl)ethan-1-one (3.97 g, 12.8 mmol, 83 %) as

a white powder. The physical and spectral data were identical to those previously reported for this compound.[6]

^{1}H NMR (400 MHz, $CDCl_3$) δ 7.95 – 7.90 (m, 2H), 7.48 – 7.42 (m, 4H), 7.15 – 7.10 (m, 2H), 4.21 (s, 2H).

General Procedure C for the synthesis of aryl diazoketones

Note: Hood lights were turned off to minimize product decomposition.

To a flame-dried 20 mL dram vial was added the corresponding ketone (1 equiv.), o-NBSA (1.5 equiv.), and acetonitrile (0.30 molar). The reaction mixture was back-filled with N_2 (x3), and then the reaction mixture was cooled to 0 ^oC via water-bath. To the cooled reaction mixture was added 2,3,4,6,7,8,9,10- octahydropyrimido[1,2-a]azepine (4 equiv.) drop-wise. The reaction mixture was stirred for 30 minutes in an ice-water bath. The wet crude material was diluted with a slurry containing SiO_2 with 1% TEA in 10% diethyl ether: 90% hexanes and concentrated in vacuo to afford a dry-load. This dry-load was then subjected to a silica-plug doped with 1% TEA in 10% diethyl ether: 90% hexanes. The colored material was collected, concentrated in vacuo to afford the corresponding diazo ketone as a yellow or orange powder.

Storage: The vial was sealed under nitrogen and placed into a -20 ^oC freezer to minimize decomposition.

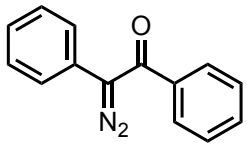

2-diazo-1,2-diphenylethan-1-one

Diazo was prepared from General Procedure C. 1,2-diphenylethan-1-one (5000 mg, 1 Eq, 25.48 mmol), o-NBSA (8.720 g, 1.5 equiv, 38.22 mmol), and 2,3,4,6,7,8,9,10- octahydropyrimido[1,2-a]azepine (15.51 g, 15.4 mL, 4 equiv, 101.9 mmol) was used. The crude material was subjected to a silica plug (15 inch silica) doped with 1% TEA in 10% diethyl ether: 90% hexanes. The dry-loaded, eluted through the silica plug (all yellow band collected). The material was concentrated in vacuo to afford 2-diazo-1,2- diphenylethan-1-one (3.65 g, 16.4 mmol, 65 %) as an orange amorphous solid. The desired diazo was sensitive to deuterated solvent and was not stable enough to obtain a pure ^{13}C NMR. The physical and spectral data were identical to those previously reported for this compound.[7]

^{1}H NMR (400 MHz, C_6D_6) δ 7.46 – 7.34 (m, 4H), 7.09 (t, 2H), 7.05 – 6.98 (m, 1H), 6.97 – 6.91 (m, 3H).

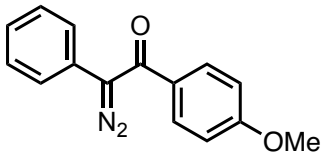

2-diazo-1-(4-methoxyphenyl)-2-phenylethan-1-one

Diazo was prepared from General Procedure C. 1-(4-methoxyphenyl)-2-phenylethan-1- one (226 mg, 1 equiv, 1.00 mmol), o-NBSA (342 mg, 1.5 equiv, 1.50 mmol), and 2,3,4,6,7,8,9,10-octahydropyrimido[1,2-a]azepine (609 mg, 603 µL, 4 equiv, 4.00 mmol) was used. The crude material was subjected to a silica plug doped with 1% TEA in 10% diethyl ether: 90% hexanes. The material was concentrated in vacuo to afford 2-diazo- 1-(4-methoxyphenyl)-2-phenylethan-1-one (158.6 mg, 628.7 µmol, 63 %) as an amorphous orange powder. The desired diazo was sensitive to deuterated solvent and was not stable enough to obtain a pure ^{13}C NMR.

^{1}H NMR (600 MHz, $CDCl_3$) δ 7.64 – 7.58 (m, 2H), 7.47 – 7.37 (m, 4H), 7.28 – 7.23 (m, 1H), 6.93 – 6.87 (m, 2H), 3.85 (s, 3H).

IR (neat): 2934, 2838, 2066 (strong), 1737, 1600, 1573, 1509, 1496, 1461, 1417, 1347, 1328, 1307, 1283, 1248, 1171, 1111, 1069, 1029, 913, 859, 839, 786, 757, 691, 645, 621, 568, 519, 497, 406 cm^{-1}.

HRMS (+p ESI): calc. mass for $C_{15}H_{13}O_2$ $[M + H - N_2]^-$ - 225.09101; obs. mass for $C_{15}H_{13}O_2$ $[M + H - N_2]^-$ - 225.09094.

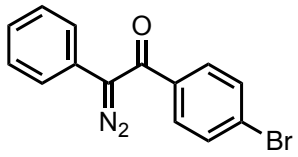

1-(4-bromophenyl)-2-diazo-2-phenylethan-1-one

Diazo was prepared from General Procedure C. 1-(4-bromophenyl)-2-phenylethan-1-one (5.73 g, 1 equiv, 20.83 mmol), o-NBSA (6.5 g, 1.3 equiv, 27.1 mmol), and 2,3,4,6,7,8,9,10-octahydropyrimido[1,2-a]azepine (6.98 g, 6.84 mL, 2.2 equiv, 45.82 mmol) was used. The crude material was subjected to a silica plug doped with 1% TEA in 10% diethyl ether: 90% hexanes. The material was concentrated in vacuo to afford 1-(4-bromophenyl)-2-diazo-2-phenylethan-1-one (4.07 g, 13.5 mmol, 65 %) as an amorphous orange powder. The desired diazo was sensitive to deuterated solvent and was not stable enough to obtain a pure ^{13}C NMR.

^{1}H NMR (600 MHz, $CDCl_3$) δ 7.58 – 7.52 (m, 2H), 7.50 – 7.45 (m, 2H), 7.45 – 7.38 (m, 4H), 7.30 – 7.27 (m, 1H).

IR (neat): 3058, 2073 (strong), 1622, 1586, 1496 1448, 1393, 1349, 1331, 1285, 1259, 1242, 1178, 1074, 1010, 910, 856, 829, 755, 739, 690, 651, 514, 490, 466, 450, 435, 417, 404 cm^{-1}.

HRMS (+p ESI): calc. mass for $C_{14}H_{10}O^{79}Br$ $[M + H - N_2]^-$ - 272.99095; obs. mass for $C_{14}H_{10}O^{79}Br$ $[M + H - N_2]^-$ - 272.99094.

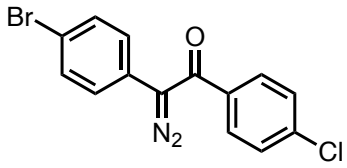

2-(4-bromophenyl)-1-(4-chlorophenyl)-2-diazoethan-1-one

Diazo was prepared from General Procedure C. 2-(4-bromophenyl)-1-(4-chlorophenyl)ethan-1-one (3.97 g, 1 equiv, 12.8 mmol), o-NBSA (4.4 g, 1.5 equiv, 19.2 mmol), and 2,3,4,6,7,8,9,10-octahydropyrimido[1,2-a]azepine (4.29 g, 4.25 mL, 2.2 equiv, 28.2 mmol) was used. The crude material was subjected to a silica plug doped with 1% TEA in 10% diethyl ether: 90% hexanes. The material was concentrated in vacuo to afford 2-(4-bromophenyl)-1-(4-chlorophenyl)-2-diazoethan-1-one (3.79 g, 11.3 mmol, 88 %) as an amorphous orange powder. The desired diazo was sensitive to deuterated solvent and was not stable enough to obtain a pure ^{13}C NMR.

^{1}H NMR (600 MHz, $CDCl_3$) δ 7.57 – 7.51 (m, 4H), 7.44 – 7.39 (m, 2H), 7.36 – 7.30 (m, 2H).

IR (neat): 2074 (strong), 1624, 1588, 1488, 1398, 1337, 1272, 1242, 1179, 1091, 1013, 911, 857, 823, 744, 674, 610, 521, 489, 474, 455, 443, 434, 409 cm^{-1}.

HRMS (+p ESI): calc. mass for $C_{14}H_9O^{79}Br^{35}Cl$ $[M + H - N_2]^-$ - 306.95198; obs. mass for $C_{14}H_9O^{79}Br^{35}Cl$ $[M + H - N_2]^-$ - 306.95205.

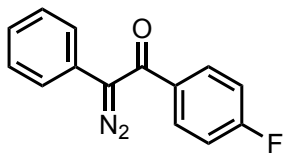

2-diazo-1-(4-fluorophenyl)-2-phenylethan-1-one

Diazo was prepared from General Procedure C. 1-(4-fluorophenyl)-2-phenylethan-1-one (1.71 g, 1 equiv, 7.98 mmol), o-NBSA (2.5 g, 1.3 equiv, 10.4 mmol), and 2,3,4,6,7,8,9,10-octahydropyrimido[1,2-a]azepine (1.45 g, 1.43 mL, 1.2 equiv, 9.57 mmol) was used. The crude material was subjected to a silica plug doped with 1% TEA in 10% diethyl ether: 90% hexanes. The material was concentrated in vacuo to afford 2-diazo-1-(4-fluorophenyl)-2-phenylethan-1-one (1.22 g, 5.06 mmol, 63 %) as an amorphous orange powder. The desired diazo was sensitive to deuterated solvent and was not stable enough to obtain a pure ^{13}C NMR.

^{1}H NMR (600 MHz, $CDCl_3$) δ 7.65 – 7.60 (m, 2H), 7.45 – 7.38 (m, 3H), 7.30 – 7.24 (m, 2H), 7.12 – 7.06 (m, 2H).

IR (neat): 3063, 2074 (strong), 1739, 1698, 1623, 1599, 1507, 1497, 1449, 1408, 1349, 1331, 1283, 1261, 1235, 1184, 1156, 1098, 1068, 1014, 980, 913, 863, 846, 757, 697, 638, 620, 609, 558, 517, 466, 453, 438, 427, 414 cm^{-1}.

HRMS (+p ESI): calc. mass for $C_{14}H_{10}OF$ $[M + H - N_2]^-$ - 213.07102; obs. mass for $C_{14}H_{10}OF$ $[M + H - N_2]^-$ - 213.07097.

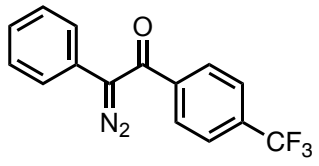

2-diazo-2-phenyl-1-(4-(trifluoromethyl)phenyl)ethan-1-one

Diazo was prepared from General Procedure C. 2-phenyl-1-(4-(trifluoromethyl)phenyl)ethan-1-one (500 mg, 1 equiv, 1.89 mmol), o-NBSA (518 mg, 1.2 equiv, 2.27 mmol), and 2,3,4,6,7,8,9,10- octahydropyrimido[1,2-a]azepine (576 mg, 0.57 mL, 2 equiv, 3.78 mmol) was used. The crude material was subjected to a silica plug doped with 1% TEA in 10% diethyl ether:

90% hexanes. The material was concentrated in vacuo to afford 2-diazo-2-phenyl-1-(4-(trifluoromethyl)phenyl)ethan-1-one (490 mg, 1.69 mmol, 89 %) as an orange powder. The desired diazo was sensitive to deuterated solvent and was not stable enough to obtain a pure ^{13}C NMR.

^{1}H NMR (400 MHz, $CDCl_3$) δ 7.74 – 7.66 (m, 4H), 7.47 – 7.37 (m, 4H), 7.33 – 7.27 (m, 1H).

^{19}F NMR (376 MHz, $CDCl_3$) δ -63.02.

IR (neat): 3015, 2970, 2098, 2078, 1738, 1614, 1590, 1573, 1495, 1448, 1407, 1363, 1323, 1284, 1241, 1217, 1176, 1124, 1111, 1075, 1062, 1024, 1015, 998, 964, 919, 866, 838, 773, 763, 753, 709, 689, 653, 653, 615, 591, 535, 512, 501, 493, 448, 407 cm^{-1}.

HRMS (+p ESI): calc. mass for $C_{15}H_{10}OF_3$ $[M + H – N_2]^-$ - 263.06783; obs. mass for $C_{15}H_{10}OF_3$ $[M + H – N_2]^-$ - 263.06783.

General procedure for the aryl diazoketone C-H insertion reactions

Note: Hood lights were turned off to minimize diazo ketone decomposition.

To a flame-dried 20 mL dram vial was added the corresponding substrate (5-10 equiv.), Rh_2(*S*-TPPTTL)4 (0.005 Eq, 1 mol %), and activated 4 Å MS (1 g/0.5 mmol diazo ketone). The mixture was back-filled with N_2 (x3). Half-portion of dry distilled DCM (0.0625 molar) was added to the mixture and the solution was allowed to stir at 25 °C for 10 minutes. Meanwhile to a separate flame-dried 20 mL dram- vial was added half-portion of dry distilled DCM (0.0625 molar) to the corresponding diazo ketone (1 equiv.) under N_2. Then both vials were sparged using an N_2 needle from the Schlenk line for 5 min. The diazo-solution was transferred to the reaction mixture containing the rhodium catalyst and trap dropwise over 2-3 min. The reaction mixture was wrapped in tin foil and was allowed to stir vigorously overnight at 25 °C. The

reaction mixture was then concentrated in vacuo for crude ^{1}H NMR to determine the regio- and diastereoselectivity. The crude was subjected to flash chromatography (0–10% hexanes:ether) to afford the corresponding C-H insertion product.

Note: Solvent must be carefully dried (distilled over CaH_2 and stored on activated 4 Å MS).

The general procedure for the aryl diazoketone C-H insertion reactions was used to accomplish the catalyst screen shown below.

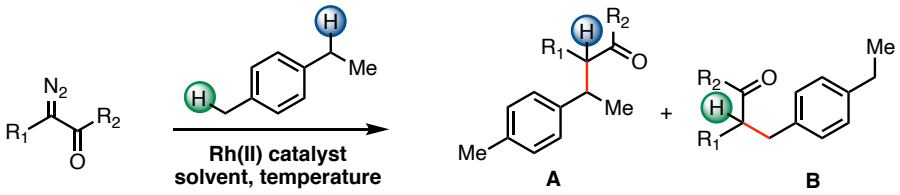

Entry	Compd.	R_1	R_2	Solvent	Conc. (M)	Catalyst	yield(%)	rr (A:B)	dr	ee(%)
1	4.7	Ph	(*p*-Br)Ph	CH_2Cl_2	0.125	Rh_2(*S*-PTAD)$_4$	15	2:1	>20:1	77
2	4.8	Ph	(*p*-CF_3)Ph	CH_2Cl_2	0.125	Rh_2(*S*-DOSP)$_4$	24[a]	>20:1	8:1	54
3	4.8	Ph	(*p*-CF_3)Ph	CH_2Cl_2	0.125	Rh_2(*S*-NTTL)$_4$	1[a]	>20:1	>20:1	32
4	4.8	Ph	(*p*-CF_3)Ph	CH_2Cl_2	0.125	Rh_2(*R*-TCPTAD)$_4$	13[a]	>20:1	>20:1	52
5	4.8	Ph	(*p*-CF_3)Ph	CH_2Cl_2	0.125	Rh_2(*R*-2-Cl 5-BrTPCP)$_4$	3[a]	5:1	>20:1	52
6	4.8	Ph	(*p*-CF_3)Ph	CH_2Cl_2	0.125	Rh_2(*S*-*p*BrTPCP)$_4$	4[a]	7:1	>20:1	86
7[b]	**4.8**	**Ph**	**(*p*-CF_3)Ph**	**CH_2Cl_2**	**0.0625**	**Rh_2(*S*-TPPTTL)$_4$**	**66**	**>20:1**	**>20:1**	**99**

[a]Yields were determined by NMR with trichloroethylene as internal standard
[b]Reaction was degassed and the diazo added all at once

Crude ^{1}H NMR of catalyst screen for the aryl diazoketone C-H insertion reactions

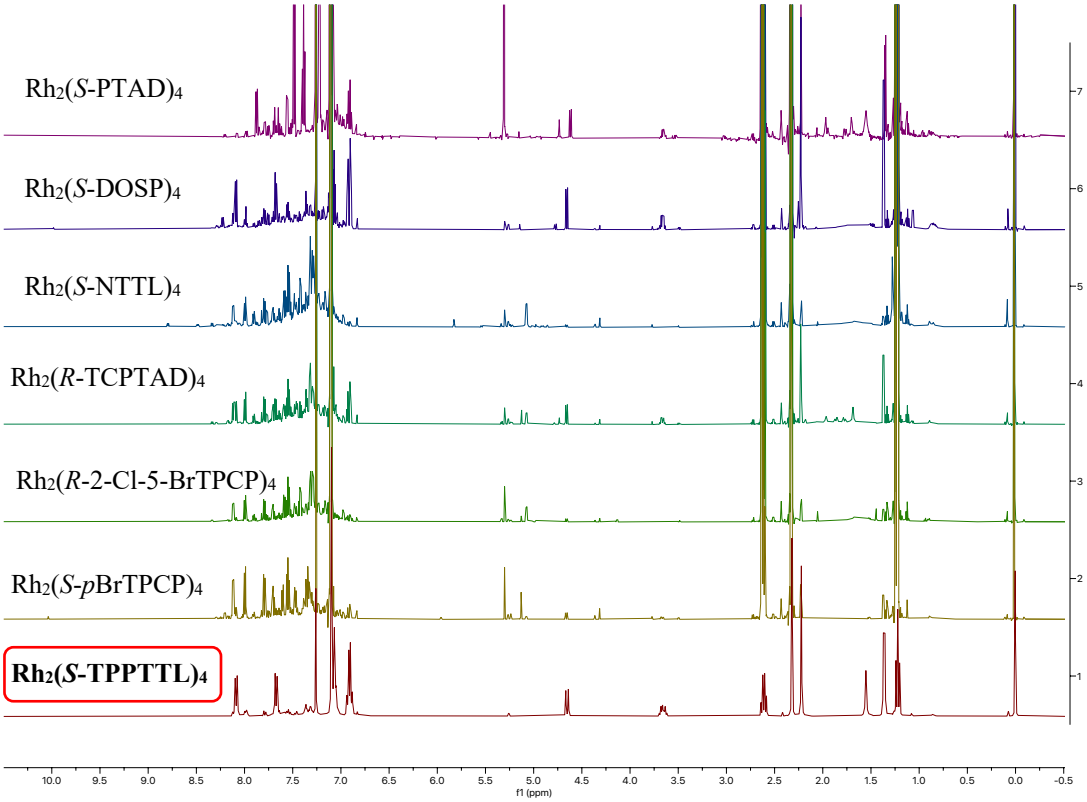

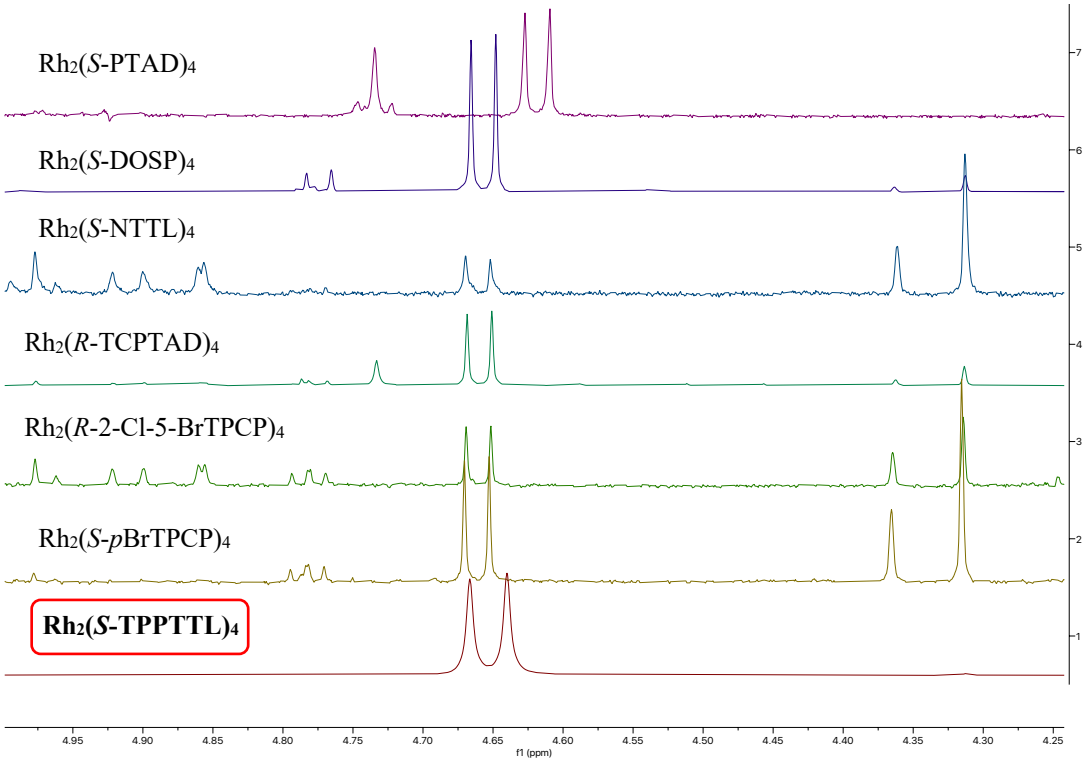

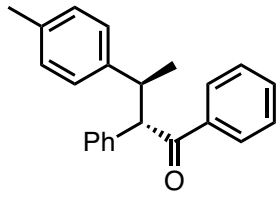

(2*S*,3*S*)-1,2-diphenyl-3-(*p*-tolyl)butan-1-one

This compound was prepared according to the general procedure for C-H insertion using 1-ethyl-4-methylbenzene (500 mg, 1.57 mL, 5 equiv, 11.25 mmol) as the substrate and 2-diazo- 1,2-diphenylethan-1-one (500 mg, 1 equiv, 2.25 mmol) under the catalyst of Rh_2(*S*-TPPTTL)$_4$ (27.7 mg, 0.005 Eq, 11.25 μmol). After flash chromatography (3% ether in hexanes) the product was obtained as an amorphous white powder (454mg 64% yield, >20:1 rr, >20:1 dr, 99% ee).

$[\alpha]^{20}_D$: -152^o (c 0.233 g/100 mL, DCM)

^{1}H NMR (600 MHz, $CDCl_3$) δ 8.04 – 7.99 (m, 2H), 7.54 – 7.48 (m, 1H), 7.42 (dd, J = 8.3, 7.2 Hz, 2H), 7.14 – 7.05 (m, 4H), 7.05 – 6.99 (m, 1H), 6.95 – 6.88 (m, 4H), 4.70 (d, J = 10.7 Hz, 1H), 3.67 (dq, J = 10.7, 6.7 Hz, 1H), 2.22 (s, 3H), 1.35 (d, J = 6.8 Hz, 3H).

^{13}C NMR (151 MHz, $CDCl_3$) δ 200.2, 141.2, 137.8, 137.6, 135.3, 132.9, 128.8, 128.7, 128.6, 128.6, 128.3, 127.6, 126.7, 61.0, 43.5, 21.1, 20.9.

IR (neat) 3024, 2963, 2923, 2873, 1671, 1596, 1579, 1514, 1492, 1447, 1373, 1346, 1288, 1267, 1233, 1202, 1175, 1102, 1074, 994, 932, 859, 813, 766, 754, 721, 698, 652, 642, 587, 555, 429, 418, 409 cm^{-1}.

HRMS (-p APCI) calc. mass for $C_{23}H_{21}O$ $[M–H]^-$ 313.1597 found 313.1598.

HPLC (OD column, 1.0 % *i*-propanol in hexane, 0.5 mL min , 0.5 mg mL , 30 min, UV 230 nm) retention times of 10.45 min (minor) and 12.3 min (major) 99% ee with Rh2(*S*-TPPTTL)4.

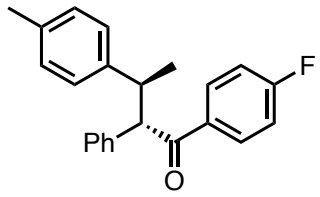

(2*R*,3*R*)-1-(4-fluorophenyl)-2-phenyl-3-(*p*-tolyl)butan-1-one

This compound was prepared according to the general procedure for C-H insertion using 1-ethyl-4-methylbenzene (601 mg, 698 μL, 10 equiv, 5.00 mmol) as the substrate and 2-diazo-1-(4-fluorophenyl)-2-phenylethan-1-one (120 mg, 1 equiv, 0.500 mmol) under the catalyst of Rh_2(*S*-TPPTTL)$_4$ (6.16 mg, 0.005 equiv, 2.50 μmol). After flash chromatography (3% ether in hexanes) the product was obtained as an amorphous white powder (60 mg, 36% yield, >20:1 rr, >20:1 dr, >99% ee).

$[\alpha]^{20}_D$: -164.6° (c 0.327 g/100 mL, EtOAc)

^{1}H NMR (600 MHz, $CDCl_3$) δ 8.04 (ddd, J = 8.9, 5.4, 1.8 Hz, 2H), 7.12 – 7.01 (m, 7H), 6.91 (qd, J = 8.1, 1.7 Hz, 4H), 4.63 (dd, J = 10.7, 1.6 Hz, 1H), 3.69 – 3.60 (m, 1H), 2.22 (s, 3H), 1.34 (dd, J = 6.9, 1.6 Hz, 3H).

^{13}C NMR (151 MHz, $CDCl_3$) δ 198.5, 166.4, 164.7, 141.0, 137.6, 135.4, 133.9, 133.9, 131.2, 131.1, 128.7, 128.7, 128.3, 127.5, 126.8, 115.7, 115.6, 61.0, 43.5, 21.0, 20.9.

^{19}F NMR (282 MHz, $CDCl_3$) δ -105.4, -105.4, -105.4, -105.4, -105.4, -105.4.

IR (neat): 3025, 2963, 2925, 1678, 1597, 1514, 1505, 1453, 1409, 1346, 1288, 1266, 1233, 1202, 1155, 995, 856, 826, 815, 761, 735, 698, 600, 551, 403 cm^{-1}.

HRMS (-p APCI): calc. mass for $C_{23}H_{20}OF$ $[M - H]^-$ 331.1503 found 331.1502

HPLC (Chiralpak AD-H column, 1.0% *i*-propanol in hexane, 1.0 mL min^{-1}, 0.5 mg mL^{-1}, 30 min, UV 210 nm) retention times of 7.0 min (major) and 7.7 min (minor), >99% e.e.

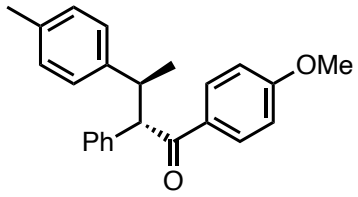

(2*S*,3*S*)-1-(4-methoxyphenyl)-2-phenyl-3-(*p*-tolyl)butan-1-one

This compound was prepared according to the general procedure for C-H insertion using 1-ethyl-4-methylbenzene (601 mg, 698 μL, 10 equiv, 5.00 mmol) as the substrate and 2-diazo-1-(4-methoxyphenyl)-2-phenylethan-1- one (126 mg, 1 equiv, 0.500 mmol) under the catalyst of Rh_2(*S*-TPPTTL)$_4$ (6.16 mg, 0.005 equiv, 2.50 μmol). After flash chromatography (3% ether in hexanes) the product was obtained as an amorphous white powder (56 mg, 30% yield, >20:1 rr, >20:1 dr, >99% ee).

$[\alpha]^{20}_D$: -60.3° (c 0.410 g/100 mL, EtOAc)

^{1}H NMR (600 MHz, $CDCl_3$) δ 8.03 – 8.00 (m, 2H), 7.12 – 7.04 (m, 4H), 7.03 – 6.96 (m, 1H), 6.93 – 6.88 (m, 6H), 4.65 (d, J = 10.7 Hz, 1H), 3.83 (s, 3H), 3.66 (dq, J = 10.9, 6.7 Hz, 1H), 2.21 (s, 3H), 1.33 (d, J = 6.7 Hz, 3H).

^{13}C NMR (151 MHz, $CDCl_3$) δ 198.5, 163.4, 141.3, 138.2, 135.3, 130.9, 130.6, 128.7, 128.6, 128.2, 127.6, 126.5, 113.7, 60.5, 55.5, 55.4, 43.5, 21.1, 20.9.

IR (neat): 2962, 2931, 1668, 1598, 1574, 1510, 1453, 1418, 1306, 1288, 1260, 1205, 1168, 1115, 1073, 1031, 993, 922, 853, 814, 762, 739, 699, 635, 609, 553, 451, 433, 405 cm^{-1}.

HRMS (+p APCI): calc. mass for $C_{24}H_{25}O_2$ $[M + H]^+$ 345.1849 found 345.1847.

HPLC (Chiralcel OD column, 0.5% *i*-propanol in hexane, 0.5 mL min^{-1}, 0.5 mg mL^{-1}, 60 min, UV 210 nm) retention times of 21.1 min and 25.5 min, >99% e.e.

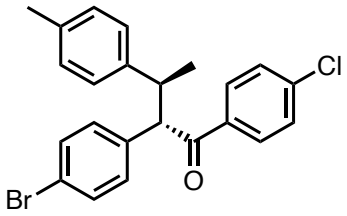

(2*S*,3*S*)-2-(4-bromophenyl)-1-(4-chlorophenyl)-3-(*p*-tolyl)butan-1-one

This compound was prepared according to the general procedure for C-H insertion using 1-ethyl-4-methylbenzene (601 mg, 698 μL, 10 equiv, 5.00 mmol) as the substrate and 2-(4-bromophenyl)-1-(4-chlorophenyl)-2- diazoethan-1-one (168 mg, 1 equiv, 0.500 mmol) under the catalyst of Rh_2(*S*-TPPTTL)$_4$ (6.16 mg, 0.005 equiv, 2.50 μmol). After flash chromatography (3% ether in hexanes) the product was obtained as an amorphous off-white powder (122 mg, 57% yield, >20:1 rr, >20:1 dr, 90% ee).

$[\alpha]^{20}_D$: -41.5^o (c 0.334 g/100 mL, EtOAc)

^{1}H NMR (600 MHz, $CDCl_3$) δ 7.93 – 7.90 (m, 2H), 7.41 – 7.38 (m, 2H), 7.22 – 7.19 (m, 2H), 6.96 – 6.93 (m, 4H), 6.90 – 6.87 (m, 2H), 4.59 (d, J = 10.7 Hz, 1H), 3.60 (dq, J = 10.6, 6.7 Hz, 1H), 2.24 (s, 3H), 1.32 (d, J = 6.8 Hz, 3H).

^{13}C NMR (151 MHz, $CDCl_3$) δ 198.6, 140.5, 139.7, 136.6, 135.7, 135.6, 132.5, 131.5, 131.3, 130.3, 129.9, 129.5, 129.0, 128.9, 127.4, 121.0, 60.3, 43.4, 21.1, 21.0.

IR (neat): 2964, 2925, 1679, 1588, 1569, 1515, 1485, 1456, 1398, 1375, 1316, 1287, 1266, 1203, 1172, 1093, 1074, 1011, 997, 854, 814, 800, 741, 721, 681, 558, 512, 471, 423, 410 cm^{-1}.

HRMS (-p APCI): calc. mass for $C_{23}H_{19}OBrCl$ $[M - H]^-$ 425.0304 found 425.0308

HPLC (Chiralpak AD-H column, 0.3% *i*-propanol in hexane, 0.8 mL min^{-1}, 0.5 mg mL^{-1}, 60 min, UV 210 nm) retention times of 25.0 min (minor) and 30.9 min (major), 90% e.e.

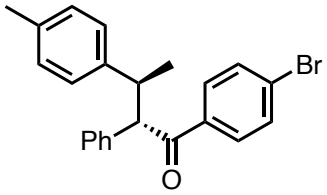

(2*S*,3*S*)-1-(4-bromophenyl)-2-phenyl-3-(*p*-tolyl)butan-1-one

This compound was prepared according to the general procedure for C-H insertion using 1-ethyl-4-methylbenzene (601 mg, 698 μL, 10 equiv, 5.00 mmol) as the substrate and 1-(4-bromophenyl)-2-diazo-2-phenylethan-1-one (151 mg, 1 equiv, 0.500 mmol) under the catalyst of Rh_2(*S*-TPPTTL)$_4$ (6.16 mg, 0.005 equiv, 2.50 μmol). After flash chromatography (3% ether in hexanes) the product was obtained as an amorphous white powder (106 mg, 54% yield, >20:1 rr, >20:1 dr, >99% ee).

$[\alpha]^{20}_D$: -62.8° (c 0.906 g/100 mL, EtOAc)

^{1}H NMR (600 MHz, $CDCl_3$) δ 7.88 – 7.84 (m, 2H), 7.57 – 7.52 (m, 2H), 7.10 – 7.01 (m, 5H), 6.94 – 6.87 (m, 4H), 4.61 (d, J = 10.6 Hz, 1H), 3.64 (dq, J = 10.6, 6.8 Hz, 1H), 2.22 (s, 3H), 1.34 (d, J = 6.8 Hz, 3H).

^{13}C NMR (151 MHz, $CDCl_3$) δ 199.1, 140.9, 137.45 136.2, 135.5, 131.9, 130.1, 128.7, 128.7, 128.4, 128.1, 127.6, 126.9, 61.1, 43.4, 20.9.

IR (neat): 2991, 2942, 1674, 1581, 1514, 1483, 1452, 1394, 1331, 1307, 1292, 1266, 1199, 1174, 1107, 1069, 993, 907, 865, 852, 815, 807, 761, 734, 705, 669, 551, 520, 450, 419, 410 cm^{-1}.

HRMS (-p APCI): calc. mass for $C_{23}H_{20}OBr$ $[M - H]^-$ 391.0703 found 391.0699

HPLC (Chiralcel OD column, 0.3% *i*-propanol in hexane, 0.8 mL min^{-1}, 0.5 mg mL^{-1}, 30 min, UV 210 nm) retention times of 9.3 min and 10.2 min, >99% e.e.

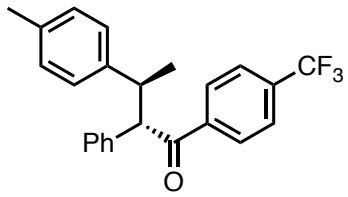

(2*S*,3*S*)-2-phenyl-3-(*p*-tolyl)-1-(4-(trifluoromethyl)phenyl)butan-1-one

This compound was prepared according to the general procedure for C-H insertion using 1-ethyl-4-methylbenzene (1.35 g, 1.57 ml, 5 equiv, 11.35 mmol) as the substrate and 2-diazo-2-phenyl-1-(4-(trifluoromethyl)phenyl)ethan-1-one (500 mg, 1 equiv, 2.25 mmol) under the catalyst of Rh_2(*S*-TPPTTL)$_4$ (27 mg, 0.005 equiv, 11.25 μmol). After flash chromatography (3% ether in hexanes) the product was obtained as an amorphous off-white powder (471 mg, 66% yield, >20:1 rr, >20:1 dr, 99% ee).

Rf = 0.65 (10% diethyl ether/hexanes)

$[\alpha]^{20}_D$: -123.8^o (c = 0.97, $CHCl_3$)

^{1}H NMR (400 MHz, $CDCl_3$) δ 8.09 (d, *J* = 8.1 Hz, 2H), 7.67 (d, *J* = 8.0 Hz, 2H), 7.13 – 7.01 (m, 5H), 6.97 – 6.86 (m, 4H), 4.66 (d, *J* = 10.6 Hz, 1H), 3.66 (dq, *J* = 10.6, 6.7 Hz, 1H), 2.22 (s, 3H), 1.36 (d, *J* = 6.7 Hz, 3H)

^{13}C NMR (101 MHz, $CDCl_3$) δ 199.1, 140.7, 140.2, 137.1, 135.5, 134.1 (q, *J* = 32.6 Hz), 128.8, 128.8, 128.7, 128.5, 127.5, 127.0, 125.6 (q, *J* = 3.8 Hz), 124.9, 122.2, 61.6, 43.4, 20.9 (d, *J* = 4.6 Hz).

^{19}F NMR (376 MHz, $CDCl_3$) δ -63.2.

IR (neat): 2919, 1678, 1580, 1514, 1495, 1453, 1408, 1380, 1321, 1265, 1199, 1166, 1130, 1109, 1065, 996, 870, 857, 813, 774, 761, 746, 718, 706, 695, 667, 588, 550, 530, 518, 475, 413, 403 cm^{-1}.

HRMS (-p APCI): calcd for $C_{24}H_{20}F_3O$ $(M-H)^-$ 381.1461 found 381.1467

HPLC (Chiralpak RRW column, 0.5% isopropanol in hexane, 0.5 mL/min, λ 230 nm) retention times of 10.6 min (major) and 12.3 min (minor), 99% ee

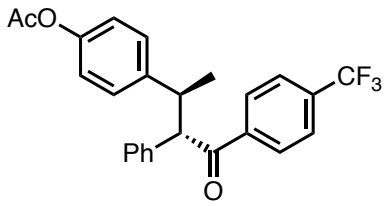

4-((2*S*,3*S*)-4-oxo-3-phenyl-4-(4-(trifluoromethyl)phenyl)butan-2-yl)phenyl acetate

This compound was prepared according to the general procedure for C-H insertion using 4-ethylphenyl acetate (0.33 ml, 5 equiv, 2.07 mmol) as the substrate and 2-diazo-2-phenyl-1-(4-(trifluoromethyl)phenyl)ethan-1-one (120 mg, 1 equiv, 0.41 mmol) under the catalyst of Rh_2(*S*-TPPTTL)$_4$ (5 mg, 0.005 equiv, 2.0 μmol). After flash chromatography (5% ether in hexanes) the product was obtained as a yellow oil (103 mg, 59% yield, >20:1 dr, 99% ee).

Rf = 0.24 (20% diethyl ether/hexanes)

$[\alpha]^{20}_D$: -68.8^o (c = 1.24, $CHCl_3$)

^{1}H NMR (400 MHz, $CDCl_3$) δ 8.07 (d, J = 8.7 Hz, 2H), 7.67 (d, J = 8.1 Hz, 2H), 7.11 – 7.01 (m, J = 1.9, 2.0, 0.9, 1.6 Hz, 5H), 6.99 – 6.83 (ddd, J = 2.0, 2.1 Hz, 4H), 4.60 (d, J = 10.5 Hz, 1H), 3.69 (dq, J = 10.6, 6.7 Hz, 1H), 2.24 (s, 3H), 1.38 (d, J = 6.8 Hz, 3H).

^{13}C NMR (101 MHz, $CDCl_3$) δ 198.7, 169.4, 148.9, 141.3, 140.0 (d, *J* = 1.4 Hz), 136.8, 134.2 (q, *J* = 32.7 Hz), 128.8, 128.7, 128.6 (d, *J* = 2.2 Hz), 127.2, 125.6 (q, *J* = 3.7 Hz), 123.5 (q, *J* = 272.8 Hz), 120.9, 61.8, 43.3, 21.1, 20.6.

^{19}F NMR (376 MHz, $CDCl_3$) δ -63.2.

IR (neat) 2931, 1763, 1684, 1582, 1507, 1454, 1427, 1409, 1368, 1266, 1203, 1166, 1127 1110, 1065, 1014, 996, 940, 910, 870, 844, 821, 775, 737, 700, 633, 596, 553, 506, 448, 436, 426, 413, 403 cm^{-1}.

HRMS (-p APCI): calcd for $C_{25}H_{20}F_3O_3$ $(M-H)^-$ 425.1359 found 425.1365

HPLC (Chiralpak RRW column, 2% isopropanol in hexane, 1 mL/min, λ 230 nm) retention times of 27.6 min (major) and 33.9 min (minor), 99% ee.

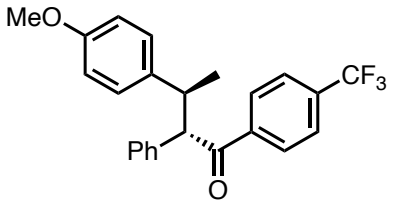

(2*S*,3*S*)-3-(4-methoxyphenyl)-2-phenyl-1-(4-(trifluoromethyl)phenyl)butan-1-one

This compound was prepared according to the general procedure for C-H insertion using 1-ethyl-4-methoxybenzene (0.25 ml, 5 equiv, 1.73 mmol) as the substrate and 2-diazo-2-phenyl-1-(4-(trifluoromethyl)phenyl)ethan-1-one (100 mg, 1 equiv, 0.35 mmol) under the catalyst of Rh_2(*S*-TPPTTL)$_4$ (5 mg, 0.005 equiv, 2.0 μmol). After flash chromatography (3% ether in hexanes) the product was obtained as an amorphous white powder (91 mg, 66% yield, >20:1 rr, >20:1 dr, 91% ee).

Rf = 0.324 (10% diethyl ether/hexanes)

$[\alpha]^{20}_D$: -142.2° (c = 1.04, $CHCl_3$)

^{1}H NMR (600 MHz, $CDCl_3$) δ 8.08 (d, J = 8.1 Hz, 2H), 7.67 (d, J = 8.1 Hz, 2H), 7.11 – 7.04 (m, 5H), 6.91 (d, J = 8.4 Hz, 2H), 6.68 – 6.64 (m, 2H), 4.61 (d, J = 10.5 Hz, 1H), 3.71 (s, 3H), 3.64 (dq, J = 10.8, 6.9 Hz, 1H), 1.36 (dd, J = 6.7, 0.9 Hz, 3H).

^{13}C NMR (151 MHz, $CDCl_3$) δ 199.1, 157.8, 140.2, 137.2, 135.9, 134.3, 134.0, 128.8, 128.8, 128.6, 128.5, 127.0, 125.6 (q, *J* = 3.8 Hz), 124.4, 122.6, 113.4, 61.9, 55.1, 43.0, 20.9.

^{19}F NMR (565 MHz, $CDCl_3$) δ -63.2.

IR (neat) 2990, 1677, 1607, 1581, 1512, 1454, 1410, 1325, 1267, 1246, 1165, 1134, 1109, 1067, 1034, 995, 869, 855, 824, 760, 747, 706, 695, 586, 558, 544, 527, 413, 403 cm^{-1}.

HRMS (–p APCI) calcd for $C_{24}H_{20}F_3O_2$ $(M-H)^-$ 397.1494 found 397.1421

HPLC (Chiralpak SSW column, 1% isopropanol in hexane, 2 mL/min, λ 230 nm) retention times of 9.58 min (minor) and 12.32 min (major), 91% ee**.**

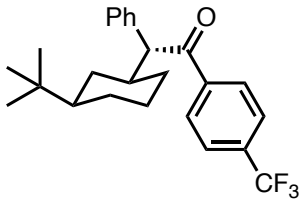

(*S*)-2-((1*S*,3*S*)-3-(*tert*-butyl)cyclohexyl)-2-phenyl-1-(4-(trifluoromethyl)phenyl)ethan-1-one

This compound was prepared according to the general procedure for C-H insertion using *tert*-butylcyclohexane (210 mg, 5 equiv, 1.5 mmol) as the substrate and 2-diazo-2-phenyl-1-(4-(trifluoromethyl)phenyl)ethan-1-one (87 mg, 1 equiv, 0.3 mmol) under the catalyst of Rh_2(*S*-TPPTTL)$_4$ (4 mg, 0.005 equiv, 1.7 μmol). After flash chromatography (3% ether in hexanes) the product was obtained as an amorphous white solid (62 mg, 51% yield, >20:1 rr, >20:1 dr, >99% ee).

Rf = 0.33 (10% diethyl ether/hexanes)

$[\alpha]^{20}_D$: -20.5° (c = 0.4, $CHCl_3$)

^{1}H NMR (400 MHz, $CDCl_3$) δ 8.05 (d, *J* = 8.1 Hz, 2H), 7.66 (d, *J* = 8.0 Hz, 2H), 7.30 – 7.28 (m, 4H), 7.24 – 7.18 (m, 1H), 4.27 (d, *J* = 9.9 Hz, 1H), 2.19 (tdt, *J* = 11.7, 9.8, 3.2 Hz, 1H), 1.86

– 1.69 (m, 3H), 1.44 – 1.23 (m, 2H), 0.96 (qt, *J* = 12.3, 3.3 Hz, 1H), 0.90 – 0.80 (m, 2H), 0.71 (s, 9H), 0.56 (q, *J* = 12.0 Hz, 1H).

^{13}C NMR (101 MHz, $CDCl_3$) δ 199.8, 140.5, 137.2, 134.0 (q, *J* = 32.6 Hz), 128.8 (d, *J* = 6.6 Hz), 127.3, 125.6 (q, *J* = 3.7 Hz), 123.6 (q, *J* = 272.7 Hz), 60.9, 47.7, 41.5, 32.5 (d, *J* = 5.1 Hz), 31.5, 27.4, 27.2, 26.4.

^{19}F NMR (565 MHz, $CDCl_3$) δ -63.2.

IR (neat) 2925, 2854, 2360, 2342, 1688, 1322, 1170, 1133, 1067, 748, 702, 418, cm^{-1}

HRMS (+p APCI) calcd for $C_{25}H_{30}F_3O$ $(M+H)^+$ 403.2249 found 403.2237

HPLC (Chiralpak RRW column, 0.5% isopropanol in hexane, 0.25 mL/min, λ 254 nm) retention time of 18.2 min, >99% ee.

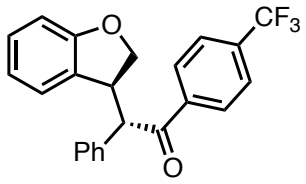

(*S*)-2-((*S*)-2,3-dihydrobenzofuran-3-yl)-2-phenyl-1-(4-(trifluoromethyl)phenyl)ethan-1-one

This compound was prepared according to the general procedure for C-H insertion using 2,3-dihydrobenzofuran (0.22 ml, 5 equiv, 1.9 mmol) as the substrate and 2-diazo-2-phenyl-1-(4-(trifluoromethyl)phenyl)ethan-1-one (110 mg, 1 equiv, 0.38 mmol) under the catalyst of Rh_2(*S*-TPPTTL)$_4$ (5 mg, 0.005 equiv, 2.0 μmol). After reaction completion and solvent removal in vacuo, the crude residue was subjected to Kugelrohr distillation (0.5 mmHg, 90 ºC) for one hour to remove excess starting material. After flash chromatography (5% ether in hexanes) the product was obtained as an amorphous yellow solid (43 mg, 30% yield. >20:1 rr, 3:1 dr, 96% ee).

Rf = 0.487 (15% diethyl ether/hexanes)

$[\alpha]^{20}_{D}$: -88.2° (c = 0.95, $CHCl_3$)

^{1}H NMR (400 MHz, $CDCl_3$) δ 8.04 (dt, *J* = 8.1, 0.9 Hz, 2H), 7.64 (dd, *J* = 8.9, 0.8 Hz, 2H), 7.32 (qt, *J* = 4.9, 2.1 Hz, 3H), 7.20 (dd, *J* = 7.7, 1.9 Hz, 2H), 7.09 (tdd, *J* = 7.4, 1.4, 0.6 Hz, 1H), 6.80 (dd, *J* = 8.1, 1.0 Hz, 1H), 6.56 (td, *J* = 7.5, 1.0 Hz, 1H), 5.87 (dp, *J* = 7.5, 0.7 Hz, 1H), 4.79 (dd, *J* = 9.5, 8.3 Hz, 1H), 4.67 (d, *J* = 10.7 Hz, 1H), 4.28 (ddd, *J* = 10.4, 8.1, 4.0 Hz, 1H), 4.22 (dd, *J* = 9.5, 4.2 Hz, 1H).

^{13}C NMR (101 MHz, $CDCl_3$) δ 198.0, 160.3, 138.8, 136.1, 134.4 (q, *J* = 32.7 Hz), 129.3, 129.2, 129.11, 128.7, 128.1, 127.4, 126.0, 125.7 (q, *J* = 3.8 Hz), 123.4 (q, *J* = 272.8 Hz), 119.8, 109.5, 59.5, 45.2.

^{19}F NMR (376 MHz, $CDCl_3$) δ -63.3.

IR (neat): 2937, 1679, 1593, 1513, 1480, 1455, 1409, 1322, 1294, 1282, 1214, 1167, 1127, 1066, 1006, 997, 971, 922, 836, 774, 748, 734, 702, 605, 518, 504, 468, 436, 426, 413, 403 cm^{-1}.

HRMS (-p APCI) calcd for $C_{23}H_{16}F_3O_2$ $(M-H)^-$ 381.1181 found 381.1105

HPLC (Chiralpak RRW column, 10.0% *i*-propanol in hexane, 0.5 mL min^{-1}, 0.5 mg mL^{-1}, 15 min, UV 254 nm) retention times of 9.4 min (major) and 10.2 min (minor), 96% ee.

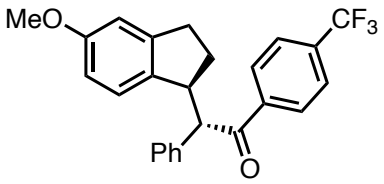

(*S*)-2-((*S*)-5-methoxy-2,3-dihydro-1*H*-inden-1-yl)-2-phenyl-1-(4-(trifluoromethyl) phenyl)ethan-1-one

This compound was prepared according to the general procedure for C-H insertion using 5-methoxy-2,3-dihydro-1H-indene (0.28 ml, 5 equiv, 1.8 mmol) as the substrate and 2-diazo-2-phenyl-1-(4-(trifluoromethyl)phenyl)ethan-1-one (110 mg, 1 equiv, 0.38 mmol) under the catalyst of Rh_2(*S*-TPPTTL)$_4$ (5 mg, 0.005 equiv, 2.0 μmol). After flash chromatography (3% ether in hexanes) the product was obtained as an amorphous off-white solid (96 mg, 62% yield, 13:1 rr, >20:1 dr, 81% ee).

Rf = 0.175 (10% diethyl ether/hexanes)

$[\alpha]^{20}_D$: -59.4^o (c = 1.05, $CHCl_3$)

^{1}H NMR (400 MHz, $CDCl_3$) δ 8.10 – 8.02 (m, 2H), 7.69 – 7.62 (m, 2H), 7.32 – 7.27 (m, 3H), 7.25 – 7.23 (m, 2H), 6.76 (d, *J* = 2.5 Hz, 1H), 6.42 – 6.34 (m, 1H), 5.90 (d, *J* = 8.4 Hz, 1H), 4.55 (d, *J* = 10.7 Hz, 1H), 4.05 (ddd, *J* = 11.2, 7.9, 3.9 Hz, 1H), 3.73 (s, 3H), 2.95 (dt, *J* = 16.1, 8.1 Hz, 1H), 2.82 (ddd, *J* = 16.1, 8.8, 4.3 Hz, 1H), 2.44 (ddt, *J* = 13.1, 8.9, 8.0 Hz, 1H), 1.85 – 1.72 (m, 1H).

^{13}C NMR (151 MHz, $CDCl_3$) δ 198.9, 159.0, 145.9, 139.8, 137.4, 136.2, 134.1, 129.4, 128.9, 128.9, 127.7, 126.1, 125.7 (q, J = 3.8 Hz), 124.4, 111.4, 109.7, 59.0, 55.3, 47.7, 32.2, 31.0.

^{19}F NMR (565 MHz, $CDCl_3$) δ -63.2.

IR (neat): 2938, 1677, 1605, 1583, 1492, 1454, 1409, 1327, 1246, 1164, 1127, 1108, 1067, 1029, 1015, 996, 922, 873, 858, 816, 773, 740, 705, 694, 589, 515, 470, 448, 435, 426, 413, 403 cm^{-1}.

HRMS (-p APCI) calcd for $C_{25}H_{20}F_3O_2$ $(M-H)^-$ 409.1494 found 409.1419

HPLC: (Chiralpak RRW column, 3.0% *i*-propanol in hexane, 0.1 mL min^{-1}, 0.1 mg mL^{-1}, 90 min, UV 230 nm) retention times of 72.4 min (major) and 78.6 (minor), 81% ee.

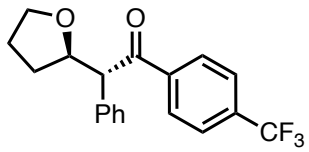

(*S*)-2-phenyl-2-((*S*)-tetrahydrofuran-2-yl)-1-(4-(trifluoromethyl)phenyl)ethan-1-one

This compound was prepared according to the general procedure for C-H insertion using THF (0.9 ml, 5 equiv, 1.5 mmol) as the substrate and 2-diazo-2-phenyl-1-(4-(trifluoromethyl) -phenyl)ethan-1-one (87 mg, 1 equiv, 0.30 mmol) under the catalyst of Rh_2(*S*-TPPTTL)$_4$ (4 mg, 0.005 equiv, 1.7 μmol). After flash chromatography (10% ether in hexanes) the product was obtained as an amorphous clear solid (75 mg, 75% yield, >20:1 rr, 7:1 dr, 78% ee).

Note: The benzylic proton and alpha to oxygen insertion proton are overlapped in the ^{1}H NMR along with the benzylic proton from the minor diastereomer. To ascertain the diastereoselectivity the quartet from the alpha to oxygen minor diastereomer was normalized to one and the overlap of the over 3 protons resulted in 15. The diastereoselectivity was then calculated as such: 15= X+X+1, resulting in a 7:1 dr.

Rf = 0.1 (10% diethyl ether/hexanes)

$[\alpha]^{20}_D$: -82.5^o (c = 1.0, $CHCl_3$)

^{1}H NMR (600 MHz, $CDCl_3$) δ 8.03 (d, *J* = 8.2 Hz, 2H), 7.65 (d, *J* = 8.2 Hz, 2H), 7.40 – 7.35 (m, 2H), 7.35 – 7.30 (m, 2H), 7.29 – 7.18 (m, 1H), 4.59 – 4.51 (m, 2H), 3.85 (dt, *J* = 8.6, 6.8 Hz, 1H), 3.71 (dt, *J* = 8.3, 6.7 Hz, 1H), 2.30 – 2.21 (m, 1H), 1.90 (dtd, *J* = 11.8, 6.2, 4.1 Hz, 2H), 1.56 (tdd, *J* = 12.5, 8.3, 6.2 Hz, 1H).

^{13}C NMR (151 MHz, $CDCl_3$) δ 197.9, 139.3, 134.2 (q, *J* = 32.8 Hz), 130.4, 129.1, 129.0, 128.9, 128.7, 127.7, 125.6 (q, *J* = 3.8 Hz), 123.5 (q, *J* = 272.9 Hz), 81.0, 68.0, 59.6, 30.8, 25.7.

^{19}F NMR (565 MHz, $CDCl_3$) δ -63.2.

IR (neat) 2923, 2854, 2360, 2342, 1687, 1325, 1170, 1129, 1066, 701, 417, cm^{-1}

HRMS (–p APCI) calcd for $C_{19}H_{16}F_3O_2$ $(M-H)^-$ 333.1097 found 333.1106

HPLC (Chiralpak OD-H column, 1% isopropanol in hexane, 1 mL/min, λ 210 nm) retention times of 8.24 min and 8.93 min, 78% ee.

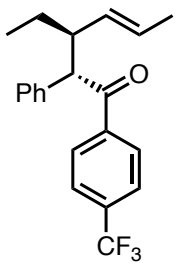

(2*R*,3*R*,*E*)-3-ethyl-2-phenyl-1-(4-(trifluoromethyl)phenyl)hex-4-en-1-one

This compound was prepared according to the general procedure for C-H insertion using *trans*-2-hexene (0.22 ml, 5 E equiv 1.7 mmol) as the substrate and 2-diazo-2-phenyl-1-(4-(trifluoromethyl) -phenyl)ethan-1-one (100 mg, 1 equiv, 0.35 mmol) under the catalyst of Rh_2(*S*-TPPTTL)$_4$ (4 mg, 0.005 Eq, 1.7 μmol). After flash chromatography (3% ether in hexanes) the product was obtained as a clear oil (69 mg, 58% yield, >20:1 rr, >20:1 dr, >99% ee).

Rf = 0.822 (5% diethyl ether/hexanes)

$[\alpha]^{20}_D$: -75.0° (c 1.996 g/100 mL, EtOAc)

^{1}H NMR (600 MHz, $CDCl_3$) δ 8.05 (d, *J* = 8.2 Hz, 2H), 7.66 (d, *J* = 8.3 Hz, 2H), 7.25 – 7.20 (m, 4H), 7.17 (td, *J* = 6.9, 1.6 Hz, 1H), 5.19 – 5.10 (m, 1H), 4.98 (ddd, *J* = 15.2, 9.4, 1.8 Hz, 1H), 4.43 (d, *J* = 9.9 Hz, 1H), 2.84 (qd, *J* = 9.6, 3.1 Hz, 1H), 1.53 (ddddd, *J* = 14.7, 11.5, 8.4, 5.3, 1.4 Hz, 1H), 1.44 (dd, *J* = 6.4, 1.6 Hz, 3H), 1.28 – 1.21 (m, 1H) 0.87 (t, *J* = 7.4 Hz, 3H).

^{13}C NMR (151 MHz, $CDCl_3$) δ 199.3, 140.3, 137.5, 134.0 (q, *J* = 32.6 Hz), 131.4, 129.1, 128.8, 128.56, 127.6, 127.0, 125.6 (q, *J* = 3.7 Hz), 123.6 (q, *J* = 272.8 Hz), 59.1, 48.1, 26.8, 17.8, 11.9.

^{19}F NMR (565 MHz, $CDCl_3$) δ -63.2.

IR (neat) 2964, 2933, 2360, 2342, 1686, 1322, 1170, 1132, 1067, 747, 410, cm^{-1}

HRMS (+p APCI) calcd for $C_{21}H_{22}F_3O$ $(M+H)^+$ 347.1623 found 347.1609

HPLC (Chiralpak RRW column, 1.0% isopropanol in hexane, 1.0 mL/min, λ 230 nm) retention times of 5.1min, >99% ee.

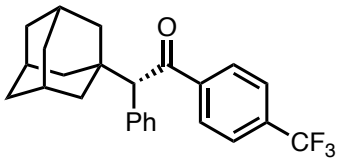

(*S*)-2-((3*S*,5*S*,7*S*)-adamantan-1-yl)-2-phenyl-1-(4-(trifluoromethyl)phenyl)ethan-1-one

This compound was prepared according to the general procedure for C-H insertion using adamantane (204 mg, 5 equiv, 1.7 mmol) as the substrate and 2-diazo-2-phenyl-1-(4-(trifluoromethyl) -phenyl)ethan-1-one (87 mg, 1 equiv, 0.3 mmol) under the catalyst of Rh_2(*S*-TPPTTL)$_4$ (4 mg, 0.005 equiv, 1.7 μmol). After flash chromatography (3% ether in hexanes) the product was obtained as an amorphous off-white solid (68 mg, 58% yield, >20:1 rr, 95% ee).

Rf = 0.822 (5% diethyl ether/hexanes)

$[\alpha]^{20}_D$: -136.7° (c = 0.98, $CHCl_3$)

^{1}H NMR (400 MHz, $CDCl_3$) δ 7.99 (d, *J* = 8.2 Hz, 2H), 7.64 (d, *J* = 8.2 Hz, 2H), 7.40 – 7.35 (m, 2H), 7.34 – 7.27 (m, 3H), 4.33 (s, 1H), 1.96 (p, *J* = 3.1 Hz, 3H), 1.83 (dq, *J* = 12.0, 2.5 Hz, 3H), 1.70 – 1.56 (m, 9H).

^{13}C NMR (101 MHz, $CDCl_3$) δ 199.9, 141.8, 134.2, 133.7 (q, *J* = 32.7 Hz), 130.5, 128.5, 128.1, 127.3, 125.5 (q, *J* = 3.8 Hz), 123.6 (q, *J* = 272.6 Hz), 64.2, 40.2, 37.6, 36.8, 28.6.

^{19}F NMR (565 MHz, $CDCl_3$) δ -63.1.

IR (neat) 2906, 2849, 2360, 2342, 1738, 1323, 1132, 1067, 668, 418, cm^{-1}

HRMS (–p APCI) calcd for $C_{25}H_{24}F_3O$ $(M-H)^-$ 397.1774 found 397.1778

HPLC (Chiralpak SSW column, 0.5% isopropanol in hexane, 0.5 mL/min, λ 230 nm) retention times of 14.2 min and 16.2 min, 95% ee.

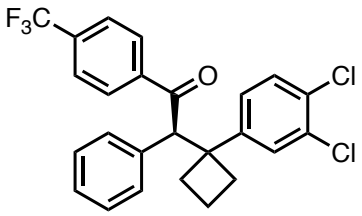

(*S*)-2-(1-(3,4-dichlorophenyl)cyclobutyl)-2-phenyl-1-(4-(trifluoromethyl)phenyl)ethan-1-one

This compound was prepared according to the general procedure for C-H insertion using 1,2-dichloro-4-cyclobutylbenzene (302 mg, 5 equiv, 1.5 mmol) as the substrate and 2-diazo-2-phenyl-1-(4-(trifluoromethyl) -phenyl)ethan-1-one (87 mg, 1 equiv, 0.3 mmol) under the catalyst of Rh_2(*S*-TPPTTL)$_4$ (4 mg, 0.005 equiv, 1.7 μmol). After flash chromatography (3% ether in hexanes) the product was obtained as a clear oil (65 mg, 47% yield, >20:1 rr, >99% ee).

Rf = 0.54 (10% diethyl ether/hexanes)

$[\alpha]^{20}_D$: -68.5^o (c = 1.2, $CHCl_3$)

^{1}H NMR (400 MHz, $CDCl_3$) δ 7.86 – 7.78 (m, 2H), 7.60 – 7.52 (m, 2H), 7.32 – 7.27 (m, 3H), 7.24 (s, 1H), 7.19 (d, *J* = 2.2 Hz, 1H), 7.17 – 7.13 (m, 2H), 6.99 (dd, *J* = 8.4, 2.2 Hz, 1H), 4.90 (s, 1H), 2.70 (ddd, *J* = 11.5, 9.1, 6.4 Hz, 1H), 2.45 (ddd, *J* = 12.6, 8.5, 7.1 Hz, 3H), 1.81 – 1.54 (m, 2H).

^{13}C NMR (101 MHz, $CDCl_3$) δ 197.9, 147.9, 140.1, 135.0, 133.9 (q, *J* = 32.8 Hz), 131.2, 130.4, 130.0, 129.6, 129.1, 128.7, 128.6, 127.9, 127.8, 125.5 (q, *J* = 3.7 Hz), 123.5 (q, *J* = 272.7 Hz), 62.7, 49.4, 32.8, 31.8, 16.4.

^{19}F NMR (376 MHz, $CDCl_3$) δ -63.2.

IR (neat) 3063, 3027, 2981, 2944, 2867, 1745, 1689, 1470, 1310, 1209, 1168, 1128, 1067, 1014, 817, 712 cm^{-1}.

HRMS (–p APCI) calcd for $C_{25}H_{18}F_3OCl_2$ $(M-H)^-$ 461.0765 found 461.0694

HPLC (Chiralpak RRW column, 1.0% isopropanol in hexane, 0.5 mL/min, λ 230 nm) retention times of 9.9 min, >99% ee.

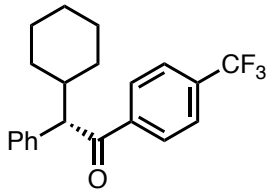

(*S*)-2-cyclohexyl-2-phenyl-1-(4-(trifluoromethyl)phenyl)ethan-1-one

This compound was prepared according to the general procedure for C-H insertion using cyclohexane (126 mg, 5 equiv, 1.5 mmol) as the substrate and 2-diazo-2-phenyl-1-(4-(trifluoromethyl) -phenyl)ethan-1-one (87 mg, 1 equiv, 0.3 mmol) under the catalyst of Rh_2(*S*-TPPTTL)$_4$ (4 mg, 0.005 equiv, 1.7 μmol). After flash chromatography (3% ether in hexanes) the product was obtained as a clear oil (60 mg, 58% yield, 99% ee).

Rf = 0.73 (10% diethyl ether/hexanes)

$[\alpha]^{20}_D$: -5.0° (c = 1.0, $CHCl_3$)

^{1}H NMR (600 MHz, $CDCl_3$) δ 8.05 (d, *J* = 8.1 Hz, 2H), 7.66 (d, *J* = 8.2 Hz, 2H), 7.33 – 7.27 (m, 4H), 7.24 – 7.19 (m, 1H), 4.28 (d, *J* = 10.1 Hz, 1H), 2.30 (qt, *J* = 10.9, 3.3 Hz, 1H), 1.83 (dt, *J* = 12.6, 3.1 Hz, 1H), 1.67 (ddt, *J* = 19.3, 12.5, 3.1 Hz, 3H), 1.39 – 1.28 (m, 2H), 1.17 (dddd, *J* = 25.2, 15.2, 12.2, 8.6 Hz, 2H), 0.98 (qd, *J* = 12.4, 3.4 Hz, 1H), 0.91 – 0.81 (m, 1H).

^{13}C NMR (151 MHz, $CDCl_3$) δ 199.7, 140.4, 137.3, 134.0 (q, *J* = 32.7 Hz), 128.9, 128.7, 127.3, 125.6 (q, *J* = 3.7 Hz), 123.6 (q, *J* = 272.6 Hz), 60.7, 41.0, 32.6, 30.6, 26.4, 26.1 (d, *J* = 5.6 Hz).

^{19}F NMR (565 MHz, $CDCl_3$) δ -63.2.

IR (neat) 2926, 2854, 2360, 2342, 1686, 1323, 1260, 1169, 1132, 1066, 802, 429, cm^{-1}

HRMS (+p APCI) calcd for $C_{21}H_{22}F_3O$ $(M+H)^+$ 347.1623 found 347.1610

HPLC (Chiralpak SSW column, 0.5% isopropanol in hexane, 0.5 mL/min, λ 230 nm) retention times of 13.4 min and 17.4 min, 99% ee.

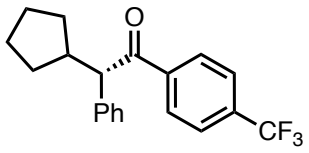

(*S*)-2-cyclopentyl-2-phenyl-1-(4-(trifluoromethyl)phenyl)ethan-1-one

This compound was prepared according to the general procedure for C-H insertion using cyclopentane (0.75 ml, 10 equiv, 3.0 mmol) as the substrate and 2-diazo-2-phenyl-1-(4-(trifluoromethyl) -phenyl)ethan-1-one (87 mg, 1 equiv, 0.3 mmol) under the catalyst of Rh_2(*S*-TPPTTL)$_4$ (4 mg, 0.005 equiv, 1.7 μmol). After flash chromatography (3% ether in hexanes) the product was obtained as a clear oil (40 mg, 40% yield, 99% ee).

Rf = 0.86 (10% diethyl ether/hexanes)

$[\alpha]^{20}_D$: -86.9° (c = 1.0, $CHCl_3$)

^{1}H NMR (400 MHz, $CDCl_3$) δ 8.05 (dt, *J* = 8.1, 1.0 Hz, 2H), 7.68 – 7.61 (m, 2H), 7.33 – 7.27 (m, 4H), 7.24 – 7.18 (m, 1H), 4.28 (d, *J* = 10.5 Hz, 1H), 2.74 (dtt, *J* = 10.4, 9.2, 7.2 Hz, 1H), 2.03 – 1.91 (m, 1H), 1.66 – 1.58 (m, 3H), 1.53 – 1.36 (m, 2H), 1.21 – 1.02 (m, 2H).

^{13}C NMR (151 MHz, $CDCl_3$) δ 199.3, 139.9, 138.6, 133.9 (q, *J* = 32.6 Hz), 128.9, 128.8, 128.4, 127.2, 125.6 (q, *J* = 3.8 Hz), 123.6 (q, *J* = 272.6 Hz), 60.2, 43.7, 31.9, 30.9, 25.2, 24.7.

^{19}F NMR (565 MHz, $CDCl_3$) δ -63.2.

IR (neat) 3064, 3027, 2954, 2868, 1685, 1599, 1581, 1510, 1495, 1452, 1408, 1315, 1274, 1209, 1166, 1126, 1111, 1080, 1031, 1015, 1006, 988, 873, 822, 773, 744, 700 cm^{-1}.

HRMS (+p APCI) calcd for $C_{20}H_{20}F_3O$ $(M+H)^+$ 333.1388 found 333.1465.

HPLC (Chiralpak RRW column, 0.5 % *i*-propanol in hexane, 0.5 mL min^{-1}, 0.5 mg mL^{-1}, 15 min, UV 230 nm) retention times of 9.6 min (major) and 11.6 min (minor) 99% ee.

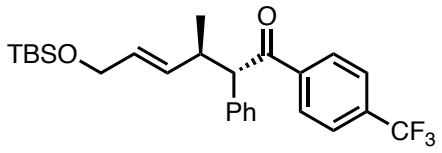

(2*S*,3*R*,*E*)-6-((*tert*-butyldimethylsilyl)oxy)-3-methyl-2-phenyl-1-(4-(trifluoromethyl) -phenyl)hex-4-en-1-one

This compound was prepared according to the general procedure for C-H insertion using (*E*)-*tert*-butyldimethyl(pent-2-en-1-yloxy)silane (301 mg, 5 equiv, 1.5 mmol) as the substrate and 2-diazo-2-phenyl-1-(4-(trifluoromethyl) -phenyl)ethan-1-one (87 mg, 1 equiv, 0.3 mmol) under the catalyst of Rh_2(*S*-TPPTTL)$_4$ (4 mg, 0.005 equiv, 1.7 μmol). After flash chromatography (2% ether in hexanes) the product was obtained as a clear oil (71 mg, 51% yield, 7:1 rr, >20:1 dr, 95% ee).

Rf = 0.5 (10% diethyl ether/hexanes)

$[\alpha]^{20}_D$: -54.5° (c = 1.0, $CHCl_3$)

^{1}H NMR (600 MHz, $CDCl_3$) δ 8.08 – 8.04 (m, 2H), 7.69 – 7.64 (m, 2H), 7.28 – 7.26 (m, 4H), 7.22 – 7.16 (m, 1H), 5.42 – 5.37 (m, 2H), 4.35 (d, *J* = 10.1 Hz, 1H), 3.97 – 3.95 (m, 2H), 3.19 (dddd, *J* = 12.4, 8.8, 6.6, 5.4 Hz, 1H), 1.13 (d, *J* = 6.5 Hz, 3H), 0.84 (s, 9H), -0.04 (d, *J* = 7.8 Hz, 6H).

^{13}C NMR (151 MHz, $CDCl_3$) δ 198.9, 140.1, 137.2, 134.1 (q, *J* = 32.7 Hz), 132.4, 129.8, 128.9, 128.8 (d, *J* = 2.7 Hz), 127.3, 125.6 (q, *J* = 3.7 Hz), 123.5 (q, *J* = 272.6 Hz), 63.5, 60.3, 39.5, 25.9, 19.1, 18.3, -5.3.

^{19}F NMR (565 MHz, $CDCl_3$) δ -63.2.

IR (neat) 3064, 3030, 2958, 2930, 2885, 2857, 1688, 1583, 1409, 1310, 1256, 1169, 1130, 835 cm^{-1}.

HRMS (+p APCI) calcd for $C_{26}H_{34}F_3O_2Si$ $(M+H)^+$ 463.2280 found 463.2274

HPLC (Chiralpak RRW column, 0.5 % *i*-propanol in hexane, 0.5 mL min^{-1}, 0.5 mg mL^{-1}, 15 min, UV 230 nm) retention times of 8.6 min (major) and 9.9 min (minor) 95% ee.

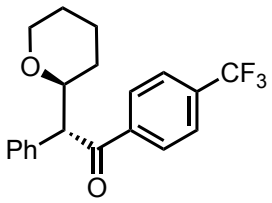

(*R*)-2-phenyl-2-((*S*)-tetrahydro-2*H*-pyran-2-yl)-1-(4-(trifluoromethyl)phenyl)ethan-1-one

This compound was prepared according to the general procedure for C-H insertion using tetrahydropyran (0.17 ml, 5 equiv, 1.7 mmol) as the substrate and 2-diazo-2-phenyl-1-(4-(trifluoromethyl) -phenyl)ethan-1-one (100 mg, 1 equiv, 0.35 mmol) under the catalyst of Rh_2(*S*-TPPTTL)$_4$ (4 mg, 0.005 equiv, 1.7 μmol). After flash chromatography (5% ether in hexanes) the product was obtained as a thick clear oil (36 mg, 30% yield,, >20:1 r.r., 10:1 d.r, 91% e.e.).

Rf = 0.158 (10% diethyl ether/hexanes)

$[\alpha]^{20}_D$: -49.5^o (c = 1.07, $CHCl_3$)

^{1}HNMR (600 MHz, CDCl3) δ 8.05 (d, *J* = 8.2 Hz, 2H), 7.67 (d, *J* = 8.2 Hz, 2H), 7.41 – 7.35 (m, 2H), 7.31 (dd, *J* = 8.4, 6.9 Hz, 2H), 7.26 – 7.22 (m, 1H), 4.65 (d, *J* = 9.1 Hz, 1H), 4.07 (ddd,

J = 10.8, 9.1, 1.8 Hz, 1H), 3.93 – 3.87 (m, 1H), 3.34 (td, *J* = 11.6, 2.5 Hz, 1H), 1.86 – 1.76 (m, 2H), 1.63 – 1.52 (m, 2H), 1.49 (dtt, *J* = 9.4, 4.4, 2.3 Hz, 1H), 1.34 (tdd, *J* = 12.6, 10.6, 4.3 Hz, 1H).

^{13}C NMR (151 MHz, $CDCl_3$) δ 197.9, 139.8, 136.1, 134.3 (q, J = 32.6 Hz), 128.9 (d, J = 8.3 Hz), 128.8, 127.5, 125.7 (q, J = 3.7 Hz), 123.5 (q, *J* = 272.6 Hz), 79.4, 69.0, 59.7, 30.45, 29.7, 25.9, 23.4.

^{19}FNMR (565 MHz, CDCl3) δ -63.2.

IR (neat): 2937, 2850, 1681, 1581, 1510, 1495, 1453, 1408, 1321, 1295, 1266, 1200, 1166, 1126, 1089, 1065, 1048, 1011, 973, 905, 871, 849, 814, 773, 745, 695, 610, 594, 550, 528, 475, 435, 426, 410, 403 cm^{-1}.

HPLC: (Chiralpak ODH column, 1.0% *i*-propanol in hexane, 1.0 mL min^{-1}, 1.0 mg mL^{-1}, 30 min, UV 230 nm) retention times of 5.2 min (minor) and 6.3 (major) 91% ee.

HRMS (+p APCI) calcd for $C_{20}H_{20}F_3O_2$ $(M+H)^+$ 349.1337 found 349.1413.

References

1. Fu, J.; Ren, Z.; Bacsa, J.; Musaev, D. G.; Davies, H. M. L., Desymmetrization of cyclohexanes by site- and stereoselective C–H functionalization. *Nature* **2018,** *564* (7736), 395-399.
2. Vaitla, J.; Boni, Y. T.; Davies, H. M. L., Distal Allylic/Benzylic C−H Functionalization of Silyl Ethers Using Donor/Acceptor Rhodium(II) Carbenes. *Angew. Chem. Int. Ed.* **2020,** *59* (19), 7397-7402.
3. Tan, Y.; Yuan, W.; Gong, L.; Meggers, E., Aerobic Asymmetric Dehydrogenative Cross-Coupling between Two C□H Groups Catalyzed by a Chiral-at-Metal Rhodium Complex. *Angew. Chem. Int. Ed.* **2015,** *54* (44), 13045-13048.
4. Landers, B.; Berini, C.; Wang, C.; Navarro, O., (N-Heterocyclic Carbene)-Pd-Catalyzed Anaerobic Oxidation of Secondary Alcohols and Domino Oxidation−Arylation Reactions. *J. Org. Chem.* **2011,** *76* (5), 1390-1397.
5. Wommack, A. J.; Moebius, D. C.; Travis, A. L.; Kingsbury, J. S., Diverse Alkanones by Catalytic Carbon Insertion into the Formyl C−H Bond. Concise Access to the Natural Precursor of Achyrofuran. *Org. Lett.* **2009,** *11* (15), 3202-3205.

6. Wu, X.; Li, K.; Wang, S.; Liu, C.; Lei, A., Acid-Promoted Cross-Dehydrative Aromatization for the Synthesis of Tetraaryl-Substituted Pyrroles. *Org. Lett.* **2016,** *18* (1), 56-59.
7. Denton, J. R.; Davies, H. M. L., Enantioselective Reactions of Donor/Acceptor Carbenoids Derived from α-Aryl-α-Diazoketones. *Org. Lett.* **2009,** *11* (4), 787-790.

Appendix

Appendix – Ch.2 NMR Spectra

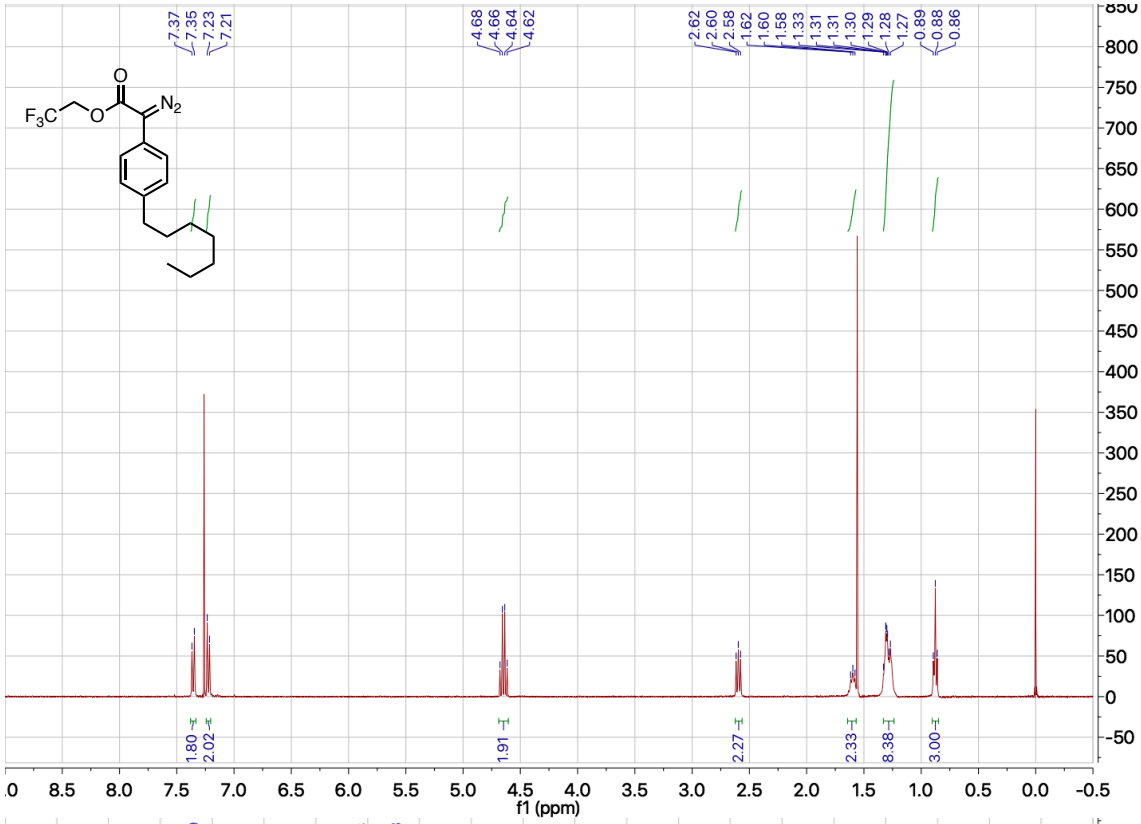

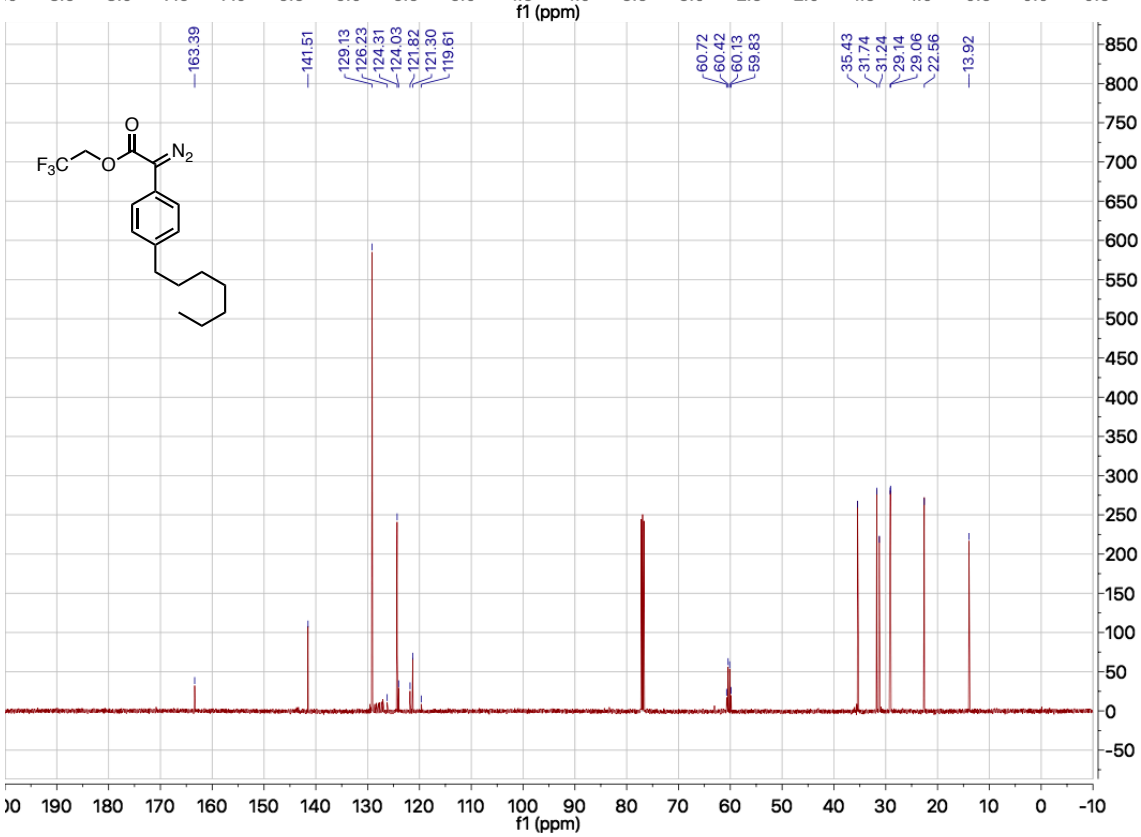

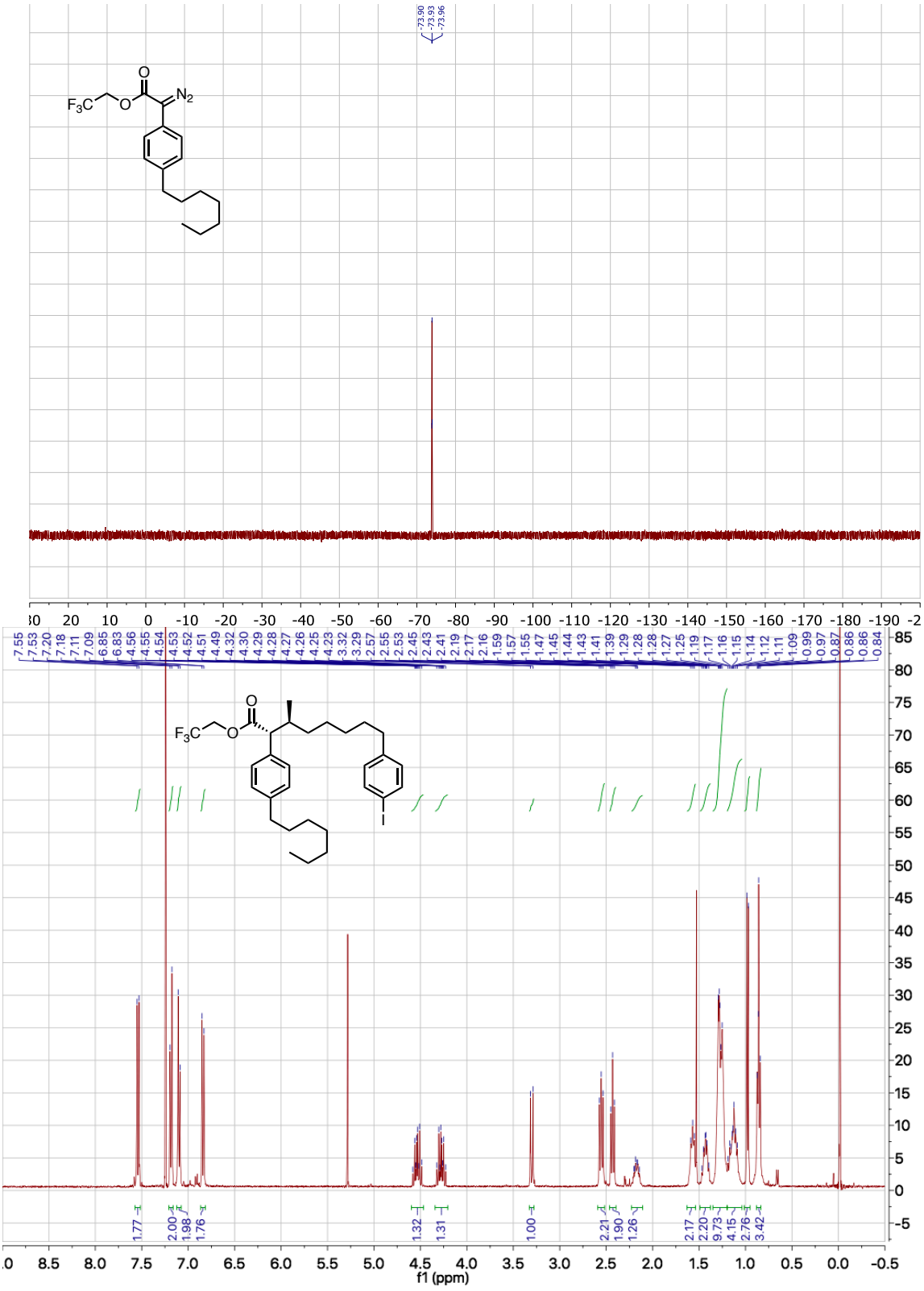
F3C
O
O
N2
-73.90
-73.93
-73.96
F3C
O
O
I
f1 (ppm)

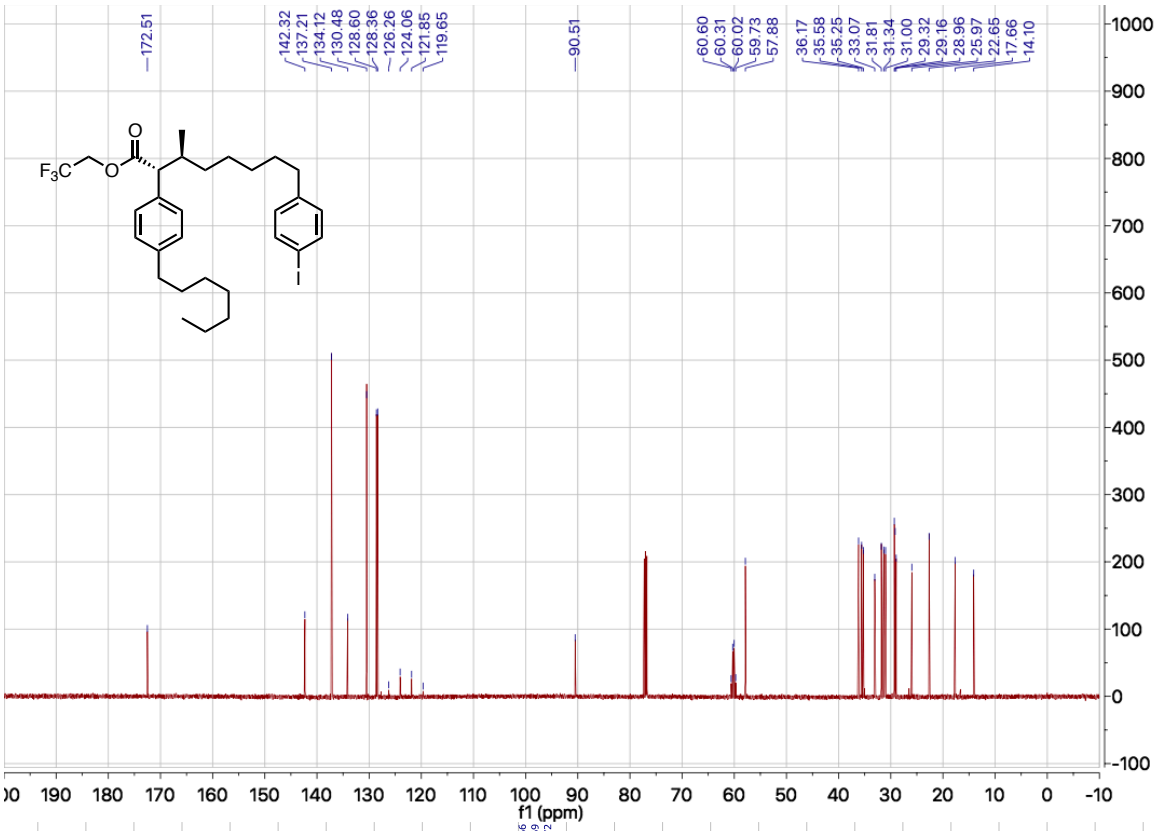
172.51
142.32
137.21
134.12
130.48
128.60
128.36
126.26
124.06
121.85
119.65
90.51
60.60
60.31
60.02
59.73
57.88
36.17
35.58
35.25
33.07
31.81
31.34
31.00
29.32
29.16
28.96
25.97
22.65
17.66
14.10
F3C
O
O
I
f1 (ppm)

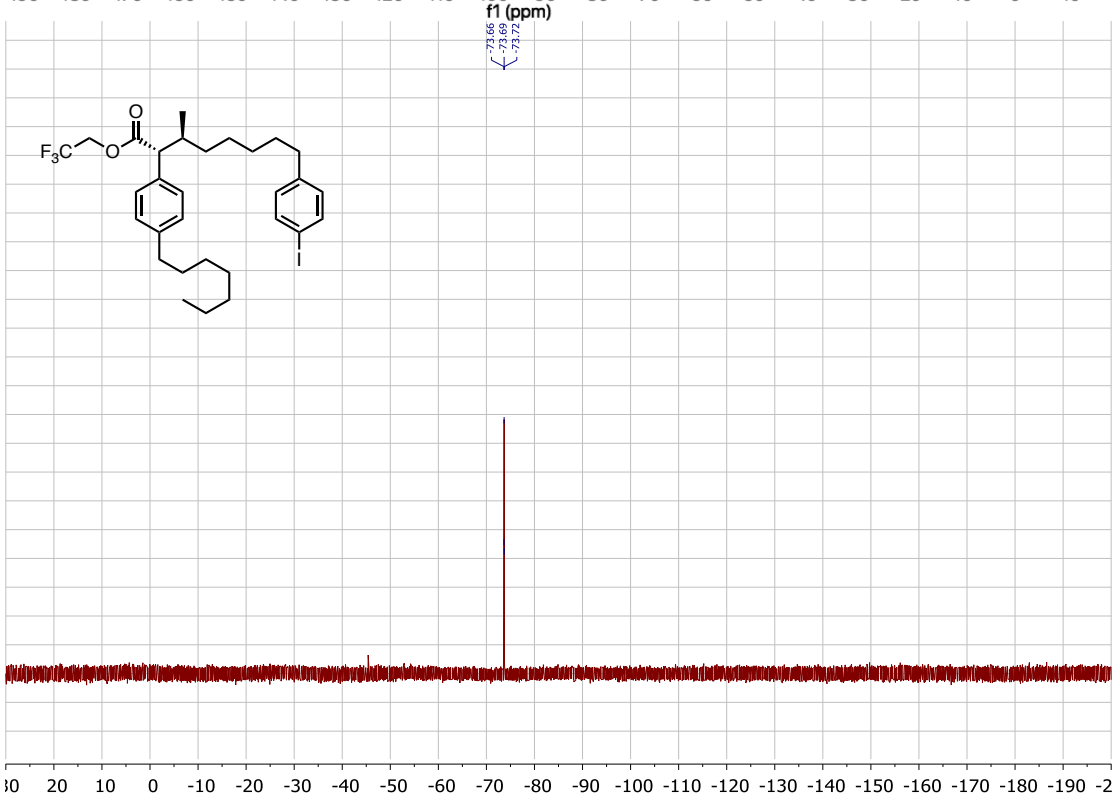
-73.66
-73.69
-73.72
F3C
O
O
I

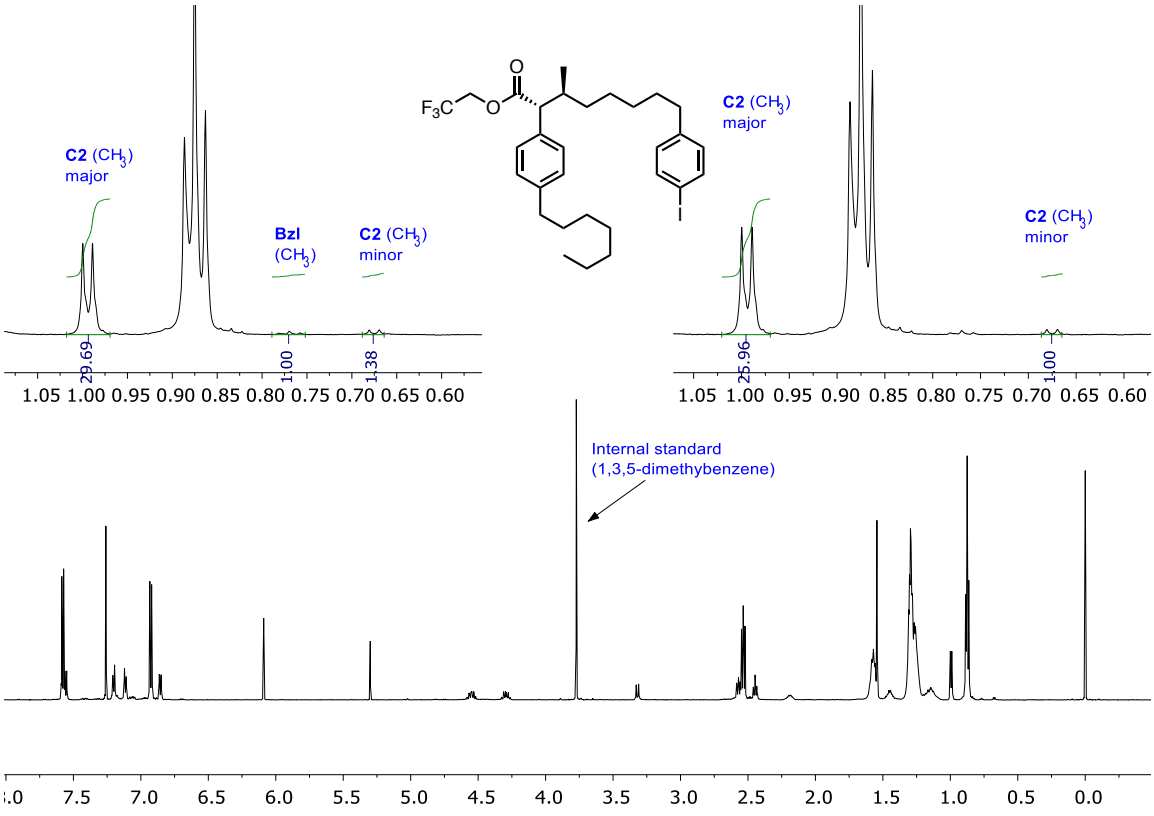
C2 (CH3)
major
Bzl
(CH3)
C2 (CH3)
minor
29.69
1.00
1.38
C2 (CH3)
major
C2 (CH3)
minor
25.96
1.00
Internal standard
(1,3,5-dimethybenzene)

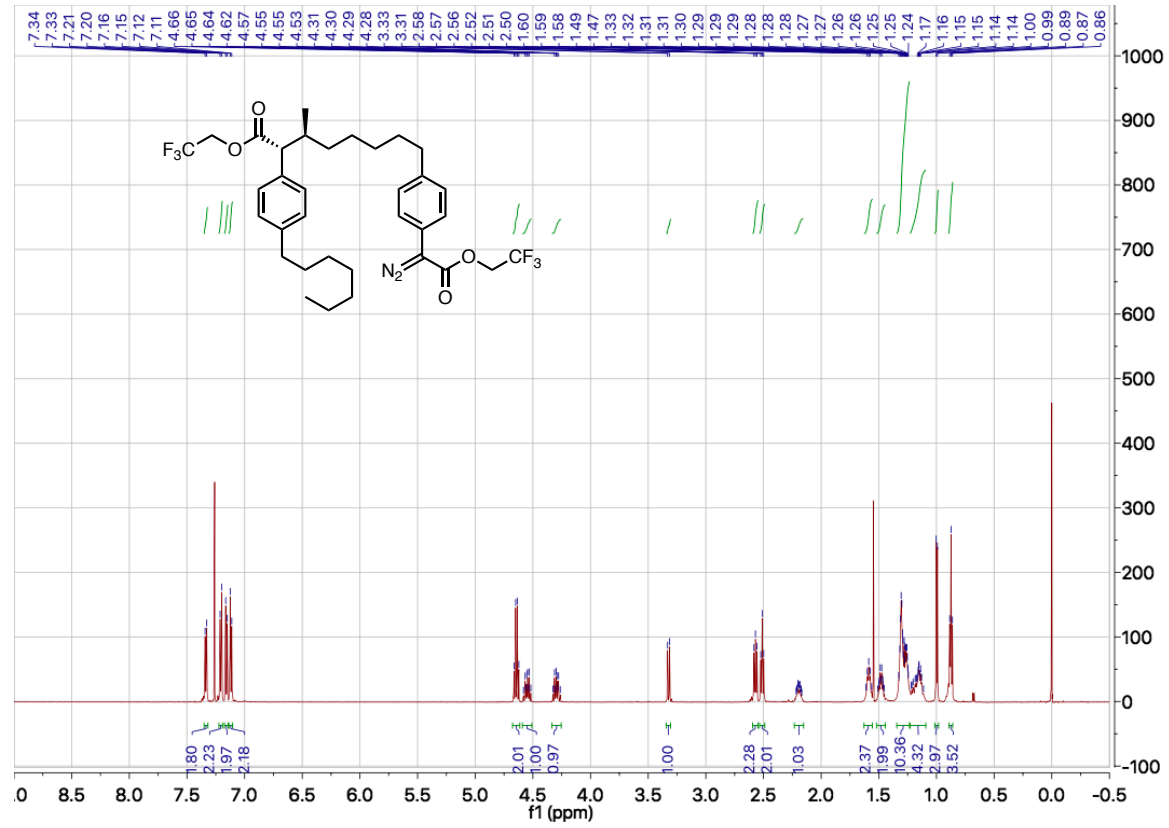
f1 (ppm)

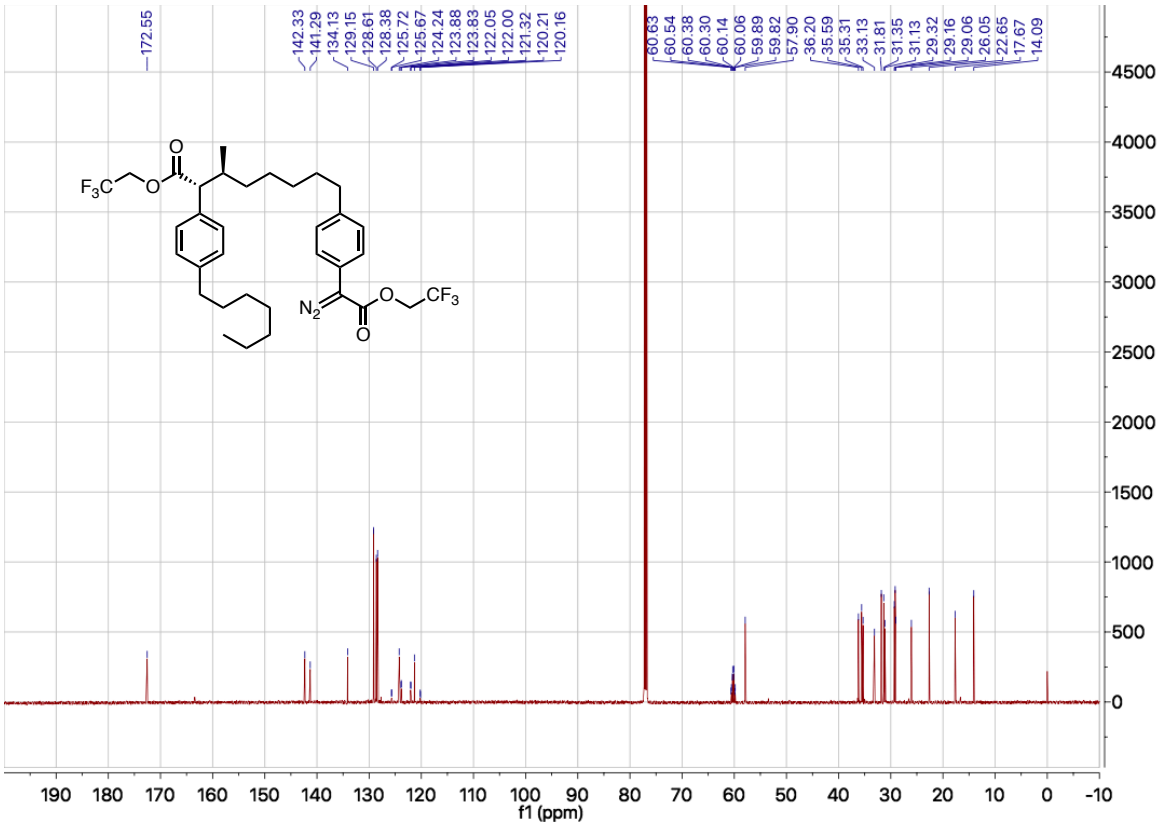
172.55
142.33
141.29
134.13
129.15
128.61
128.38
125.72
125.67
124.24
123.88
123.83
122.05
122.00
121.32
120.21
120.16
60.63
60.54
60.38
60.30
60.14
60.06
59.89
59.82
57.90
36.20
35.59
35.31
33.13
31.81
31.35
31.13
29.32
29.16
29.06
26.05
22.65
17.67
14.09
F3C
O
N2
CF3
f1 (ppm)

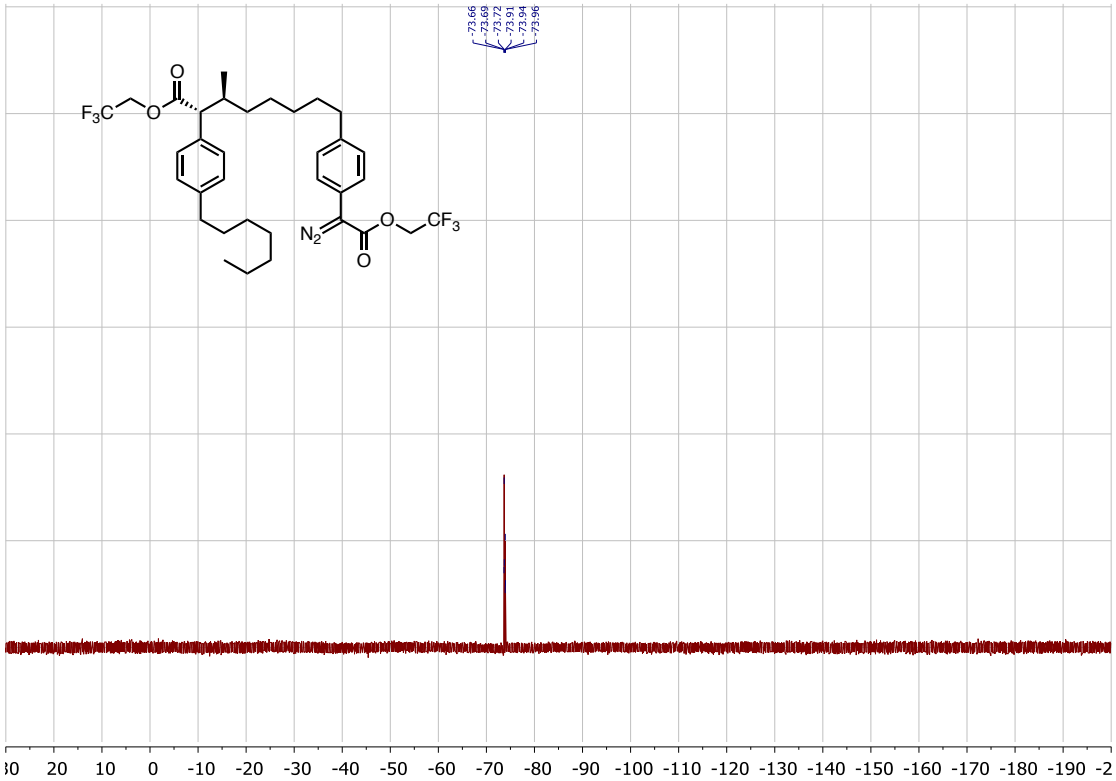
-73.66
-73.69
-73.72
-73.91
-73.94
-73.96
F3C
O
N2
CF3

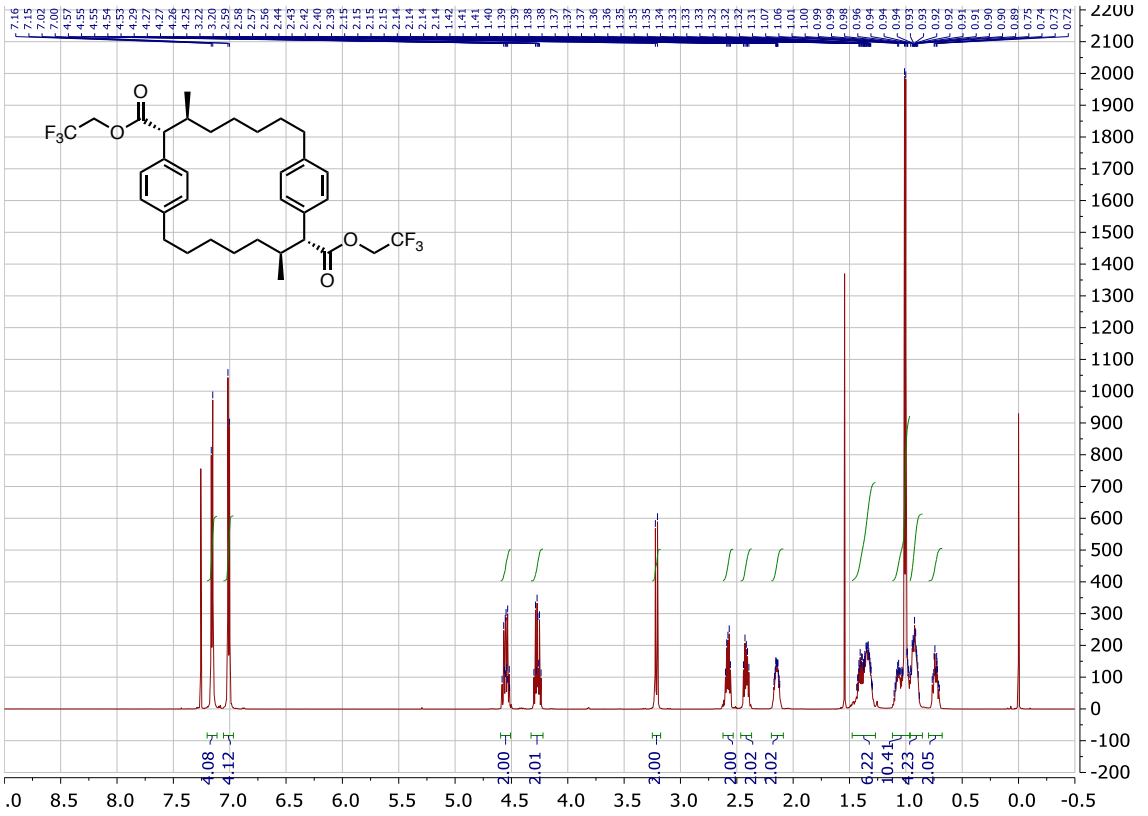
F3C
O
O
O
O
CF3
4.08
4.12
2.00
2.01
2.00
2.00
2.02
2.02
6.22
10.41
4.23
2.05

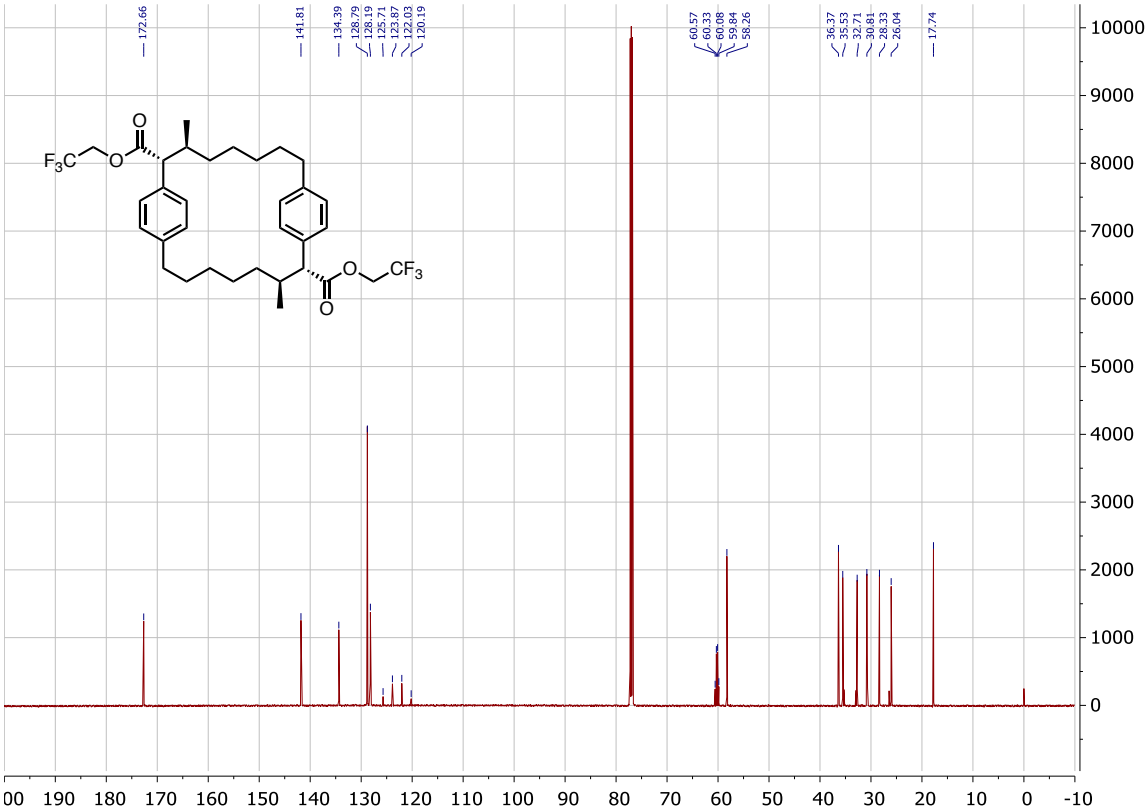
F3C
O
O
O
O
CF3
172.66
141.81
134.39
128.79
128.19
125.71
123.87
122.03
120.19
60.57
60.33
60.08
59.84
58.26
36.37
35.53
32.71
30.81
28.33
26.04
17.74

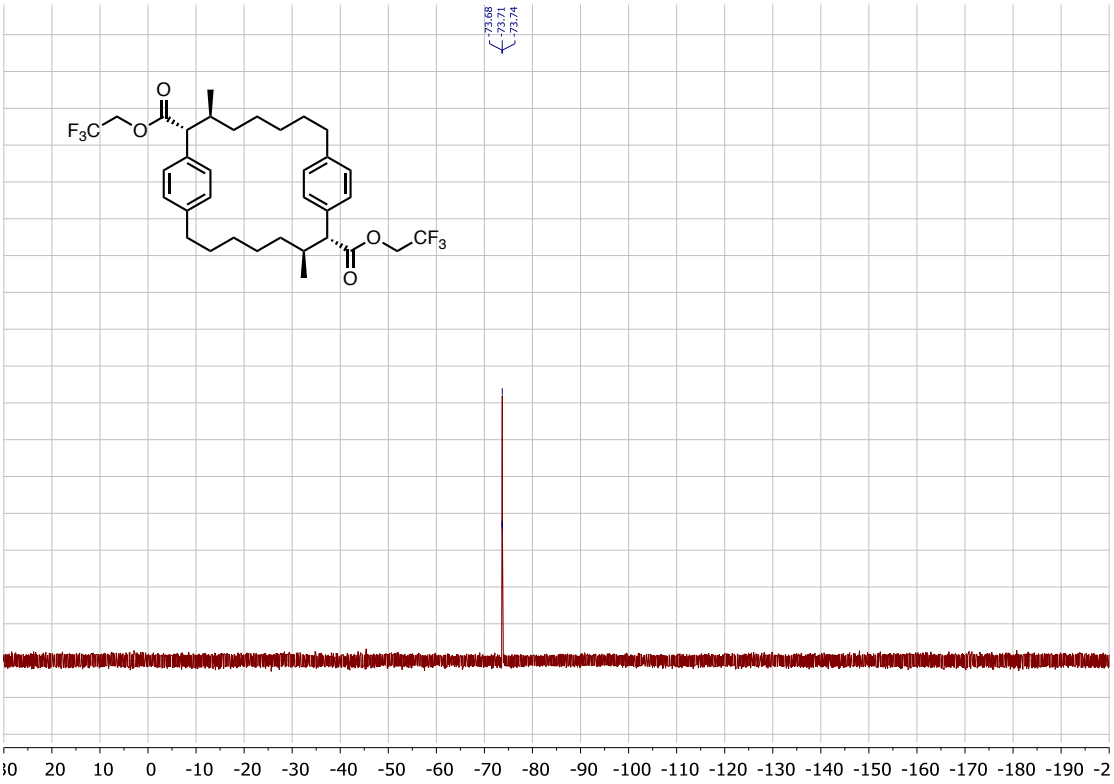
-73.68
-73.71
-73.74
F3C
O
O
O
O
CF3
30 20 10 0 -10 -20 -30 -40 -50 -60 -70 -80 -90 -100 -110 -120 -130 -140 -150 -160 -170 -180 -190 -2

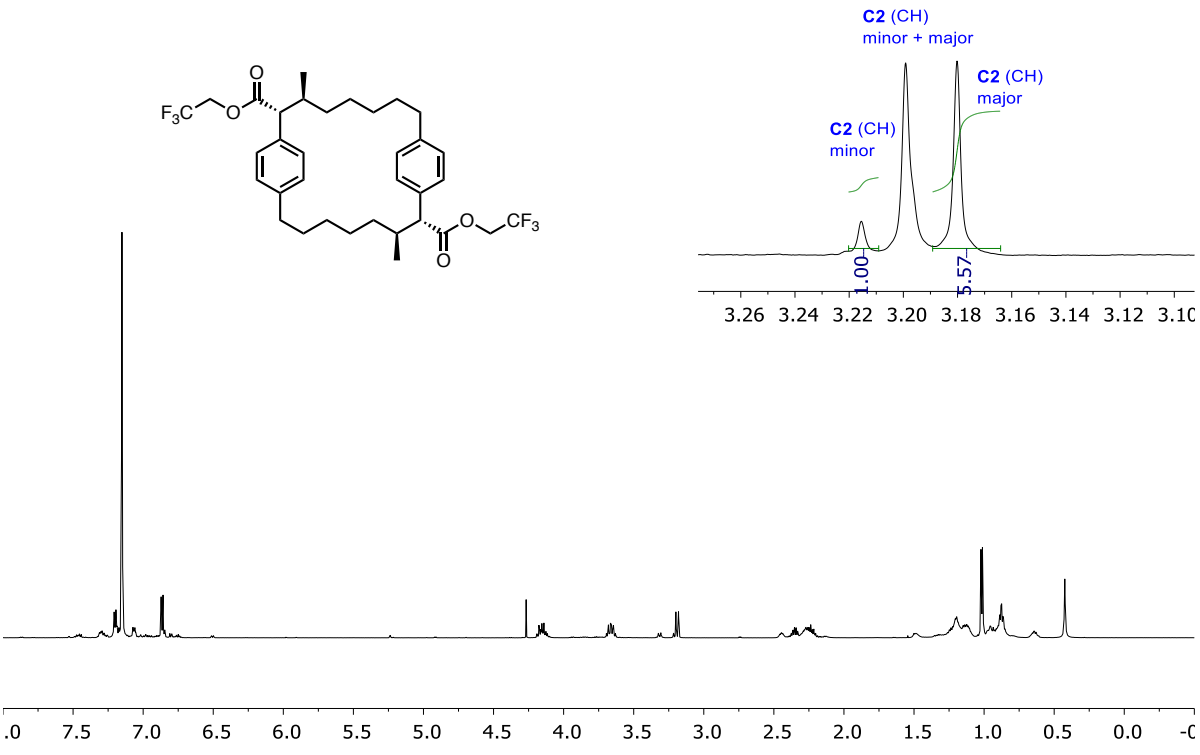
F3C
O
O
O
O
CF3
C2 (CH)
minor + major
C2 (CH)
major
C2 (CH)
minor
1.00
5.57
3.26 3.24 3.22 3.20 3.18 3.16 3.14 3.12 3.10
.0 7.5 7.0 6.5 6.0 5.5 5.0 4.5 4.0 3.5 3.0 2.5 2.0 1.5 1.0 0.5 0.0 -0

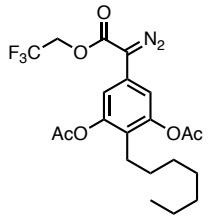
O
F3C
O
N2
AcO
OAc

7.26 cdcl3
7.08
4.66
4.64
4.62
4.60
2.42
2.40
2.38
1.43
1.28
0.89
0.88
0.86
1.41
2.00
2.31
6.73
2.30
7.46
3.42
f1 (ppm)

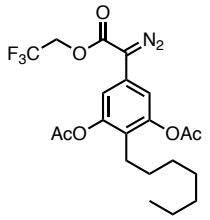
O
F3C
O
N2
AcO
OAc

169.0
162.6
150.3
125.9
125.5
123.7
123.5
121.9
120.0
115.5
77.0 CDCl3
60.7
60.4
60.2
59.9
31.7
29.6
29.0
28.9
24.7
22.6
20.8
20.8
14.1
f1 (ppm)

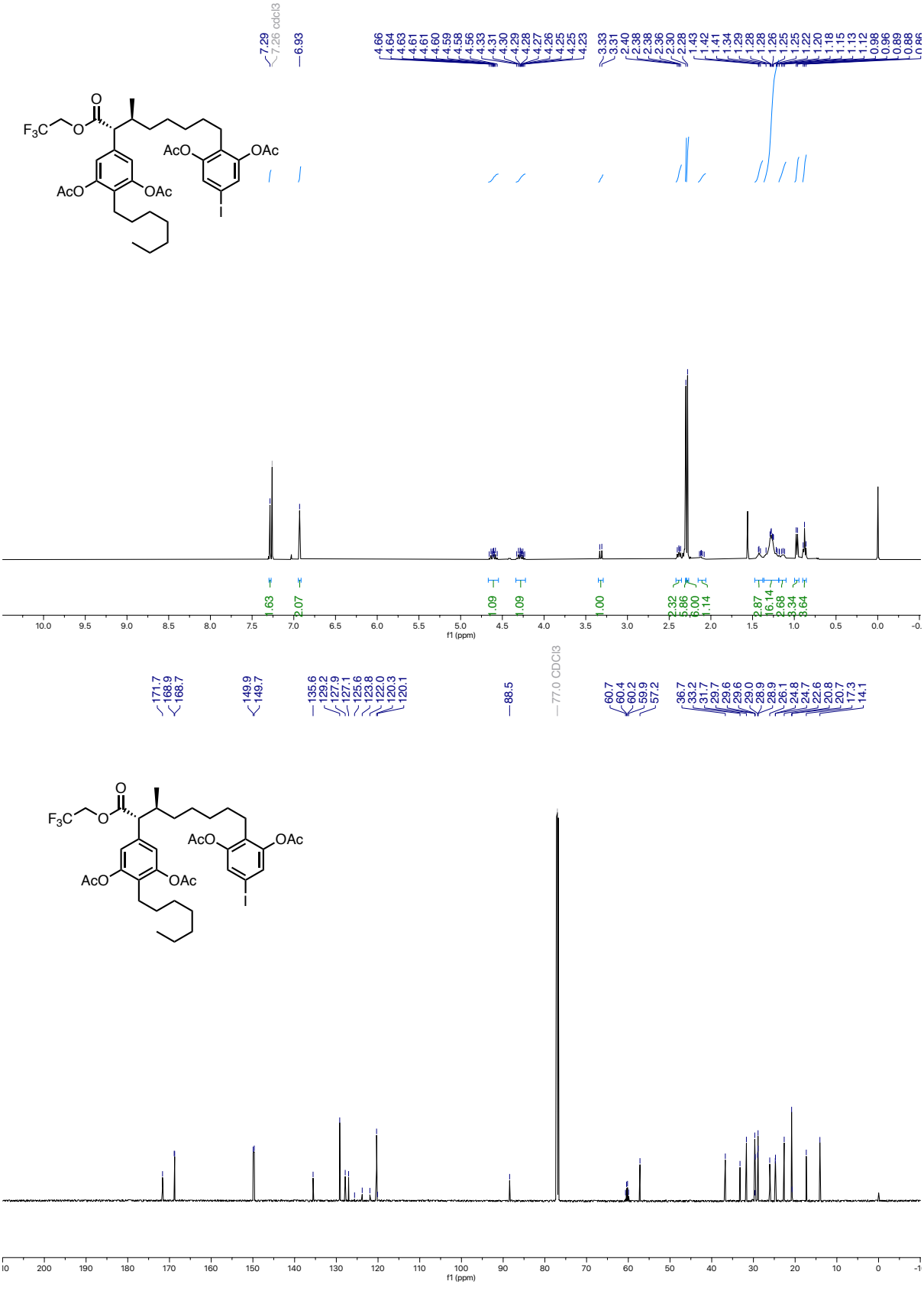
F3C
O
AcO
OAc
AcO
OAc
I
7.29
7.26 cdcl3
6.93
f1 (ppm)
77.0 CDCl3
f1 (ppm)

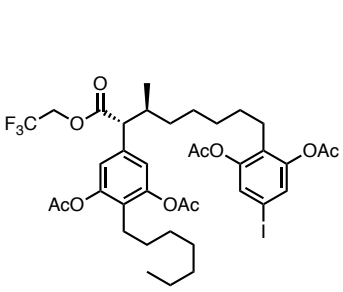
O
F3C
O
AcO
OAc
AcO
OAc
I


-73.5
-73.6
-73.6
-73.6
-73.6
-73.6

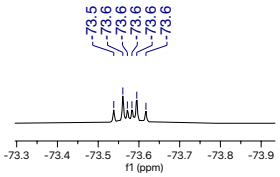
-73.5
-73.6
-73.6
-73.6
-73.6
-73.6
-73.3
-73.4
-73.5
-73.6
-73.7
-73.8
-73.9
f1 (ppm)

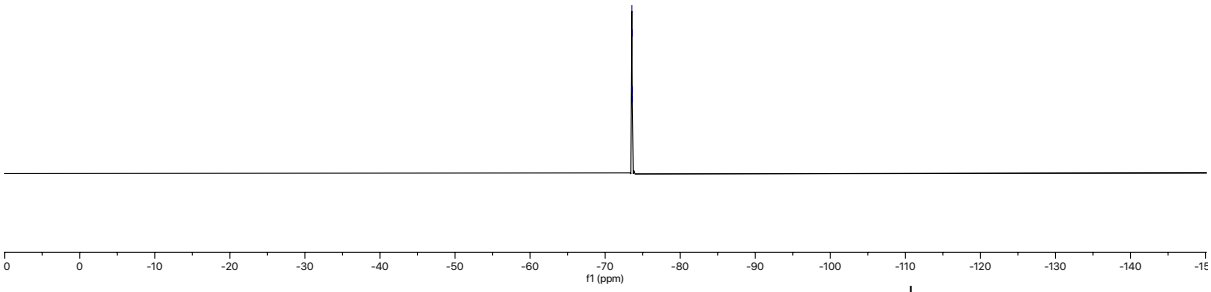
0
-10
-20
-30
-40
-50
-60
-70
-80
-90
-100
-110
-120
-130
-140
f1 (ppm)

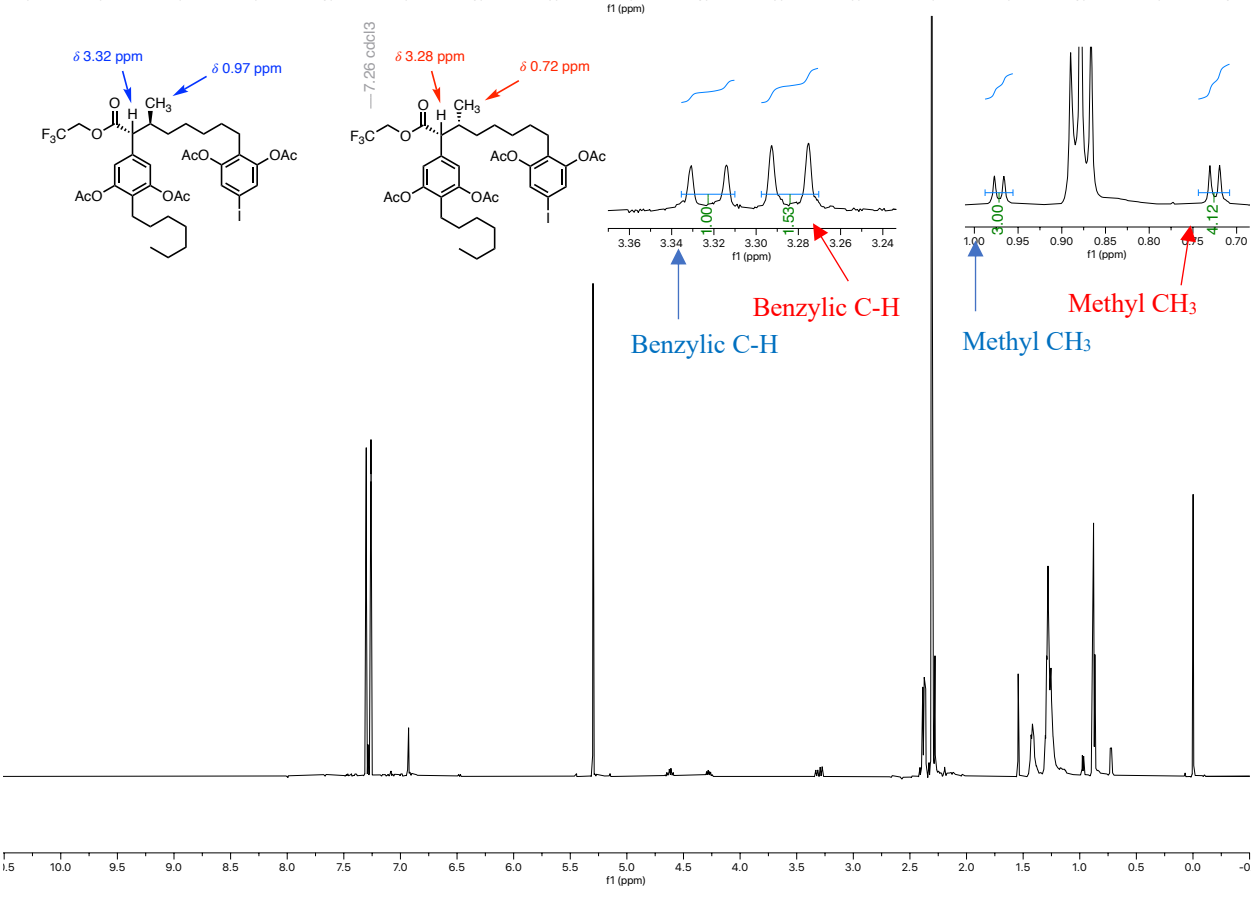
δ 3.32 ppm
δ 0.97 ppm
δ 3.28 ppm
δ 0.72 ppm
7.26 cdcl3
1.00
1.53
3.00
4.12
Benzylic C-H
Methyl CH3
Benzylic C-H
Methyl CH3
f1 (ppm)

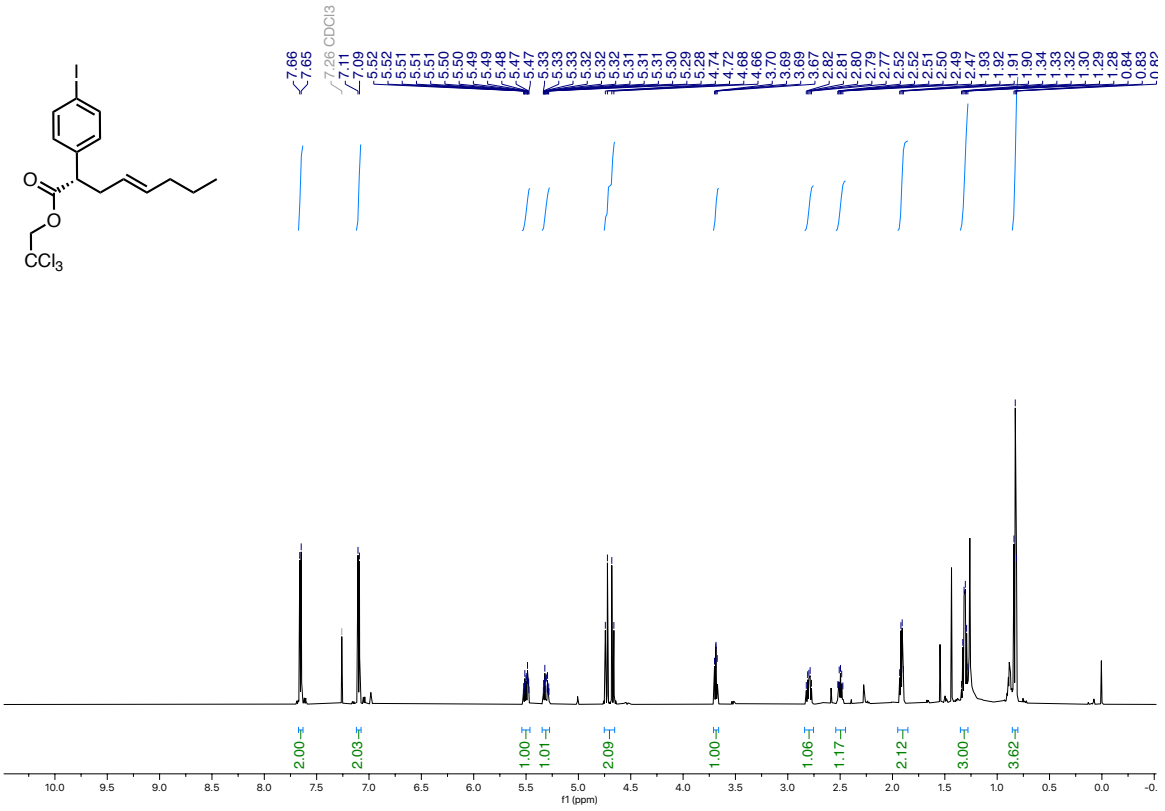
7.66
7.65
7.26 CDCl3
7.11
7.09
2.00
2.03
1.00
1.01
2.09
1.00
1.06
1.17
2.12
3.00
3.62
f1 (ppm)

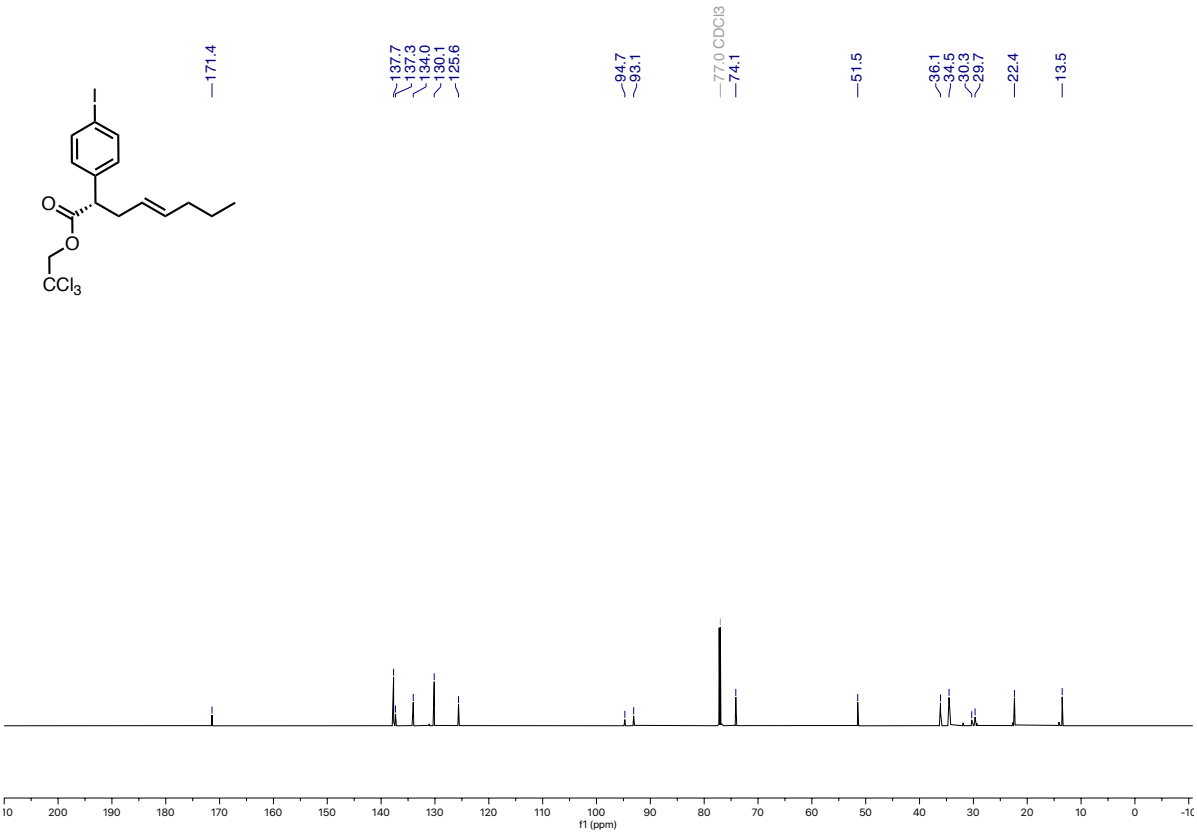
171.4
137.7
137.3
134.0
130.1
125.6
94.7
93.1
77.0 CDCl3
74.1
51.5
36.1
34.5
30.3
29.7
22.4
13.5
f1 (ppm)

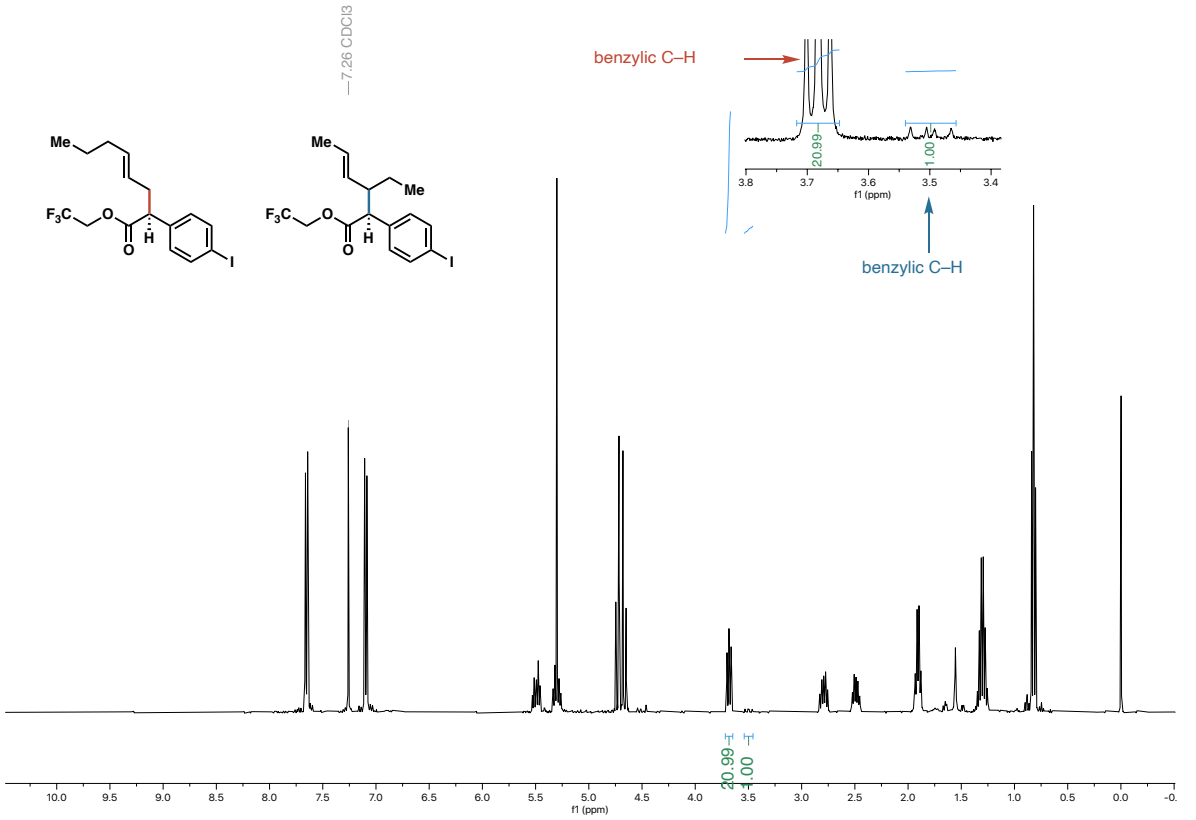
7.26 CDCl3
benzylic C–H
benzylic C–H
20.99
1.00
f1 (ppm)

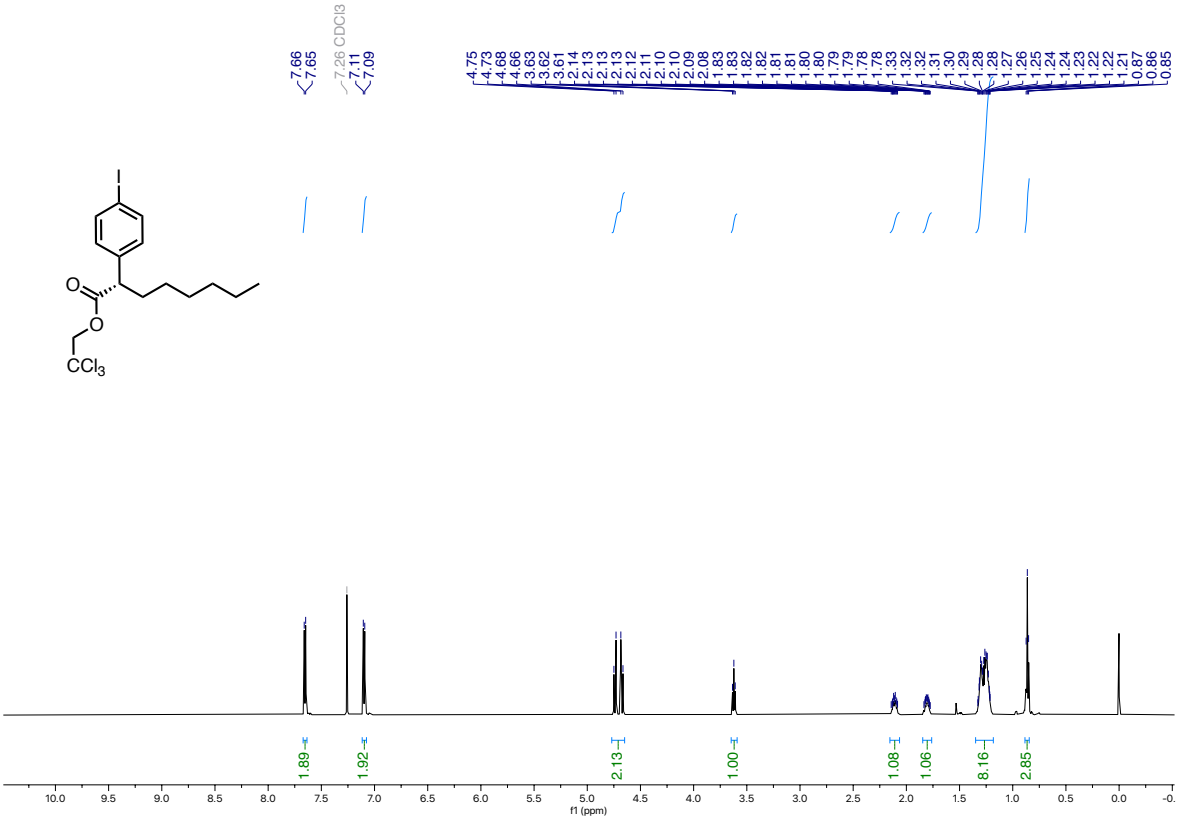
7.26 CDCl3
f1 (ppm)

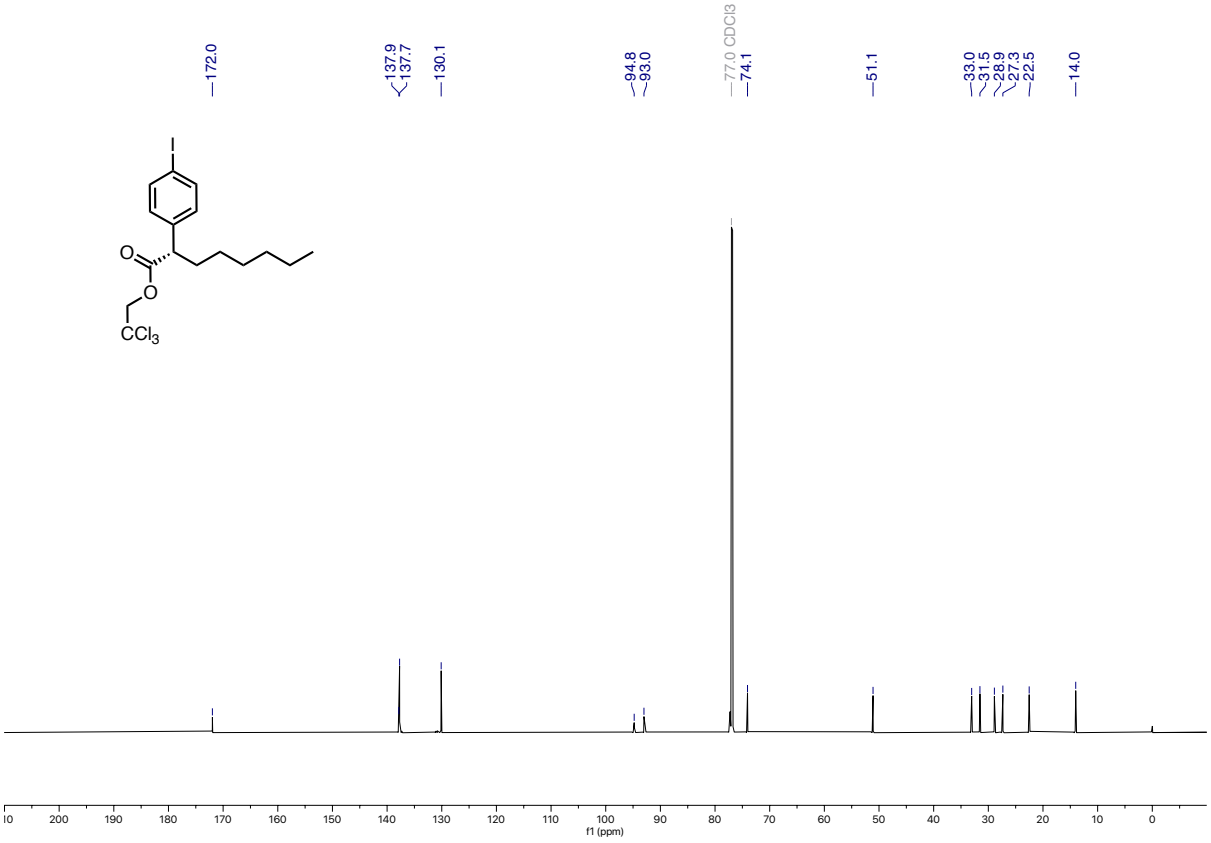
172.0
137.9
137.7
130.1
94.8
93.0
77.0 CDCl3
74.1
51.1
33.0
31.5
28.9
27.3
22.5
14.0
I
O
O
CCl3
f1 (ppm)

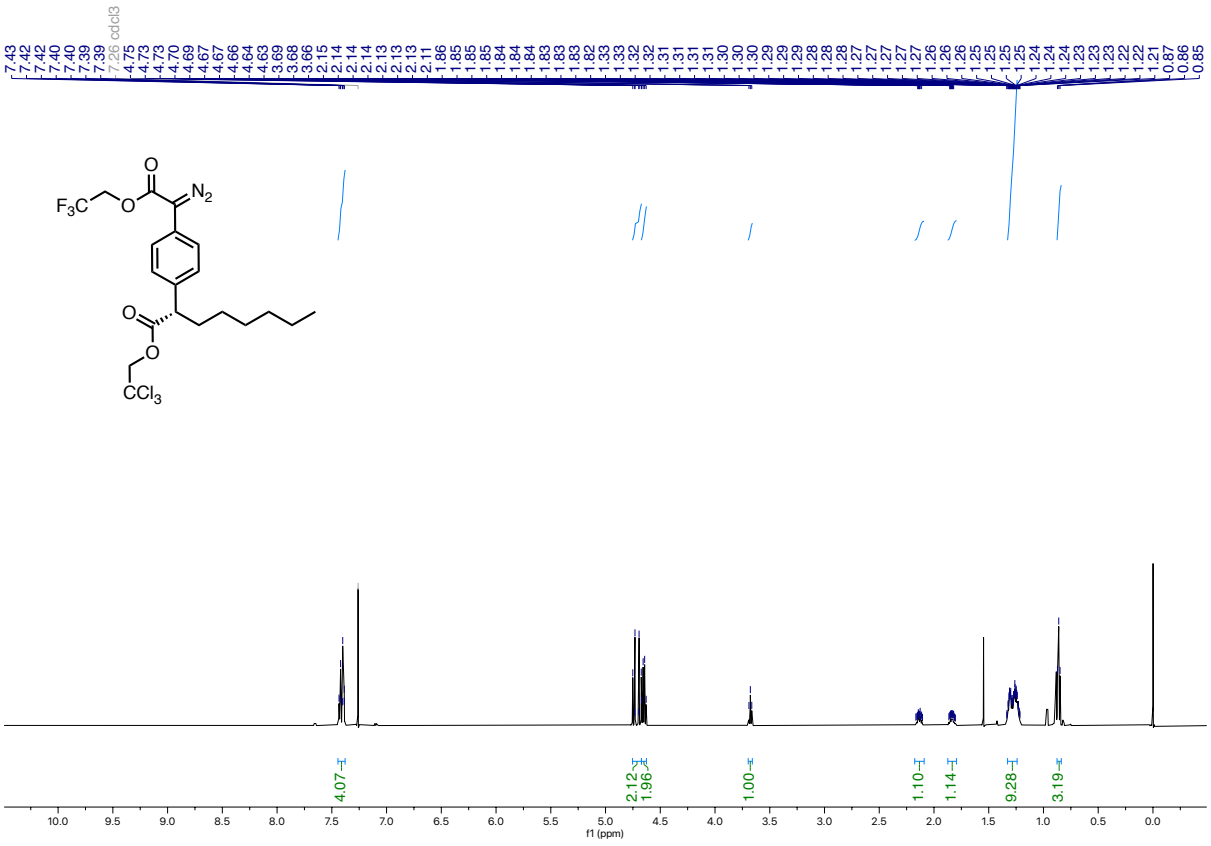
7.26 cdcl3
F3C
O
O
N2
O
O
CCl3
4.07
2.12
1.96
1.00
1.10
1.14
9.28
3.19
f1 (ppm)

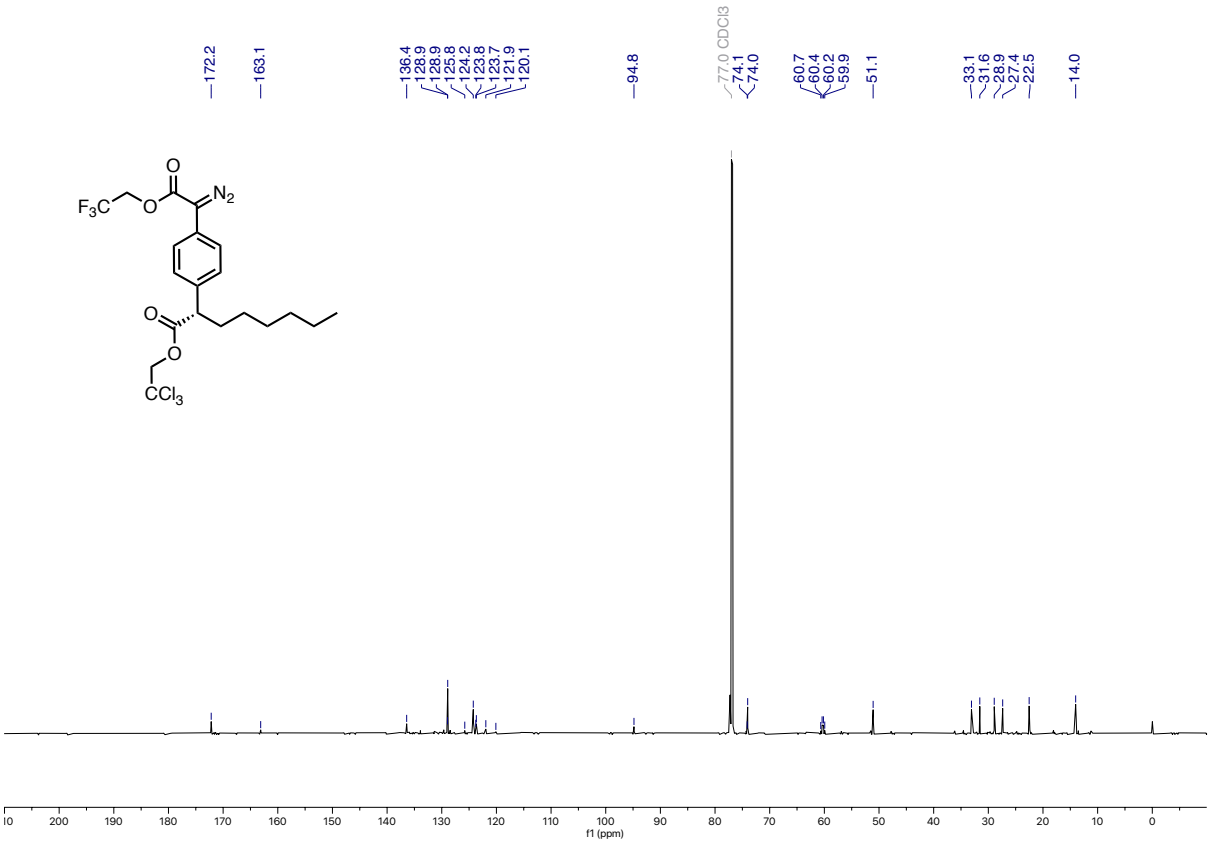
172.2
163.1
136.4
128.9
128.9
125.8
124.2
123.8
123.7
121.9
120.1
94.8
77.0 CDCl3
74.1
74.0
60.7
60.4
60.2
59.9
51.1
33.1
31.6
28.9
27.4
22.5
14.0
f1 (ppm)

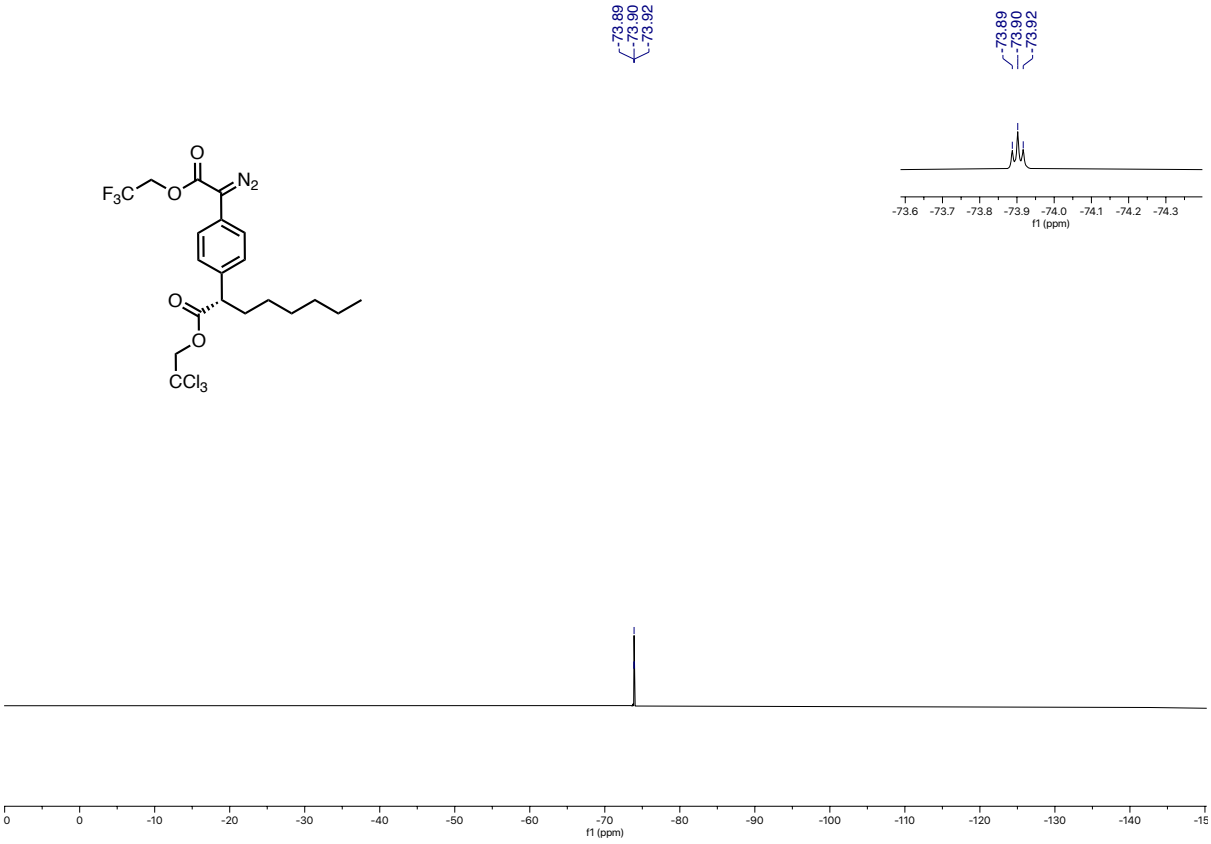
-73.89
-73.90
-73.92
-73.89
-73.90
-73.92
-73.6 -73.7 -73.8 -73.9 -74.0 -74.1 -74.2 -74.3
f1 (ppm)
f1 (ppm)

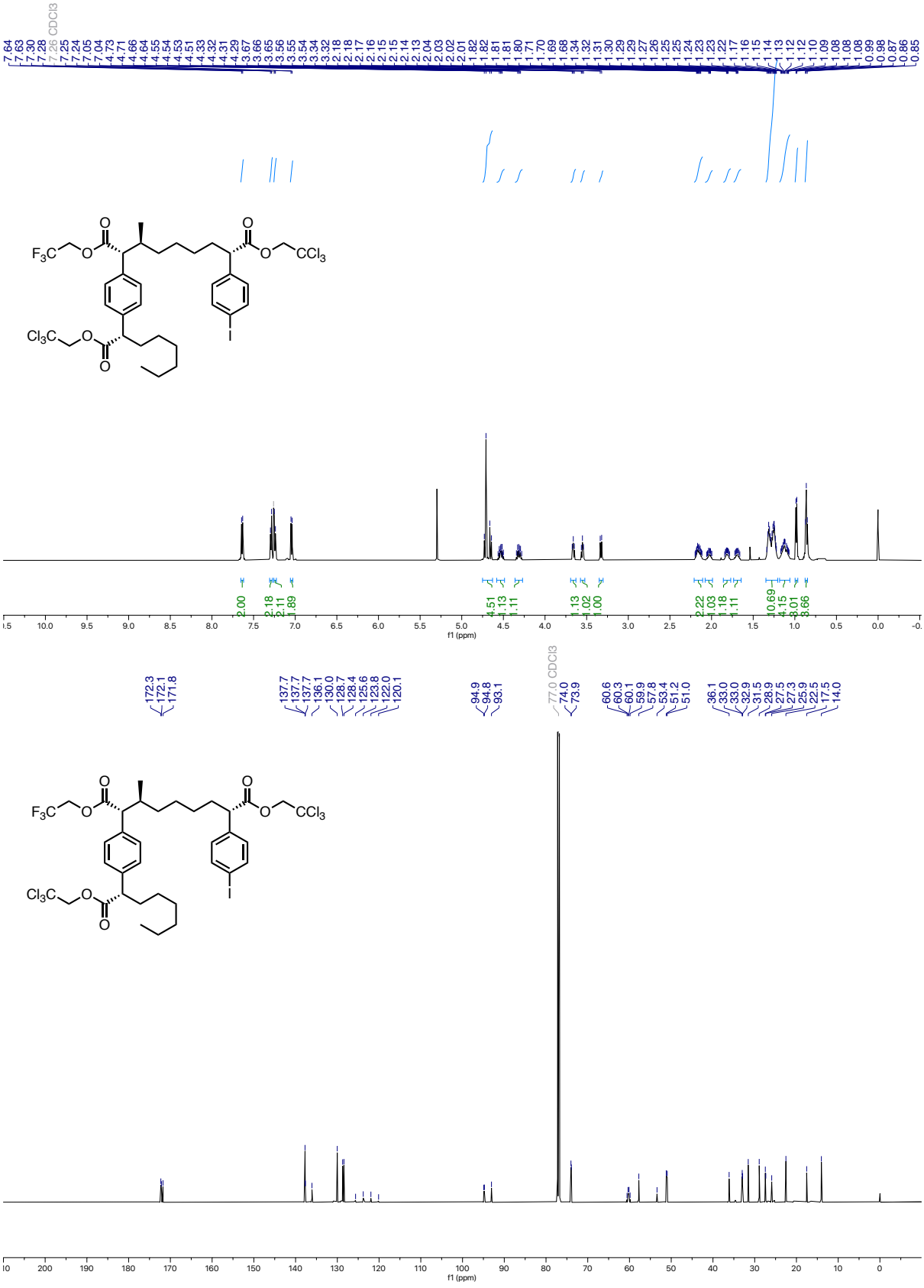
7.64
7.63
7.30
7.28
7.26 CDCl3
7.25
7.24
7.05
7.04
4.73
4.71
4.66
4.64
4.55
4.54
4.53
4.51
4.33
4.32
4.31
4.29
3.67
3.66
3.65
3.56
3.55
3.54
3.34
3.32
2.18
2.18
2.17
2.16
2.15
2.15
2.14
2.13
2.04
2.03
2.02
2.01
1.82
1.82
1.81
1.81
1.80
1.71
1.70
1.69
1.68
1.34
1.32
1.31
1.30
1.29
1.29
1.27
1.26
1.25
1.25
1.24
1.23
1.23
1.22
1.17
1.16
1.15
1.14
1.13
1.12
1.10
1.09
1.08
1.08
0.99
0.98
0.87
0.86
0.85
F3C
O
O
O
CCl3
Cl3C
O
O
I
2.00
2.18
2.11
1.89
4.51
1.13
1.11
1.13
1.02
1.00
2.22
1.03
1.18
1.11
10.69
4.15
3.01
8.66
f1 (ppm)
172.3
172.1
171.8
137.7
137.7
137.7
136.1
130.0
128.7
128.4
125.6
123.8
122.0
120.1
94.9
94.8
93.1
77.0 CDCl3
74.0
73.9
60.6
60.3
60.1
59.9
57.8
53.4
51.2
51.0
36.1
33.0
33.0
32.9
31.5
28.9
27.5
27.3
25.9
22.5
17.5
14.0
f1 (ppm)

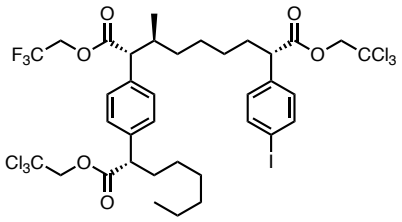
O
O
F3C
O
O
CCl3
Cl3C
O
O
I


-73.6
-73.7
-73.7

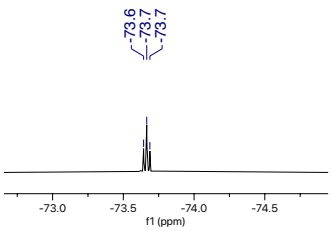
-73.6
-73.7
-73.7
-73.0
-73.5
-74.0
-74.5
f1 (ppm)

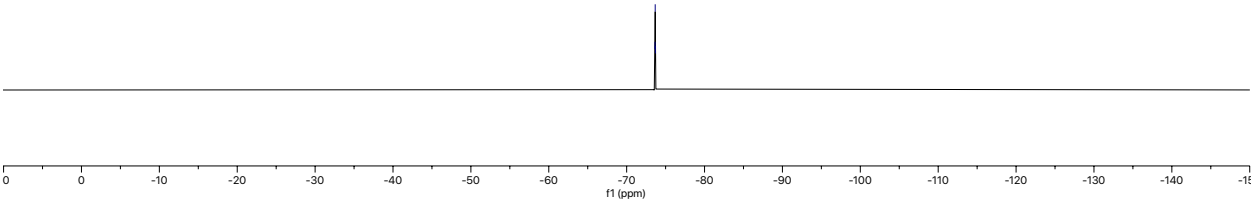
0
-10
-20
-30
-40
-50
-60
-70
-80
-90
-100
-110
-120
-130
-140
f1 (ppm)

7.26 CDCl3

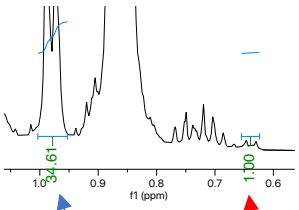
34.61
1.00
1.0
0.9
0.8
0.7
0.6
f1 (ppm)

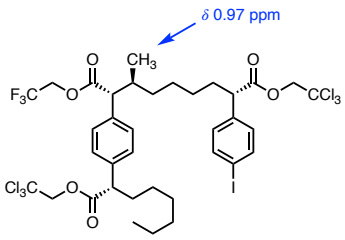
δ 0.97 ppm
CH3
O
O
F3C
O
O
CCl3
Cl3C
O
O
I

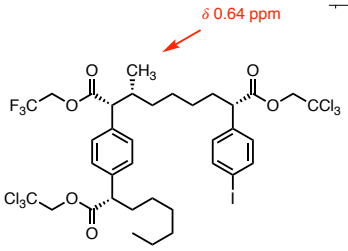
δ 0.64 ppm
CH3
O
O
F3C
O
O
CCl3
Cl3C
O
O
I


Methyl CH3
Methyl CH3

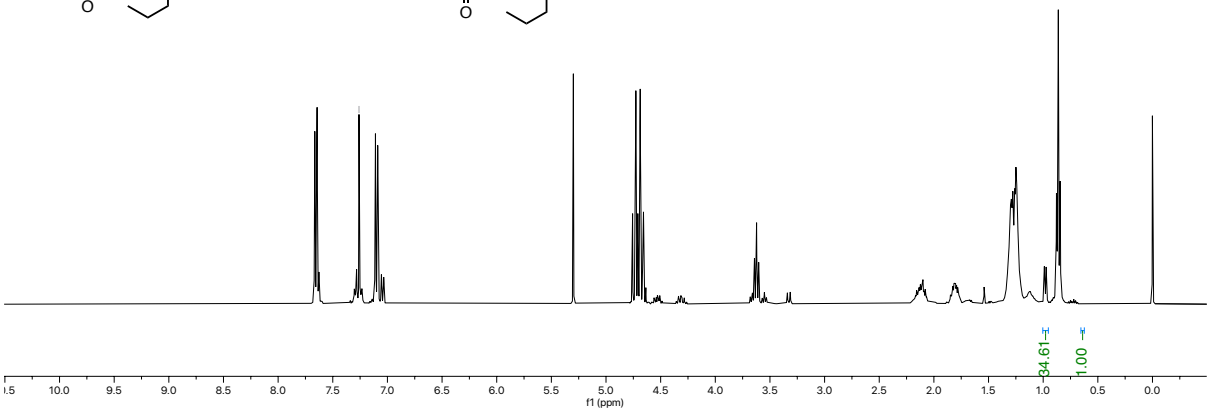
34.61
1.00
10.0
9.5
9.0
8.5
8.0
7.5
7.0
6.5
6.0
5.5
5.0
4.5
4.0
3.5
3.0
2.5
2.0
1.5
1.0
0.5
0.0
f1 (ppm)

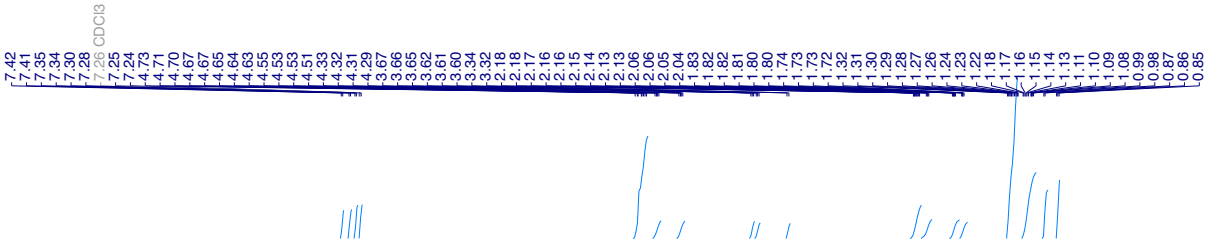
CDCl3

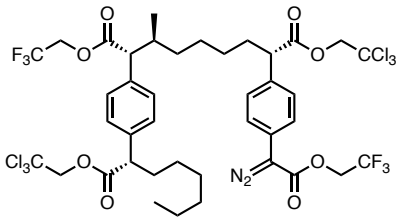
F3C
O
O
O
CCl3
Cl3C
O
O
N2
O
CF3
O

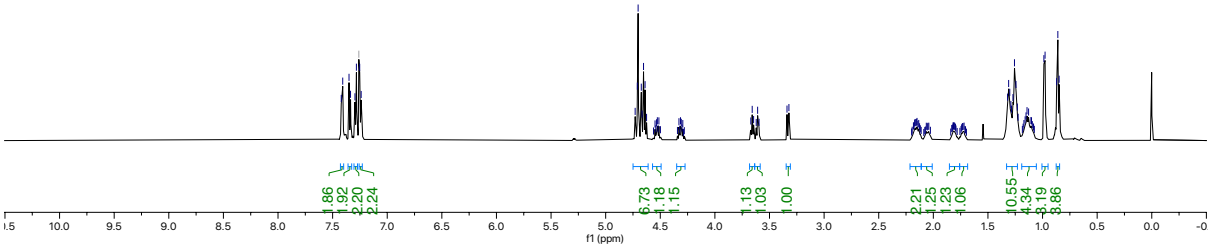
1.86
1.92
2.20
2.24
6.73
4.18
1.15
1.13
1.03
1.00
2.21
1.25
1.23
1.06
10.55
4.34
3.19
3.86
f1 (ppm)

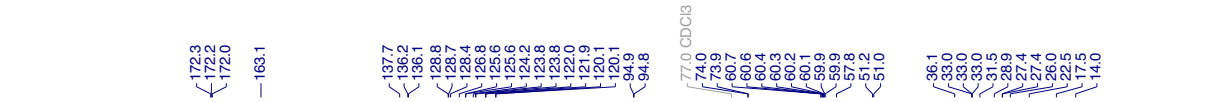
172.3
172.2
172.0
163.1
137.7
136.2
136.1
128.8
128.7
128.4
126.8
125.6
125.6
124.2
123.8
123.8
122.0
121.9
120.1
120.1
94.9
94.8
77.0 CDCl3
74.0
73.9
60.7
60.6
60.4
60.3
60.2
60.1
59.9
59.9
57.8
51.2
51.0
36.1
33.0
33.0
33.0
31.5
28.9
28.9
27.4
27.4
26.0
22.5
17.5
14.0

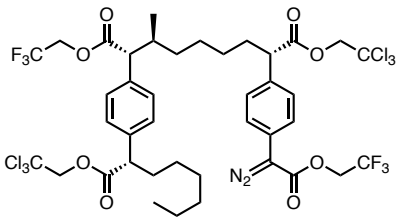
F3C
O
O
O
CCl3
Cl3C
O
O
N2
O
CF3
O

f1 (ppm)

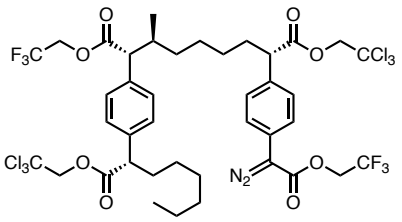
F3C
O
O
O
CCl3
Cl3C
O
O
N2
O
O
CF3


-73.7
-73.7
-73.7
-73.9
-73.9
-73.9

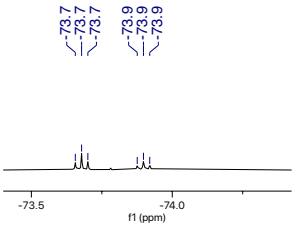
-73.7
-73.7
-73.7
-73.9
-73.9
-73.9
-73.5
-74.0
f1 (ppm)

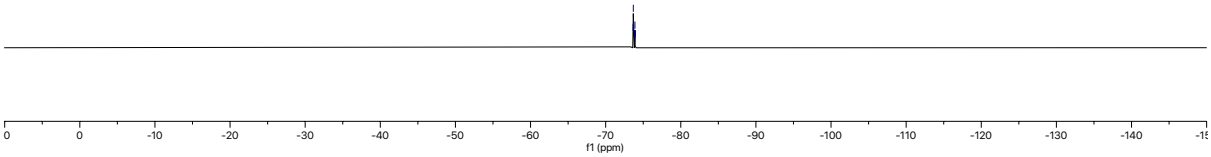
0
-10
-20
-30
-40
-50
-60
-70
-80
-90
-100
-110
-120
-130
-140
f1 (ppm)

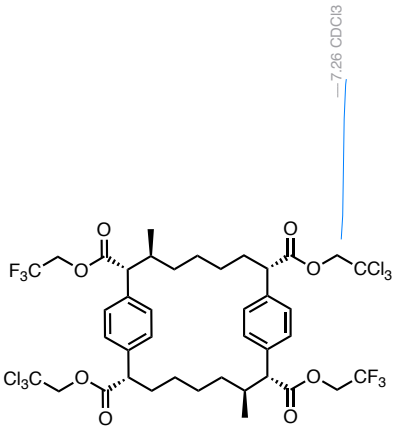
F3C
O
O
O
CCl3
Cl3C
O
O
O
CF3

7.26 CDCl3
8.12
1.99
2.06
2.30
2.25
2.14
2.00
2.05
4.32
2.20
6.24
4.09
2.25
4.00
f1 (ppm)

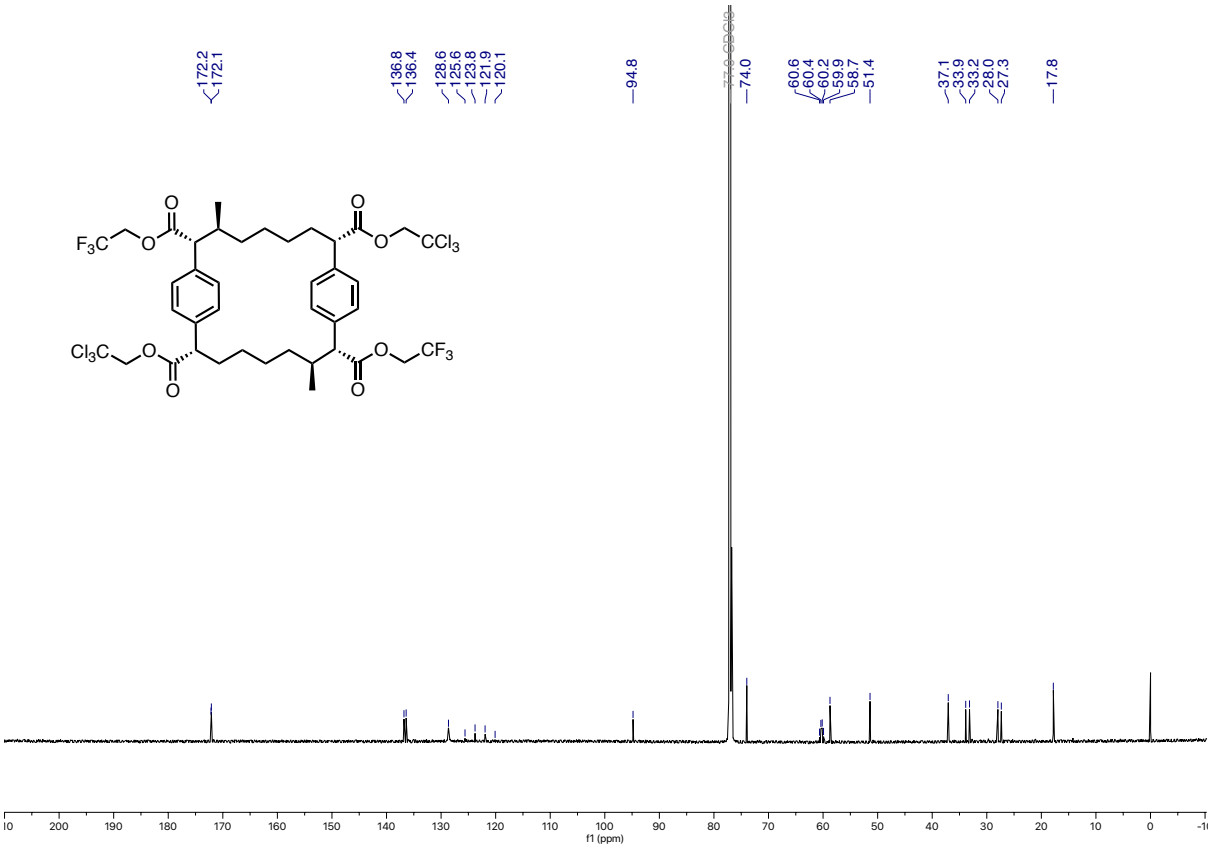
172.2
172.1
136.8
136.4
128.6
125.6
123.8
121.9
120.1
94.8
77.0 CDCl3
74.0
60.6
60.4
60.2
59.9
58.7
51.4
37.1
33.9
33.2
28.0
27.3
17.8
f1 (ppm)

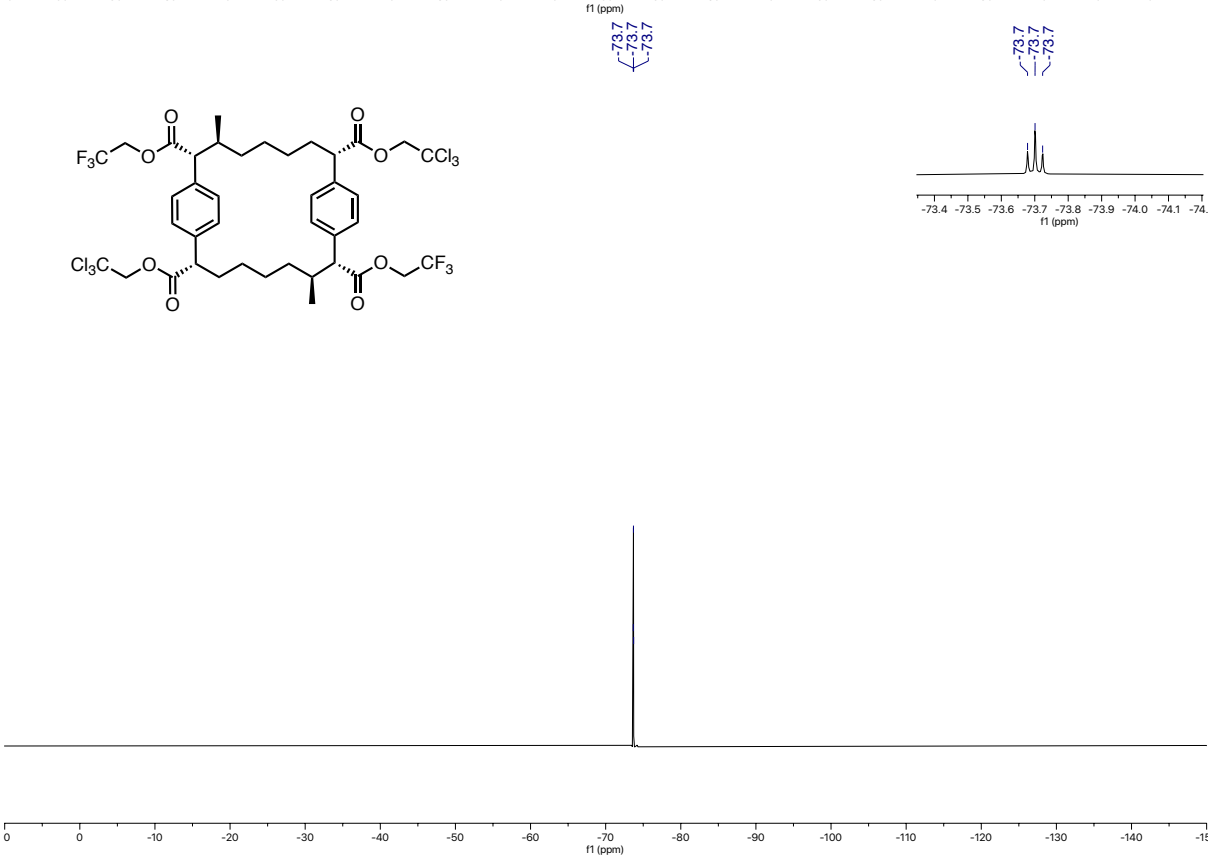
-73.7
-73.7
-73.7
-73.7
-73.7
-73.7
f1 (ppm)

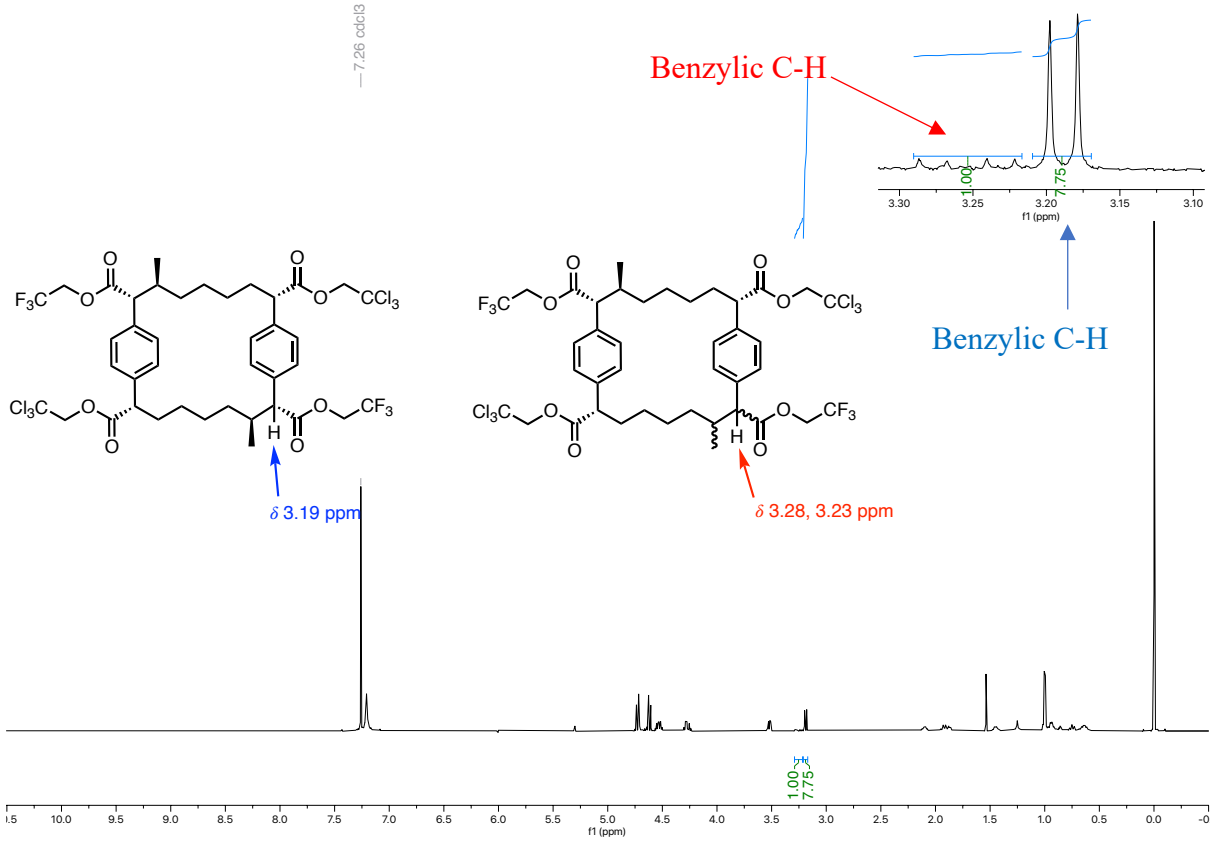
Benzylic C-H
Benzylic C-H
δ 3.19 ppm
δ 3.28, 3.23 ppm
f1 (ppm)

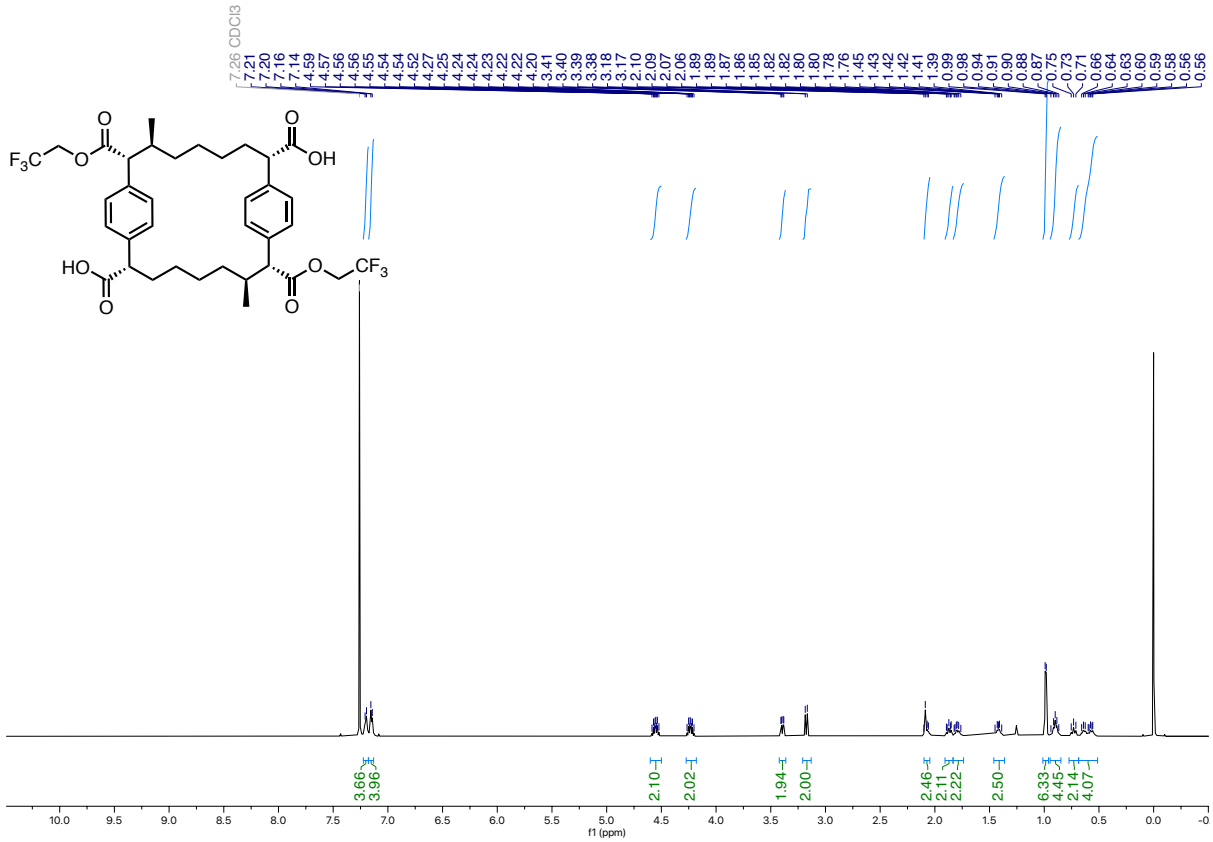
f1 (ppm)

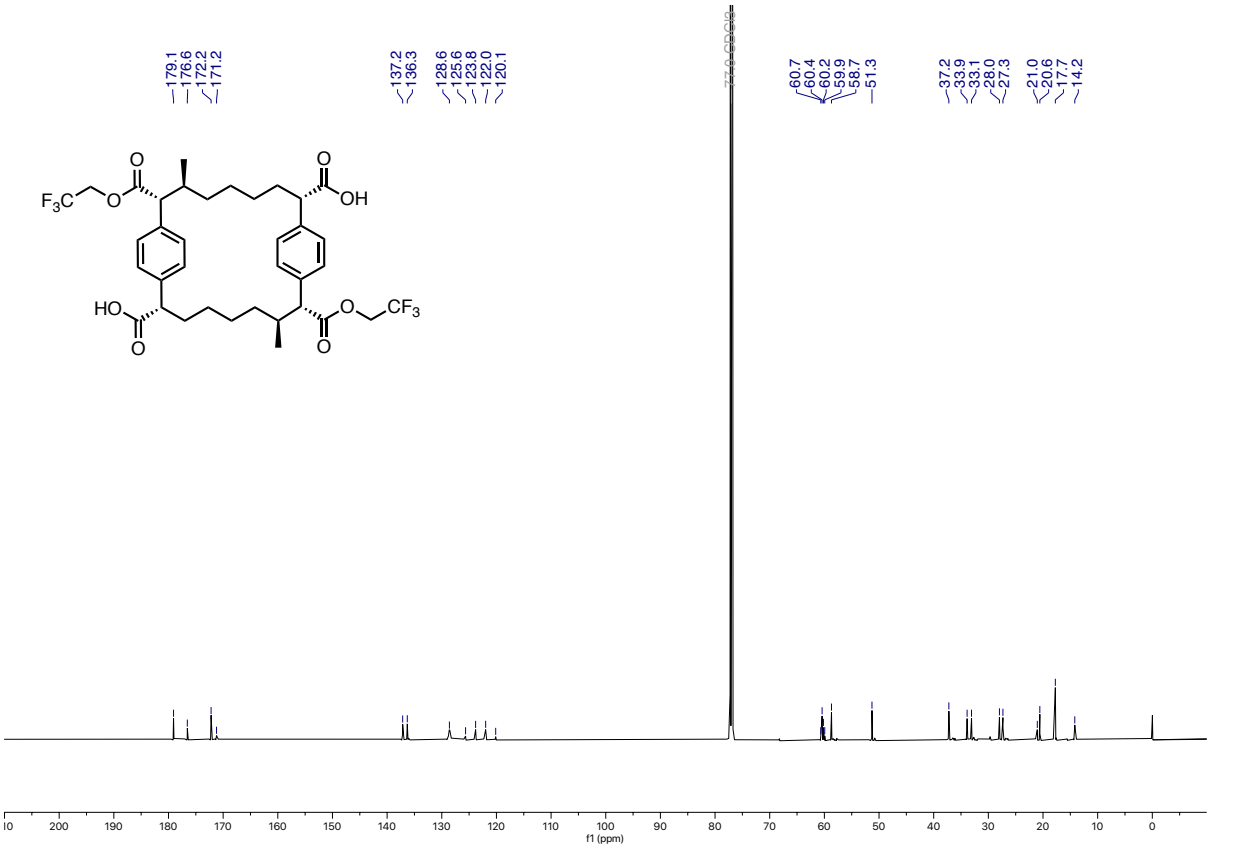
179.1
176.6
172.2
171.2
137.2
136.3
128.6
125.6
123.8
122.0
120.1
77.0
60.7
60.4
60.2
59.9
58.7
51.3
37.2
33.9
33.1
28.0
27.3
21.0
20.6
17.7
14.2
F3C
O
OH
HO
CF3
f1 (ppm)

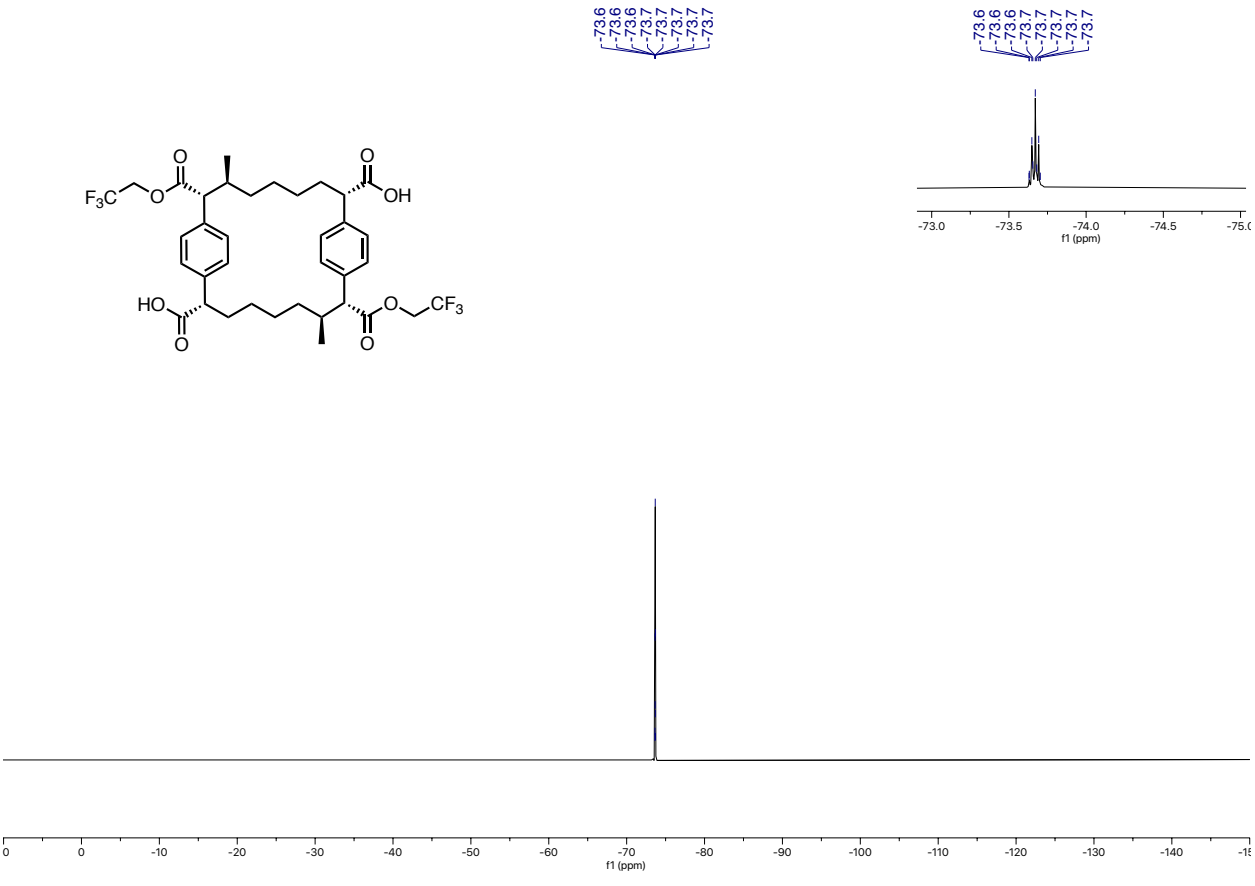
-73.6
-73.6
-73.6
-73.7
-73.7
-73.7
-73.7
-73.7
F3C
O
OH
HO
CF3
f1 (ppm)

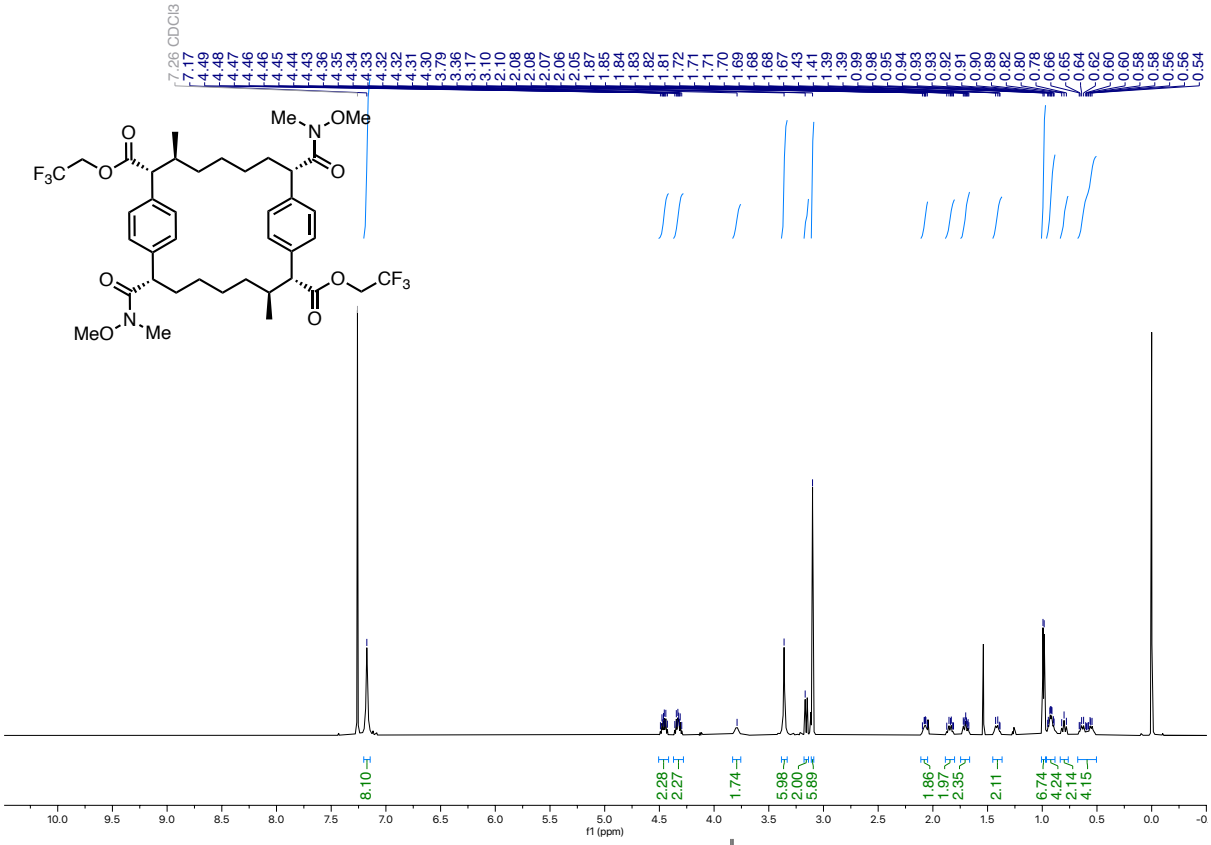
7.26 CDCl3
Me
N
OMe
F3C
O
CF3
MeO
N
Me
8.10
2.28
2.27
1.74
5.98
2.00
5.89
1.86
1.97
2.35
2.11
6.74
4.24
2.14
4.15
f1 (ppm)

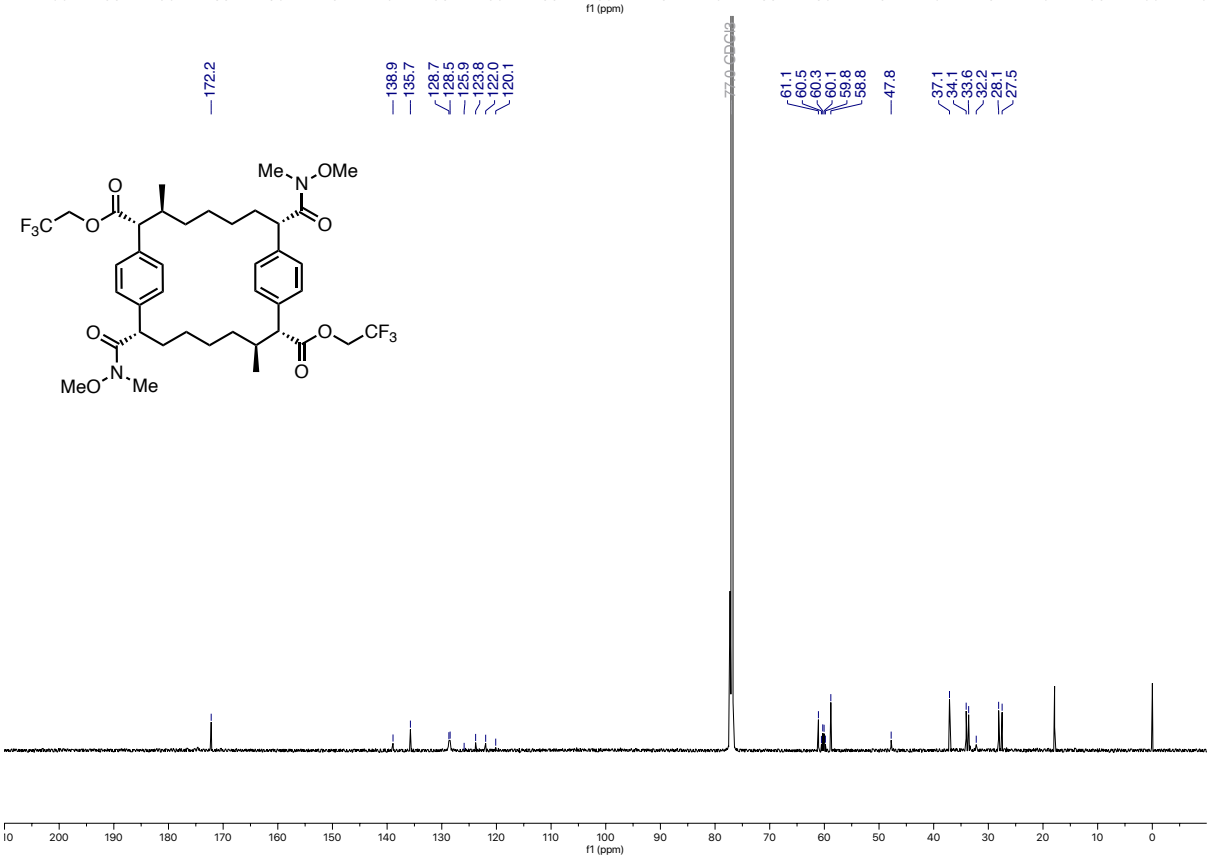
172.2
138.9
135.7
128.7
128.5
125.9
123.8
122.0
120.1
77.0 CDCl3
61.1
60.5
60.3
60.1
59.8
58.8
47.8
37.1
34.1
33.6
32.2
28.1
27.5
Me
N
OMe
F3C
O
CF3
MeO
N
Me
f1 (ppm)

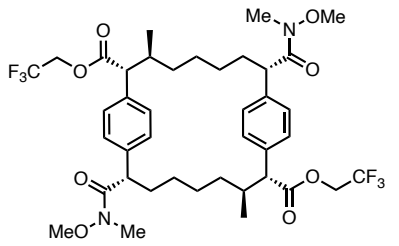
Me
N
OMe
O
F3C
O
O
O
O
O
CF3
MeO
N
Me

-73.7
-73.8
-73.8
-73.5 -73.6 -73.7 -73.8 -73.9 -74.0 -74.1 -74.2
f1 (ppm)
0 -10 -20 -30 -40 -50 -60 -70 -80 -90 -100 -110 -120 -130 -140
f1 (ppm)

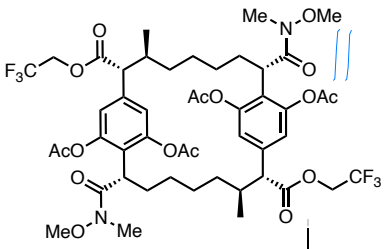
Me
N
OMe
O
F3C
O
O
AcO
OAc
AcO
OAc
O
O
CF3
MeO
N
Me

7.26 CDCl3
7.00 7.00 6.89 6.89 4.47 4.45 4.44 4.42 4.42 4.40 4.40 4.00 3.99 3.97 3.96 3.17 3.14 3.00 2.91 2.32 2.21 1.99 1.99 1.98 1.96 1.95 1.93 1.92 1.90 1.89 1.82 1.81 1.80 1.79 1.78 1.77 1.76 1.49 1.46 1.44 1.43 1.42 1.41 1.40 0.99 0.98 0.92 0.89 0.88 0.88 0.86 0.83 0.80 0.71 0.69 0.66 0.65 0.63 0.57 0.54 0.51 0.48
1.99 1.96 4.19 2.00 2.07 6.20 5.53 6.11 6.24 3.95 2.20 2.58 6.15 4.94 2.14 1.91
f1 (ppm)

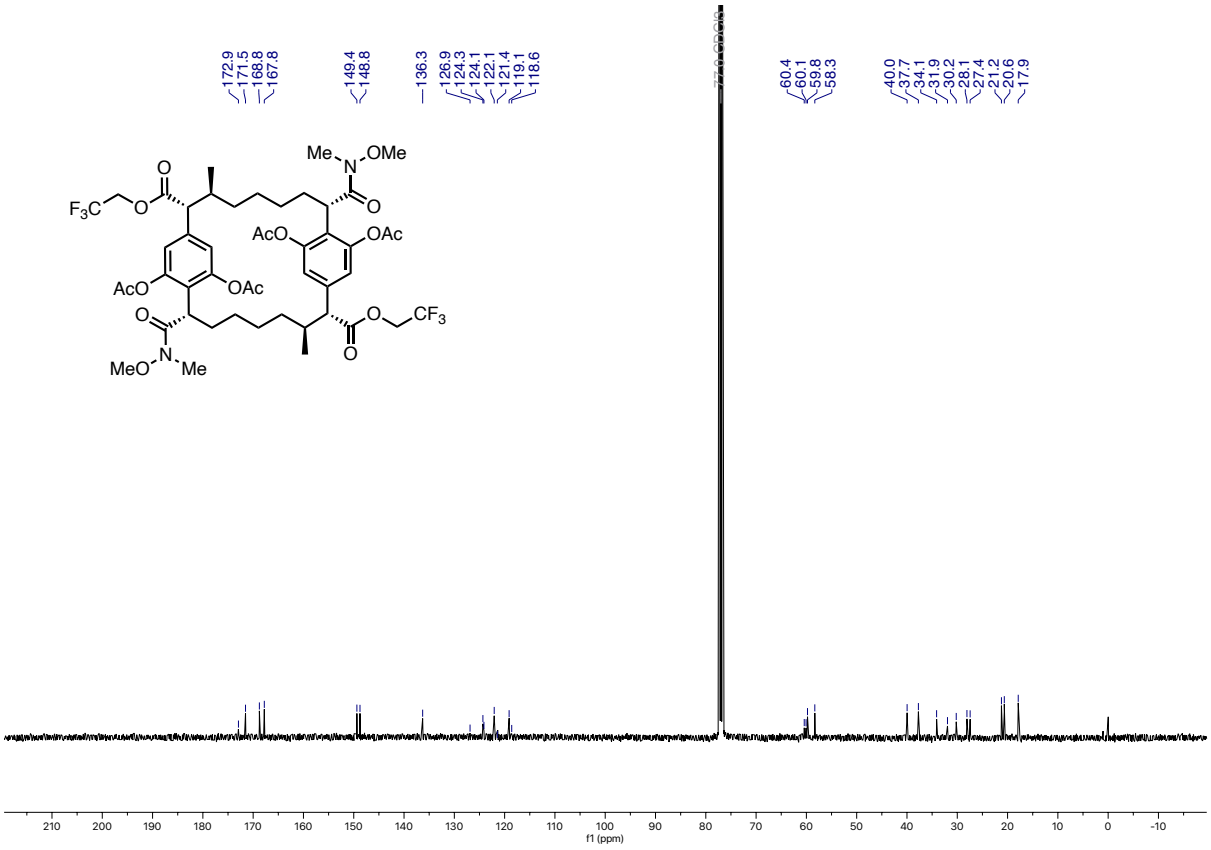
172.9
171.5
168.8
167.8
149.4
148.8
136.3
126.9
124.3
124.1
122.1
121.4
119.1
118.6
77.0
60.4
60.1
59.8
58.3
40.0
37.7
34.1
31.9
30.2
28.1
27.4
21.2
20.6
17.9
Me
N
OMe
O
F3C
AcO
OAc
CF3
MeO
Me
f1 (ppm)

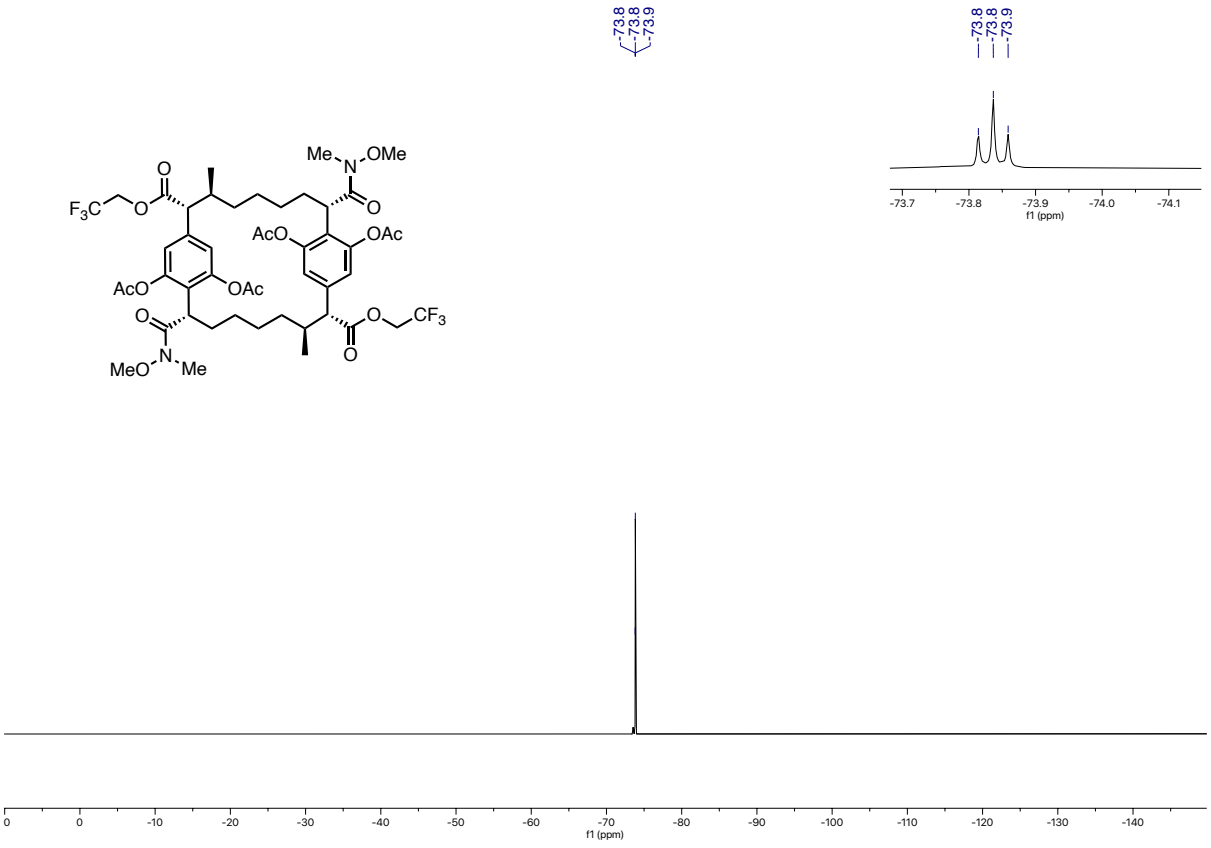
-73.8
-73.8
-73.9
-73.7
-73.8
-73.9
-74.0
-74.1
f1 (ppm)
Me
N
OMe
O
F3C
AcO
OAc
CF3
MeO
Me
f1 (ppm)

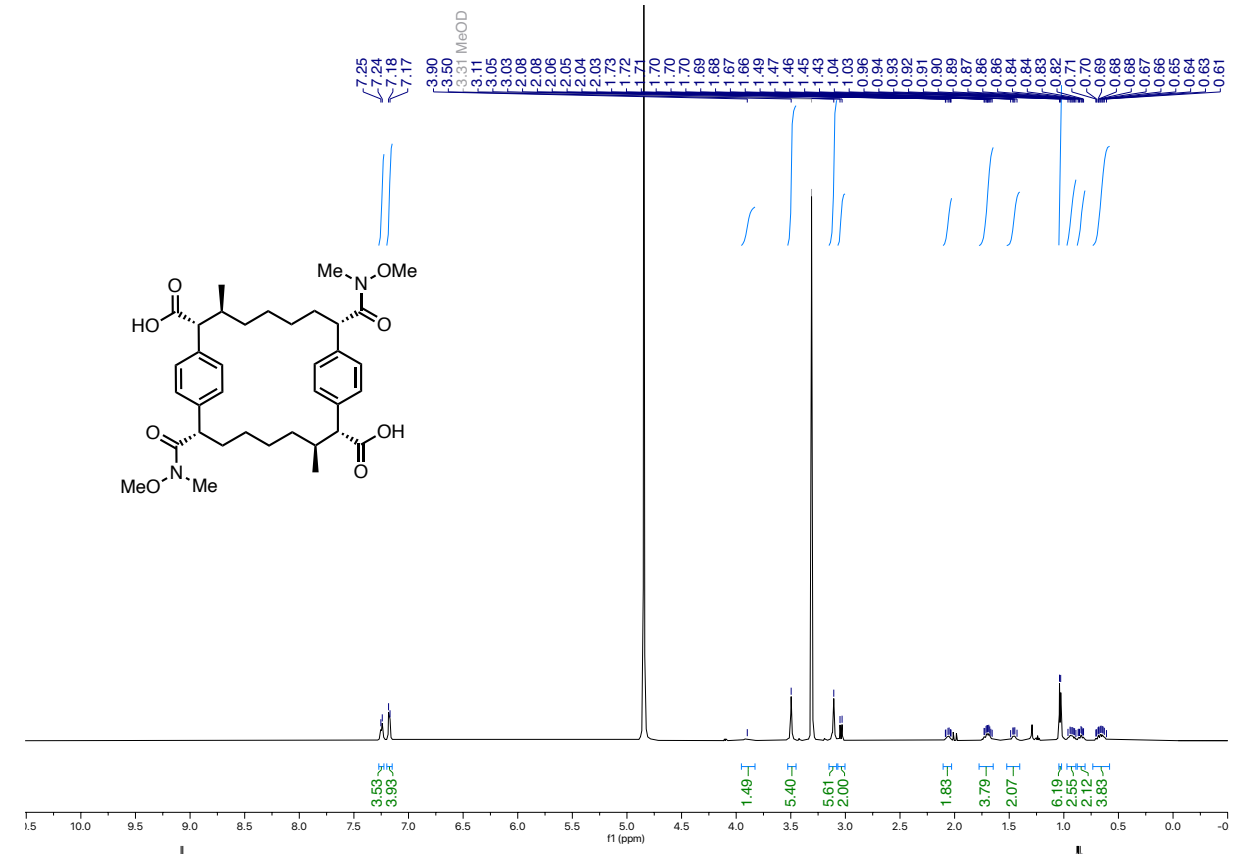
7.25
7.24
7.18
7.17
3.90
3.50
3.31 MeOD
3.11
3.05
3.03
2.08
2.08
2.06
2.05
2.04
2.03
1.73
1.72
1.71
1.70
1.70
1.70
1.69
1.68
1.67
1.66
1.49
1.47
1.46
1.45
1.43
1.04
1.03
0.96
0.94
0.93
0.92
0.91
0.90
0.90
0.89
0.87
0.86
0.86
0.84
0.84
0.83
0.82
0.71
0.70
0.69
0.68
0.68
0.67
0.66
0.65
0.64
0.63
0.61
Me
N
OMe
O
HO
O
O
OH
O
MeO
N
Me
3.53
3.93
1.49
5.40
5.61
2.00
1.83
3.79
2.07
6.19
2.55
2.12
3.83
f1 (ppm)

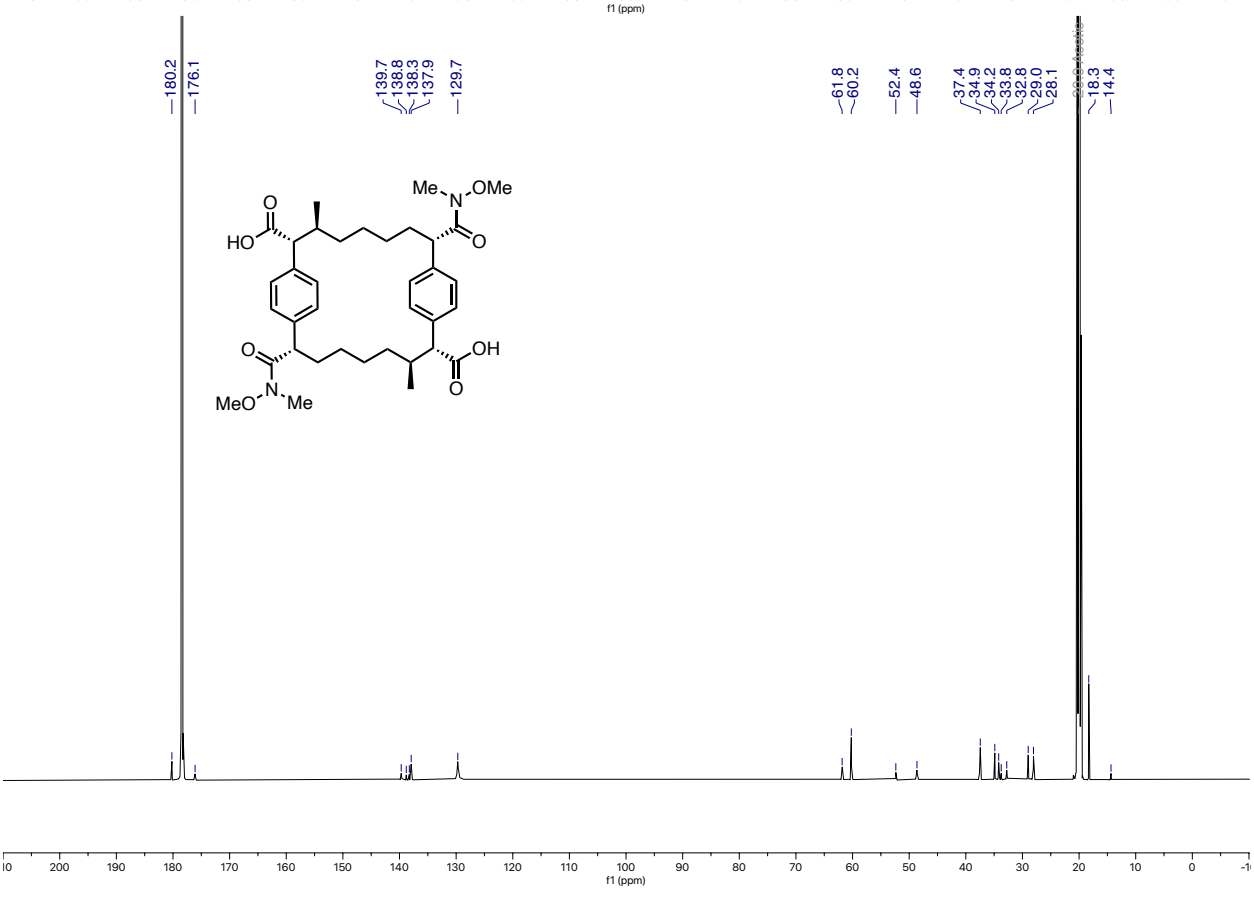
180.2
176.1
139.7
138.8
138.3
137.9
129.7
61.8
60.2
52.4
48.6
37.4
34.9
34.2
33.8
32.8
29.0
28.1
18.3
14.4
Me
N
OMe
O
HO
O
O
OH
O
MeO
N
Me
f1 (ppm)

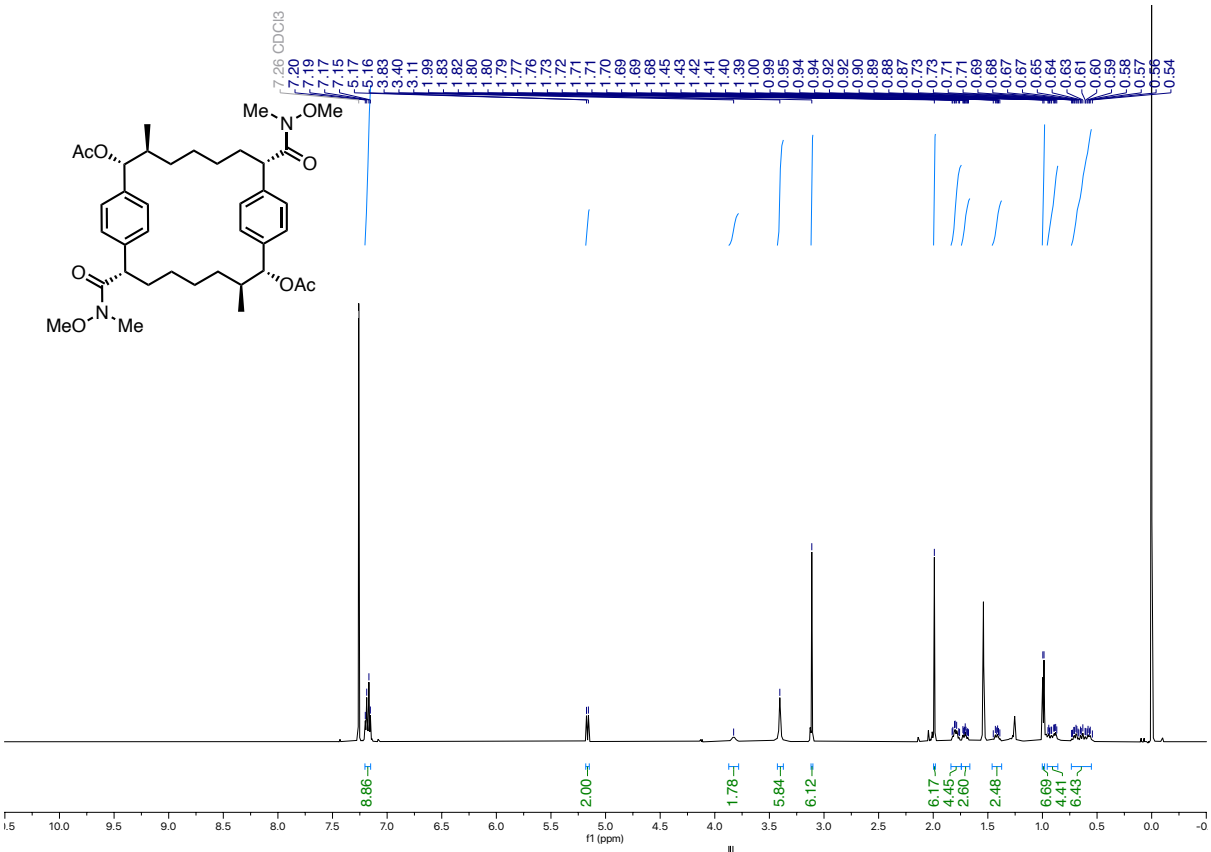
7.26 CDCl3
7.20
7.19
7.17
7.15
5.17
5.16
3.83
3.40
3.11
1.99
1.83
1.82
1.80
1.80
1.79
1.77
1.76
1.73
1.72
1.71
1.71
1.70
1.69
1.69
1.68
1.45
1.43
1.42
1.41
1.40
1.39
1.00
0.99
0.95
0.94
0.94
0.92
0.90
0.89
0.88
0.87
0.73
0.73
0.71
0.71
0.69
0.68
0.67
0.67
0.65
0.64
0.63
0.61
0.60
0.59
0.58
0.57
0.56
0.54
Me
N
OMe
O
AcO
O
OAc
MeO
N
Me
8.86
2.00
1.78
5.84
6.12
6.17
4.45
2.60
2.48
6.69
4.41
6.43
f1 (ppm)

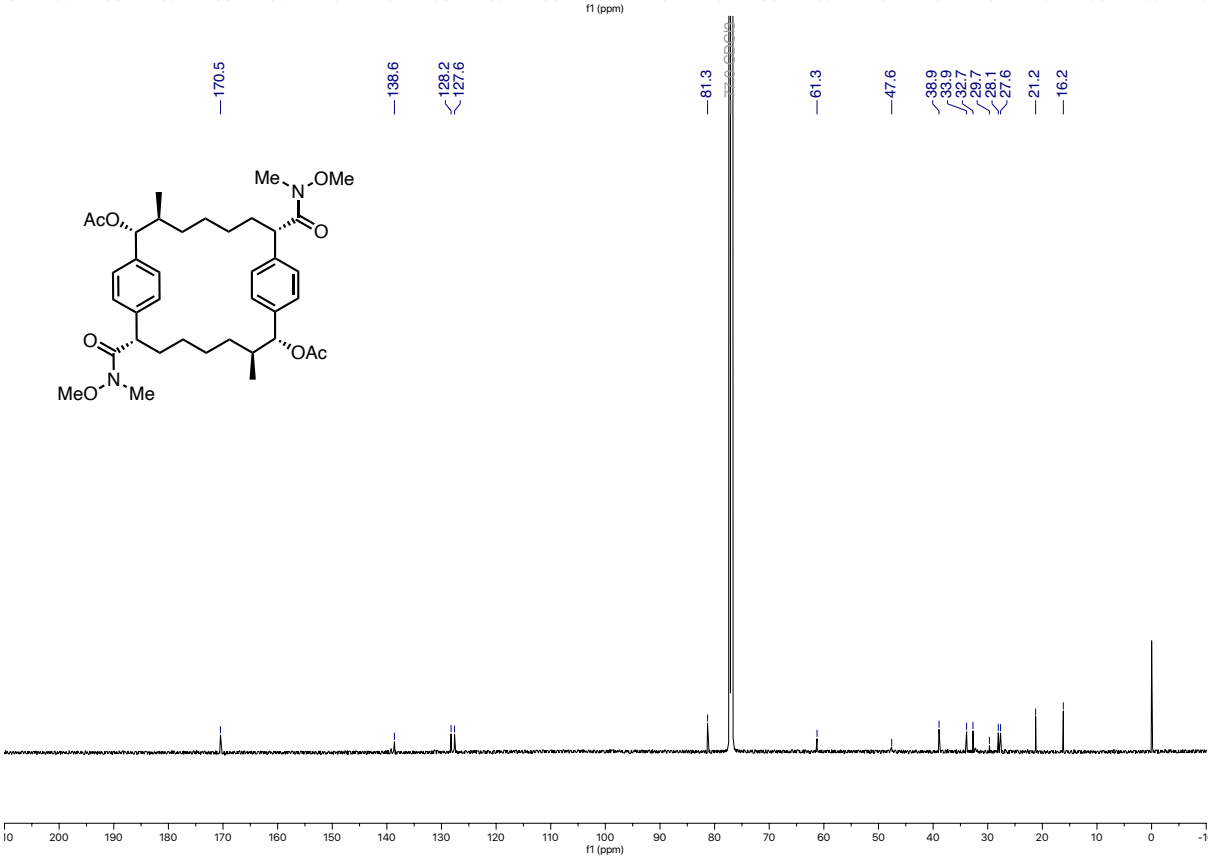
170.5
138.6
128.2
127.6
81.3
77.0 CDCl3
61.3
47.6
38.9
33.9
32.7
29.7
28.1
27.6
21.2
16.2
Me
N
OMe
O
AcO
O
OAc
MeO
N
Me
f1 (ppm)

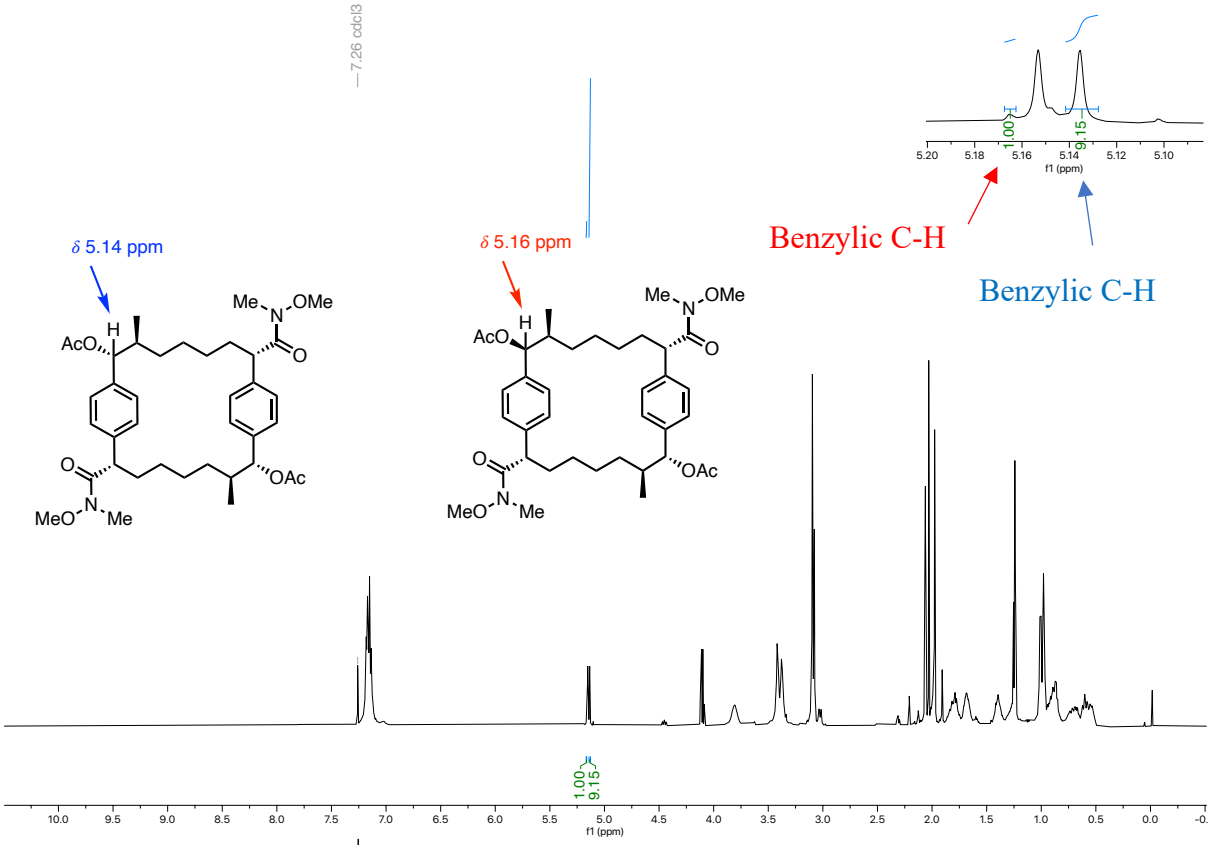
δ 5.14 ppm
δ 5.16 ppm
Benzylic C-H
Benzylic C-H
f1 (ppm)

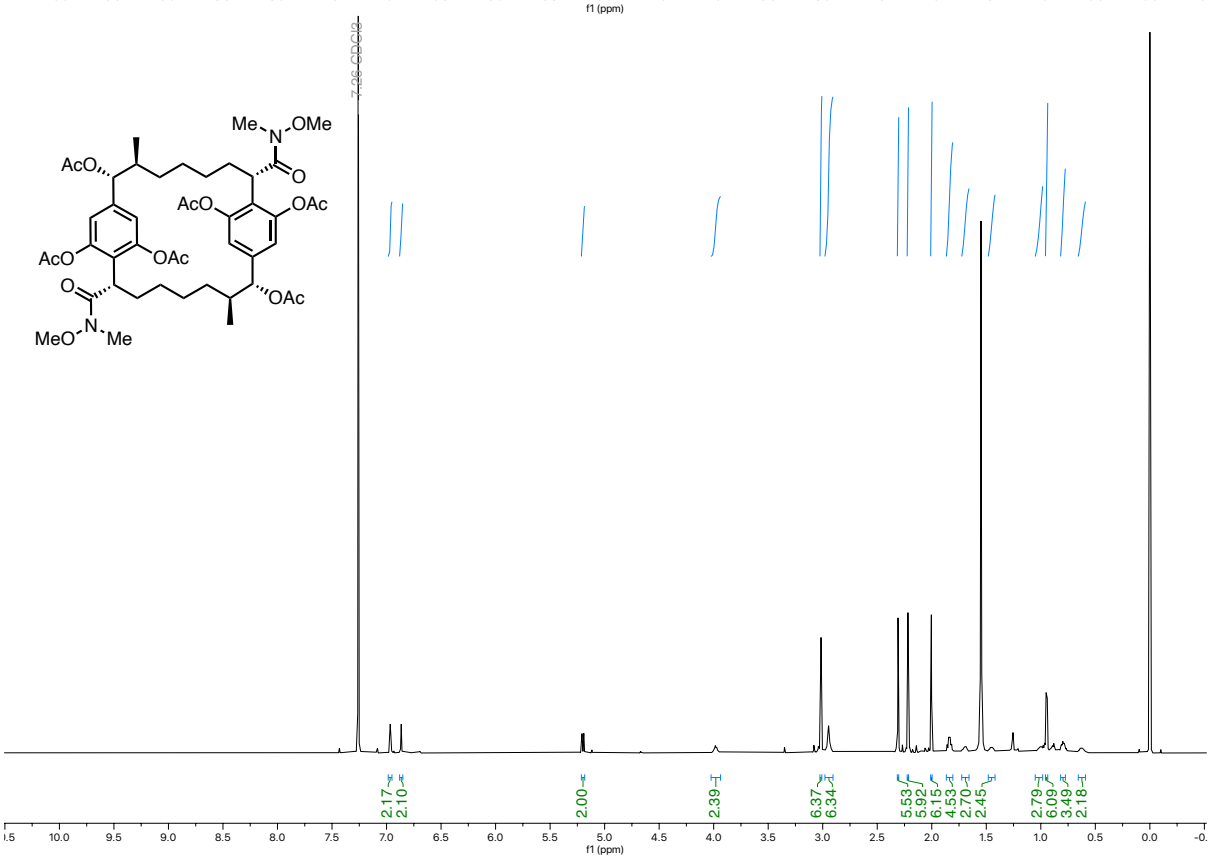
f1 (ppm)

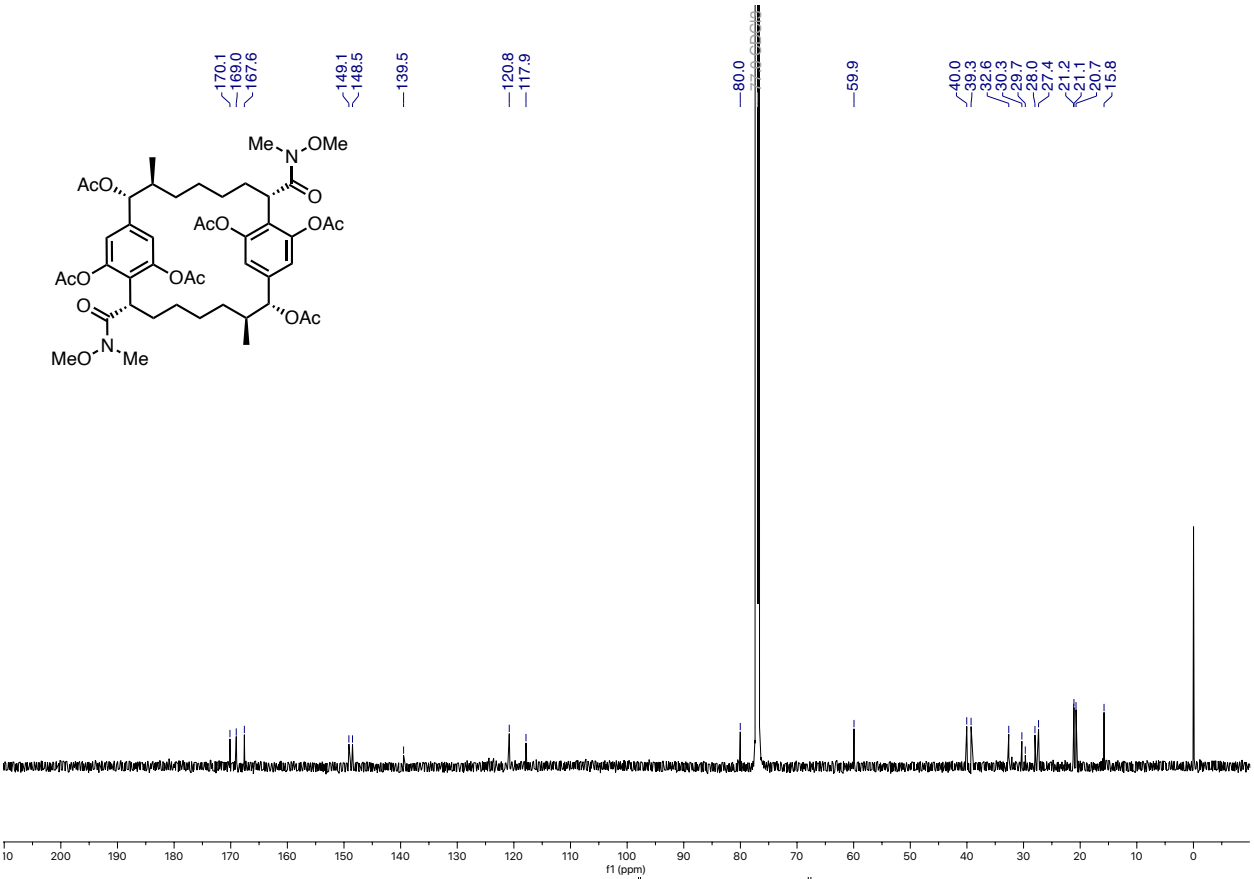
170.1
169.0
167.6
149.1
148.5
139.5
120.8
117.9
80.0
59.9
40.0
39.3
32.6
30.3
29.7
28.0
27.4
21.2
21.1
20.7
15.8
Me
N
OMe
O
AcO
AcO
OAc
AcO
OAc
O
OAc
N
MeO
Me
f1 (ppm)

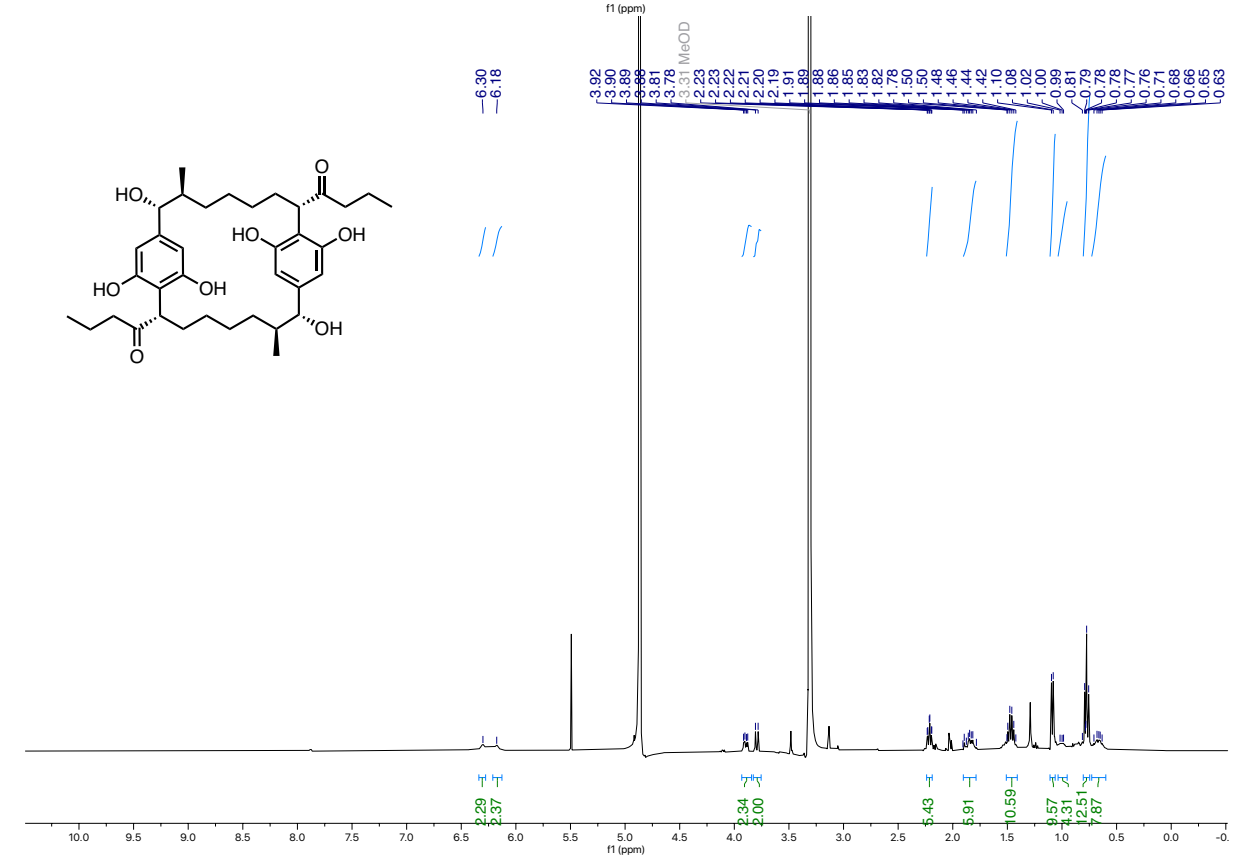
6.30
6.18
3.92
3.90
3.89
3.88
3.81
3.78
3.31 MeOD
2.23
2.22
2.21
2.20
2.19
1.91
1.89
1.88
1.86
1.85
1.83
1.82
1.78
1.50
1.50
1.48
1.46
1.44
1.42
1.10
1.08
1.02
1.00
0.99
0.81
0.79
0.78
0.78
0.77
0.76
0.71
0.68
0.66
0.65
0.63
HO
O
HO
OH
HO
OH
OH
O
2.29
2.37
2.34
2.00
5.43
5.91
10.59
9.57
4.31
12.51
7.87
f1 (ppm)

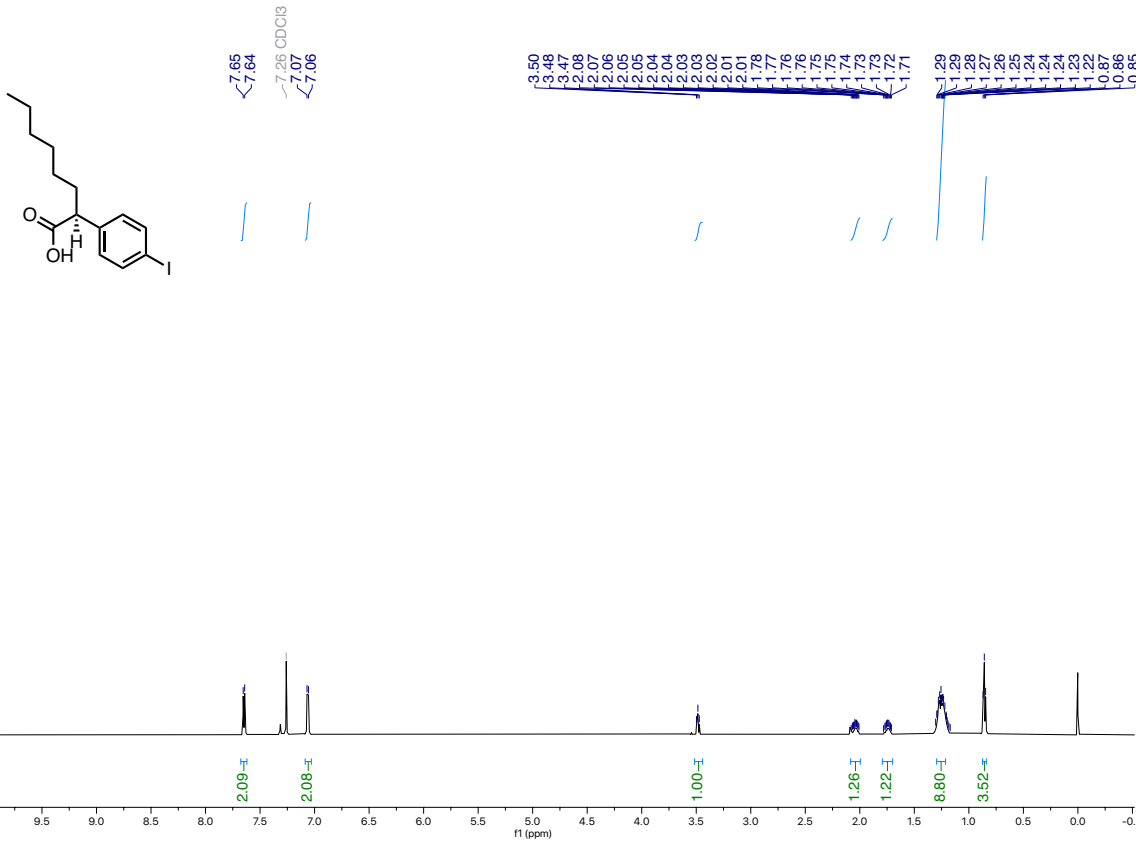
7.65
7.64
7.26 CDCl3
7.07
7.06
3.50
3.48
3.47
2.08
2.07
2.06
2.05
2.05
2.04
2.04
2.03
2.02
2.01
1.78
1.77
1.76
1.76
1.75
1.75
1.74
1.73
1.73
1.72
1.71
1.29
1.29
1.28
1.27
1.26
1.25
1.24
1.24
1.24
1.23
1.22
0.87
0.86
O
OH
H
I
2.09
2.08
1.00
1.26
1.22
8.80
3.52
f1 (ppm)

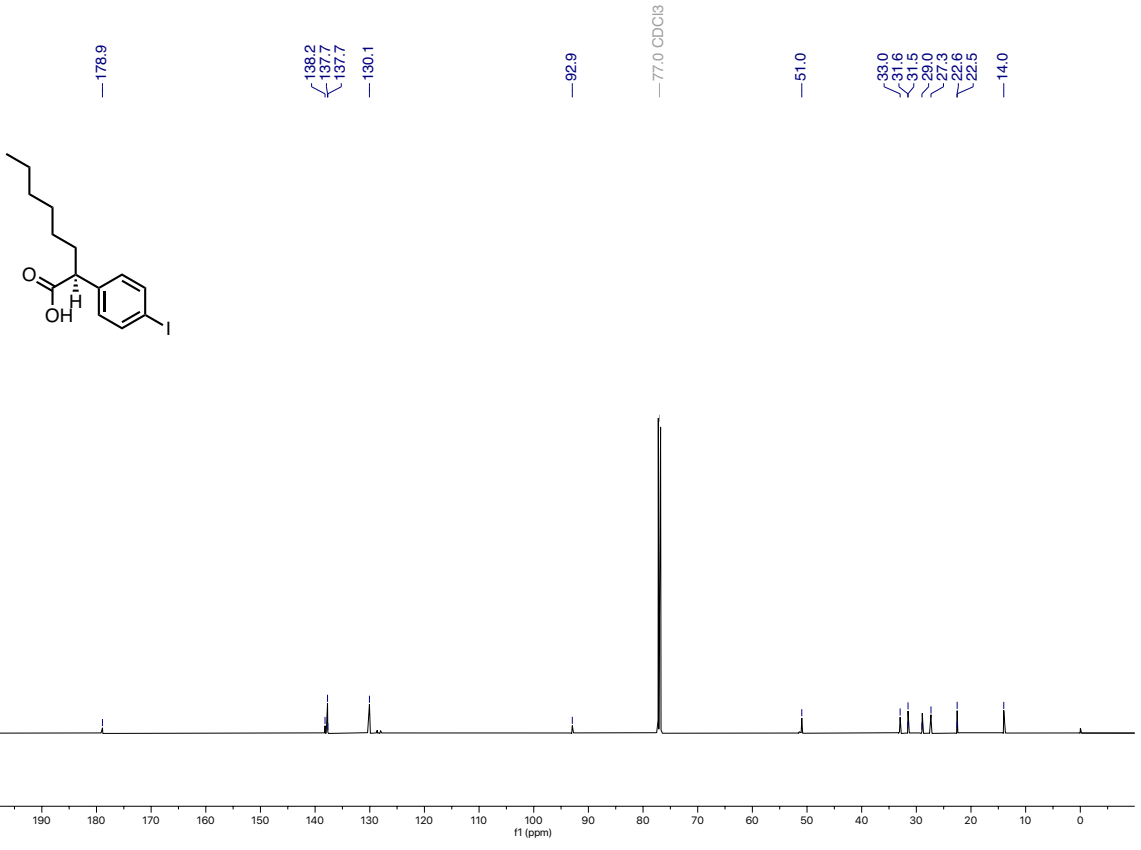
178.9
138.2
137.7
137.7
130.1
92.9
77.0 CDCl3
51.0
33.0
31.6
31.5
29.0
27.3
22.6
22.5
14.0
O
OH
H
I
f1 (ppm)

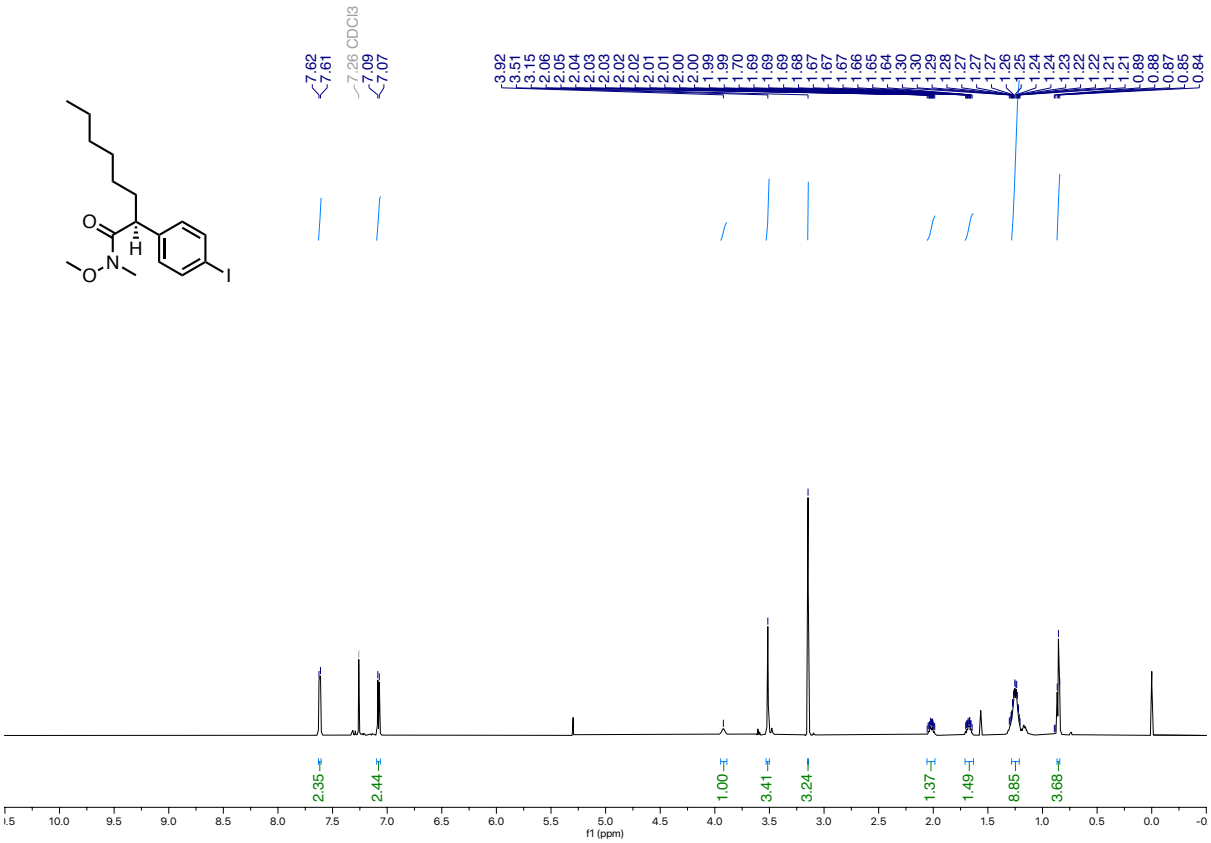
7.62
7.61
7.26 CDCl3
7.09
7.07
3.92
3.51
3.15
2.06
2.05
2.04
2.03
2.02
2.02
2.01
2.01
2.00
2.00
1.99
1.99
1.70
1.69
1.69
1.68
1.68
1.67
1.67
1.66
1.65
1.64
1.30
1.30
1.29
1.28
1.27
1.27
1.27
1.26
1.25
1.24
1.24
1.23
1.22
1.22
1.21
1.21
0.89
0.88
0.87
0.85
0.84
O
H
N
O
I
2.35
2.44
1.00
3.41
3.24
1.37
1.49
8.85
3.68
f1 (ppm)

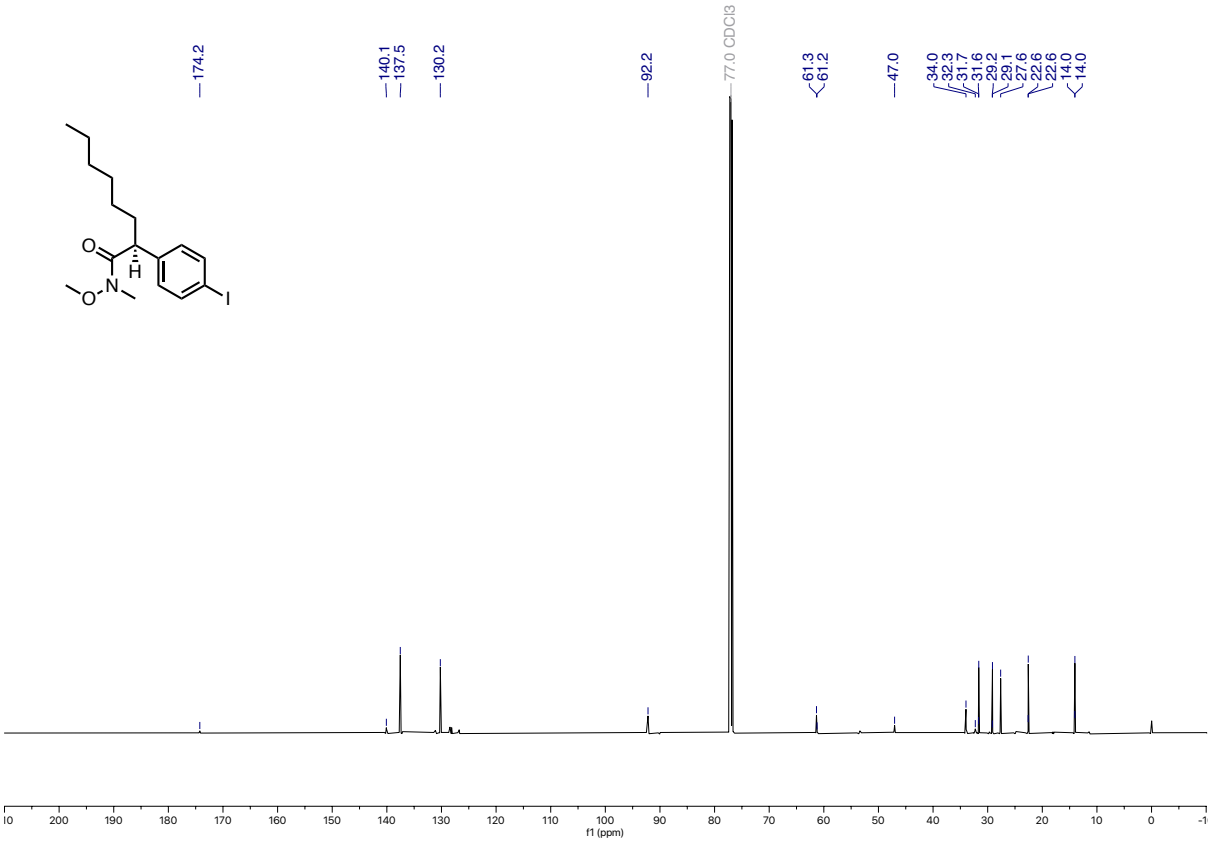
174.2
140.1
137.5
130.2
92.2
77.0 CDCl3
61.3
61.2
47.0
34.0
32.3
31.7
31.6
29.2
29.1
27.6
22.6
14.0
14.0
O
H
N
O
I
f1 (ppm)

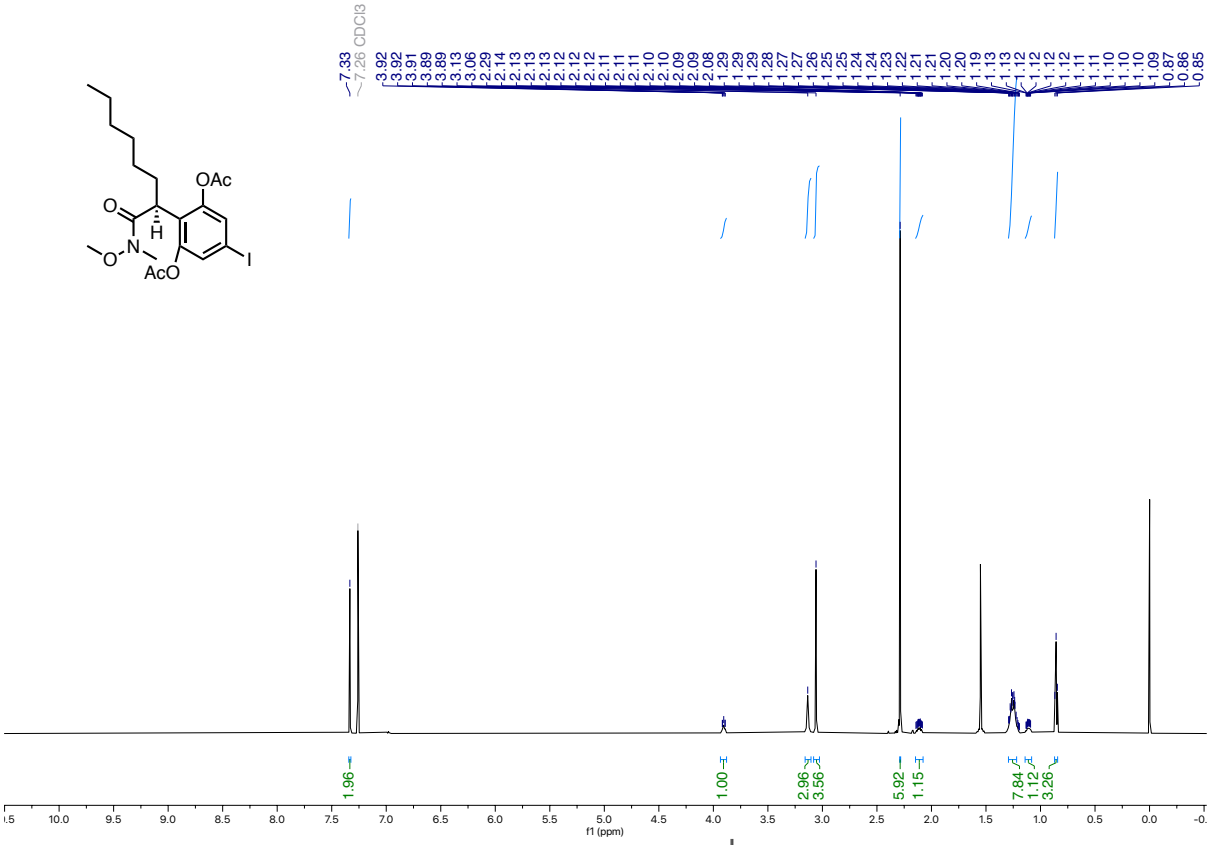
7.33
7.26 CDCl3
3.92
3.91
3.89
3.13
3.06
2.29
2.14
2.13
2.12
2.11
2.10
2.09
2.08
1.29
1.28
1.27
1.26
1.25
1.24
1.23
1.22
1.21
1.20
1.19
1.13
1.12
1.11
1.10
1.09
0.87
0.86
0.85
OAc
O
H
N
O
AcO
I
1.96
1.00
2.96
3.56
5.92
1.15
7.84
1.12
3.26
f1 (ppm)

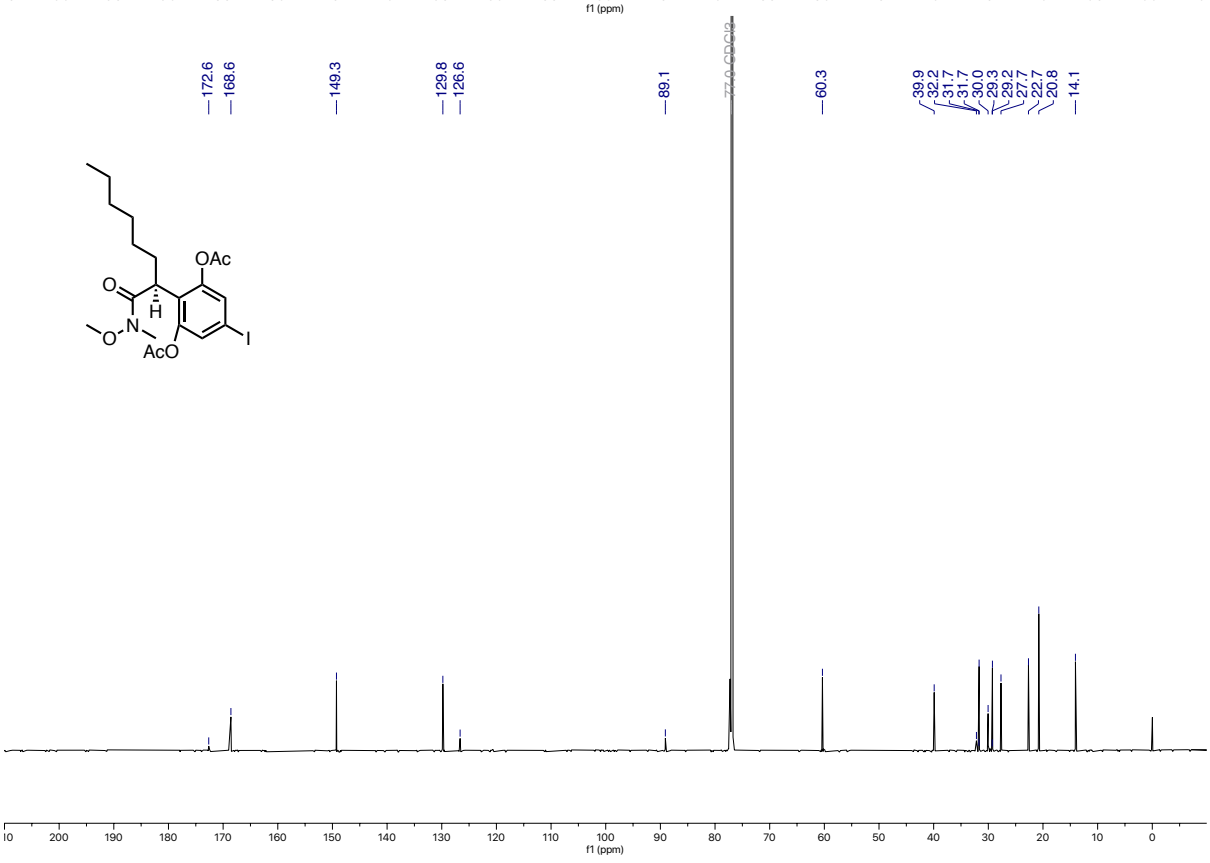
172.6
168.6
149.3
129.8
126.6
89.1
77.0 CDCl3
60.3
39.9
32.2
31.7
31.7
30.0
29.3
29.2
27.7
22.7
20.8
14.1
OAc
O
H
N
O
AcO
I
f1 (ppm)

Appendix – Ch.3 NMR Spectra

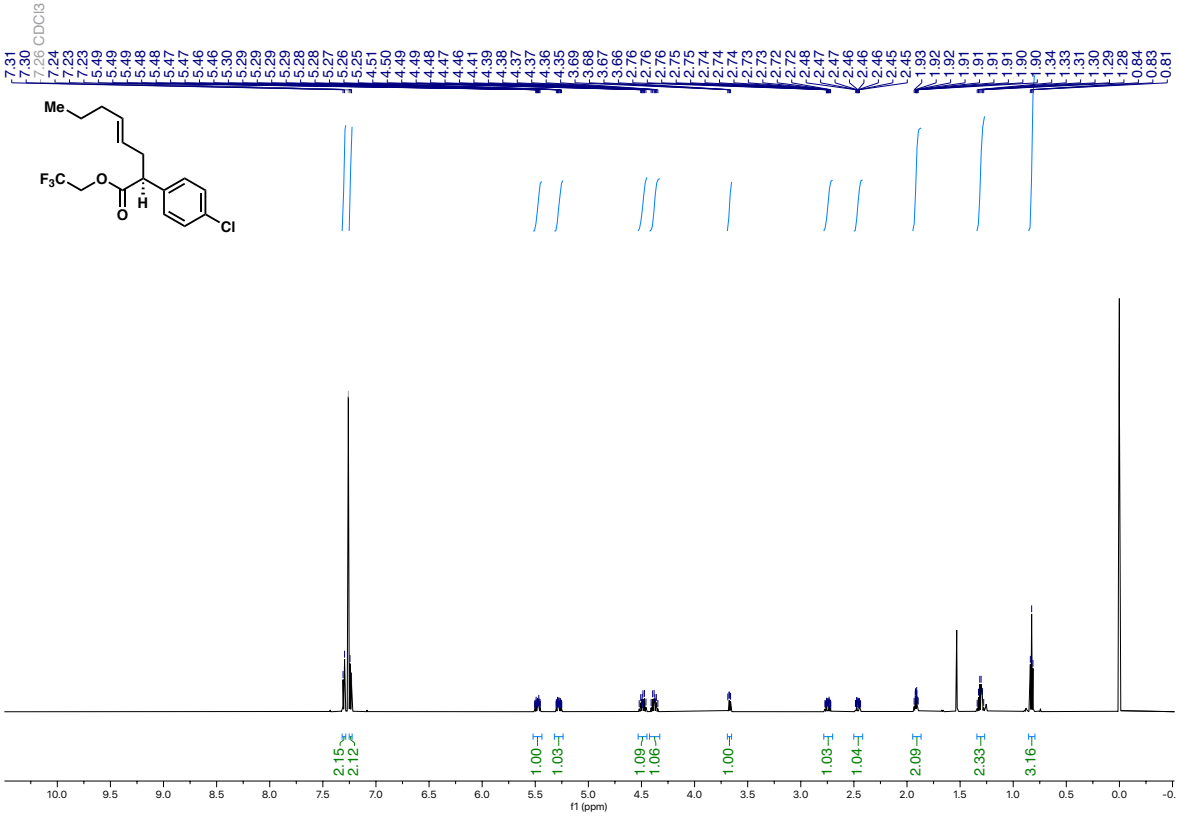

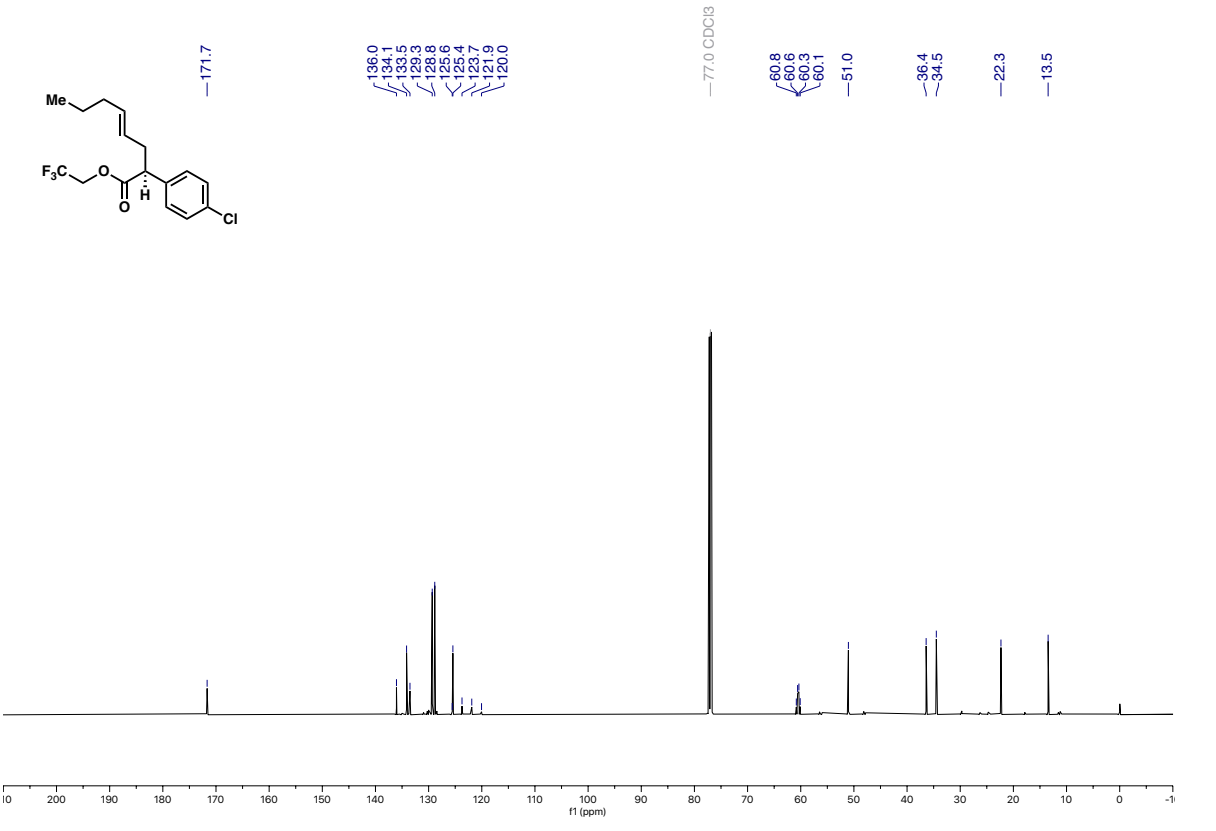

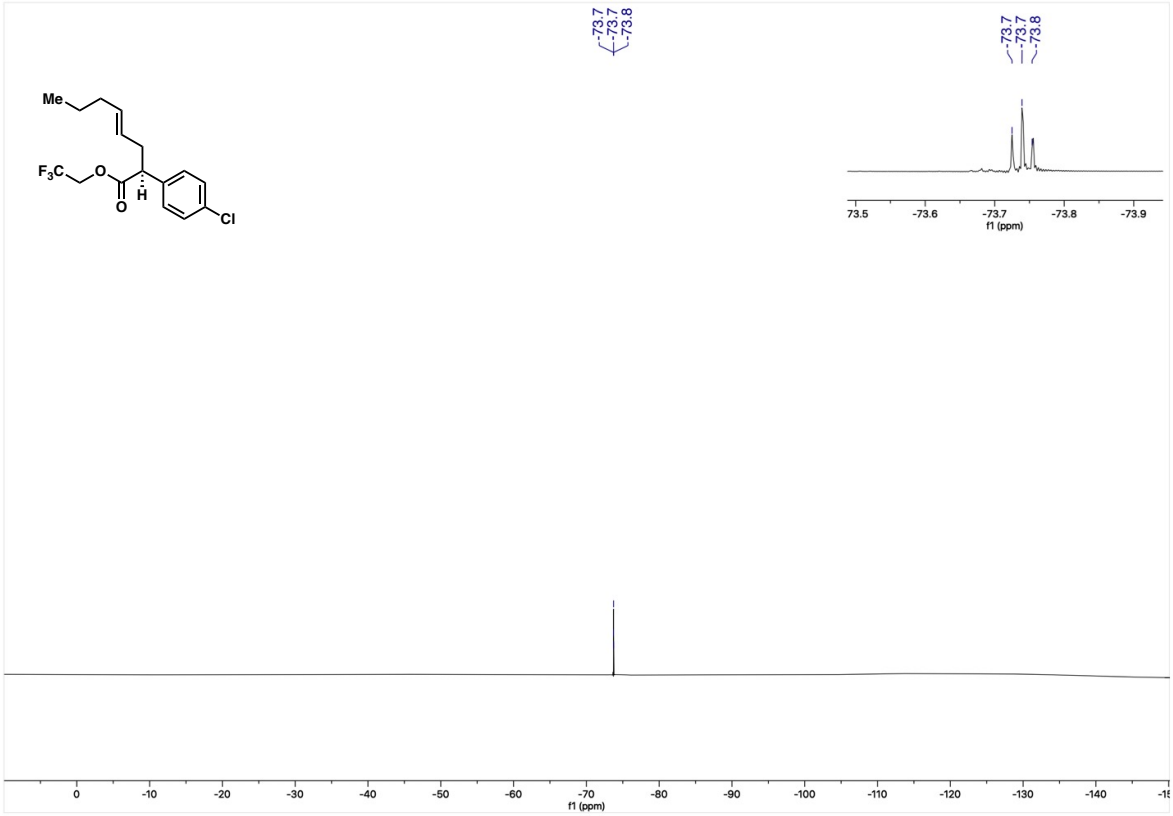
-73.7
-73.7
-73.8
Me
F3C
O
O
H
Cl
73.5
-73.6
-73.7
-73.8
-73.9
f1 (ppm)
0
-10
-20
-30
-40
-50
-60
-70
-80
-90
-100
-110
-120
-130
-140
f1 (ppm)

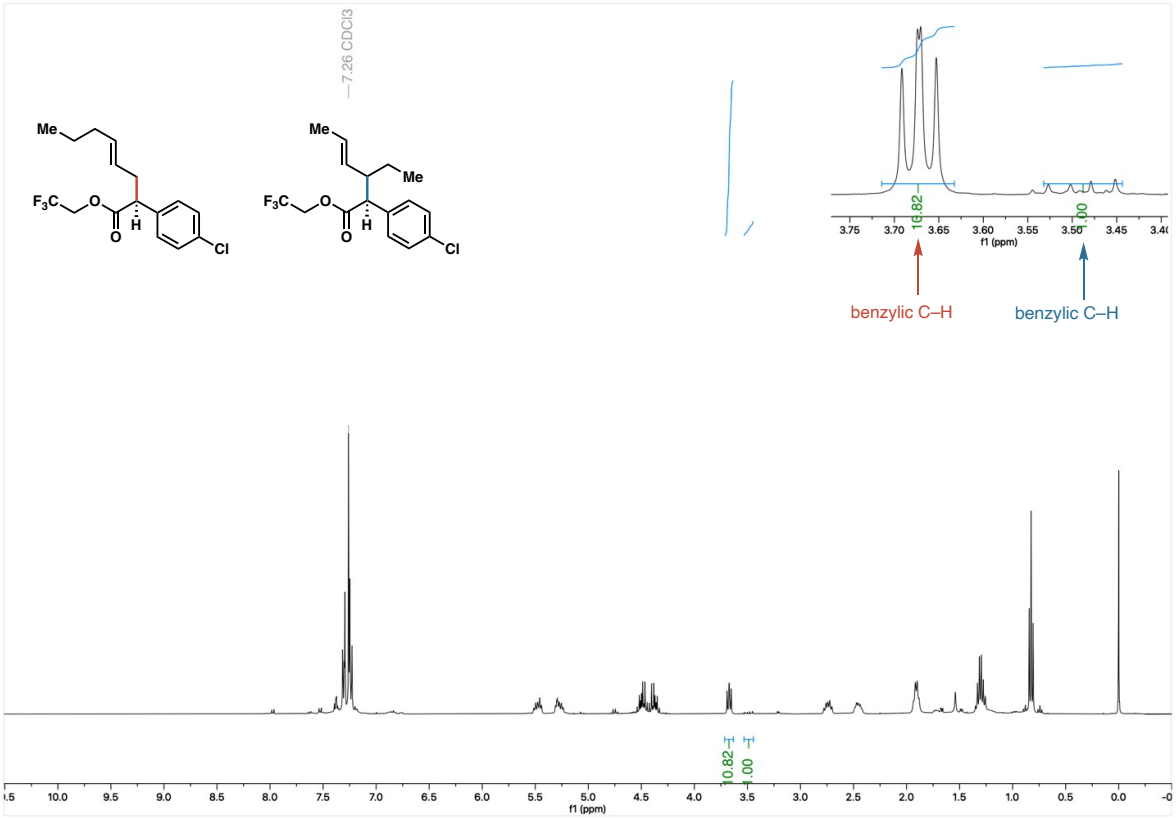
7.26 CDCl3
Me
F3C
O
O
H
Cl
Me
Me
F3C
O
O
H
Cl
1.82
1.00
3.75
3.70
3.65
3.60
3.55
3.50
3.45
f1 (ppm)
benzylic C–H
benzylic C–H
1.82
1.00
10.0
9.5
9.0
8.5
8.0
7.5
7.0
6.5
6.0
5.5
5.0
4.5
4.0
3.5
3.0
2.5
2.0
1.5
1.0
0.5
0.0
f1 (ppm)

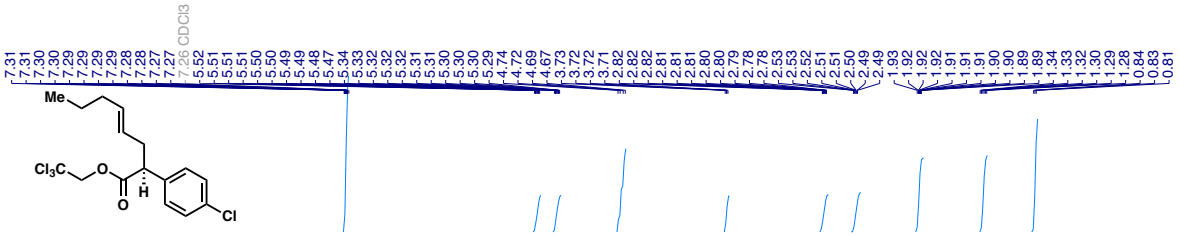
7.26 CDCl3
Me
Cl3C
O
H
Cl

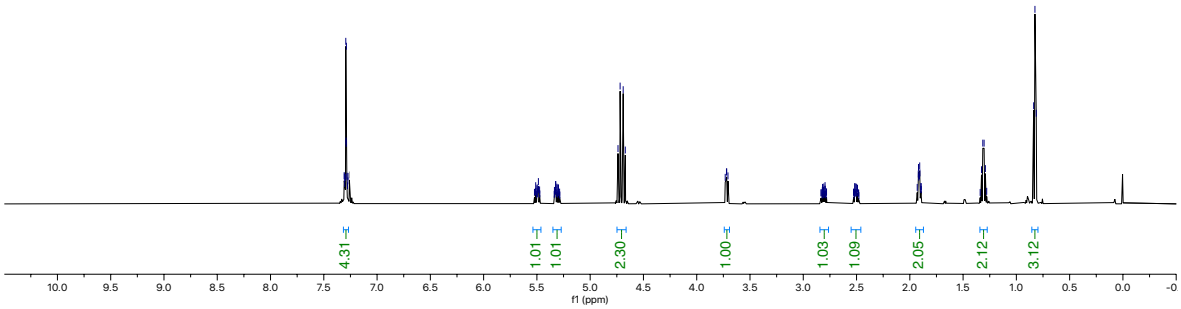
4.31
1.01
1.01
2.30
1.00
1.03
1.09
2.05
2.12
3.12
f1 (ppm)

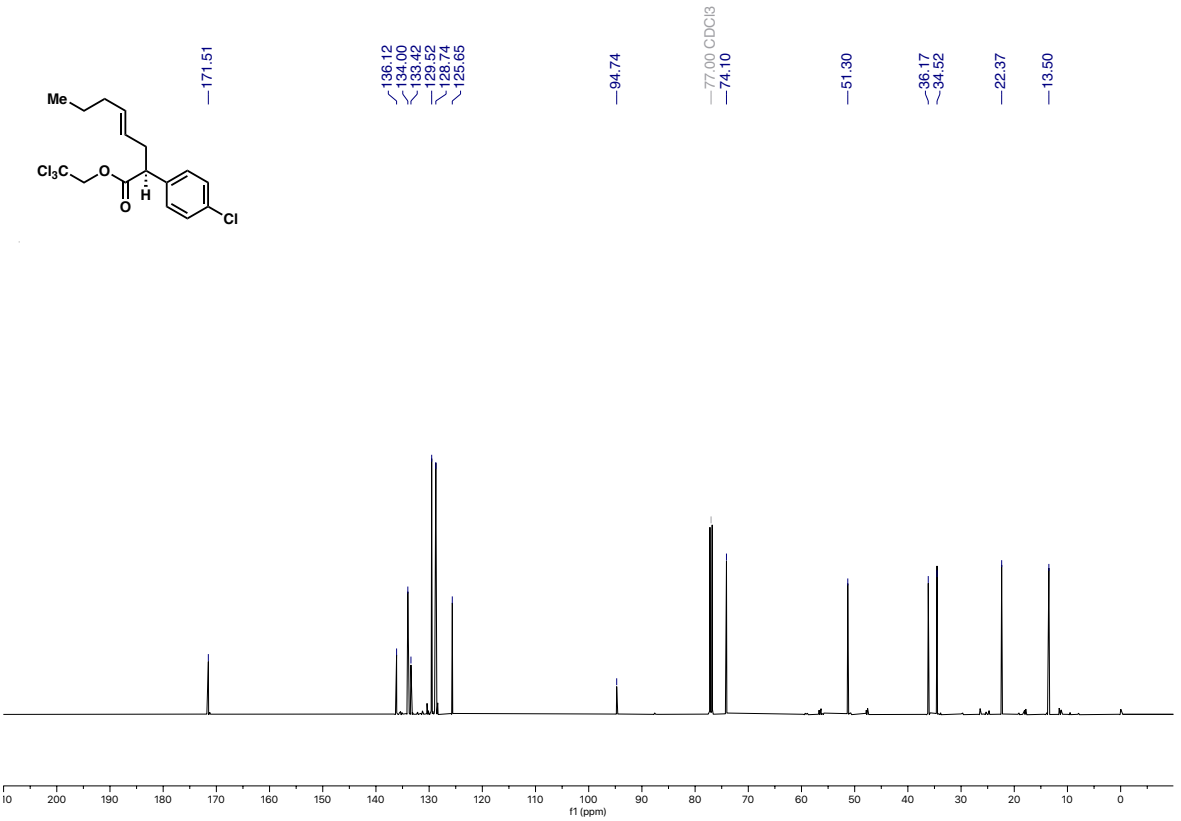
171.51
136.12
134.00
133.42
129.52
128.74
125.65
94.74
77.00 CDCl3
74.10
51.30
36.17
34.52
22.37
13.50
Me
Cl3C
O
H
Cl
f1 (ppm)

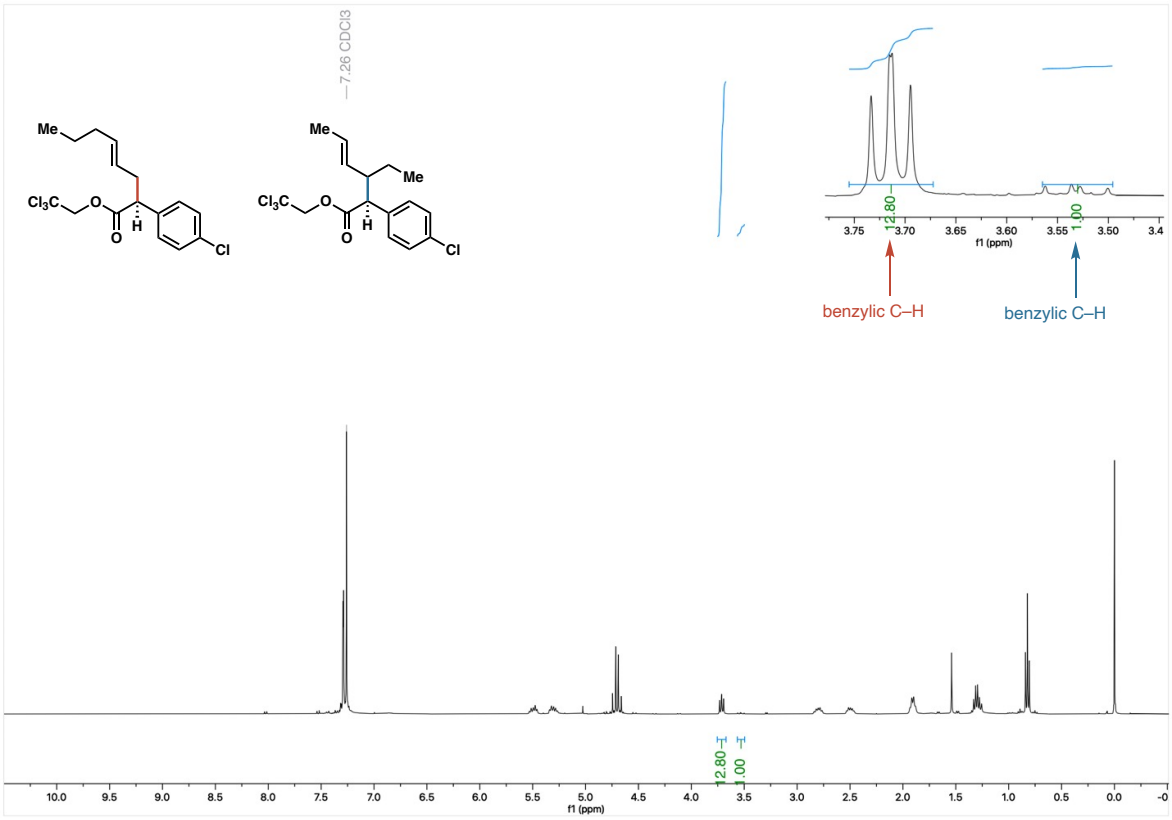
Me
Cl3C
O
O
H
Cl
Me
Me
Cl3C
O
O
H
Cl
7.26 CDCl3
benzylic C–H
benzylic C–H
12.80
1.00
f1 (ppm)

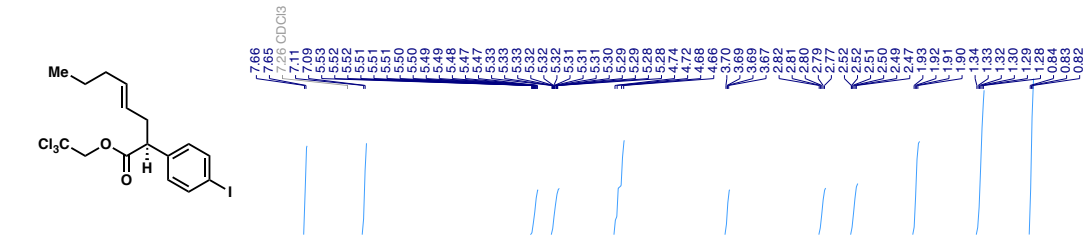
Me
Cl3C
O
O
H
I
7.26 CDCl3

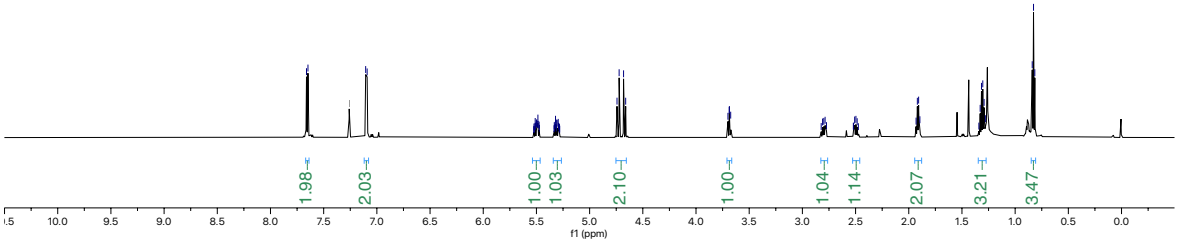
1.98
2.03
1.00
1.03
2.10
1.00
1.04
1.14
2.07
3.21
3.47
f1 (ppm)

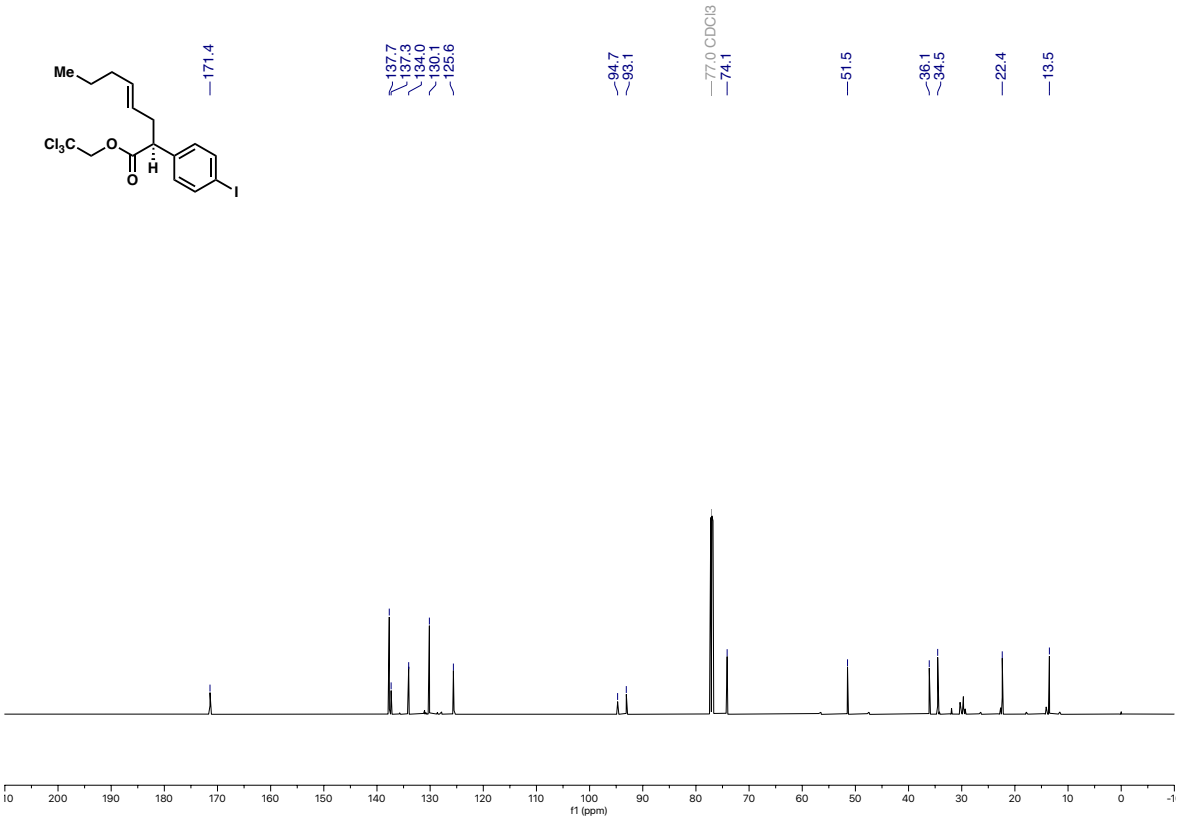
Me
Cl3C
O
O
H
I
171.4
137.7
137.3
134.0
130.1
125.6
94.7
93.1
77.0 CDCl3
74.1
51.5
36.1
34.5
22.4
13.5
f1 (ppm)

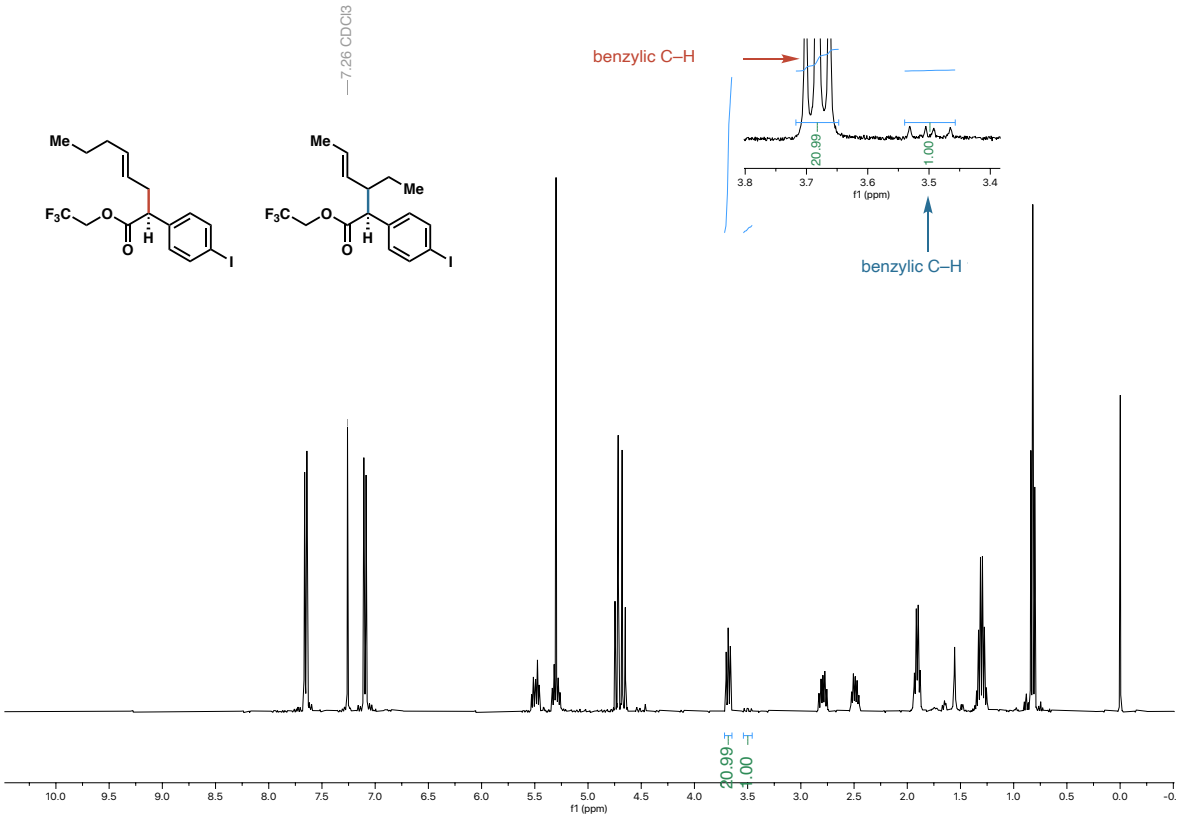
7.26 CDCl3
Me
F3C
O
O
H
I
Me
F3C
O
O
H
I
Me
benzylic C–H
20.99
1.00
f1 (ppm)
benzylic C–H
20.99
1.00
f1 (ppm)

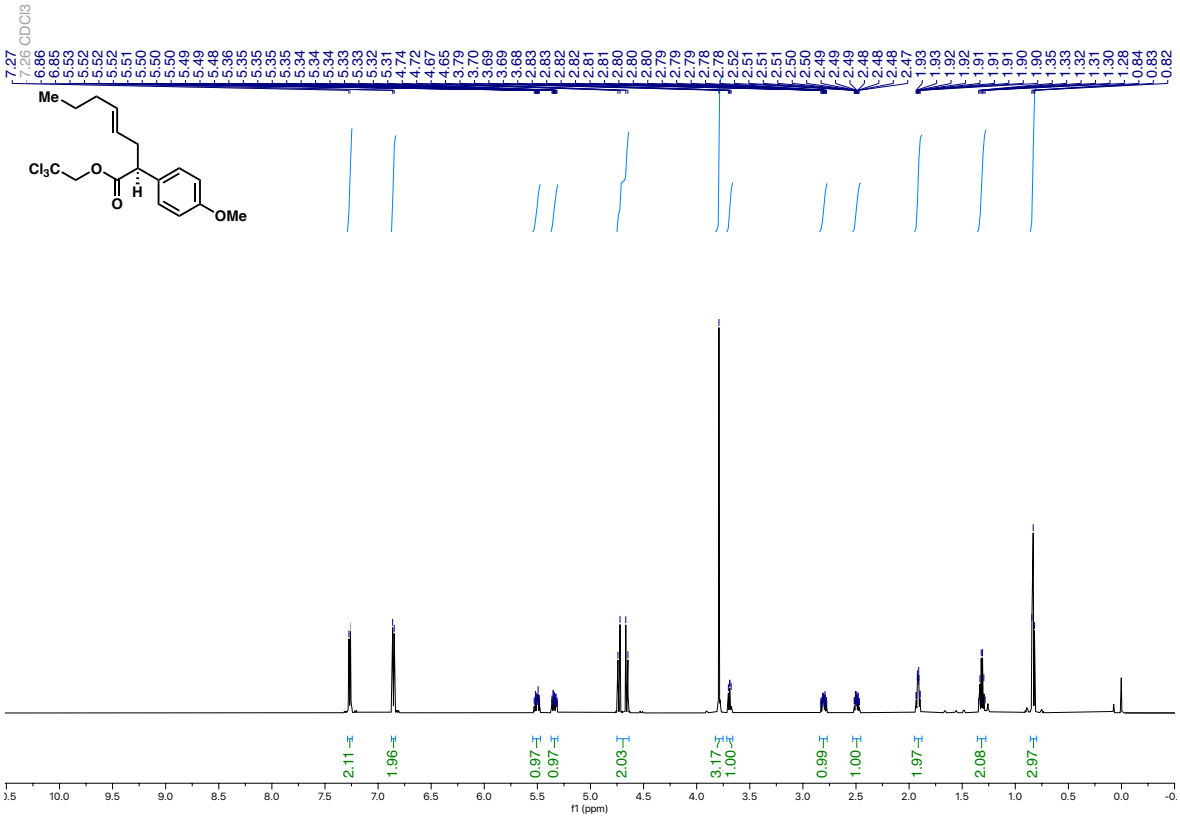
7.27
7.26 CDCl3
Me
Cl3C
O
O
H
OMe
2.11
1.96
0.97
0.97
2.03
3.17
1.00
0.99
1.00
1.97
2.08
2.97
f1 (ppm)

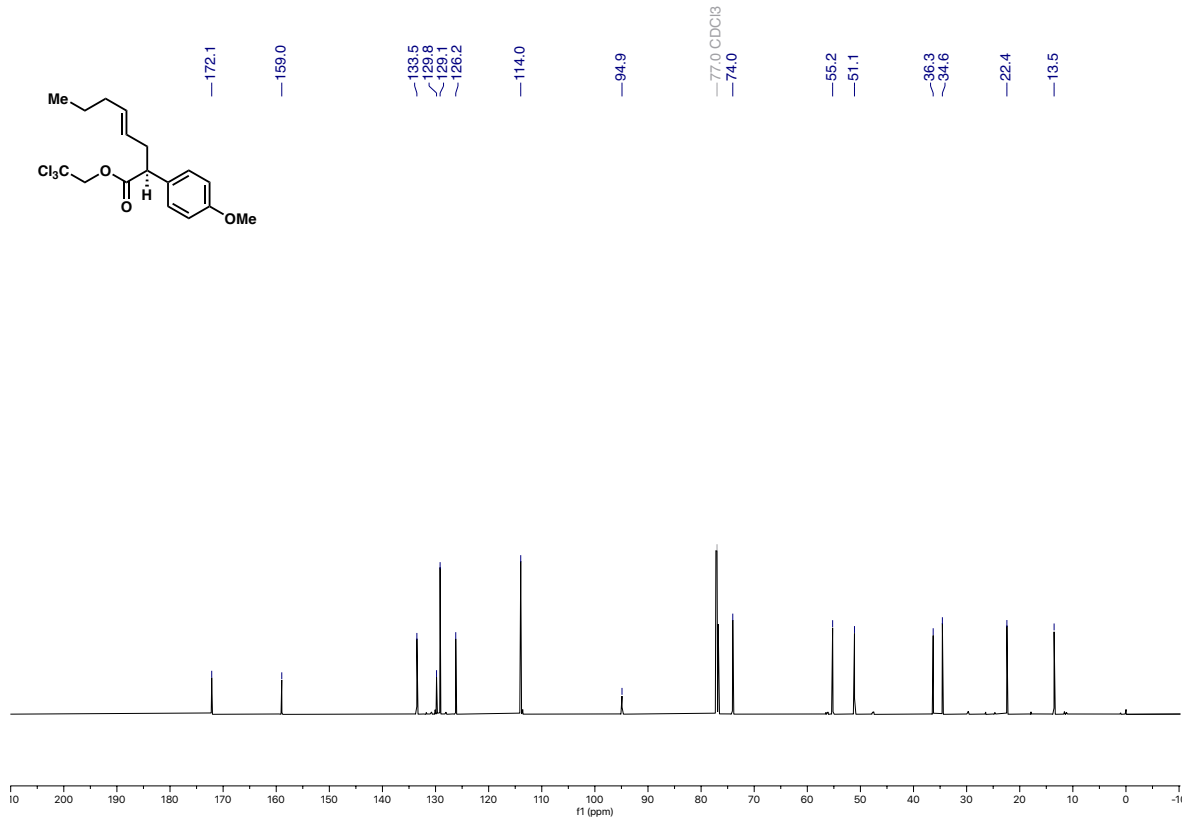
172.1
159.0
133.5
129.8
129.1
126.2
114.0
94.9
77.0 CDCl3
74.0
55.2
51.1
36.3
34.6
22.4
13.5
Me
Cl3C
O
O
H
OMe
f1 (ppm)

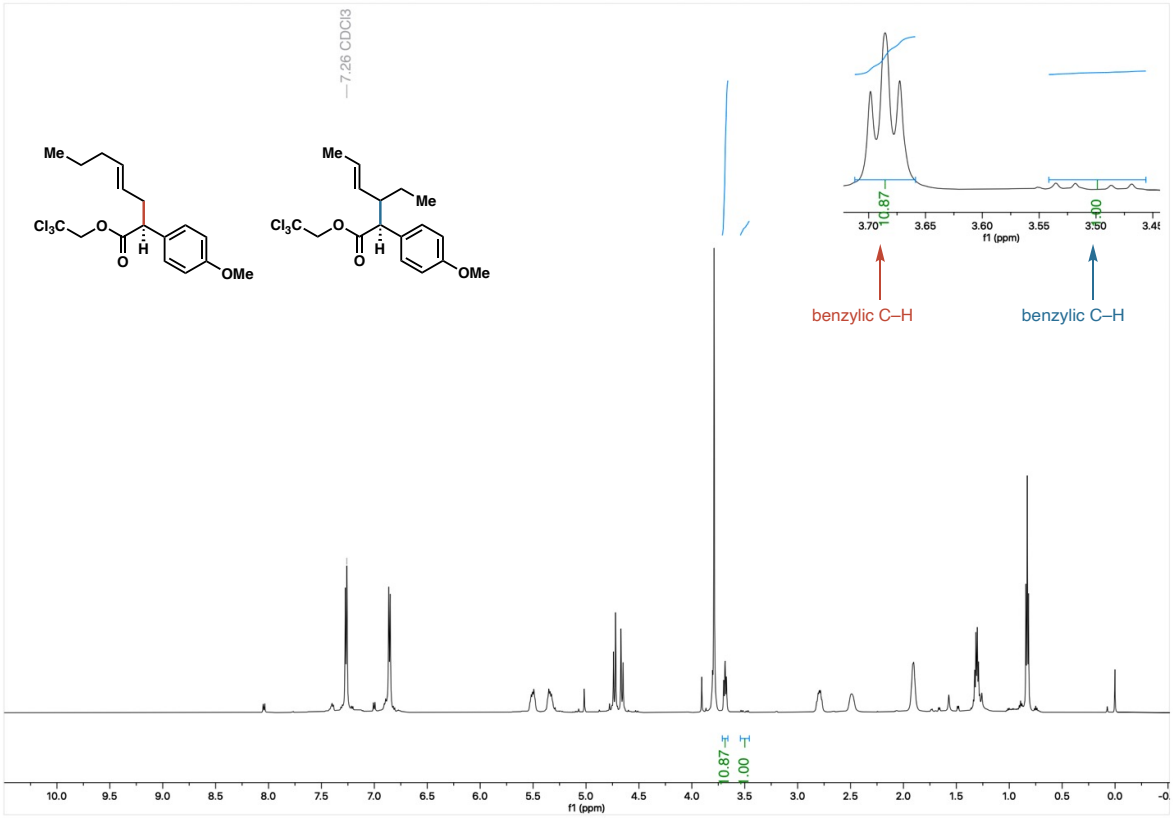
7.26 CDCl3
Me
Cl3C
O
O
H
OMe
Me
Me
Cl3C
O
O
H
OMe
benzylic C–H
benzylic C–H
10.87
1.00
f1 (ppm)

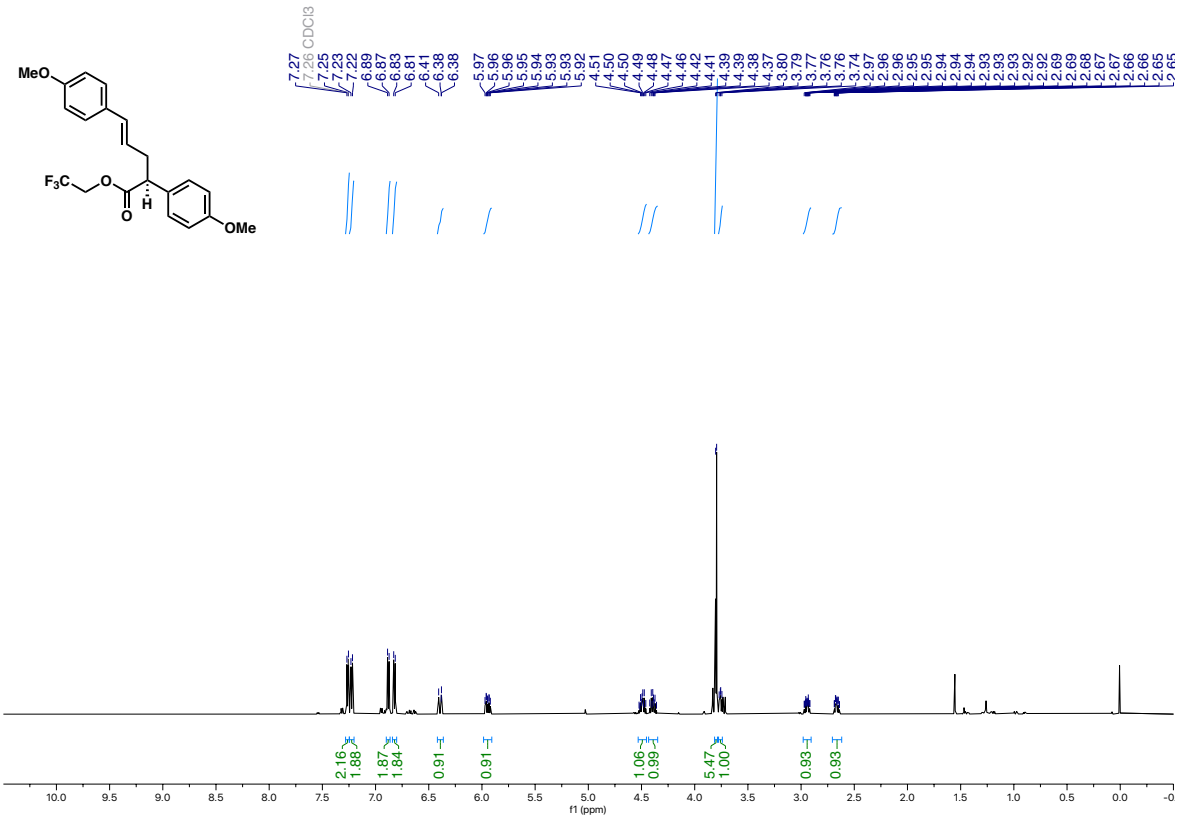
MeO
F3C
O
O
H
OMe
7.27
7.26 CDCl3
2.16
1.88
1.87
1.84
0.91
0.91
1.06
0.99
5.47
1.00
0.93
0.93
f1 (ppm)

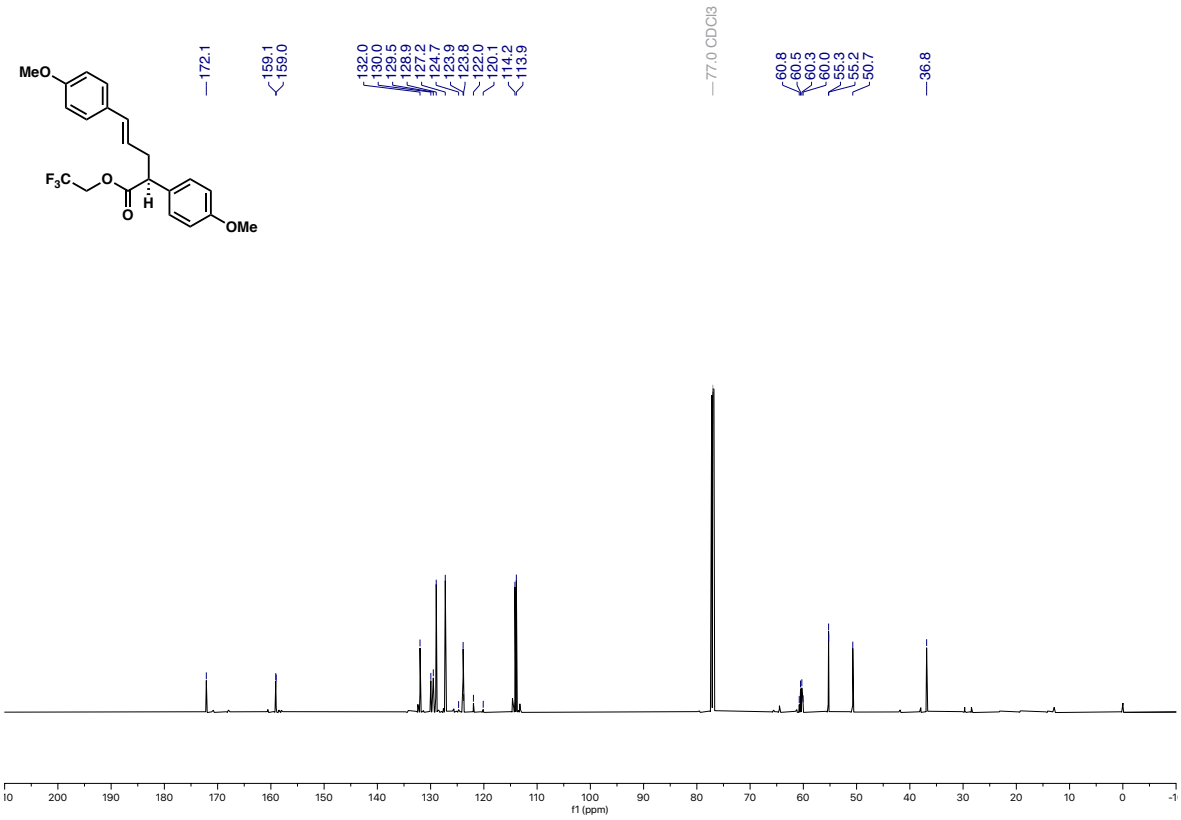
MeO
F3C
O
O
H
OMe
172.1
159.1
159.0
132.0
130.0
128.5
128.9
127.2
124.7
123.9
123.8
122.0
120.1
114.2
113.9
77.0 CDCl3
60.8
60.5
60.3
60.0
55.3
55.2
50.7
36.8
f1 (ppm)

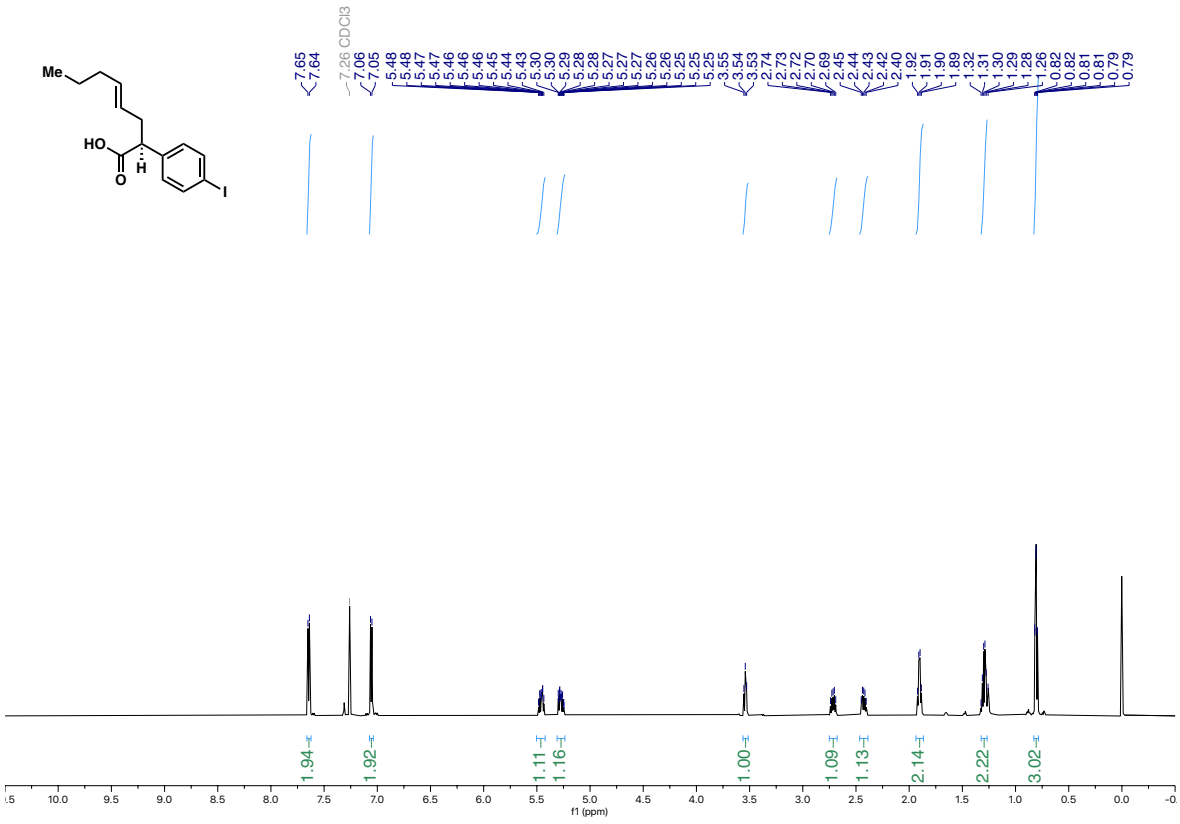
Me
HO
O
H
I
7.65
7.64
7.26 CDCl3
7.06
7.05
5.48
5.47
5.46
5.45
5.44
5.43
5.30
5.29
5.28
5.27
5.26
5.25
3.55
3.54
3.53
2.74
2.73
2.72
2.70
2.69
2.45
2.44
2.43
2.42
2.40
1.92
1.91
1.90
1.89
1.32
1.31
1.30
1.29
1.28
1.26
0.82
0.81
0.79
1.94
1.92
1.11
1.16
1.00
1.09
1.13
2.14
2.22
3.02
f1 (ppm)

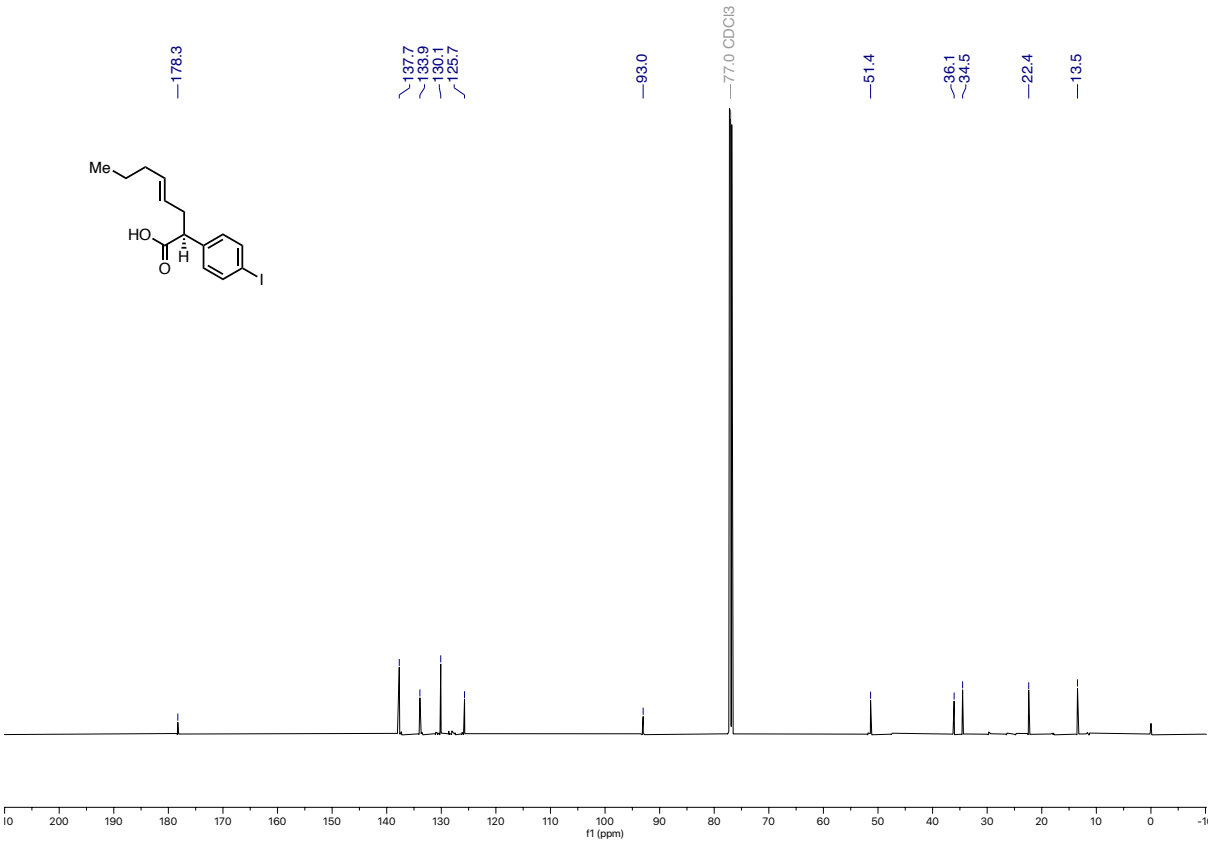
178.3
137.7
133.9
130.1
125.7
93.0
77.0 CDCl3
51.4
36.1
34.5
22.4
13.5
Me
HO
O
H
I
f1 (ppm)

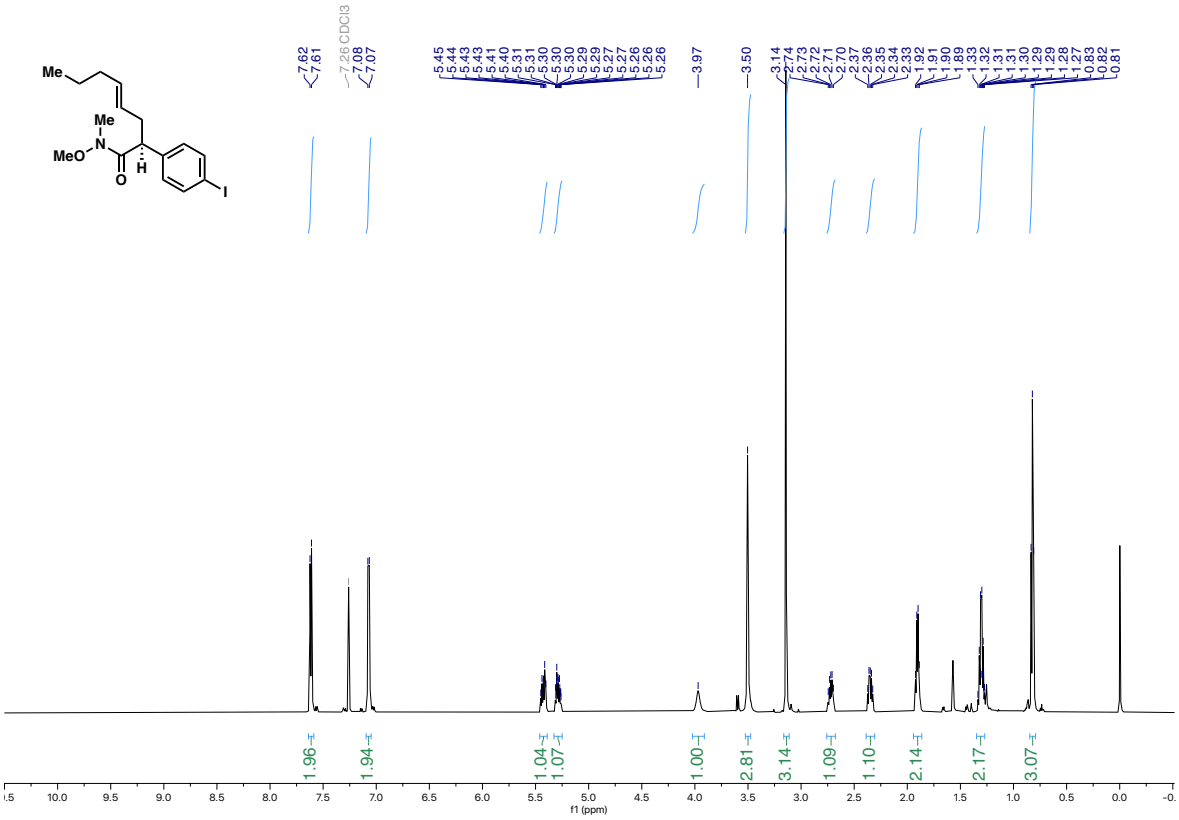
Me
Me
N
MeO
O
H
I
7.62
7.61
7.26 CDCl3
7.08
7.07
5.45
5.44
5.43
5.43
5.41
5.40
5.31
5.31
5.30
5.30
5.29
5.29
5.27
5.27
5.26
5.26
5.26
3.97
3.50
3.14
2.74
2.73
2.72
2.71
2.70
2.37
2.36
2.35
2.34
2.33
1.92
1.91
1.90
1.89
1.33
1.32
1.31
1.31
1.30
1.29
1.29
1.28
1.27
0.83
0.82
0.81
1.96
1.94
1.04
1.07
1.00
2.81
3.14
1.09
1.10
2.14
2.17
3.07
f1 (ppm)

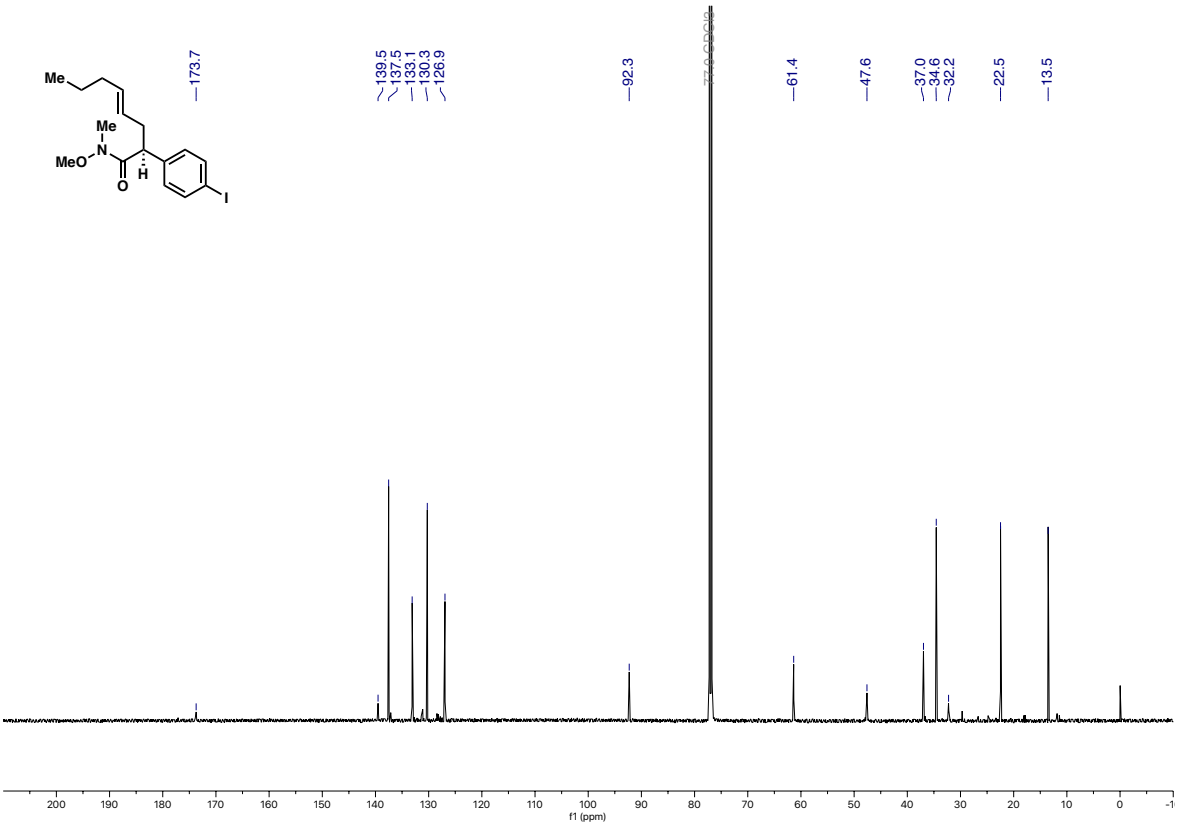
Me
Me
N
MeO
O
H
I
173.7
139.5
137.5
133.1
130.3
126.9
92.3
77.0 CDCl3
61.4
47.6
37.0
34.6
32.2
22.5
13.5
f1 (ppm)

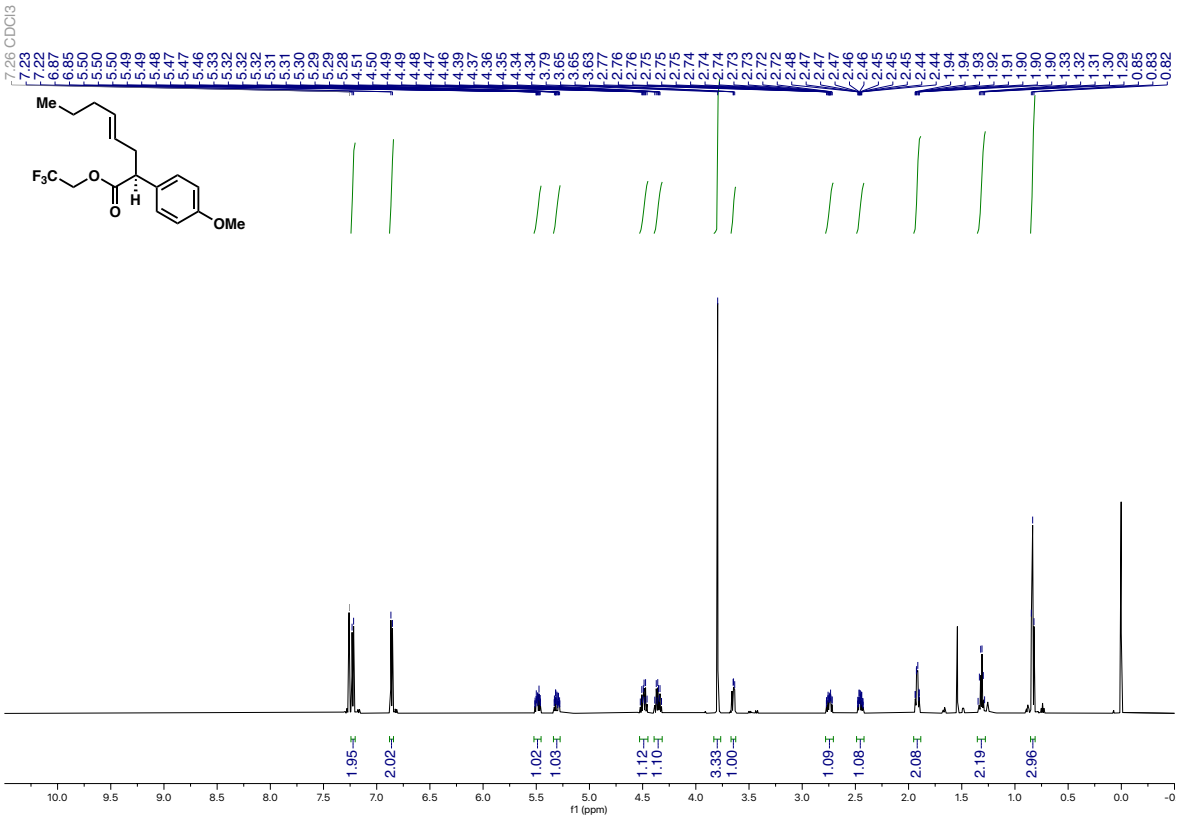
7.26 CDCl3
Me
F3C
O
O
H
OMe
1.95
2.02
1.02
1.03
1.12
1.10
3.33
1.00
1.09
1.08
2.08
2.19
2.96
f1 (ppm)

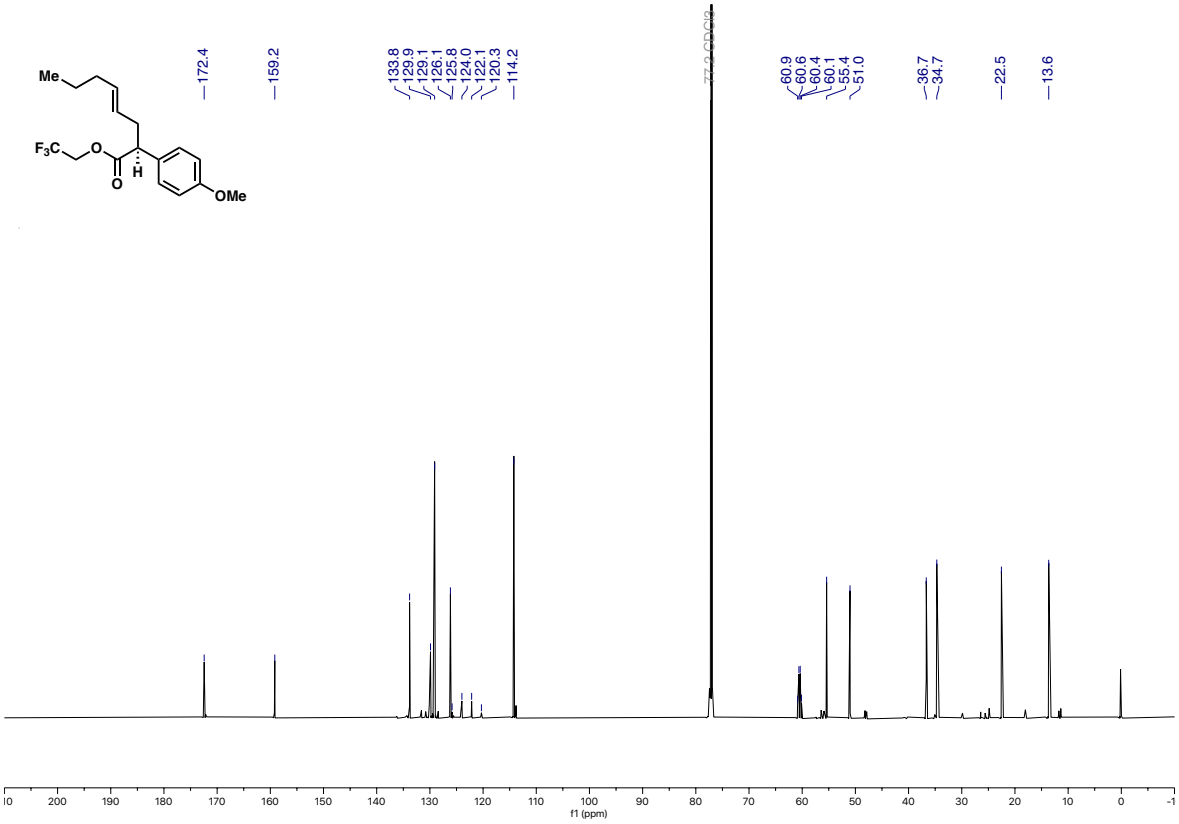
Me
F3C
O
O
H
OMe
172.4
159.2
133.8
129.9
129.1
126.1
125.8
124.0
122.1
120.3
114.2
77.2 CDCl3
60.9
60.6
60.4
60.1
55.4
51.0
36.7
34.7
22.5
13.6
f1 (ppm)

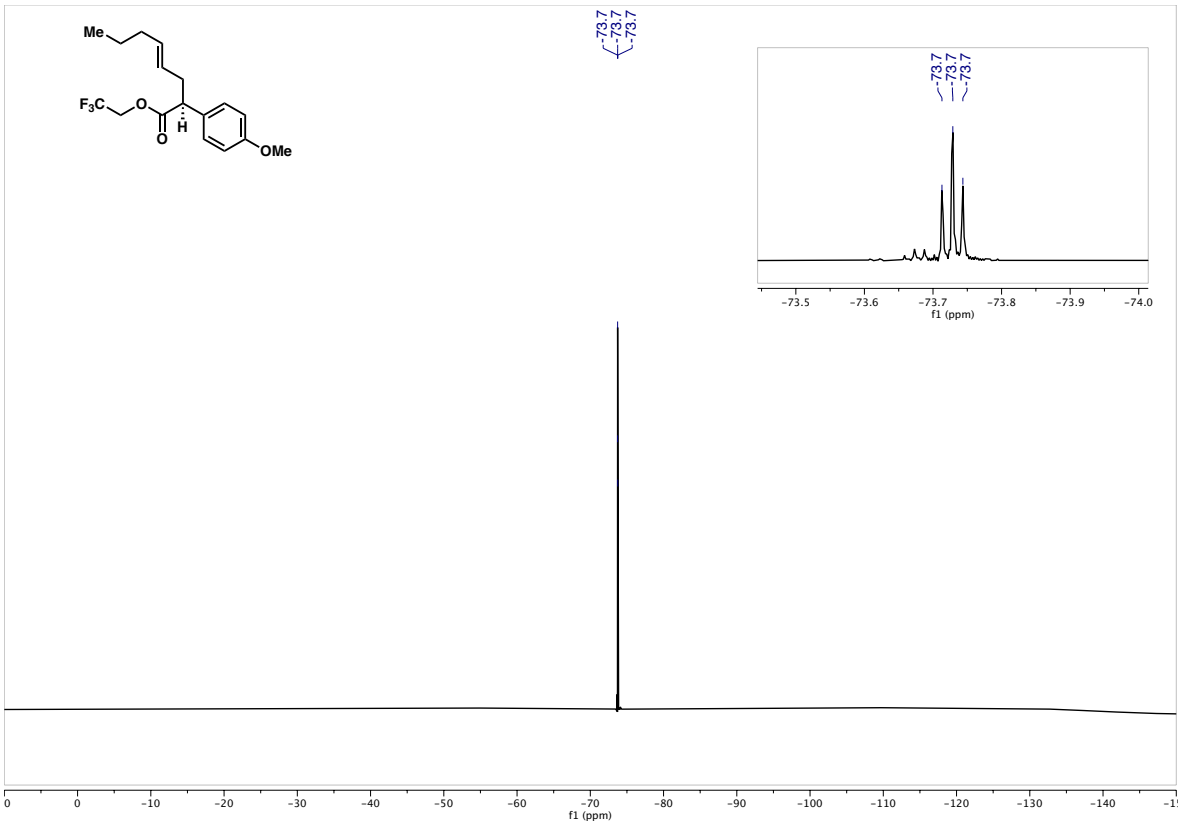
Me
F3C
O
O
H
OMe
-73.7
-73.7
-73.7
-73.5
-73.6
-73.7
-73.8
-73.9
-74.0
f1 (ppm)
0
-10
-20
-30
-40
-50
-60
-70
-80
-90
-100
-110
-120
-130
-140
f1 (ppm)

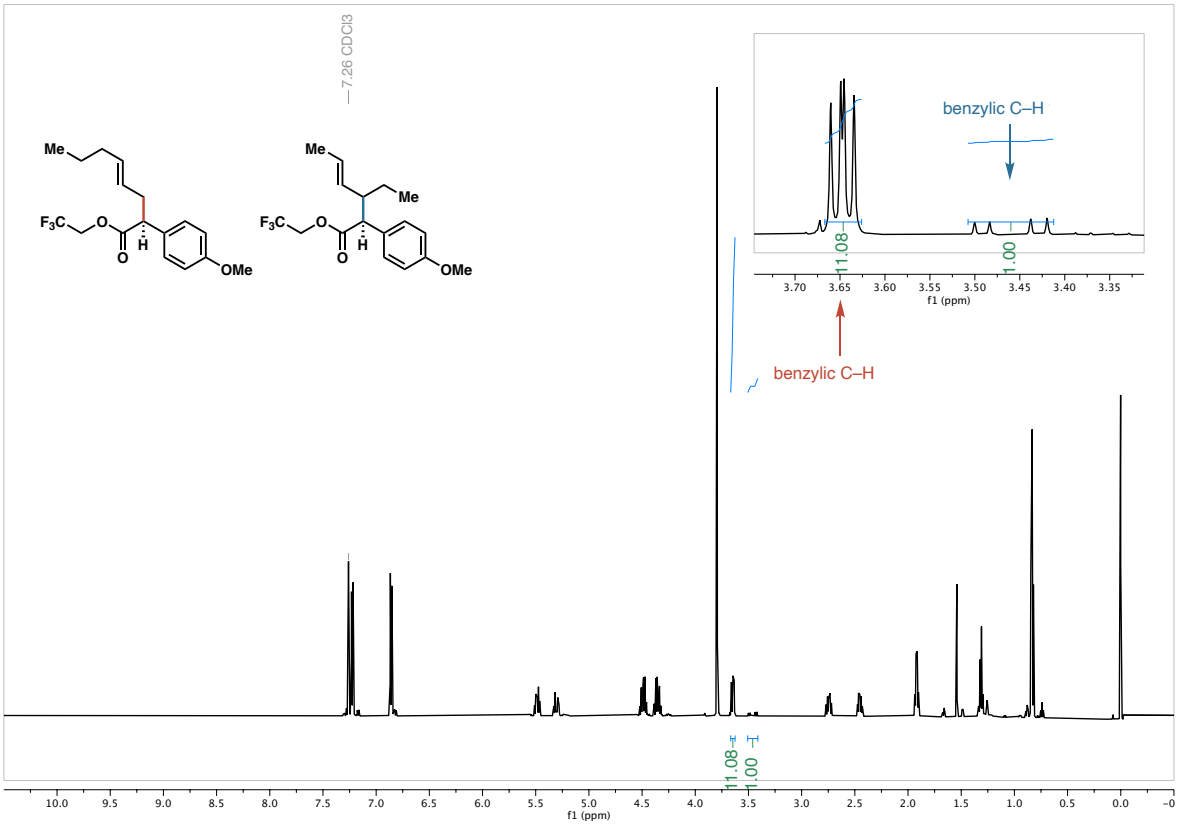
7.26 CDCl3
Me
F3C
O
O
H
OMe
Me
F3C
O
O
H
Me
OMe
benzylic C–H
11.08
1.00
3.70
3.65
3.60
3.55
3.50
3.45
3.40
3.35
f1 (ppm)
benzylic C–H
11.08
1.00
10.0
9.5
9.0
8.5
8.0
7.5
7.0
6.5
6.0
5.5
5.0
4.5
4.0
3.5
3.0
2.5
2.0
1.5
1.0
0.5
0.0
f1 (ppm)

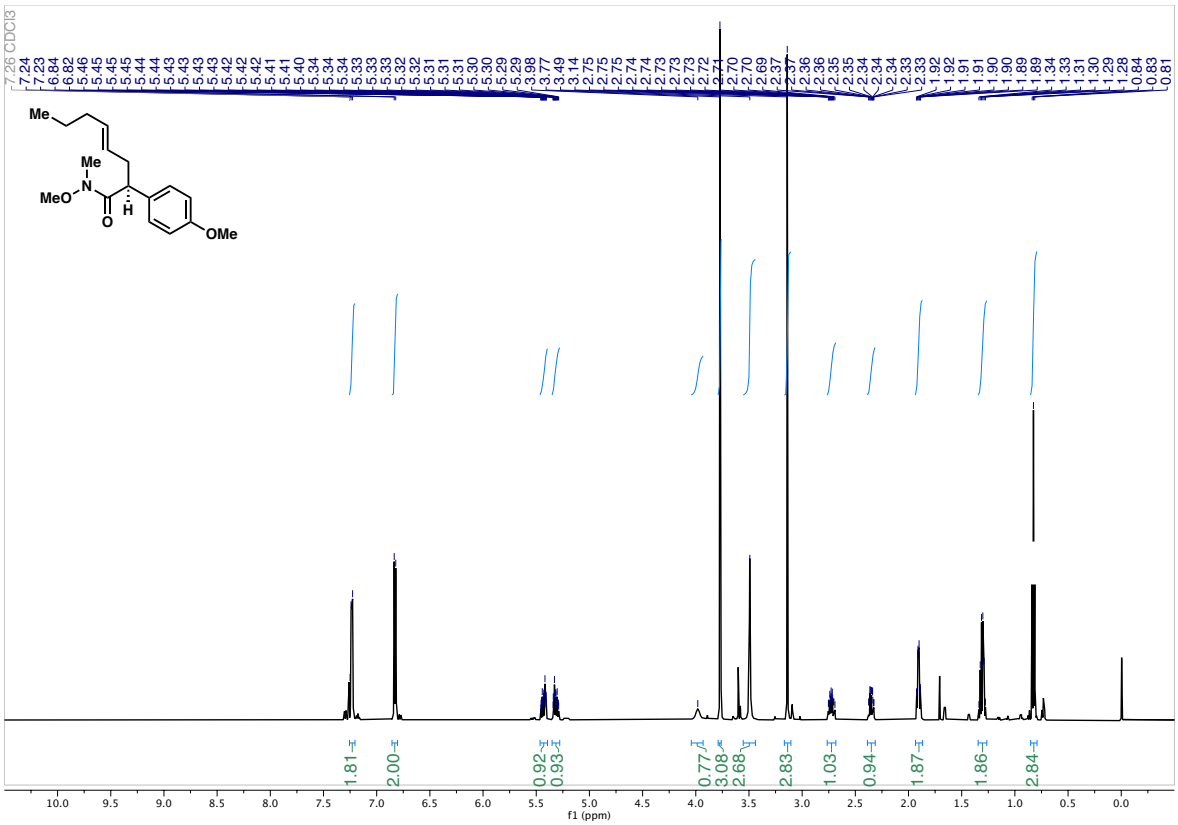
Me
Me
N
MeO
O
H
OMe
f1 (ppm)

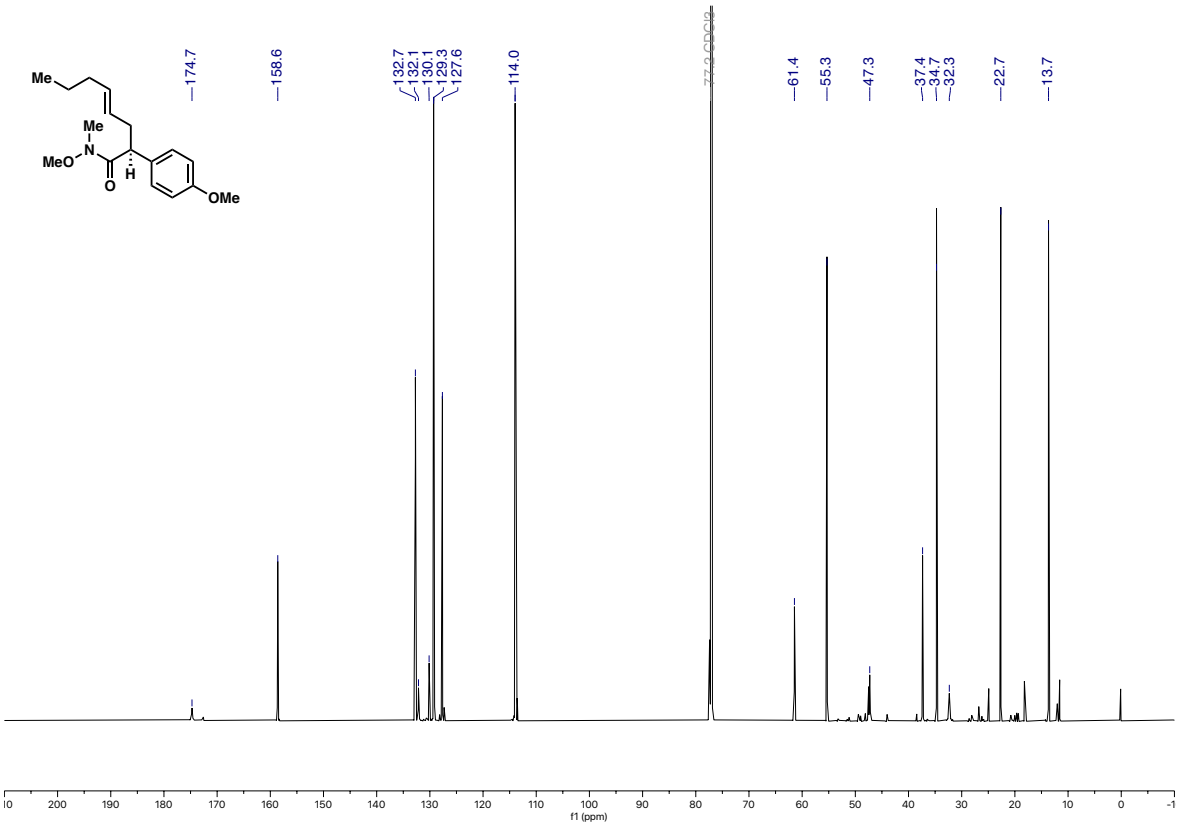
Me
Me
N
MeO
O
H
OMe
174.7
158.6
132.7
132.1
130.1
129.3
127.6
114.0
61.4
55.3
47.3
37.4
34.7
32.3
22.7
13.7
f1 (ppm)

Appendix – Ch.4 NMR Spectra

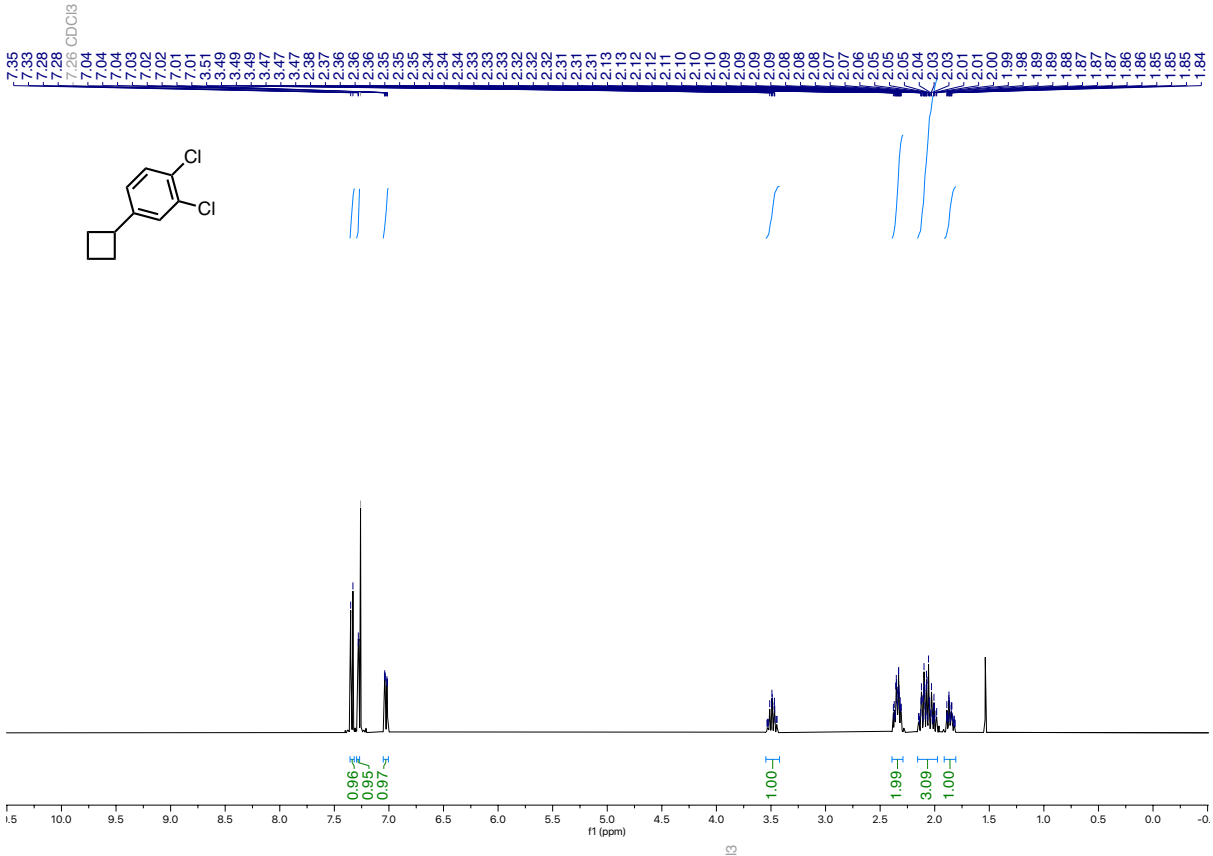

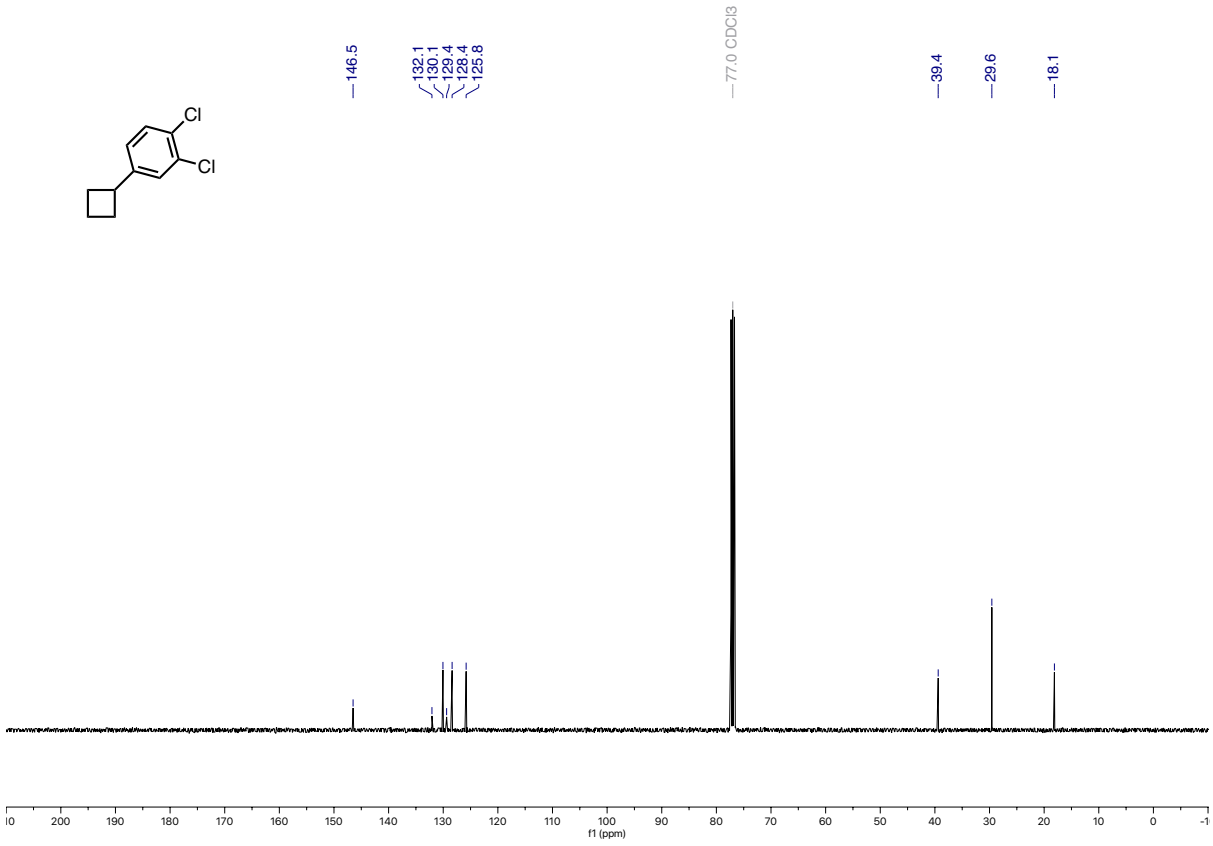

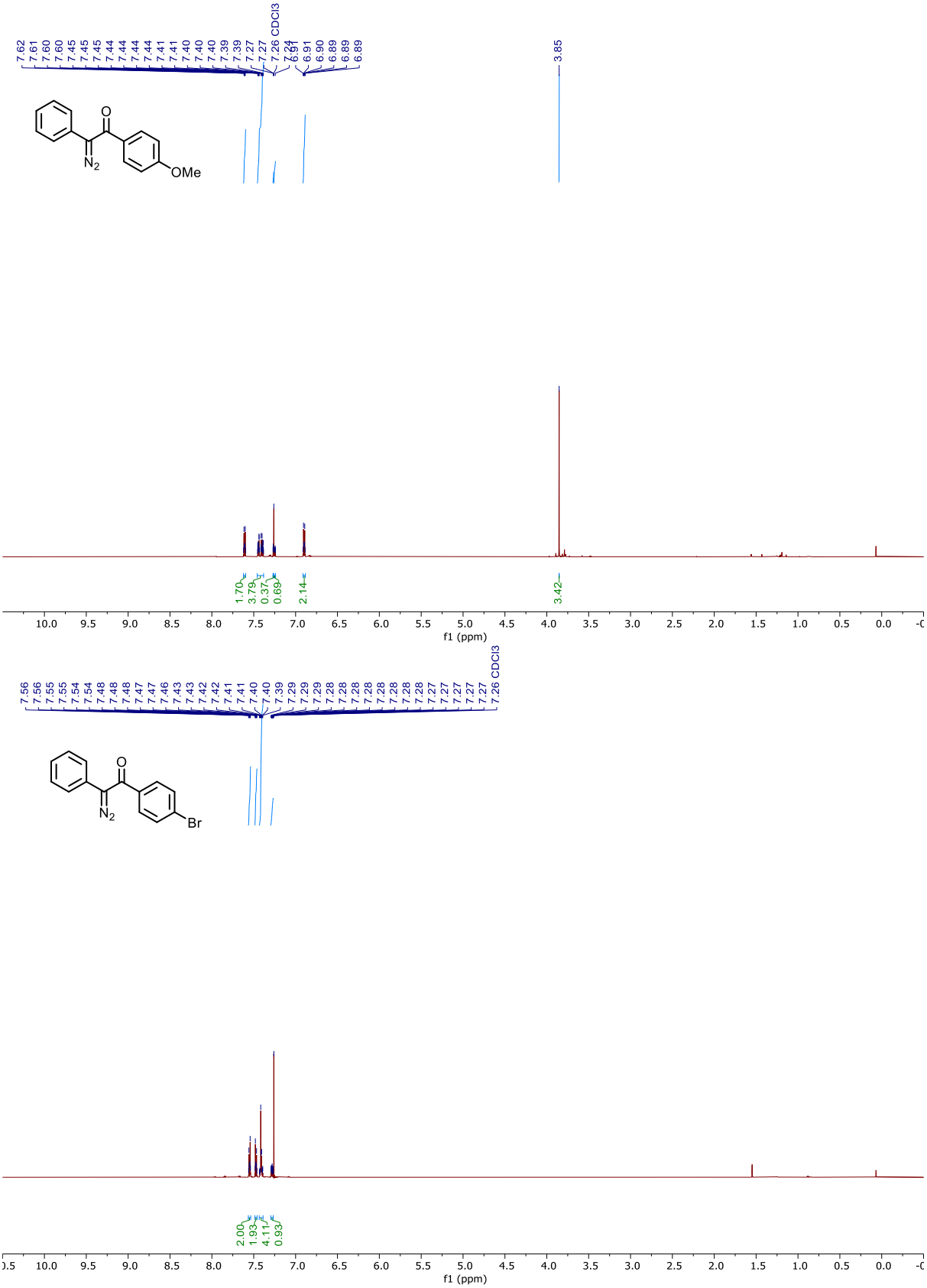
7.62
7.61
7.60
7.60
7.45
7.45
7.45
7.44
7.44
7.44
7.44
7.41
7.41
7.40
7.40
7.40
7.39
7.39
7.27
7.27
7.26 CDCl3
7.24
6.91
6.91
6.90
6.89
6.89
6.89
3.85
O
N2
OMe
1.70
3.79
0.37
0.69
2.14
3.42
10.0
9.5
9.0
8.5
8.0
7.5
7.0
6.5
6.0
5.5
5.0
4.5
4.0
3.5
3.0
2.5
2.0
1.5
1.0
0.5
0.0
f1 (ppm)
7.56
7.56
7.55
7.55
7.54
7.54
7.48
7.48
7.48
7.47
7.47
7.46
7.43
7.43
7.42
7.42
7.41
7.41
7.40
7.40
7.39
7.29
7.29
7.29
7.28
7.28
7.28
7.28
7.28
7.28
7.28
7.27
7.27
7.27
7.27
7.26 CDCl3
O
N2
Br
2.00
1.93
4.11
0.93
f1 (ppm)

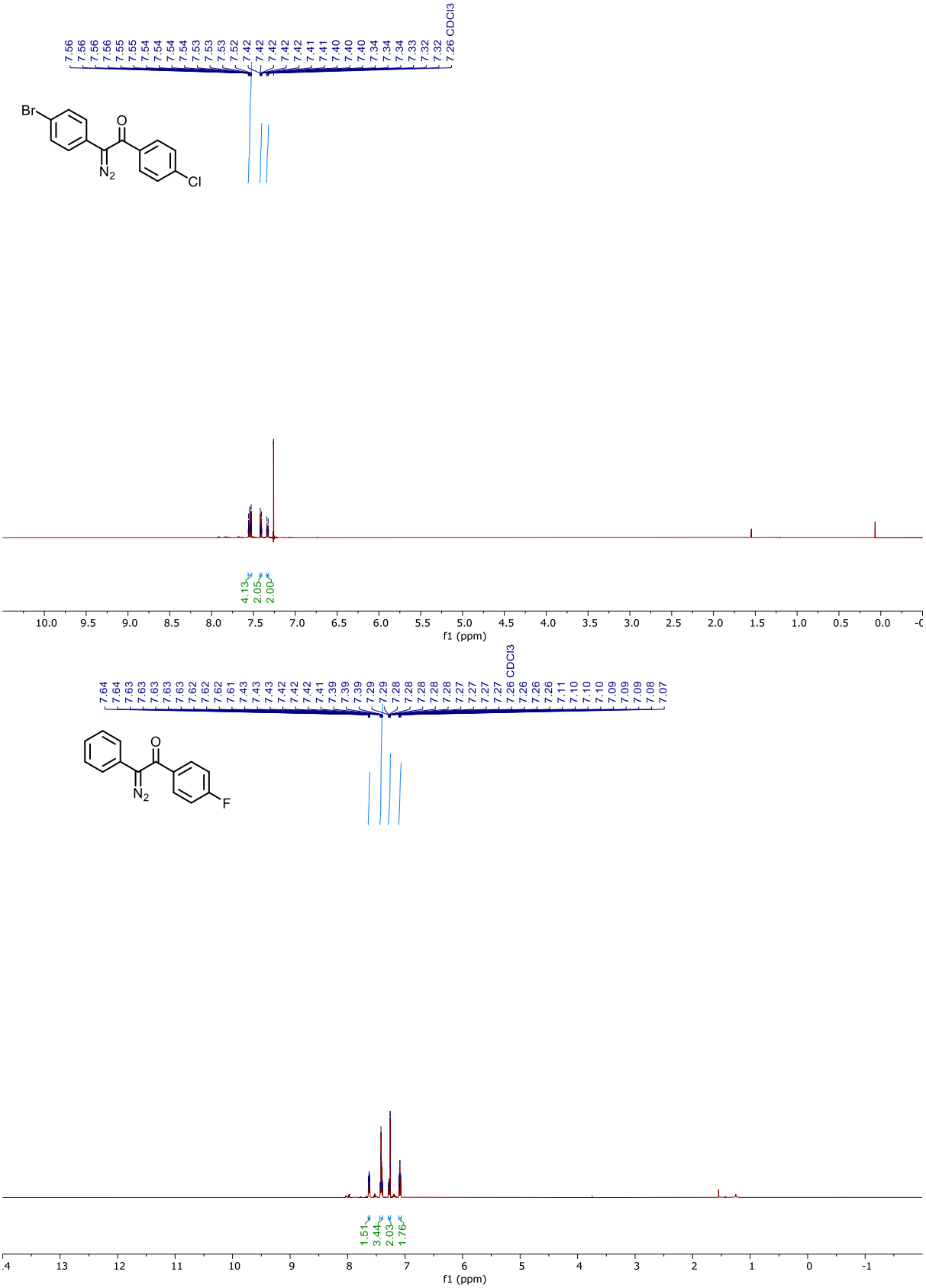
7.56 7.56 7.56 7.56 7.55 7.54 7.54 7.54 7.53 7.53 7.52 7.42 7.42 7.42 7.42 7.41 7.41 7.40 7.40 7.34 7.34 7.33 7.32 7.26 CDCl3
Br
O
N2
Cl
4.13
2.05
2.00
f1 (ppm)
7.64 7.64 7.63 7.63 7.63 7.63 7.62 7.62 7.62 7.61 7.43 7.43 7.42 7.42 7.42 7.41 7.39 7.39 7.39 7.29 7.29 7.28 7.28 7.28 7.28 7.28 7.27 7.27 7.27 7.27 7.26 CDCl3 7.26 7.26 7.26 7.11 7.10 7.10 7.10 7.09 7.09 7.09 7.08 7.07
O
N2
F
1.51
3.44
2.03
1.76
f1 (ppm)

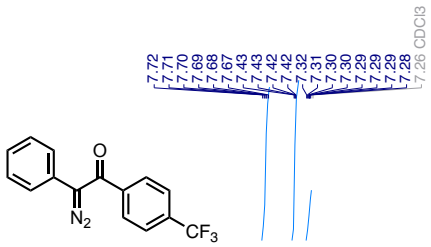
7.72
7.71
7.70
7.69
7.68
7.67
7.43
7.43
7.42
7.42
7.32
7.31
7.31
7.30
7.30
7.29
7.29
7.29
7.28
7.26 CDCl3
O
N2
CF3

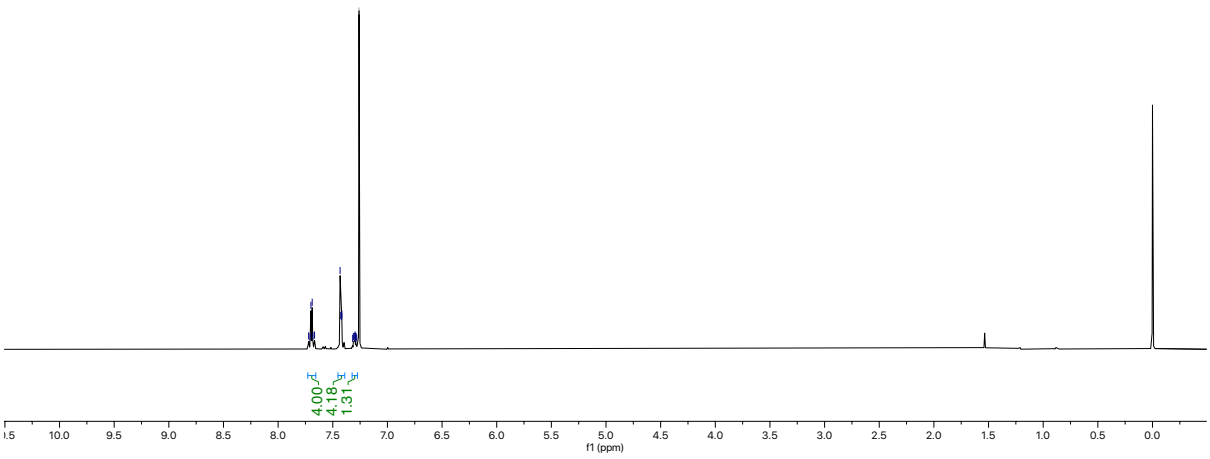
4.00
4.18
1.31
10.0
9.5
9.0
8.5
8.0
7.5
7.0
6.5
6.0
5.5
5.0
4.5
4.0
3.5
3.0
2.5
2.0
1.5
1.0
0.5
0.0
f1 (ppm)

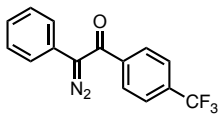
O
N2
CF3

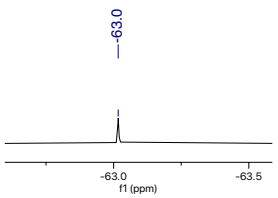
-63.0
-63.0
-63.0
-63.5
f1 (ppm)

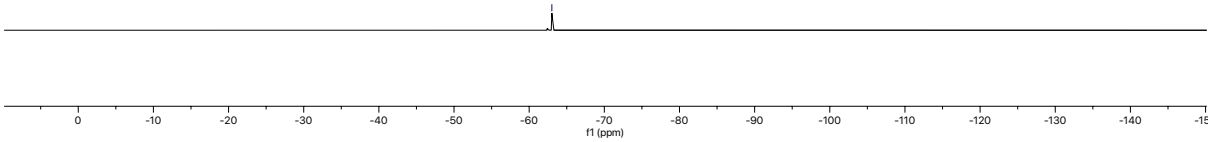
0
-10
-20
-30
-40
-50
-60
-70
-80
-90
-100
-110
-120
-130
-140
f1 (ppm)

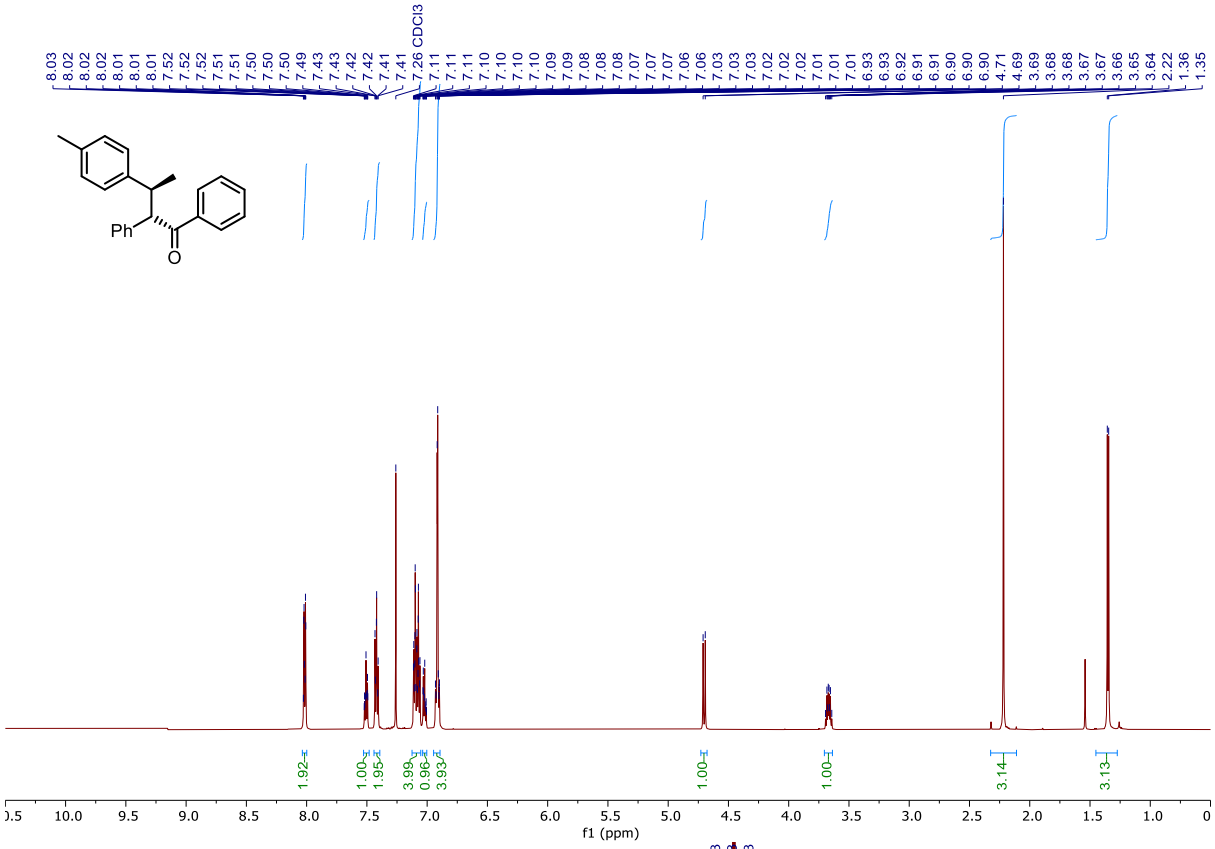
8.03 8.02 8.02 8.02 8.01 8.01 8.01 7.52 7.52 7.52 7.51 7.51 7.50 7.50 7.50 7.49 7.43 7.43 7.42 7.42 7.41 7.41 7.26 CDCl3 7.11 7.11 7.11 7.10 7.10 7.10 7.10 7.09 7.09 7.08 7.08 7.08 7.07 7.07 7.07 7.06 7.06 7.03 7.03 7.03 7.02 7.02 7.02 7.01 7.01 7.01 6.93 6.93 6.92 6.91 6.91 6.90 6.90 6.90 4.71 4.69 3.69 3.68 3.68 3.67 3.67 3.66 3.65 3.64 2.22 1.36 1.35
Ph
O
1.92 1.00 1.95 3.99 0.96 3.93 1.00 1.00 3.14 3.13
f1 (ppm)

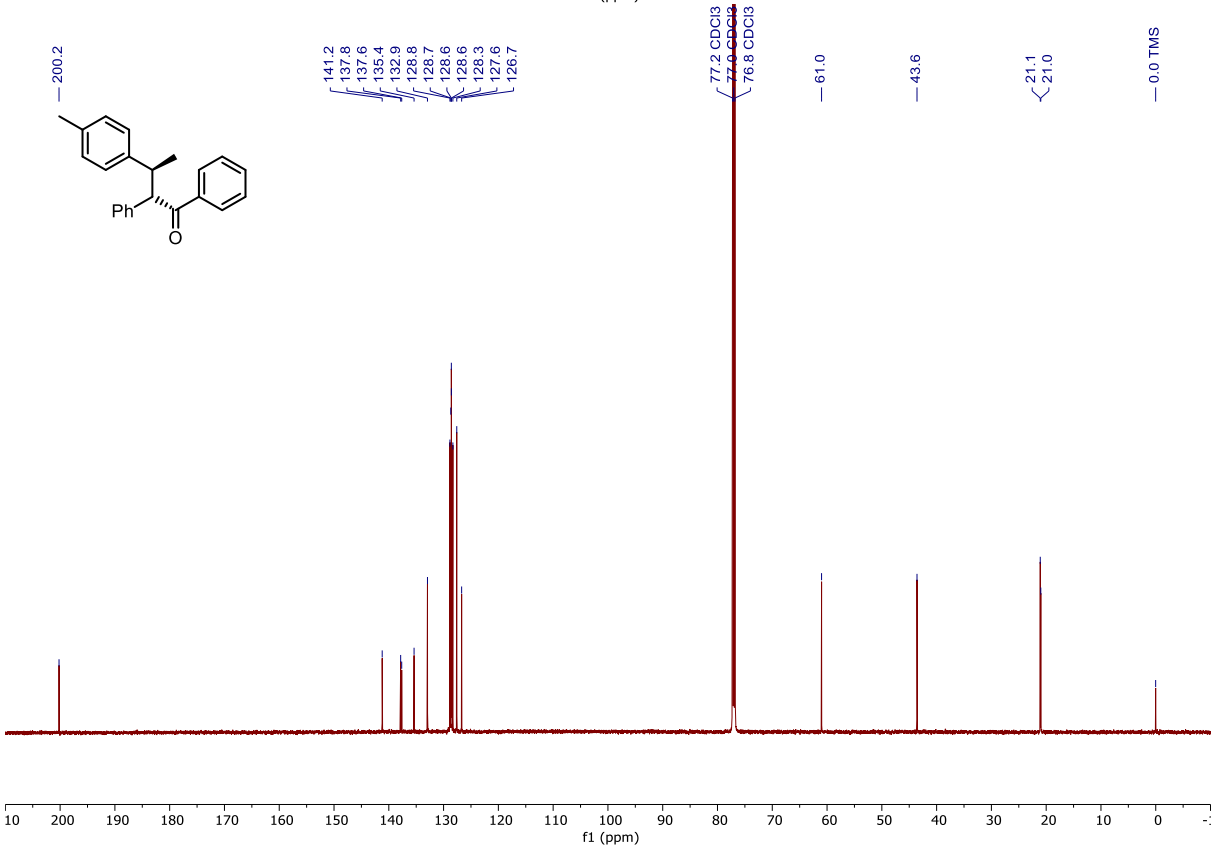
200.2
141.2 137.8 137.6 135.4 132.9 128.8 128.7 128.6 128.6 128.3 127.6 126.7
77.2 CDCl3 77.0 CDCl3 76.8 CDCl3
61.0
43.6
21.1 21.0
0.0 TMS
Ph
O
f1 (ppm)

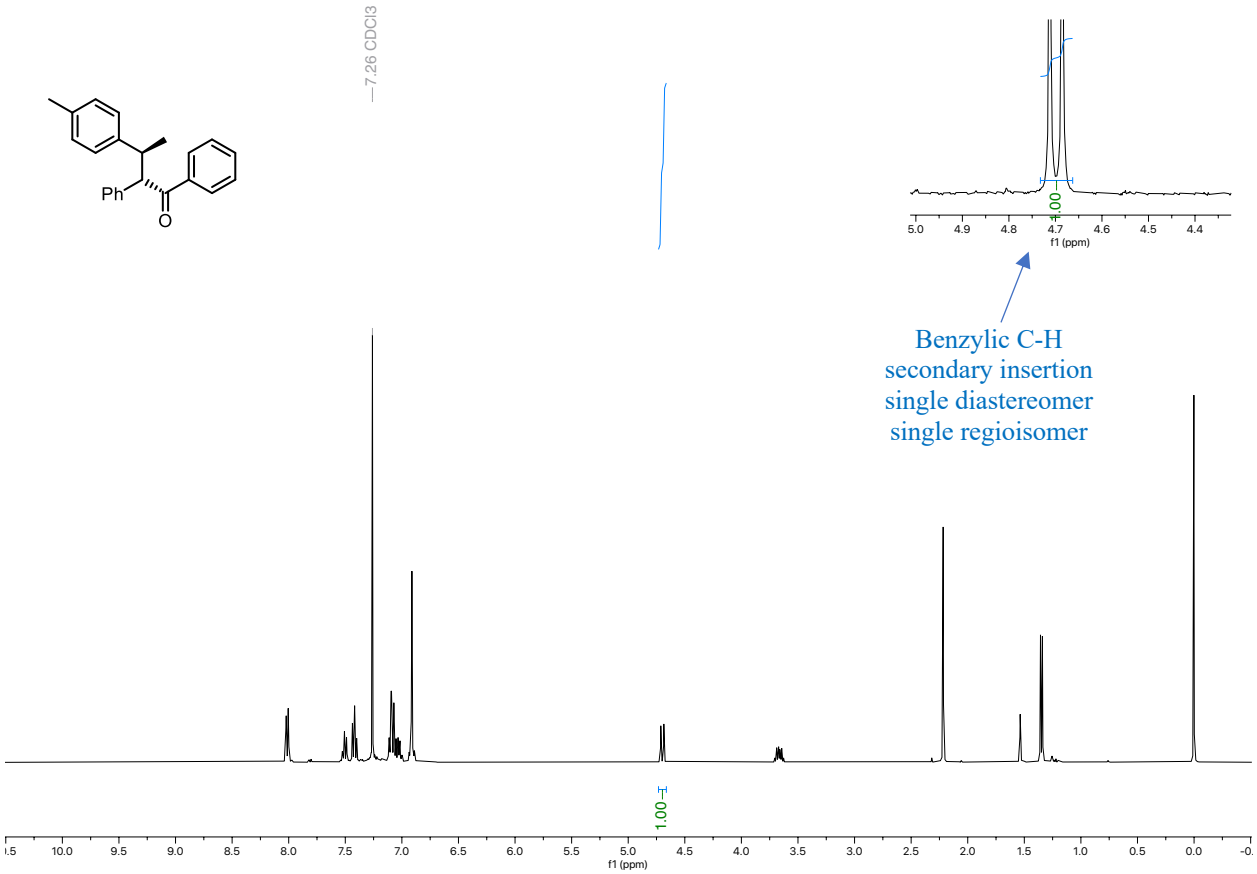
7.26 CDCl3
Ph
O
1.00
f1 (ppm)
Benzylic C-H
secondary insertion
single diastereomer
single regioisomer

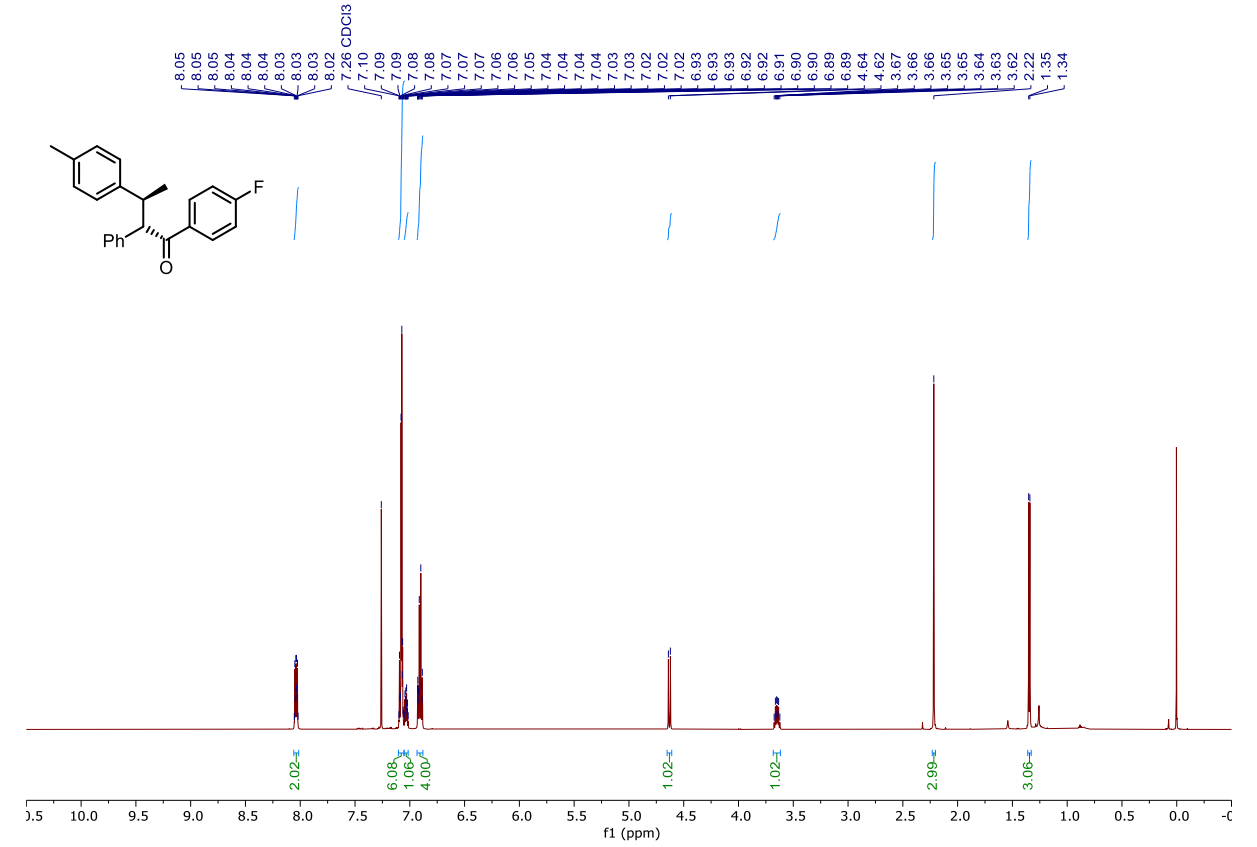
CDCl3
F
Ph
O
2.02
6.08
1.06
4.00
1.02
1.02
2.99
3.06
f1 (ppm)

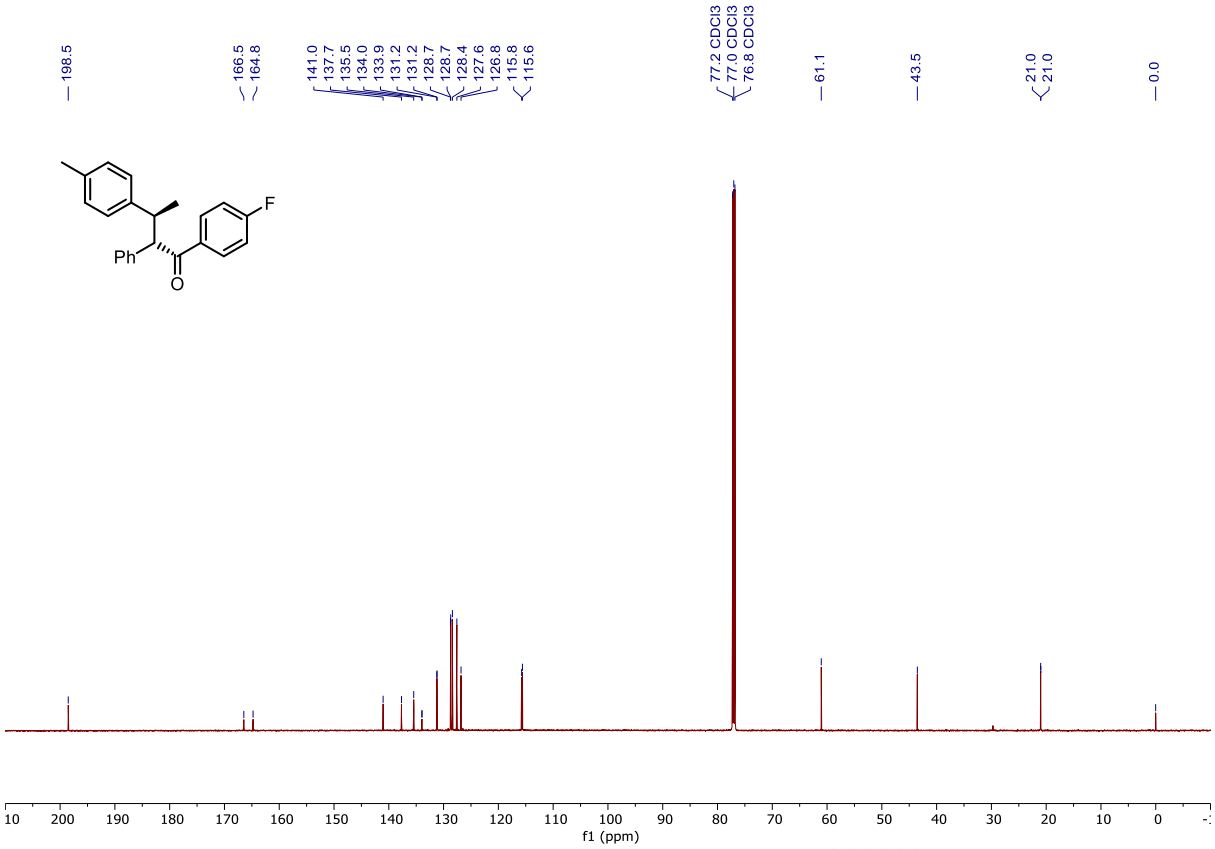
198.5
166.5
164.8
141.0
137.7
135.5
134.0
133.9
131.2
131.2
128.7
128.7
128.4
127.6
126.8
115.8
115.6
77.2 CDCl3
77.0 CDCl3
76.8 CDCl3
61.1
43.5
21.0
21.0
0.0
F
Ph
O
f1 (ppm)

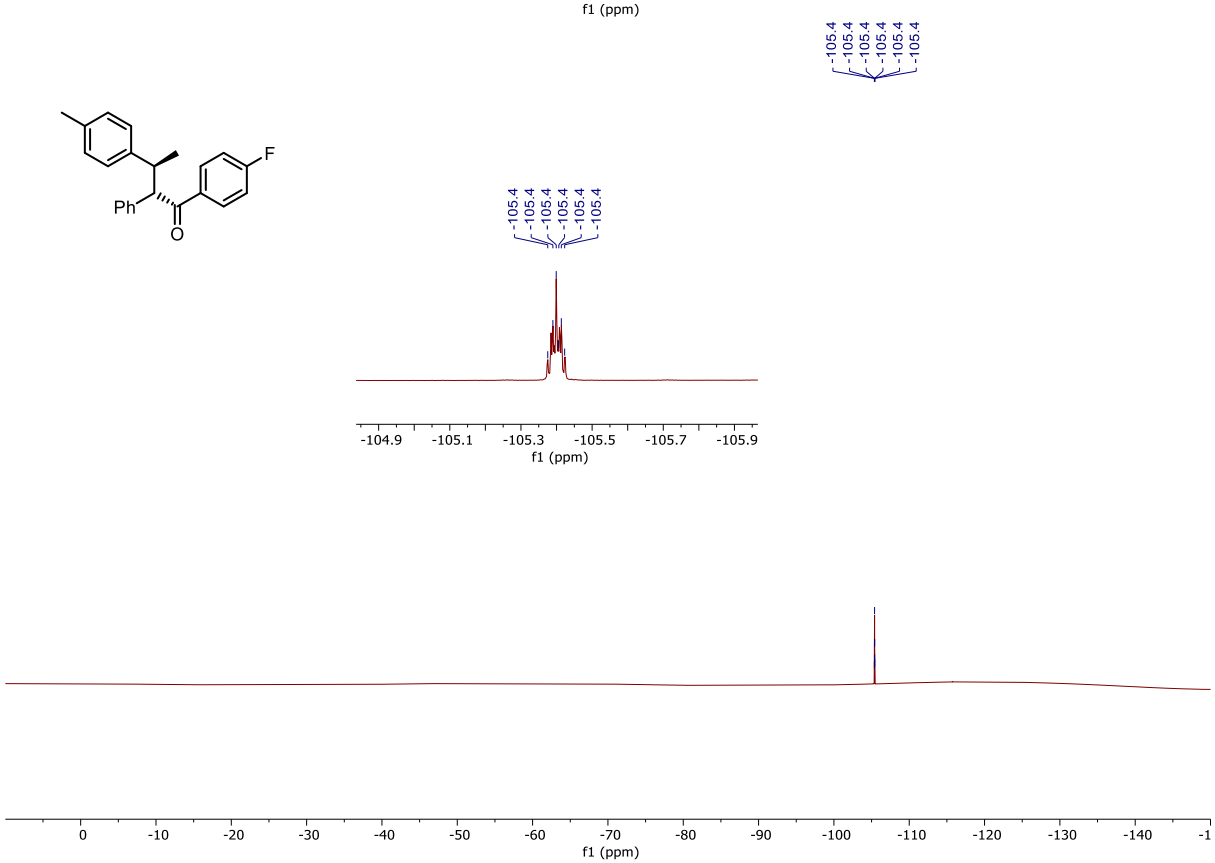
-105.4
-105.4
-105.4
-105.4
-105.4
-105.4
F
Ph
O
-104.9
-105.1
-105.3
-105.5
-105.7
-105.9
f1 (ppm)
f1 (ppm)

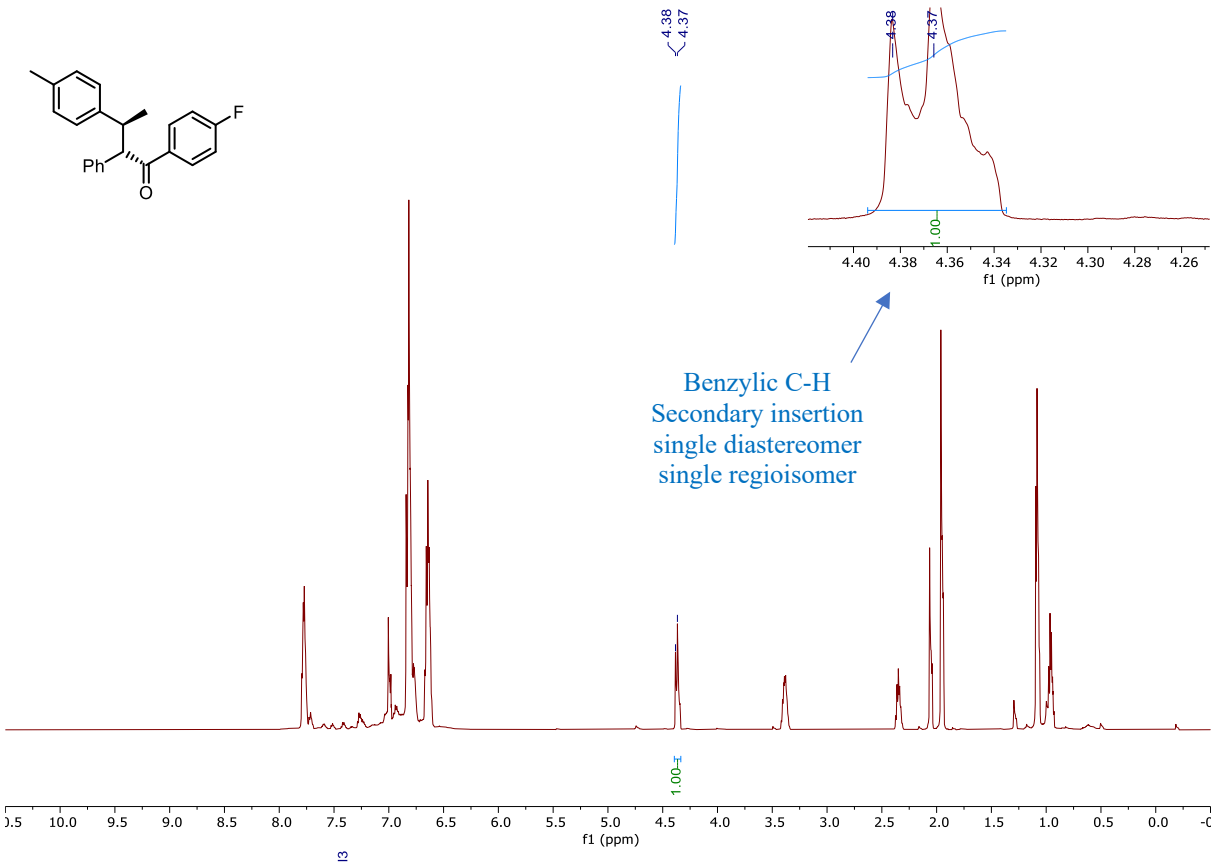
F
Ph
O
4.38
4.37
1.00
4.40 4.38 4.36 4.34 4.32 4.30 4.28 4.26
f1 (ppm)
Benzylic C-H
Secondary insertion
single diastereomer
single regioisomer
1.00
f1 (ppm)

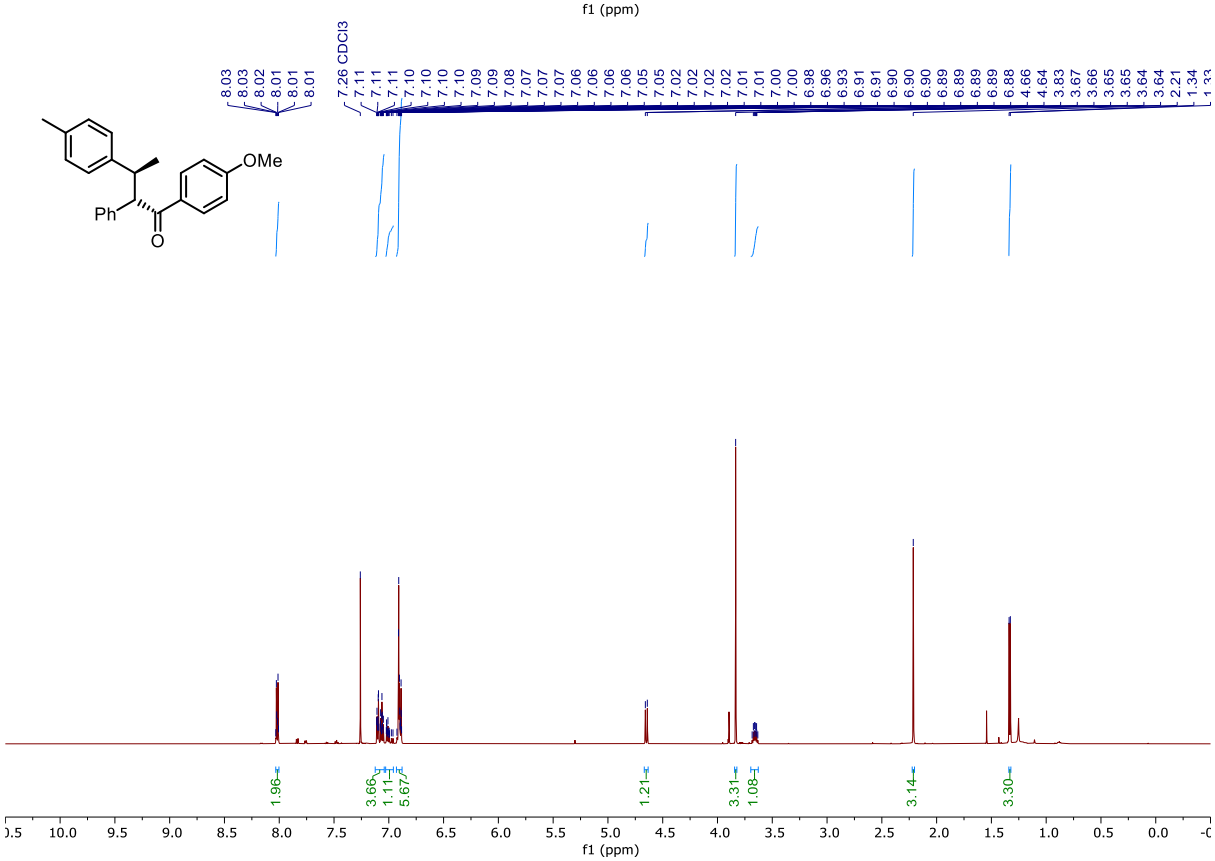
OMe
Ph
O
7.26 CDCl3
1.96
3.66
1.11
5.67
1.21
3.31
1.08
3.14
3.30
f1 (ppm)

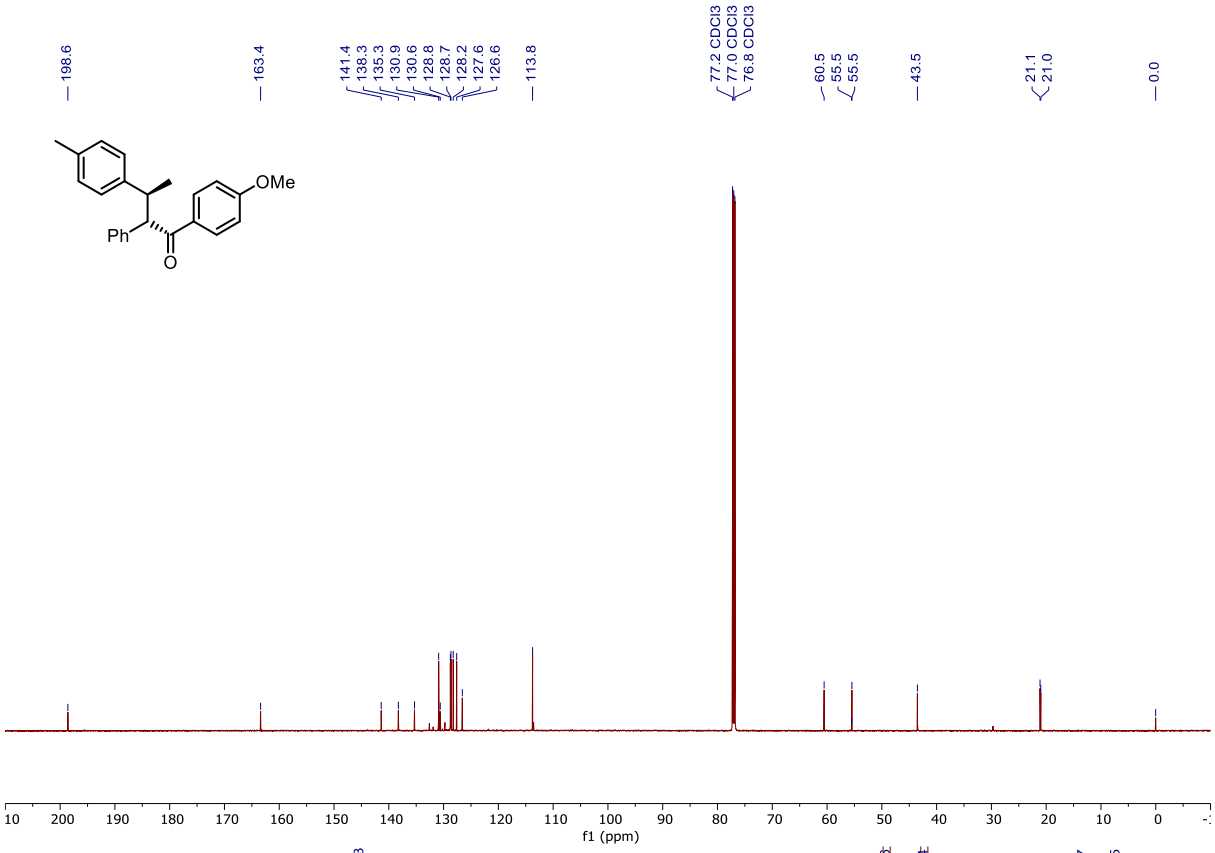
198.6
163.4
141.4
138.3
135.3
130.9
130.6
128.8
128.7
128.2
127.6
126.6
113.8
77.2 CDCl3
77.0 CDCl3
76.8 CDCl3
60.5
55.5
55.5
43.5
21.1
21.0
0.0
OMe
Ph
O
f1 (ppm)

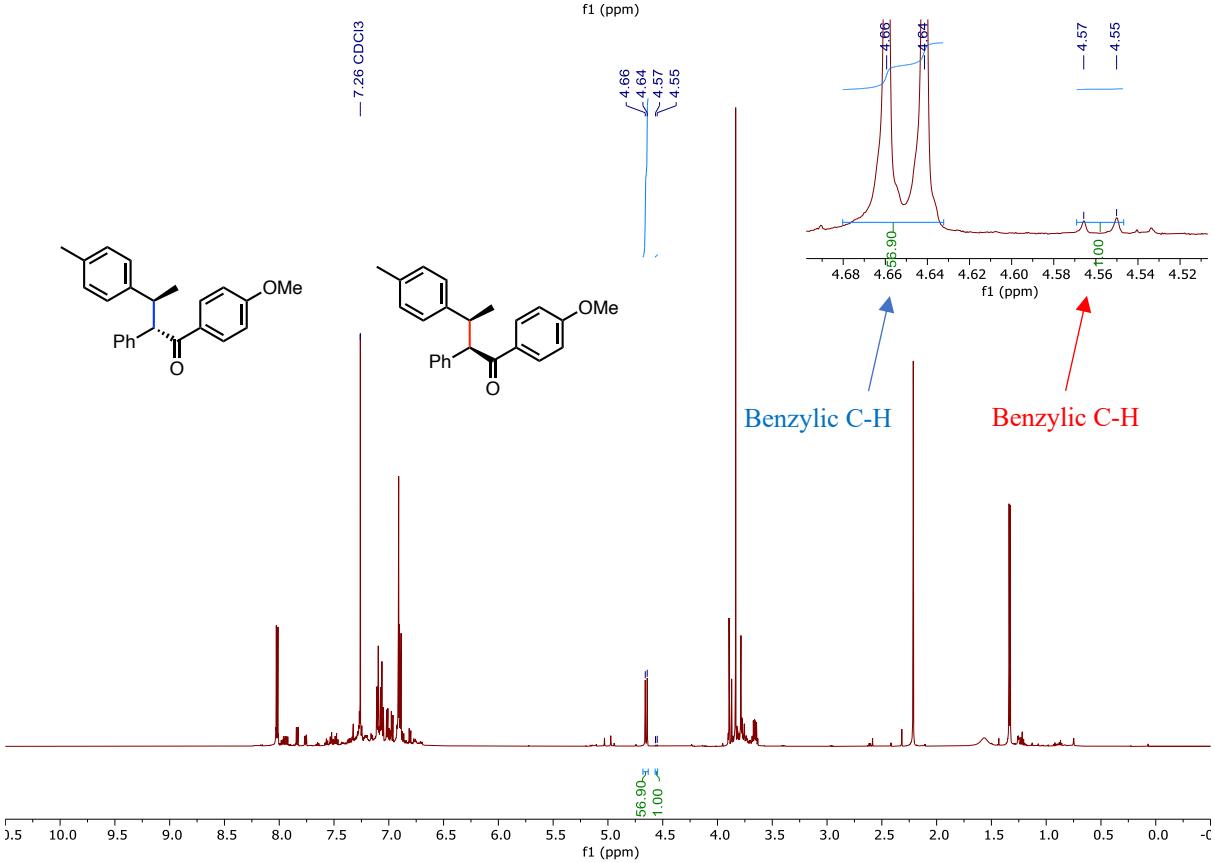
7.26 CDCl3
4.66
4.64
4.57
4.55
OMe
Ph
O
56.90
1.00
f1 (ppm)
Benzylic C-H
Benzylic C-H

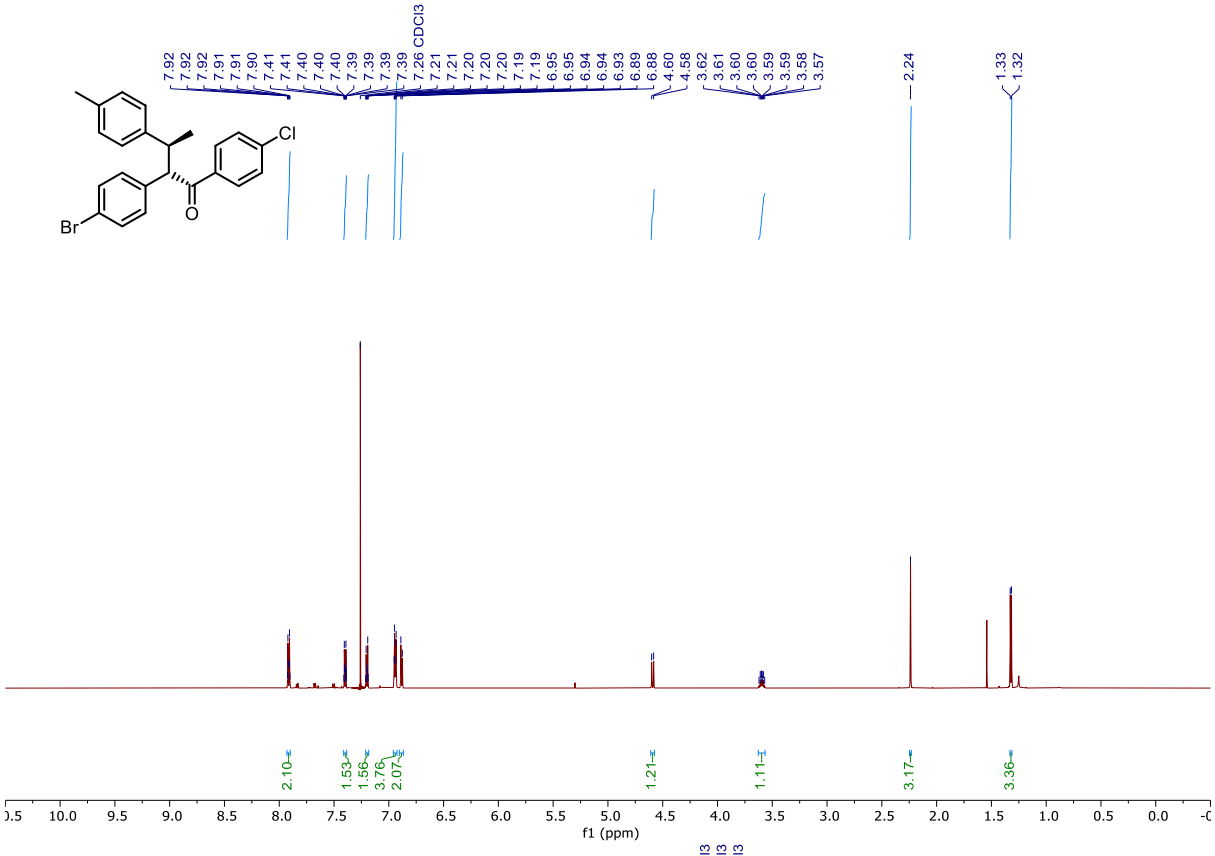
7.92
7.92
7.92
7.91
7.91
7.90
7.41
7.41
7.40
7.40
7.40
7.39
7.39
7.39
7.39
7.26 CDCl3
7.21
7.21
7.20
7.20
7.20
7.19
7.19
6.95
6.95
6.94
6.94
6.93
6.89
6.88
4.60
4.58
3.62
3.61
3.60
3.60
3.59
3.59
3.58
3.57
2.24
1.33
1.32
Cl
Br
O
2.10
1.53
1.56
3.76
2.07
1.21
1.11
3.17
3.36
f1 (ppm)

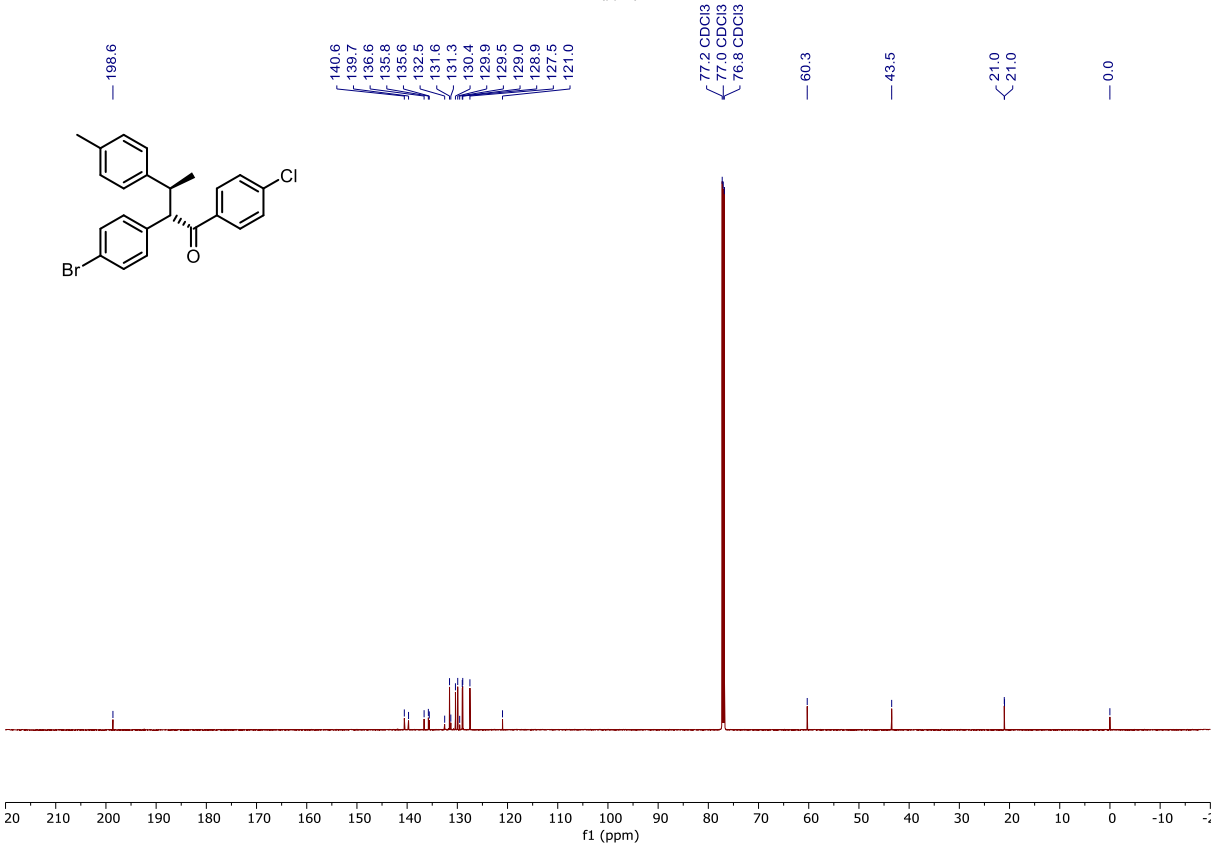
198.6
140.6
139.7
136.6
135.8
135.6
132.5
131.6
131.3
130.4
129.9
129.5
129.0
128.9
127.5
121.0
77.2 CDCl3
77.0 CDCl3
76.8 CDCl3
60.3
43.5
21.0
21.0
0.0
Cl
Br
O
f1 (ppm)

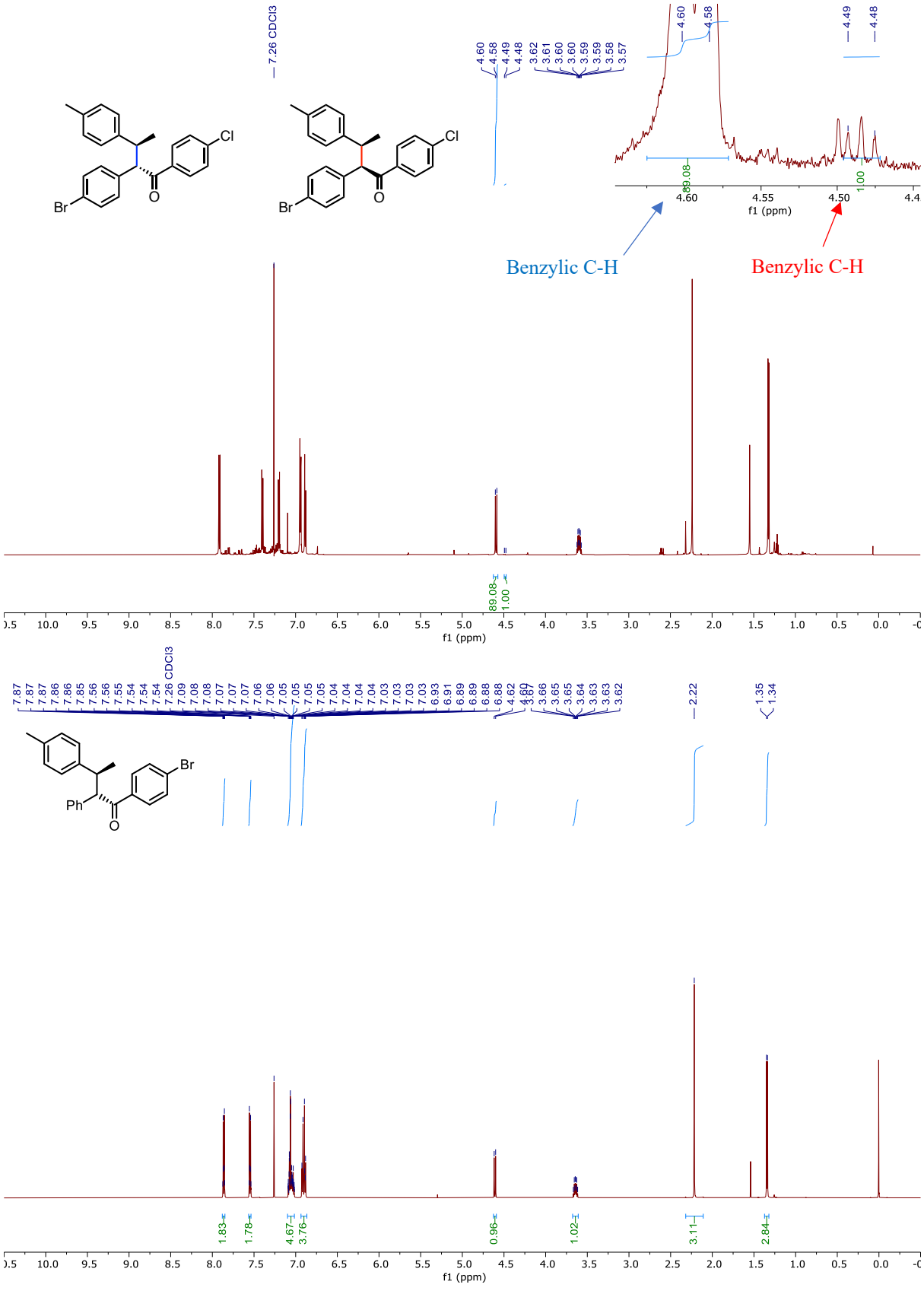
Cl
Br
O
7.26 CDCl3
4.60
4.58
4.49
4.48
3.62
3.61
3.60
3.59
3.59
3.58
3.57
89.08
1.00
f1 (ppm)
Benzylic C-H
Benzylic C-H
Br
Ph
O
7.87
7.87
7.87
7.86
7.86
7.85
7.56
7.56
7.55
7.54
7.54
7.54
7.26 CDCl3
7.09
7.08
7.08
7.07
7.07
7.07
7.06
7.06
7.05
7.05
7.05
7.05
7.04
7.04
7.04
7.04
7.03
7.03
7.03
7.03
6.93
6.91
6.89
6.89
6.88
6.88
4.62
3.66
3.65
3.65
3.64
3.63
3.63
3.62
2.22
1.35
1.34
1.83
1.78
4.67
3.76
0.96
1.02
3.11
2.84

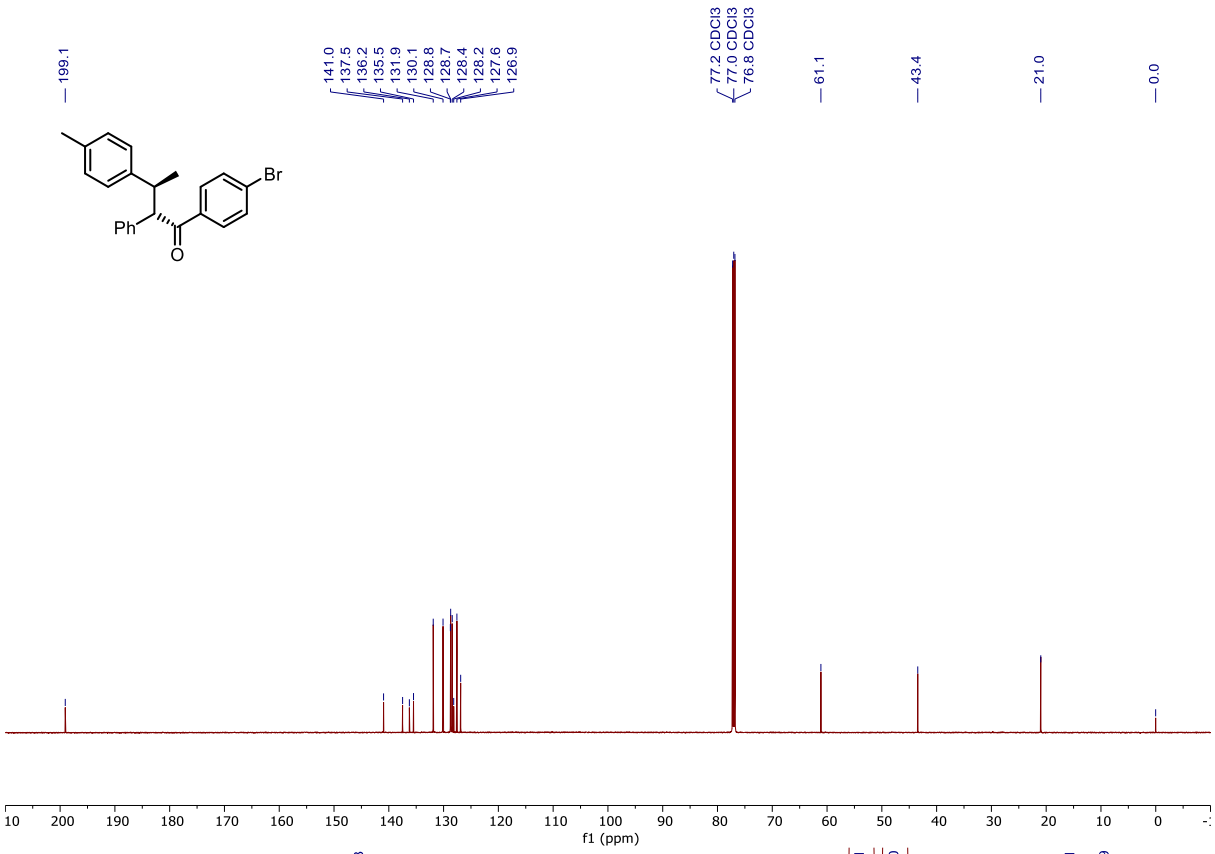
199.1
141.0
137.5
136.2
135.5
131.9
130.1
128.8
128.7
128.4
128.2
127.6
126.9
77.2 CDCl3
77.0 CDCl3
76.8 CDCl3
61.1
43.4
21.0
0.0
Br
Ph
O
f1 (ppm)

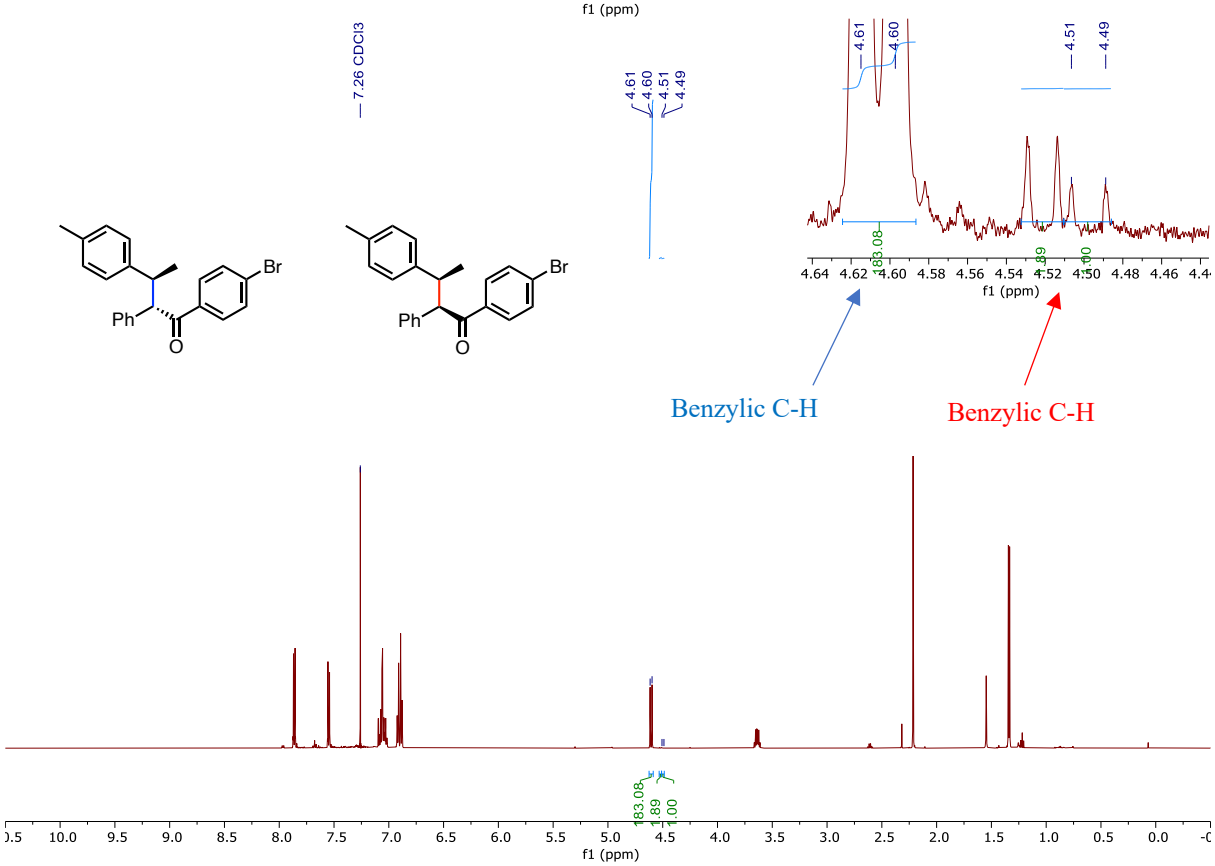
7.26 CDCl3
4.61
4.60
4.51
4.49
183.08
1.89
1.00
Br
Ph
O
Benzylic C-H
Benzylic C-H
f1 (ppm)

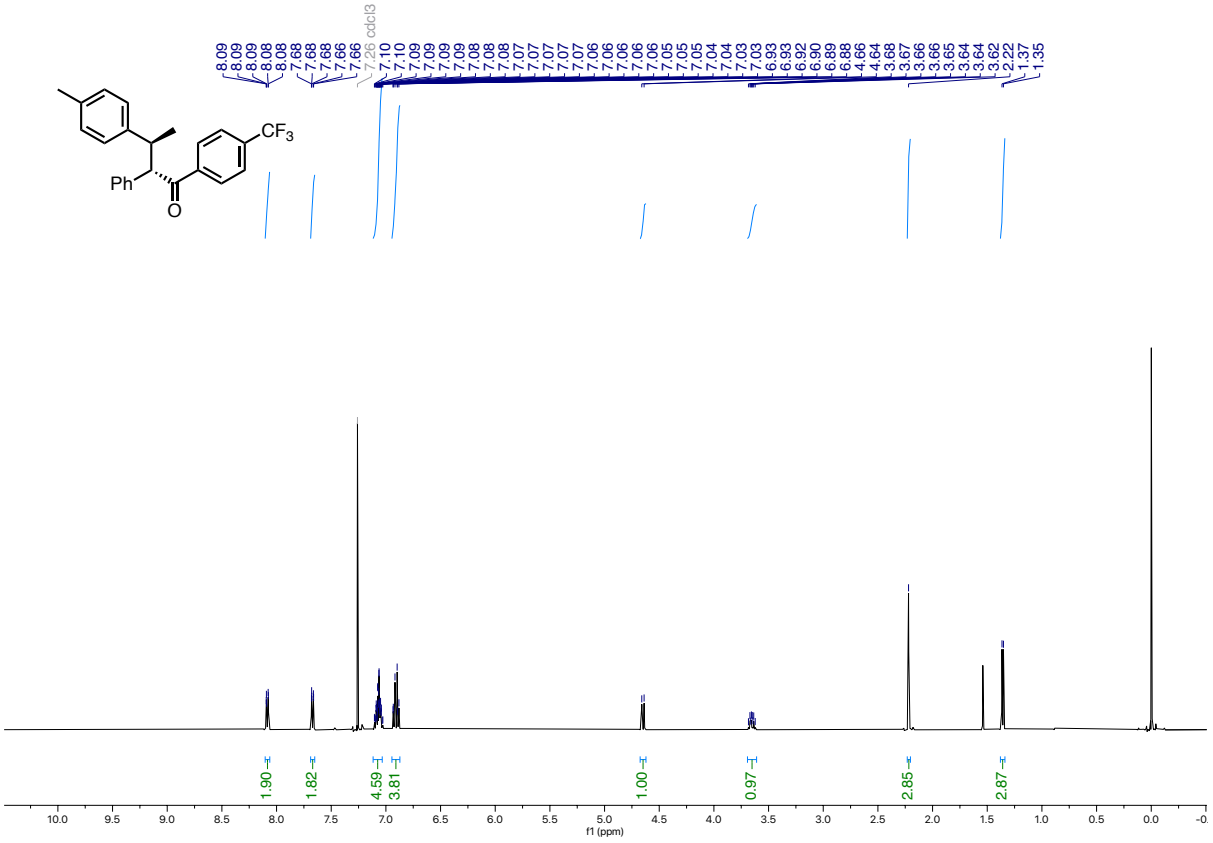
8.09
8.09
8.09
8.08
8.08
7.88
7.88
7.88
7.66
7.66
7.26 cdcl3
7.10
7.10
7.09
7.09
7.09
7.09
7.08
7.08
7.08
7.07
7.07
7.07
7.07
7.07
7.06
7.06
7.06
7.06
7.06
7.06
7.05
7.05
7.05
7.04
7.04
7.03
7.03
6.93
6.93
6.92
6.90
6.89
6.88
4.66
4.64
3.68
3.67
3.66
3.66
3.65
3.64
3.62
2.22
1.37
1.35
CF3
Ph
O
1.90
1.82
4.59
3.81
1.00
0.97
2.85
2.87
f1 (ppm)

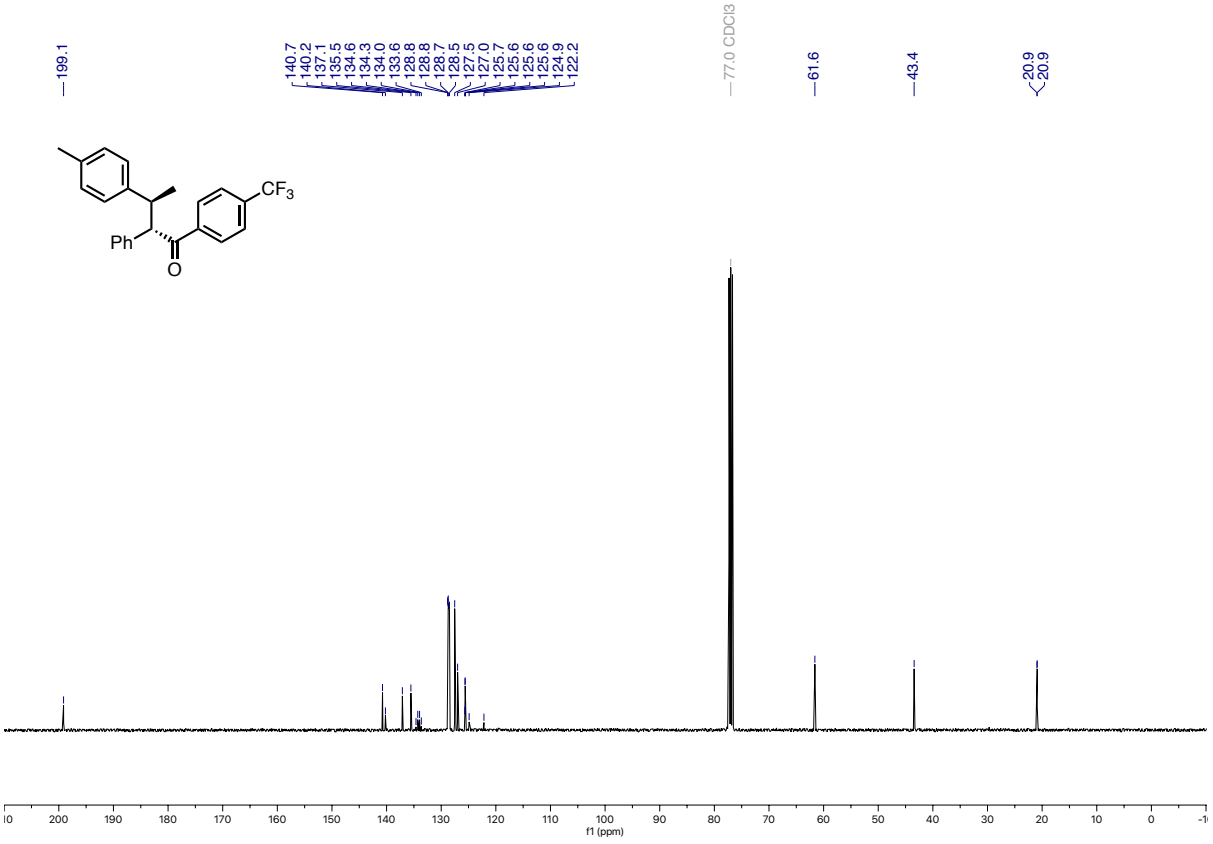
199.1
140.7
140.2
137.1
135.5
134.6
134.3
134.0
133.6
128.8
128.8
128.7
128.5
127.5
127.0
125.7
125.6
125.6
125.6
124.9
122.2
77.0 CDCl3
61.6
43.4
20.9
20.9
CF3
Ph
O
f1 (ppm)

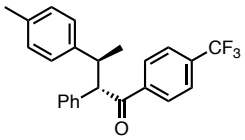
CF3
Ph
O

-63.2
-63.2
-61.5 -62.0 -62.5 -63.0 -63.5 -64.0 -64.5 -65.0
f1 (ppm)
0 -10 -20 -30 -40 -50 -60 -70 -80 -90 -100 -110 -120 -130 -140
f1 (ppm)

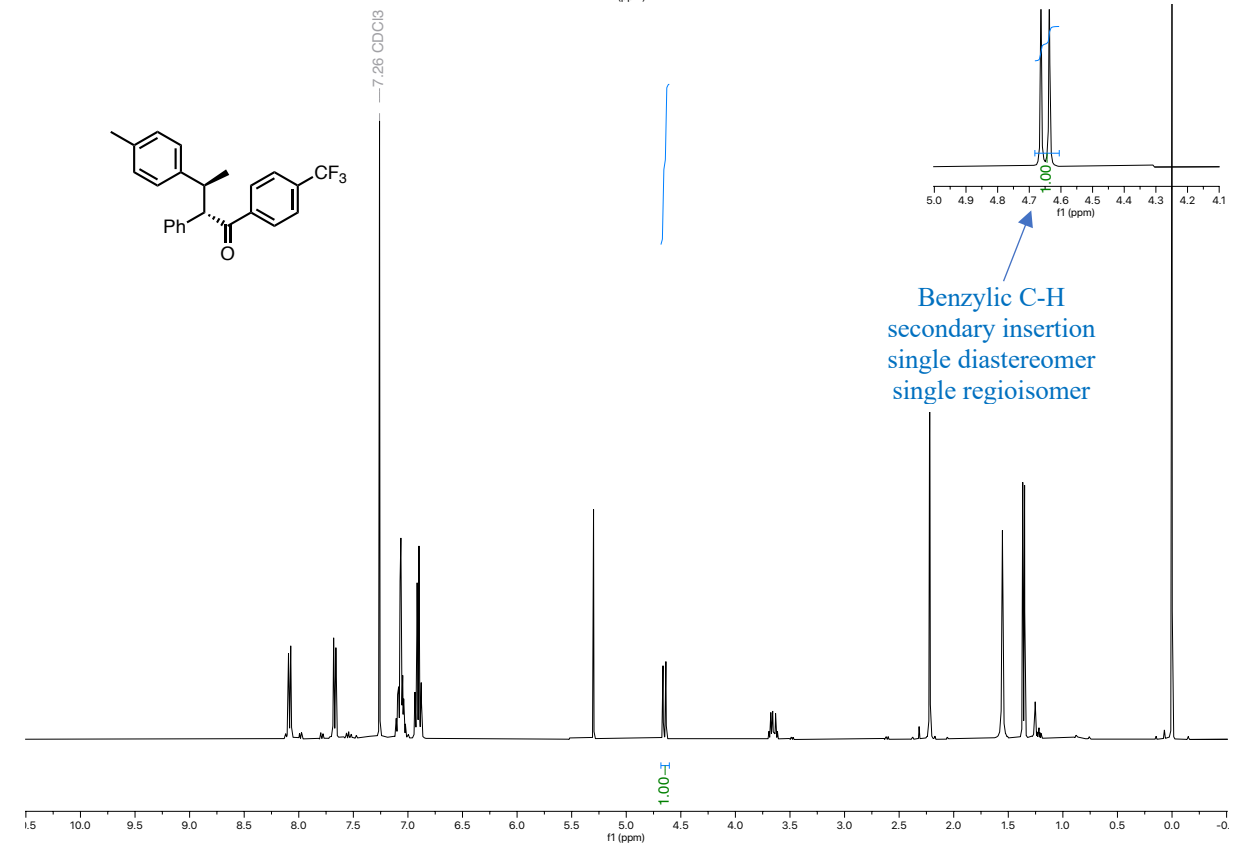
7.26 CDCl3
CF3
Ph
O
1.00
5.0 4.9 4.8 4.7 4.6 4.5 4.4 4.3 4.2
f1 (ppm)
Benzylic C-H
secondary insertion
single diastereomer
single regioisomer
1.00
10.0 9.5 9.0 8.5 8.0 7.5 7.0 6.5 6.0 5.5 5.0 4.5 4.0 3.5 3.0 2.5 2.0 1.5 1.0 0.5 0.0
f1 (ppm)

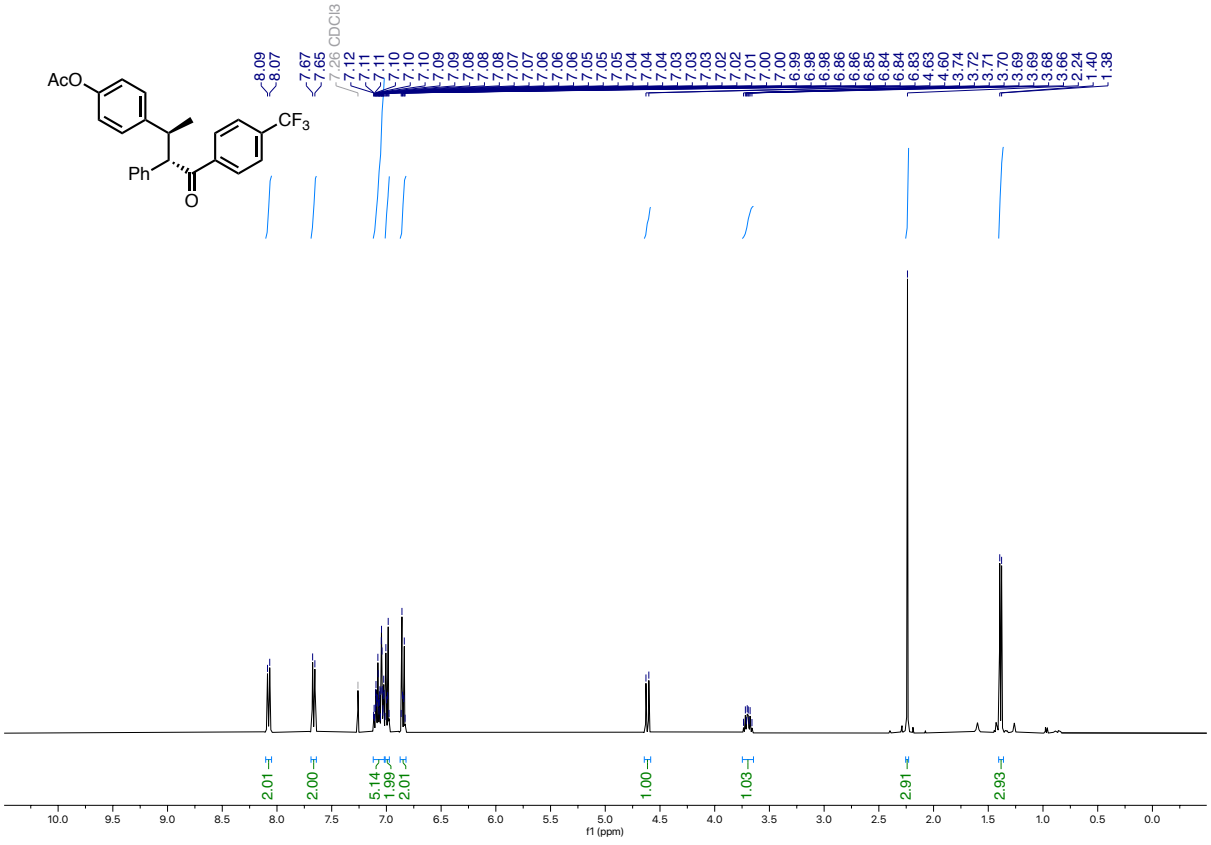
AcO
CF3
Ph
O
8.09
8.07
7.67
7.65
7.26 CDCl3
7.12
7.11
7.10
7.10
7.10
7.09
7.09
7.08
7.08
7.07
7.07
7.06
7.06
7.06
7.05
7.05
7.04
7.04
7.04
7.03
7.03
7.02
7.02
7.01
7.00
7.00
6.99
6.98
6.98
6.86
6.85
6.84
6.84
6.83
4.63
4.60
3.74
3.72
3.71
3.70
3.69
3.69
3.68
3.66
2.24
1.40
1.38
2.01
2.00
5.14
1.99
2.01
1.00
1.03
2.91
2.93
f1 (ppm)

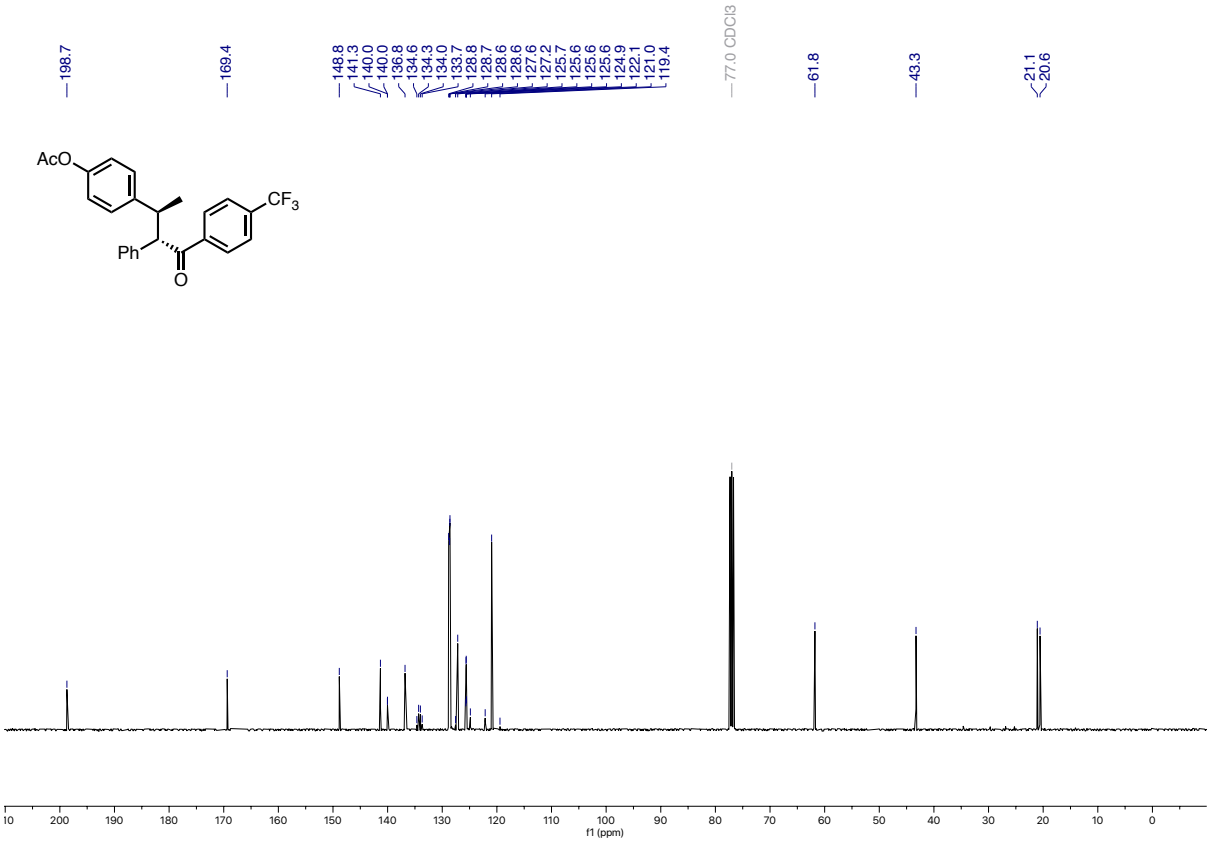
198.7
169.4
148.8
141.3
140.0
140.0
136.8
134.6
134.3
134.0
133.7
128.8
128.7
128.6
128.6
127.6
127.2
125.7
125.6
125.6
125.6
124.9
122.1
121.0
119.4
77.0 CDCl3
61.8
43.3
21.1
20.6
AcO
CF3
Ph
O
f1 (ppm)

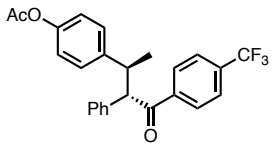
AcO
CF3
Ph
O

-63.2
-63.2
-62.5
-63.0
-63.5
-64.0
f1 (ppm)

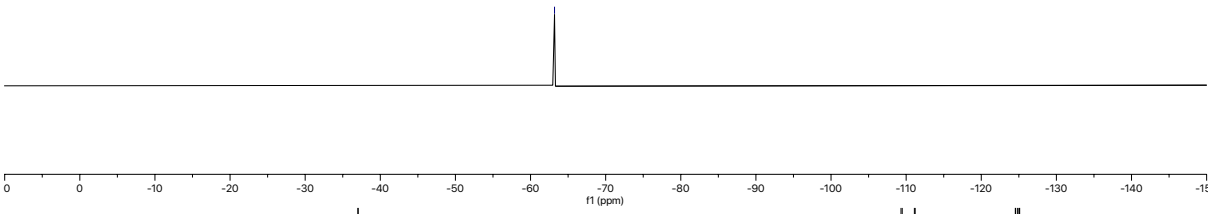
0
-10
-20
-30
-40
-50
-60
-70
-80
-90
-100
-110
-120
-130
-140
f1 (ppm)

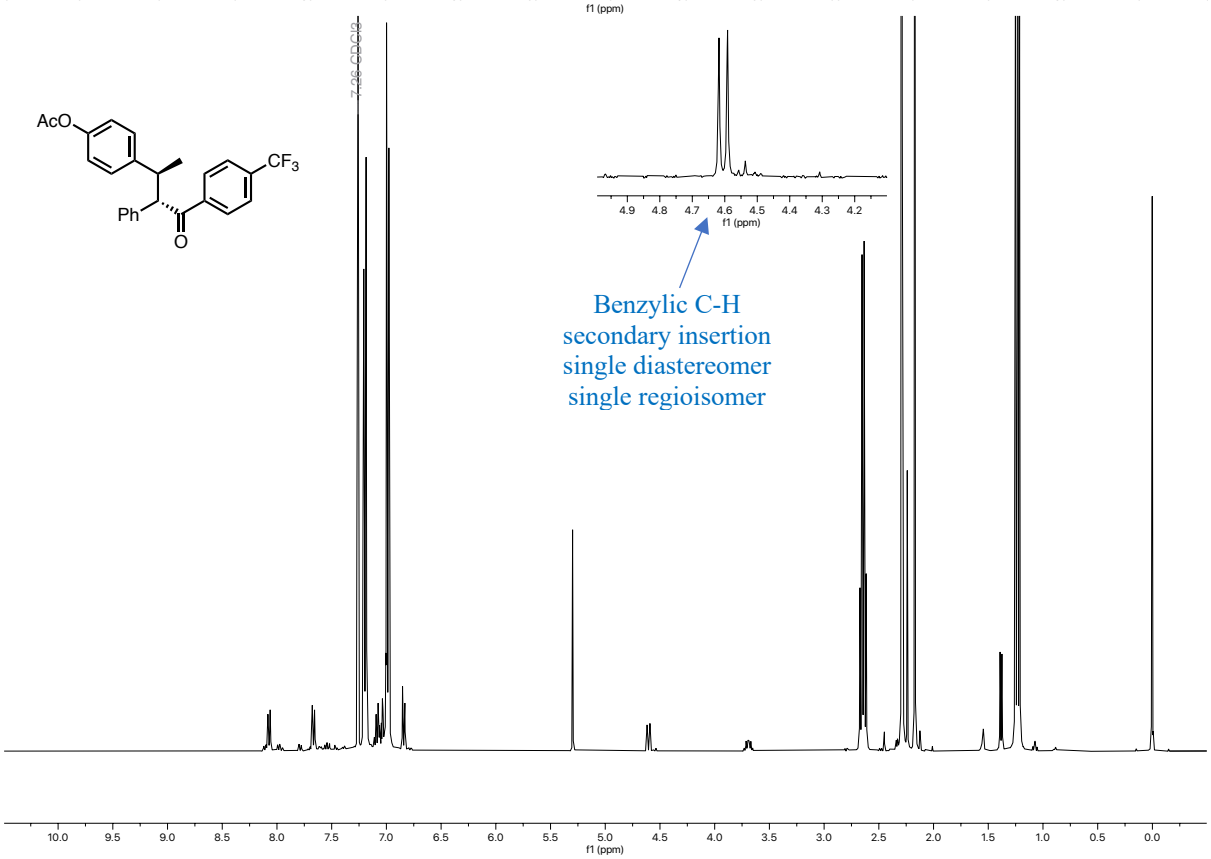
AcO
CF3
Ph
O
7.26 CDCl3
4.9
4.8
4.7
4.6
4.5
4.4
4.3
4.2
f1 (ppm)
Benzylic C-H
secondary insertion
single diastereomer
single regioisomer
10.0
9.5
9.0
8.5
8.0
7.5
7.0
6.5
6.0
5.5
5.0
4.5
4.0
3.5
3.0
2.5
2.0
1.5
1.0
0.5
0.0
f1 (ppm)

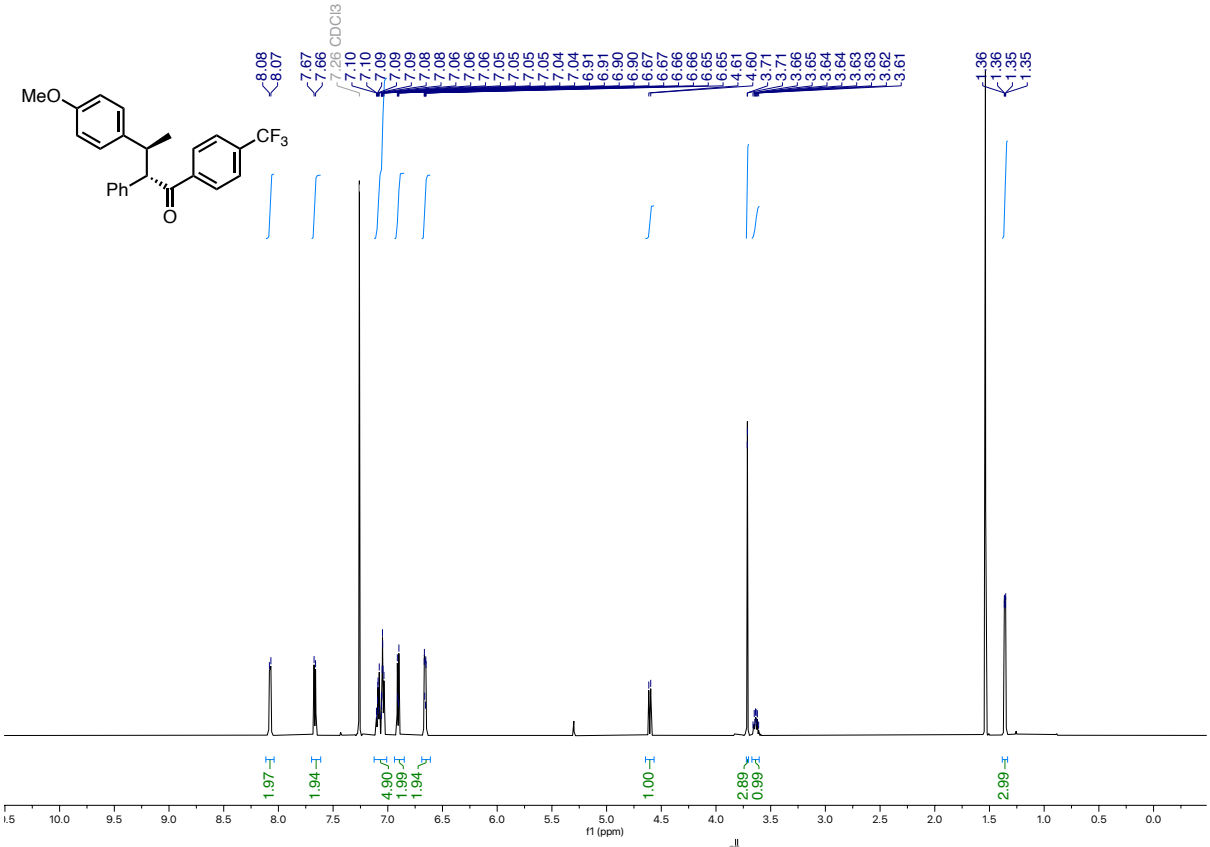
MeO
CF3
Ph
O
8.08
8.07
7.67
7.66
7.26 CDCl3
7.10
7.09
7.08
7.06
7.05
7.04
6.91
6.90
6.67
6.66
6.65
4.61
4.60
3.71
3.66
3.65
3.64
3.63
3.62
3.61
1.36
1.35
1.97
1.94
4.90
1.99
1.94
1.00
2.89
0.99
2.99
f1 (ppm)

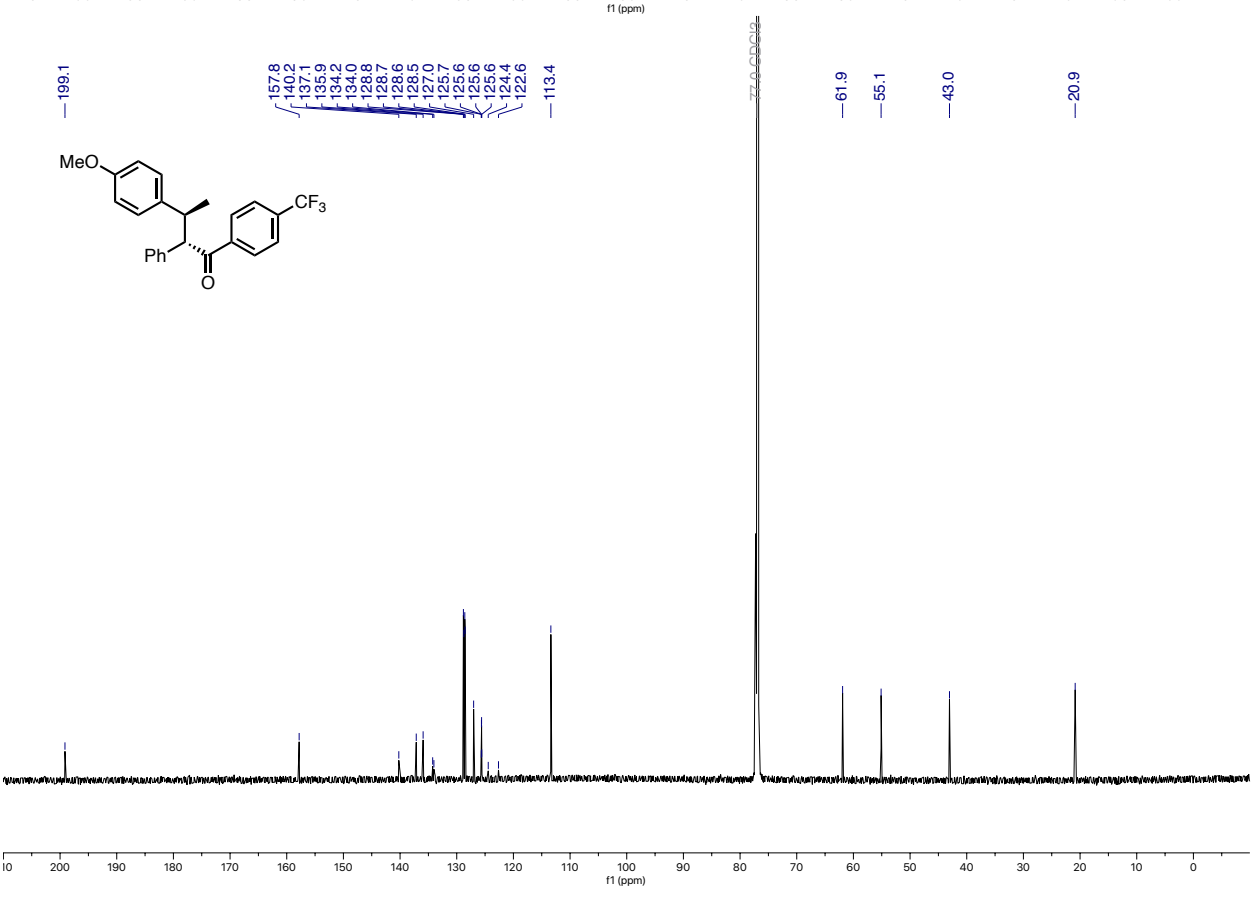
MeO
CF3
Ph
O
199.1
157.8
140.2
137.1
135.9
134.2
134.0
128.8
128.7
128.6
128.5
127.0
125.7
125.6
125.6
125.6
124.4
122.6
113.4
77.0 CDCl3
61.9
55.1
43.0
20.9
f1 (ppm)

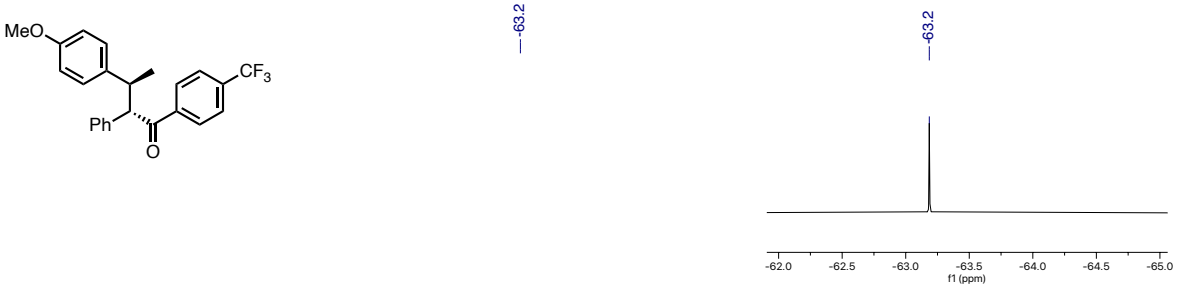
MeO
CF3
Ph
O
-63.2
-63.2
-62.0
-62.5
-63.0
-63.5
-64.0
-64.5
-65.0
f1 (ppm)

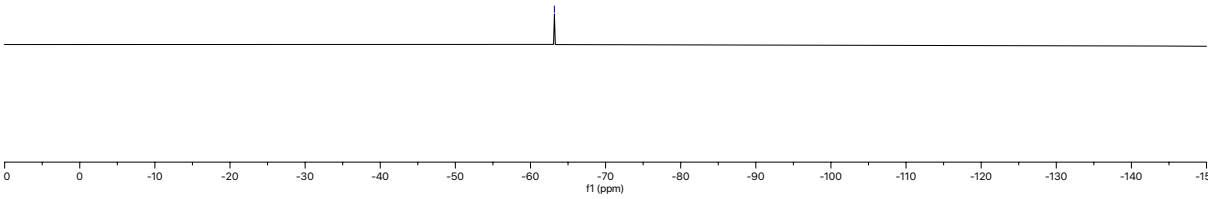
0
-10
-20
-30
-40
-50
-60
-70
-80
-90
-100
-110
-120
-130
-140
f1 (ppm)

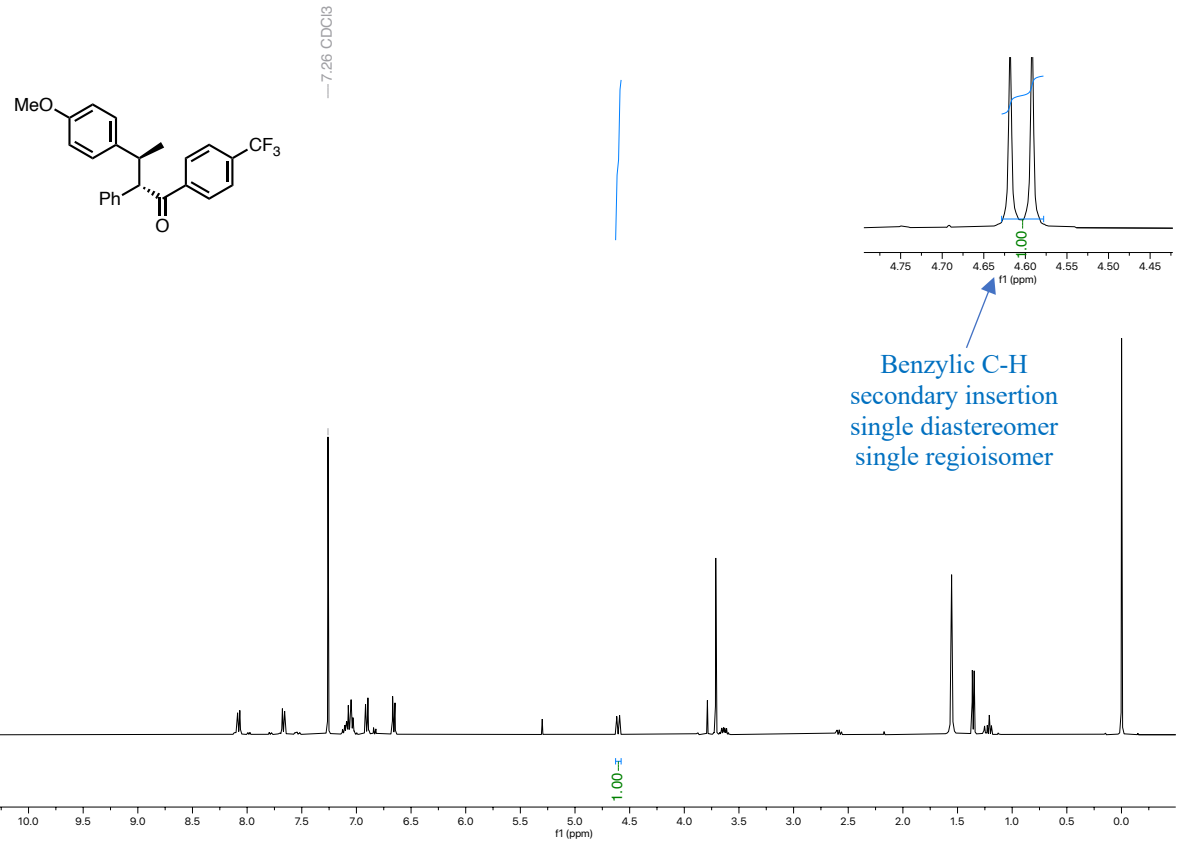
7.26 CDCl3
MeO
CF3
Ph
O
1.00
4.75
4.70
4.65
4.60
4.55
4.50
4.45
f1 (ppm)
Benzylic C-H
secondary insertion
single diastereomer
single regioisomer
1.00
10.0
9.5
9.0
8.5
8.0
7.5
7.0
6.5
6.0
5.5
5.0
4.5
4.0
3.5
3.0
2.5
2.0
1.5
1.0
0.5
0.0
f1 (ppm)

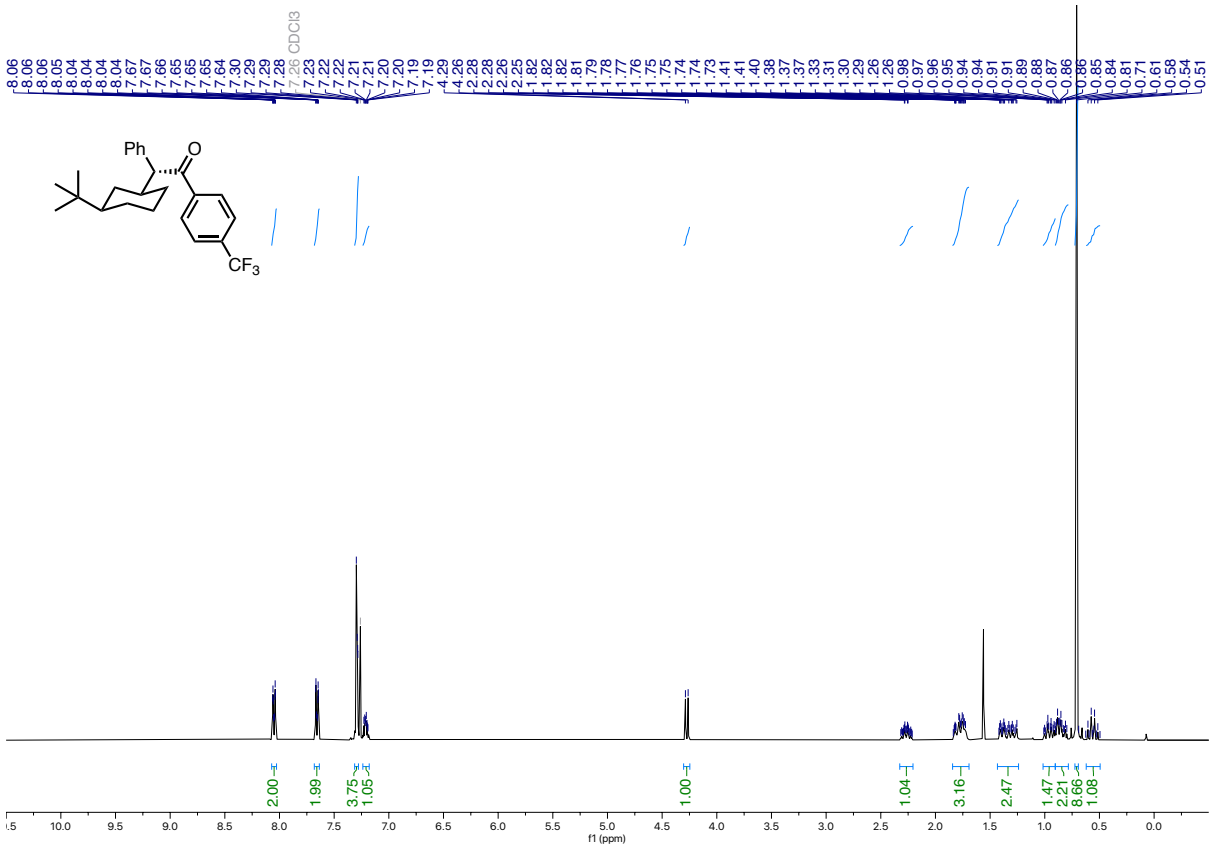
Ph
O
CF3
CDCl3
f1 (ppm)

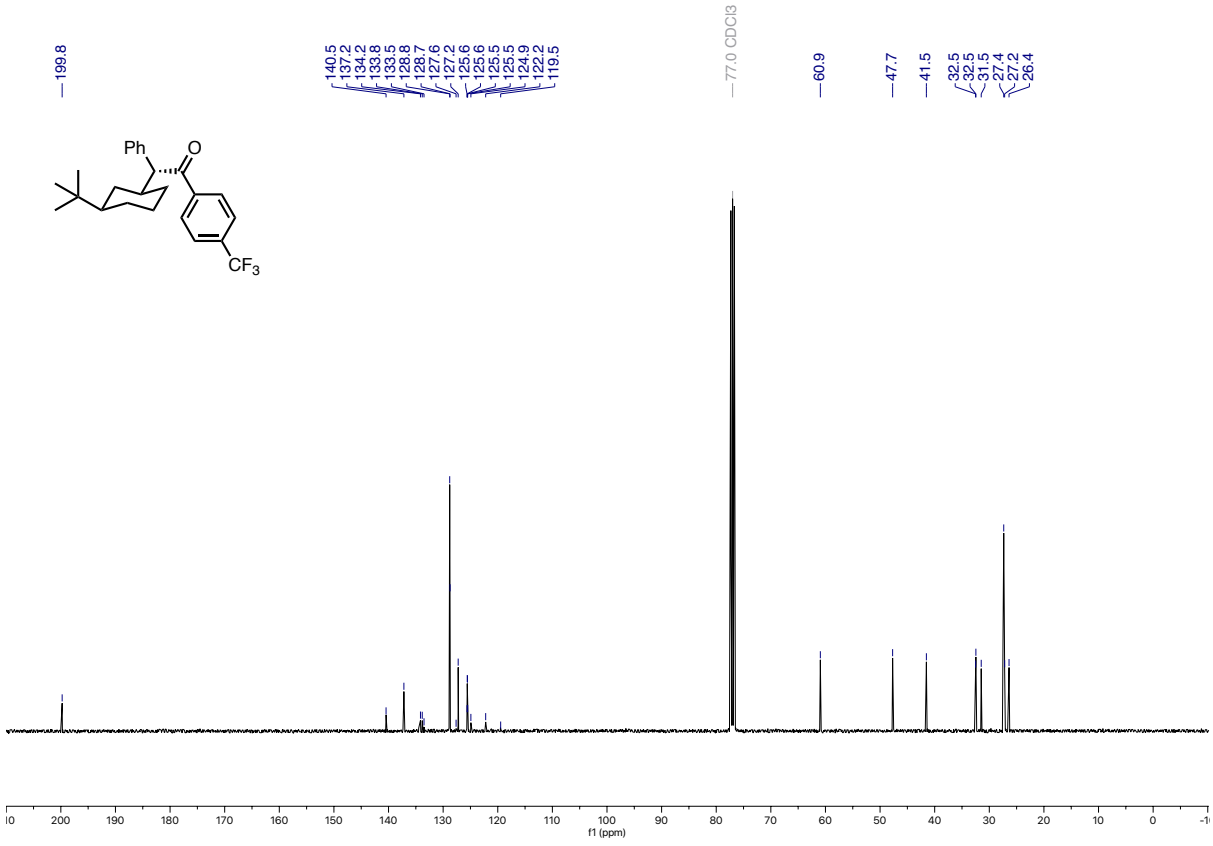
Ph
O
CF3
CDCl3
f1 (ppm)

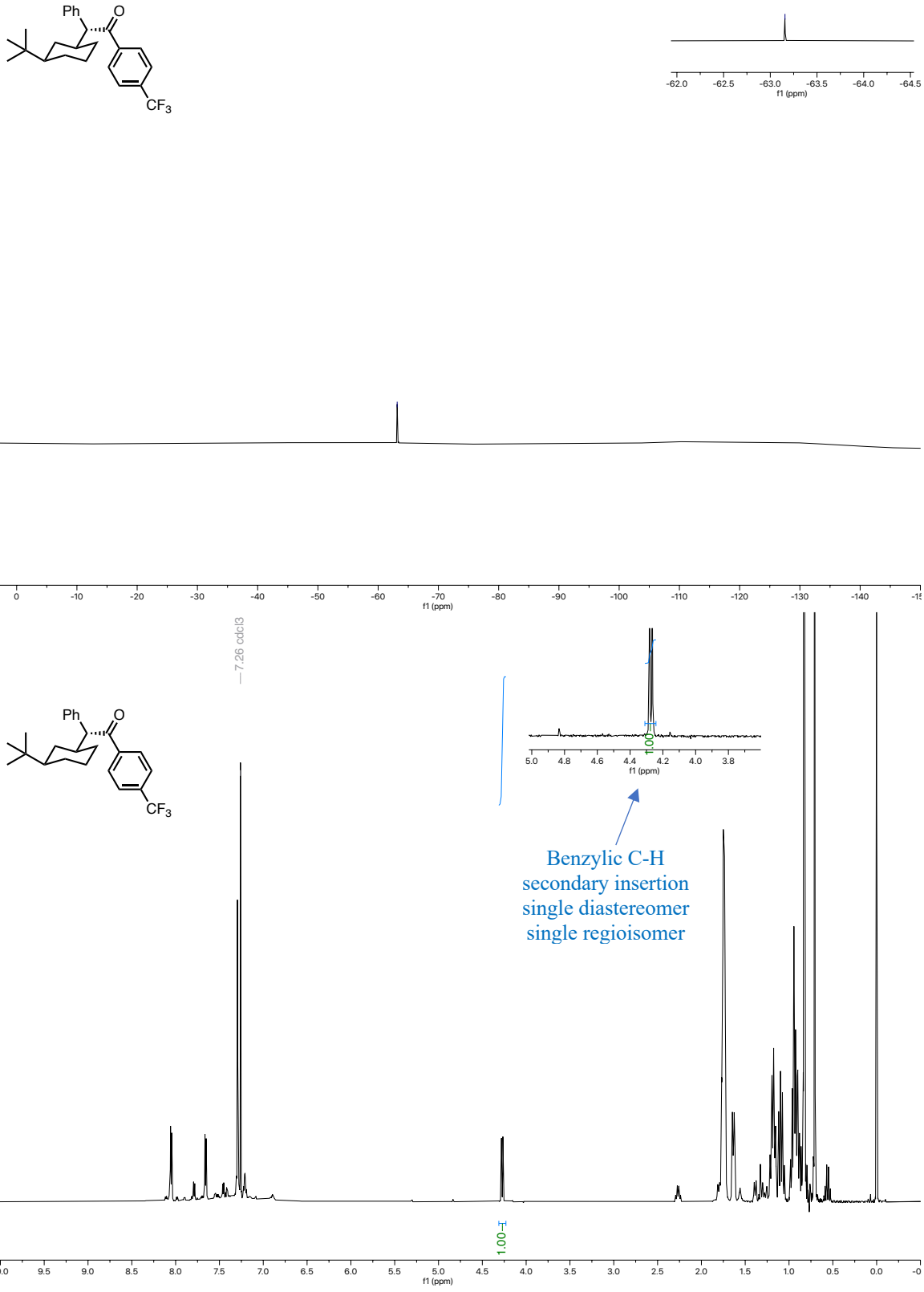
-63.2
-63.2
Ph
O
CF3
-62.0
-62.5
-63.0
-63.5
-64.0
-64.5
f1 (ppm)
0
-10
-20
-30
-40
-50
-60
-70
-80
-90
-100
-110
-120
-130
-140
7.26 cdcl3
1.00
5.0
4.8
4.6
4.4
4.2
4.0
3.8
Benzylic C-H
secondary insertion
single diastereomer
single regioisomer
10.0
9.5
9.0
8.5
8.0
7.5
7.0
6.5
6.0
5.5
5.0
4.5
4.0
3.5
3.0
2.5
2.0
1.5
1.0
0.5
0.0

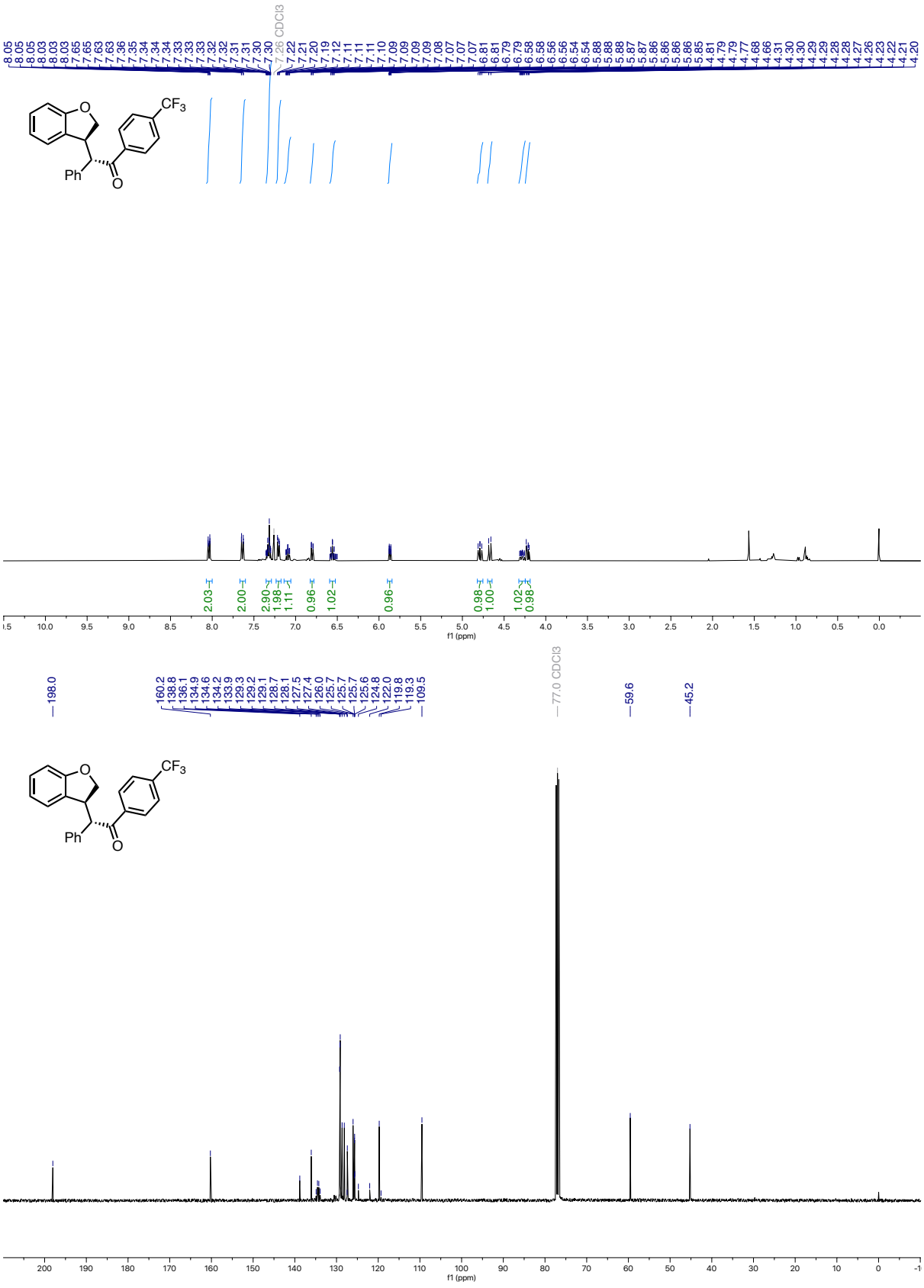
CDCl3
CF3
O
Ph
O
f1 (ppm)
CDCl3
CF3
O
Ph
O
f1 (ppm)

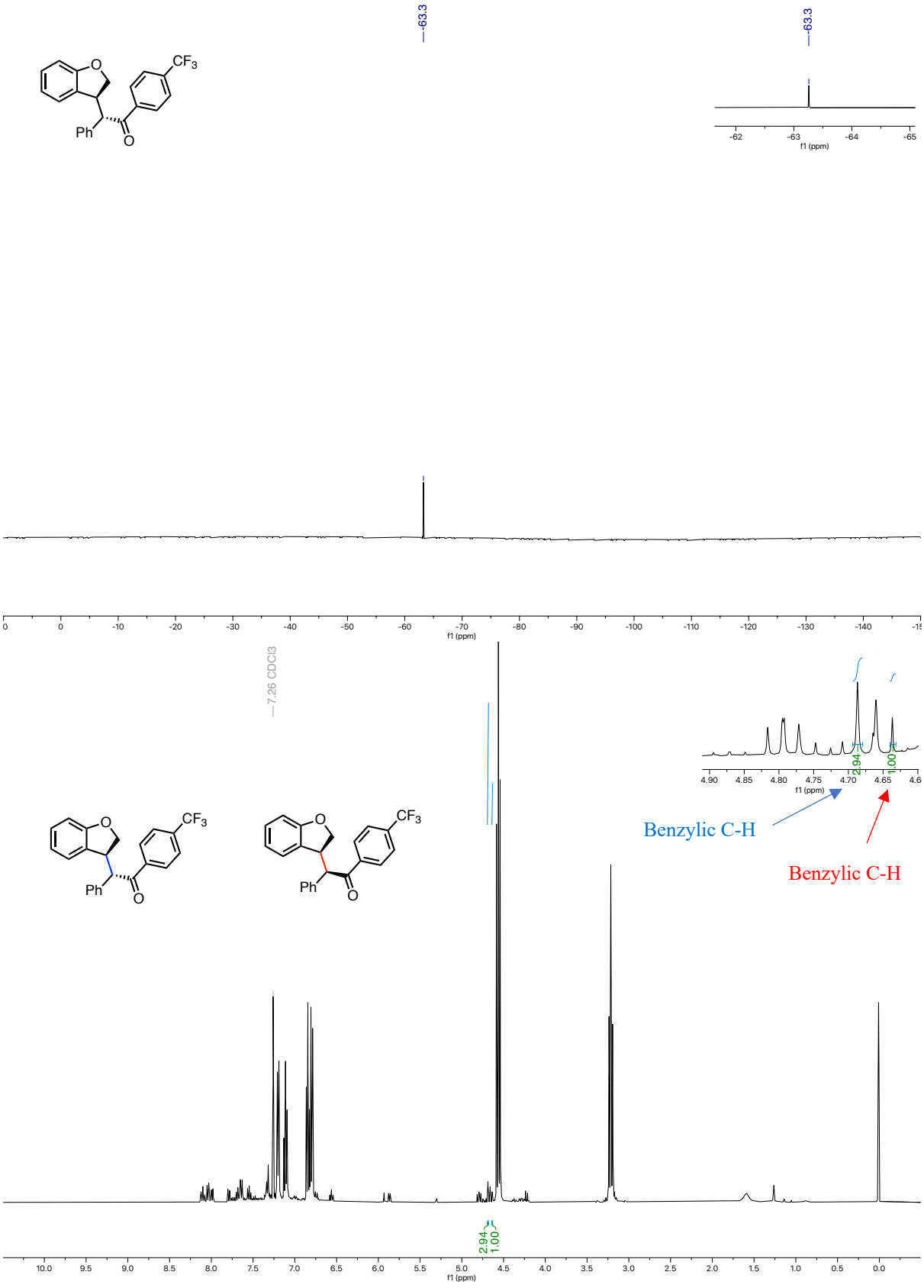
-63.3
-63.3
CF3
O
Ph
O
f1 (ppm)
7.26 CDCl3
2.94
1.00
Benzylic C-H
Benzylic C-H

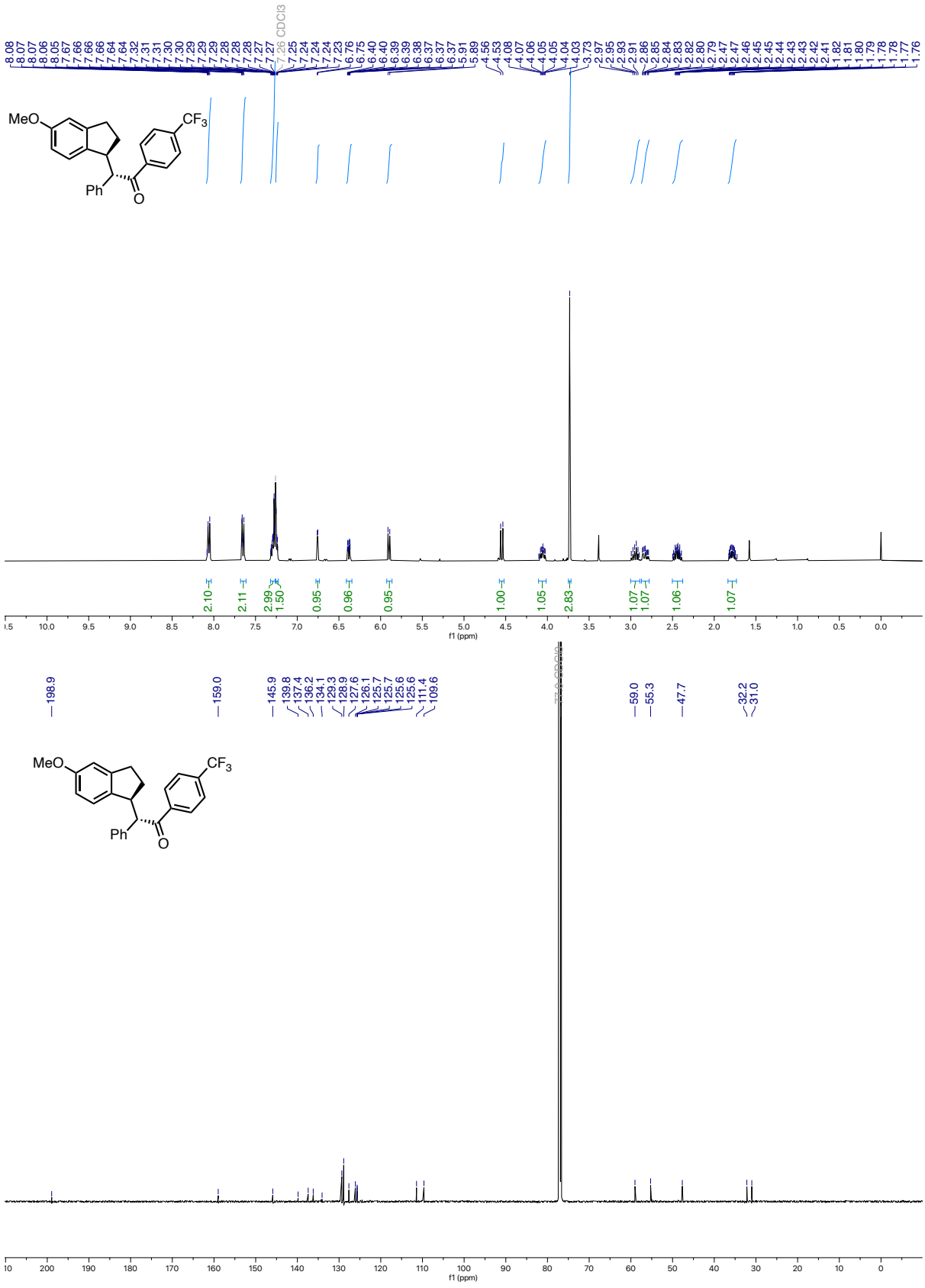
CDCl3
MeO
CF3
Ph
O
f1 (ppm)

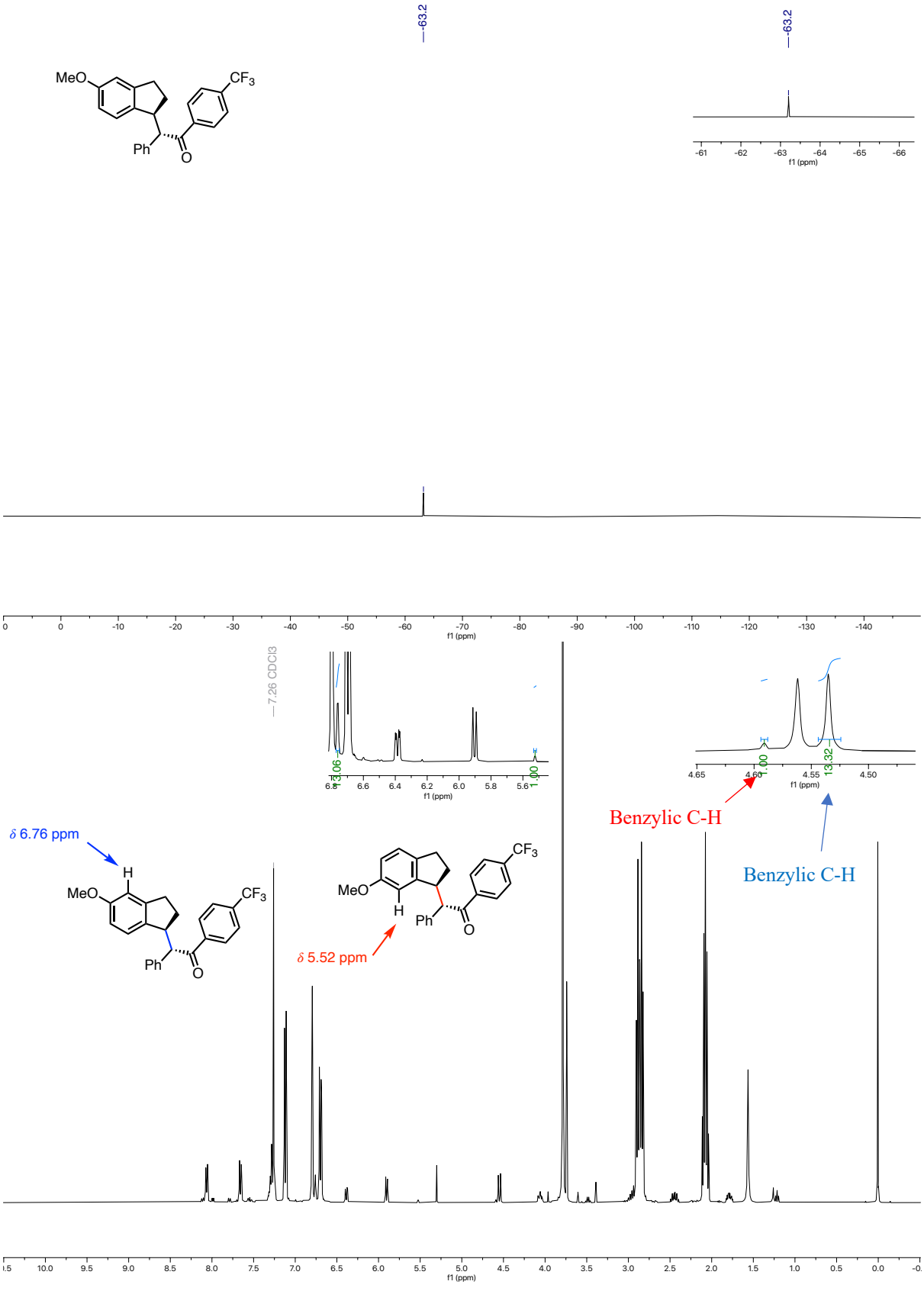
MeO
CF3
Ph
O
-63.2
-63.2
f1 (ppm)
7.26 CDCl3
δ 6.76 ppm
δ 5.52 ppm
Benzylic C-H
Benzylic C-H

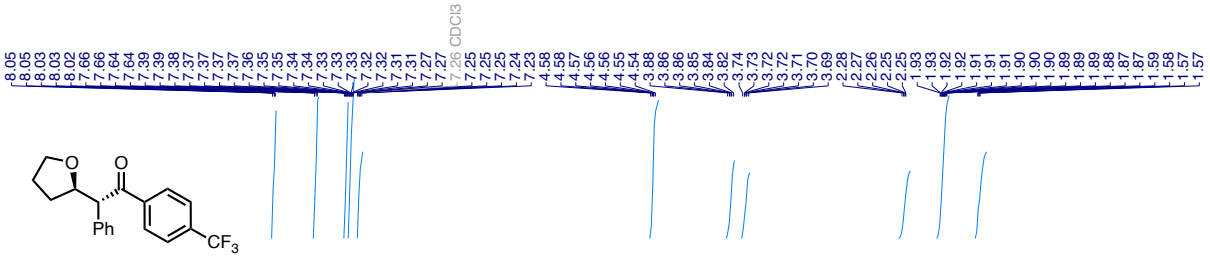
8.05
8.05
8.03
8.03
8.02
7.66
7.64
7.64
7.39
7.38
7.37
7.37
7.37
7.36
7.35
7.35
7.34
7.34
7.33
7.33
7.32
7.31
7.31
7.27
7.26 CDCl3
7.25
7.25
7.24
7.23
4.58
4.58
4.57
4.56
4.56
4.55
4.54
3.88
3.86
3.86
3.85
3.84
3.82
3.74
3.73
3.72
3.72
3.71
3.70
3.69
2.28
2.27
2.26
2.25
2.25
1.93
1.93
1.92
1.92
1.91
1.91
1.91
1.90
1.90
1.90
1.89
1.89
1.89
1.88
1.87
1.87
1.59
1.58
1.57
1.57
O
O
Ph
CF3

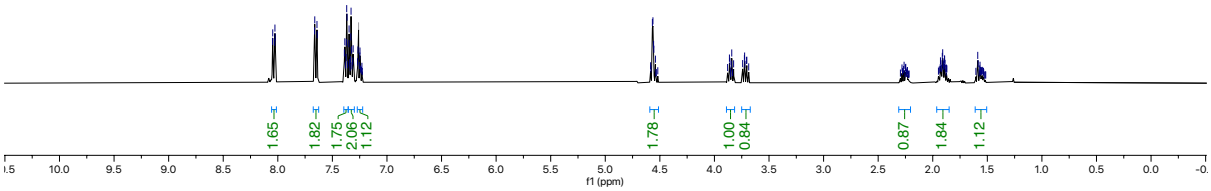
1.65
1.82
1.75
2.06
1.12
1.78
1.00
0.84
0.87
1.84
1.12
f1 (ppm)


197.9
139.4
136.6
134.7
134.4
134.0
133.7
129.1
129.0
129.0
128.7
127.7
127.5
125.7
125.6
125.6
125.6
124.8
122.1
119.4
81.0
77.0 CDCl3
68.0
59.6
30.8
25.7

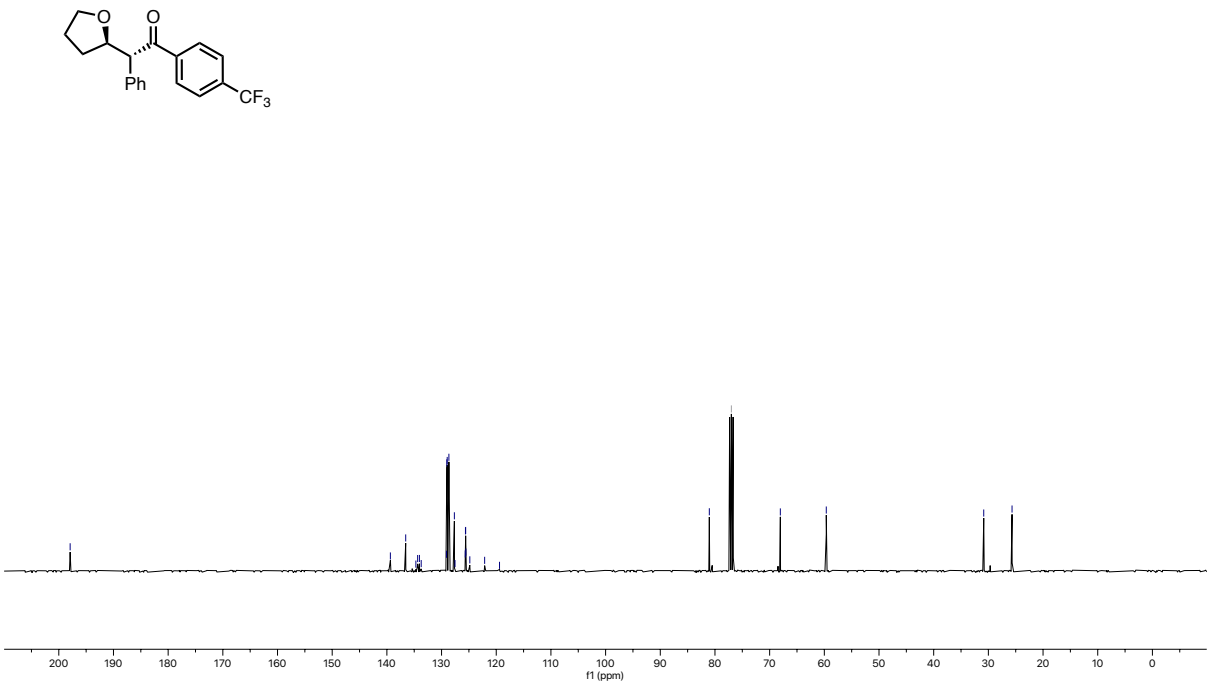
O
O
Ph
CF3
f1 (ppm)

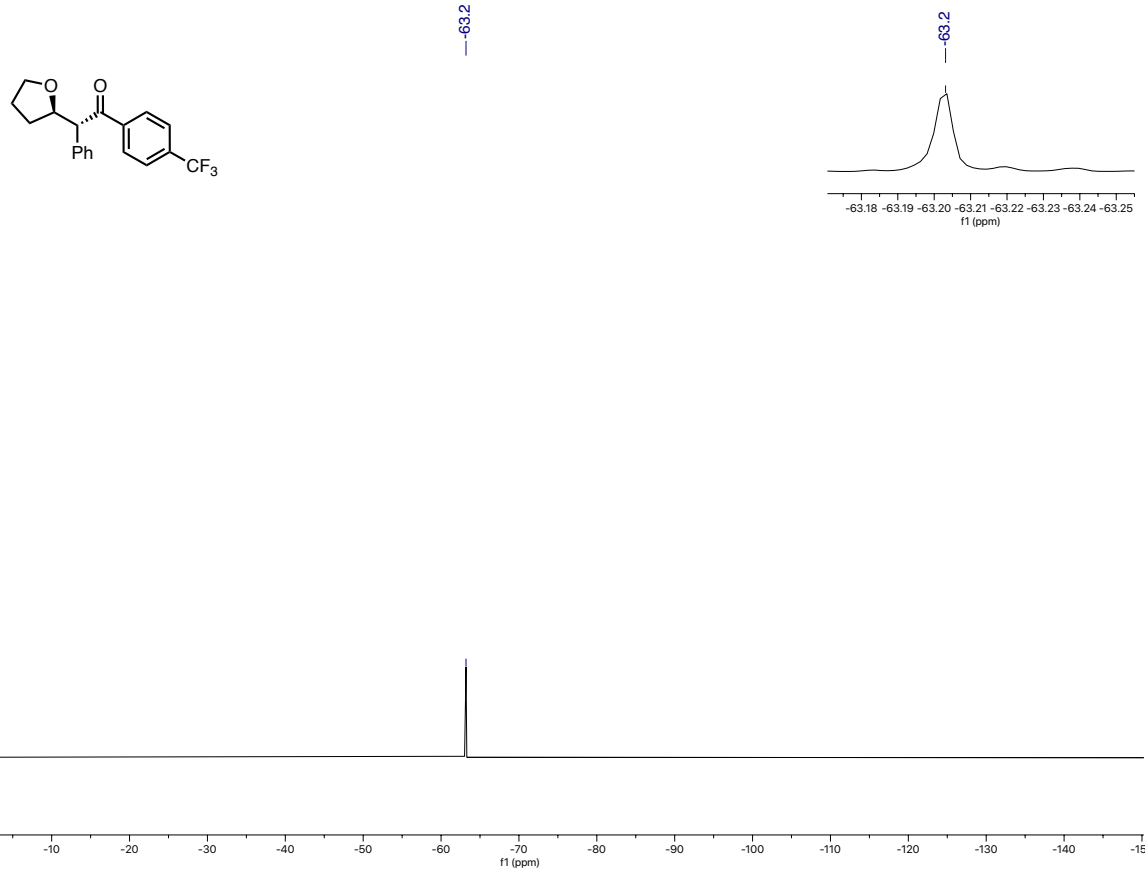
-63.2
-63.2
-63.18 -63.19 -63.20 -63.21 -63.22 -63.23 -63.24 -63.25
f1 (ppm)
0 -10 -20 -30 -40 -50 -60 -70 -80 -90 -100 -110 -120 -130 -140
f1 (ppm)

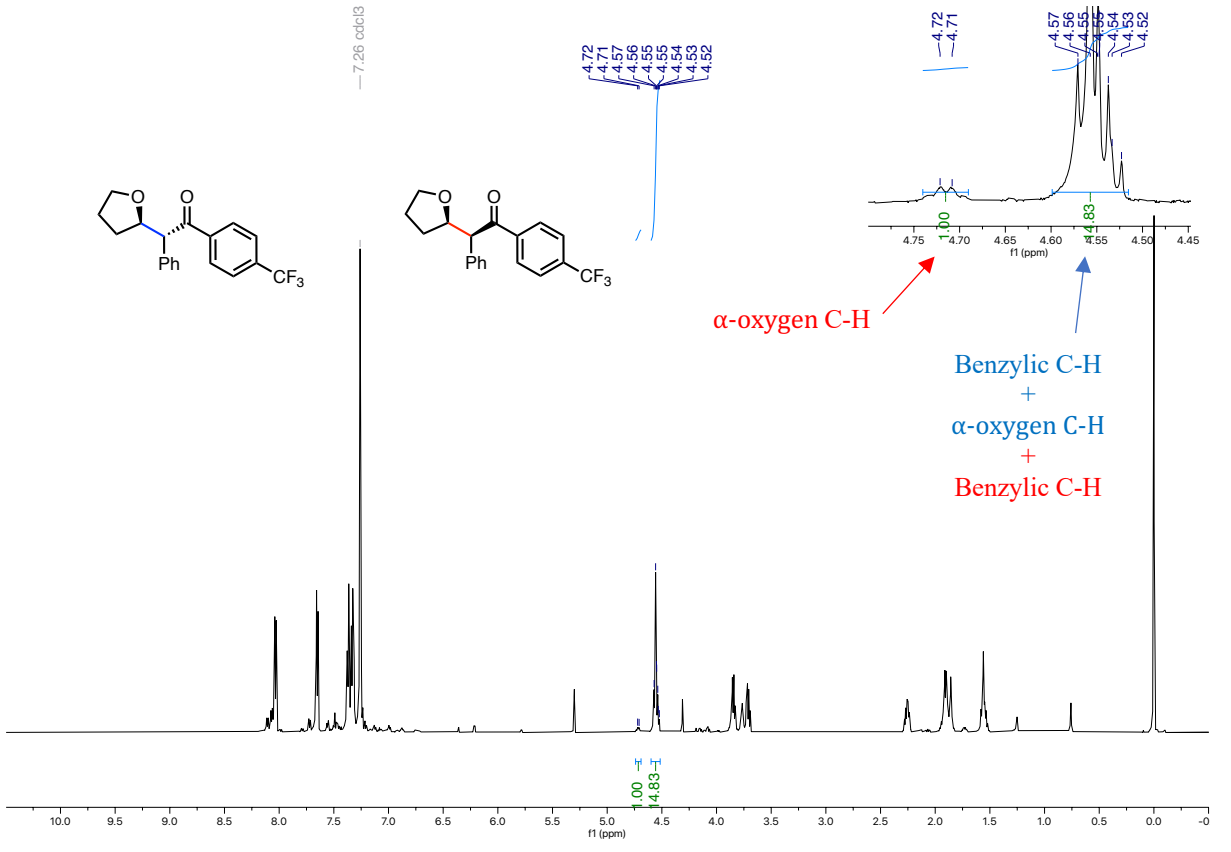
7.26 cdcl3
4.72
4.71
4.57
4.56
4.55
4.54
4.53
4.52
1.00
4.83
4.75 4.70 4.65 4.60 4.55 4.50 4.45
f1 (ppm)
α-oxygen C-H
Benzylic C-H
+
α-oxygen C-H
+
Benzylic C-H
10.0 9.5 9.0 8.5 8.0 7.5 7.0 6.5 6.0 5.5 5.0 4.5 4.0 3.5 3.0 2.5 2.0 1.5 1.0 0.5 0.0
f1 (ppm)

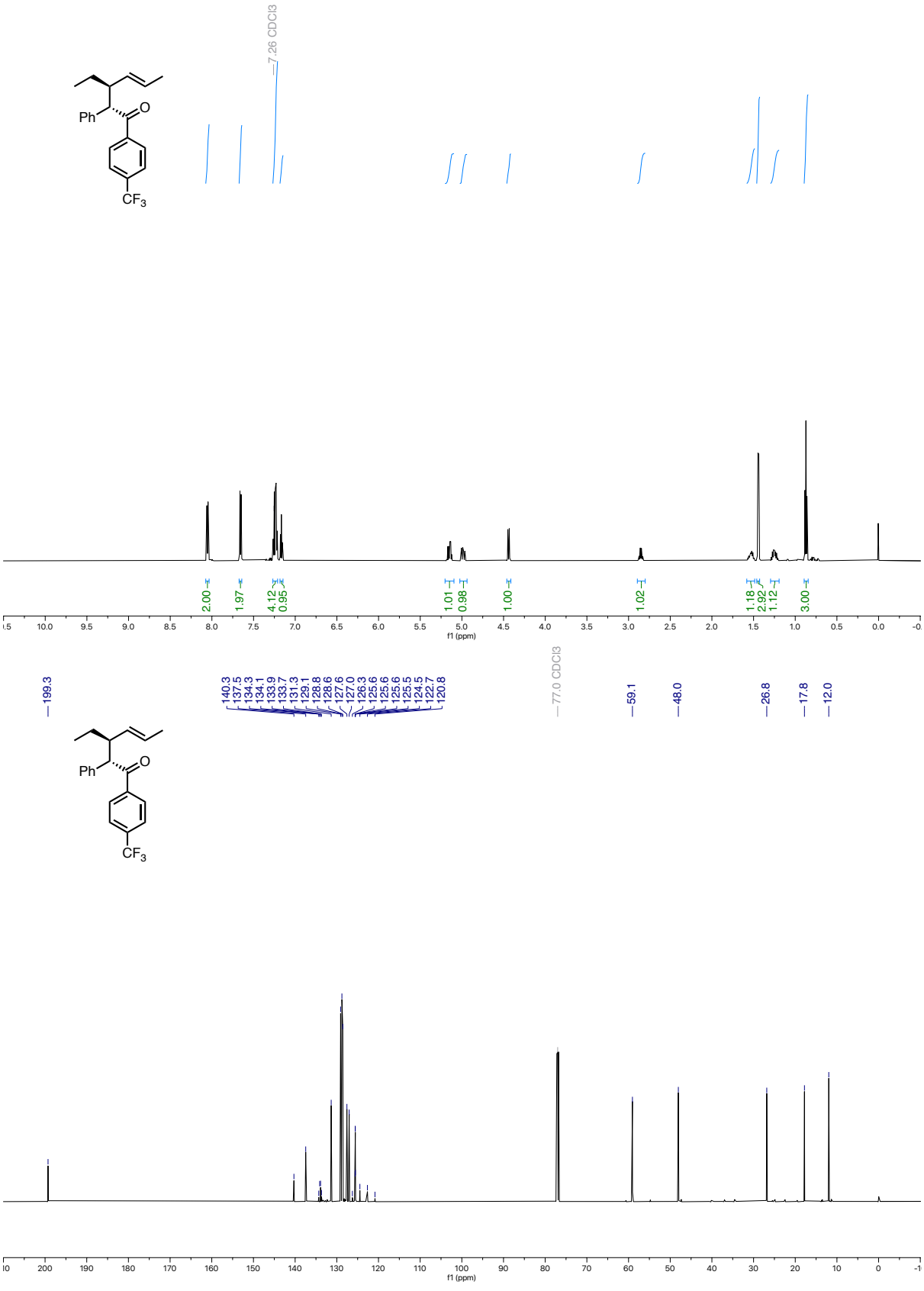
7.26 CDCl3
Ph
O
CF3
2.00
1.97
4.12
0.95
1.01
0.98
1.00
1.02
1.18
2.92
1.12
3.00
f1 (ppm)
199.3
140.3
137.5
134.3
134.1
133.9
133.7
131.3
129.1
128.8
128.6
127.6
127.0
126.3
125.6
125.6
125.6
125.5
124.5
122.7
120.8
77.0 CDCl3
59.1
48.0
26.8
17.8
12.0
f1 (ppm)

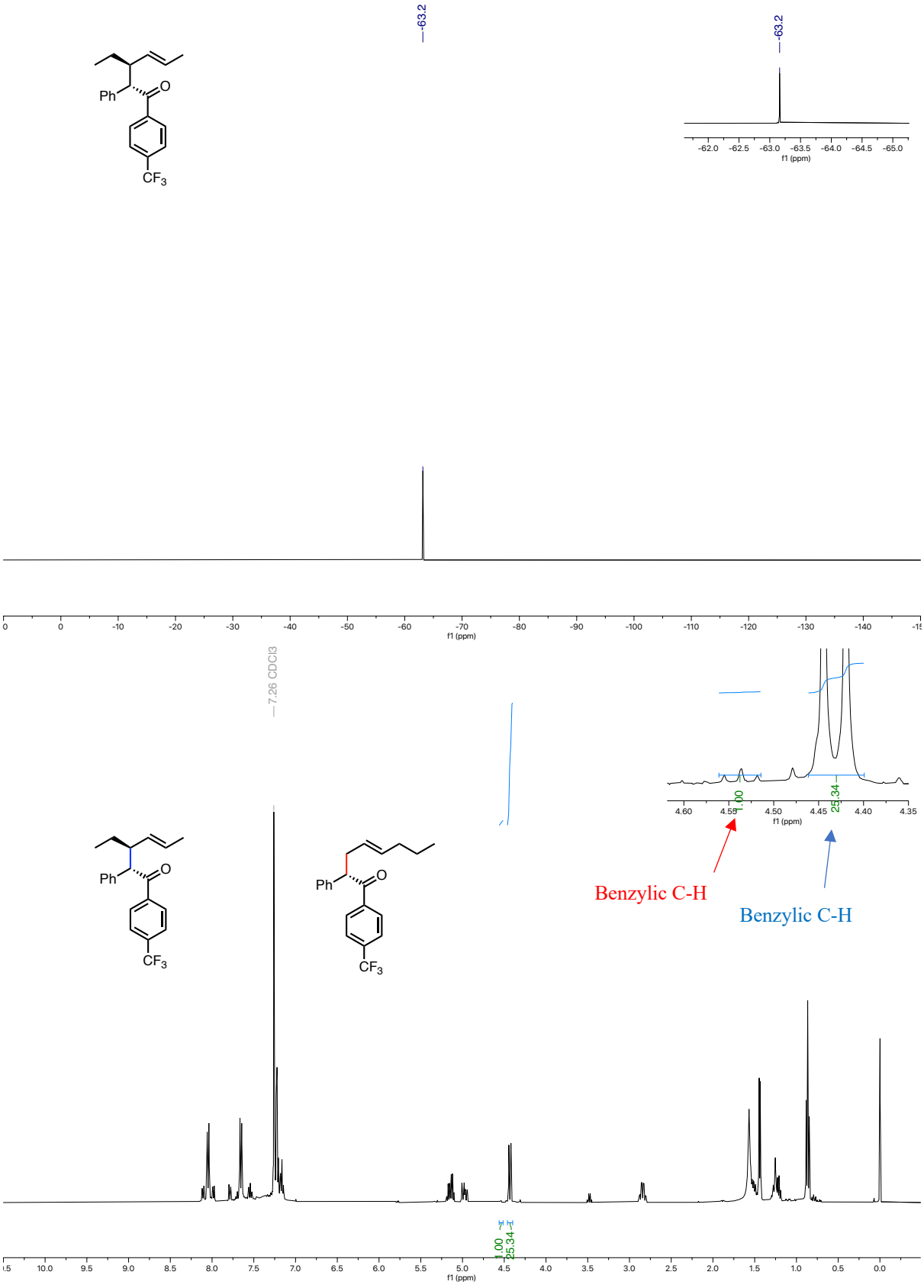
-63.2
-63.2
Ph
O
CF3
f1 (ppm)
7.26 CDCl3
1.00
25.34
Benzylic C-H
Benzylic C-H

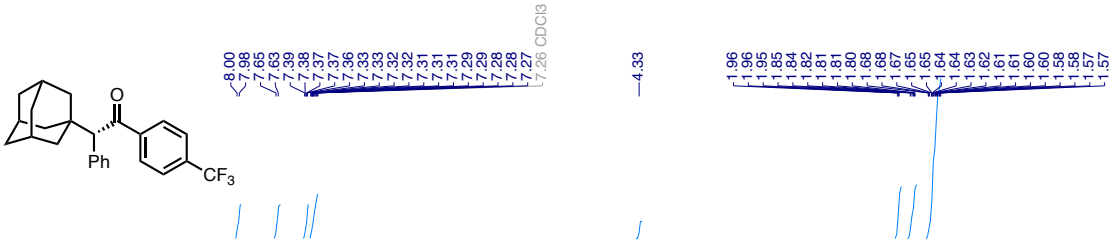
8.00
7.98
7.65
7.63
7.39
7.38
7.37
7.37
7.36
7.33
7.32
7.32
7.31
7.31
7.29
7.28
7.28
7.27
7.26 CDCl3
4.33
1.96
1.96
1.95
1.85
1.84
1.82
1.81
1.81
1.80
1.68
1.68
1.67
1.65
1.65
1.64
1.64
1.63
1.62
1.61
1.61
1.60
1.60
1.58
1.58
1.57
1.57
O
Ph
CF3

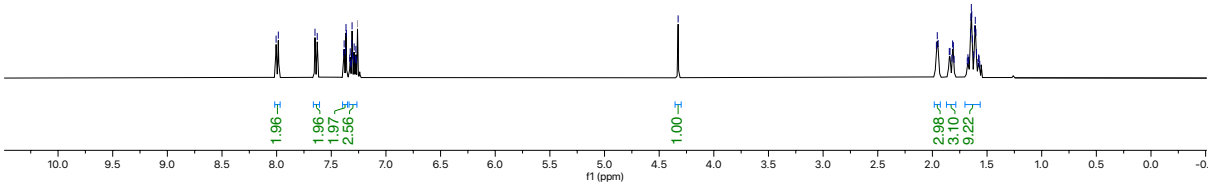
1.96
1.96
1.97
2.56
1.00
2.98
3.10
9.22
f1 (ppm)

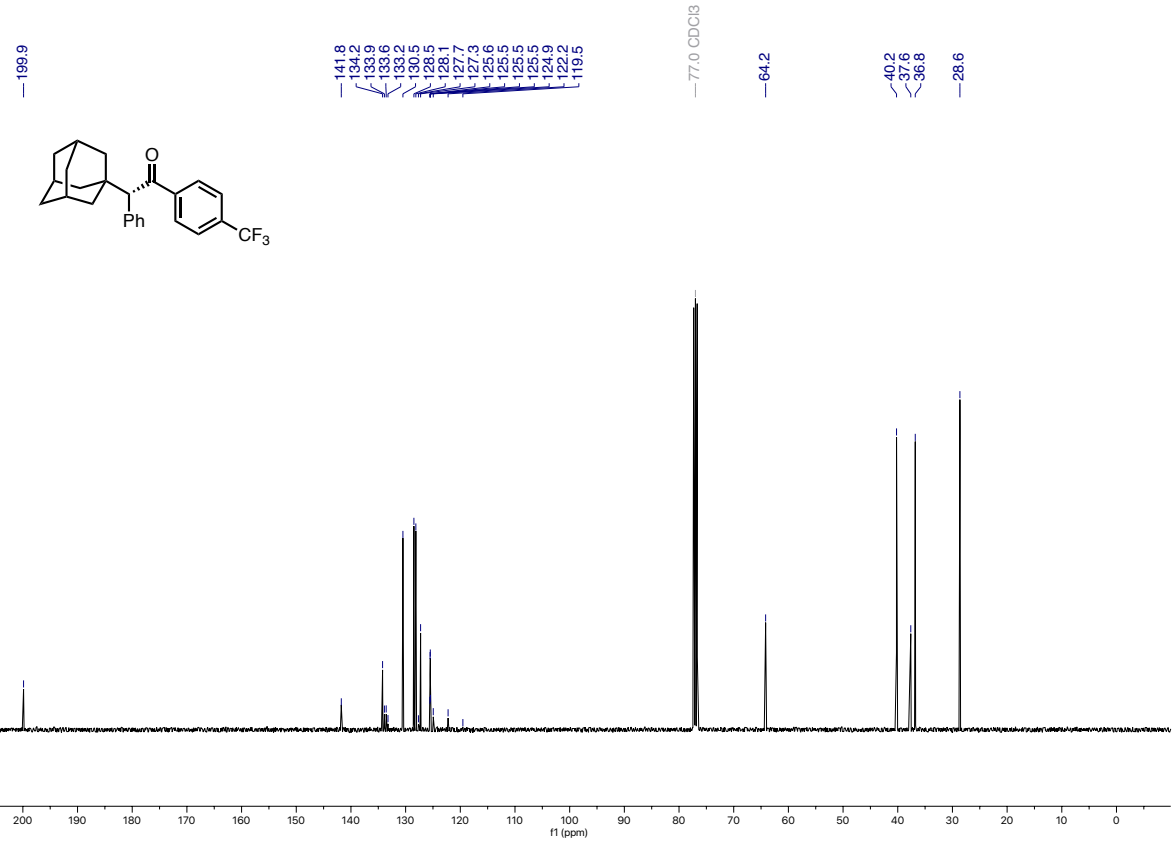
199.9
141.8
134.2
133.9
133.6
133.2
130.5
128.5
128.1
127.7
127.3
125.6
125.5
125.5
125.5
124.9
122.2
119.5
77.0 CDCl3
64.2
40.2
37.6
36.8
28.6
O
Ph
CF3
f1 (ppm)

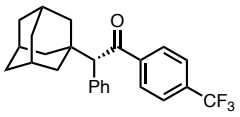
O
Ph
CF3

-63.1
-63.1
-62
-63
-64
-65
f1 (ppm)

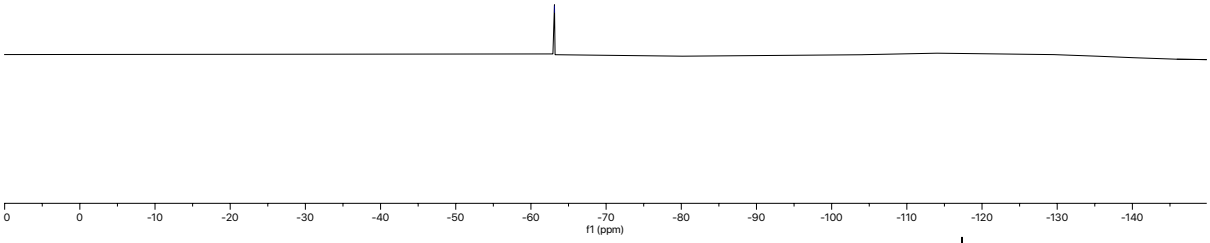
0
-10
-20
-30
-40
-50
-60
-70
-80
-90
-100
-110
-120
-130
-140
f1 (ppm)

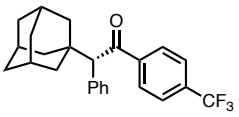
O
Ph
CF3

7.26 cdcl3
1.01
4.7
4.6
4.5
4.4
4.3
4.2
4.1
4.0
3.9
f1 (ppm)
Benzylic C-H
secondary insertion
single diastereomer
single regioisomer
1.00
10.5
10.0
9.5
9.0
8.5
8.0
7.5
7.0
6.5
6.0
5.5
5.0
4.5
4.0
3.5
3.0
2.5
2.0
1.5
1.0
0.5
0.0
f1 (ppm)

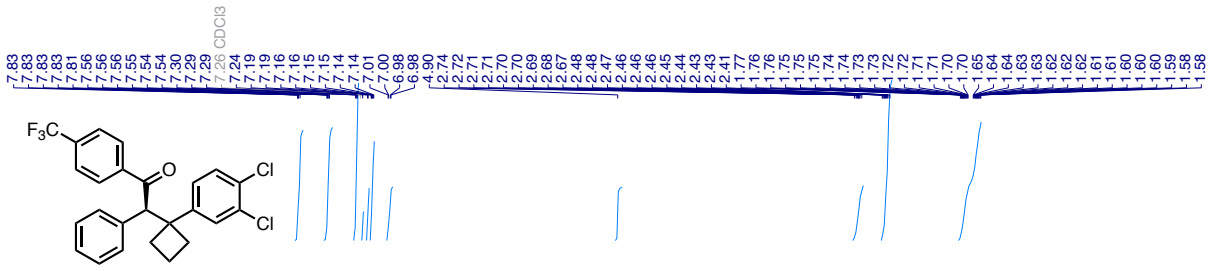
7.26 CDCl3
F3C
O
Cl
Cl

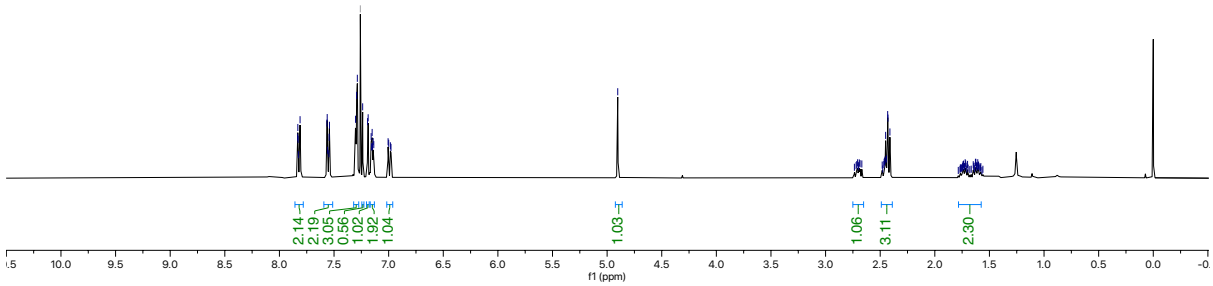
2.14
2.19
3.05
0.56
1.02
1.92
1.04
1.03
1.06
3.11
2.30
f1 (ppm)

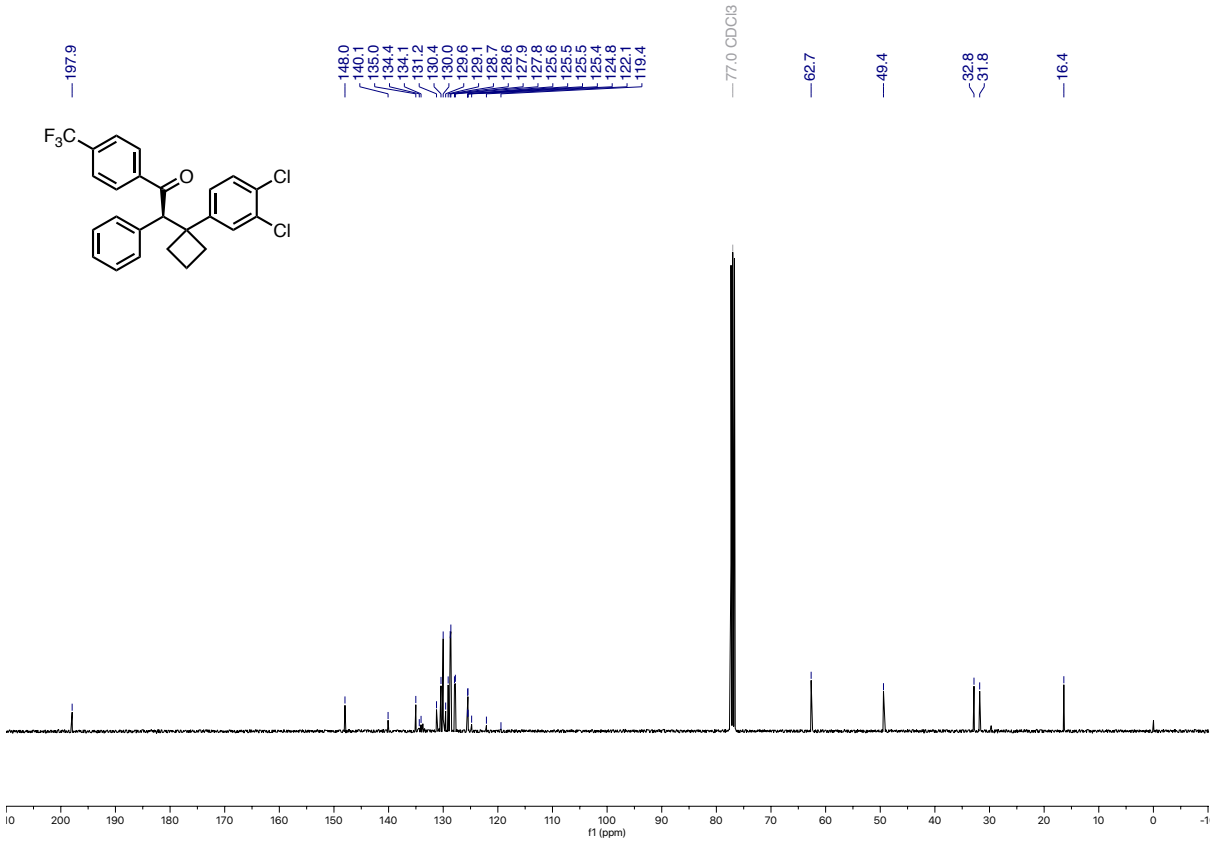
197.9
148.0
140.1
135.0
134.4
134.1
131.2
130.4
130.0
129.6
129.1
128.7
128.6
127.9
127.8
125.6
125.5
125.5
125.4
124.8
122.1
119.4
77.0 CDCl3
62.7
49.4
32.8
31.8
16.4
F3C
O
Cl
Cl
f1 (ppm)

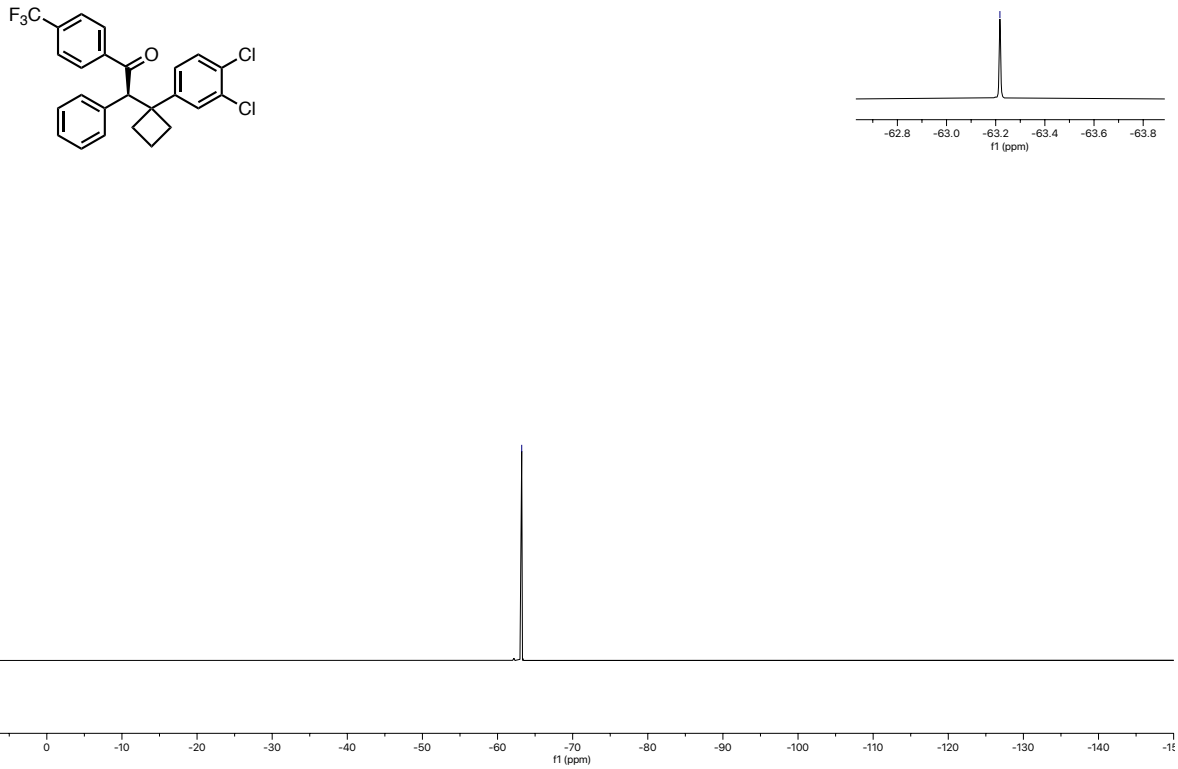
F3C
O
Cl
Cl
-63.2
-63.2
-62.8
-63.0
-63.2
-63.4
-63.6
-63.8
f1 (ppm)
0
-10
-20
-30
-40
-50
-60
-70
-80
-90
-100
-110
-120
-130
-140
f1 (ppm)

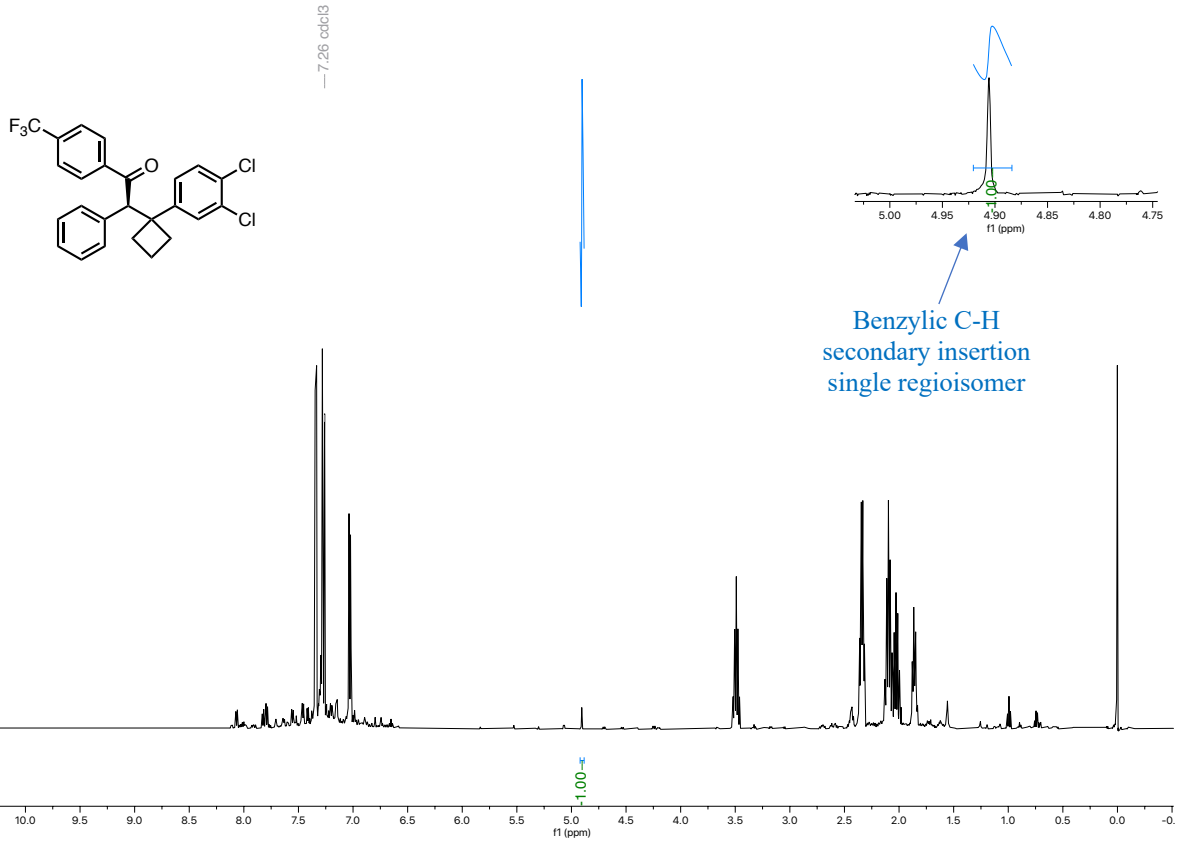
7.26 cdcl3
F3C
O
Cl
Cl
1.00
5.00
4.95
4.90
4.85
4.80
4.75
f1 (ppm)
Benzylic C-H
secondary insertion
single regioisomer
1.00
10.0
9.5
9.0
8.5
8.0
7.5
7.0
6.5
6.0
5.5
5.0
4.5
4.0
3.5
3.0
2.5
2.0
1.5
1.0
0.5
0.0
f1 (ppm)

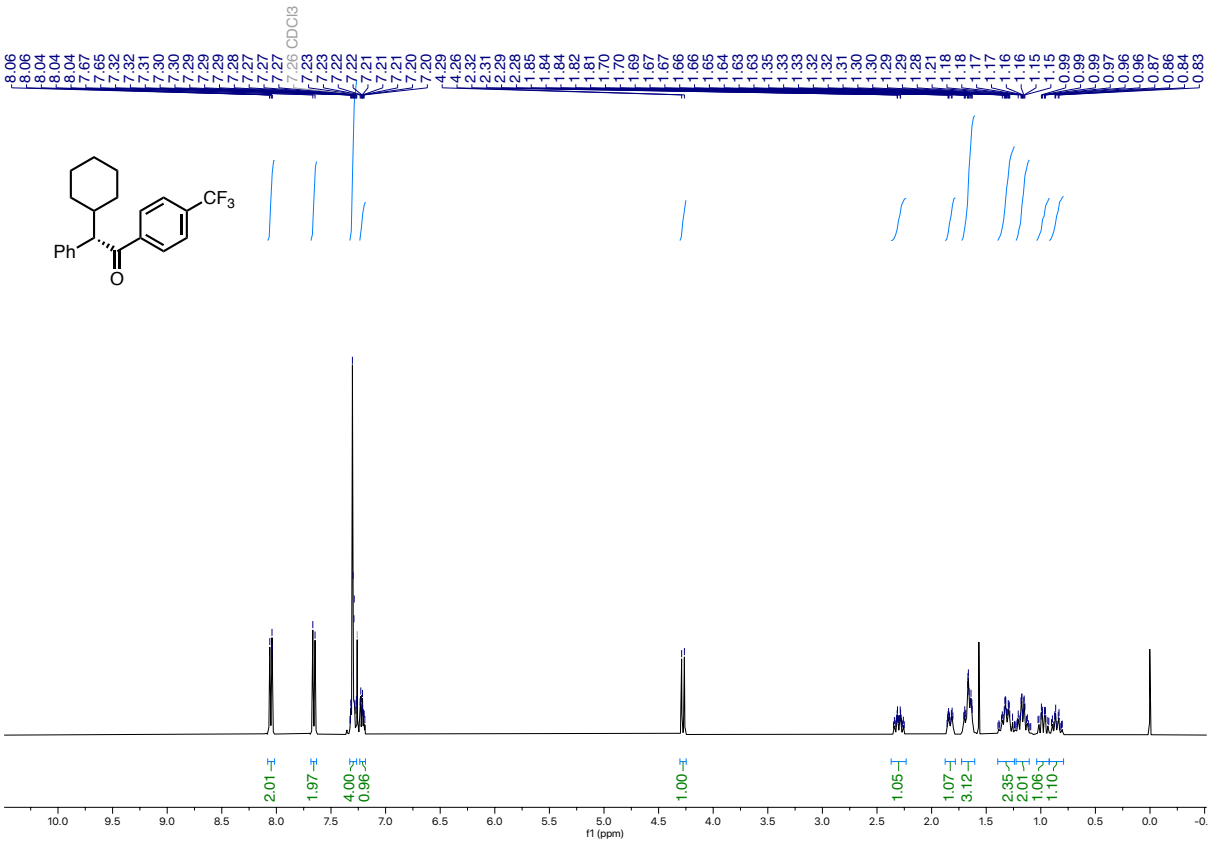
CF3
Ph
O
f1 (ppm)

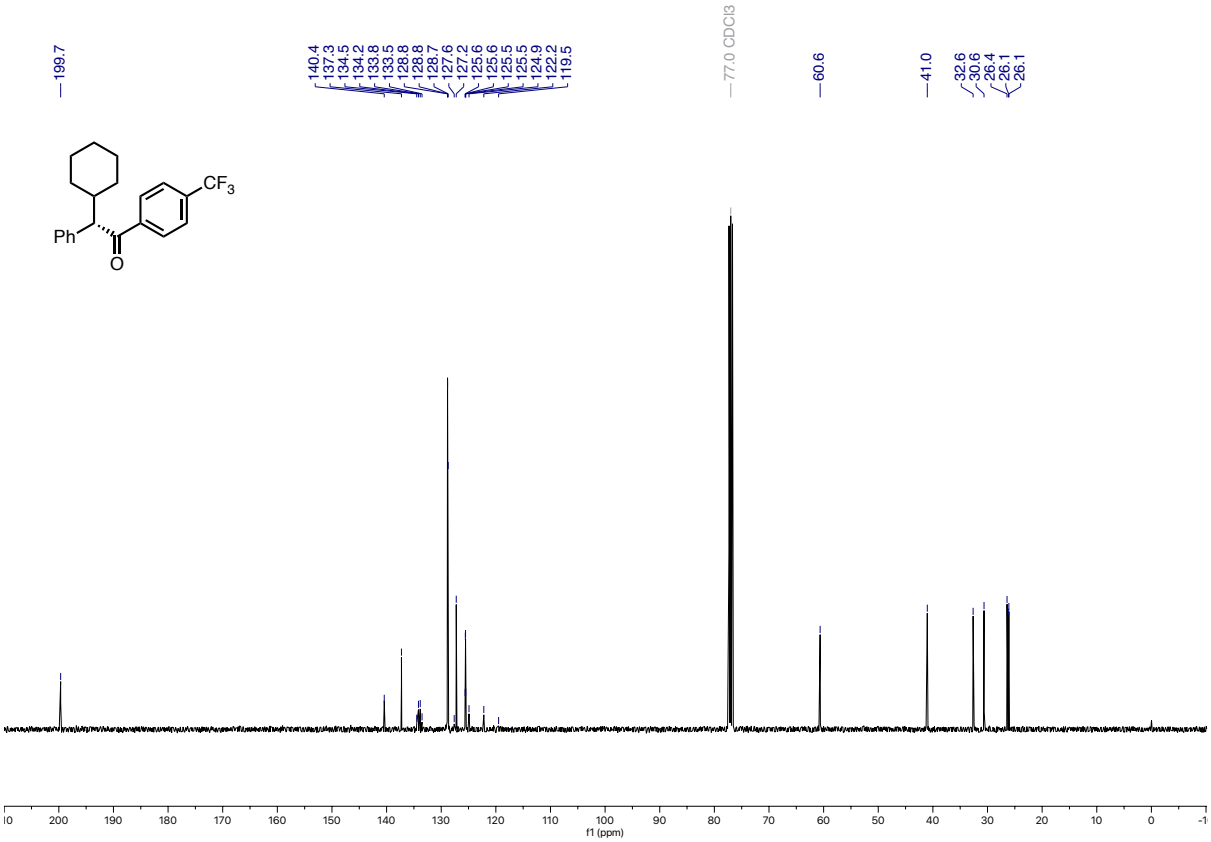
CF3
Ph
O
f1 (ppm)

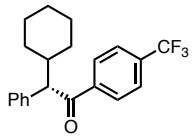
CF3
Ph
O

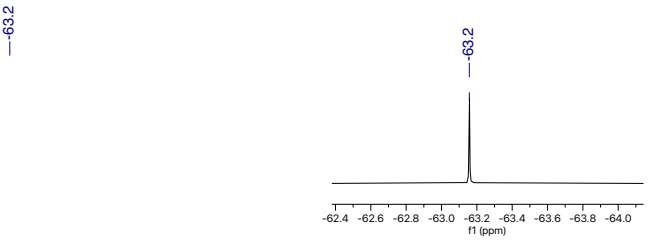
-63.2
-63.2
-62.4 -62.6 -62.8 -63.0 -63.2 -63.4 -63.6 -63.8 -64.0
f1 (ppm)

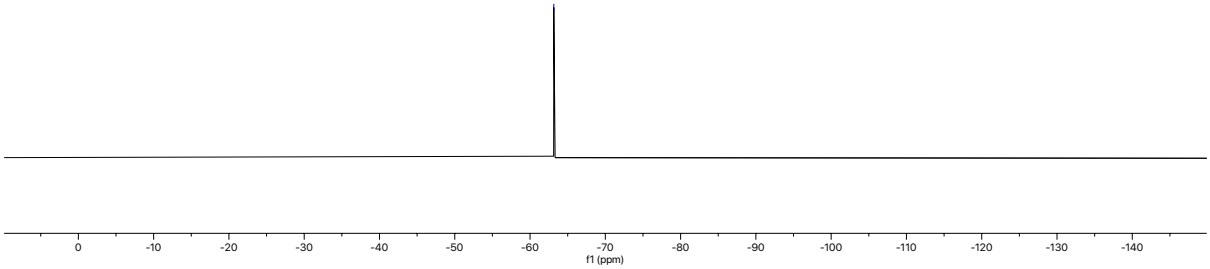
0 -10 -20 -30 -40 -50 -60 -70 -80 -90 -100 -110 -120 -130 -140
f1 (ppm)

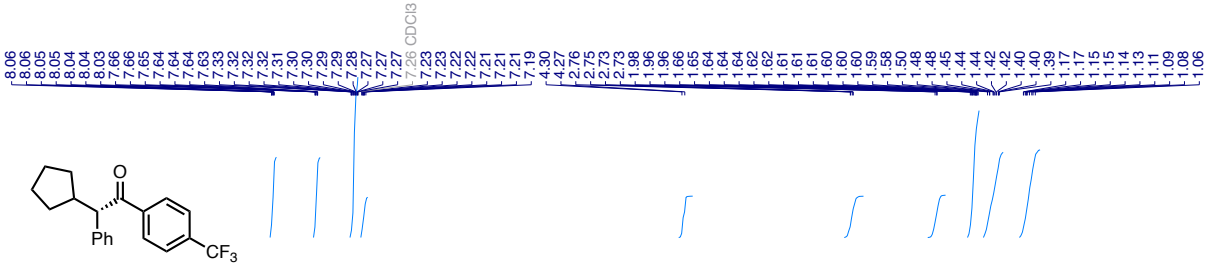
7.26 CDCl3
O
Ph
CF3

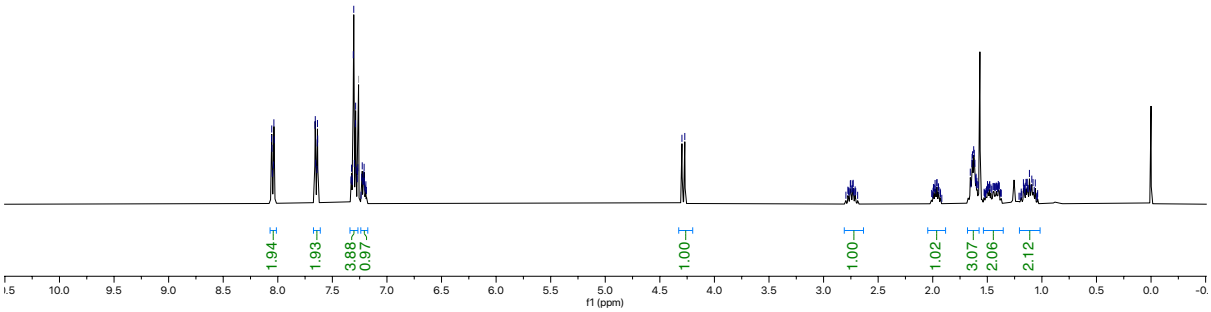
1.94
1.93
3.88
0.97
1.00
1.00
1.02
3.07
2.06
2.12
f1 (ppm)

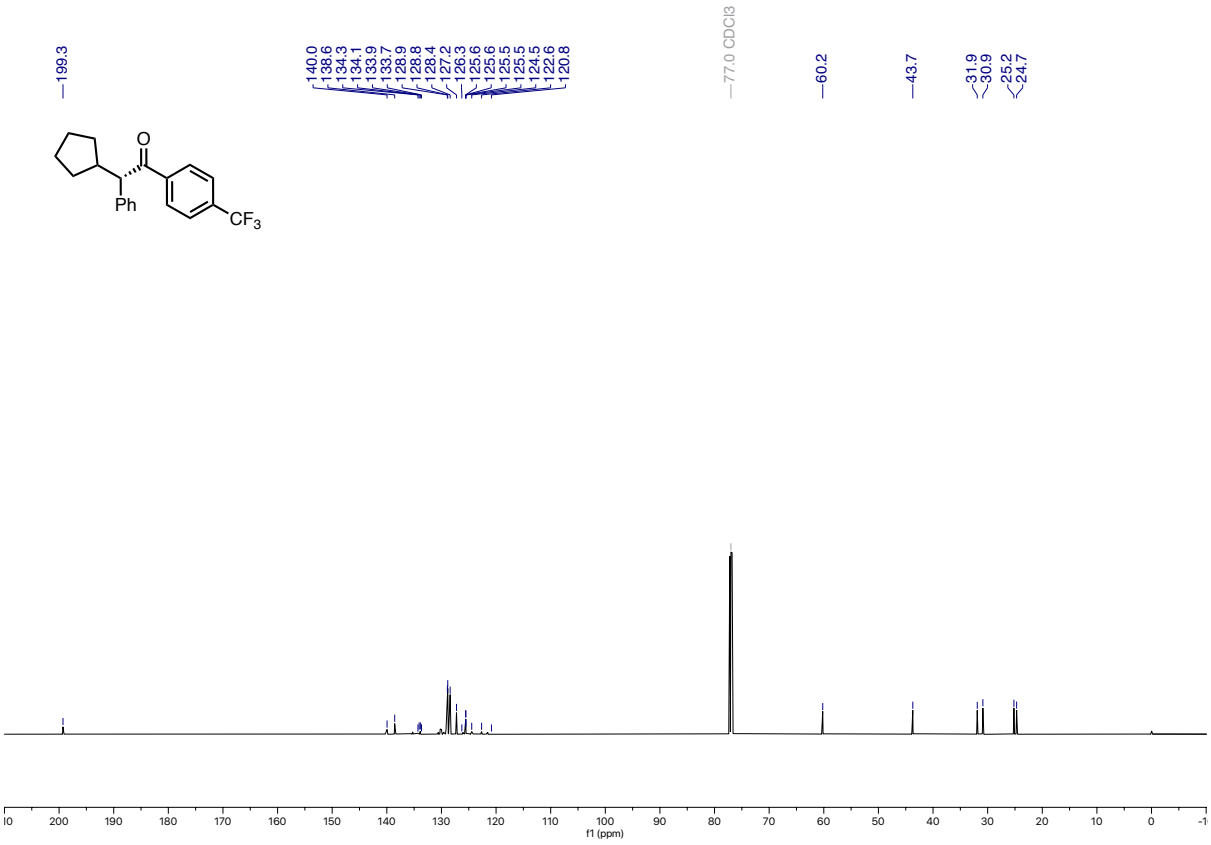
199.3
140.0
138.6
134.3
134.1
133.9
133.7
128.9
128.8
128.4
127.2
126.3
125.6
125.6
125.5
125.5
124.5
122.6
120.8
77.0 CDCl3
60.2
43.7
31.9
30.9
25.2
24.7
O
Ph
CF3
f1 (ppm)

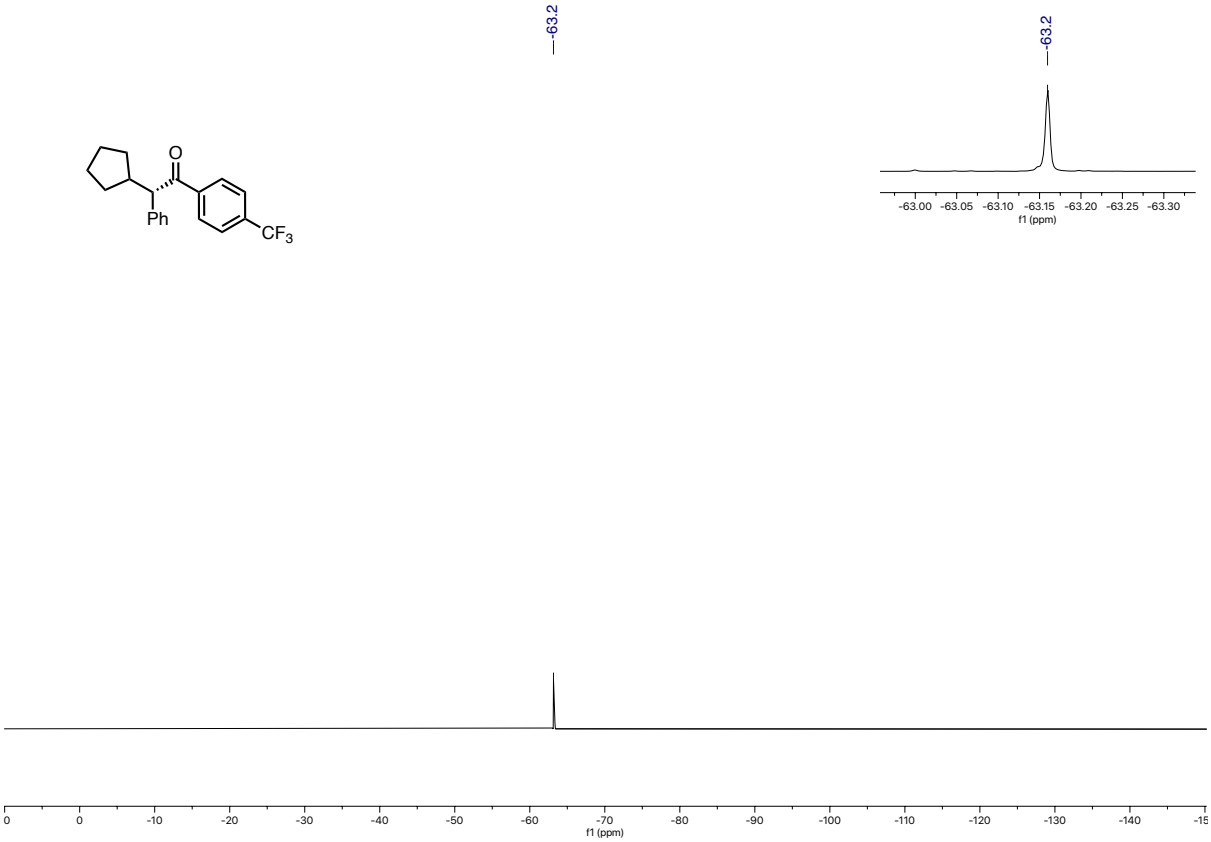
63.2
63.2
O
Ph
CF3
-63.00 -63.05 -63.10 -63.15 -63.20 -63.25 -63.30
f1 (ppm)
f1 (ppm)

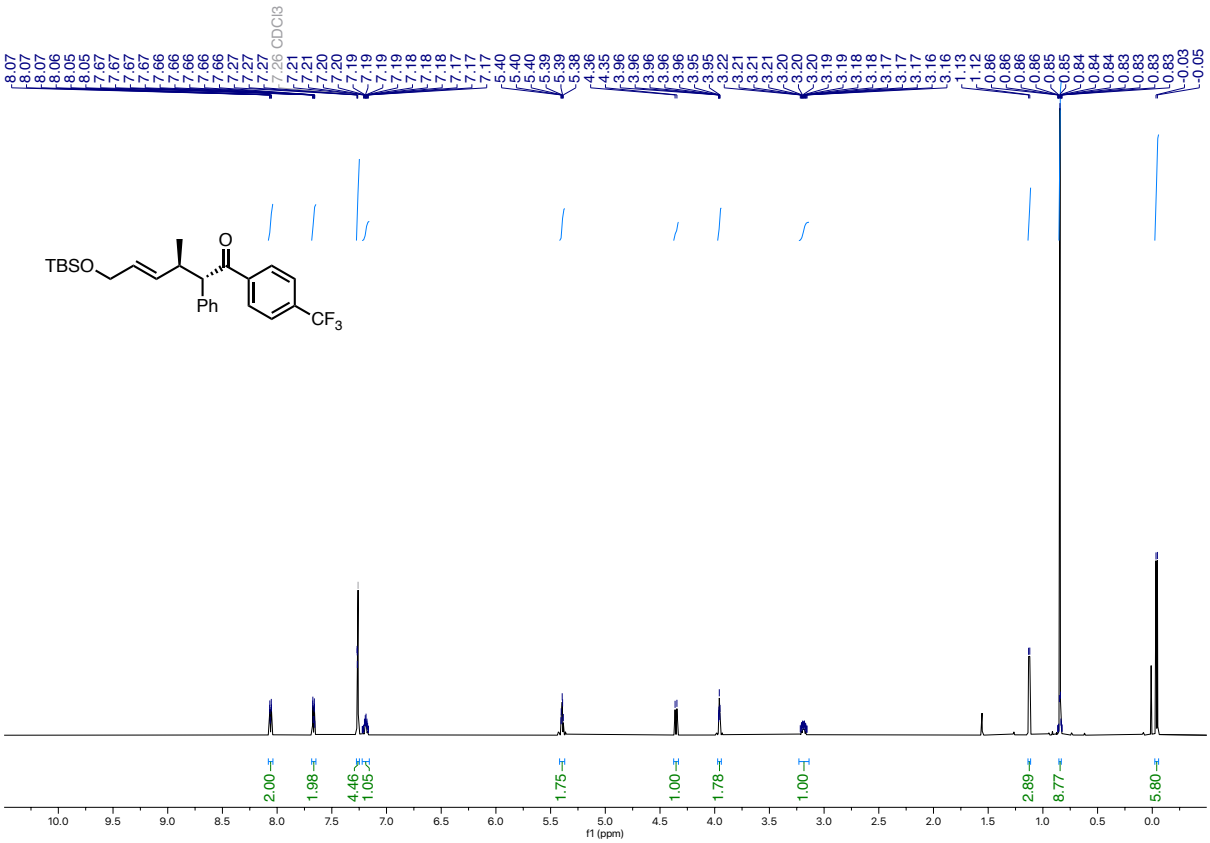
TBSO
O
Ph
CF3
7.26 CDCl3
f1 (ppm)

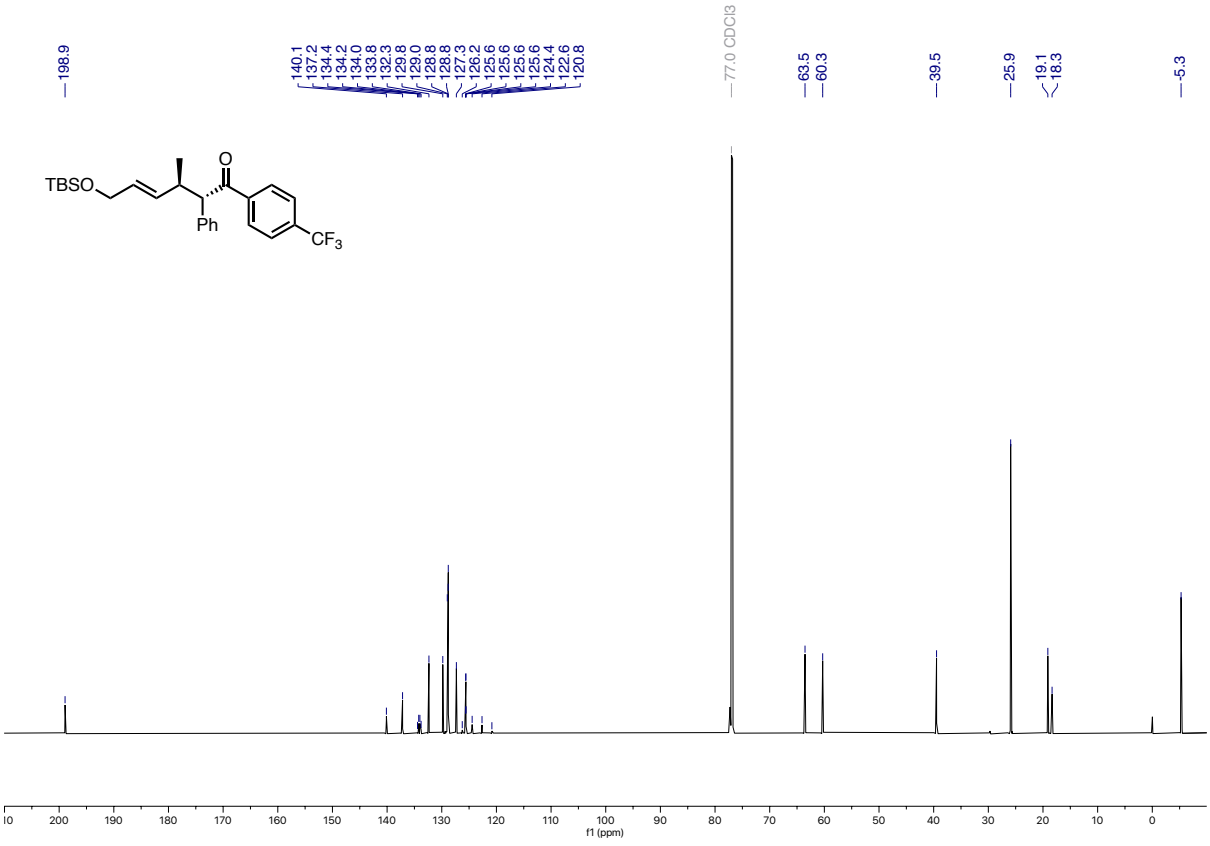
TBSO
O
Ph
CF3
77.0 CDCl3
f1 (ppm)

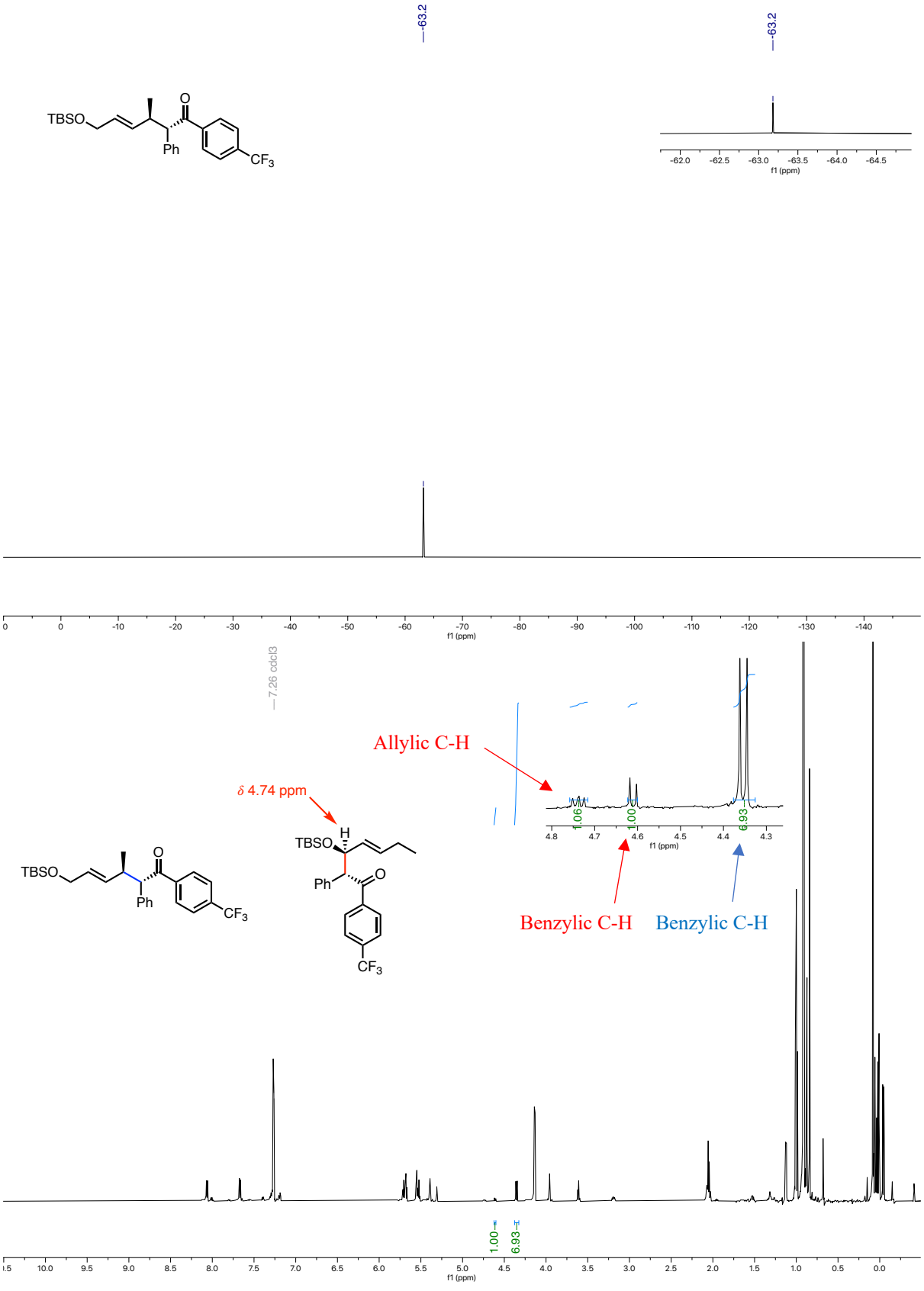
TBSO
Ph
CF3
O
-63.2
-63.2
f1 (ppm)
f1 (ppm)
7.26 cdcl3
Allylic C-H
δ 4.74 ppm
H
Benzylic C-H
Benzylic C-H
1.00
6.93
f1 (ppm)

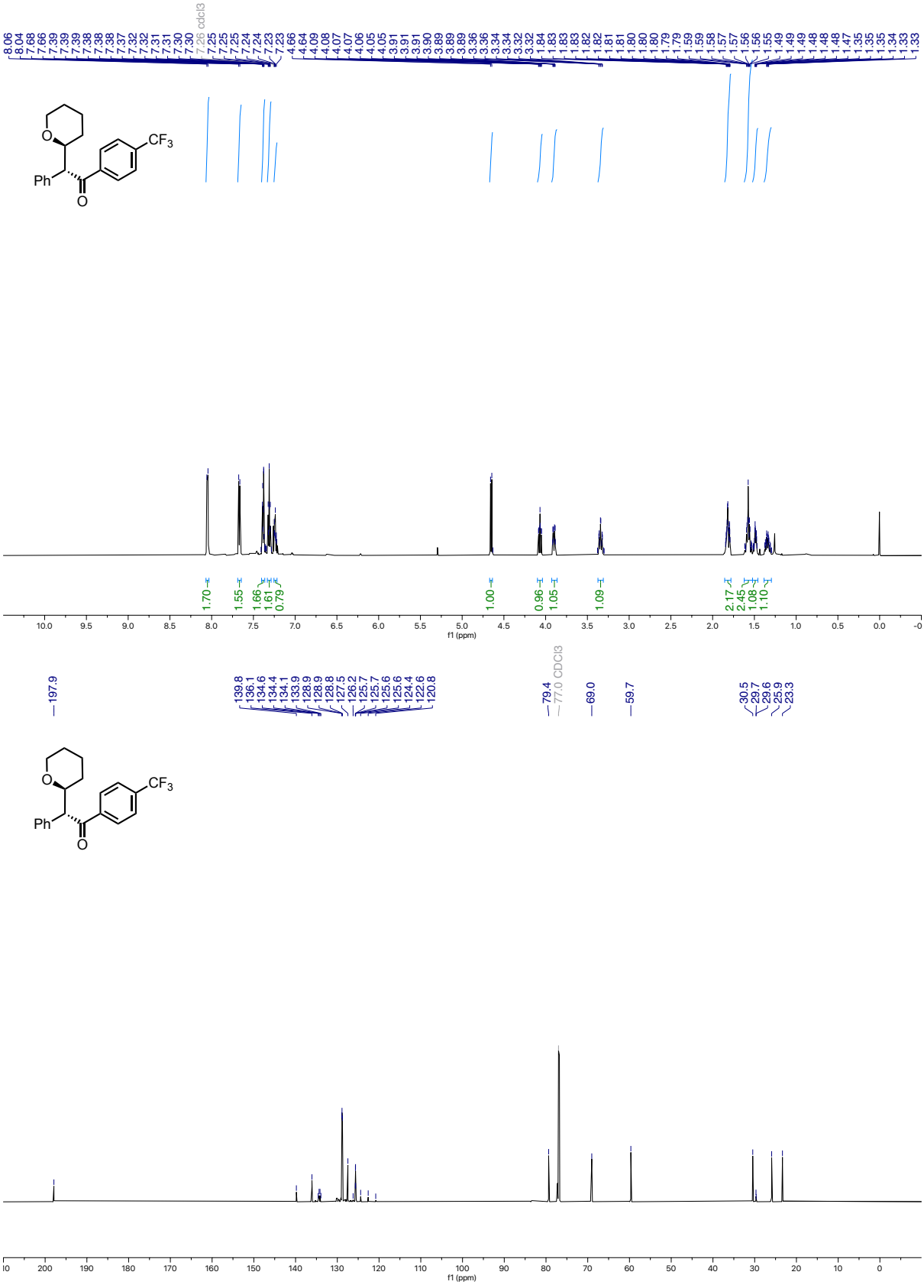
8.06 8.04 7.68 7.66 7.39 7.39 7.39 7.38 7.38 7.38 7.37 7.32 7.32 7.31 7.31 7.30 7.30 7.26 cdcl3 7.25 7.25 7.25 7.24 7.24 7.23 7.23 4.66 4.64 4.09 4.08 4.07 4.07 4.06 4.05 4.05 3.91 3.91 3.90 3.89 3.89 3.89 3.36 3.34 3.34 3.32 3.32 1.84 1.83 1.83 1.83 1.82 1.82 1.81 1.81 1.80 1.80 1.80 1.79 1.79 1.59 1.59 1.58 1.57 1.57 1.56 1.56 1.55 1.49 1.49 1.49 1.48 1.48 1.48 1.47 1.35 1.35 1.35 1.34 1.33 1.33
O
CF3
Ph
O
1.70
1.55
1.66
1.61
0.79
1.00
0.96
1.05
1.09
2.17
2.45
1.08
1.10
10.0 9.5 9.0 8.5 8.0 7.5 7.0 6.5 6.0 5.5 5.0 4.5 4.0 3.5 3.0 2.5 2.0 1.5 1.0 0.5 0.0 -0
f1 (ppm)
197.9
139.8 136.1 134.6 134.4 134.1 133.9 128.9 128.9 128.8 127.5 126.2 125.7 125.7 125.6 125.6 124.4 122.6 120.8
79.4
77.0 CDCl3
69.0
59.7
30.5 29.7 29.6 25.9 23.3
O
CF3
Ph
O
10 200 190 180 170 160 150 140 130 120 110 100 90 80 70 60 50 40 30 20 10 0
f1 (ppm)

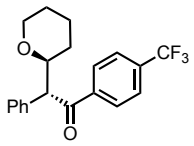
O
CF3
Ph
O

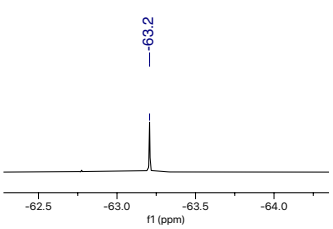
-63.2
-62.5
-63.0
-63.5
-64.0
f1 (ppm)

-63.2
0
-10
-20
-30
-40
-50
-60
-70
-80
-90
-100
-110
-120
-130
-140
f1 (ppm)

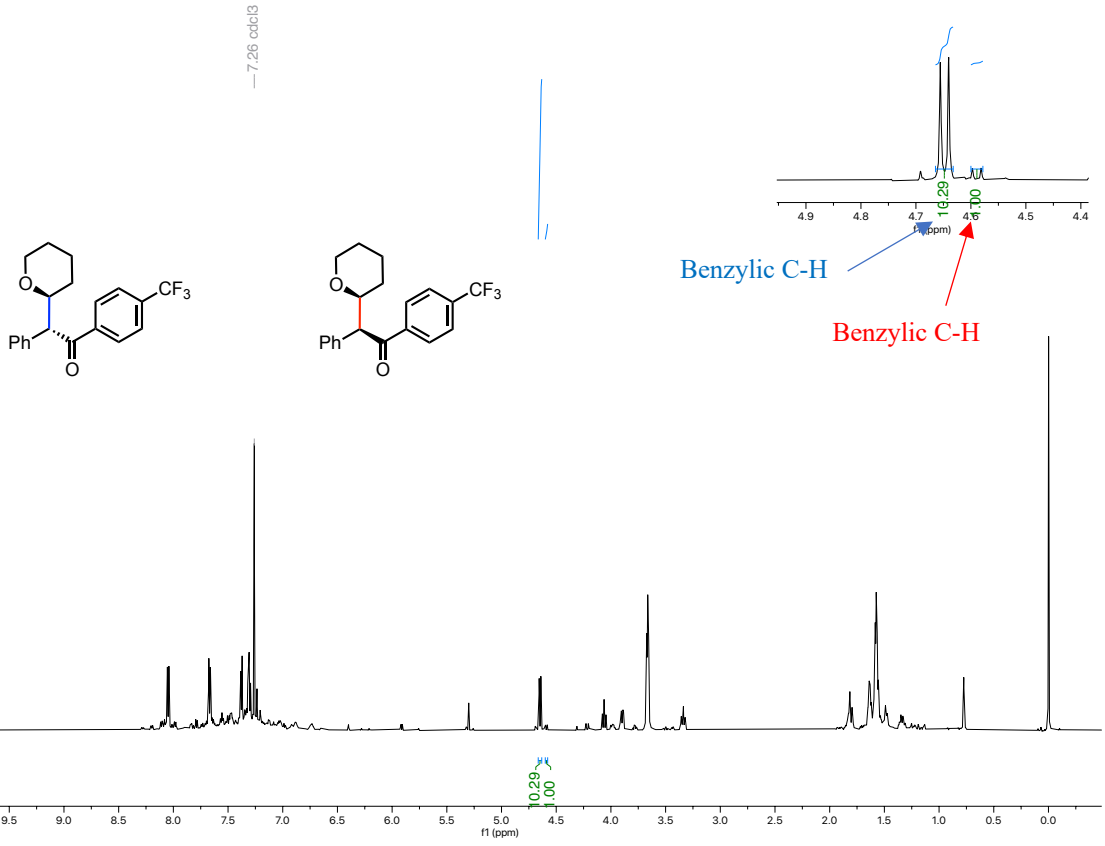
7.26 cdcl3
O
CF3
Ph
O
O
CF3
Ph
O
16.29
1.00
4.9
4.8
4.7
4.6
4.5
4.4
Benzylic C-H
Benzylic C-H
10.29
1.00
10.0
9.5
9.0
8.5
8.0
7.5
7.0
6.5
6.0
5.5
5.0
4.5
4.0
3.5
3.0
2.5
2.0
1.5
1.0
0.5
0.0
f1 (ppm)

Appendix – Ch.2 HPLC Data

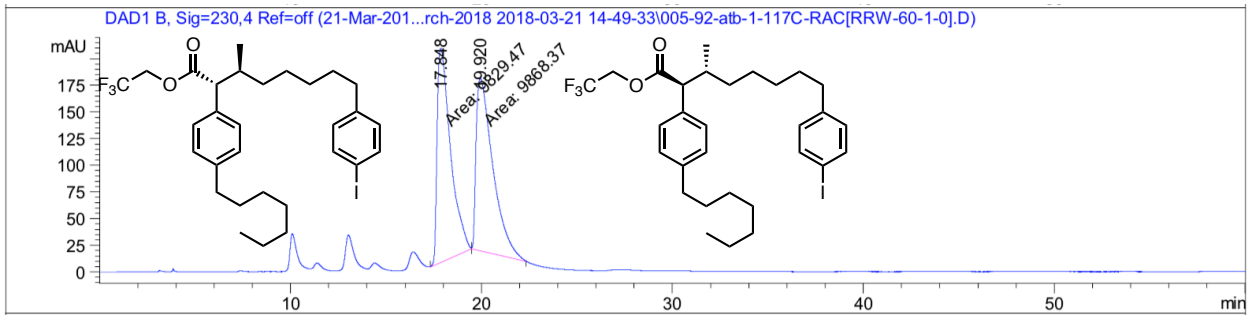

Signal 2: DAD1 B, Sig=230,4 Ref=off

Peak #	RetTime [min]	Type	Width [min]	Area [mAU*s]	Height [mAU]	Area %
1	17.848	MM	0.5750	9829.47168	200.90695	49.9013
2	19.920	MM	1.0183	9868.37109	161.51624	50.0987
Totals :				1.96978e4	362.42319	

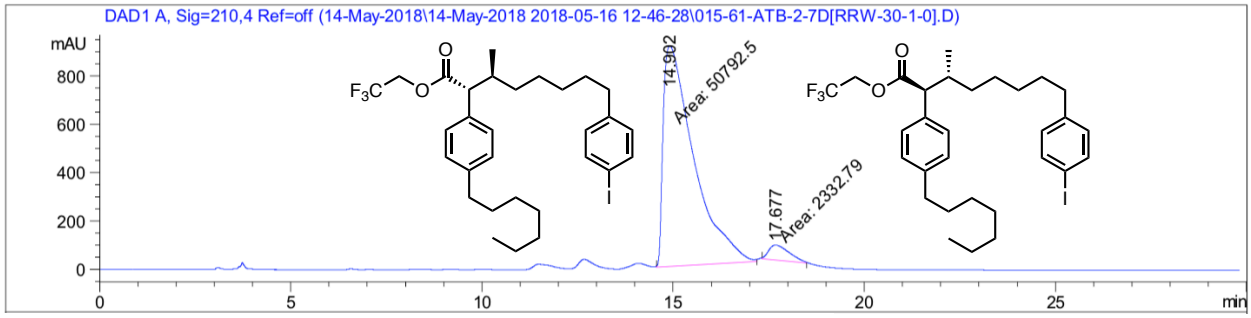

Signal 1: DAD1 A, Sig=210,4 Ref=off

Peak #	RetTime [min]	Type	Width [min]	Area [mAU*s]	Height [mAU]	Area %
1	14.902	MM	0.9260	5.07925e4	914.16620	95.6089
2	17.677	MM	0.6274	2332.78857	61.97265	4.3911
Totals :				5.31253e4	976.13885	

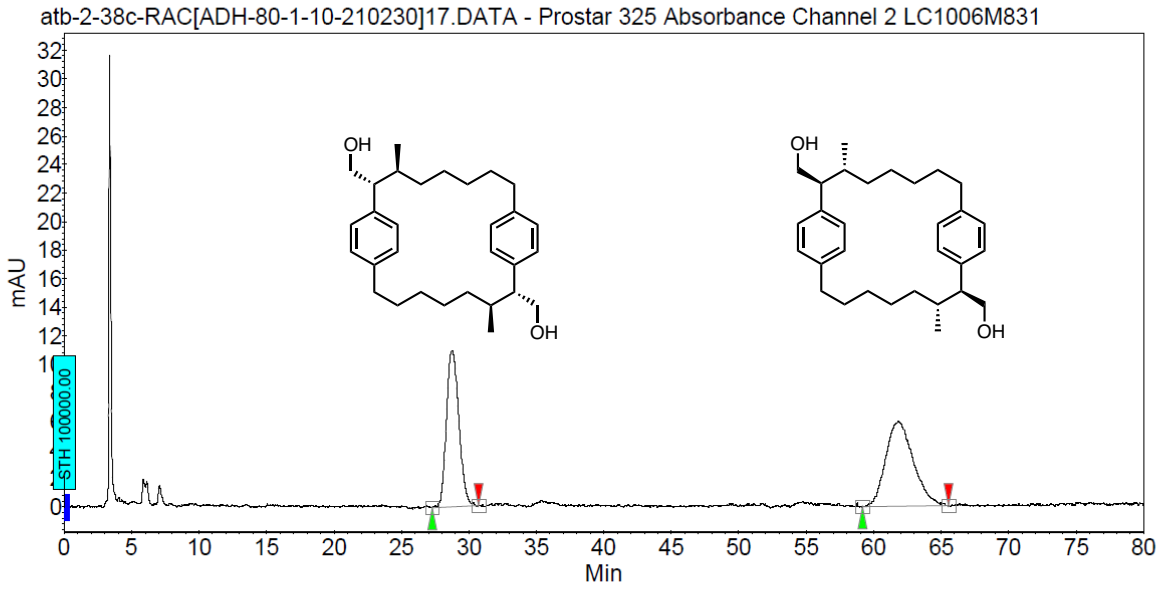

Peak results :

Index	Name	Time [Min]	Quantity [% Area]	Height [mAU]	Area [mAU.Min]	Area % [%]
1	UNKNOWN	28.74	45.33	11.0	11.7	45.329
2	UNKNOWN	61.84	54.67	6.0	14.1	54.671
Total			100.00	16.9	25.8	100.000

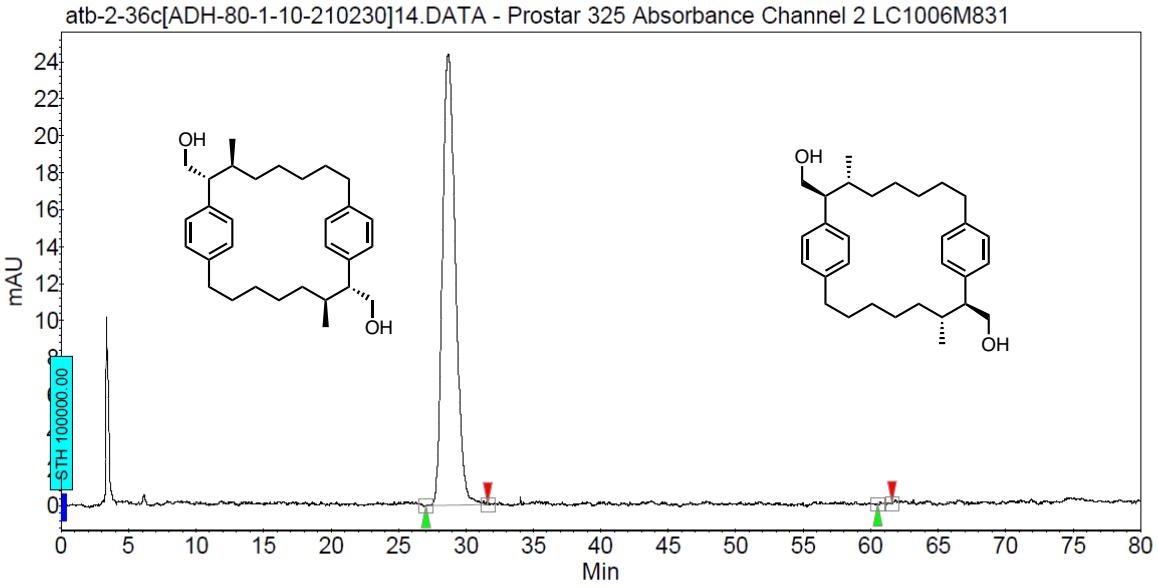

Peak results :

Index	Name	Time [Min]	Quantity [% Area]	Height [mAU]	Area [mAU.Min]	Area % [%]
1	UNKNOWN	28.69	99.92	24.3	27.2	99.923
2	UNKNOWN	60.71	0.08	0.1	0.0	0.077
Total			100.00	24.4	27.2	100.000

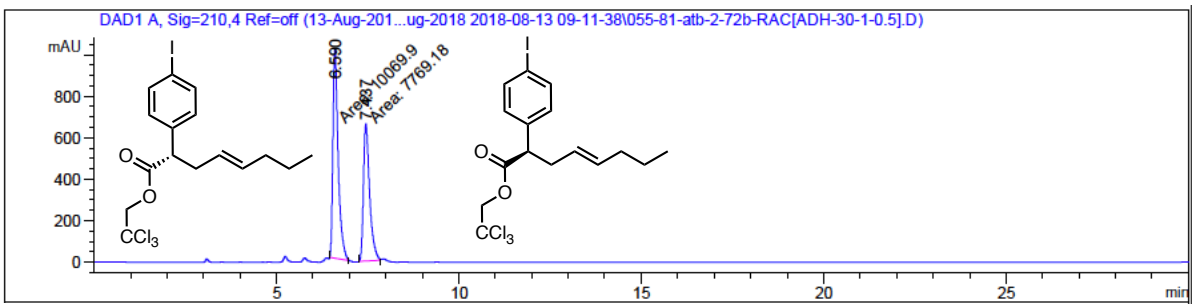

Signal 1: DAD1 A, Sig=210,4 Ref=off

Peak #	RetTime [min]	Type	Width [min]	Area [mAU*s]	Height [mAU]	Area %
1	6.590	MM	0.1665	1.00699e4	1008.00983	56.4484
2	7.437	MM	0.1958	7769.18262	661.15894	43.5516
Totals :				1.78390e4	1669.16876	

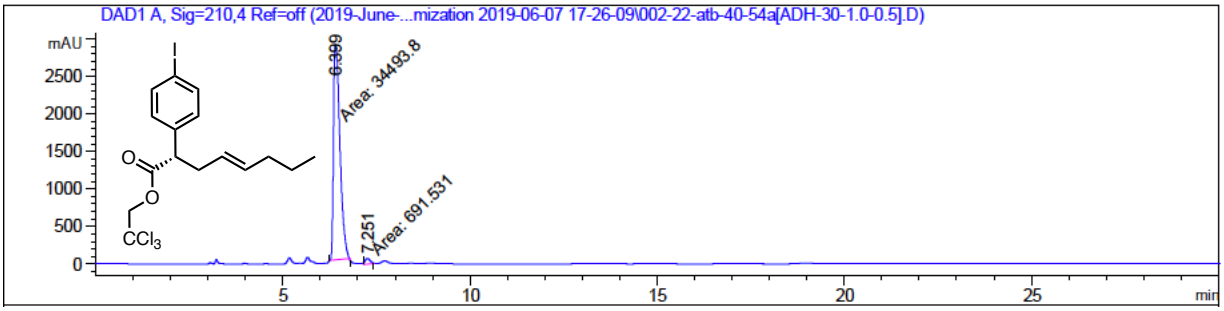

Signal 1: DAD1 A, Sig=210,4 Ref=off

Peak #	RetTime [min]	Type	Width [min]	Area [mAU*s]	Height [mAU]	Area %
1	6.399	MM	0.2007	3.44938e4	2864.12842	98.0346
2	7.251	MM	0.1539	691.53064	74.86881	1.9654
Totals :				3.51854e4	2938.99723	

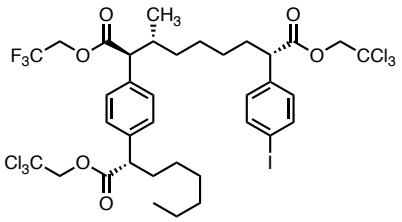

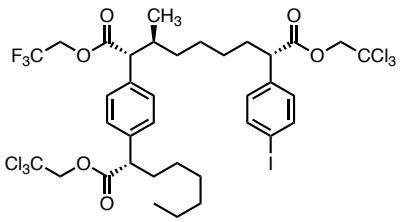

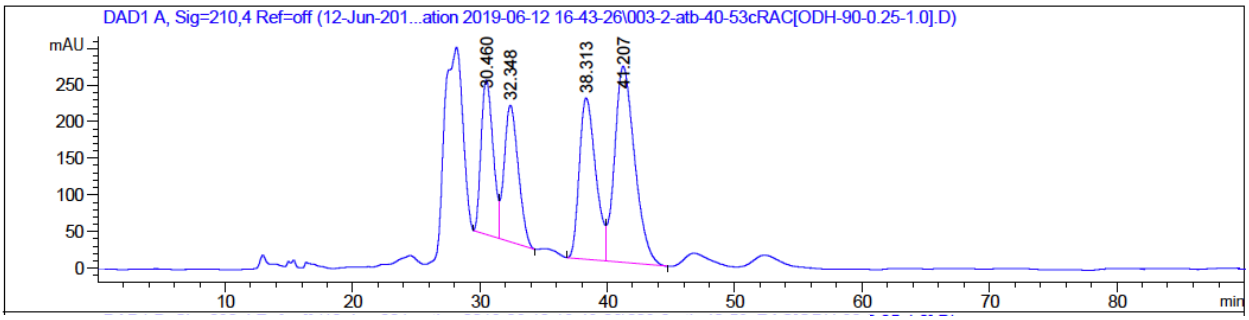

Signal 1: DAD1 A, Sig=210,4 Ref=off

Peak #	RetTime [min]	Type	Width [min]	Area [mAU*s]	Height [mAU]	Area %
1	30.460	BV	0.7695	1.38123e4	210.79062	17.8661
2	32.348	VB	0.9000	1.43233e4	186.40335	18.5271
3	38.313	BV	1.0523	1.97767e4	219.99544	25.5811
4	41.207	VB	1.2827	2.93976e4	267.69070	38.0257
Totals :				7.73100e4	884.88011	

HPLC of the product from Rh_2(*S*-2-Cl-5-BrTPCP)$_4$

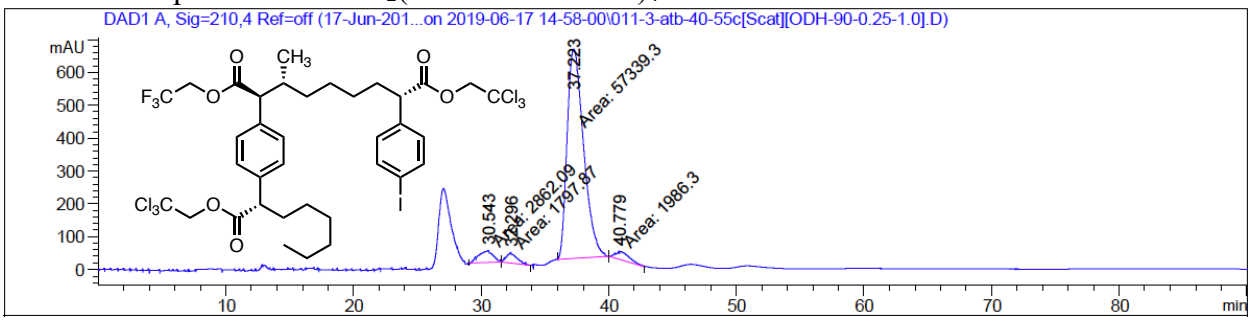

Signal 1: DAD1 A, Sig=210,4 Ref=off

Peak #	RetTime [min]	Type	Width [min]	Area [mAU*s]	Height [mAU]	Area %
1	30.543	MM	1.2717	2862.08569	37.51070	4.4730
2	32.296	MM	0.8968	1797.86963	33.41164	2.8098
3	37.223	MM	1.5001	5.73393e4	637.06042	89.6129
4	40.779	MM	1.2771	1986.30420	25.92206	3.1043
Totals :				6.39855e4	733.90483	

HPLC of the product from Rh_2(*R*-2-Cl-5-BrTPCP)$_4$

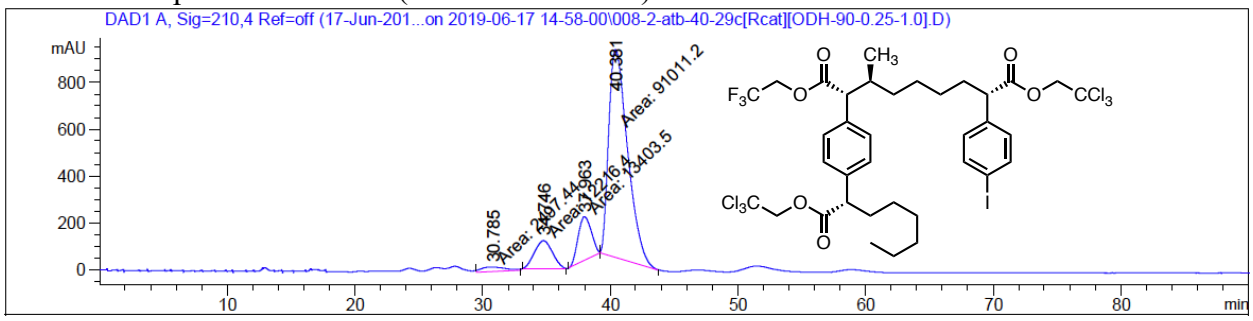

Signal 1: DAD1 A, Sig=210,4 Ref=off

Peak #	RetTime [min]	Type	Width [min]	Area [mAU*s]	Height [mAU]	Area %
1	30.785	MM	2.3329	2497.43896	17.84183	2.0964
2	34.746	MM	1.6694	1.22164e4	121.96550	10.2548
3	37.963	MM	0.8470	1.34035e4	184.94353	11.2513
4	40.381	MM	1.7119	9.10112e4	886.05078	76.3975
Totals :				1.19129e5	1210.80164	

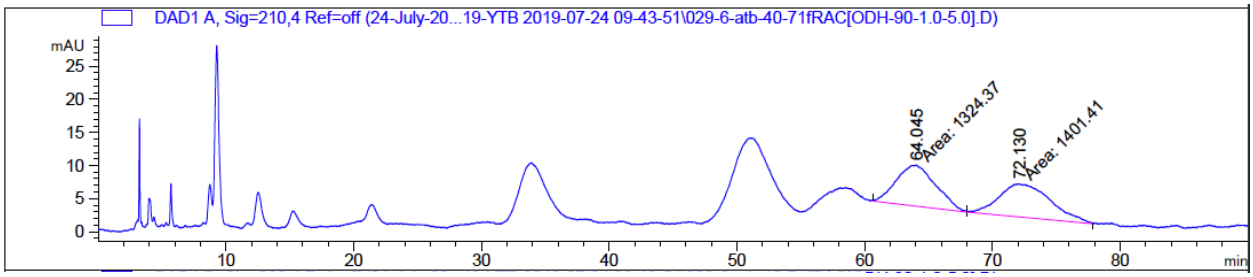

Signal 1: DAD1 A, Sig=210,4 Ref=off

Peak #	RetTime [min]	Type	Width [min]	Area [mAU*s]	Height [mAU]	Area %
1	64.045	MM	3.5470	1324.36804	6.22297	48.5868
2	72.130	MM	4.6690	1401.40820	5.00255	51.4132
Totals :				2725.77625	11.22552	

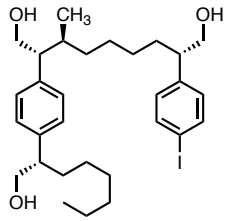

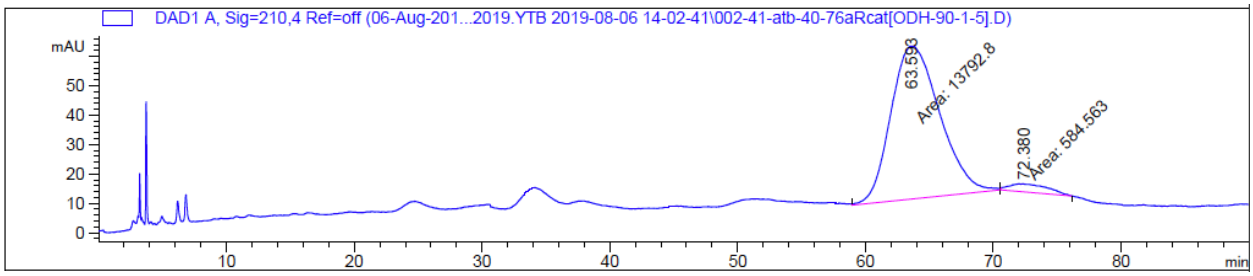

Signal 1: DAD1 A, Sig=210,4 Ref=off

Peak #	RetTime [min]	Type	Width [min]	Area [mAU*s]	Height [mAU]	Area %
1	63.593	MM	4.4228	1.37928e4	51.97662	95.9341
2	72.380	MM	3.5399	584.56274	2.75227	4.0659
Totals :				1.43774e4	54.72889	

Appendix – Ch.3 HPLC Data

(*S*,*E*)-2-(4-chlorophenyl)oct-4-en-1-ol HPLC:

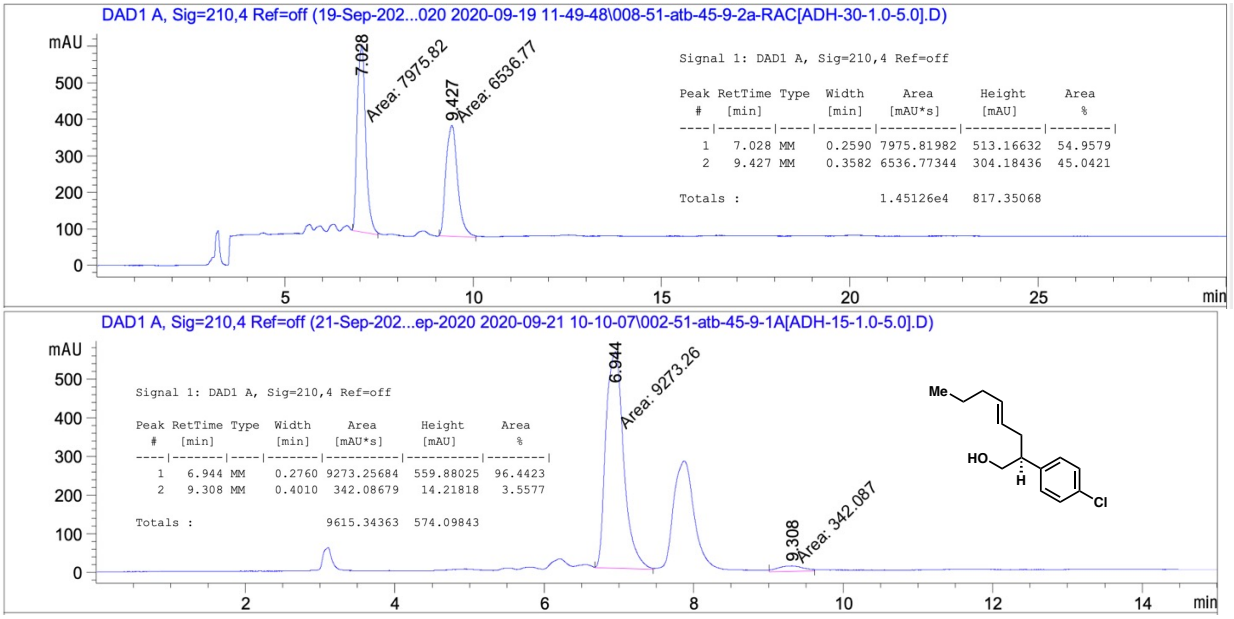

2,2,2-trichloroethyl (*S*,*E*)-2-(4-chlorophenyl)oct-4-enoate HPLC:

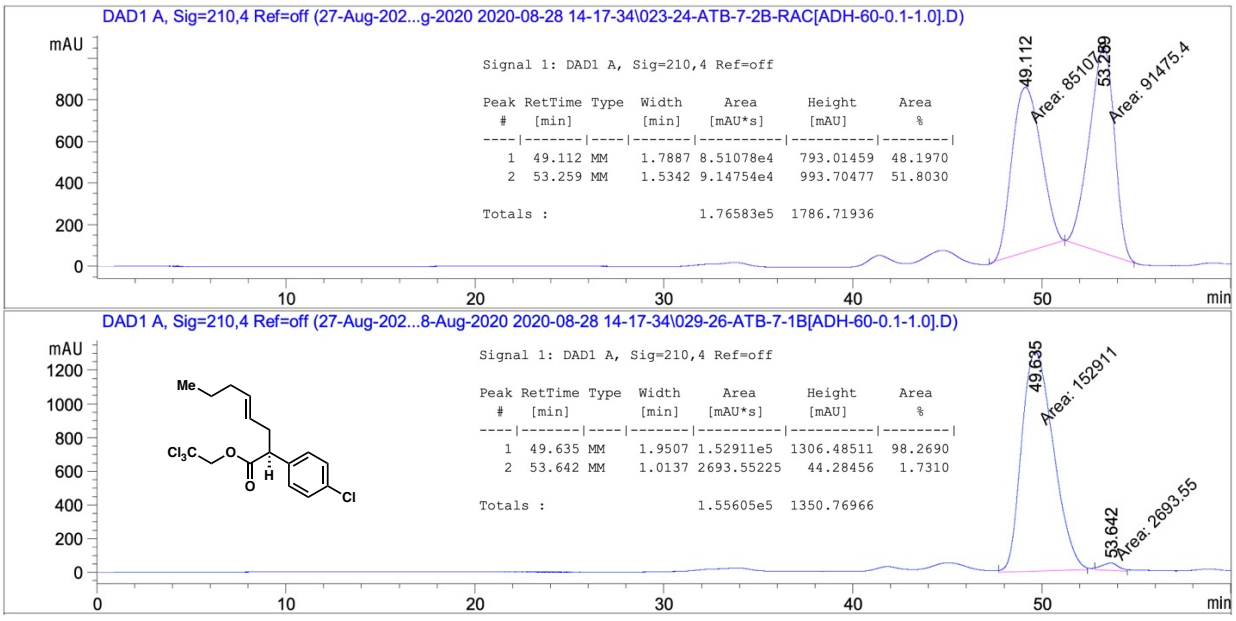

2,2,2-trichloroethyl (*S*,*E*)-2-(4-iodophenyl)oct-4-enoate HPLC:

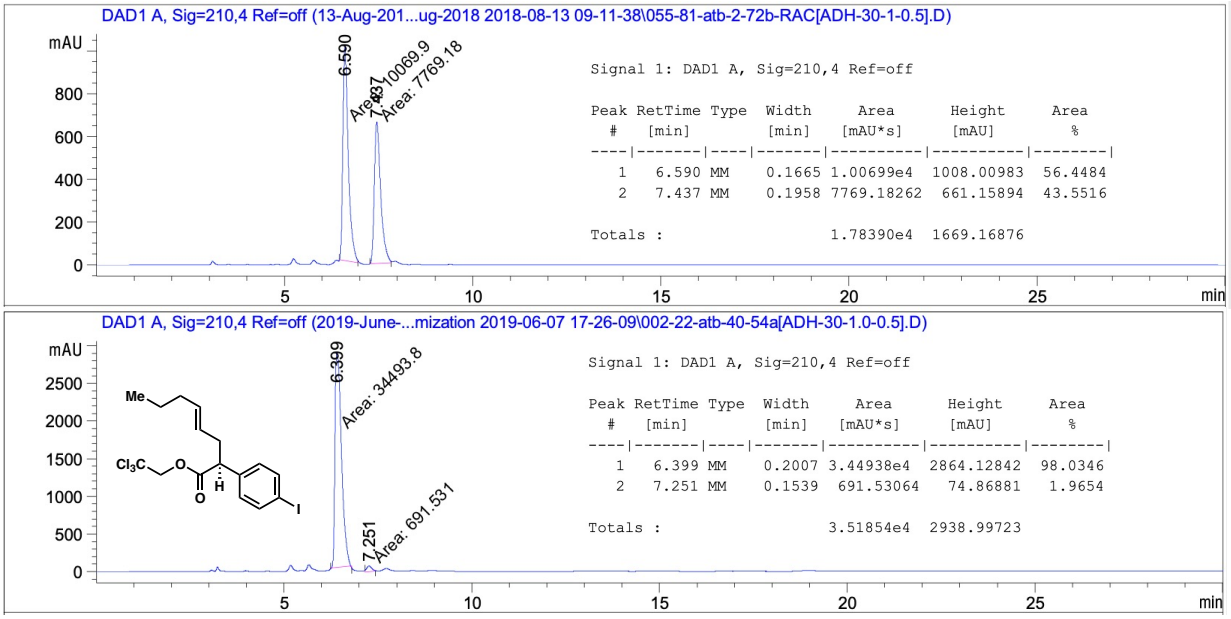

2,2,2-trifluoroethyl (*S*,*E*)-2-(4-methoxyphenyl)oct-4-enoate HPLC:

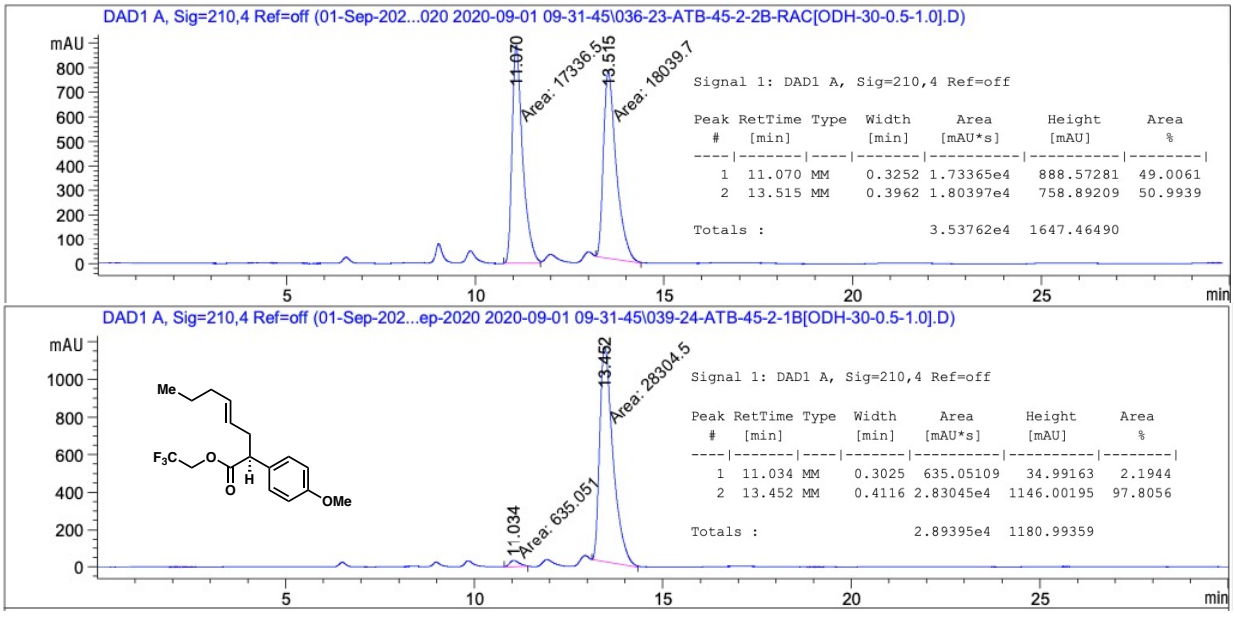

2,2,2-trichloroethyl (*S*,*E*)-2-(4-methoxyphenyl)oct-4-enoate HPLC:

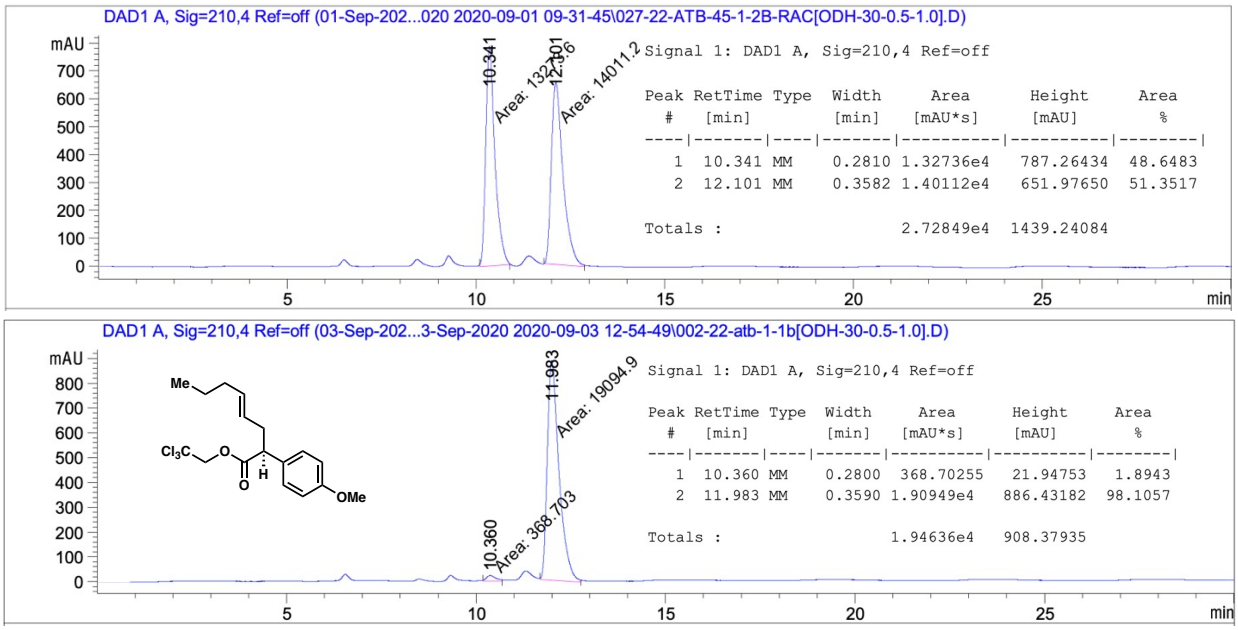

2,2,2-trifluoroethyl (*S*,*E*)-2,5-bis(4-methoxyphenyl)pent-4-enoate HPLC:

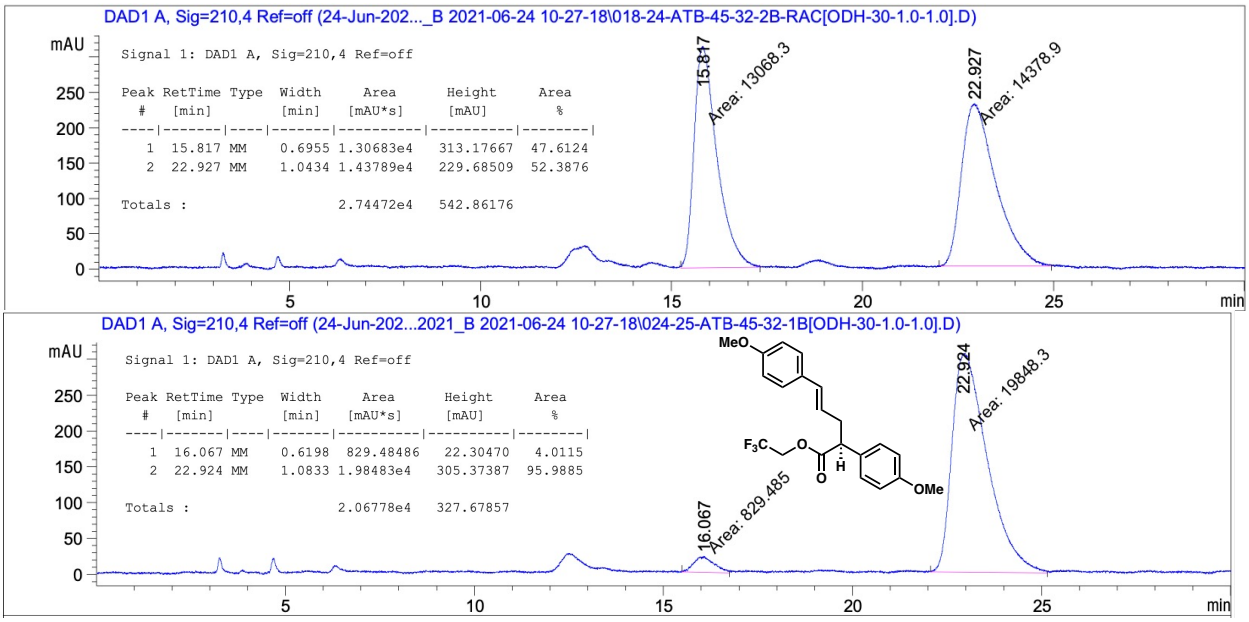

(*S*,*E*)-2-(4-iodophenyl)oct-4-enoic acid HPLC:

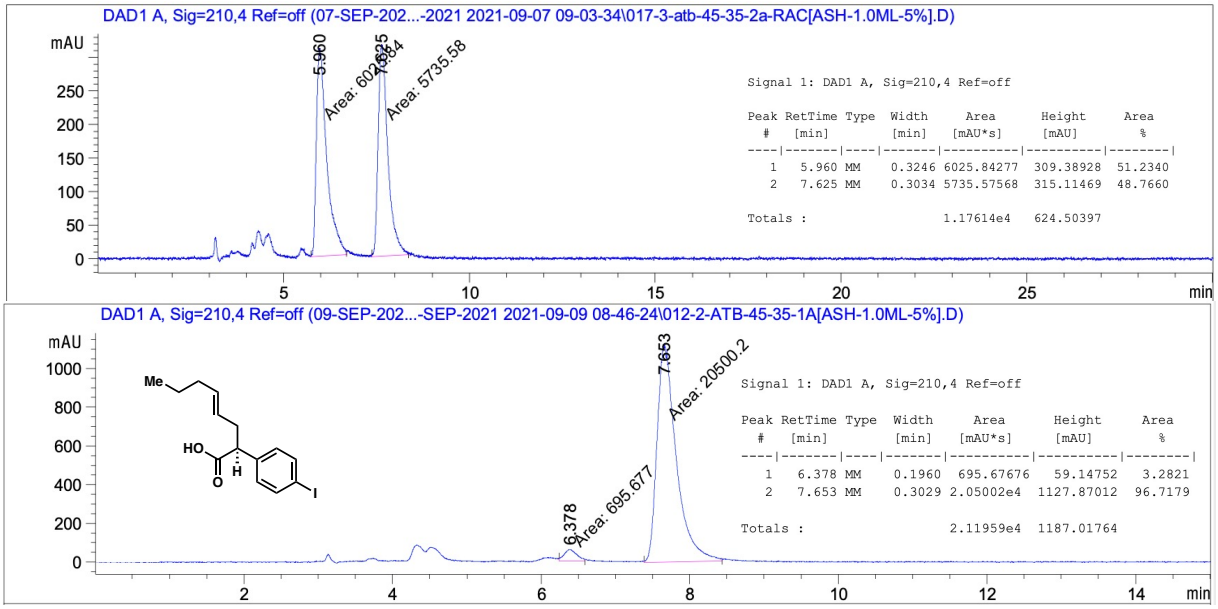

(*S*,*E*)-2-(4-iodophenyl)-*N*-methoxy-*N*-methyloct-4-enamide HPLC (via HATU coupling):

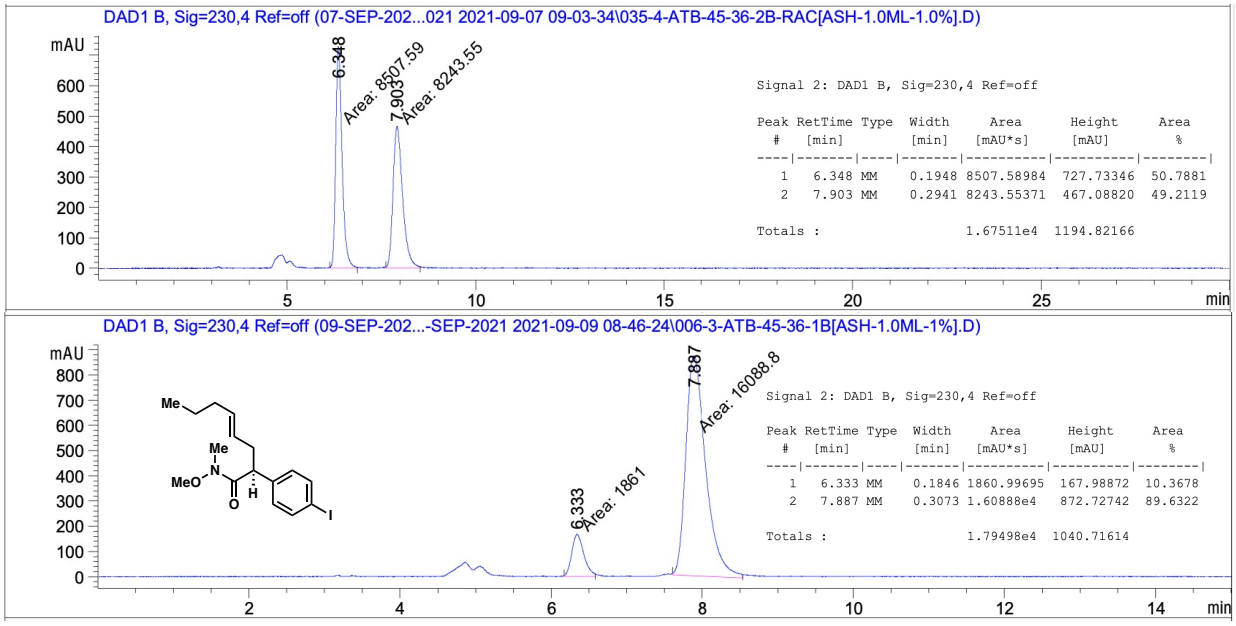

(*S*,*E*)-*N*-methoxy-2-(4-methoxyphenyl)-*N*-methyloct-4-enamide HPLC (via C–O coupling):

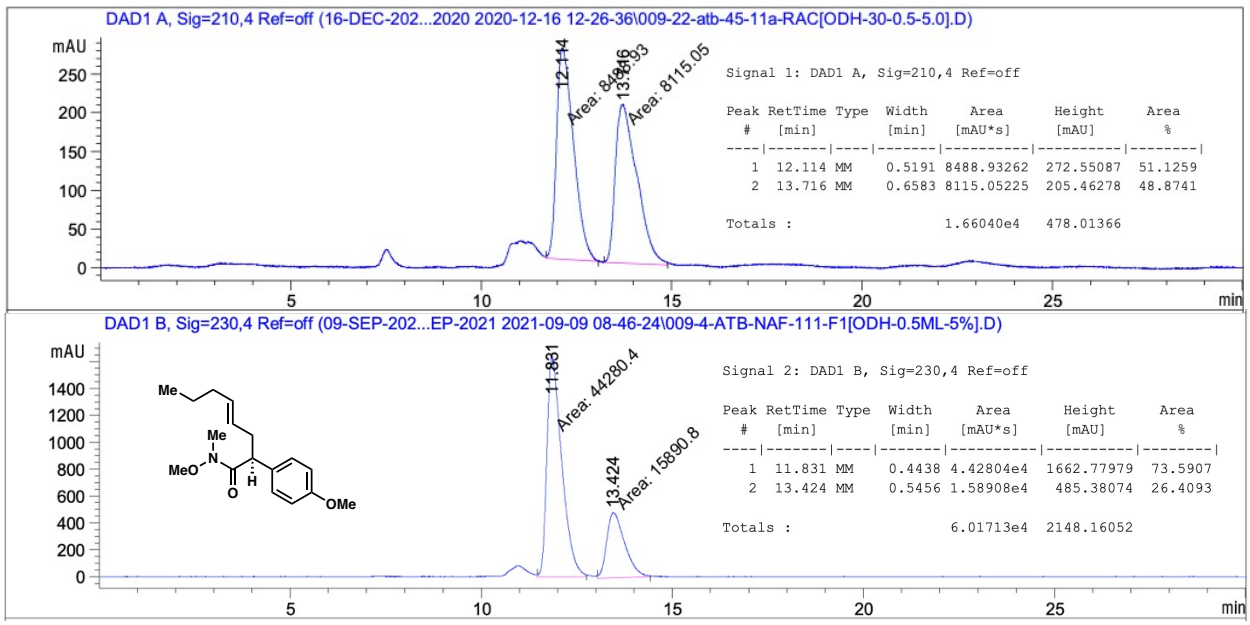

(*S*,*E*)-*N*-methoxy-2-(4-methoxyphenyl)-*N*-methyloct-4-enamide HPLC (via amide coupling with *i*PrMgCl):

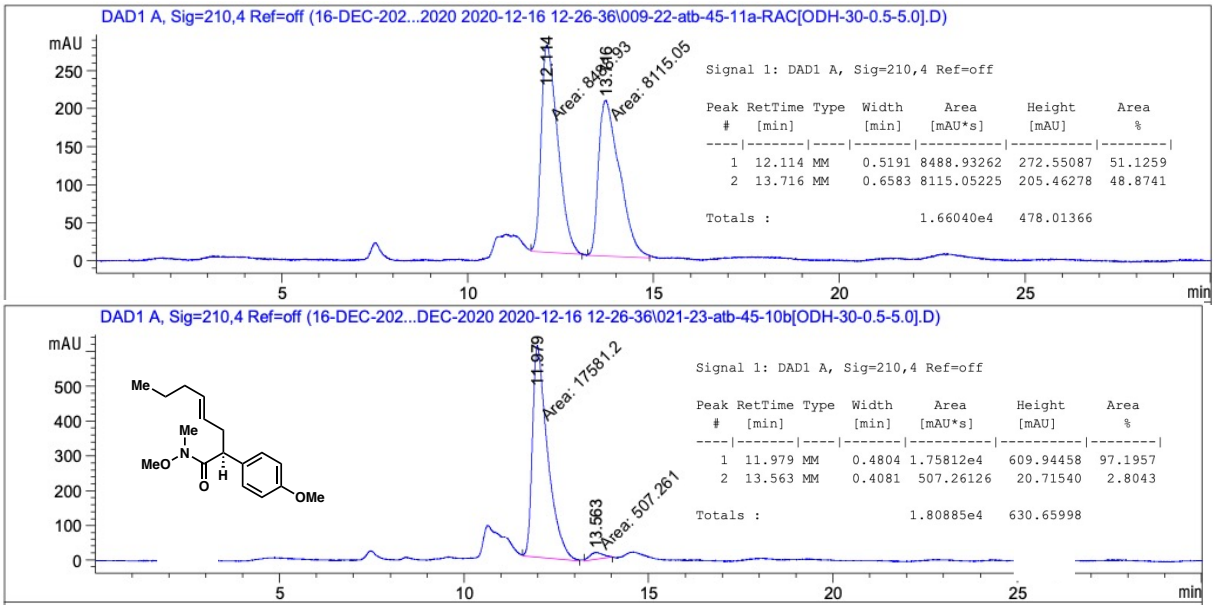

Appendix – Ch.4 HPLC Data

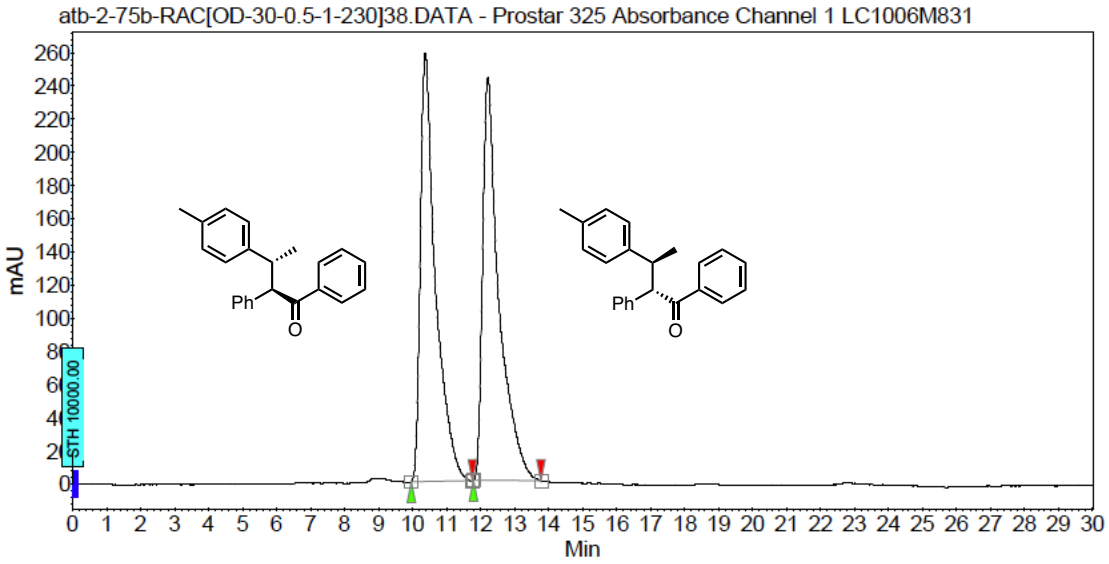

Peak results :

Index	Name	Time [Min]	Quantity [% Area]	Height [mAU]	Area [mAU.Min]	Area % [%]
1	UNKNOWN	10.38	49.51	257.7	133.4	49.515
2	UNKNOWN	12.22	50.49	243.1	136.0	50.485
Total			100.00	500.8	269.5	100.000

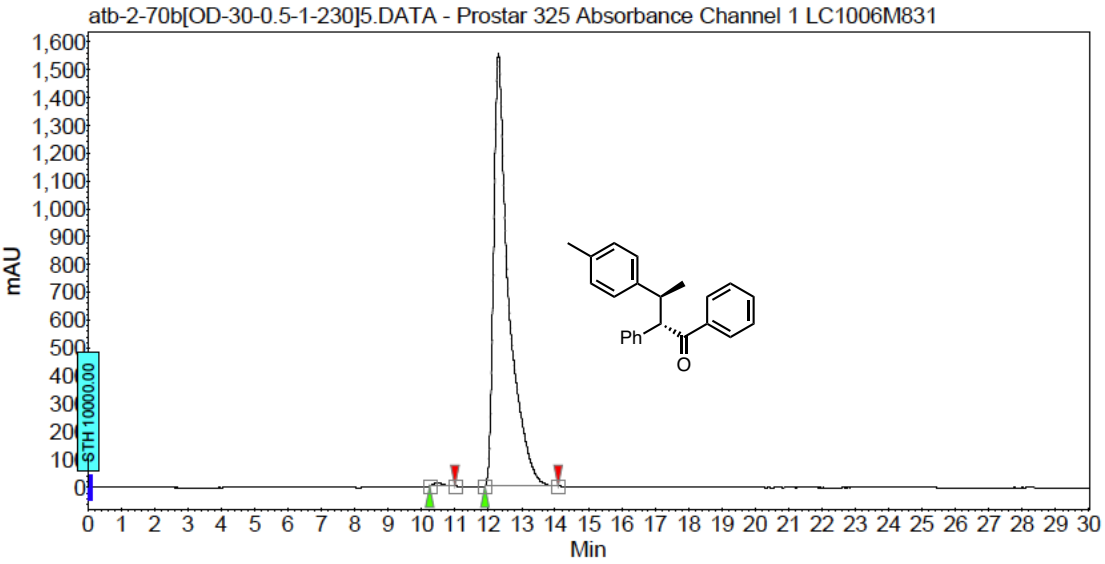

Peak results :

Index	Name	Time [Min]	Quantity [% Area]	Height [mAU]	Area [mAU.Min]	Area % [%]
1	UNKNOWN	10.45	0.55	12.2	4.5	0.549
2	UNKNOWN	12.30	99.45	1554.0	809.9	99.451
Total			100.00	1566.2	814.4	100.000

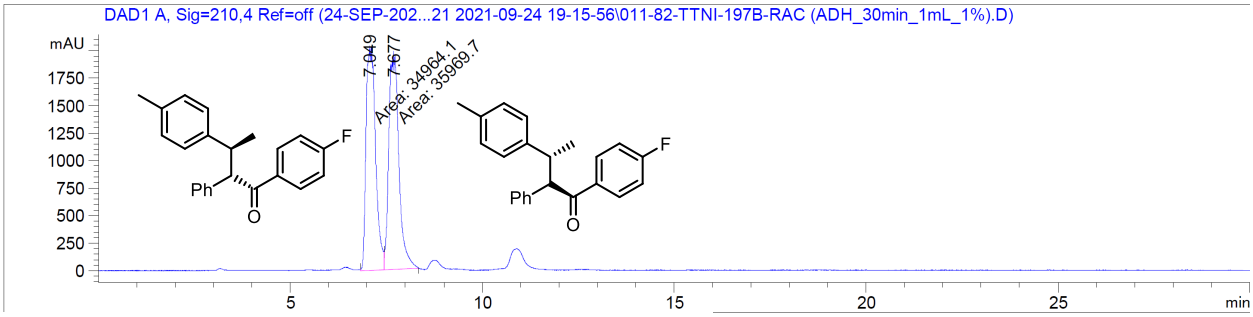

Signal 1: DAD1 A, Sig=210,4 Ref=off

Peak #	RetTime [min]	Type	Width [min]	Area [mAU*s]	Height [mAU]	Area %
1	7.049	MF	0.2850	3.49641e4	2044.89453	49.2912
2	7.677	FM	0.3014	3.59697e4	1989.03772	50.7088
Totals :				7.09338e4	4033.93225	

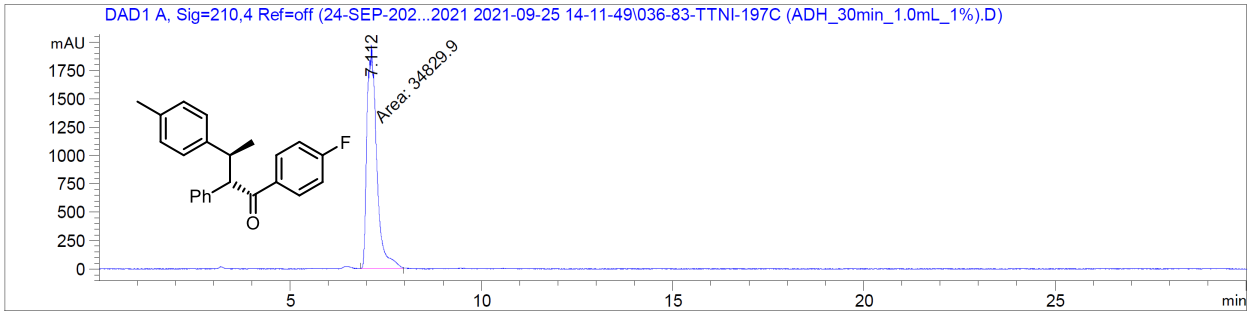

Signal 1: DAD1 A, Sig=210,4 Ref=off

Peak #	RetTime [min]	Type	Width [min]	Area [mAU*s]	Height [mAU]	Area %
1	7.112	MM	0.2947	3.48299e4	1969.95215	100.0000
Totals :				3.48299e4	1969.95215	

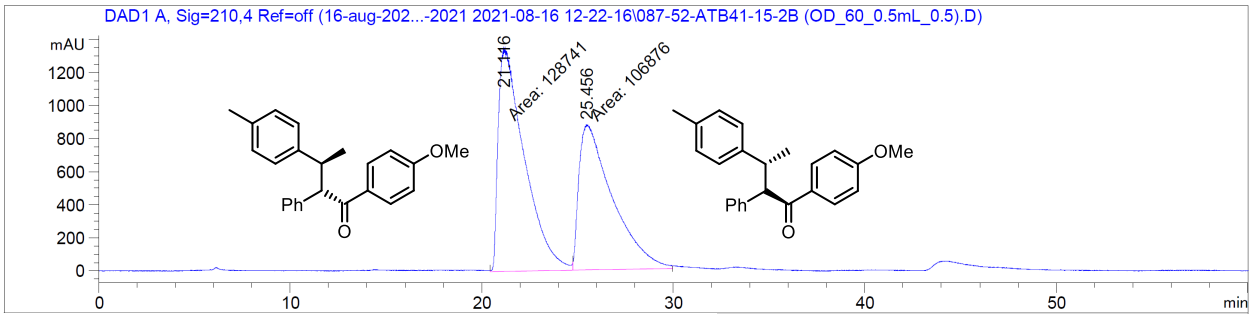

Signal 1: DAD1 A, Sig=210,4 Ref=off

Peak #	RetTime [min]	Type	Width [min]	Area [mAU*s]	Height [mAU]	Area %
1	21.116	MF	1.5730	1.28741e5	1364.04260	54.6401
2	25.456	FM	2.0181	1.06876e5	882.66443	45.3599
Totals :				2.35617e5	2246.70703	

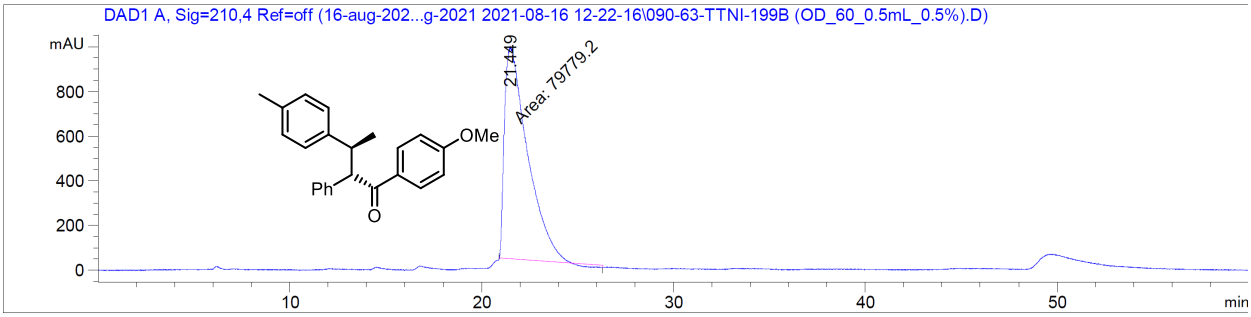

Signal 1: DAD1 A, Sig=210,4 Ref=off

Peak #	RetTime [min]	Type	Width [min]	Area [mAU*s]	Height [mAU]	Area %
1	21.449	MM	1.3925	7.97792e4	954.89221	100.0000
Totals :				7.97792e4	954.89221	

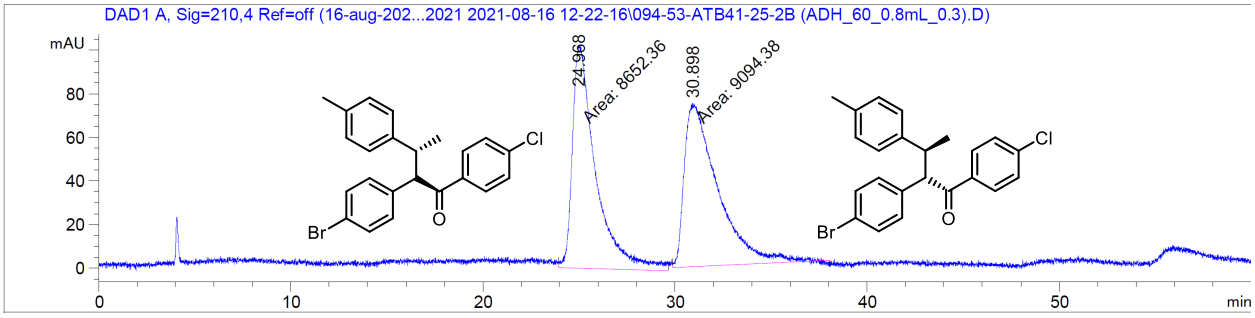

Signal 1: DAD1 A, Sig=210,4 Ref=off

Peak #	RetTime [min]	Type	Width [min]	Area [mAU*s]	Height [mAU]	Area %
1	24.968	MM	1.4103	8652.35742	102.25462	48.7547
2	30.898	MM	2.0190	9094.37500	75.07294	51.2453
Totals :				1.77467e4	177.32756	

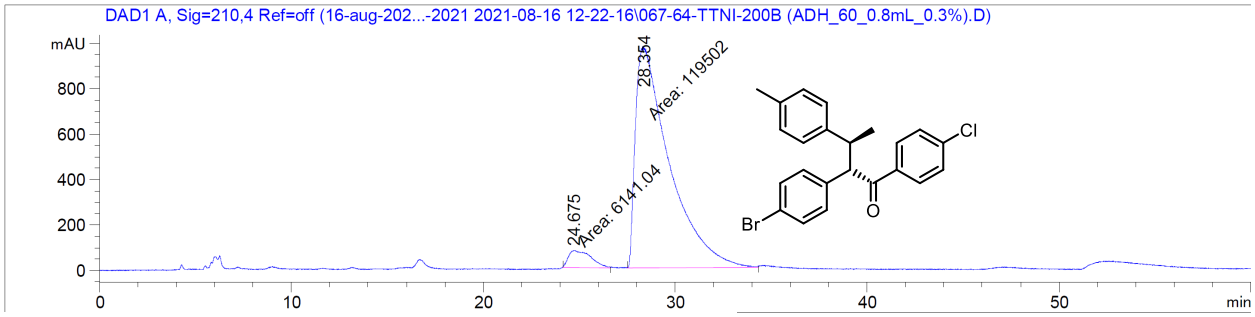

Signal 1: DAD1 A, Sig=210,4 Ref=off

Peak #	RetTime [min]	Type	Width [min]	Area [mAU*s]	Height [mAU]	Area %
1	24.675	MM	1.3670	6141.03760	74.87107	4.8877
2	28.354	MM	2.0366	1.19502e5	977.93500	95.1123
Totals :				1.25643e5	1052.80607	

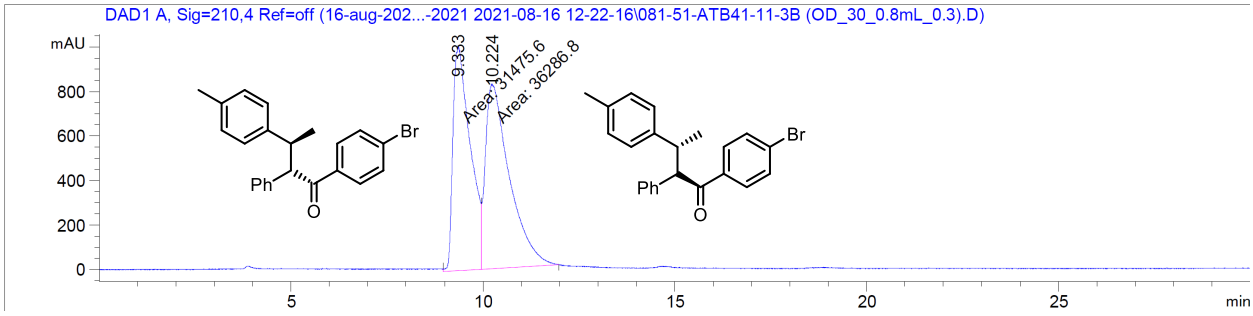

Signal 1: DAD1 A, Sig=210,4 Ref=off

Peak #	RetTime [min]	Type	Width [min]	Area [mAU*s]	Height [mAU]	Area %
1	9.333	MF	0.5183	3.14756e4	1012.05969	46.4500
2	10.224	FM	0.7267	3.62868e4	832.25238	53.5500
Totals :				6.77624e4	1844.31207	

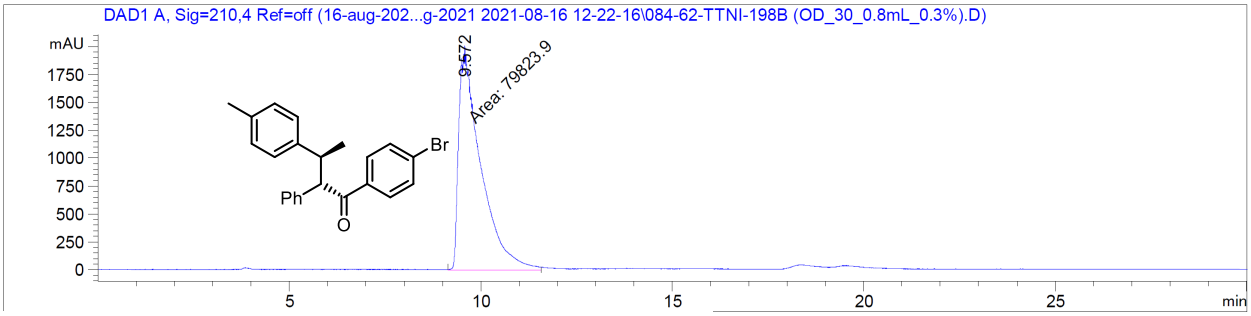

Signal 1: DAD1 A, Sig=210,4 Ref=off

Peak #	RetTime [min]	Type	Width [min]	Area [mAU*s]	Height [mAU]	Area %
1	9.572	MM	0.6591	7.98239e4	2018.53711	100.0000
Totals :				7.98239e4	2018.53711	

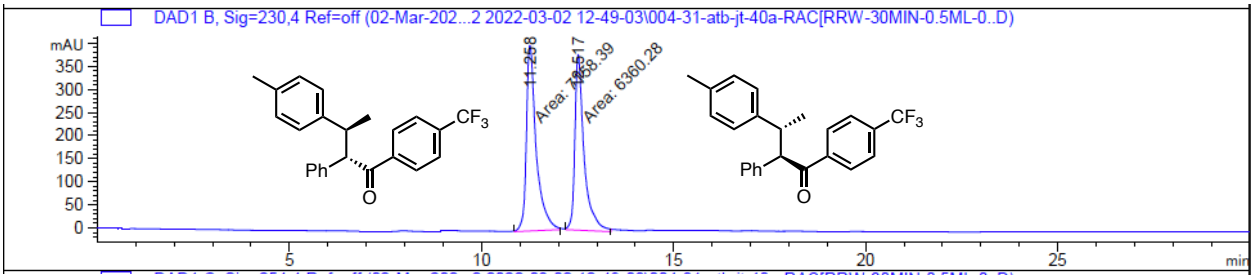

Signal 2: DAD1 B, Sig=230,4 Ref=off

Peak #	RetTime [min]	Type	Width [min]	Area [mAU*s]	Height [mAU]	Area %
1	11.258	MM	0.2971	7158.38770	401.52637	52.9519
2	12.517	MM	0.2790	6360.27539	379.92096	47.0481
Totals :				1.35187e4	781.44733	

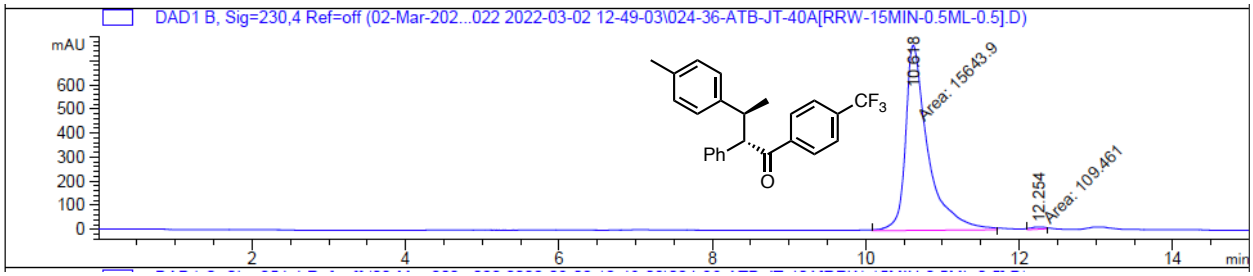

Signal 2: DAD1 B, Sig=230,4 Ref=off

Peak #	RetTime [min]	Type	Width [min]	Area [mAU*s]	Height [mAU]	Area %
1	10.618	MM	0.3393	1.56439e4	768.34760	99.3052
2	12.254	MM	0.1433	109.46097	9.15441	0.6948
Totals :				1.57534e4	777.50201	

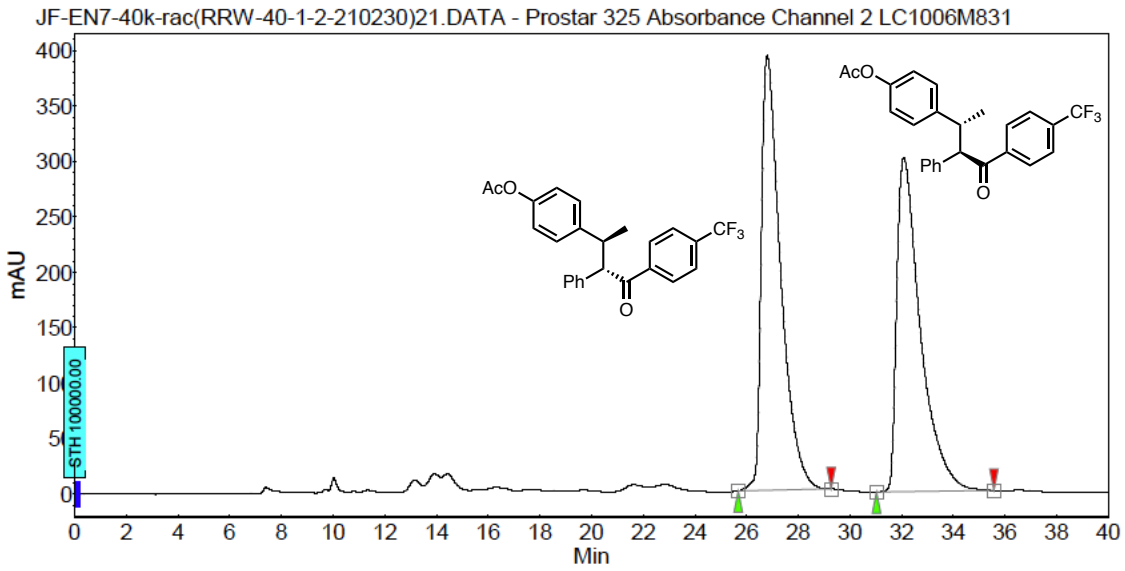

Peak results :

Index	Name	Time [Min]	Quantity [% Area]	Height [mAU]	Area [mAU.Min]	Area % [%]
1	UNKNOWN	26.81	51.59	392.4	340.2	51.591
2	UNKNOWN	32.09	48.41	301.2	319.2	48.409
Total			100.00	693.7	659.5	100.000

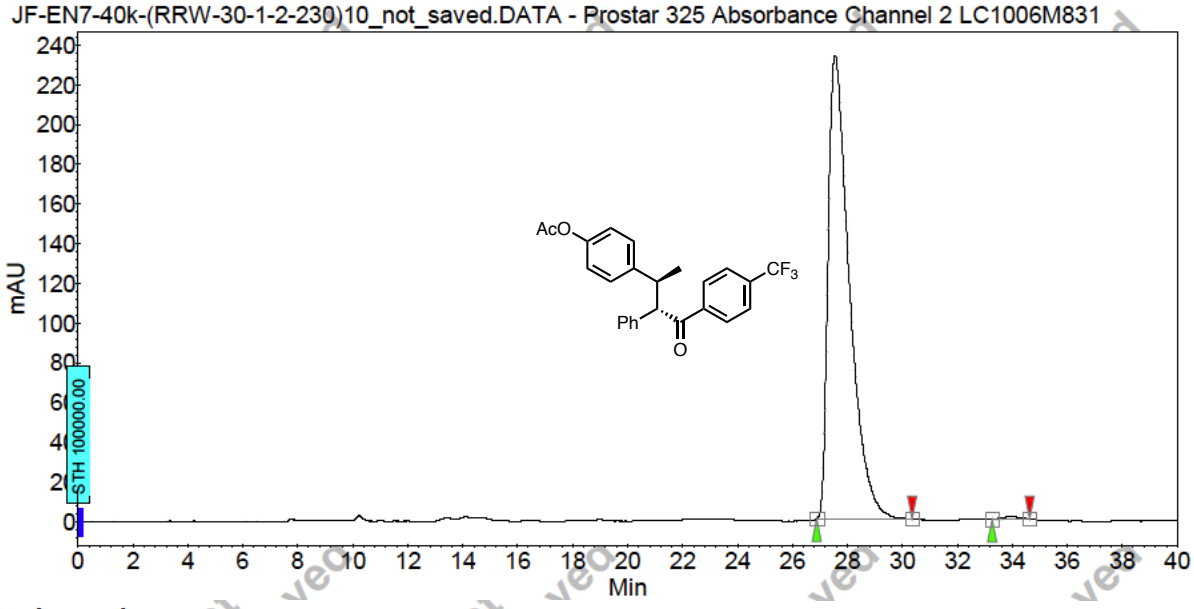

Peak results :

Index	Name	Time [Min]	Quantity [% Area]	Height [mAU]	Area [mAU.Min]	Area % [%]
1	UNKNOWN	27.55	99.50	233.8	209.8	99.498
2	UNKNOWN	33.89	0.50	1.5	1.1	0.502
Total			100.00	235.3	210.9	100.000

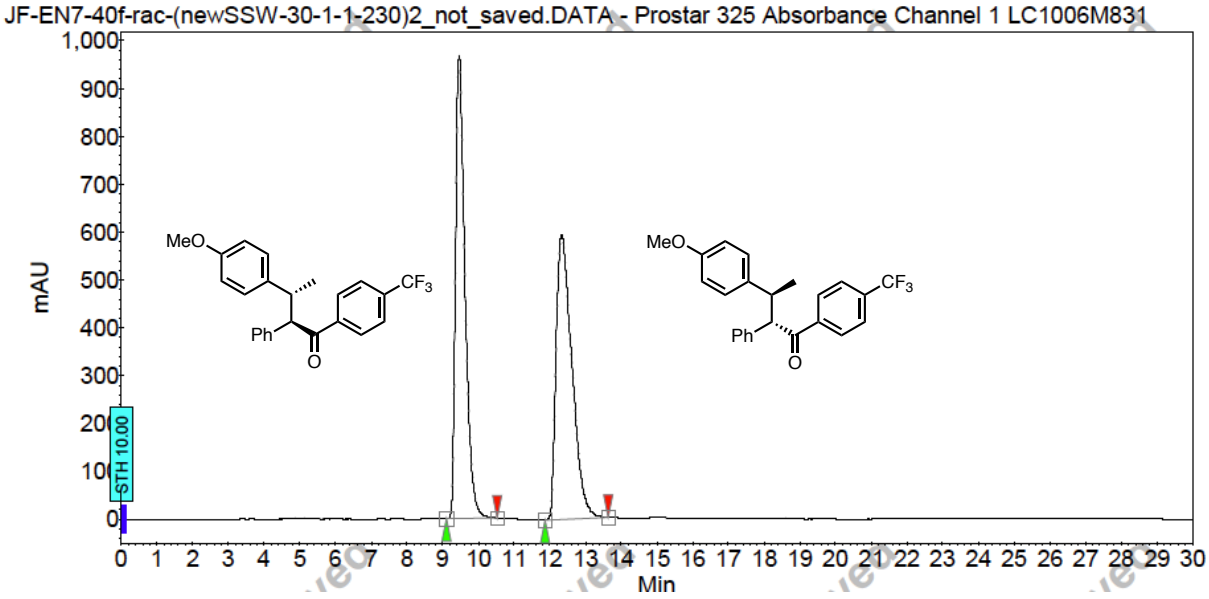

Peak results :

Index	Name	Time [Min]	Quantity [% Area]	Height [mAU]	Area [mAU.Min]	Area % [%]
1	UNKNOWN	9.46	49.28	968.3	297.0	49.282
2	UNKNOWN	12.33	50.72	595.3	305.6	50.718
Total			100.00	1563.6	602.6	100.000

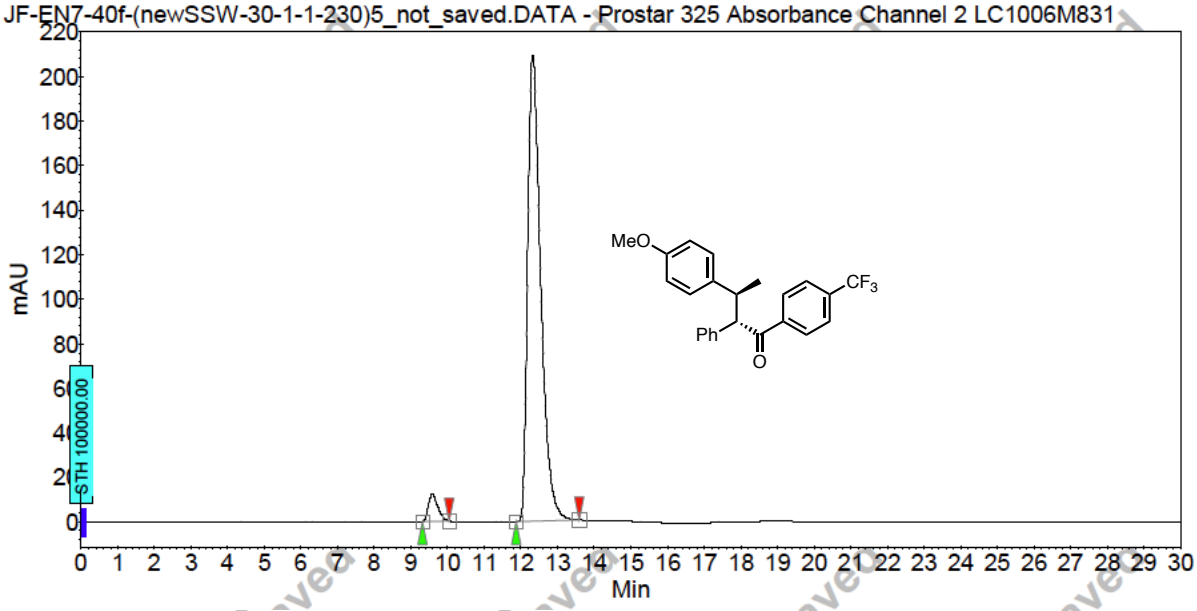

Peak results :

Index	Name	Time [Min]	Quantity [% Area]	Height [mAU]	Area [mAU.Min]	Area % [%]
1	UNKNOWN	9.58	4.03	12.3	3.6	4.034
2	UNKNOWN	12.32	95.97	209.3	86.1	95.966
Total			100.00	221.6	89.7	100.000

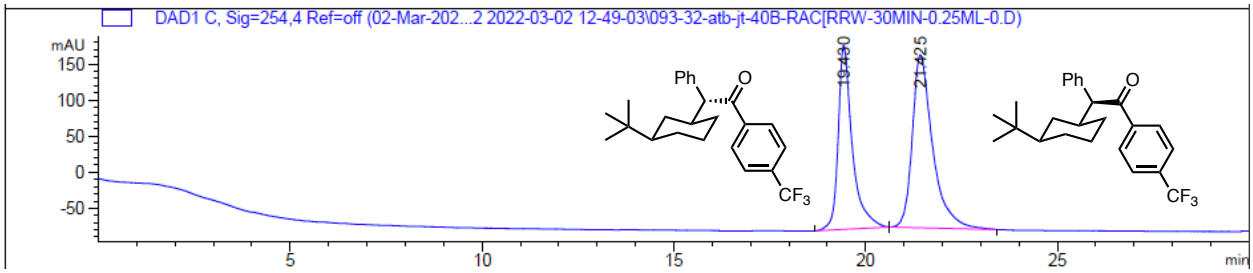

Signal 3: DAD1 C, Sig=254,4 Ref=off

Peak #	RetTime [min]	Type	Width [min]	Area [mAU*s]	Height [mAU]	Area %
1	19.430	BB	0.3554	6523.17822	255.00546	42.3810
2	21.425	BB	0.4518	8868.58594	239.63199	57.6190
Totals :				1.53918e4	494.63745	

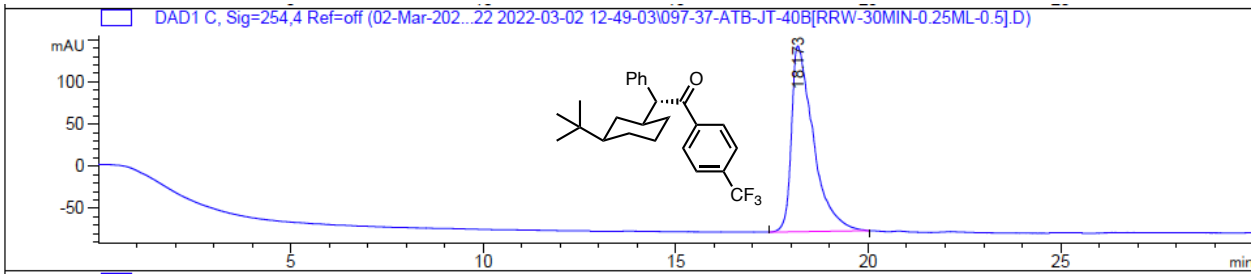

Signal 3: DAD1 C, Sig=254,4 Ref=off

Peak #	RetTime [min]	Type	Width [min]	Area [mAU*s]	Height [mAU]	Area %
1	18.173	BB	0.4717	8701.77051	219.88354	100.0000
Totals :				8701.77051	219.88354	

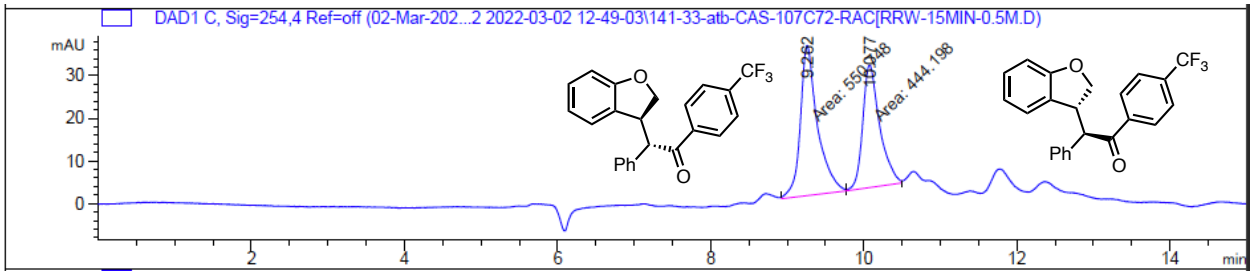

Signal 3: DAD1 C, Sig=254,4 Ref=off

Peak #	RetTime [min]	Type	Width [min]	Area [mAU*s]	Height [mAU]	Area %
1	9.262	MM	0.2603	550.74811	35.25984	55.3546
2	10.077	MM	0.2576	444.19769	28.73804	44.6454
Totals :				994.94580	63.99788	

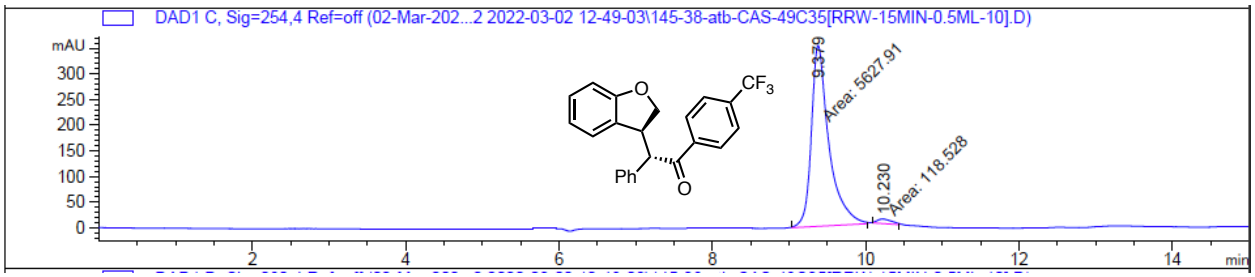

Signal 3: DAD1 C, Sig=254,4 Ref=off

Peak #	RetTime [min]	Type	Width [min]	Area [mAU*s]	Height [mAU]	Area %
1	9.379	MM	0.2666	5627.91016	351.82410	97.9374
2	10.230	MM	0.2215	118.52838	8.91872	2.0626
Totals :				5746.43854	360.74282	

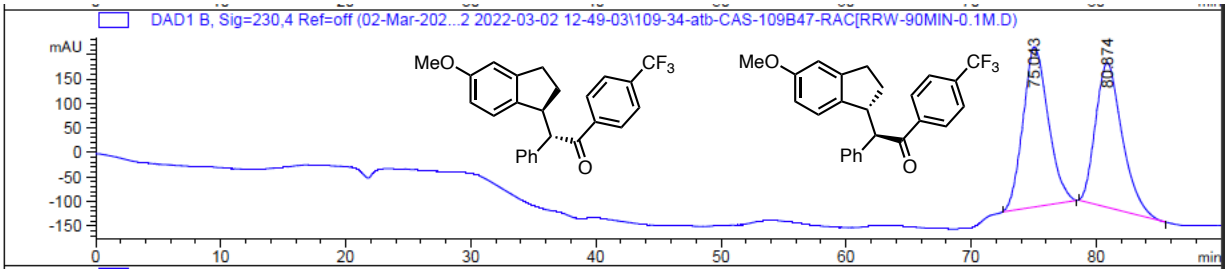

Signal 2: DAD1 B, Sig=230,4 Ref=off

Peak #	RetTime [min]	Type	Width [min]	Area [mAU*s]	Height [mAU]	Area %
1	75.043	BB	1.6340	4.56618e4	326.31503	51.1236
2	80.874	BB	1.7343	4.36547e4	294.26077	48.8764
Totals :				8.93165e4	620.57581	

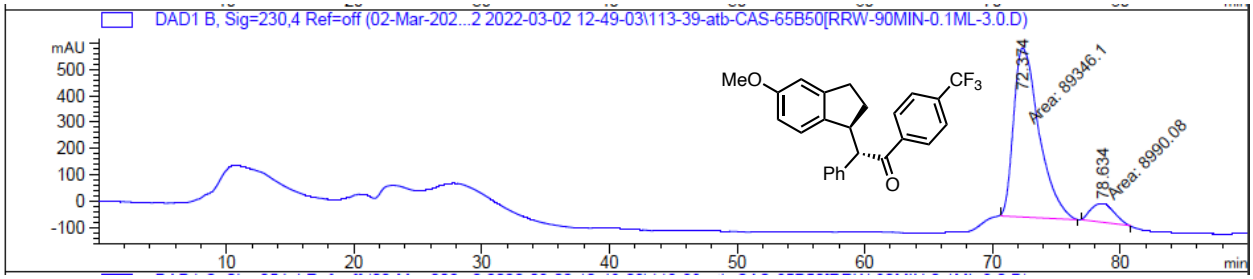

Signal 2: DAD1 B, Sig=230,4 Ref=off

Peak #	RetTime [min]	Type	Width [min]	Area [mAU*s]	Height [mAU]	Area %
1	72.374	MM	2.3145	8.93461e4	643.37170	90.8578
2	78.634	MM	2.0799	8990.08203	72.03977	9.1422
Totals :				9.83362e4	715.41148	

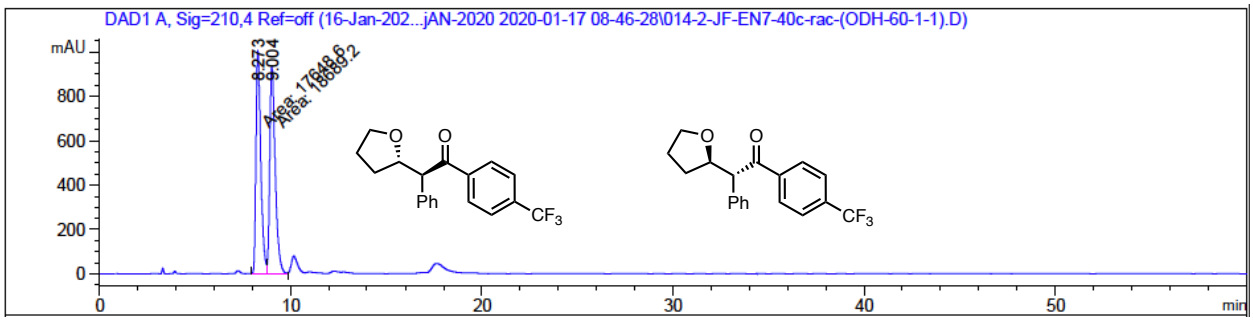

Signal 1: DAD1 A, Sig=210,4 Ref=off

Peak #	RetTime [min]	Type	Width [min]	Area [mAU*s]	Height [mAU]	Area %
1	8.273	MF	0.2915	1.76486e4	1009.18073	48.5682
2	9.004	FM	0.3341	1.86892e4	932.24548	51.4318
Totals :				3.63379e4	1941.42621	

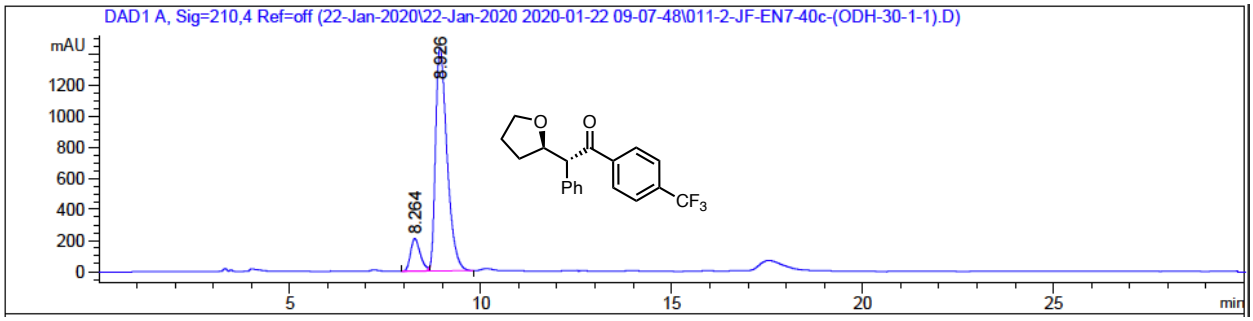

Signal 1: DAD1 A, Sig=210,4 Ref=off

Peak #	RetTime [min]	Type	Width [min]	Area [mAU*s]	Height [mAU]	Area %
1	8.264	BV E	0.2671	3717.57568	209.89127	10.9328
2	8.926	VB R	0.2980	3.02862e4	1439.06470	89.0672
Totals :				3.40038e4	1648.95596	

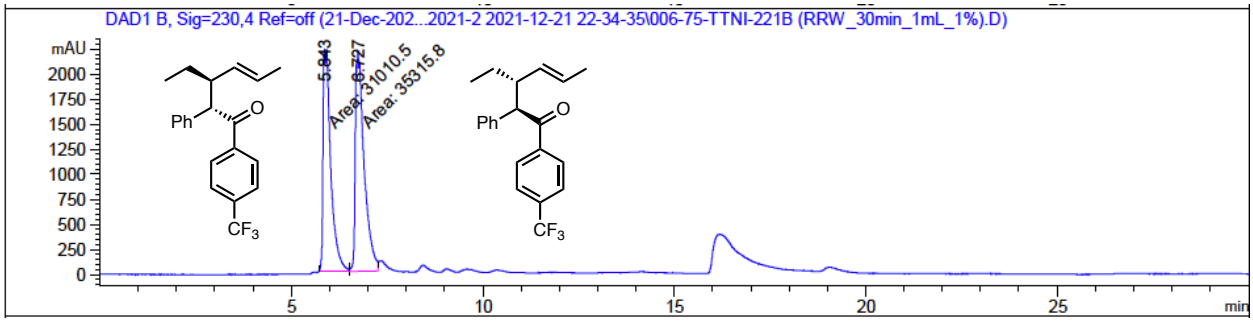

Signal 2: DAD1 B, Sig=230,4 Ref=off

Peak #	RetTime [min]	Type	Width [min]	Area [mAU*s]	Height [mAU]	Area %
1	5.843	MF	0.2332	3.10105e4	2216.41772	46.7544
2	6.727	FM	0.2666	3.53158e4	2207.50488	53.2456
Totals :				6.63263e4	4423.92261	

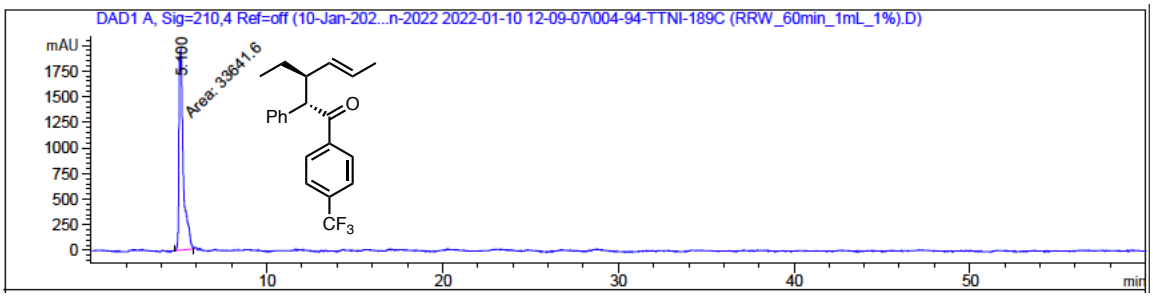

Signal 1: DAD1 A, Sig=210,4 Ref=off

Peak #	RetTime [min]	Type	Width [min]	Area [mAU*s]	Height [mAU]	Area %
1	5.100	MM	0.2826	3.36416e4	1983.71790	100.0000
Totals :				3.36416e4	1983.71790	

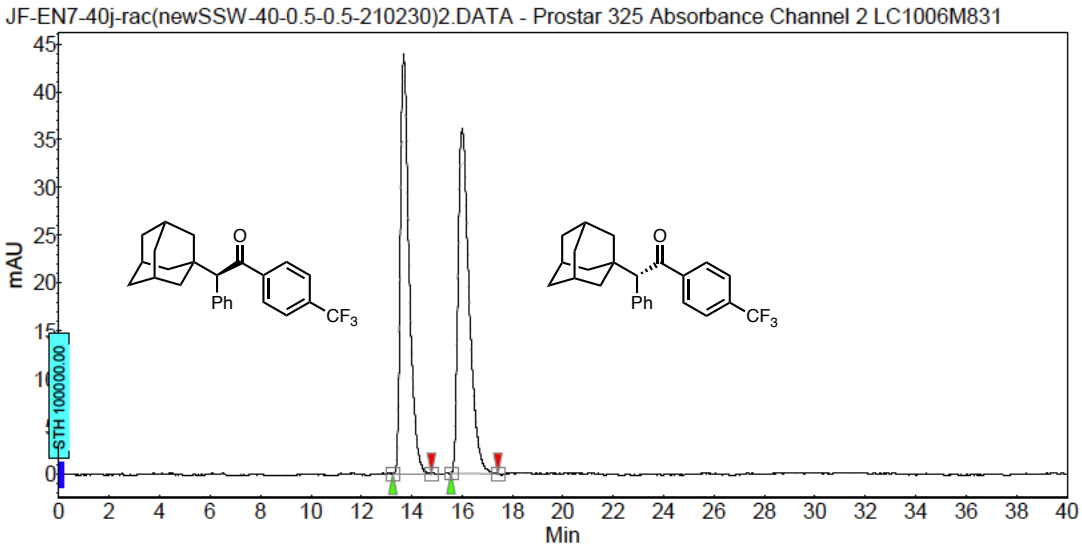

Peak results :

Index	Name	Time [Min]	Quantity [% Area]	Height [mAU]	Area [mAU.Min]	Area % [%]
1	UNKNOWN	13.68	48.76	44.0	17.6	48.761
2	UNKNOWN	16.00	51.24	36.1	18.5	51.239
Total			100.00	80.0	36.1	100.000

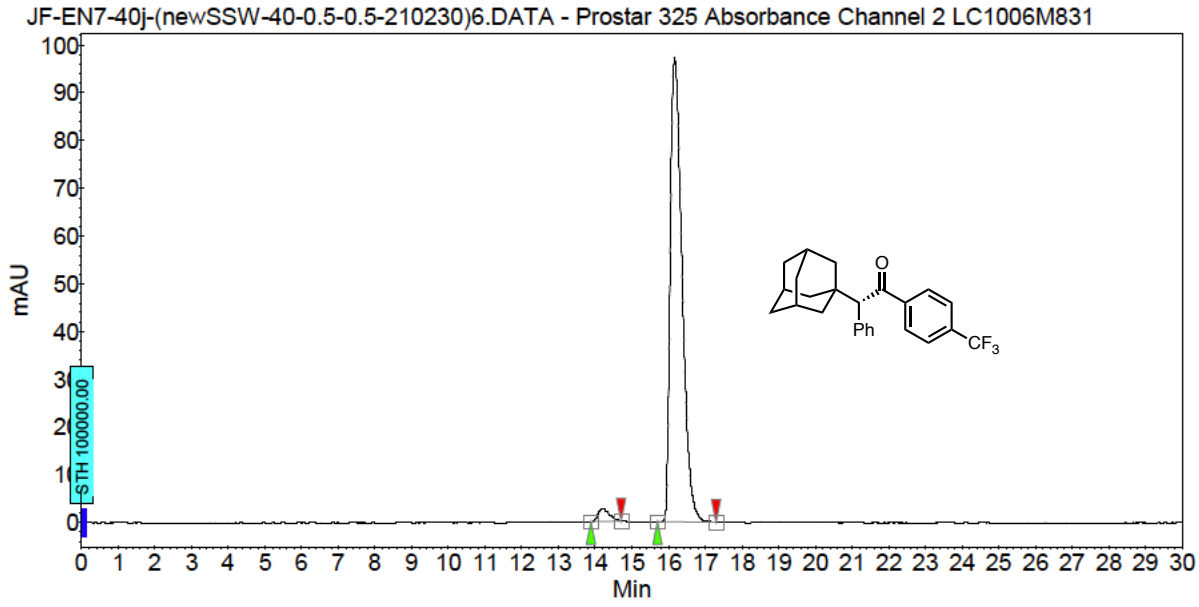

Peak results :

Index	Name	Time [Min]	Quantity [% Area]	Height [mAU]	Area [mAU.Min]	Area % [%]
1	UNKNOWN	14.20	2.62	2.8	1.0	2.622
2	UNKNOWN	16.16	97.38	97.4	36.2	97.378
Total			100.00	100.2	37.2	100.000

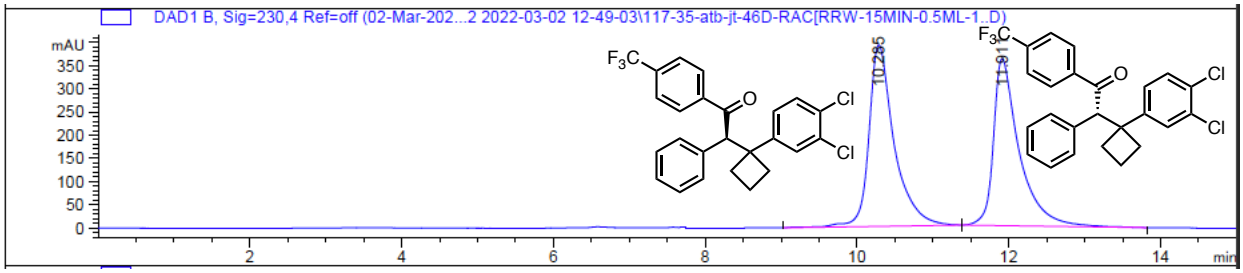

Signal 2: DAD1 B, Sig=230,4 Ref=off

Peak #	RetTime [min]	Type	Width [min]	Area [mAU*s]	Height [mAU]	Area %
1	10.285	BB	0.3330	9042.07227	390.73837	51.6616
2	11.911	BB	0.3379	8460.42480	359.68314	48.3384
Totals :				1.75025e4	750.42151	

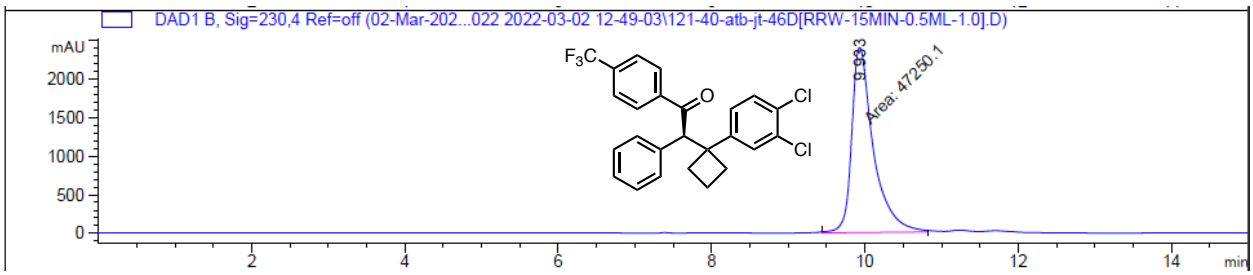

Signal 2: DAD1 B, Sig=230,4 Ref=off

Peak #	RetTime [min]	Type	Width [min]	Area [mAU*s]	Height [mAU]	Area %
1	9.933	MM	0.3282	4.72501e4	2399.23218	100.0000
Totals :				4.72501e4	2399.23218	

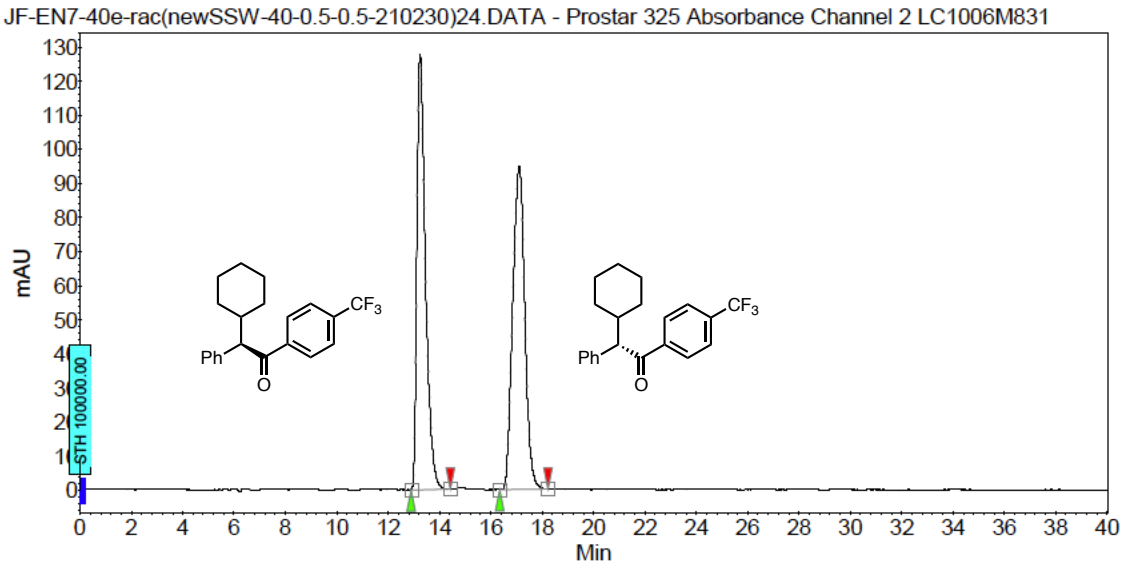

Peak results :

Index	Name	Time [Min]	Quantity [% Area]	Height [mAU]	Area [mAU.Min]	Area % [%]
1	UNKNOWN	13.24	48.93	127.6	49.7	48.929
2	UNKNOWN	17.10	51.07	94.8	51.9	51.071
Total			100.00	222.5	101.6	100.000

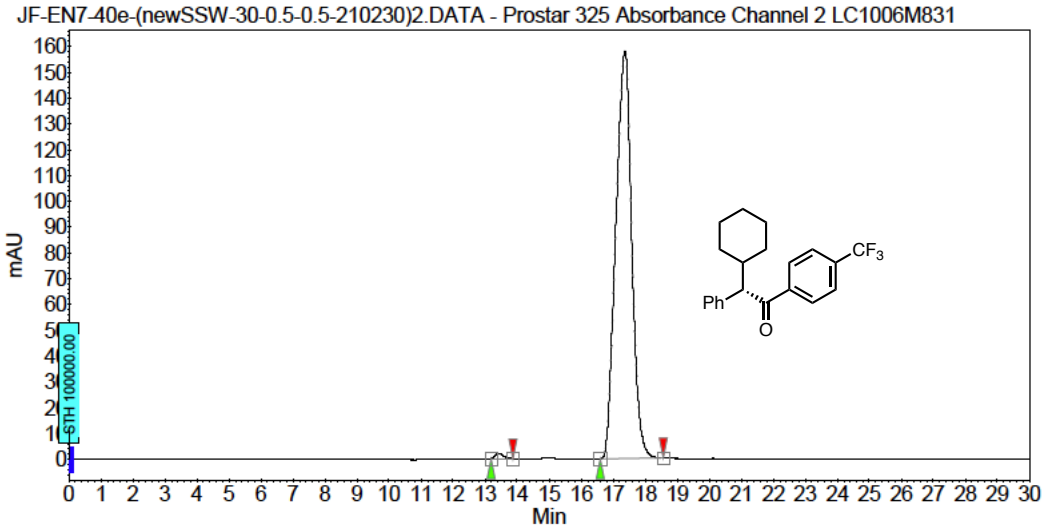

Peak results :

Index	Name	Time [Min]	Quantity [% Area]	Height [mAU]	Area [mAU.Min]	Area % [%]
1	UNKNOWN	13.43	0.69	2.0	0.6	0.688
2	UNKNOWN	17.37	99.31	157.8	90.9	99.312
Total			100.00	159.9	91.5	100.000

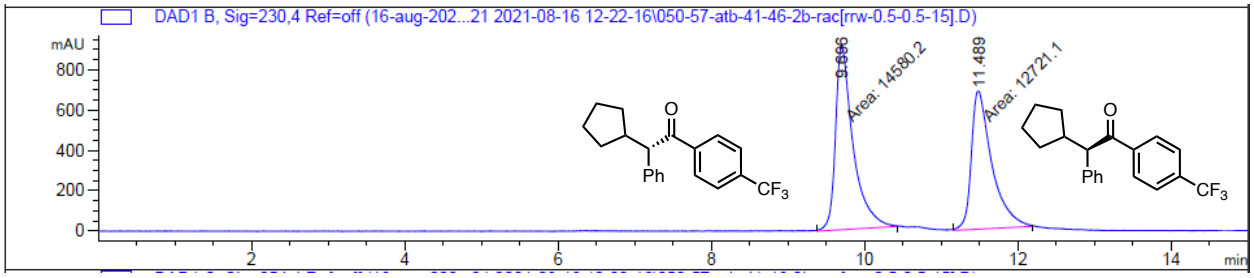

Signal 2: DAD1 B, Sig=230,4 Ref=off

Peak #	RetTime [min]	Type	Width [min]	Area [mAU*s]	Height [mAU]	Area %
1	9.696	MM	0.2651	1.45802e4	916.55933	53.4049
2	11.489	MM	0.3100	1.27211e4	683.90594	46.5951
Totals :				2.73013e4	1600.46527	

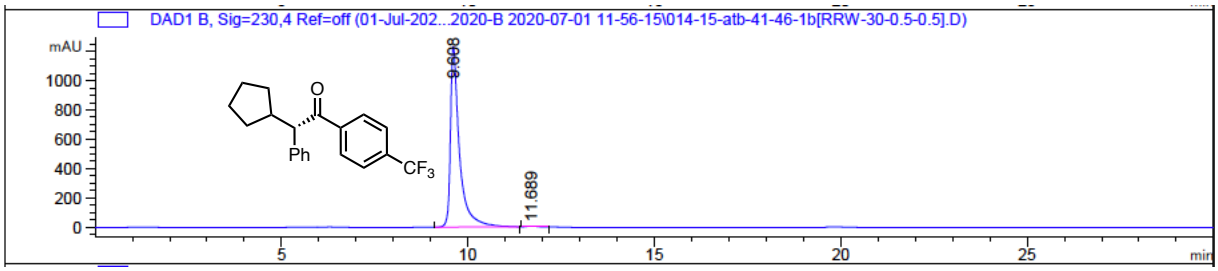

Signal 2: DAD1 B, Sig=230,4 Ref=off

Peak #	RetTime [min]	Type	Width [min]	Area [mAU*s]	Height [mAU]	Area %
1	9.608	VV R	0.2366	2.08042e4	1231.51782	99.5537
2	11.689	VB R	0.1912	93.26826	5.78229	0.4463
Totals :				2.08975e4	1237.30011	

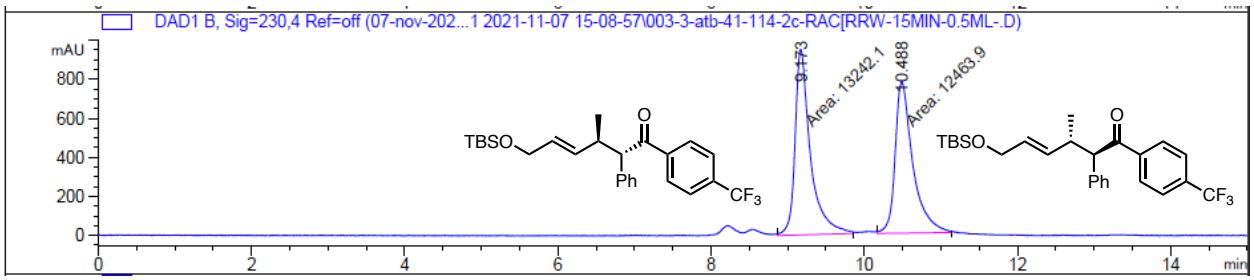

Signal 2: DAD1 B, Sig=230,4 Ref=off

Peak #	RetTime [min]	Type	Width [min]	Area [mAU*s]	Height [mAU]	Area %
1	9.173	MM	0.2322	1.32421e4	950.63538	51.5137
2	10.488	MM	0.2663	1.24639e4	780.21088	48.4863

Totals : 2.57060e4 1730.84625

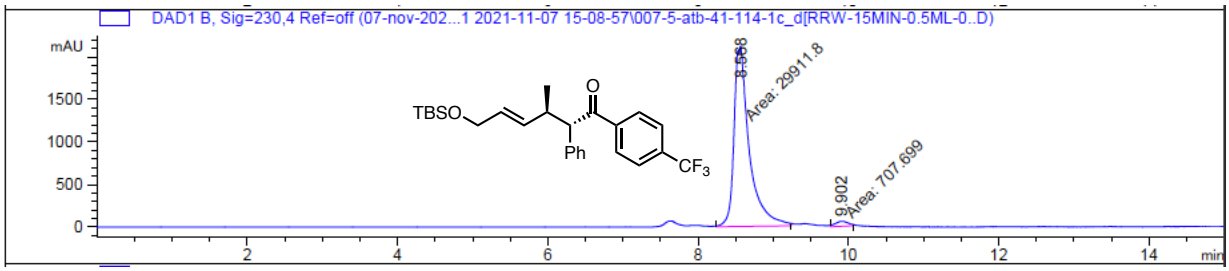

Signal 2: DAD1 B, Sig=230,4 Ref=off

Peak #	RetTime [min]	Type	Width [min]	Area [mAU*s]	Height [mAU]	Area %
1	8.568	MM	0.2344	2.99118e4	2126.39966	97.6887
2	9.902	MM	0.1947	707.69910	60.58871	2.3113

Totals : 3.06195e4 2186.98837

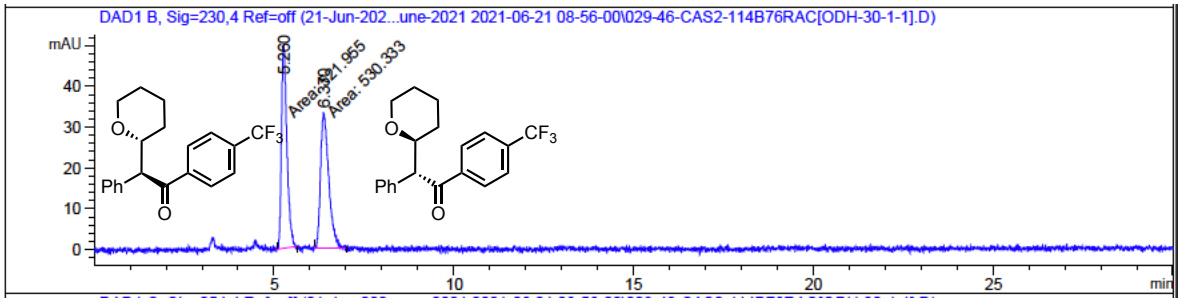

Signal 2: DAD1 B, Sig=230,4 Ref=off

Peak #	RetTime [min]	Type	Width [min]	Area [mAU*s]	Height [mAU]	Area %
1	5.260	MM	0.1745	521.95471	49.86419	49.6019
2	6.370	MM	0.2647	530.33270	33.39367	50.3981
Totals :				1052.28741	83.25787	

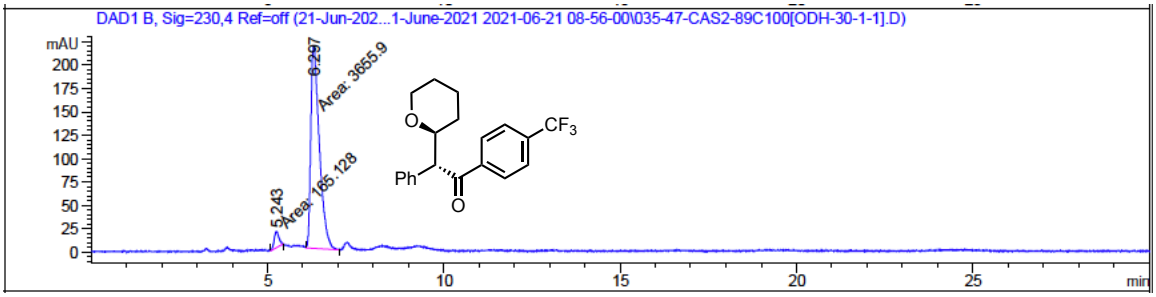

Signal 2: DAD1 B, Sig=230,4 Ref=off

Peak #	RetTime [min]	Type	Width [min]	Area [mAU*s]	Height [mAU]	Area %
1	5.243	MM	0.1578	165.12849	17.43653	4.3216
2	6.297	MM	0.2817	3655.89624	216.27599	95.6784
Totals :				3821.02473	233.71252	

Appendix – Ch.2 X-ray Crystallographic Data

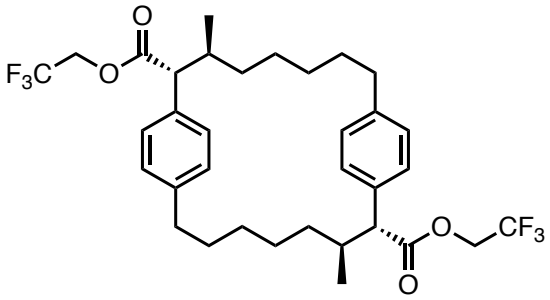

bis(2,2,2-trifluoroethyl) (2*R*,3*S*,10*R*,11*S*)-3,11-dimethyl-1,9(1,4)-dibenzenacyclohexadecaphane-2,10-dicarboxylate

Crystal Data and Experimental

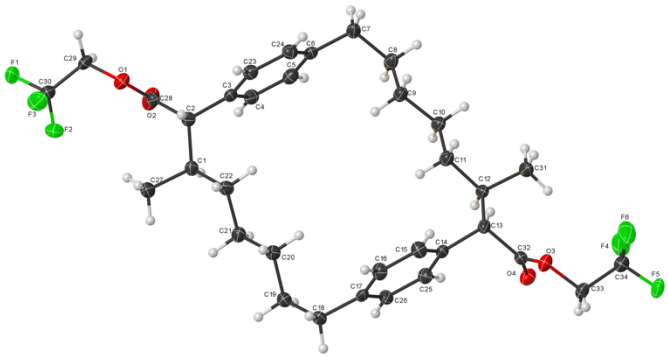

Experimental. Single colorless needle-shaped crystals of **Aaron-macrocycle** were recrystallized from hexane by slow evaporation. A suitable crystal 0.57×0.06×0.04 mm^3 was selected and mounted on a loopon a XtaLAB Synergy, Dualflex, HyPix diffractometer. The crystal was kept at a steady T = 100(2) K during data collection.The structure was solved with the **ShelXT** (Sheldrick, 2015) structure solution program usingthe Intrinsic Phasing solution method and by using **Olex2** (Dolomanov et al., 2009) as the graphical interface. The model was refined with version 2018/3 of **ShelXL** (Sheldrick, 2015)using Least Squares minimisation.

Crystal Data. $C_{34}H_{42}F_6O_4$, M_r = 628.67, monoclinic, $P2$ (No. 3), a = 25.1525(4) Å, b = 5.53398(4) Å, c = 27.2474(4) Å, β = 117.4652(19)°, α = γ = 90°, V = 3365.19(9) Å^3, T = 100(2) K, Z = 4, Z' = 2, μ(CuK$_\alpha$) = 0.866 mm^{-1}, 42058 reflections measured, 10947 unique (R_{int} = 0.0510) which were used in all calculations. The final wR_2 was 0.0885 (all data) and R_1 was 0.0363 (I > 2σ(I)).

Compound	**Aaron-macrocycle**
Formula	$C_{34}H_{42}F_6O_4$
$D_{calc.}$/ g cm^{-3}	1.241
μ/mm^{-1}	0.866
Formula Weight	628.67
Colour	colourless
Shape	needle
Size/mm^3	0.57×0.06×0.04
T/K	100(2)
Crystal System	monoclinic
Flack Parameter	-0.02(6)
Hooft Parameter	-0.00(5)
Space Group	$P2$
a/Å	25.1525(4)
b/Å	5.53398(4)
c/Å	27.2474(4)
α/°	90
β/°	117.4652(19)
γ/°	90
V/Å^3	3365.19(9)
Z	4
Z'	2
Wavelength/Å	1.54184
Radiation type	CuK$_\alpha$
Θ_{min}/°	1.980
Θ_{max}/°	73.814
Measured Refl.	42058
Independent Refl.	10947
Reflections with I > 2σ(I)	9975
R_{int}	0.0510
Parameters	797
Restraints	1
Largest Peak	0.323
Deepest Hole	-0.205
GooF	0.985
wR_2 (all data)	0.0885
wR_2	0.0853
R_1 (all data)	0.0412
R_1	0.0363

Structure Quality Indicators

Reflections: d min (Cu) 0.80 | I/σ 23.6 | Rint 5.10%

Refinement: Shift -0.008 | Max Peak 0.3 | Min Peak -0.2 | GooF 0.985 | Flack -.02(6)

A colourless needle-shaped crystal with dimensions 0.57×0.06×0.04 mm^3 was mounted on a loop. Data were collected using an XtaLAB Synergy, Dualflex, HyPix diffractometer equipped with an Oxford Cryosystems low-temperature device operating at T = 100(2) K.

Data were measured using ω scans with a narrow frame width of 0.5° per frame for 3.5/3.7/10.0 s using CuK_α radiation. The total number of runs and images was based on the strategy calculation from the program **CrysAlisPro** (Rigaku, V1.171.39.43c, 2018). The maximum resolution that was achieved was Θ = 73.814°.

The diffraction pattern was indexed using **CrysAlisPro** (Rigaku, V1.171.39.43c, 2018) and the unit cell was refined using **CrysAlisPro** (Rigaku, V1.171.39.43c, 2018) on 24772 reflections, 59% of the observed reflections.

Data reduction, scaling and absorption corrections were performed using **CrysAlisPro** (Rigaku, V1.171.39.43c, 2018). The final completeness is 98.70 % out to 73.814° in Θ. A numerical absorption correction based on Gaussian integration over a multifaceted crystal model was applied using CrysAlisPro 1.171.39.43c (Rigaku Oxford Diffraction, 2018). An empirical absorption correction using spherical harmonics as implemented by SCALE3 ABSPACK algorithm was applied. The absorption coefficient μ of this material is 0.866 mm^{-1} at this wavelength (λ = 1.54184Å) and the minimum and maximum transmissions are 0.487 and 1.000.

The structure was solved and the space group $P2$ (# 3) determined by the **ShelXT** (Sheldrick, 2015) structure solution program using Intrinsic Phasing and refined by Least Squares using version 2018/3 of **ShelXL-2014** (Sheldrick, 2015). All non-hydrogen atoms were refined anisotropically. Hydrogen atom positions were calculated geometrically and refined using the riding model.Hydrogen atom positions were calculated geometrically and refined using the riding model.

The value of Z' is 2. This means that there are two independent molecules in the asymmetric unit.

The Flack parameter was refined to -0.02(6). Determination of absolute structure using Bayesian statistics on Bijvoet differences using the Olex2 results in -0.00(5). Note: The Flack parameter is used to determine chirality of the crystal studied, the value should be near 0, a value of 1 means that the stereochemistry is wrong and the model should be inverted. A value of 0.5 means that the crystal consists of a racemic mixture of the two enantiomers.

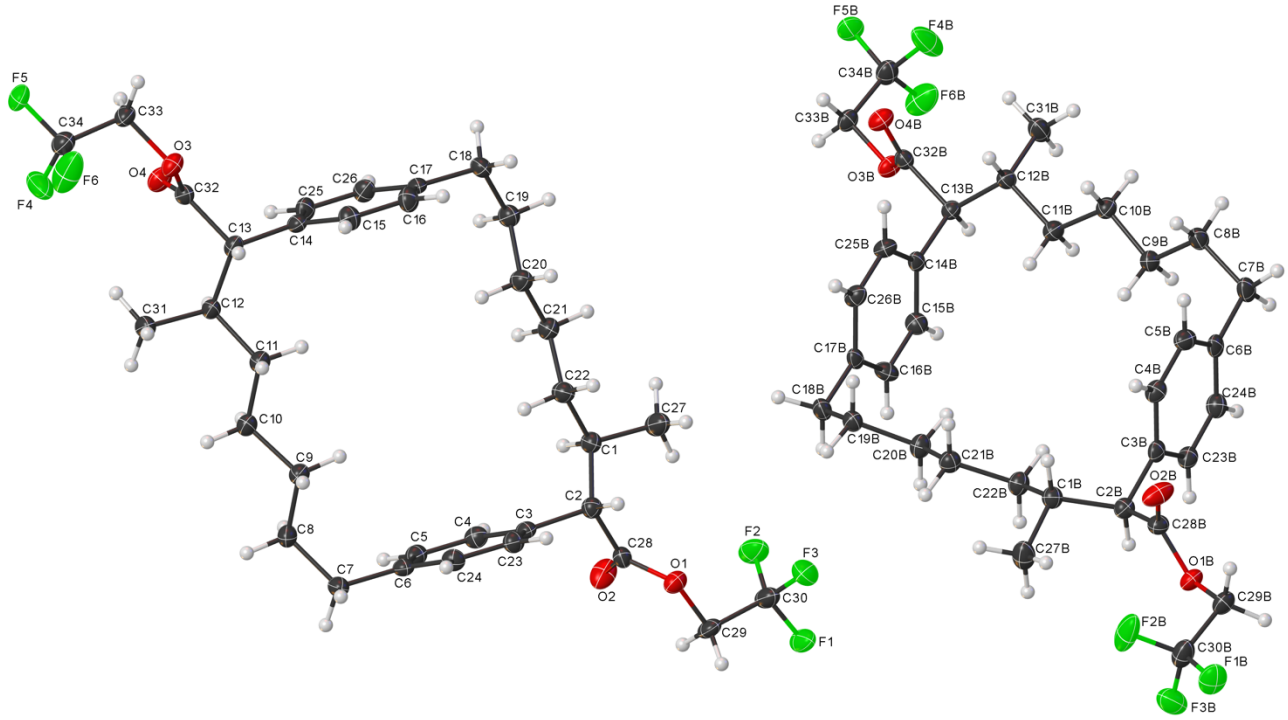

Figure 1: The asymmetric unit contains two molecules of the compound.

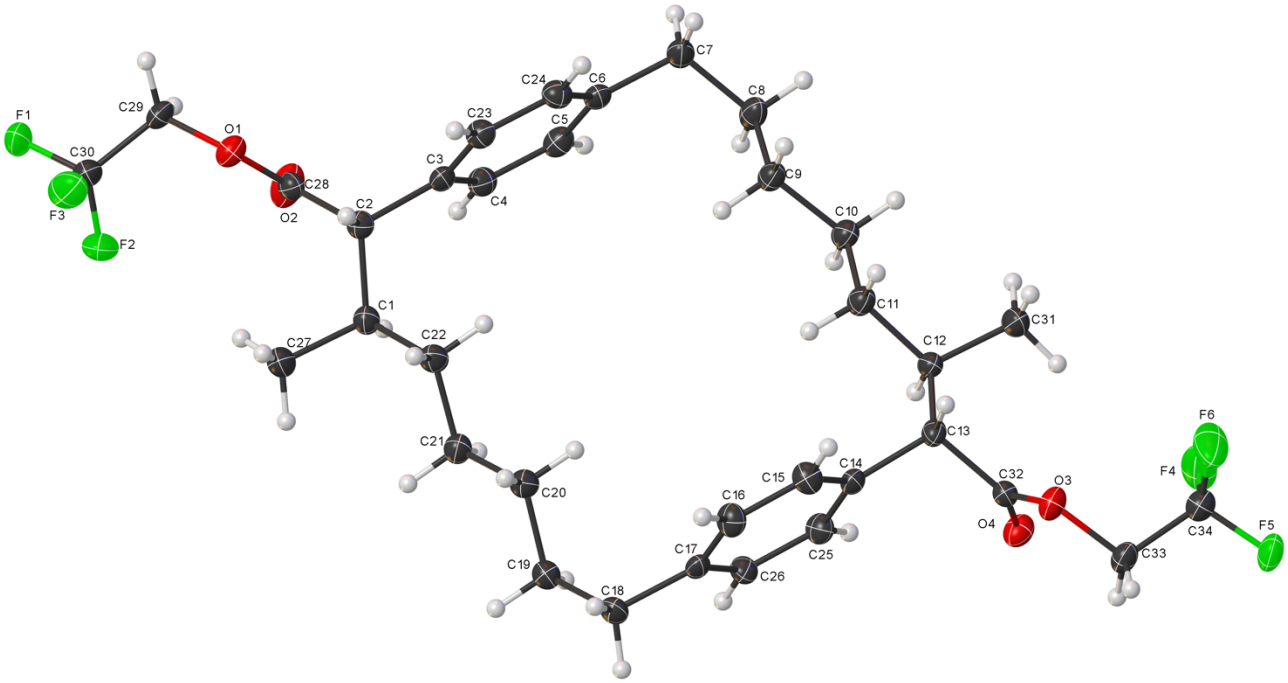

Figure 2:

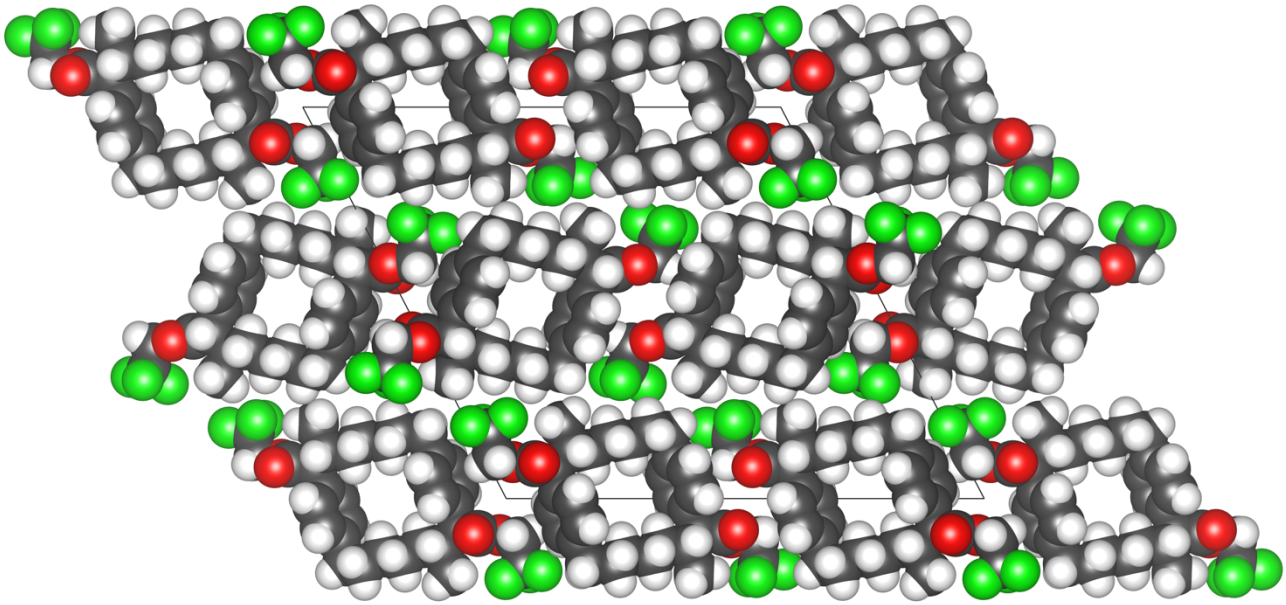

Figure 3:

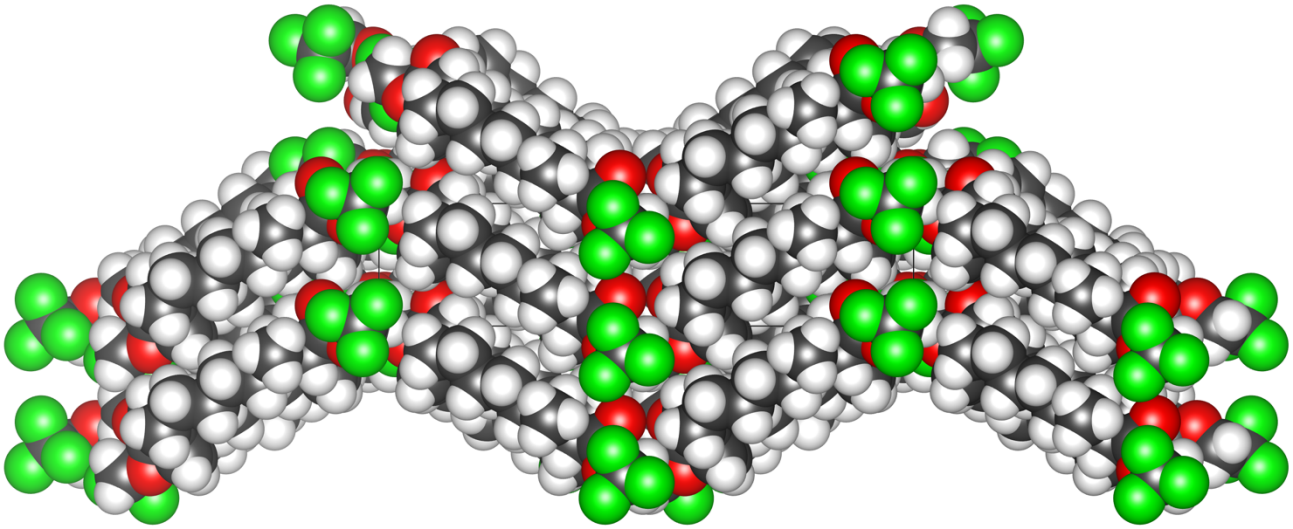

Figure 4:

Data Plots: Diffraction Data

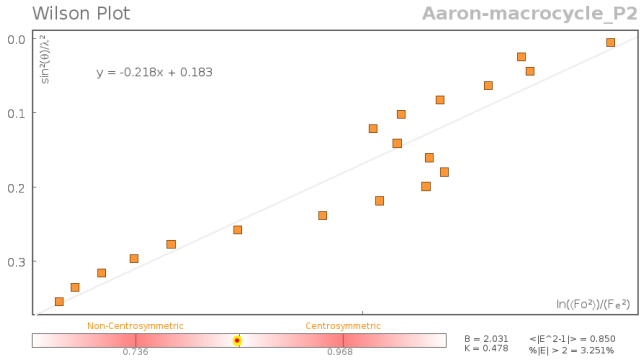

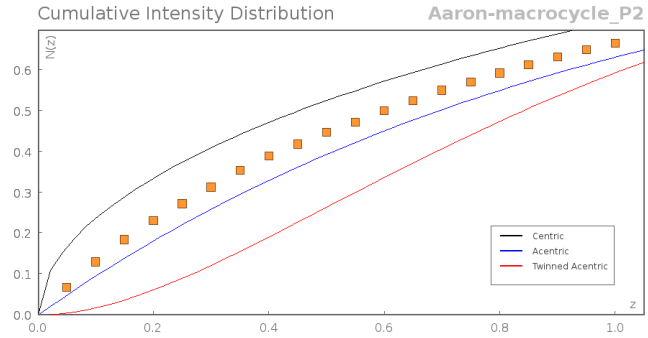

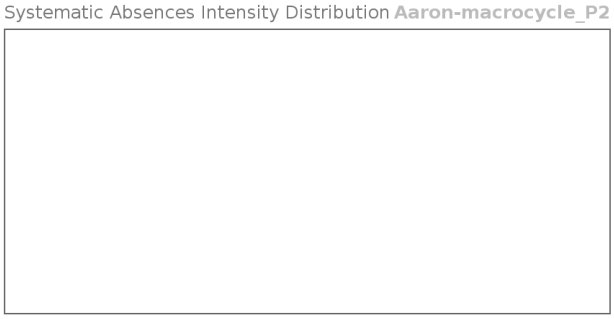

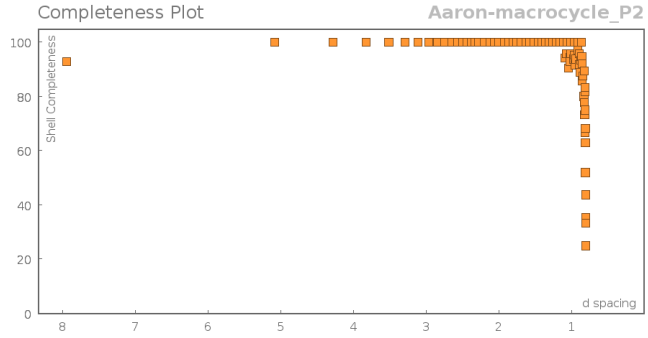

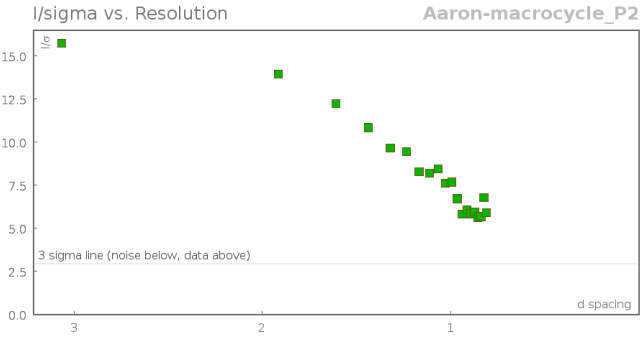

Data Plots: Refinement and Data

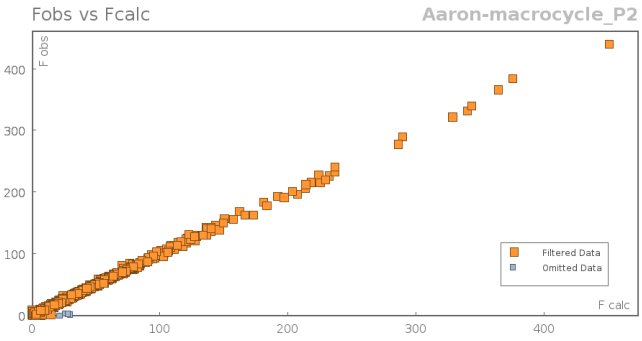

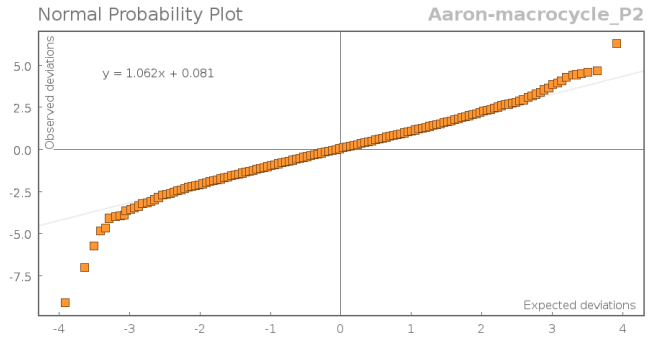

Reflection Statistics

Total reflections (after filtering)	42062	Unique reflections	10947
Completeness	0.804	Mean I/σ	16.19
hkl_{max} collected	(30, 6, 33)	hkl_{min} collected	(-30, -6, -33)
hkl_{max} used	(27, 6, 33)	hkl_{min} used	(-30, -6, 0)
Lim d_{max} collected	100.0	Lim d_{min} collected	0.77
d_{max} used	22.32	d_{min} used	0.8
Friedel pairs	5250	Friedel pairs merged	0

Inconsistent equivalents	10	R_{int}	0.051
R_{sigma}	0.0423	Intensity transformed	0
Omitted reflections	0	Omitted by user (OMIT hkl)	4
Multiplicity	(6310, 4911, 3058, 1507, 1006, 519, 204, 88, 40, 7, 2)	Maximum multiplicity	18
Removed systematic absences	0	Filtered off (Shel/OMIT)	0

Images of the Crystal on the Diffractometer

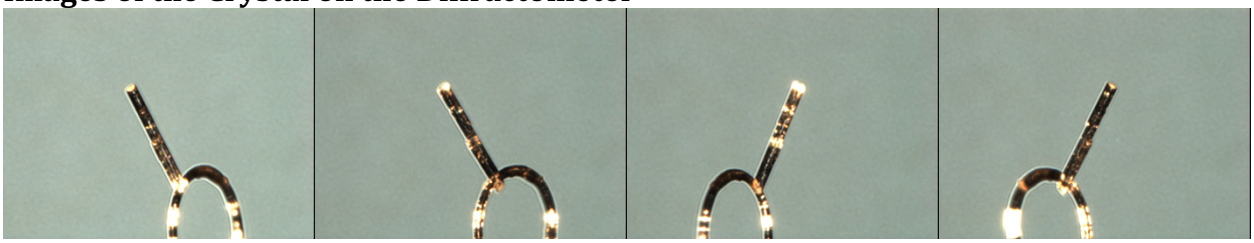

Table 1: Fractional Atomic Coordinates (×10^4) and Equivalent Isotropic Displacement Parameters (Å^2×10^3) for **Aaron-macrocycle_P2**. U_{eq} is defined as 1/3 of the trace of the orthogonalised U_{ij}.

Atom	x	y	z	U_{eq}
F1	3107.8(7)	-1535(3)	3482.8(6)	40.3(4)
F2	2927.5(7)	-699(4)	4163.9(7)	43.1(5)
F3	3029.6(8)	2168(3)	3682.3(7)	44.3(5)
F4	6931.1(8)	10422(4)	11116.2(8)	54.0(5)
F5	6790.1(7)	13309(3)	11567.5(6)	34.1(4)
F6	7051.5(9)	14083(5)	10937.5(8)	63.2(7)
O1	4027.6(8)	1790(3)	4704.1(7)	24.9(4)
O2	4161.9(10)	-1186(3)	5309.5(8)	34.6(5)
O3	6006.0(8)	12270(3)	10110.3(7)	24.8(4)
O4	5755.0(8)	8401(3)	10163.3(7)	26.6(4)
C1	3780.7(11)	2906(5)	5830.5(10)	22.6(5)
C2	4251.8(11)	2953(5)	5616.8(10)	21.2(5)
C3	4891.6(11)	2815(5)	6079.4(10)	19.9(5)
C4	5096.8(12)	917(5)	6458.4(10)	23.7(6)
C5	5675.7(12)	905(5)	6887.6(10)	24.0(6)
C6	6074.6(11)	2778(5)	6953.4(10)	21.4(5)
C7	6704.0(11)	2795(5)	7419.2(10)	27.1(6)
C8	6739.8(12)	2951(5)	7994.2(10)	27.6(6)
C9	6465.4(12)	5221(5)	8095.4(10)	23.7(6)
C10	6516.9(12)	5313(5)	8675.3(10)	24.1(5)
C11	6212.8(12)	7497(5)	8772.7(10)	24.6(6)
C12	6209.5(11)	7575(5)	9334.4(9)	21.0(5)
C13	5839.4(11)	9758(5)	9353.0(10)	20.3(5)
C14	5191.4(11)	9689(5)	8912.1(10)	20.0(5)
C15	4964.7(12)	11456(5)	8505.7(11)	25.0(6)
C16	4377.1(12)	11353(5)	8087.6(11)	26.2(6)
C17	3996.1(11)	9483(5)	8059.1(10)	20.1(5)
C18	3362.9(11)	9314(5)	7599.5(10)	23.9(6)
C19	3252.2(12)	7142(5)	7217.6(11)	25.3(6)
C20	3625.5(12)	7131(5)	6911.5(11)	26.0(6)
C21	3517.0(12)	4965(5)	6538.5(11)	25.0(6)
C22	3874.2(12)	5034(5)	6215.9(11)	24.8(6)
C23	5287.2(11)	4679(5)	6142.9(10)	22.6(5)
C24	5865.8(12)	4667(5)	6573.4(10)	23.7(5)
C25	4809.6(11)	7819(5)	8889.4(10)	23.6(5)
C26	4225.4(11)	7726(5)	8470.6(10)	23.9(5)
C27	3147.2(12)	2864(6)	5349.5(11)	35.0(7)
C28	4147.1(11)	936(5)	5211.2(10)	21.4(5)

Atom	x	y	z	U_{eq}
C29	3900.7(12)	18(5)	4278.4(10)	26.0(6)
C30	3240.7(12)	-13(6)	3906.9(11)	32.9(7)
C31	6844.6(11)	7687(6)	9811.7(10)	31.4(6)
C32	5860.6(11)	9970(5)	9917.2(10)	20.3(5)
C33	6063.6(11)	12761(5)	10649.8(10)	24.3(5)
C34	6708.7(12)	12639(5)	11063.1(11)	29.0(6)
F1B	1848.2(8)	11712(3)	49.8(7)	39.7(4)
F2B	2053.5(8)	10844(4)	890.5(7)	53.2(6)
F3B	1882.0(8)	7990(3)	307.4(7)	43.7(4)
F4B	-2001.3(8)	-248(4)	4376.9(8)	50.5(5)
F5B	-1810.7(7)	-2763(3)	5035.6(6)	32.3(4)
F6B	-1985.5(8)	-4054(4)	4231.7(8)	51.2(5)
O1B	934.2(8)	8649(3)	534.8(7)	23.6(4)
O2B	917.9(10)	11669(3)	1080.3(8)	33.4(5)
O3B	-990.6(8)	-1732(3)	4282.2(7)	22.4(4)
O4B	-804.5(8)	2223(3)	4505.0(7)	26.6(4)
C1B	1271.4(11)	7679(5)	1922.1(10)	21.6(5)
C2B	793.8(11)	7555(5)	1304.6(10)	20.6(5)
C3B	155.1(11)	7692(5)	1223.3(9)	20.3(5)
C4B	-47.0(12)	9629(5)	1421.8(10)	22.4(5)
C5B	-630.8(12)	9684(5)	1349.5(10)	24.4(6)
C6B	-1030.0(11)	7828(5)	1080.7(9)	22.0(5)
C7B	-1664.2(11)	7860(5)	1009.2(10)	26.5(6)
C8B	-1693.1(11)	7697(5)	1557.4(10)	24.2(5)
C9B	-1433.2(11)	5398(5)	1880.1(10)	22.5(5)
C10B	-1508.1(12)	5231(5)	2401.0(10)	22.6(5)
C11B	-1201.5(12)	3046(5)	2755.0(10)	24.1(5)
C12B	-1242.2(11)	2857(5)	3298.8(10)	20.4(5)
C13B	-849.3(11)	741(5)	3648.3(9)	18.1(5)
C14B	-199.2(11)	914(4)	3765.3(9)	17.7(5)
C15B	47.6(12)	-830(5)	3567.6(10)	22.8(5)
C16B	638.0(12)	-664(5)	3658.9(11)	24.7(6)
C17B	1001.5(11)	1259(4)	3953.6(10)	19.3(5)
C18B	1643.5(11)	1494(5)	4061.0(10)	23.3(5)
C19B	1755.6(11)	3697(5)	3779.4(10)	21.7(5)
C20B	1415.4(12)	3584(5)	3151.1(10)	23.7(5)
C21B	1548.4(12)	5680(5)	2863.7(10)	23.4(5)
C22B	1177.7(12)	5569(5)	2236.1(10)	23.1(5)
C23B	-247.0(11)	5842(5)	950.0(10)	22.5(5)
C24B	-828.8(12)	5903(5)	881.9(10)	24.0(6)
C25B	163.1(11)	2841(5)	4062.7(10)	23.3(5)
C26B	749.2(11)	3003(5)	4151.5(10)	23.4(5)
C27B	1901.1(12)	7665(6)	1970.6(11)	33.0(6)
C28B	890.5(12)	9560(5)	978.9(10)	21.7(5)
C29B	1057.3(12)	10354(5)	202.4(10)	25.5(6)
C30B	1713.3(13)	10234(6)	369.5(11)	33.1(7)
C31B	-1887.4(12)	2491(6)	3189.4(11)	31.1(6)
C32B	-879.9(11)	590(4)	4189.4(10)	19.0(5)
C33B	-1060.2(11)	-2166(5)	4766.7(10)	21.9(5)
C34B	-1714.1(12)	-2286(5)	4600.9(10)	27.8(6)

Table 2: Anisotropic Displacement Parameters (×10^4) **Aaron-macrocycle_P2**. The anisotropic displacement factor exponent takes the form: $-2\pi^2[h^2a^{*2} \times U_{11} + ... + 2hka^* \times b^* \times U_{12}]$

Atom	U_{11}	U_{22}	U_{33}	U_{23}	U_{13}	U_{12}
F1	28.1(9)	59.4(12)	28.7(8)	-19.7(8)	9.1(7)	0.2(8)
F2	27.6(9)	68.3(13)	39.7(10)	-10.2(9)	21.0(8)	-6.9(9)

Atom	U_{11}	U_{22}	U_{33}	U_{23}	U_{13}	U_{12}
F3	40.1(11)	53.9(12)	37.5(10)	7.1(9)	16.6(8)	20.2(9)
F4	39.0(11)	61.0(13)	43.9(11)	-12.8(10)	3.6(9)	25.4(10)
F5	36.5(9)	41.8(10)	18.0(7)	-5.3(7)	7.4(7)	3.0(8)
F6	46.0(12)	105.8(19)	36.2(10)	-6.7(11)	17.7(10)	-38.8(12)
O1	32.9(11)	22.1(9)	22.0(9)	0.3(7)	14.5(8)	0.7(8)
O2	54.7(14)	16.9(10)	29.3(10)	-1.3(8)	16.8(10)	-1.8(9)
O3	33.2(11)	21.3(9)	19.2(9)	-2.1(7)	11.6(8)	-1.9(8)
O4	34.1(11)	25.2(10)	23.5(9)	0.3(8)	15.9(8)	-5.2(8)
C1	21.1(13)	24.2(13)	20.9(12)	-2.6(11)	8.2(11)	-0.1(11)
C2	21.6(13)	20.5(12)	20.7(12)	0.1(10)	9.2(11)	0.2(11)
C3	20.2(13)	22.0(12)	18.5(11)	-4.1(10)	9.9(10)	1.0(11)
C4	24.9(15)	22.7(13)	24.7(13)	-3.7(11)	12.3(12)	-3.6(11)
C5	31.0(15)	20.8(13)	21.8(12)	3.5(10)	13.6(12)	5.5(11)
C6	21.6(13)	24.1(13)	20.5(12)	-3.5(11)	11.4(11)	2.4(11)
C7	22.3(14)	34.1(15)	22.5(13)	-4.3(12)	8.3(11)	6.3(12)
C8	27.9(15)	32.6(15)	18.6(12)	1.8(11)	7.7(11)	8.8(12)
C9	25.7(14)	25.8(14)	19.4(12)	0.3(11)	10.1(11)	4.1(12)
C10	24.2(14)	29.1(14)	19.3(12)	1.2(11)	10.3(11)	1.7(11)
C11	25.9(14)	27.7(14)	19.9(12)	1.0(11)	10.4(11)	3.5(12)
C12	18.4(12)	27.5(13)	17.2(11)	0.0(10)	8.2(10)	1.2(11)
C13	20.8(13)	23.6(13)	16.1(12)	-0.3(10)	8.3(11)	-3.1(11)
C14	20.1(13)	22.8(13)	17.2(12)	-4.3(10)	8.7(11)	0.5(10)
C15	24.9(15)	21.2(13)	26.5(13)	2.5(11)	9.7(12)	0.3(11)
C16	27.6(15)	24.3(14)	22.7(13)	4.1(11)	8.1(12)	3.2(12)
C17	19.4(13)	24.8(13)	16.8(12)	-3.9(10)	9.0(11)	4.0(11)
C18	18.1(13)	28.1(14)	24.0(13)	-1.3(11)	8.4(11)	3.3(11)
C19	21.0(14)	29.5(15)	23.8(13)	-2.2(11)	9.2(11)	-0.6(11)
C20	22.9(14)	30.3(15)	25.1(13)	-3.4(11)	11.4(12)	-0.9(11)
C21	24.1(14)	27.7(14)	21.8(13)	-2.1(11)	9.4(12)	1.0(11)
C22	22.0(14)	26.5(14)	25.8(13)	-3.4(11)	11.0(12)	0.3(11)
C23	24.9(14)	21.1(12)	22.3(13)	2.5(10)	11.4(12)	2.2(11)
C24	23.1(14)	22.8(13)	26.5(13)	-0.6(11)	12.6(12)	-1.8(11)
C25	25.1(14)	24.7(13)	19.3(12)	5.2(11)	8.9(11)	2.4(11)
C26	20.0(13)	29.3(14)	22.6(12)	-2.0(11)	10.0(11)	-5.5(12)
C27	22.9(14)	52.3(19)	28.1(14)	-11.8(14)	10.4(12)	-3.4(14)
C28	18.8(13)	23.8(14)	19.3(12)	2.4(10)	7.0(11)	2.7(10)
C29	28.5(15)	32.3(15)	20.6(13)	-7.7(11)	14.2(12)	-1.8(12)
C30	24.8(15)	49.4(19)	26.5(14)	-9.8(13)	13.6(13)	-0.6(14)
C31	21.5(14)	48.2(18)	22.0(13)	-2.5(13)	7.7(12)	5.9(13)
C32	16.9(13)	23.8(13)	18.8(12)	-1.7(10)	7.0(11)	-0.3(11)
C33	28.6(14)	25.0(13)	18.5(12)	-2.4(11)	10.2(11)	2.8(12)
C34	29.8(15)	34.0(15)	23.7(13)	-3.8(12)	12.7(12)	-1.1(13)
F1B	38.2(10)	52.4(11)	34.2(9)	6.0(8)	21.7(8)	-8.8(8)
F2B	37.3(11)	92.0(16)	23.4(8)	-7.7(10)	8.3(8)	-25.9(11)
F3B	38.2(10)	50.4(11)	49.1(10)	11.1(9)	25.6(9)	12.8(9)
F4B	39.5(11)	60.0(12)	61.5(12)	34.4(10)	31.4(10)	23.2(9)
F5B	33.3(9)	40.6(10)	31.5(8)	7.2(7)	22.1(7)	1.0(7)
F6B	40.4(11)	73.9(14)	41.0(10)	-22.3(10)	20.3(9)	-26.3(10)
O1B	30.8(10)	23.9(9)	19.2(8)	-2.0(7)	14.1(8)	-1.5(8)
O2B	60.9(14)	17.3(9)	35.3(11)	-0.6(8)	33.5(11)	-0.6(9)
O3B	32.1(10)	18.1(9)	21.2(9)	1.5(7)	15.9(8)	-1.6(8)
O4B	35.2(11)	24.0(10)	24.3(9)	-5.2(8)	16.8(9)	-3.6(8)
C1B	22.4(13)	20.6(12)	21.2(12)	1.5(10)	9.5(11)	0.0(11)
C2B	23.0(13)	18.3(12)	20.8(12)	0.7(10)	10.3(11)	0.1(11)
C3B	24.2(13)	19.8(12)	15.0(11)	5.0(10)	7.4(10)	3.0(11)
C4B	27.5(15)	18.8(13)	20.4(12)	-1.6(10)	10.5(12)	-2.2(11)
C5B	30.8(15)	22.1(13)	23.1(13)	3.8(11)	14.6(12)	5.9(11)
C6B	22.8(13)	25.5(13)	15.1(11)	8.0(10)	6.7(10)	4.3(11)

Atom	U_{11}	U_{22}	U_{33}	U_{23}	U_{13}	U_{12}
C7B	22.2(13)	34.2(15)	21.2(12)	9.7(12)	8.4(11)	4.6(12)
C8B	21.1(13)	27.8(14)	22.9(12)	4.8(11)	9.5(11)	4.1(11)
C9B	22.6(14)	25.2(13)	19.1(12)	2.6(11)	9.0(11)	4.1(11)
C10B	24.5(14)	22.3(13)	19.8(12)	-0.9(10)	9.3(11)	1.4(11)
C11B	26.1(14)	26.8(14)	20.6(12)	1.0(11)	11.7(11)	4.4(11)
C12B	20.5(13)	21.6(12)	19.6(12)	2.4(10)	9.7(10)	3.7(11)
C13B	19.2(13)	18.2(12)	16.9(11)	-1.8(10)	8.5(10)	-1.4(10)
C14B	17.3(13)	19.8(12)	15.4(11)	4.7(10)	7.1(10)	1.9(10)
C15B	23.7(14)	18.3(13)	25.2(13)	-1.8(10)	10.2(12)	-0.7(10)
C16B	23.2(14)	22.7(13)	30.8(14)	1.0(11)	14.8(12)	5.8(11)
C17B	16.8(13)	23.6(13)	16.6(11)	7.1(10)	7.0(11)	3.6(10)
C18B	18.4(14)	28.9(14)	20.9(12)	4.7(11)	7.6(11)	3.6(11)
C19B	18.4(13)	24.7(13)	20.9(12)	0.6(10)	8.2(11)	0.8(11)
C20B	25.2(14)	24.0(13)	20.4(12)	1.3(11)	9.0(11)	-2.7(11)
C21B	23.8(14)	24.0(13)	22.9(13)	1.3(11)	11.3(11)	-0.4(11)
C22B	25.2(14)	21.7(13)	21.0(12)	1.2(11)	9.6(12)	-2.2(11)
C23B	26.9(15)	19.1(12)	19.3(12)	-0.2(10)	8.8(11)	2.3(11)
C24B	24.3(15)	22.2(13)	21.4(13)	0.1(11)	7.1(12)	-2.4(11)
C25B	26.9(14)	24.9(13)	22.3(12)	-3.2(11)	15.0(11)	0.0(12)
C26B	22.4(13)	26.8(13)	21.3(12)	-5.6(11)	10.4(11)	-5.9(11)
C27B	23.8(15)	45.9(18)	27.8(14)	6.3(14)	10.4(12)	-4.1(14)
C28B	24.0(14)	20.3(13)	21.7(13)	-0.2(10)	11.3(11)	3.1(11)
C29B	31.3(16)	28.1(14)	19.4(12)	1.3(11)	13.8(12)	-1.2(12)
C30B	31.0(16)	45.9(18)	22.1(14)	1.6(13)	11.9(13)	-6.7(14)
C31B	23.8(14)	42.4(17)	28.2(14)	9.0(13)	12.9(12)	6.4(13)
C32B	16.8(13)	20.0(12)	19.6(12)	2.1(10)	7.9(10)	1.2(10)
C33B	26.8(14)	23.0(13)	17.8(12)	3.4(10)	11.7(11)	-0.3(11)
C34B	27.1(14)	34.8(15)	23.0(13)	3.9(12)	12.7(12)	-1.9(13)

Table 3: Bond Lengths in Å for **Aaron-macrocycle_P2**.

Atom	Atom	Length/Å
F1	C30	1.342(3)
F2	C30	1.328(3)
F3	C30	1.347(4)
F4	C34	1.328(3)
F5	C34	1.345(3)
F6	C34	1.331(3)
O1	C28	1.356(3)
O1	C29	1.438(3)
O2	C28	1.201(3)
O3	C32	1.361(3)
O3	C33	1.435(3)
O4	C32	1.199(3)
C1	C2	1.543(3)
C1	C22	1.522(4)
C1	C27	1.527(4)
C2	C3	1.521(3)
C2	C28	1.506(3)
C3	C4	1.394(4)
C3	C23	1.388(4)
C4	C5	1.385(4)
C5	C6	1.395(4)
C6	C7	1.505(4)
C6	C24	1.393(4)
C7	C8	1.530(3)
C8	C9	1.518(4)

Atom	Atom	Length/Å
C9	C10	1.525(3)
C10	C11	1.517(4)
C11	C12	1.535(3)
C12	C13	1.540(3)
C12	C31	1.527(3)
C13	C14	1.515(3)
C13	C32	1.518(3)
C14	C15	1.388(4)
C14	C25	1.393(4)
C15	C16	1.390(4)
C16	C17	1.388(4)
C17	C18	1.508(4)
C17	C26	1.392(4)
C18	C19	1.529(4)
C19	C20	1.516(3)
C20	C21	1.513(4)
C21	C22	1.520(3)
C23	C24	1.385(4)
C25	C26	1.385(4)
C29	C30	1.494(4)
C33	C34	1.490(4)
F1B	C30B	1.347(3)
F2B	C30B	1.319(3)
F3B	C30B	1.348(4)
F4B	C34B	1.326(3)

Atom	Atom	Length/Å
F5B	C34B	1.341(3)
F6B	C34B	1.342(3)
O1B	C28B	1.361(3)
O1B	C29B	1.437(3)
O2B	C28B	1.194(3)
O3B	C32B	1.363(3)
O3B	C33B	1.430(3)
O4B	C32B	1.201(3)
C1B	C2B	1.554(3)
C1B	C22B	1.528(3)
C1B	C27B	1.527(3)
C2B	C3B	1.519(3)
C2B	C28B	1.509(3)
C3B	C4B	1.398(3)
C3B	C23B	1.390(4)
C4B	C5B	1.389(3)
C5B	C6B	1.386(4)
C6B	C7B	1.515(3)
C6B	C24B	1.392(4)
C7B	C8B	1.531(3)
C8B	C9B	1.513(4)
C9B	C10B	1.518(3)
C10B	C11B	1.517(4)
C11B	C12B	1.535(3)
C12B	C13B	1.545(3)
C12B	C31B	1.522(3)
C13B	C14B	1.518(3)
C13B	C32B	1.514(3)
C14B	C15B	1.384(3)
C14B	C25B	1.394(4)
C15B	C16B	1.391(3)
C16B	C17B	1.391(4)
C17B	C18B	1.508(3)
C17B	C26B	1.393(3)
C18B	C19B	1.534(3)
C19B	C20B	1.522(3)
C20B	C21B	1.520(3)
C21B	C22B	1.525(3)
C23B	C24B	1.388(4)
C25B	C26B	1.382(3)
C29B	C30B	1.497(4)
C33B	C34B	1.493(3)

Table 4: Bond Angles in ° for **Aaron-macrocycle_P2**.

Atom	Atom	Atom	Angle/°
C28	O1	C29	116.5(2)
C32	O3	C33	117.09(19)
C22	C1	C2	110.3(2)
C22	C1	C27	111.9(2)
C27	C1	C2	110.8(2)
C3	C2	C1	112.92(19)
C28	C2	C1	111.1(2)
C28	C2	C3	109.3(2)
C4	C3	C2	122.7(2)
C23	C3	C2	119.3(2)
C23	C3	C4	117.9(2)
C5	C4	C3	121.0(2)
C4	C5	C6	121.2(2)
C5	C6	C7	121.8(2)
C24	C6	C5	117.4(2)
C24	C6	C7	120.8(2)
C6	C7	C8	114.0(2)
C9	C8	C7	114.6(2)
C8	C9	C10	112.8(2)
C11	C10	C9	113.5(2)
C10	C11	C12	115.6(2)
C11	C12	C13	109.6(2)
C31	C12	C11	111.5(2)
C31	C12	C13	110.5(2)
C14	C13	C12	113.5(2)
C14	C13	C32	109.11(19)
C32	C13	C12	110.7(2)
C15	C14	C13	120.7(2)
C15	C14	C25	117.8(2)
C25	C14	C13	121.4(2)
C16	C15	C14	121.0(2)
C15	C16	C17	121.5(2)
C16	C17	C18	122.0(2)
C26	C17	C16	117.2(2)
C26	C17	C18	120.8(2)
C17	C18	C19	113.9(2)
C20	C19	C18	114.4(2)
C21	C20	C19	114.0(2)
C20	C21	C22	113.4(2)
C21	C22	C1	115.8(2)
C24	C23	C3	121.0(2)
C23	C24	C6	121.5(2)
C26	C25	C14	120.8(2)
C25	C26	C17	121.7(2)
O1	C28	C2	111.8(2)
O2	C28	O1	122.5(2)
O2	C28	C2	125.7(2)
O1	C29	C30	108.6(2)
F1	C30	F3	106.4(2)
F1	C30	C29	110.4(2)
F2	C30	F1	107.6(2)
F2	C30	F3	106.9(2)
F2	C30	C29	112.9(2)
F3	C30	C29	112.3(3)
O3	C32	C13	110.0(2)
O4	C32	O3	123.4(2)
O4	C32	C13	126.7(2)
O3	C33	C34	109.0(2)
F4	C34	F5	106.6(2)
F4	C34	F6	107.0(2)

Atom	Atom	Atom	Angle/°
F4	C34	C33	112.4(2)
F5	C34	C33	111.1(2)
F6	C34	F5	106.6(2)
F6	C34	C33	112.8(2)
C28B	O1B	C29B	116.5(2)
C32B	O3B	C33B	116.90(19)
C22B	C1B	C2B	109.3(2)
C27B	C1B	C2B	110.27(19)
C27B	C1B	C22B	111.7(2)
C3B	C2B	C1B	113.15(18)
C28B	C2B	C1B	110.5(2)
C28B	C2B	C3B	108.9(2)
C4B	C3B	C2B	122.1(2)
C23B	C3B	C2B	120.1(2)
C23B	C3B	C4B	117.9(2)
C5B	C4B	C3B	120.8(2)
C6B	C5B	C4B	121.3(2)
C5B	C6B	C7B	121.5(2)
C5B	C6B	C24B	117.9(2)
C24B	C6B	C7B	120.6(2)
C6B	C7B	C8B	113.2(2)
C9B	C8B	C7B	114.5(2)
C8B	C9B	C10B	112.8(2)
C11B	C10B	C9B	113.4(2)
C10B	C11B	C12B	115.3(2)
C11B	C12B	C13B	109.76(19)
C31B	C12B	C11B	111.1(2)
C31B	C12B	C13B	109.9(2)
C14B	C13B	C12B	113.73(19)
C32B	C13B	C12B	109.69(19)
C32B	C13B	C14B	109.43(19)
C15B	C14B	C13B	120.5(2)
C15B	C14B	C25B	118.0(2)
C25B	C14B	C13B	121.5(2)

Atom	Atom	Atom	Angle/°
C14B	C15B	C16B	121.2(2)
C15B	C16B	C17B	121.1(2)
C16B	C17B	C18B	122.5(2)
C16B	C17B	C26B	117.2(2)
C26B	C17B	C18B	120.2(2)
C17B	C18B	C19B	113.5(2)
C20B	C19B	C18B	113.1(2)
C21B	C20B	C19B	113.9(2)
C20B	C21B	C22B	112.4(2)
C21B	C22B	C1B	115.1(2)
C3B	C23B	C24B	121.0(2)
C23B	C24B	C6B	121.1(2)
C26B	C25B	C14B	120.7(2)
C25B	C26B	C17B	121.8(2)
O1B	C28B	C2B	110.6(2)
O2B	C28B	O1B	123.2(2)
O2B	C28B	C2B	126.2(2)
O1B	C29B	C30B	107.9(2)
F1B	C30B	C29B	110.3(2)
F2B	C30B	F1B	108.0(2)
F2B	C30B	F3B	106.6(3)
F2B	C30B	C29B	113.1(2)
F3B	C30B	F1B	106.9(2)
F3B	C30B	C29B	111.6(2)
O3B	C32B	C13B	109.8(2)
O4B	C32B	O3B	123.7(2)
O4B	C32B	C13B	126.4(2)
O3B	C33B	C34B	108.36(19)
F4B	C34B	F5B	107.0(2)
F4B	C34B	F6B	107.1(2)
F4B	C34B	C33B	113.1(2)
F5B	C34B	F6B	106.4(2)
F5B	C34B	C33B	111.4(2)
F6B	C34B	C33B	111.6(2)

Table 5: Torsion Angles in ° for **Aaron-macrocycle_P2**.

Atom	Atom	Atom	Atom	Angle/°
O1	C29	C30	F1	176.0(2)
O1	C29	C30	F2	-63.5(3)
O1	C29	C30	F3	57.5(3)
O3	C33	C34	F4	-66.4(3)
O3	C33	C34	F5	174.3(2)
O3	C33	C34	F6	54.6(3)
C1	C2	C3	C4	57.5(3)
C1	C2	C3	C23	-120.4(2)
C1	C2	C28	O1	118.2(2)
C1	C2	C28	O2	-61.6(3)
C2	C1	C22	C21	-169.3(2)
C2	C3	C4	C5	-177.3(2)
C2	C3	C23	C24	177.3(2)
C3	C2	C28	O1	-116.5(2)
C3	C2	C28	O2	63.7(3)
C3	C4	C5	C6	-0.5(4)
C3	C23	C24	C6	0.8(4)

Atom	Atom	Atom	Atom	Angle/°
C4	C3	C23	C24	-0.7(3)
C4	C5	C6	C7	179.7(2)
C4	C5	C6	C24	0.5(3)
C5	C6	C7	C8	-63.9(3)
C5	C6	C24	C23	-0.7(3)
C6	C7	C8	C9	-61.2(3)
C7	C6	C24	C23	-179.9(2)
C7	C8	C9	C10	-179.4(2)
C8	C9	C10	C11	-176.6(2)
C9	C10	C11	C12	175.5(2)
C10	C11	C12	C13	-175.0(2)
C10	C11	C12	C31	62.3(3)
C11	C12	C13	C14	60.4(3)
C11	C12	C13	C32	-176.5(2)
C12	C13	C14	C15	-116.8(3)
C12	C13	C14	C25	61.1(3)
C12	C13	C32	O3	130.1(2)
C12	C13	C32	O4	-51.4(3)
C13	C14	C15	C16	177.5(2)
C13	C14	C25	C26	-177.3(2)
C14	C13	C32	O3	-104.2(2)
C14	C13	C32	O4	74.3(3)
C14	C15	C16	C17	-0.2(4)
C14	C25	C26	C17	-0.2(4)
C15	C14	C25	C26	0.6(4)
C15	C16	C17	C18	-178.4(2)
C15	C16	C17	C26	0.7(4)
C16	C17	C18	C19	113.9(3)
C16	C17	C26	C25	-0.5(3)
C17	C18	C19	C20	-61.7(3)
C18	C17	C26	C25	178.6(2)
C18	C19	C20	C21	179.5(2)
C19	C20	C21	C22	177.5(2)
C20	C21	C22	C1	-179.7(2)
C22	C1	C2	C3	59.7(3)
C22	C1	C2	C28	-177.0(2)
C23	C3	C4	C5	0.6(3)
C24	C6	C7	C8	115.2(3)
C25	C14	C15	C16	-0.4(4)
C26	C17	C18	C19	-65.1(3)
C27	C1	C2	C3	-175.9(2)
C27	C1	C2	C28	-52.6(3)
C27	C1	C22	C21	66.9(3)
C28	O1	C29	C30	103.6(3)
C28	C2	C3	C4	-66.7(3)
C28	C2	C3	C23	115.4(2)
C29	O1	C28	O2	1.7(4)
C29	O1	C28	C2	-178.0(2)
C31	C12	C13	C14	-176.4(2)
C31	C12	C13	C32	-53.2(3)
C32	O3	C33	C34	97.2(3)
C32	C13	C14	C15	119.2(2)
C32	C13	C14	C25	-62.9(3)
C33	O3	C32	O4	3.4(4)
C33	O3	C32	C13	-178.11(19)
O1B	C29B	C30B	F1B	176.8(2)
O1B	C29B	C30B	F2B	-62.1(3)

Atom	Atom	Atom	Atom	Angle/°
O1B	C29B	C30B	F3B	58.1(3)
O3B	C33B	C34B	F4B	-61.4(3)
O3B	C33B	C34B	F5B	178.1(2)
O3B	C33B	C34B	F6B	59.4(3)
C1B	C2B	C3B	C4B	57.0(3)
C1B	C2B	C3B	C23B	-122.2(2)
C1B	C2B	C28B	O1B	126.1(2)
C1B	C2B	C28B	O2B	-55.0(4)
C2B	C1B	C22B	C21B	-170.6(2)
C2B	C3B	C4B	C5B	-178.9(2)
C2B	C3B	C23B	C24B	178.6(2)
C3B	C2B	C28B	O1B	-109.0(2)
C3B	C2B	C28B	O2B	69.9(3)
C3B	C4B	C5B	C6B	0.1(4)
C3B	C23B	C24B	C6B	0.5(4)
C4B	C3B	C23B	C24B	-0.7(4)
C4B	C5B	C6B	C7B	179.0(2)
C4B	C5B	C6B	C24B	-0.3(3)
C5B	C6B	C7B	C8B	-65.2(3)
C5B	C6B	C24B	C23B	0.0(3)
C6B	C7B	C8B	C9B	-61.8(3)
C7B	C6B	C24B	C23B	-179.3(2)
C7B	C8B	C9B	C10B	-176.1(2)
C8B	C9B	C10B	C11B	-174.9(2)
C9B	C10B	C11B	C12B	177.5(2)
C10B	C11B	C12B	C13B	-173.2(2)
C10B	C11B	C12B	C31B	65.1(3)
C11B	C12B	C13B	C14B	55.9(3)
C11B	C12B	C13B	C32B	178.8(2)
C12B	C13B	C14B	C15B	-117.0(2)
C12B	C13B	C14B	C25B	61.6(3)
C12B	C13B	C32B	O3B	131.5(2)
C12B	C13B	C32B	O4B	-50.3(3)
C13B	C14B	C15B	C16B	178.3(2)
C13B	C14B	C25B	C26B	-178.1(2)
C14B	C13B	C32B	O3B	-103.0(2)
C14B	C13B	C32B	O4B	75.1(3)
C14B	C15B	C16B	C17B	0.2(4)
C14B	C25B	C26B	C17B	-0.5(4)
C15B	C14B	C25B	C26B	0.6(4)
C15B	C16B	C17B	C18B	179.9(2)
C15B	C16B	C17B	C26B	-0.1(4)
C16B	C17B	C18B	C19B	115.1(3)
C16B	C17B	C26B	C25B	0.2(4)
C17B	C18B	C19B	C20B	-63.6(3)
C18B	C17B	C26B	C25B	-179.7(2)
C18B	C19B	C20B	C21B	-176.7(2)
C19B	C20B	C21B	C22B	-177.3(2)
C20B	C21B	C22B	C1B	177.7(2)
C22B	C1B	C2B	C3B	59.8(3)
C22B	C1B	C2B	C28B	-177.7(2)
C23B	C3B	C4B	C5B	0.4(3)
C24B	C6B	C7B	C8B	114.1(3)
C25B	C14B	C15B	C16B	-0.4(4)
C26B	C17B	C18B	C19B	-64.9(3)
C27B	C1B	C2B	C3B	-177.0(2)
C27B	C1B	C2B	C28B	-54.6(3)
C27B	C1B	C22B	C21B	67.1(3)

Atom	Atom	Atom	Atom	Angle/°
C28B	O1B	C29B	C30B	99.4(3)
C28B	C2B	C3B	C4B	-66.3(3)
C28B	C2B	C3B	C23B	114.5(2)
C29B	O1B	C28B	O2B	4.0(4)
C29B	O1B	C28B	C2B	-177.0(2)
C31B	C12B	C13B	C14B	178.4(2)
C31B	C12B	C13B	C32B	-58.7(3)
C32B	O3B	C33B	C34B	99.1(2)
C32B	C13B	C14B	C15B	119.9(2)
C32B	C13B	C14B	C25B	-61.4(3)
C33B	O3B	C32B	O4B	4.5(3)
C33B	O3B	C32B	C13B	-177.24(19)

Table 6: Hydrogen Fractional Atomic Coordinates (×10⁴) and Equivalent Isotropic Displacement Parameters (Å²×10³) for **Aaron-macrocycle_P2**. U_{eq} is defined as 1/3 of the trace of the orthogonalised U_{ij}.

Atom	x	y	z	U_{eq}
H1	3838.87	1417.26	6044.01	27
H2	4207.62	4485.31	5421.4	25
H4	4840.99	-360.14	6422.28	28
H5	5801.05	-375.76	7136.72	29
H7A	6916.88	4159.71	7370.2	33
H7B	6906.2	1334.9	7398.66	33
H8A	6538.59	1555.85	8047.23	33
H8B	7157.54	2870.15	8269.03	33
H9A	6045.69	5298.2	7825.73	28
H9B	6663.7	6623.82	8041.48	28
H10A	6340.63	3858.89	8736.64	29
H10B	6937.65	5329.69	8943.77	29
H11A	5801.39	7546.94	8483.22	30
H11B	6410.9	8941.41	8737.19	30
H12	6017.59	6097.78	9373.73	25
H13	6022.18	11219.04	9293.16	24
H15	5209.75	12729.35	8513.21	30
H16	4236.17	12564.47	7821	31
H18A	3269.88	10780.41	7380.3	29
H18B	3091.16	9221.46	7761.05	29
H19A	3335.86	5676.06	7435.97	30
H19B	2831.8	7113.21	6948.5	30
H20A	3539.25	8588.14	6690.01	31
H20B	4046.03	7171.75	7180.08	31
H21A	3093.65	4881.95	6279.45	30
H21B	3620.75	3509.13	6761.73	30
H22A	4296.5	5121.09	6477.84	30
H22B	3772.08	6505.72	5998.13	30
H23	5162.07	5955.91	5892.69	27
H24	6120.38	5949.12	6609.47	28
H25	4948.78	6619.38	9158.69	28
H26	3979.76	6457.4	8463.97	29
H27A	3082.42	4291.05	5128.85	52
H27B	2861.64	2813.75	5491.26	52
H27C	3099.11	1459.46	5125.95	52
H29A	4033.67	-1564.23	4443.05	31
H29B	4111.57	420.45	4067.88	31
H31A	7042.46	9106.84	9774.92	47
H31B	7063.15	6277.03	9804.09	47
H31C	6827.48	7745.84	10156.27	47
H33A	5836.99	11583.49	10740.57	29
H33B	5905.86	14354.71	10655.57	29
H1B	1216.17	9191.66	2079.88	26
H2B	842	6011.03	1153.47	25
H4B	212.4	10895.87	1604.28	27
H5B	-756.36	10992.28	1484.09	29
H7BA	-1884.57	6514.62	775.82	32
H7BB	-1859.37	9339.1	821.4	32
H8BA	-1479.64	9064.2	1786.17	29
H8BB	-2108.59	7825.21	1481.74	29
H9BA	-1009.95	5319.97	1980.83	27
H9BB	-1627.82	4021.27	1645.32	27

Atom	x	y	z	U_{eq}
H10C	-1346.11	6682.04	2619.1	27
H10D	-1932.21	5164.79	2297.27	27
H11C	-781.77	3079.64	2841.42	29
H11D	-1376.03	1600.41	2538.96	29
H12B	-1091.09	4361.57	3506.93	24
H13B	-1015.29	-759.67	3443.49	22
H15B	-185.46	-2136.09	3370.18	27
H16B	792.41	-1858.43	3520.68	30
H18C	1755.56	43.85	3930.99	28
H18D	1899.36	1608.16	4456.72	28
H19C	1637.8	5146.66	3904.52	26
H19D	2181.16	3813.56	3892.11	26
H20C	1515.18	2084.57	3028.49	28
H20D	989.07	3560.12	3038.74	28
H21C	1970.68	5661.14	2959.15	28
H21D	1465.5	7188.06	2996.65	28
H22C	757.11	5506.24	2145.69	28
H22D	1272.99	4079.35	2106.12	28
H23B	-124.41	4542.27	810.61	27
H24B	-1088.59	4636.94	700.23	29
H25B	8.95	4029.39	4202.81	28
H26B	981.32	4312.22	4348.7	28
H27D	1963.79	6182.78	1821.78	50
H27E	2191.46	7799.8	2352.75	50
H27F	1943.79	9005.6	1767.83	50
H29C	949.16	11971.7	260.87	31
H29D	825.95	9956.17	-186.45	31
H31D	-2039.34	1012.82	2988.64	47
H31E	-2127.92	3820.41	2975.5	47
H31F	-1901.78	2409.07	3534.97	47
H33C	-874.84	-872.72	5031.91	26
H33D	-868.03	-3675.15	4937.83	26

Citations

CrysAlisPro Software System, Rigaku Oxford Diffraction, (2018).

O.V. Dolomanov and L.J. Bourhis and R.J. Gildea and J.A.K. Howard and H. Puschmann, Olex2: A complete structure solution, refinement and analysis program, *J. Appl. Cryst.*, (2009), **42**, 339-341.

Sheldrick, G.M., Crystal structure refinement with ShelXL, *Acta Cryst.*, (2015), **C27**, 3-8.

Sheldrick, G.M., ShelXT-Integrated space-group and crystal-structure determination, *Acta Cryst.*, (2015), **A71**, 3-8.

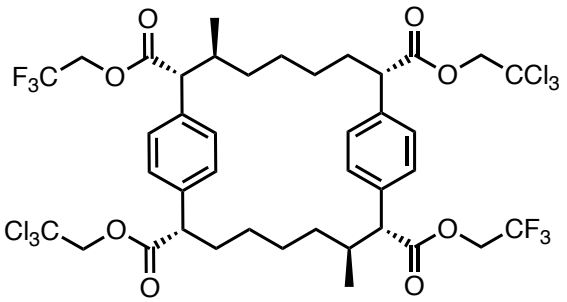

Macrocycle 2.23

Crystal Data and Experimental

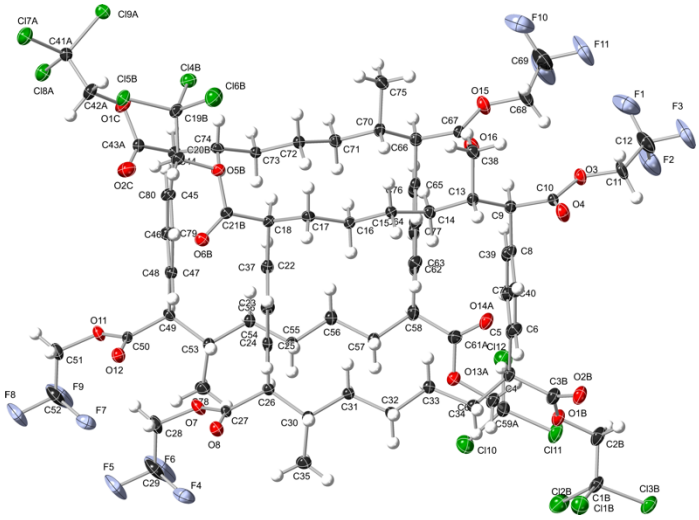

Experimental. Single colorless prism-shaped crystals of **atb-40-48** were chosen from the sample as supplied. A suitable crystal with dimensions 0.28 × 0.21 × 0.17 mm^3 was selected and mounted on a loop with paratone on a Rigaku Synergy-S diffractometer. The crystal was kept at a steady T = 100.0(2) K during data collection. The structure was solved with the **ShelXT** 2018/2 (Sheldrick, 2018) solution program using dual methods and by using **Olex2** 1.3-alpha (Dolomanov et al., 2009) as the graphical interface. The model was refined with **ShelXL** 2018/3 (Sheldrick, 2015) using full matrix least squares minimisation on $\boldsymbol{F^2}$.

Crystal Data. $C_{40}H_{44}Cl_6F_6O_8$, M_r = 979.45, monoclinic, $P2_1$ (No. 4), a = 11.00854(7) Å, b = 27.37588(17) Å, c = 15.61807(10) Å, β = 104.1223(7)°, α = γ = 90°, V = 4564.54(5) Å^3, T = 100.0(2) K, Z = 4, Z' = 2, μ(Cu K$_\alpha$) = 4.074 mm^{-1}, 61888 reflections measured, 17396 unique (R_{int} = 0.0415) which were used in all calculations. The final wR_2 was 0.0911 (all data) and R_1 was 0.0343 (I≥2 σ(I)).

Compound	**atb-40-48**
Formula	$C_{40}H_{44}Cl_6F_6O_8$
$D_{calc.}$/ g cm^{-3}	1.425
μ/mm^{-1}	4.074
Formula Weight	979.45
Color	colorless
Shape	prism-shaped
Size/mm^3	0.28×0.21×0.17
T/K	100.0(2)
Crystal System	monoclinic
Flack Parameter	0.005(4)
Hooft Parameter	0.005(4)
Space Group	$P2_1$
a/Å	11.00854(7)
b/Å	27.37588(17)
c/Å	15.61807(10)
α/°	90
β/°	104.1223(7)
γ/°	90
V/Å^3	4564.54(5)
Z	4
Z'	2
Wavelength/Å	1.54184
Radiation type	Cu K$_\alpha$
Θ_{min}/°	2.918
Θ_{max}/°	72.888
Measured Refl's.	61888
Indep't Refl's	17396
Refl's I≥2 σ(I)	16862
R_{int}	0.0415
Parameters	1177
Restraints	732
Largest Peak	0.460
Deepest Hole	-0.390
GooF	1.045
wR_2 (all data)	0.0911
wR_2	0.0903
R_1 (all data)	0.0354
R_1	0.0343

Structure Quality Indicators

Reflections:	d min (Cu\a) 2Θ=145.8°	0.81	I/σ(I) CIF	29.0	Rint CIF	4.15%	Full 135.4° 98% to 145.8°	99.8
Refinement:	Shift CIF	0.006	Max Peak CIF	0.5	Min Peak CIF	-0.4	GooF CIF	1.045	Hooft CIF	.005(4)

A colorless prism-shaped-shaped crystal with dimensions 0.28 × 0.21 × 0.17 mm^3 was mounted on a loop with paratone. Data were collected using a XtaLAB Synergy, Dualflex, HyPix diffractometer operating at T = 100.0(2) K.

Data were measured using ω scans with Cu K_α radiation. The diffraction pattern was indexed and the total number of runs and images was based on the strategy calculation from the program CrysAlisPro 1.171.40.53 (Rigaku OD, 2019). The maximum resolution that was achieved was Θ = 72.888° (0.83 Å).

The unit cell was refined using CrysAlisPro 1.171.40.53 (Rigaku OD, 2019) on 50795 reflections, 82% of the observed reflections.

Data reduction, scaling and absorption corrections were performed using CrysAlisPro 1.171.40.53 (Rigaku OD, 2019). The final completeness is 99.80 % out to 72.888° in Θ. A numerical absorption correction based on gaussian integration over a multifaceted crystal model was performed using CrysAlisPro 1.171.41.108a (Rigaku Oxford Diffraction, 2021). An empirical absorption correction using spherical harmonics, implemented in SCALE3 ABSPACK scaling algorithm was also applied. The absorption coefficient μ of this material is 4.074 mm^{-1} at this wavelength (λ = 1.54184Å) and the minimum and maximum transmissions are 0.453 and 1.000.

The structure was solved and the space group $P2_1$ (# 4) determined by the ShelXT 2018/2 (Sheldrick, 2018) structure solution program and refined by full matrix least squares minimisation on F^2 using version 2018/3 of **ShelXL** 2018/3 (Sheldrick, 2015). All non-hydrogen atoms were refined anisotropically. Hydrogen atom positions were calculated geometrically and refined using the riding model.

The X-ray structure is disordered and the asymmetric unit contains two equivalent forms of the trichloro acetate with two major spatial arrangements. The group pivots about the macrocycle with the C of the CCl_3 group in an almost fixed position and is readily interpreted as 2 conformers. There is less than a 10% contribution from the second conformer to the overall structure.

The Flack parameter was refined to 0.005(4). Determination of absolute structure using Bayesian statistics on Bijvoet differences using the Olex2 results in 0.005(4). Note: The Flack parameter is used to determine chirality of the crystal studied, the value should be near 0, a value of 1 means that the stereochemistry is wrong and the model should be inverted. A value of 0.5 means that the crystal consists of a racemic mixture of the two enantiomers.

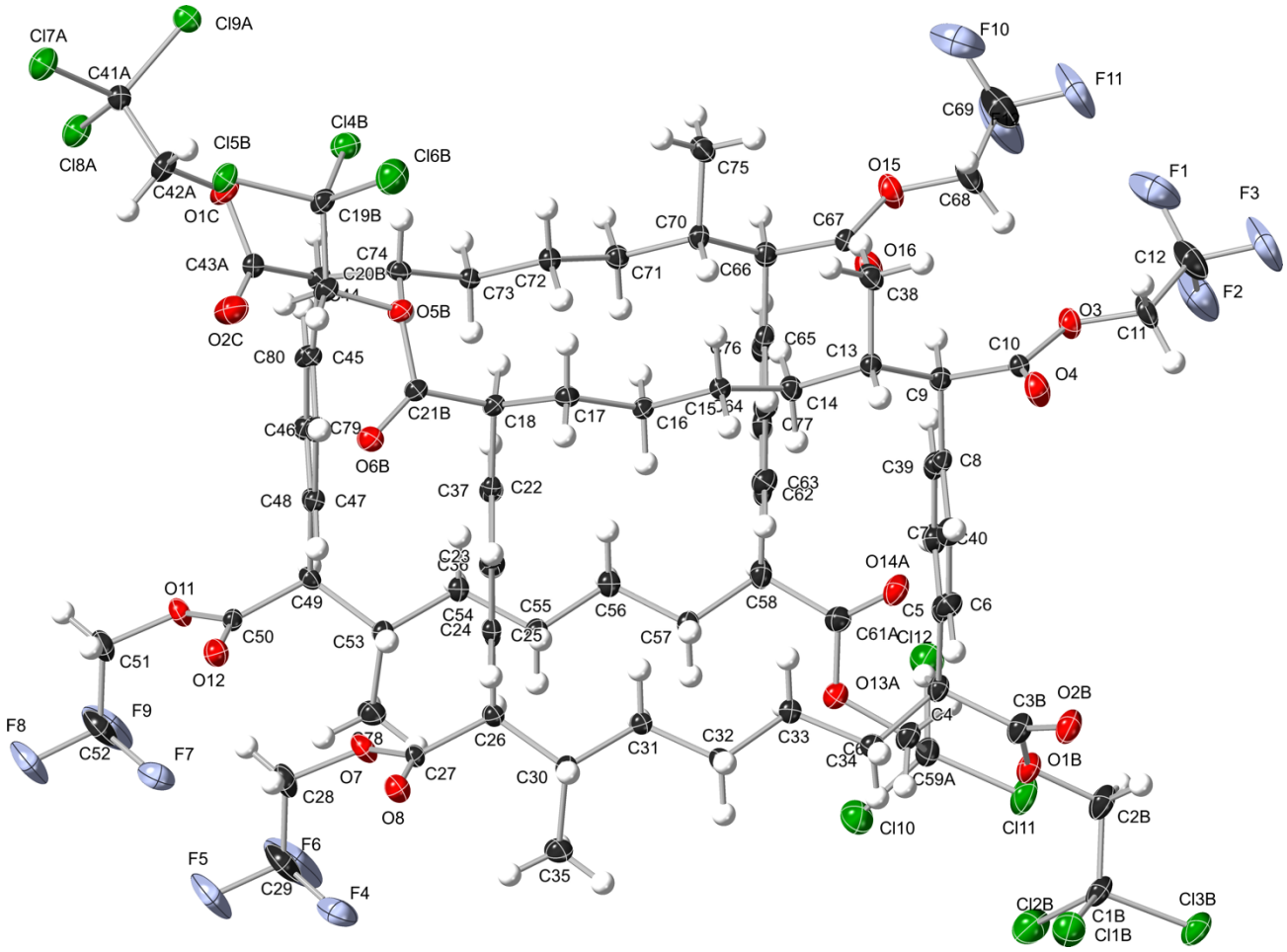

Figure 5: A thermal ellipsoid representation of the asymmetric unit showing the orientation of the major substituents. The value of Z' is 2. This means that there are two independent molecules in the asymmetric unit.

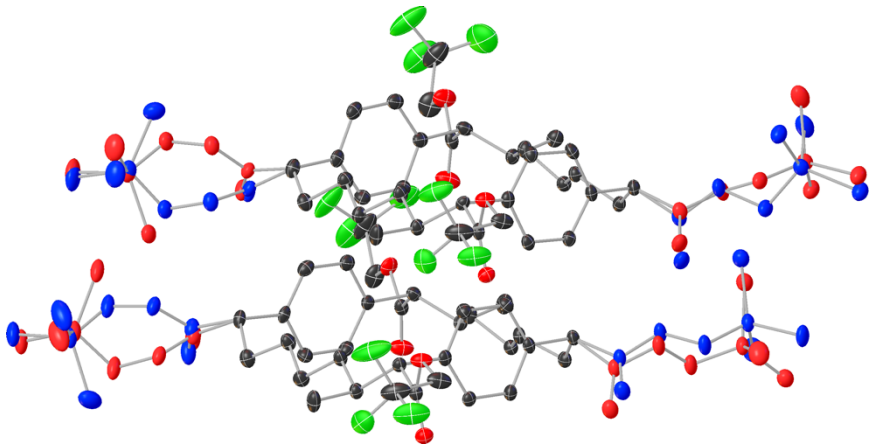

Figure 6: The disorder model showing the major (blue) and minor (red) substituents.

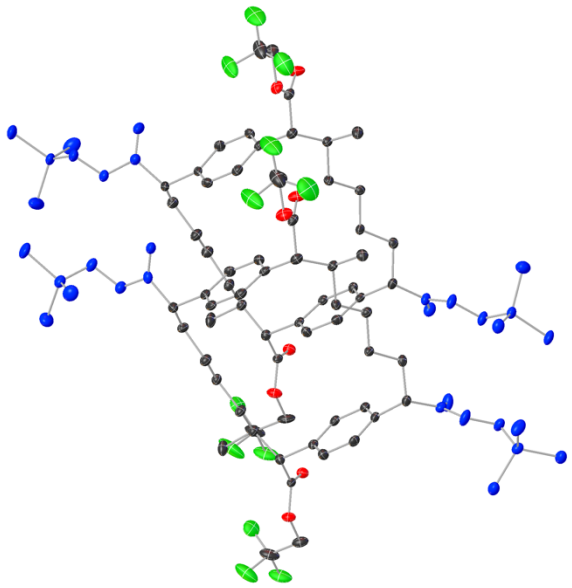

Figure 7: The structure with its major components (91-93%).

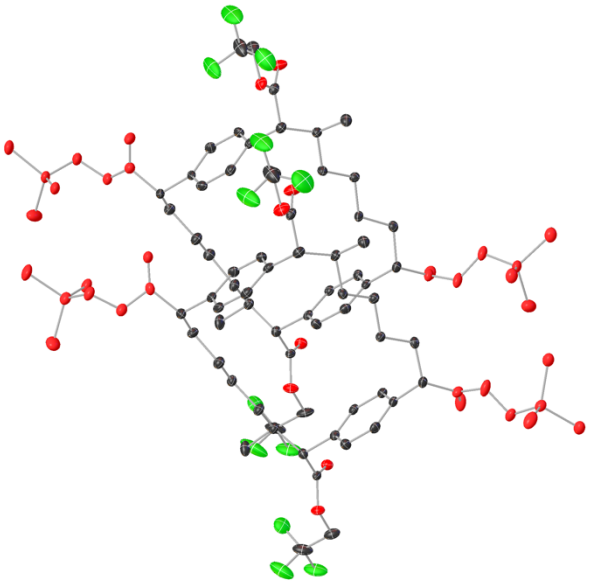

Figure 8: The structure with its minor components (7-9%).

Data Plots: Diffraction Data

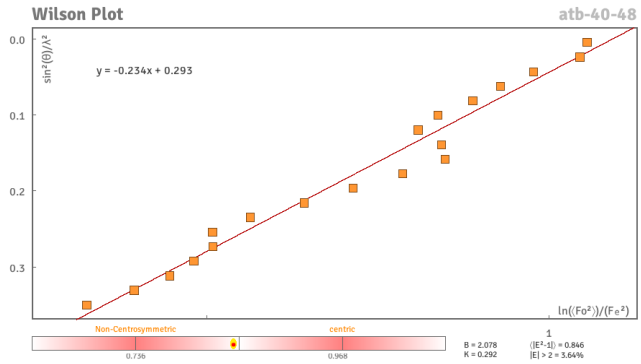

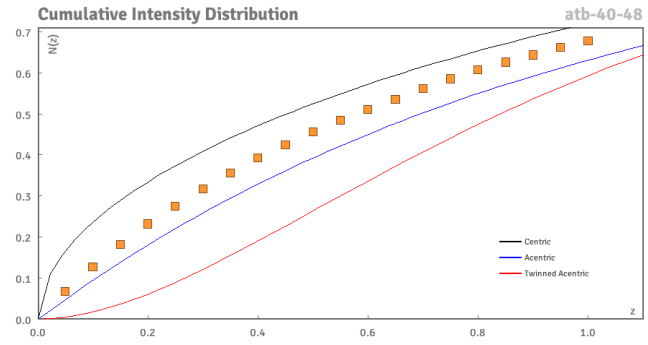

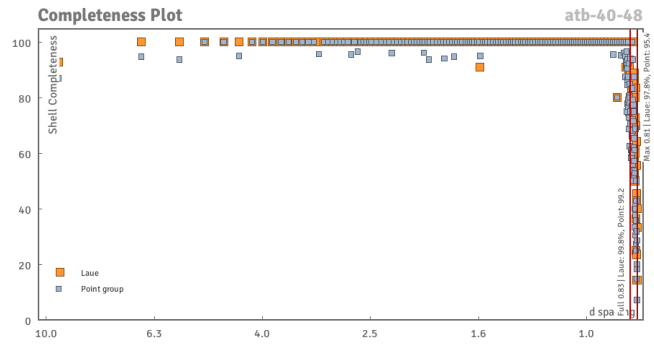

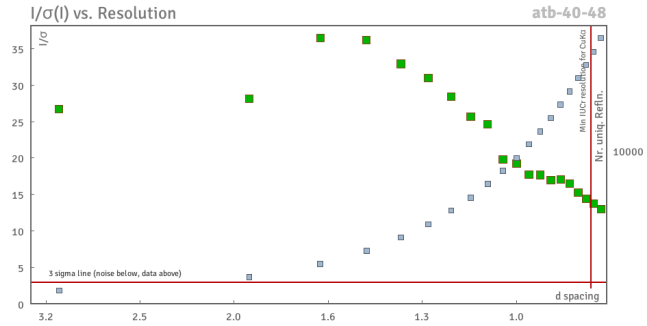

Data Plots: Refinement and Data

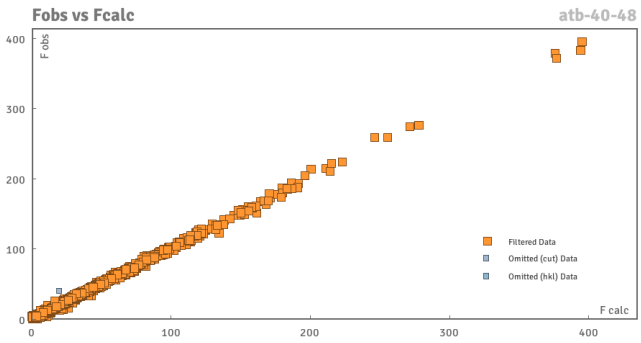

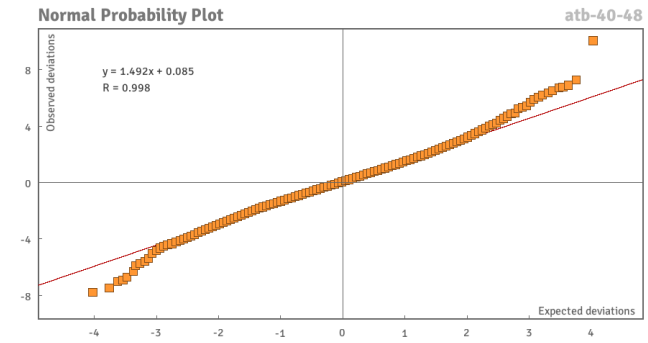

Reflection Statistics

Total reflections (after filtering)	61922	Unique reflections	17396
Completeness	0.954	Mean I/σ	23.01

hkl_{max} collected	(10, 33, 18)	hkl_{min} collected	(-13, -32, -19)
hkl_{max} used	(13, 33, 19)	hkl_{min} used	(-13, -32, 0)
Lim d_{max} collected	100.0	Lim d_{min} collected	0.77
d_{max} used	15.15	d_{min} used	0.81
Friedel pairs	4597	Friedel pairs merged	0
Inconsistent equivalents	63	R_{int}	0.0415
R_{sigma}	0.0345	Intensity transformed	0
Omitted reflections	0	Omitted by user (OMIT hkl)	34
Multiplicity	(6157, 5992, 3763, 2350, 1471, 892, 508, 372, 225, 103, 43, 26, 1)	Maximum multiplicity	13
Removed systematic absences	0	Filtered off (Shel/OMIT)	0

Table 7: Fractional Atomic Coordinates (×10⁴) and Equivalent Isotropic Displacement Parameters (Å²×10³) for **atb-40-48**. U_{eq} is defined as 1/3 of the trace of the orthogonalised U_{ij}.

Atom	x	y	z	U_{eq}
F1	13332(3)	-3089.1(11)	10089(2)	58.5(7)
F2	14008(3)	-2533.0(11)	11049.7(15)	59.5(8)
F3	15263(3)	-3097.8(11)	10822.2(18)	65.6(9)
F4	8045(2)	2937.1(9)	5431.3(16)	39.6(5)
F5	6399(2)	3160.6(10)	4461(2)	52.6(7)
F6	6251(3)	2912.7(11)	5740(2)	66.3(9)
O3	13627(2)	-2210.8(10)	9351.1(14)	23.9(5)
O4	14707(2)	-1920.7(10)	8418.6(17)	28.6(5)
O7	7177(2)	1981.1(9)	5403.4(15)	22.3(5)
O8	8919(2)	1962.6(9)	4888.4(14)	21.8(4)
C4	13224(2)	315.6(12)	10022.2(17)	18.2(6)
C5	13121(3)	-185.0(12)	9581.7(18)	16.2(6)
C6	13925(3)	-339.5(13)	9056(2)	20.3(6)
C7	13773(3)	-794.1(12)	8662(2)	19.2(6)
C8	12832(3)	-1111.9(12)	8774.2(19)	16.2(6)
C9	12612(3)	-1612.7(12)	8338.9(19)	17.5(6)
C10	13766(3)	-1922.5(12)	8679.6(19)	17.9(6)
C11	14699(4)	-2497.1(14)	9736(2)	29.8(8)
C12	14318(5)	-2805.0(15)	10425(2)	41.8(10)
C13	12280(3)	-1608.5(12)	7314.7(19)	17.0(6)
C14	11219(3)	-1245.9(12)	6954.6(19)	18.2(6)
C15	10942(3)	-1159.9(11)	5961.4(19)	16.0(6)
C16	9836(3)	-815.5(11)	5660.5(19)	16.6(6)
C17	9344(3)	-768.5(11)	4660.7(19)	17.7(6)
C18	8104(3)	-477.7(12)	4454.7(15)	16.6(6)
C22	8262(3)	26.1(11)	4866.8(19)	15.3(6)
C23	9134(3)	356.1(12)	4679.9(19)	17.5(6)
C24	9287(3)	812.6(12)	5077.3(18)	16.0(6)
C25	8585(3)	947.0(11)	5677.5(18)	15.5(6)
C26	8768(3)	1445.1(11)	6124.6(19)	16.2(6)
C27	8353(3)	1822.2(11)	5405.7(19)	15.7(6)
C28	6625(3)	2324.7(14)	4728(2)	27.7(7)
C29	6843(4)	2831.3(14)	5105(3)	36.2(9)

Atom	x	y	z	U_{eq}
C30	10122(3)	1534.2(12)	6670(2)	17.8(6)
C31	10404(3)	1157.2(12)	7414.7(19)	18.6(6)
C32	11736(3)	1146.8(12)	7990(2)	20.2(6)
C33	11882(3)	761.8(12)	8710(2)	20.6(6)
C34	13166(3)	742.0(12)	9349(2)	21.0(6)
C35	10265(3)	2059.9(13)	7020(2)	27.1(7)
C36	7717(3)	618.5(12)	5856(2)	18.7(6)
C37	7552(3)	160.1(12)	5448(2)	18.9(6)
C38	11899(3)	-2126.7(12)	6990(2)	23.7(7)
C39	12051(3)	-959.7(12)	9296(2)	19.9(6)
C40	12191(3)	-504.9(13)	9699(2)	20.2(6)
Cl1A	14844(14)	1686(3)	12243(12)	45.0(3)
Cl2A	16877(10)	1106(6)	13266(8)	32.7(2)
Cl3A	14418(9)	678(4)	12635(7)	28.6(5)
O1A	14794(15)	838(5)	10884(6)	22.6(4)
O2A	15180(20)	30(5)	10930(30)	31.5(7)
C1A	15514(8)	1097(4)	12378(6)	25.0(6)
C2A	15863(11)	931(6)	11554(8)	28.6(5)
C3A	14464(12)	366(5)	10710(11)	23.7(6)
Cl1B	16332.9(9)	1338.0(6)	11512.5(6)	38.5(2)
Cl2B	14407.9(10)	1631.0(6)	12361.0(8)	45.0(3)
Cl3B	16697.1(9)	1198.2(6)	13397.1(6)	32.7(2)
O1B	14120.6(18)	642.3(9)	11424.9(13)	22.6(4)
O2B	15364(2)	160.9(11)	10833.2(19)	31.5(7)
C1B	15579(2)	1184.5(10)	12353.1(14)	25.0(6)
C2B	15012(2)	685.5(9)	12219.7(13)	28.6(5)
C3B	14372(2)	352.7(14)	10791.4(17)	23.7(6)
Cl10	9804.3(10)	1717.8(6)	12236.7(7)	37.7(3)
Cl11	11830.8(12)	1164.3(8)	13337.2(7)	38.7(3)
Cl12	9436.2(9)	703.6(6)	12609.2(6)	34.9(2)
O13A	9962(2)	914.0(9)	10886.1(13)	23.2(5)
O14A	10427(3)	118.4(15)	10802(2)	25.0(5)
C59A	10531(2)	1137.9(10)	12405.1(14)	24.1(7)
C60A	10979(2)	980.4(10)	11612.2(14)	24.4(7)
C61A	9712(2)	452.8(10)	10582.8(19)	19.5(7)
Cl4	11260(7)	1317(3)	11524(5)	24.4(7)
Cl5	11783(11)	1129(6)	13399(5)	38.7(3)
Cl6	9450(9)	1588(4)	12503(7)	37.7(3)
O13B	9153(8)	635(4)	11405(11)	23.2(5)
O14B	10480(30)	149(18)	10906(15)	25.0(5)
C59B	10592(8)	1146(3)	12399(4)	24.1(7)
C60B	9981(12)	653(3)	12237(7)	24.4(7)
C61B	9492(8)	360(3)	10782(6)	19.5(7)
Cl4B	4794.7(7)	-1581.1(5)	2684.3(5)	26.56(18)
Cl5B	4742.2(7)	-1286.3(5)	894.3(5)	27.51(18)
Cl6B	6965.1(8)	-1733.5(6)	1992.6(6)	36.2(2)
O5B	6847(2)	-847.8(8)	3172.4(12)	23.2(4)
O6B	7589(2)	-100.9(9)	2993.6(15)	24.9(5)
C19B	5687(2)	-1336.2(9)	1988.7(13)	20.7(6)
C20B	6171(2)	-836.2(9)	2290.8(13)	24.0(5)
C21B	7527(3)	-441.2(10)	3470.3(15)	19.0(5)
Cl4A	6940(20)	-1732(8)	1230(14)	26.56(18)
Cl5A	5500(20)	-1703(9)	2548(15)	26.56(18)
Cl6A	5350(20)	-904(7)	1313(16)	36.2(2)
O5A	6948(18)	-727(10)	3040(9)	23.2(4)
O6A	8270(50)	-95(14)	3087(11)	24.9(5)
C19A	6364(15)	-1348(5)	1947(11)	20.7(6)
C20A	7415(14)	-1092(8)	2584(17)	24.0(5)

Atom	x	y	z	U_{eq}
C21A	7770(30)	-387(6)	3464(3)	19.0(5)
Cl7A	-7.3(8)	-1204.2(6)	723.1(5)	27.12(15)
Cl8A	-569.5(7)	-705.8(6)	2212.1(5)	27.12(15)
Cl9A	527.8(9)	-1670.4(6)	2436.4(6)	33.8(2)
O1AC	2161(2)	-815.8(11)	3013.7(15)	28.2(6)
O2AC	3584(3)	-255.1(11)	2857.4(16)	30.5(6)
C41A	491(2)	-1106.3(9)	1868.3(13)	20.6(7)
C42A	1781(2)	-881.2(10)	2099.9(13)	23.6(7)
C43A	3066(3)	-483.6(12)	3321.1(15)	19.2(6)
Cl7B	1940(7)	-1709(4)	1945(6)	27.12(15)
Cl8B	-271(8)	-1241(4)	882(5)	27.12(15)
Cl9B	-240(8)	-1579(4)	2643(6)	33.8(2)
O1AB	2270(20)	-868(4)	2973(17)	28.2(6)
O2AB	2920(30)	-95(7)	2897(13)	30.5(6)
C41B	679(6)	-1315(3)	1971(5)	20.6(7)
C42B	1141(9)	-824(3)	2337(8)	23.6(7)
C43B	2833(14)	-451(4)	3328(3)	19.2(6)
F7	3005(2)	2918.9(9)	5342.4(16)	39.1(5)
F8	1406(2)	3152.1(9)	4338.3(18)	45.1(6)
F9	1176(3)	2907.5(10)	5600(2)	54.9(7)
F10	8134(3)	-3161.8(11)	9753(2)	69.2(9)
F11	9878(3)	-3174.1(12)	10743.5(19)	67.0(9)
F12	8399(4)	-2691.3(12)	10877.7(19)	69.9(10)
O11	2110.3(19)	1968.3(9)	5289.3(14)	20.4(4)
O12	3874.9(19)	1945.6(9)	4802.2(14)	20.3(4)
O15	8484(2)	-2190.5(10)	9410.4(16)	31.1(6)
O16	9699(2)	-1860.8(10)	8613.9(18)	32.0(6)
C44	3328(3)	-484.5(12)	4323.8(15)	17.4(6)
C45	3390(3)	22.1(11)	4715(2)	15.8(6)
C46	4282(3)	362.8(12)	4600.2(19)	17.0(6)
C47	4379(3)	814.1(12)	5011.3(19)	16.9(6)
C48	3587(3)	932.7(11)	5566.7(19)	16.5(6)
C49	3686(3)	1426.8(11)	6024.5(19)	15.5(6)
C50	3290(3)	1808.3(11)	5311.2(19)	15.7(6)
C51	1589(3)	2314.4(13)	4618(2)	25.4(7)
C52	1805(4)	2818.0(14)	4982(3)	34.4(9)
C53	5004(3)	1536.3(12)	6614.3(19)	18.1(6)
C54	5289(3)	1161.7(12)	7370(2)	20.0(6)
C55	6604(3)	1188.6(12)	7968.4(19)	18.4(6)
C56	6833(3)	798.3(13)	8685(2)	21.4(6)
C57	8172(3)	809.7(12)	9266(2)	20.0(6)
C58	8414(2)	401.8(12)	9965.3(19)	20.9(6)
C62	8212(3)	-109.3(12)	9570.9(19)	18.7(6)
C63	8902(3)	-276.7(12)	8985(2)	20.0(6)
C64	8709(3)	-740.8(12)	8621(2)	18.9(6)
C65	7810(3)	-1052.8(12)	8825(2)	18.1(6)
C66	7573(3)	-1561.9(12)	8440(2)	19.2(6)
C67	8704(3)	-1875.3(12)	8806(2)	19.8(6)
C68	9512(4)	-2494.6(15)	9826(3)	37.0(9)
C69	8961(5)	-2879.7(16)	10296(3)	45.0(11)
C70	7259(3)	-1585.0(12)	7420.1(19)	17.5(6)
C71	6171(3)	-1239.1(12)	7022.2(19)	18.3(6)
C72	5982(3)	-1150.6(12)	6040(2)	17.6(6)
C73	4879(3)	-813.3(11)	5676.9(19)	16.0(6)
C74	4557(3)	-767.8(11)	4669.7(19)	16.8(6)
C75	6933(3)	-2110.8(12)	7120(2)	21.7(6)
C76	7123(3)	-883.8(13)	9403(2)	21.3(6)
C77	7323(3)	-418.7(13)	9772(2)	21.0(6)

Atom	x	y	z	U_{eq}
C78	5053(4)	2061.6(12)	6959(2)	26.5(7)
C79	2695(3)	595.1(12)	5675(2)	19.8(6)
C80	2597(3)	142.6(12)	5245(2)	19.0(6)

Table 8: Anisotropic Displacement Parameters (×10^4) for **atb-40-48**. The anisotropic displacement factor exponent takes the form: $-2\pi^2[h^2a^{*2} \times U_{11} + ... + 2hka^* \times b^* \times U_{12}]$

Atom	U_{11}	U_{22}	U_{33}	U_{23}	U_{13}	U_{12}
F1	96(2)	33.2(14)	57.3(16)	11.0(12)	41.0(16)	-3.7(14)
F2	115(2)	45.0(15)	23.5(11)	11.7(10)	27.4(14)	28.4(15)
F3	108(2)	45.8(16)	42.9(15)	26.5(12)	18.5(15)	40.5(16)
F4	57.6(14)	17.7(10)	46.1(13)	-1.2(9)	17.4(11)	0.2(9)
F5	57.6(15)	33.5(13)	76.9(18)	34.4(12)	36.1(14)	26.3(11)
F6	102(2)	35.7(14)	89(2)	20.1(14)	77(2)	28.6(14)
O3	29.9(12)	26.0(12)	13.9(10)	6.4(9)	1.7(9)	2.5(9)
O4	17.9(11)	33.8(13)	34.9(13)	14.7(11)	8.0(10)	6.0(9)
O7	20.7(10)	18.9(11)	30.1(12)	9.9(9)	11.5(9)	6.1(8)
O8	22.4(11)	21.4(11)	22.2(11)	3.5(9)	6.9(9)	2.3(9)
C4	17.6(14)	20.5(15)	14.2(14)	-4.9(11)	-0.3(11)	4.3(11)
C5	18.7(13)	17.9(14)	10.0(13)	-0.7(11)	-0.6(11)	5.7(11)
C6	16.0(14)	23.5(16)	21.5(15)	-2.0(12)	5.2(12)	-1.9(11)
C7	17.7(13)	23.3(16)	17.4(14)	-2.6(11)	5.8(11)	3.2(11)
C8	15.3(13)	19.5(14)	12.2(13)	0.7(11)	0.4(11)	-0.2(11)
C9	16.5(13)	18.5(14)	16.3(14)	2.2(11)	1.9(11)	-1.7(11)
C10	20.7(15)	15.5(14)	14.9(14)	3.3(11)	-0.5(11)	-1.3(11)
C11	42(2)	21.2(16)	21.6(16)	8.1(13)	-0.5(15)	10.5(14)
C12	79(3)	27.4(19)	20.3(17)	9.0(15)	14.1(19)	13(2)
C13	17.2(13)	16.8(14)	15.7(14)	-0.2(11)	1.7(11)	1.6(11)
C14	20.7(14)	15.7(14)	16.9(14)	-1.4(11)	1.9(11)	4.3(11)
C15	15.9(13)	14.2(13)	16.7(14)	1.0(11)	1.8(11)	0.5(11)
C16	18.1(13)	14.3(14)	15.2(14)	-2.1(10)	-0.4(11)	0.1(11)
C17	20.5(14)	14.1(14)	17.7(14)	-2.4(11)	3.2(11)	-0.9(11)
C18	16.5(13)	16.6(14)	14.9(14)	-0.9(11)	0.5(11)	-2.7(11)
C22	15.4(13)	13.0(13)	14.3(14)	1.2(10)	-2.6(11)	0.4(10)
C23	19.6(14)	17.1(14)	14.4(14)	-1.0(11)	1.4(11)	-0.7(11)
C24	17.1(13)	16.5(14)	12.8(13)	2.0(11)	0.5(11)	0.9(11)
C25	16.5(13)	15.7(14)	11.6(13)	2.9(10)	-1.9(11)	1.9(10)
C26	18.7(14)	15.0(14)	14.2(13)	1.6(11)	2.9(11)	-0.6(11)
C27	15.9(13)	12.5(13)	16.7(14)	0.9(11)	0.2(11)	2.9(10)
C28	17.2(14)	28.5(18)	37.2(19)	16.8(15)	6.5(13)	8.0(12)
C29	41(2)	24.3(19)	52(2)	18.7(16)	28.0(18)	17.7(15)
C30	18.3(14)	17.6(14)	15.6(14)	0.6(11)	0.5(11)	-0.4(11)
C31	21.7(14)	16.1(14)	15.8(14)	2.0(11)	0.4(12)	-2.7(11)
C32	22.2(15)	17.5(14)	19.8(15)	3.7(12)	3.2(12)	-1.0(11)
C33	20.5(14)	19.1(15)	19.3(15)	2.7(12)	-0.7(12)	-2.0(11)
C34	21.9(14)	16.4(15)	22.5(15)	-0.6(12)	0.9(12)	0.5(11)
C35	39.0(19)	17.7(16)	20.4(16)	-3.1(12)	-0.8(14)	-3.6(13)
C36	18.0(14)	19.1(15)	19.7(14)	-2.7(11)	5.7(11)	0.6(11)
C37	15.6(13)	17.6(14)	22.3(15)	0.9(12)	2.3(11)	-0.3(11)
C38	32.0(17)	16.0(15)	20.7(15)	1.1(12)	1.7(13)	3.7(12)
C39	18.4(14)	24.2(16)	15.3(14)	2.3(12)	0.8(11)	0.2(12)
C40	18.7(14)	25.5(16)	16.6(14)	1.4(12)	5.0(11)	5.8(12)
Cl1A	30.8(5)	32.6(5)	64.4(7)	-19.5(4)	-2.3(5)	10.0(4)
Cl2A	30.5(4)	36.4(6)	25.2(5)	-13.6(4)	-4.6(3)	0.3(4)
Cl3A	24.3(8)	37.0(10)	20.2(9)	-11.0(8)	-2.9(7)	5.2(8)

Atom	U_{11}	U_{22}	U_{33}	U_{23}	U_{13}	U_{12}
O1A	21.6(8)	29.0(8)	15.0(8)	-4.9(7)	0.4(7)	2.7(7)
O2A	26.7(11)	32.1(9)	28.5(13)	-10.2(10)	-7.0(10)	8.2(9)
C1A	19.2(11)	31.3(14)	20.7(9)	-10.9(9)	-2.4(9)	1.0(11)
C2A	24.3(8)	37.0(10)	20.2(9)	-11.0(8)	-2.9(7)	5.2(8)
C3A	20.3(10)	28.7(9)	19.9(14)	-5.6(8)	0.8(9)	3.7(6)
Cl1B	32.8(5)	44.6(6)	36.7(5)	12.0(4)	6.0(4)	-9.6(4)
Cl2B	30.8(5)	32.6(5)	64.4(7)	-19.5(4)	-2.3(5)	10.0(4)
Cl3B	30.5(4)	36.4(6)	25.2(5)	-13.6(4)	-4.6(3)	0.3(4)
O1B	21.6(8)	29.0(8)	15.0(8)	-4.9(7)	0.4(7)	2.7(7)
O2B	26.7(11)	32.1(9)	28.5(13)	-10.2(10)	-7.0(10)	8.2(9)
C1B	19.2(11)	31.3(14)	20.7(9)	-10.9(9)	-2.4(9)	1.0(11)
C2B	24.3(8)	37.0(10)	20.2(9)	-11.0(8)	-2.9(7)	5.2(8)
C3B	20.3(10)	28.7(9)	19.9(14)	-5.6(8)	0.8(9)	3.7(6)
Cl10	45.3(6)	25.7(5)	38.0(6)	-5.2(4)	2.2(4)	9.5(4)
Cl11	39.1(5)	47.0(6)	21.2(4)	-7.6(4)	-9.6(4)	3.7(4)
Cl12	36.0(5)	40.2(5)	30.5(5)	6.1(4)	11.8(4)	-3.8(4)
O13A	23.3(12)	23.1(13)	20.5(12)	-1.3(10)	0.0(10)	-0.8(9)
O14A	22.8(11)	29.3(14)	19.6(13)	-7.9(11)	-1.1(10)	4.0(10)
C59A	24.9(16)	24.6(16)	19.5(15)	-0.1(12)	-0.7(13)	1.2(12)
C60A	23.7(16)	28.4(17)	17.7(15)	-0.2(13)	-1.4(12)	-3.9(13)
C61A	23.9(17)	20.7(17)	14.2(15)	-2.5(12)	5.1(13)	-1.7(13)
Cl4	23.7(16)	28.4(17)	17.7(15)	-0.2(13)	-1.4(12)	-3.9(13)
Cl5	39.1(5)	47.0(6)	21.2(4)	-7.6(4)	-9.6(4)	3.7(4)
Cl6	45.3(6)	25.7(5)	38.0(6)	-5.2(4)	2.2(4)	9.5(4)
O13B	23.3(12)	23.1(13)	20.5(12)	-1.3(10)	0.0(10)	-0.8(9)
O14B	22.8(11)	29.3(14)	19.6(13)	-7.9(11)	-1.1(10)	4.0(10)
C59B	24.9(16)	24.6(16)	19.5(15)	-0.1(12)	-0.7(13)	1.2(12)
C60B	23.7(16)	28.4(17)	17.7(15)	-0.2(13)	-1.4(12)	-3.9(13)
C61B	23.9(17)	20.7(17)	14.2(15)	-2.5(12)	5.1(13)	-1.7(13)
Cl4B	29.9(4)	25.3(4)	23.5(4)	-0.4(3)	4.7(3)	-5.9(3)
Cl5B	31.1(4)	29.7(4)	16.1(3)	-3.2(3)	-5.1(3)	-2.8(3)
Cl6B	29.5(4)	35.2(5)	41.4(5)	-6.6(4)	4.0(4)	7.7(3)
O5B	29.8(9)	19.0(8)	16.3(8)	-0.7(6)	-3.2(7)	-6.8(7)
O6B	29.5(10)	21.0(9)	21.5(10)	2.4(7)	1.2(8)	-4.5(8)
C19B	20.9(9)	21.6(9)	17.1(9)	-4.3(7)	-0.5(7)	-1.6(8)
C20B	28.7(11)	21.7(9)	16.7(9)	-1.5(7)	-3.8(7)	-5.1(8)
C21B	22.2(10)	16.2(8)	16.0(10)	-1.7(6)	-0.8(8)	-2.3(7)
Cl4A	29.9(4)	25.3(4)	23.5(4)	-0.4(3)	4.7(3)	-5.9(3)
Cl5A	29.9(4)	25.3(4)	23.5(4)	-0.4(3)	4.7(3)	-5.9(3)
Cl6A	29.5(4)	35.2(5)	41.4(5)	-6.6(4)	4.0(4)	7.7(3)
O5A	29.8(9)	19.0(8)	16.3(8)	-0.7(6)	-3.2(7)	-6.8(7)
O6A	29.5(10)	21.0(9)	21.5(10)	2.4(7)	1.2(8)	-4.5(8)
C19A	20.9(9)	21.6(9)	17.1(9)	-4.3(7)	-0.5(7)	-1.6(8)
C20A	28.7(11)	21.7(9)	16.7(9)	-1.5(7)	-3.8(7)	-5.1(8)
C21A	22.2(10)	16.2(8)	16.0(10)	-1.7(6)	-0.8(8)	-2.3(7)
Cl7A	24.1(3)	35.9(3)	20.7(3)	-4.0(2)	4.0(2)	-0.3(2)
Cl8A	24.1(3)	35.9(3)	20.7(3)	-4.0(2)	4.0(2)	-0.3(2)
Cl9A	39.4(5)	25.6(4)	29.9(5)	7.2(3)	-4.2(4)	-7.8(4)
O1AC	29.1(12)	33.6(13)	17.8(11)	-1.9(10)	-1.9(9)	-12.4(10)
O2AC	41.2(16)	33.8(14)	16.8(12)	-1.6(10)	7.4(11)	-13.3(12)
C41A	20.0(14)	20.5(16)	19.6(15)	2.5(12)	1.6(12)	-1.1(12)
C42A	18.4(15)	33.8(18)	16.9(15)	-1.9(13)	1.0(12)	-2.3(13)
C43A	18.6(14)	17.4(14)	18.8(14)	1.6(11)	-0.6(11)	0.3(11)
Cl7B	24.1(3)	35.9(3)	20.7(3)	-4.0(2)	4.0(2)	-0.3(2)
Cl8B	24.1(3)	35.9(3)	20.7(3)	-4.0(2)	4.0(2)	-0.3(2)
Cl9B	39.4(5)	25.6(4)	29.9(5)	7.2(3)	-4.2(4)	-7.8(4)
O1AB	29.1(12)	33.6(13)	17.8(11)	-1.9(10)	-1.9(9)	-12.4(10)
O2AB	41.2(16)	33.8(14)	16.8(12)	-1.6(10)	7.4(11)	-13.3(12)

Atom	U_{11}	U_{22}	U_{33}	U_{23}	U_{13}	U_{12}
C41B	20.0(14)	20.5(16)	19.6(15)	2.5(12)	1.6(12)	-1.1(12)
C42B	18.4(15)	33.8(18)	16.9(15)	-1.9(13)	1.0(12)	-2.3(13)
C43B	18.6(14)	17.4(14)	18.8(14)	1.6(11)	-0.6(11)	0.3(11)
F7	49.4(13)	18.6(10)	47.6(13)	1.1(9)	8.5(11)	-0.3(9)
F8	50.2(13)	31.1(12)	62.8(16)	28.7(11)	30.6(12)	21.3(10)
F9	83.9(19)	32.5(13)	67.2(17)	14.4(12)	54.5(16)	20.5(12)
F10	93(2)	31.1(14)	88(2)	2.2(14)	29.9(19)	-9.1(14)
F11	109(2)	45.5(16)	50.8(16)	28.5(13)	27.4(16)	41.9(16)
F12	118(3)	61.9(19)	44.4(15)	27.7(14)	47.6(17)	46.5(18)
O11	18.5(10)	19.1(11)	24.1(11)	8.2(9)	6.5(8)	5.8(8)
O12	19.5(10)	21.6(11)	20.2(11)	1.6(9)	5.8(9)	2.9(8)
O15	30.3(12)	32.2(13)	29.4(13)	16.2(11)	4.8(10)	4.0(10)
O16	20.2(11)	32.7(14)	42.6(15)	14.3(11)	6.6(10)	4.0(9)
C44	17.6(13)	17.7(14)	15.3(13)	-2.1(11)	0.9(11)	-2.0(11)
C45	17.1(13)	12.8(13)	14.6(14)	-0.6(10)	-1.7(11)	-0.5(10)
C46	15.4(13)	19.1(14)	14.9(14)	-0.7(11)	0.6(11)	1.0(11)
C47	16.4(13)	16.8(14)	14.7(13)	1.5(11)	-1.8(11)	-0.9(11)
C48	18.7(14)	13.8(14)	14.4(13)	1.8(11)	-1.0(11)	3.0(11)
C49	21.2(14)	12.9(13)	12.8(13)	2.0(10)	4.7(11)	1.2(11)
C50	16.1(13)	13.1(13)	15.2(14)	-2.1(11)	-1.6(11)	2.6(10)
C51	19.6(14)	25.8(17)	30.3(17)	14.3(14)	5.0(13)	4.0(12)
C52	35.0(19)	23.4(18)	51(2)	18.2(16)	22.6(17)	13.6(14)
C53	20.3(14)	17.3(14)	14.7(14)	1.5(11)	0.4(11)	-0.9(11)
C54	21.4(15)	19.1(15)	16.4(14)	2.6(11)	-1.2(12)	-0.7(11)
C55	20.5(14)	18.2(14)	14.8(14)	0.0(11)	1.3(11)	0.8(11)
C56	22.4(15)	21.2(15)	18.4(15)	2.4(12)	0.6(12)	0.1(12)
C57	16.6(14)	19.2(15)	21.1(15)	0.3(12)	-1.0(12)	2.1(11)
C58	22.4(15)	22.0(16)	16.0(14)	-2.2(12)	0.4(12)	6.2(12)
C62	18.0(14)	22.7(16)	12.6(14)	0.1(11)	-1.7(11)	4.0(11)
C63	14.9(14)	23.9(16)	21.6(15)	-0.7(12)	5.1(12)	-0.1(11)
C64	16.4(13)	21.5(15)	18.6(14)	-1.7(12)	3.9(11)	1.2(11)
C65	13.2(13)	24.1(16)	15.2(14)	3.0(11)	-0.1(11)	1.1(11)
C66	16.0(13)	20.9(15)	19.7(15)	4.9(12)	2.8(11)	-2.3(11)
C67	20.7(15)	15.8(14)	18.2(14)	1.1(11)	-4.1(12)	-1.5(11)
C68	47(2)	23.9(18)	37(2)	11.3(15)	3.0(17)	13.1(16)
C69	77(3)	31(2)	32(2)	9.1(16)	21(2)	16(2)
C70	17.6(13)	19.9(15)	13.3(13)	1.4(11)	0.5(11)	-0.1(11)
C71	21.6(14)	15.5(14)	16.8(14)	-1.5(11)	3.1(11)	1.9(11)
C72	17.7(13)	17.2(14)	16.6(14)	1.4(11)	1.9(11)	0.0(11)
C73	17.2(13)	13.1(14)	16.1(14)	-0.4(10)	0.8(11)	0.2(10)
C74	23.0(14)	12.7(13)	14.3(13)	-0.8(10)	3.7(11)	-1.8(11)
C75	27.2(16)	16.9(15)	20.3(15)	2.5(12)	4.7(13)	2.2(12)
C76	17.7(14)	27.4(16)	17.6(15)	4.9(12)	1.6(12)	-0.3(12)
C77	19.0(14)	28.8(17)	13.4(14)	1.8(12)	0.1(11)	6.2(12)
C78	40.2(19)	17.6(16)	18.3(16)	-2.1(12)	0.3(14)	-3.2(13)
C79	19.7(14)	18.6(15)	20.8(15)	-2.6(12)	4.3(12)	0.9(11)
C80	15.4(13)	19.0(15)	20.3(15)	-1.0(12)	-0.2(11)	-3.8(11)

Table 9: Bond Lengths in Å for **atb-40-48**.

Atom	Atom	Length/Å
F1	C12	1.335(6)
F2	C12	1.337(5)
F3	C12	1.339(5)
F4	C29	1.329(5)
F5	C29	1.351(4)
F6	C29	1.332(5)
O3	C10	1.351(4)
O3	C11	1.422(4)

Atom	Atom	Length/Å
O4	C10	1.202(4)
O7	C27	1.364(4)
O7	C28	1.434(4)
O8	C27	1.198(4)
C4	C5	1.525(4)
C4	C34	1.561(4)
C4	C3A	1.524(3)
C4	C3B	1.520(3)
C5	C6	1.411(4)
C5	C40	1.393(4)
C6	C7	1.381(4)
C7	C8	1.396(4)
C8	C9	1.523(4)
C8	C39	1.386(4)
C9	C10	1.512(4)
C9	C13	1.552(4)
C11	C12	1.504(5)
C13	C14	1.532(4)
C13	C38	1.530(4)
C14	C15	1.524(4)
C15	C16	1.521(4)
C16	C17	1.528(4)
C17	C18	1.545(4)
C18	C22	1.514(4)
C18	C21B	1.517(3)
C18	C21A	1.521(3)
C22	C23	1.400(4)
C22	C37	1.384(4)
C23	C24	1.387(4)
C24	C25	1.402(4)
C25	C26	1.523(4)
C25	C36	1.389(4)
C26	C27	1.512(4)
C26	C30	1.545(4)
C28	C29	1.503(6)
C30	C31	1.529(4)
C30	C35	1.534(4)
C31	C32	1.522(4)
C32	C33	1.521(4)
C33	C34	1.520(4)
C36	C37	1.399(4)
C39	C40	1.387(5)
Cl1A	C1A	1.765(3)
Cl2A	C1A	1.777(3)
Cl3A	C1A	1.780(3)
O1A	C2A	1.394(3)
O1A	C3A	1.352(3)
O2A	C3A	1.202(3)
C1A	C2A	1.502(3)
Cl1B	C1B	1.767(2)
Cl2B	C1B	1.779(2)
Cl3B	C1B	1.788(2)
O1B	C2B	1.387(2)
O1B	C3B	1.348(2)
O2B	C3B	1.199(3)
C1B	C2B	1.495(3)
Cl10	C59A	1.768(2)
Cl11	C59A	1.776(2)
Cl12	C59A	1.776(2)
O13A	C60A	1.397(2)
O13A	C61A	1.353(2)
O14A	C61A	1.202(3)
C59A	C60A	1.503(3)
C61A	C58	1.523(3)
Cl4	C59B	1.765(3)
Cl5	C59B	1.777(3)
Cl6	C59B	1.780(3)
O13B	C60B	1.394(3)
O13B	C61B	1.353(3)
O14B	C61B	1.202(3)
C59B	C60B	1.502(3)
C61B	C58	1.520(3)
Cl4B	C19B	1.765(2)
Cl5B	C19B	1.7761(19)
Cl6B	C19B	1.777(2)
O5B	C20B	1.397(2)
O5B	C21B	1.358(2)
O6B	C21B	1.205(3)
C19B	C20B	1.502(3)
Cl4A	C19A	1.765(3)
Cl5A	C19A	1.777(3)
Cl6A	C19A	1.780(3)
O5A	C20A	1.395(3)
O5A	C21A	1.352(3)
O6A	C21A	1.202(3)
C19A	C20A	1.502(3)
Cl7A	C41A	1.759(2)
Cl8A	C41A	1.777(2)
Cl9A	C41A	1.777(2)
O1AC	C42A	1.397(2)
O1AC	C43A	1.348(2)
O2AC	C43A	1.201(3)
C41A	C42A	1.509(3)
C43A	C44	1.521(3)
Cl7B	C41B	1.765(3)
Cl8B	C41B	1.777(3)
Cl9B	C41B	1.780(3)
O1AB	C42B	1.394(3)
O1AB	C43B	1.353(3)
O2AB	C43B	1.202(3)
C41B	C42B	1.502(3)
C43B	C44	1.520(3)
F7	C52	1.333(5)
F8	C52	1.351(4)
F9	C52	1.341(4)
F10	C69	1.329(6)
F11	C69	1.346(5)
F12	C69	1.323(5)
O11	C50	1.363(4)
O11	C51	1.426(4)
O12	C50	1.199(4)
O15	C67	1.344(4)
O15	C68	1.427(4)
O16	C67	1.205(4)
C44	C45	1.510(4)
C44	C74	1.539(4)

Atom	Atom	Length/Å
C45	C46	1.397(4)
C45	C80	1.383(4)
C46	C47	1.384(4)
C47	C48	1.410(4)
C48	C49	1.521(4)
C48	C79	1.389(4)
C49	C50	1.512(4)
C49	C53	1.546(4)
C51	C52	1.488(5)
C53	C54	1.537(4)
C53	C78	1.532(4)
C54	C55	1.521(4)
C55	C56	1.523(4)
C56	C57	1.532(4)
C57	C58	1.539(4)
C58	C62	1.523(4)
C62	C63	1.401(4)
C62	C77	1.387(5)
C63	C64	1.387(4)
C64	C65	1.403(4)
C65	C66	1.515(4)
C65	C76	1.390(4)
C66	C67	1.506(4)
C66	C70	1.546(4)
C68	C69	1.495(6)
C70	C71	1.534(4)
C70	C75	1.529(4)
C71	C72	1.517(4)
C72	C73	1.520(4)
C73	C74	1.531(4)
C76	C77	1.393(5)
C79	C80	1.401(4)

Table 10: Bond Angles in ° for **atb-40-48**.

Atom	Atom	Atom	Angle/°
C10	O3	C11	114.3(3)
C27	O7	C28	116.3(2)
C5	C4	C34	112.4(2)
C3A	C4	C5	110.7(8)
C3A	C4	C34	106.9(5)
C3B	C4	C5	111.9(2)
C3B	C4	C34	111.8(3)
C6	C5	C4	122.9(3)
C40	C5	C4	118.8(3)
C40	C5	C6	118.3(3)
C7	C6	C5	120.4(3)
C6	C7	C8	121.2(3)
C7	C8	C9	123.1(3)
C39	C8	C7	118.2(3)
C39	C8	C9	118.6(3)
C8	C9	C13	115.2(2)
C10	C9	C8	108.6(2)
C10	C9	C13	109.5(2)
O3	C10	C9	110.9(3)
O4	C10	O3	122.4(3)
O4	C10	C9	126.7(3)
O3	C11	C12	105.3(3)
F1	C12	F2	106.4(4)
F1	C12	F3	107.4(3)
F1	C12	C11	112.8(3)
F2	C12	F3	107.6(3)
F2	C12	C11	112.1(3)
F3	C12	C11	110.3(4)
C14	C13	C9	110.5(2)
C38	C13	C9	108.1(2)
C38	C13	C14	110.9(2)
C15	C14	C13	114.8(2)
C16	C15	C14	110.9(2)
C15	C16	C17	115.1(2)
C16	C17	C18	109.3(2)
C22	C18	C17	112.1(2)
C22	C18	C21B	110.3(2)
C22	C18	C21A	105.0(7)
C21B	C18	C17	112.1(2)
C21A	C18	C17	106.2(11)
C23	C22	C18	120.8(3)
C37	C22	C18	119.7(3)
C37	C22	C23	119.4(3)
C24	C23	C22	120.2(3)
C23	C24	C25	120.6(3)
C24	C25	C26	120.6(3)
C36	C25	C24	118.9(3)
C36	C25	C26	120.5(3)
C25	C26	C30	113.3(2)
C27	C26	C25	106.8(2)
C27	C26	C30	112.2(2)
O7	C27	C26	109.5(2)
O8	C27	O7	123.0(3)
O8	C27	C26	127.4(3)
O7	C28	C29	108.6(3)
F4	C29	F5	106.6(3)
F4	C29	F6	107.5(4)
F4	C29	C28	113.6(3)
F5	C29	C28	109.2(4)
F6	C29	F5	106.8(3)
F6	C29	C28	112.7(3)
C31	C30	C26	107.6(2)
C31	C30	C35	112.2(3)
C35	C30	C26	110.3(2)
C32	C31	C30	116.7(3)
C33	C32	C31	111.2(2)
C34	C33	C32	115.1(3)
C33	C34	C4	110.3(2)
C25	C36	C37	120.6(3)
C22	C37	C36	120.3(3)

Atom	Atom	Atom	Angle/°
C8	C39	C40	121.4(3)
C39	C40	C5	120.6(3)
C3A	O1A	C2A	117.4(3)
Cl1A	C1A	Cl2A	109.22(19)
Cl1A	C1A	Cl3A	109.24(18)
Cl2A	C1A	Cl3A	108.84(18)
C2A	C1A	Cl1A	111.2(2)
C2A	C1A	Cl2A	109.2(2)
C2A	C1A	Cl3A	109.1(2)
O1A	C2A	C1A	110.7(3)
O1A	C3A	C4	112.2(10)
O2A	C3A	C4	122.9(15)
O2A	C3A	O1A	123.2(4)
C3B	O1B	C2B	118.68(18)
Cl1B	C1B	Cl2B	108.33(14)
Cl1B	C1B	Cl3B	109.20(12)
Cl2B	C1B	Cl3B	108.56(12)
C2B	C1B	Cl1B	111.68(15)
C2B	C1B	Cl2B	110.51(15)
C2B	C1B	Cl3B	108.50(15)
O1B	C2B	C1B	112.50(17)
O1B	C3B	C4	109.8(2)
O2B	C3B	C4	125.7(2)
O2B	C3B	O1B	124.4(2)
C61A	O13A	C60A	117.38(19)
Cl10	C59A	Cl11	109.28(13)
Cl10	C59A	Cl12	108.98(13)
Cl11	C59A	Cl12	109.05(13)
C60A	C59A	Cl10	111.24(16)
C60A	C59A	Cl11	109.06(15)
C60A	C59A	Cl12	109.21(15)
O13A	C60A	C59A	110.34(17)
O13A	C61A	C58	112.7(2)
O14A	C61A	O13A	123.2(2)
O14A	C61A	C58	124.0(3)
C61B	O13B	C60B	117.2(3)
Cl4	C59B	Cl5	109.24(19)
Cl4	C59B	Cl6	109.18(18)
Cl5	C59B	Cl6	108.87(18)
C60B	C59B	Cl4	111.2(2)
C60B	C59B	Cl5	109.2(2)
C60B	C59B	Cl6	109.2(2)
O13B	C60B	C59B	110.7(3)
O13B	C61B	C58	105.4(9)
O14B	C61B	O13B	123.2(4)
O14B	C61B	C58	131.3(10)
C21B	O5B	C20B	115.82(17)
Cl4B	C19B	Cl5B	109.77(12)
Cl4B	C19B	Cl6B	108.93(12)
Cl5B	C19B	Cl6B	109.13(11)
C20B	C19B	Cl4B	111.13(15)
C20B	C19B	Cl5B	108.16(14)
C20B	C19B	Cl6B	109.70(15)
O5B	C20B	C19B	110.59(16)
O5B	C21B	C18	110.6(2)
O6B	C21B	C18	127.2(2)
O6B	C21B	O5B	122.1(2)
C21A	O5A	C20A	117.3(3)

Atom	Atom	Atom	Angle/°
Cl4A	C19A	Cl5A	109.27(18)
Cl4A	C19A	Cl6A	109.22(18)
Cl5A	C19A	Cl6A	108.88(18)
C20A	C19A	Cl4A	111.1(2)
C20A	C19A	Cl5A	109.2(2)
C20A	C19A	Cl6A	109.1(2)
O5A	C20A	C19A	110.6(3)
O5A	C21A	C18	110.7(4)
O6A	C21A	C18	125.4(8)
O6A	C21A	O5A	123.3(4)
C43A	O1AC	C42A	117.5(2)
Cl7A	C41A	Cl8A	109.65(12)
Cl7A	C41A	Cl9A	109.81(12)
Cl9A	C41A	Cl8A	108.78(12)
C42A	C41A	Cl7A	110.35(14)
C42A	C41A	Cl8A	108.96(15)
C42A	C41A	Cl9A	109.26(15)
O1AC	C42A	C41A	109.06(16)
O1AC	C43A	C44	107.7(2)
O2AC	C43A	O1AC	123.7(2)
O2AC	C43A	C44	128.5(2)
C43B	O1AB	C42B	117.2(3)
Cl7B	C41B	Cl8B	109.30(18)
Cl7B	C41B	Cl9B	109.21(18)
Cl8B	C41B	Cl9B	108.94(18)
C42B	C41B	Cl7B	111.1(2)
C42B	C41B	Cl8B	109.1(2)
C42B	C41B	Cl9B	109.1(2)
O1AB	C42B	C41B	110.6(3)
O1AB	C43B	C44	112.5(11)
O2AB	C43B	O1AB	123.1(4)
O2AB	C43B	C44	124.4(12)
C50	O11	C51	116.2(2)
C67	O15	C68	115.8(3)
C43A	C44	C74	107.0(2)
C43B	C44	C74	117.1(7)
C45	C44	C43A	113.2(2)
C45	C44	C43B	109.1(5)
C45	C44	C74	111.8(2)
C46	C45	C44	121.7(3)
C80	C45	C44	119.2(3)
C80	C45	C46	118.9(3)
C47	C46	C45	120.9(3)
C46	C47	C48	120.1(3)
C47	C48	C49	120.6(3)
C79	C48	C47	119.0(3)
C79	C48	C49	120.4(3)
C48	C49	C53	113.7(2)
C50	C49	C48	107.0(2)
C50	C49	C53	111.4(2)
O11	C50	C49	110.0(2)
O12	C50	O11	123.0(3)
O12	C50	C49	126.9(3)
O11	C51	C52	109.6(3)
F7	C52	F8	106.5(3)
F7	C52	F9	106.9(4)
F7	C52	C51	113.8(3)
F8	C52	C51	110.5(3)

Atom	Atom	Atom	Angle/°
F9	C52	F8	106.3(3)
F9	C52	C51	112.4(3)
C54	C53	C49	108.3(2)
C78	C53	C49	109.8(3)
C78	C53	C54	111.9(3)
C55	C54	C53	115.1(3)
C54	C55	C56	112.3(3)
C55	C56	C57	112.6(3)
C56	C57	C58	112.3(2)
C61A	C58	C57	110.8(2)
C61B	C58	C57	127.9(3)
C61B	C58	C62	106.1(4)
C62	C58	C61A	111.2(2)
C62	C58	C57	113.4(2)
C63	C62	C58	121.0(3)
C77	C62	C58	120.7(3)
C77	C62	C63	118.2(3)
C64	C63	C62	121.0(3)
C63	C64	C65	120.7(3)
C64	C65	C66	122.1(3)
C76	C65	C64	118.1(3)
C76	C65	C66	119.7(3)
C65	C66	C70	114.9(2)
C67	C66	C65	109.1(2)
C67	C66	C70	108.9(3)
O15	C67	C66	111.0(3)
O16	C67	O15	121.8(3)
O16	C67	C66	127.2(3)
O15	C68	C69	105.2(3)
F10	C69	F11	107.1(4)
F10	C69	C68	113.2(4)
F11	C69	C68	109.5(4)
F12	C69	F10	107.6(4)
F12	C69	F11	107.1(3)
F12	C69	C68	112.1(4)
C71	C70	C66	110.4(2)
C75	C70	C66	109.3(2)
C75	C70	C71	110.8(2)
C72	C71	C70	114.2(2)
C71	C72	C73	112.0(2)
C72	C73	C74	113.3(2)
C73	C74	C44	111.4(2)
C65	C76	C77	121.1(3)
C62	C77	C76	120.9(3)
C48	C79	C80	120.3(3)
C45	C80	C79	120.8(3)

Table 11: Torsion Angles in ° for **atb-40-48**.

Atom	Atom	Atom	Atom	Angle/°
O3	C11	C12	F1	58.9(4)
O3	C11	C12	F2	-61.2(4)
O3	C11	C12	F3	179.0(3)
O7	C28	C29	F4	57.2(4)
O7	C28	C29	F5	176.0(3)
O7	C28	C29	F6	-65.4(4)
C4	C5	C6	C7	-178.9(3)
C4	C5	C40	C39	178.8(3)
C5	C4	C34	C33	66.1(3)
C5	C4	C3A	O1A	157.9(15)
C5	C4	C3A	O2A	-8(3)
C5	C4	C3B	O1B	-146.4(3)
C5	C4	C3B	O2B	34.5(5)
C5	C6	C7	C8	-0.3(5)
C6	C5	C40	C39	-1.0(4)
C6	C7	C8	C9	178.8(3)
C6	C7	C8	C39	-0.1(4)
C7	C8	C9	C10	62.5(4)
C7	C8	C9	C13	-60.6(4)
C7	C8	C39	C40	0.0(4)
C8	C9	C10	O3	96.6(3)
C8	C9	C10	O4	-82.5(4)
C8	C9	C13	C14	-50.0(3)
C8	C9	C13	C38	-171.6(2)
C8	C39	C40	C5	0.6(4)
C9	C8	C39	C40	-179.0(3)
C9	C13	C14	C15	171.8(2)
C10	O3	C11	C12	-177.0(3)

Atom	Atom	Atom	Atom	Angle/°
C10	C9	C13	C14	-172.8(2)
C10	C9	C13	C38	65.7(3)
C11	O3	C10	O4	1.9(4)
C11	O3	C10	C9	-177.2(3)
C13	C9	C10	O3	-136.9(3)
C13	C9	C10	O4	44.1(4)
C13	C14	C15	C16	177.1(2)
C14	C15	C16	C17	-170.6(2)
C15	C16	C17	C18	170.9(2)
C16	C17	C18	C22	58.4(3)
C16	C17	C18	C21B	-176.9(2)
C16	C17	C18	C21A	172.6(7)
C17	C18	C22	C23	56.9(3)
C17	C18	C22	C37	-121.9(3)
C17	C18	C21B	O5B	83.5(3)
C17	C18	C21B	O6B	-99.3(4)
C17	C18	C21A	O5A	96.3(13)
C17	C18	C21A	O6A	-75(3)
C18	C22	C23	C24	-178.6(2)
C18	C22	C37	C36	177.9(3)
C22	C18	C21B	O5B	-150.8(3)
C22	C18	C21B	O6B	26.4(4)
C22	C18	C21A	O5A	-144.7(9)
C22	C18	C21A	O6A	44(3)
C22	C23	C24	C25	0.8(4)
C23	C22	C37	C36	-0.9(4)
C23	C24	C25	C26	179.1(3)
C23	C24	C25	C36	-1.1(4)
C24	C25	C26	C27	65.0(3)
C24	C25	C26	C30	-59.1(3)
C24	C25	C36	C37	0.4(4)
C25	C26	C27	O7	100.8(3)
C25	C26	C27	O8	-77.4(4)
C25	C26	C30	C31	-63.1(3)
C25	C26	C30	C35	174.2(3)
C25	C36	C37	C22	0.6(4)
C26	C25	C36	C37	-179.8(3)
C26	C30	C31	C32	174.6(3)
C27	O7	C28	C29	-96.2(3)
C27	C26	C30	C31	175.9(2)
C27	C26	C30	C35	53.2(3)
C28	O7	C27	O8	1.2(4)
C28	O7	C27	C26	-177.1(3)
C30	C26	C27	O7	-134.5(3)
C30	C26	C27	O8	47.3(4)
C30	C31	C32	C33	179.1(3)
C31	C32	C33	C34	-177.0(3)
C32	C33	C34	C4	-176.8(3)
C34	C4	C5	C6	54.9(4)
C34	C4	C5	C40	-124.9(3)
C34	C4	C3A	O1A	35(2)
C34	C4	C3A	O2A	-130(3)
C34	C4	C3B	O1B	86.5(3)
C34	C4	C3B	O2B	-92.6(4)
C35	C30	C31	C32	-63.9(4)
C36	C25	C26	C27	-114.9(3)
C36	C25	C26	C30	121.1(3)
C37	C22	C23	C24	0.2(4)

Atom	Atom	Atom	Atom	Angle/°
C38	C13	C14	C15	-68.3(3)
C39	C8	C9	C10	-118.6(3)
C39	C8	C9	C13	118.3(3)
C40	C5	C6	C7	0.9(4)
Cl1A	C1A	C2A	O1A	-69.7(8)
Cl2A	C1A	C2A	O1A	169.7(8)
Cl3A	C1A	C2A	O1A	50.8(8)
C2A	O1A	C3A	C4	175.1(10)
C2A	O1A	C3A	O2A	-19(3)
C3A	C4	C5	C6	-64.6(9)
C3A	C4	C5	C40	115.6(8)
C3A	C4	C34	C33	-172.2(10)
C3A	O1A	C2A	C1A	-103.0(16)
Cl1B	C1B	C2B	O1B	-60.1(2)
Cl2B	C1B	C2B	O1B	60.6(2)
Cl3B	C1B	C2B	O1B	179.49(17)
C2B	O1B	C3B	C4	173.9(2)
C2B	O1B	C3B	O2B	-7.0(5)
C3B	C4	C5	C6	-72.0(4)
C3B	C4	C5	C40	108.3(3)
C3B	C4	C34	C33	-167.1(2)
C3B	O1B	C2B	C1B	111.9(3)
Cl10	C59A	C60A	O13A	-64.7(2)
Cl11	C59A	C60A	O13A	174.70(17)
Cl12	C59A	C60A	O13A	55.6(2)
O13A	C61A	C58	C57	47.6(4)
O13A	C61A	C58	C62	174.7(3)
O14A	C61A	C58	C57	-134.5(4)
O14A	C61A	C58	C62	-7.5(5)
C60A	O13A	C61A	O14A	-13.1(5)
C60A	O13A	C61A	C58	164.7(2)
C61A	O13A	C60A	C59A	-112.3(3)
C61A	C58	C62	C63	-66.5(4)
C61A	C58	C62	C77	114.5(3)
Cl4	C59B	C60B	O13B	-51.9(8)
Cl5	C59B	C60B	O13B	-172.5(7)
Cl6	C59B	C60B	O13B	68.6(7)
O13B	C61B	C58	C57	83.4(5)
O13B	C61B	C58	C62	-138.2(5)
O14B	C61B	C58	C57	-95(4)
O14B	C61B	C58	C62	44(4)
C60B	O13B	C61B	O14B	-3(4)
C60B	O13B	C61B	C58	178.9(8)
C61B	O13B	C60B	C59B	108.9(6)
C61B	C58	C62	C63	-86.1(6)
C61B	C58	C62	C77	94.9(6)
Cl4B	C19B	C20B	O5B	55.1(2)
Cl5B	C19B	C20B	O5B	175.70(18)
Cl6B	C19B	C20B	O5B	-65.4(2)
C20B	O5B	C21B	C18	174.0(2)
C20B	O5B	C21B	O6B	-3.4(4)
C21B	C18	C22	C23	-68.7(3)
C21B	C18	C22	C37	112.5(3)
C21B	O5B	C20B	C19B	168.0(2)
Cl4A	C19A	C20A	O5A	170(2)
Cl5A	C19A	C20A	O5A	-70(2)
Cl6A	C19A	C20A	O5A	49(2)
C20A	O5A	C21A	C18	-105(2)

Atom	Atom	Atom	Atom	Angle/°
C20A	O5A	C21A	O6A	67(4)
C21A	C18	C22	C23	-57.9(12)
C21A	C18	C22	C37	123.3(12)
C21A	O5A	C20A	C19A	-163.6(13)
Cl7A	C41A	C42A	O1AC	-178.95(19)
Cl8A	C41A	C42A	O1AC	60.6(2)
Cl9A	C41A	C42A	O1AC	-58.1(2)
O1AC	C43A	C44	C45	-133.3(3)
O1AC	C43A	C44	C74	103.1(3)
O2AC	C43A	C44	C45	50.2(5)
O2AC	C43A	C44	C74	-73.4(4)
C42A	O1AC	C43A	O2AC	-2.4(5)
C42A	O1AC	C43A	C44	-179.2(3)
C43A	O1AC	C42A	C41A	-158.6(3)
C43A	C44	C45	C46	-61.2(4)
C43A	C44	C45	C80	122.8(3)
C43A	C44	C74	C73	-177.2(2)
Cl7B	C41B	C42B	O1AB	-32.8(19)
Cl8B	C41B	C42B	O1AB	-153.4(19)
Cl9B	C41B	C42B	O1AB	87.7(19)
O1AB	C43B	C44	C45	-154.5(12)
O1AB	C43B	C44	C74	77.3(12)
O2AB	C43B	C44	C45	25.3(13)
O2AB	C43B	C44	C74	-102.9(13)
C42B	O1AB	C43B	O2AB	-44(3)
C42B	O1AB	C43B	C44	136(3)
C43B	O1AB	C42B	C41B	176.7(19)
C43B	C44	C45	C46	-71.5(7)
C43B	C44	C45	C80	112.6(7)
C43B	C44	C74	C73	-174.7(4)
O11	C51	C52	F7	55.5(4)
O11	C51	C52	F8	175.2(3)
O11	C51	C52	F9	-66.3(4)
O15	C68	C69	F10	63.3(4)
O15	C68	C69	F11	-177.3(3)
O15	C68	C69	F12	-58.6(5)
C44	C45	C46	C47	-175.7(3)
C44	C45	C80	C79	174.9(3)
C45	C44	C74	C73	58.4(3)
C45	C46	C47	C48	1.1(4)
C46	C45	C80	C79	-1.1(4)
C46	C47	C48	C49	179.8(3)
C46	C47	C48	C79	-1.5(4)
C47	C48	C49	C50	66.1(3)
C47	C48	C49	C53	-57.4(3)
C47	C48	C79	C80	0.6(4)
C48	C49	C50	O11	103.8(3)
C48	C49	C50	O12	-73.2(4)
C48	C49	C53	C54	-64.0(3)
C48	C49	C53	C78	173.5(3)
C48	C79	C80	C45	0.7(5)
C49	C48	C79	C80	179.3(3)
C49	C53	C54	C55	174.7(3)
C50	O11	C51	C52	-95.2(3)
C50	C49	C53	C54	174.9(2)
C50	C49	C53	C78	52.5(3)
C51	O11	C50	O12	0.0(4)
C51	O11	C50	C49	-177.2(3)

Atom	Atom	Atom	Atom	Angle/°
C53	C49	C50	O11	-131.3(3)
C53	C49	C50	O12	51.6(4)
C53	C54	C55	C56	-178.4(3)
C54	C55	C56	C57	177.6(3)
C55	C56	C57	C58	-177.7(3)
C56	C57	C58	C61A	-174.8(2)
C56	C57	C58	C61B	-164.7(8)
C56	C57	C58	C62	59.3(3)
C57	C58	C62	C63	59.1(3)
C57	C58	C62	C77	-119.8(3)
C58	C62	C63	C64	-179.5(3)
C58	C62	C77	C76	179.1(3)
C62	C63	C64	C65	0.5(5)
C63	C62	C77	C76	0.1(4)
C63	C64	C65	C66	180.0(3)
C63	C64	C65	C76	-0.2(4)
C64	C65	C66	C67	67.6(4)
C64	C65	C66	C70	-55.0(4)
C64	C65	C76	C77	-0.3(4)
C65	C66	C67	O15	105.6(3)
C65	C66	C67	O16	-74.0(4)
C65	C66	C70	C71	-53.0(3)
C65	C66	C70	C75	-175.2(2)
C65	C76	C77	C62	0.3(4)
C66	C65	C76	C77	179.6(3)
C66	C70	C71	C72	167.2(2)
C67	O15	C68	C69	-167.3(3)
C67	C66	C70	C71	-175.7(2)
C67	C66	C70	C75	62.2(3)
C68	O15	C67	O16	1.8(5)
C68	O15	C67	C66	-177.8(3)
C70	C66	C67	O15	-128.3(3)
C70	C66	C67	O16	52.1(4)
C70	C71	C72	C73	178.9(2)
C71	C72	C73	C74	-172.7(2)
C72	C73	C74	C44	171.8(2)
C74	C44	C45	C46	59.7(3)
C74	C44	C45	C80	-116.3(3)
C75	C70	C71	C72	-71.6(3)
C76	C65	C66	C67	-112.3(3)
C76	C65	C66	C70	125.1(3)
C77	C62	C63	C64	-0.5(4)
C78	C53	C54	C55	-64.1(4)
C79	C48	C49	C50	-112.6(3)
C79	C48	C49	C53	124.0(3)
C80	C45	C46	C47	0.2(4)

Table 12: Hydrogen Fractional Atomic Coordinates (×10⁴) and Equivalent Isotropic Displacement Parameters (Å²×10³) for **atb-40-48**. U_{eq} is defined as 1/3 of the trace of the orthogonalised U_{ij}.

Atom	x	y	z	U_{eq}
H4	12491.1	350.96	10268.84	22
H6	14560.11	-134.02	8974.95	24
H7	14307.76	-890.4	8314.56	23
H9	11915.42	-1766.75	8525.76	21

Atom	x	y	z	U_{eq}
H11A	15403.89	-2289.61	10003.42	36
H11B	14931.76	-2701.55	9294.15	36
H13	13021.08	-1511.64	7113.5	20
H14A	10462.33	-1364.57	7098.93	22
H14B	11430.92	-935.51	7253.07	22
H15A	11674.93	-1021.17	5812.44	19
H15B	10757.49	-1469.4	5654.76	19
H16A	10080.06	-493.88	5902.44	20
H16B	9156.88	-927.88	5906.69	20
H17A	9204.4	-1090.56	4395.88	21
H17B	9957.35	-601.19	4413.76	21
H18	7512.74	-657.01	4715.91	20
H23	9612.57	269.05	4288.41	21
H24	9861.03	1031.46	4944.3	19
H26	8208.1	1465.75	6524.59	19
H28A	5732.96	2263.03	4523.36	33
H28B	7000.1	2291.76	4229.78	33
H30	10698.42	1483.23	6289.47	21
H31A	9839.77	1215.7	7793.58	22
H31B	10211.2	835.92	7155.06	22
H32A	12313.19	1077.17	7625.54	24
H32B	11945.72	1465.1	8258.39	24
H33A	11261.01	822.85	9044.52	25
H33B	11701.44	444.22	8432.87	25
H34A	13335.18	1049.34	9664.88	25
H34B	13801.95	693.71	9023.3	25
H35A	11120.22	2115.97	7330.61	33
H35B	9729.92	2108.82	7414.3	33
H35C	10036.1	2283.85	6534.44	33
H36	7241.78	704.04	6250.12	22
H37	6962.61	-55.67	5568.37	23
H38A	11157.13	-2219.86	7169.5	28
H38B	12565.22	-2349.25	7239.45	28
H38C	11734.87	-2136.22	6357.78	28
H39	11418.69	-1166.88	9377.47	24
H40	11659.19	-412.6	10050.52	24
H2AA	16361.82	1180.78	11361.55	34
H2AB	16365.42	636.12	11677.45	34
H2BA	15669.86	447.32	12236.36	34
H2BB	14625.72	612.55	12700.64	34
H60A	11535.98	1226.58	11474.71	29
H60B	11443.23	677.25	11742.04	29
H60C	10618.86	404.04	12277.75	29
H60D	9530.69	586.79	12686.38	29
H20A	6705.77	-719.54	1924.44	29
H20B	5472.72	-611.56	2226.93	29
H20C	7885.56	-1326.73	3000.71	29
H20D	7978.7	-948.16	2264.02	29
H42A	2367.51	-1093.2	1905.76	28
H42B	1765.98	-568.92	1803.97	28
H42C	1259.08	-614.43	1862.18	28
H42D	521.02	-672.75	2598.94	28
H44	2652.35	-663.79	4493.41	21
H46	4818.19	285.43	4242.86	20
H47	4968.22	1039.33	4921.12	20
H49	3087.6	1432.64	6397.29	19
H51A	696.72	2256.41	4402.84	30
H51B	1975.76	2277.81	4126.04	30

Atom	x	y	z	U_{eq}
H53	5622.12	1499.8	6261.18	22
H54A	4691.46	1207.17	7728.41	24
H54B	5160.59	836.59	7117.19	24
H55A	6730.09	1508.42	8243.18	22
H55B	7209.18	1149.67	7614.61	22
H56A	6670.46	479.38	8410.43	26
H56B	6249.58	845.95	9053.65	26
H57A	8324.11	1123.92	9559.37	24
H57B	8757.09	774.84	8894.85	24
H58	7805.85	446.17	10324.48	25
H63	9497.43	-73.7	8838.19	24
H64	9181.38	-846.13	8236.89	23
H66	6864.42	-1701.15	8633.5	23
H68A	10141.03	-2307.71	10240.35	44
H68B	9896.54	-2639.99	9390.25	44
H70	7997.8	-1482.94	7220.54	21
H71A	5405.75	-1374.16	7126.96	22
H71B	6321.16	-927.95	7326.77	22
H72A	5839.73	-1460.62	5730.59	21
H72B	6735.89	-1007.33	5930.91	21
H73A	5070.55	-491.45	5934.17	19
H73B	4151.13	-935.24	5856.09	19
H74A	4477.42	-1091.49	4409.19	20
H74B	5232.68	-600.43	4491.9	20
H75A	6217.83	-2216.41	7319.96	26
H75B	7632.54	-2319.58	7364.1	26
H75C	6744.81	-2126.46	6487.06	26
H76	6519.32	-1084.54	9545.48	26
H77	6855.27	-314.29	10159.53	25
H78A	4839.63	2283.6	6469.83	40
H78B	5882.26	2132.22	7304.26	40
H78C	4466.49	2098	7320.34	40
H79	2160.23	669.76	6035.15	24
H80	1990.06	-79.47	5317.33	23

Table 13: Atomic Occupancies for all atoms that are not fully occupied in **atb-40-48**.

Atom	Occupancy	Atom	Occupancy	Atom	Occupancy	Atom	Occupancy
Cl1A	0.0657(18)	H2BA	0.9343(18)	O14B	0.0907(17)	Cl5A	0.0214(12)
Cl2A	0.0657(18)	H2BB	0.9343(18)	C59B	0.0907(17)	Cl6A	0.0214(12)
Cl3A	0.0657(18)	C3B	0.9343(18)	C60B	0.0907(17)	O5A	0.0214(12)
O1A	0.0657(18)	Cl10	0.9093(17)	H60C	0.0907(17)	O6A	0.0214(12)
O2A	0.0657(18)	Cl11	0.9093(17)	H60D	0.0907(17)	C19A	0.0214(12)
C1A	0.0657(18)	Cl12	0.9093(17)	C61B	0.0907(17)	C20A	0.0214(12)
C2A	0.0657(18)	O13A	0.9093(17)	Cl4B	0.9786(12)	H20C	0.0214(12)
H2AA	0.0657(18)	O14A	0.9093(17)	Cl5B	0.9786(12)	H20D	0.0214(12)
H2AB	0.0657(18)	C59A	0.9093(17)	Cl6B	0.9786(12)	C21A	0.0214(12)
C3A	0.0657(18)	C60A	0.9093(17)	O5B	0.9786(12)	Cl7A	0.9262(14)
Cl1B	0.9343(18)	H60A	0.9093(17)	O6B	0.9786(12)	Cl8A	0.9262(14)
Cl2B	0.9343(18)	H60B	0.9093(17)	C19B	0.9786(12)	Cl9A	0.9262(14)
Cl3B	0.9343(18)	C61A	0.9093(17)	C20B	0.9786(12)	O1AC	0.9262(14)
O1B	0.9343(18)	Cl4	0.0907(17)	H20A	0.9786(12)	O2AC	0.9262(14)
O2B	0.9343(18)	Cl5	0.0907(17)	H20B	0.9786(12)	C41A	0.9262(14)
C1B	0.9343(18)	Cl6	0.0907(17)	C21B	0.9786(12)	C42A	0.9262(14)
C2B	0.9343(18)	O13B	0.0907(17)	Cl4A	0.0214(12)	H42A	0.9262(14)

Atom	Occupancy	Atom	Occupancy	Atom	Occupancy	Atom	Occupancy
H42B	0.9262(14)	Cl8B	0.0738(14)	O2AB	0.0738(14)	H42C	0.0738(14)
C43A	0.9262(14)	Cl9B	0.0738(14)	C41B	0.0738(14)	H42D	0.0738(14)
Cl7B	0.0738(14)	O1AB	0.0738(14)	C42B	0.0738(14)	C43B	0.0738(14)

Table 14: Solvent masking (PLATON/SQUEEZE) information for **atb-40-48**.

No	x	y	z	V	e	Content
1	-0.148	-0.223	-0.032	1531.0	11.3	?
2	0.067	0.396	0.037	0.0	0.0	?
3	0.083	0.389	0.037	0.0	0.0	?
4	0.083	0.444	0.675	0.0	0.0	?
5	0.083	0.535	0.650	0.0	0.0	?
6	0.083	0.972	0.025	0.0	0.0	?
7	0.083	0.972	0.150	0.0	0.0	?
8	0.083	0.979	0.013	0.0	0.0	?
9	0.133	0.743	0.463	0.0	0.0	?
10	0.133	0.972	0.062	0.0	0.0	?
11	0.150	0.979	0.062	0.0	0.0	?
12	0.167	0.354	0.887	0.0	0.0	?
13	0.183	0.590	0.588	0.0	0.0	?
14	0.183	0.632	0.713	0.0	0.0	?
15	0.200	0.278	0.875	0.0	0.0	?
16	0.200	0.451	0.762	0.0	0.0	?
17	0.200	0.597	0.575	0.0	0.0	?
18	0.250	0.271	0.912	0.0	0.0	?
19	0.283	0.146	0.200	0.0	0.0	?
20	0.300	0.090	0.287	0.0	0.0	?
21	0.300	0.090	0.425	0.0	0.0	?
22	0.300	0.514	0.125	0.0	0.0	?
23	0.317	0.097	0.300	0.0	0.0	?
24	0.333	0.889	0.013	0.0	0.0	?
25	0.350	0.500	0.950	0.0	0.0	?
26	0.367	0.035	0.338	0.0	0.0	?
27	0.367	0.285	0.963	0.0	0.0	?
28	0.367	0.681	0.925	0.0	0.0	?
29	0.417	0.812	0.350	0.0	0.0	?
30	0.433	0.819	0.362	0.0	0.0	?
31	0.467	0.951	0.250	0.0	0.0	?
32	0.533	0.451	0.750	0.0	0.0	?
33	0.567	0.319	0.637	0.0	0.0	?
34	0.583	0.312	0.650	0.0	0.0	?
35	0.633	0.181	0.075	0.0	-0.0	?
36	0.633	0.535	0.662	0.0	0.0	?
37	0.633	0.785	0.037	0.0	0.0	?
38	0.650	0.000	0.050	0.0	0.0	?
39	0.667	0.389	0.988	0.0	0.0	?
40	0.683	0.597	0.700	0.0	0.0	?
41	0.700	0.014	0.875	0.0	0.0	?
42	0.700	0.590	0.575	0.0	0.0	?
43	0.700	0.590	0.713	0.0	0.0	?
44	0.717	0.646	0.800	0.0	0.0	?
45	0.750	0.771	0.087	0.0	0.0	?
46	0.800	0.097	0.425	0.0	0.0	?
47	0.800	0.778	0.125	0.0	0.0	?
48	0.800	0.951	0.237	0.0	0.0	?

No	x	y	z	V	e	Content
49	0.817	0.090	0.412	0.0	0.0	?
50	0.817	0.132	0.287	0.0	0.0	?
51	0.833	0.854	0.113	0.0	0.0	?
52	0.850	0.479	0.938	0.0	0.0	?
53	0.867	0.243	0.537	0.0	0.0	?
54	0.867	0.472	0.938	0.0	0.0	?
55	0.917	0.035	0.350	0.0	0.0	?
56	0.917	0.472	0.850	0.0	0.0	?
57	0.917	0.472	0.975	0.0	0.0	?
58	0.917	0.479	0.988	0.0	0.0	?
59	0.917	0.889	0.963	0.0	0.0	?
60	0.917	0.944	0.325	0.0	0.0	?
61	0.933	0.896	0.963	0.0	0.0	?

Citations

CrysAlisPro (Rigaku, V1.171.40.53, 2019)

CrysAlisPro (ROD), Rigaku Oxford Diffraction, Poland (?).

O.V. Dolomanov and L.J. Bourhis and R.J. Gildea and J.A.K. Howard and H. Puschmann, Olex2: A complete structure solution, refinement and analysis program, *J. Appl. Cryst.*, (2009), **42**, 339-341.

Sheldrick, G.M., Crystal structure refinement with ShelXL, *Acta Cryst.*, (2015), **C71**, 3-8.

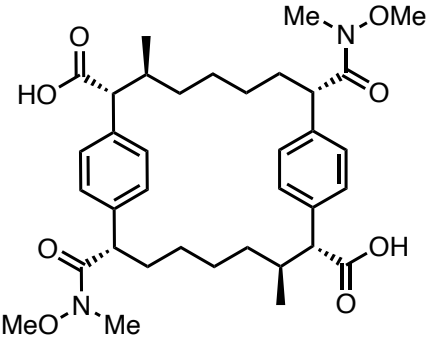

(2*R*,3*S*,8*S*,10*R*,11*S*,16*S*)-8,16-bis(methoxy(methyl)carbamoyl)-3,11-dimethyl-1,9(1,4)-dibenzenacyclohexadecaphane-2,10-dicarboxylic acid

Crystal Data and Experimental

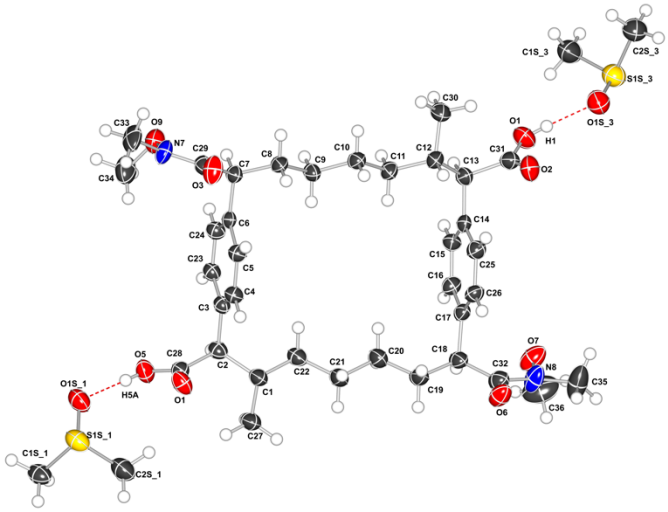

Experimental. Single colorless plate crystals of **ATB-40-192A** were recrystallised from DMSO by slow evaporation. A suitable crystal with dimensions 0.15 × 0.08 × 0.05 mm^3 was selected and mounted on a loop with paratone on a XtaLAB Synergy-S diffractometer. The crystal was kept at a steady T = 100(1) K during data collection. The structure was solved with the ShelXT (Sheldrick, 2015) solution program using dual methods and by using Olex2 (Dolomanov et al., 2009) as the graphical interface. The model was refined with ShelXL 2018/3 (Sheldrick, 2015) using full matrix least squares minimisation on $\boldsymbol{F^2}$.

Crystal Data. $C_{40}H_{61}N_2O_{10}S_2$, M_r = 794.02, triclinic, $P\bar{1}$ (No. 1), a = 9.4562(4) Å, b = 10.7610(4) Å, c = 11.0648(3) Å, α = 102.582(3)°, β = 91.056(3)°, γ = 102.482(4)°, V = 1070.38(7) Å^3, T = 100(1) K, Z = 1, Z' = 1, μ(Cu K$_\alpha$) = 1.585 mm^{-1}, 12500 reflections measured, 5691 unique (R_{int} = 0.0441) which were used in all calculations. The final wR_2 was 0.2422 (all data) and R_1 was 0.0816 (I≥2 σ(I)).

Compound	**ATB-40-192A**
Formula	$C_{40}H_{61}N_2O_{10}S_2$
$D_{calc.}$/ g cm^{-3}	1.232
μ/mm^{-1}	1.585
Formula Weight	794.02
Color	colorless
Shape	plate
Size/mm^3	0.15×0.08×0.05
T/K	100(1)
Crystal System	triclinic
Flack Parameter	0.09(5)
Hooft Parameter	0.096(16)
Space Group	$P\bar{1}$
a/Å	9.4562(4)
b/Å	10.7610(4)
c/Å	11.0648(3)
α/°	102.582(3)
β/°	91.056(3)
γ/°	102.482(4)
V/Å^3	1070.38(7)
Z	1
Z'	1
Wavelength/Å	1.54184
Radiation type	Cu K_α
Θ_{min}/°	4.103
Θ_{max}/°	73.009
Measured Refl's.	12500
Indep't Refl's	5691
Refl's I≥2 σ(I)	4681
R_{int}	0.0441
Parameters	585
Restraints	547
Largest Peak	0.630
Deepest Hole	-0.505
GooF	1.048
wR_2 (all data)	0.2422
wR_2	0.2233
R_1 (all data)	0.0935
R_1	0.0816

Structure Quality Indicators

Reflections:	d min (Cu) 0.81	I/σ(I) 19.3	Rint 4.41%	complete 99% (IUCr) 71%
Refinement:	Shift 0.000	Max Peak 0.6	Min Peak -0.5	GooF 1.048

A colorless plate-shaped crystal with dimensions 0.15 × 0.08 × 0.05 mm^3 was mounted on a loop with paratone. Data were collected using a XtaLAB Synergy, Dualflex, HyPix diffractometer equipped with an Oxford Cryosystems low-temperature device operating at T = 100(1) K.

Data were measured using ω scans using Cu K_α radiation. The diffraction pattern was indexed and the total number of runs and images was based on the strategy calculation from the program CrysAlisPro (Rigaku, V1.171.40.84a, 2020). The maximum resolution that was achieved was Θ = 73.009° (0.81 Å).

The unit cell was refined using CrysAlisPro (Rigaku, V1.171.40.84a, 2020) on 6641 reflections, 53% of the observed reflections.

Data reduction, scaling and absorption corrections were performed using CrysAlisPro (Rigaku, V1.171.40.84a, 2020). The final completeness is 98.70 % out to 73.009° in Θ. A numerical absorption correction based on a Gaussian integration over a multifaceted crystal model absorption correction was performed using CrysAlisPro 1.171.40.79a (Rigaku Oxford Diffraction, 2020). An empirical absorption correction using spherical harmonics, implemented in SCALE3 ABSPACK scaling algorithm was also applied. The absorption coefficient μ of this material is 1.585 mm^{-1} at this wavelength (λ = 1.54184Å) and the minimum and maximum transmissions are 0.764 and 1.000.

The structure was solved and the space group $P1$ (# 1 determined by the ShelXT (Sheldrick, 2015) structure solution program using dual methods and refined by full matrix least squares minimisation on F^2 using version 2018/3 of ShelXL 2018/3 (Sheldrick, 2015). All non-hydrogen atoms were refined anisotropically. Hydrogen atom positions were calculated geometrically and refined using the riding model. Their distances were refined.

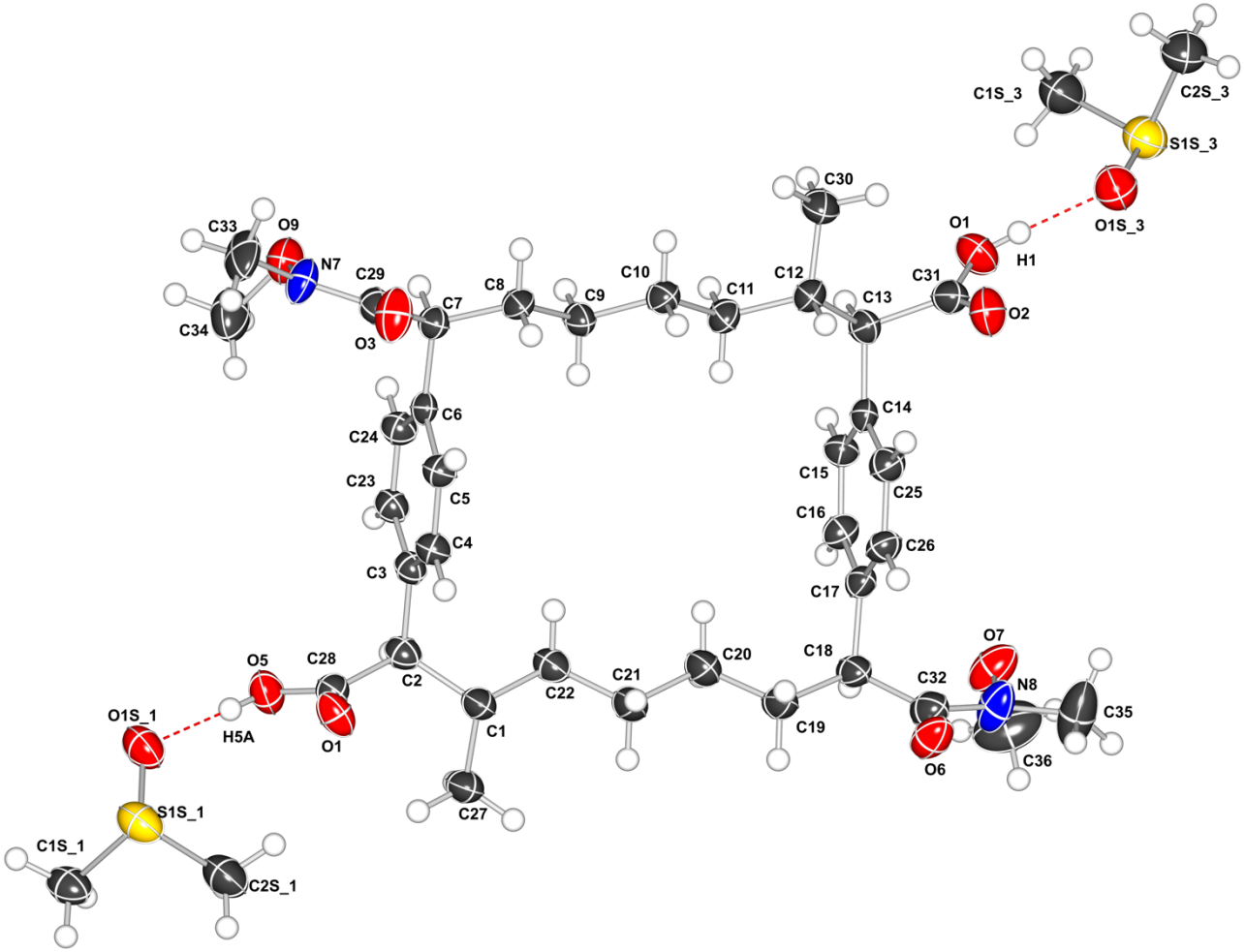

Figure 9: Thermal ellipsoid plot of the asymmetric unit. There are two disordered solvent molecules hydrogen bonded to the main molecule. Although the structure this type is expected to have two-fold rotational symmetry, there is no rotational symmetry in the crystal and the point group of the crystal is C_1.

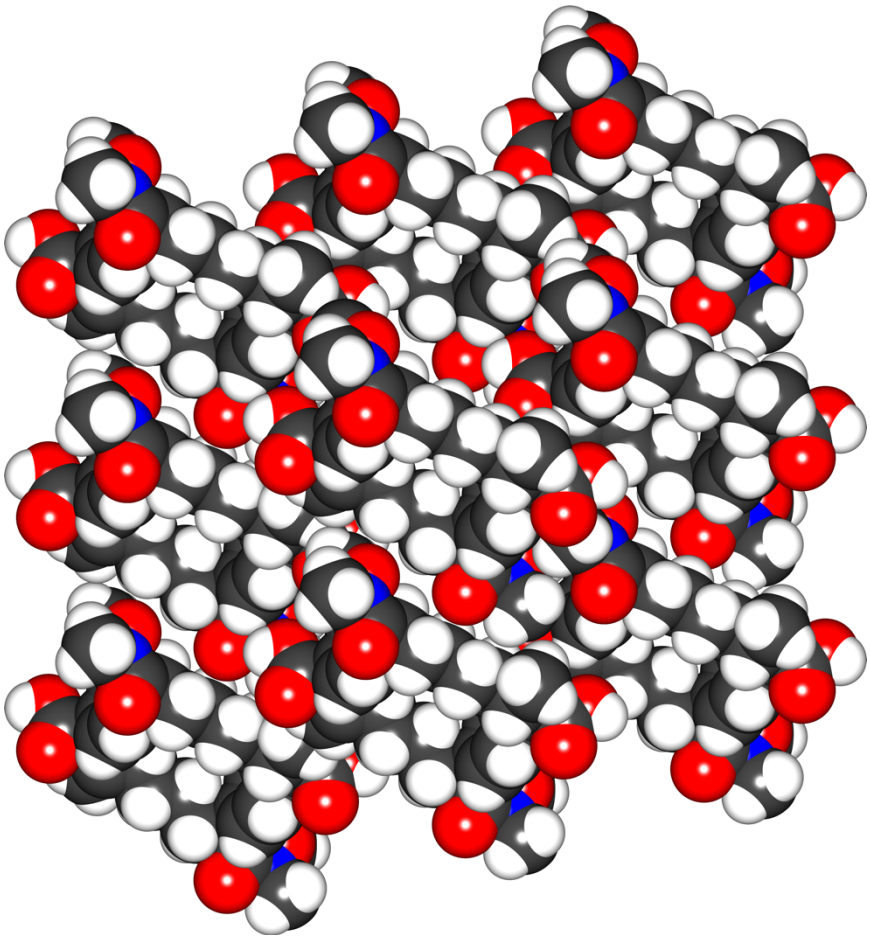

Figure 10: Molecular packing viewed along the a-axis.

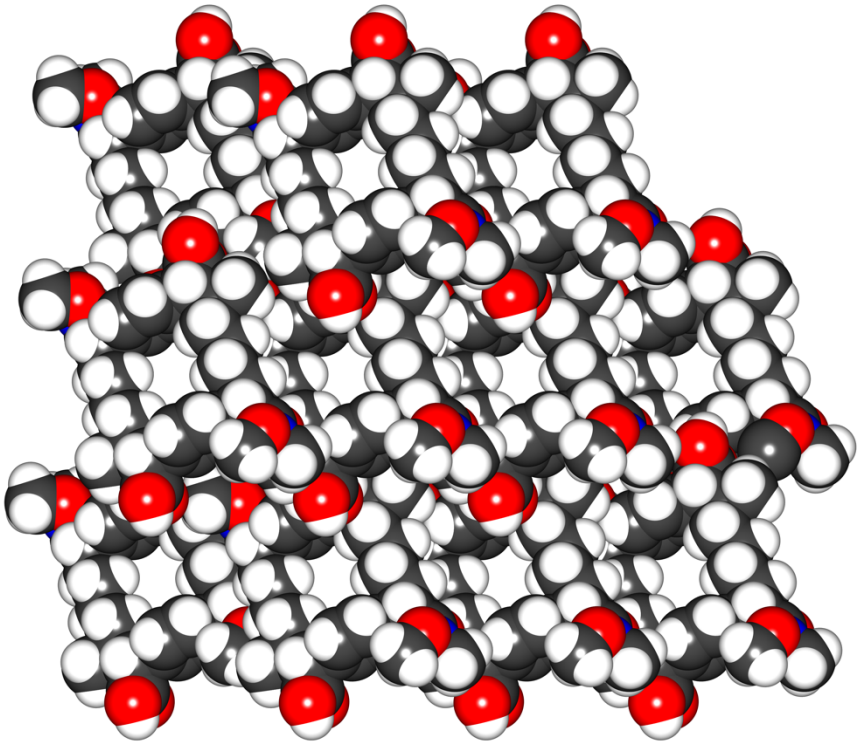

Figure 11: Molecular packing viewed along the b-axis reveals a channel structure.

_refine_special_details: Refined as a 2-component inversion twin.

Data Plots: Diffraction Data

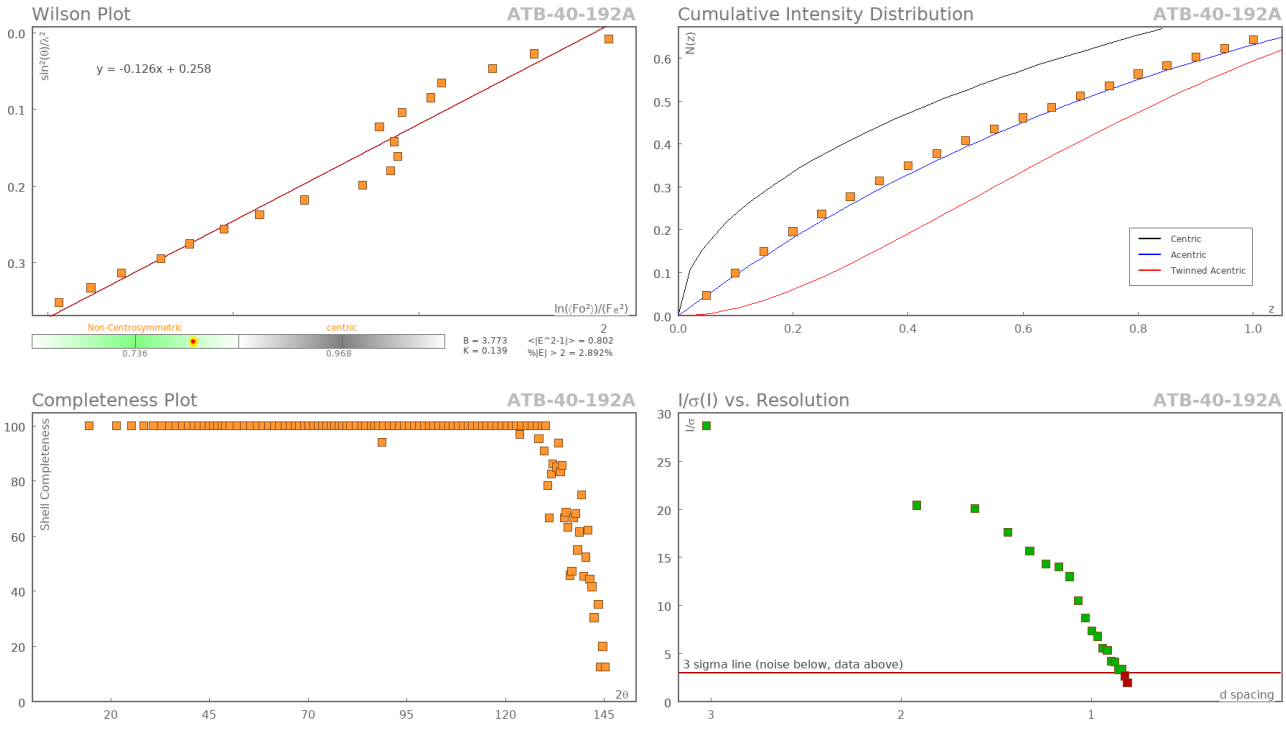

Data Plots: Refinement and Data

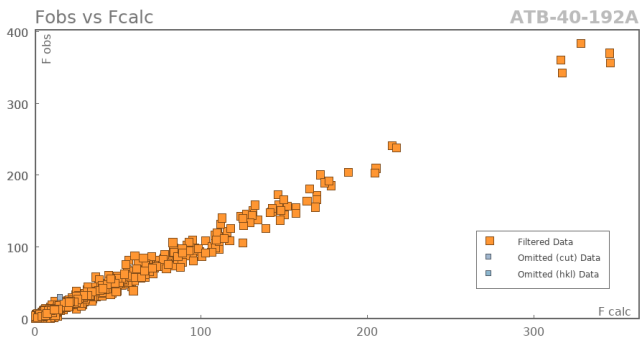

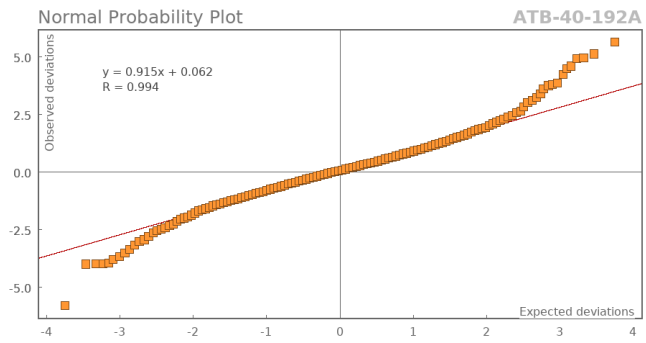

Reflection Statistics

Total reflections (after filtering)	12502	Unique reflections	5691
Completeness	0.665	Mean I/σ	12.1
hkl_{max} collected	(11, 13, 13)	hkl_{min} collected	(-11, -12, -11)
hkl_{max} used	(11, 13, 13)	hkl_{min} used	(-11, -12, -11)
Lim d_{max} collected	100.0	Lim d_{min} collected	0.77
d_{max} used	10.77	d_{min} used	0.81
Friedel pairs	1681	Friedel pairs merged	0
Inconsistent equivalents	37	R_{int}	0.0441
R_{sigma}	0.0519	Intensity transformed	0
Omitted reflections	0	Omitted by user (OMIT hkl)	2
Multiplicity	(2066, 2064, 801, 377, 166, 80, 62, 44, 22, 8, 1, 1)	Maximum multiplicity	12
Removed systematic absences	0	Filtered off (Shel/OMIT)	0

Images of the Crystal on the Diffractometer

Table 15: Fractional Atomic Coordinates (×10⁴) and Equivalent Isotropic Displacement Parameters (Å²×10³) for **ATB-40-192A**. U_{eq} is defined as 1/3 of the trace of the orthogonalised U_{ij}.

Atom	x	y	z	U_{eq}
C1	3051(8)	5798(7)	8750(7)	40.0(13)
C2	3899(7)	7238(7)	9191(7)	35.6(11)
C3	5300(7)	7573(6)	8564(6)	31.7(10)
C4	6369(7)	6864(7)	8553(6)	34.1(11)
C5	7645(7)	7175(7)	7979(6)	33.8(11)
C6	7878(7)	8226(6)	7371(6)	28.7(10)

Atom	x	y	z	U_{eq}
C7	9234(7)	8552(7)	6700(6)	33.1(12)
C8	9393(7)	7417(7)	5656(7)	36.7(14)
C9	8142(8)	6973(7)	4688(6)	36.7(13)
C10	8325(8)	5886(7)	3617(7)	38.1(14)
C11	7010(8)	5429(7)	2675(7)	36.8(14)
C12	7121(8)	4329(7)	1570(7)	37.5(14)
C13	5643(8)	3878(7)	787(6)	35.8(13)
C14	4408(7)	3290(6)	1469(6)	32.3(12)
C15	3192(8)	3832(7)	1639(6)	35.2(13)
C16	2058(8)	3300(7)	2263(7)	37.2(14)
C17	2090(7)	2220(6)	2771(6)	34.3(13)
C18	901(8)	1694(7)	3544(7)	39.8(15)
C19	1360(9)	2100(8)	4938(7)	45.1(16)
C20	1802(9)	3567(8)	5429(7)	46.6(16)
C21	2151(9)	3961(8)	6827(7)	48.5(17)
C22	2729(8)	5420(8)	7337(7)	40.7(15)
C23	5556(7)	8634(7)	8012(6)	34.2(11)
C24	6803(8)	8947(7)	7421(6)	35.3(12)
C25	4431(8)	2177(7)	1929(7)	39.0(14)
C26	3287(8)	1673(7)	2589(7)	36.3(14)
C27	1642(8)	5610(8)	9405(7)	44.5(15)
C28	4280(8)	7559(7)	10596(7)	35.1(13)
C29	10536(8)	8946(7)	7636(7)	38.5(15)
C30	8356(9)	4768(8)	781(8)	47.8(17)
C31	5826(8)	2884(8)	-407(7)	42.2(15)
C32	473(9)	193(8)	3120(8)	46.2(16)
C33	12280(9)	10739(10)	9071(9)	66(2)
C34	9479(11)	11696(10)	8754(10)	70(3)
C35	-416(15)	-1655(9)	1284(11)	85(4)
C36	-2272(11)	332(13)	1330(14)	94(4)
N7	10972(7)	10203(6)	8237(7)	47.5(15)
N8	-336(9)	-320(7)	2040(7)	57.3(18)
O1	5517(8)	3281(7)	-1413(6)	62.3(15)
O4	4781(7)	6852(6)	11122(5)	49.7(12)
O2	6151(7)	1877(6)	-438(6)	56.6(14)
O3	11185(7)	8140(6)	7871(6)	56.7(14)
O5	4040(7)	8698(6)	11176(5)	50.5(13)
O6	914(7)	-528(6)	3682(6)	56.1(14)
O7	-706(7)	512(6)	1371(7)	63.6(16)
O9	10355(8)	11129(6)	7842(6)	60.2(15)
C1S_3	6140(19)	3997(9)	-4235(14)	70(4)
C2S_3	7202(14)	2078(15)	-5555(13)	65(3)
O1S_3	6047(14)	1794(11)	-3499(8)	62.8(19)
S1S_3	5742(5)	2272(5)	-4628(4)	58.8(9)
C1S_4	4310(40)	7180(30)	14370(40)	62.2(17)
C2S_4	3130(50)	9060(30)	15600(20)	52.4(18)
O1S_4	4360(30)	9340(20)	13571(19)	57.7(15)
S1S_4	3338(14)	8315(14)	14054(12)	57.6(6)
C1S_5	5710(20)	3420(30)	-4620(30)	74(6)
C2S_5	8270(20)	4050(18)	-3360(20)	58(5)
O1S_5	6530(30)	1818(14)	-3382(15)	62.8(19)
S1S_5	7090(10)	2657(9)	-4266(8)	58.8(9)
C1S_1	3485(10)	9218(10)	15606(8)	52.4(18)
C2S_1	3082(10)	7156(10)	13719(9)	62.2(17)
O1S_1	4889(7)	9299(7)	13570(5)	57.7(15)
S1S_1	4506(4)	8446(4)	14477(3)	57.6(6)
C1S_2	7830(30)	950(20)	-5330(20)	65(3)
C2S_2	6250(30)	2700(30)	-5340(20)	60(5)

Atom	x	y	z	U_{eq}
O1S_2	6320(30)	1703(19)	-3418(17)	62.8(19)
S1S_2	7343(11)	2257(9)	-4287(9)	58.8(9)

Table 16: Anisotropic Displacement Parameters (×10⁴) for **ATB-40-192A**. The anisotropic displacement factor exponent takes the form: $-2\pi^2[h^2a^{*2} \times U_{11} + ... + 2hka^* \times b^* \times U_{12}]$

Atom	U_{11}	U_{22}	U_{33}	U_{23}	U_{13}	U_{12}
C1	38(3)	47(2)	31(3)	7(2)	7(2)	4.8(19)
C2	31(2)	44(2)	33(2)	9.2(18)	3.3(16)	9.9(17)
C3	30(2)	37(2)	26(2)	4.4(18)	0.3(17)	7.7(16)
C4	33(2)	38(3)	33(3)	10(2)	4.9(18)	9.3(18)
C5	33(2)	37(2)	33(3)	9(2)	4(2)	8.0(18)
C6	28(2)	30(2)	23(2)	1.5(17)	-3.8(16)	1.2(15)
C7	30(2)	37(3)	29(3)	5(2)	0(2)	3(2)
C8	27(3)	42(3)	34(3)	3(3)	2(2)	-3(2)
C9	33(3)	44(3)	28(3)	4(3)	1(2)	3(3)
C10	35(3)	41(3)	34(3)	8(3)	1(3)	-1(3)
C11	28(3)	41(3)	36(3)	2(3)	-1(3)	1(2)
C12	35(3)	35(3)	37(3)	4(3)	2(3)	0(2)
C13	38(3)	39(3)	27(3)	7(3)	-1(3)	3(3)
C14	35(3)	29(3)	27(3)	1(2)	-2(2)	-1(2)
C15	39(3)	35(3)	32(3)	10(2)	4(3)	6(3)
C16	34(3)	36(3)	42(4)	10(3)	2(3)	7(2)
C17	34(3)	32(3)	31(3)	6(2)	-2(2)	-2(2)
C18	31(3)	49(4)	33(3)	8(3)	1(3)	-2(3)
C19	44(4)	51(4)	32(3)	10(3)	3(3)	-6(3)
C20	50(4)	52(4)	34(4)	9(3)	5(3)	5(3)
C21	49(4)	55(4)	33(4)	6(3)	7(3)	-2(3)
C22	35(3)	54(4)	32(3)	10(3)	4(3)	10(3)
C23	35(2)	39(2)	29(3)	7(2)	2(2)	9.6(18)
C24	35(2)	39(3)	33(3)	10(2)	2.8(18)	9.1(18)
C25	37(3)	39(3)	40(4)	10(3)	2(3)	5(3)
C26	37(3)	32(3)	39(3)	13(3)	2(3)	2(2)
C27	40(3)	54(4)	37(3)	9(3)	9(2)	4(3)
C28	33(3)	38(3)	33(2)	7(2)	2(2)	5(2)
C29	32(3)	44(3)	34(3)	0(3)	1(3)	5(3)
C30	39(4)	55(4)	44(4)	3(3)	11(3)	4(3)
C31	41(4)	46(4)	36(4)	11(3)	4(3)	0(3)
C32	41(4)	51(4)	41(4)	13(3)	-2(3)	-2(3)
C33	37(4)	70(5)	66(6)	-18(4)	-13(4)	-5(4)
C34	61(6)	63(5)	74(6)	-13(4)	3(5)	17(4)
C35	124(10)	44(4)	77(7)	4(4)	-46(7)	9(5)
C36	50(6)	111(9)	133(11)	58(8)	-9(6)	14(6)
N7	40(3)	37(3)	54(4)	-3(3)	-12(3)	0(2)
N8	67(4)	47(3)	49(4)	11(3)	-30(3)	-2(3)
O1	79(4)	67(3)	38(3)	13(3)	10(3)	9(3)
O4	64(3)	59(3)	31(2)	10(2)	4(2)	25(3)
O2	65(4)	51(3)	49(3)	-2(2)	1(3)	17(3)
O3	49(3)	55(3)	59(3)	-2(3)	-21(3)	16(2)
O5	68(3)	45(3)	38(3)	2(2)	6(2)	17(2)
O6	66(3)	48(3)	50(3)	21(2)	-12(3)	-6(2)
O7	53(3)	56(3)	79(4)	25(3)	-19(3)	-3(2)
O9	70(4)	45(3)	58(3)	1(2)	5(3)	7(3)
C1S_3	80(11)	66(6)	65(9)	14(3)	21(7)	14(3)
C2S_3	57(5)	70(4)	64(4)	11(3)	11(4)	10(4)

Atom	U_{11}	U_{22}	U_{33}	U_{23}	U_{13}	U_{12}
O1S_3	64(3)	65(3)	56(2)	7(2)	5.8(19)	13(2)
S1S_3	54.7(17)	67.3(19)	54.5(16)	14.1(15)	6.9(13)	13.6(14)
C1S_4	62(3)	82(3)	44(3)	13(2)	11(3)	19(2)
C2S_4	38(4)	74(4)	44(3)	14(2)	4(2)	11(3)
O1S_4	58(3)	76(2)	37(2)	7(2)	5(2)	17(2)
S1S_4	53.0(11)	79.7(13)	44.1(11)	16.4(9)	7.7(8)	21.0(10)
C1S_5	60(7)	82(13)	83(18)	27(11)	6(7)	17(10)
C2S_5	58(9)	74(5)	47(9)	24(8)	17(8)	18(6)
O1S_5	64(3)	65(3)	56(2)	7(2)	5.8(19)	13(2)
S1S_5	54.7(17)	67.3(19)	54.5(16)	14.1(15)	6.9(13)	13.6(14)
C1S_1	38(4)	74(4)	44(3)	14(2)	4(2)	11(3)
C2S_1	62(3)	82(3)	44(3)	13(2)	11(3)	19(2)
O1S_1	58(3)	76(2)	37(2)	7(2)	5(2)	17(2)
S1S_1	53.0(11)	79.7(13)	44.1(11)	16.4(9)	7.7(8)	21.0(10)
C1S_2	57(5)	70(4)	64(4)	11(3)	11(4)	10(4)
C2S_2	52(7)	57(13)	67(6)	16(7)	11(7)	-1(9)
O1S_2	64(3)	65(3)	56(2)	7(2)	5.8(19)	13(2)
S1S_2	54.7(17)	67.3(19)	54.5(16)	14.1(15)	6.9(13)	13.6(14)

Table 17: Bond Lengths in Å for **ATB-40-192A**.

Atom	Atom	Length/Å
C1	C2	1.549(9)
C1	C22	1.535(9)
C1	C27	1.524(10)
C2	C3	1.517(9)
C2	C28	1.535(9)
C3	C4	1.391(8)
C3	C23	1.388(8)
C4	C5	1.384(9)
C5	C6	1.417(8)
C6	C7	1.508(8)
C6	C24	1.400(8)
C7	C8	1.523(9)
C7	C29	1.518(9)
C8	C9	1.504(9)
C9	C10	1.514(9)
C10	C11	1.529(8)
C11	C12	1.528(9)
C12	C13	1.555(9)
C12	C30	1.527(9)
C13	C14	1.501(8)
C13	C31	1.546(10)
C14	C15	1.396(9)
C14	C25	1.404(9)
C15	C16	1.375(9)
C16	C17	1.402(8)
C17	C18	1.512(9)
C17	C26	1.383(10)
C18	C19	1.536(9)
C18	C32	1.540(10)
C19	C20	1.515(10)
C20	C21	1.522(10)
C21	C22	1.522(10)
C23	C24	1.373(9)
C25	C26	1.395(9)
C28	O4	1.216(8)
C28	O5	1.323(8)
C29	N7	1.341(8)
C29	O3	1.233(8)
C31	O1	1.325(9)
C31	O2	1.182(9)
C32	N8	1.347(9)
C32	O6	1.226(9)
C33	N7	1.460(9)
C34	O9	1.435(11)
C35	N8	1.482(12)
C36	O7	1.449(12)
N7	O9	1.398(8)
N8	O7	1.374(8)
C1S_3	S1S_3	1.765(8)
C2S_3	S1S_3	1.756(9)
O1S_3	S1S_3	1.498(6)
C1S_4	S1S_4	1.766(8)
C2S_4	S1S_4	1.757(9)
O1S_4	S1S_4	1.499(6)
C1S_5	S1S_5	1.766(8)
C2S_5	S1S_5	1.756(9)
O1S_5	S1S_5	1.498(6)
C1S_1	S1S_1	1.767(8)
C2S_1	S1S_1	1.757(9)
O1S_1	S1S_1	1.501(5)
C1S_2	S1S_2	1.766(8)
C2S_2	S1S_2	1.756(9)
O1S_2	S1S_2	1.499(6)

Table 18: Bond Angles in ° for **ATB-40-192A**.

Atom	Atom	Atom	Angle/°
C22	C1	C2	111.4(5)
C27	C1	C2	109.0(6)
C27	C1	C22	110.4(6)
C3	C2	C1	114.4(5)
C3	C2	C28	107.7(5)
C28	C2	C1	110.0(5)
C4	C3	C2	121.8(5)
C23	C3	C2	119.9(5)
C23	C3	C4	118.3(6)
C5	C4	C3	121.5(6)
C4	C5	C6	120.1(6)
C5	C6	C7	121.1(5)
C24	C6	C5	117.5(6)
C24	C6	C7	121.5(5)
C6	C7	C8	112.3(5)
C6	C7	C29	108.6(5)
C29	C7	C8	110.5(5)
C9	C8	C7	113.6(5)
C8	C9	C10	113.9(6)
C9	C10	C11	112.4(6)
C12	C11	C10	115.1(5)
C11	C12	C13	108.6(5)
C30	C12	C11	111.3(5)
C30	C12	C13	110.9(5)
C14	C13	C12	113.5(5)
C14	C13	C31	110.3(5)
C31	C13	C12	108.1(5)
C15	C14	C13	120.2(5)
C15	C14	C25	118.4(6)
C25	C14	C13	121.3(6)
C16	C15	C14	120.6(6)
C15	C16	C17	121.6(6)
C16	C17	C18	121.9(6)
C26	C17	C16	117.8(6)
C26	C17	C18	120.3(6)
C17	C18	C19	112.2(5)
C17	C18	C32	109.2(6)
C19	C18	C32	110.1(6)
C20	C19	C18	113.4(6)
C19	C20	C21	112.9(6)
C22	C21	C20	114.4(6)
C21	C22	C1	113.5(6)
C24	C23	C3	121.1(6)
C23	C24	C6	121.5(6)
C26	C25	C14	120.1(6)
C17	C26	C25	121.4(6)
O4	C28	C2	123.5(6)
O4	C28	O5	123.2(6)
O5	C28	C2	113.2(5)
N7	C29	C7	118.9(6)
O3	C29	C7	121.8(6)
O3	C29	N7	119.3(6)
O1	C31	C13	111.2(6)
O2	C31	C13	125.3(7)
O2	C31	O1	123.5(7)
N8	C32	C18	117.4(6)
O6	C32	C18	122.6(6)
O6	C32	N8	119.8(7)
C29	N7	C33	124.7(7)
C29	N7	O9	118.4(5)
O9	N7	C33	115.2(6)
C32	N8	C35	124.0(7)
C32	N8	O7	118.8(6)
O7	N8	C35	113.4(6)
N8	O7	C36	107.7(7)
N7	O9	C34	111.9(7)
C2S_3	S1S_3	C1S_3	97.8(5)
O1S_3	S1S_3	C1S_3	108.6(5)
O1S_3	S1S_3	C2S_3	105.3(5)
C2S_4	S1S_4	C1S_4	97.6(5)
O1S_4	S1S_4	C1S_4	108.3(5)
O1S_4	S1S_4	C2S_4	105.2(5)
C2S_5	S1S_5	C1S_5	97.6(5)
O1S_5	S1S_5	C1S_5	108.4(5)
O1S_5	S1S_5	C2S_5	105.4(5)
C2S_1	S1S_1	C1S_1	97.5(4)
O1S_1	S1S_1	C1S_1	107.7(4)
O1S_1	S1S_1	C2S_1	105.4(4)
C2S_2	S1S_2	C1S_2	97.6(5)
O1S_2	S1S_2	C1S_2	108.3(5)
O1S_2	S1S_2	C2S_2	105.4(5)

Table 19: Torsion Angles in ° for **ATB-40-192A**.

Atom	Atom	Atom	Atom	Angle/°
C1	C2	C3	C4	-54.3(8)
C1	C2	C3	C23	127.6(6)
C1	C2	C28	O4	45.9(8)
C1	C2	C28	O5	-135.5(6)
C2	C1	C22	C21	169.3(6)
C2	C3	C4	C5	180.0(6)
C2	C3	C23	C24	-178.9(6)
C3	C2	C28	O4	-79.4(8)
C3	C2	C28	O5	99.2(6)

Atom	Atom	Atom	Atom	Angle/°
C3	C4	C5	C6	-0.8(9)
C3	C23	C24	C6	-1.3(9)
C4	C3	C23	C24	2.9(9)
C4	C5	C6	C7	-177.8(5)
C4	C5	C6	C24	2.3(9)
C5	C6	C7	C8	59.8(7)
C5	C6	C7	C29	-62.7(7)
C5	C6	C24	C23	-1.3(9)
C6	C7	C8	C9	58.8(7)
C6	C7	C29	N7	-88.3(7)
C6	C7	C29	O3	90.5(8)
C7	C6	C24	C23	178.7(5)
C7	C8	C9	C10	177.3(5)
C7	C29	N7	C33	-174.0(8)
C7	C29	N7	O9	-9.7(10)
C8	C7	C29	N7	148.2(6)
C8	C7	C29	O3	-33.0(9)
C8	C9	C10	C11	178.0(5)
C9	C10	C11	C12	-179.8(6)
C10	C11	C12	C13	173.8(5)
C10	C11	C12	C30	-63.8(8)
C11	C12	C13	C14	-64.0(7)
C11	C12	C13	C31	173.4(5)
C12	C13	C14	C15	121.4(6)
C12	C13	C14	C25	-59.7(7)
C12	C13	C31	O1	-121.8(6)
C12	C13	C31	O2	60.5(9)
C13	C14	C15	C16	-179.9(5)
C13	C14	C25	C26	178.2(6)
C14	C13	C31	O1	113.6(6)
C14	C13	C31	O2	-64.1(9)
C14	C15	C16	C17	1.3(9)
C14	C25	C26	C17	2.2(10)
C15	C14	C25	C26	-2.9(9)
C15	C16	C17	C18	175.2(6)
C15	C16	C17	C26	-2.1(9)
C16	C17	C18	C19	-103.0(7)
C16	C17	C18	C32	134.7(6)
C16	C17	C26	C25	0.3(9)
C17	C18	C19	C20	58.1(8)
C17	C18	C32	N8	-75.0(9)
C17	C18	C32	O6	100.2(8)
C18	C17	C26	C25	-177.0(6)
C18	C19	C20	C21	175.9(6)
C18	C32	N8	C35	157.8(9)
C18	C32	N8	O7	1.3(11)
C19	C18	C32	N8	161.4(7)
C19	C18	C32	O6	-23.3(10)
C19	C20	C21	C22	174.7(6)
C20	C21	C22	C1	179.1(6)
C22	C1	C2	C3	-55.3(7)
C22	C1	C2	C28	-176.7(5)
C23	C3	C4	C5	-1.8(9)
C24	C6	C7	C8	-120.3(6)
C24	C6	C7	C29	117.3(6)
C25	C14	C15	C16	1.2(9)
C26	C17	C18	C19	74.2(8)
C26	C17	C18	C32	-48.1(8)

Atom	Atom	Atom	Atom	Angle/°
C27	C1	C2	C3	-177.4(6)
C27	C1	C2	C28	61.2(7)
C27	C1	C22	C21	-69.4(8)
C28	C2	C3	C4	68.4(7)
C28	C2	C3	C23	-109.7(6)
C29	C7	C8	C9	-179.9(5)
C29	N7	O9	C34	113.2(8)
C30	C12	C13	C14	173.4(5)
C30	C12	C13	C31	50.7(7)
C31	C13	C14	C15	-117.2(6)
C31	C13	C14	C25	61.7(8)
C32	C18	C19	C20	179.9(6)
C32	N8	O7	C36	-115.8(10)
C33	N7	O9	C34	-81.1(9)
C35	N8	O7	C36	85.4(11)
O3	C29	N7	C33	7.2(12)
O3	C29	N7	O9	171.4(7)
O6	C32	N8	C35	-17.6(14)
O6	C32	N8	O7	-174.1(7)

Table 20: Hydrogen Fractional Atomic Coordinates ($\times 10^4$) and Equivalent Isotropic Displacement Parameters ($Å^2 \times 10^3$) for **ATB-40-192A**. U_{eq} is defined as 1/3 of the trace of the orthogonalised U_{ij}.

Atom	x	y	z	U_{eq}
H2	3227(19)	7841(17)	9011(8)	43
H4	6223(8)	6160(16)	8943(10)	41
H5	8355(16)	6690(12)	7992(6)	41
H7	9182(8)	9350(20)	6317(12)	40
H8A	10269(17)	7674(8)	5264(9)	44
H8B	9484(8)	6696(14)	6005(9)	44
H9A	8022(8)	7704(14)	4368(8)	44
H9B	7273(17)	6679(9)	5074(9)	44
H10A	8472(8)	5161(14)	3934(9)	46
H10B	9171(16)	6187(9)	3207(9)	46
H11A	6168(16)	5141(9)	3096(10)	44
H11B	6867(8)	6162(14)	2367(9)	44
H12	7322(9)	3540(20)	1905(11)	45
H13	5392(19)	4710(60)	525(19)	43
H15	3148(8)	4565(16)	1324(9)	42
H16	1243(18)	3668(10)	2352(7)	45
H18	-10(20)	2065(12)	3390(8)	48
H19A	570(16)	1751(10)	5385(10)	54
H19B	2158(16)	1726(10)	5091(7)	54
H20A	1030(16)	3950(11)	5225(8)	56
H20B	2636(17)	3910(10)	5026(10)	56
H21A	1289(17)	3682(9)	7228(10)	58
H21B	2855(15)	3509(11)	7035(8)	58
H22A	2033(14)	5876(11)	7120(8)	49
H22B	3602(17)	5699(9)	6949(10)	49
H23	4866(16)	9146(12)	8044(6)	41
H24	6939(8)	9659(16)	7042(10)	42
H25	5216(18)	1772(11)	1793(8)	47
H26	3331(8)	948(16)	2917(9)	44
H27A	1035(11)	6193(10)	9184(8)	67
H27B	1870(9)	5836(8)	10324(13)	67

Atom	x	y	z	U_{eq}
H27C	1097(11)	4678(13)	9137(8)	67
H30A	8424(9)	4020(12)	83(11)	72
H30B	9292(14)	5067(9)	1306(10)	72
H30C	8163(9)	5505(12)	435(9)	72
H33A	12217(9)	10290(11)	9776(13)	99
H33B	12368(9)	11697(15)	9401(10)	99
H33C	13150(14)	10598(10)	8606(11)	99
H34A	8650(15)	11910(10)	8329(11)	105
H34B	10082(13)	12514(14)	9298(12)	105
H34C	9094(12)	11060(12)	9273(12)	105
H35A	-1427(19)	-2040(10)	902(12)	128
H35B	-151(15)	-2214(11)	1825(13)	128
H35C	276(17)	-1612(9)	613(14)	128
H36A	-2672(12)	80(14)	446(18)	141
H36B	-2529(12)	1167(16)	1754(15)	141
H36C	-2695(12)	-374(16)	1763(15)	141
H1	5753(18)	2810(30)	-2030(40)	93
H5A	4320(20)	8851(12)	11910(50)	76
H1SA_3	5940(20)	4330(10)	-4982(16)	106
H1SB_3	5520(20)	4302(10)	-3562(16)	106
H1SC_3	7190(20)	4335(10)	-3937(14)	106
H2SA_3	7066(14)	2382(15)	-6332(16)	97
H2SB_3	8129(18)	2607(16)	-5087(14)	97
H2SC_3	7243(14)	1135(18)	-5773(13)	97
H1SA_4	3640(40)	6490(30)	14700(40)	93
H1SB_4	4700(40)	6770(30)	13590(50)	93
H1SC_4	5120(50)	7640(30)	15010(50)	93
H2SA_4	2450(50)	8430(30)	15980(20)	79
H2SB_4	4090(60)	9330(30)	16080(20)	79
H2SC_4	2720(50)	9850(40)	15610(20)	79
H1SA_5	6060(20)	3990(30)	-5210(30)	111
H1SB_5	4830(20)	2740(30)	-5010(30)	111
H1SC_5	5460(20)	3970(30)	-3840(30)	111
H2SA_5	8680(20)	4655(19)	-3900(20)	86
H2SB_5	7720(20)	4504(19)	-2700(20)	86
H2SC_5	9080(30)	3783(18)	-2950(20)	86
H1SA_1	3214(11)	8669(12)	16224(11)	79
H1SB_1	4079(12)	10095(14)	16039(10)	79
H1SC_1	2584(15)	9327(10)	15193(9)	79
H2SA_1	2773(11)	6546(12)	14278(11)	93
H2SB_1	2242(14)	7515(10)	13506(9)	93
H2SC_1	3420(11)	6673(11)	12941(13)	93
H1SA_2	8510(30)	1300(20)	-5920(20)	97
H1SB_2	8310(30)	440(20)	-4860(20)	97
H1SC_2	6930(30)	360(20)	-5810(20)	97
H2SA_2	6870(30)	3080(30)	-5950(20)	91
H2SB_2	5510(30)	1910(30)	-5790(20)	91
H2SC_2	5740(30)	3370(30)	-4880(20)	91

Table 21: Hydrogen Bond information for **ATB-40-192A**.

D	H	A	d(D-H)/Å	d(H-A)/Å	d(D-A)/Å	D-H-A/deg
O1	H1	O1S_3	0.82	1.81	2.630(12)	171.8
O1	H1	O1S_5	0.82	1.90	2.718(17)	173.1
O1	H1	O1S_2	0.82	1.89	2.714(17)	178.6

D	H	A	d(D-H)/Å	d(H-A)/Å	d(D-A)/Å	D-H-A/deg
O5	H5A	O1S_4	0.82	1.79	2.58(2)	161.0
O5	H5A	O1S_1	0.82	1.83	2.651(8)	175.8

Table 22: Atomic Occupancies for all atoms that are not fully occupied in **ATB-40-192A**.

Atom	Occupancy
C1S_3	0.516(3)
H1SA_3	0.516(3)
H1SB_3	0.516(3)
H1SC_3	0.516(3)
C2S_3	0.516(3)
H2SA_3	0.516(3)
H2SB_3	0.516(3)
H2SC_3	0.516(3)
O1S_3	0.516(3)
S1S_3	0.516(3)
C1S_4	0.129(4)
H1SA_4	0.129(4)
H1SB_4	0.129(4)
H1SC_4	0.129(4)
C2S_4	0.129(4)
H2SA_4	0.129(4)
H2SB_4	0.129(4)
H2SC_4	0.129(4)
O1S_4	0.129(4)
S1S_4	0.129(4)
C1S_5	0.258(3)
H1SA_5	0.258(3)
H1SB_5	0.258(3)
H1SC_5	0.258(3)
C2S_5	0.258(3)
H2SA_5	0.258(3)
H2SB_5	0.258(3)
H2SC_5	0.258(3)
O1S_5	0.258(3)
S1S_5	0.258(3)
C1S_1	0.871(4)
H1SA_1	0.871(4)
H1SB_1	0.871(4)
H1SC_1	0.871(4)
C2S_1	0.871(4)
H2SA_1	0.871(4)
H2SB_1	0.871(4)
H2SC_1	0.871(4)
O1S_1	0.871(4)
S1S_1	0.871(4)
C1S_2	0.225(3)
H1SA_2	0.225(3)
H1SB_2	0.225(3)
H1SC_2	0.225(3)
C2S_2	0.225(3)
H2SA_2	0.225(3)
H2SB_2	0.225(3)
H2SC_2	0.225(3)
O1S_2	0.225(3)
S1S_2	0.225(3)

Citations

CrysAlisPro (ROD), Rigaku Oxford Diffraction, Poland (?).

CrysAlisPro Software System, Rigaku Oxford Diffraction, (2020).

O.V. Dolomanov and L.J. Bourhis and R.J. Gildea and J.A.K. Howard and H. Puschmann, Olex2: A complete structure solution, refinement and analysis program, *J. Appl. Cryst.*, (2009), **42**, 339-341.

Sheldrick, G.M., Crystal structure refinement with ShelXL, *Acta Cryst.*, (2015), **C71**, 3-8.